Resolving the intersection of HIV and F-actin in the context of cell-cell viral spread

Author:
Ospina Stella, Alberto

Publication Date:
2020

DOI:
https://doi.org/10.26190/unsworks/2103

Resolving the intersection of HIV and F-Actin in the context of cell-cell viral spread

Alberto Ospina Stella
BSc, MSc

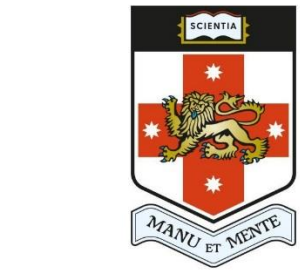

UNSW
SYDNEY

A thesis in fulfilment of the requirements for the degree of Doctor of Philosophy

Kirby Institute
Faculty of Medicine
The University of New South Wales, Australia

March 2020

UNSW SYDNEY | Australia's Global University

Thesis/Dissertation Sheet

Surname/Family Name	:	**Ospina Stella**
Given Name/s	:	**Alberto**
Abbreviation for degree as give in the University calendar	:	**PhD**
Faculty	:	**Medicine**
School	:	**Kirby Institute**
Thesis Title	:	**Resolving the intersection of HIV and F-actin in the context of cell-cell viral spread**

Abstract:

HIV has evolved elaborate mechanisms to manipulate the host cell's actin cytoskeleton. This supports specific steps of the viral life cycle but also leads to cell-type specific changes in leukocyte shape and behaviour that promote overall spread of the infection. In particular, actin manipulation is important for direct cell-cell transfer of HIV (CCTH), which is now recognized as a highly efficient mode of viral spread. This study aimed to further resolve the molecular players and mechanisms involved in this process.

Through the use of CRISPR–Cas9-mediated gene editing, herein we systematically interrogated the loss-of-function phenotype of over 50 cytoskeletal regulators, in both HIV-donor and target cells during CCTH. This was then combined with a portfolio of complementary assays ranging from live cell microscopy through to the ultrastructural resolution of focused ion beam scanning electron microscopy. This approach identified several core actin regulators to be required on both sides of viral transfer, including the Rho-GTPases Cdc42/Rac1 (signalling), upstream of the Arp2/3 complex (actin nucleator), and Profilin (which indirectly supports F-actin elongation, e.g. via Formins). In infected myeloid cells, Cdc42-Arp2/3 and Formins collaborated to form distinct "HIV-Filopodia", which were shown to be important for CCTH.

The overall findings of this work support that, while HIV uses diverse strategies to influence numerous cytoskeletal targets, there is a high tolerance for the individual loss of many manipulated regulators in the context of CCTH. However, core regulators that secure the cellular ability to mediate F-actin polymerization remain essential to this process, in particular via their contribution to cortical F-actin membrane protrusions that facilitate intercellular contacts and later maturation of the virological synapse. To conclude, we have mapped a landscape of complex interactions between HIV and the actin cytoskeleton. This not only builds on our understanding of F-actin regulation in cells of our immune system but will also facilitate the continued development of host-directed therapeutics for lentiviral and/or other pathogenic infections.

ORIGINALITY STATEMENT

‘I hereby declare that this submission is my own work and to the best of my knowledge it contains no materials previously published or written by another person, or substantial proportions of material which have been accepted for the award of any other degree or diploma at UNSW or any other educational institution, except where due acknowledgement is made in the thesis. Any contribution made to the research by others, with whom I have worked at UNSW or elsewhere, is explicitly acknowledged in the thesis. I also declare that the intellectual content of this thesis is the product of my own work, except to the extent that assistance from others in the project's design and conception or in style, presentation and linguistic expression is acknowledged.’

Signed …….....

Date …… 18th March 2020…….....

INCLUSION OF PUBLICATIONS STATEMENT

UNSW is supportive of candidates publishing their research results during their candidature as detailed in the UNSW Thesis Examination Procedure.

Publications can be used in their thesis in lieu of a Chapter if:

- The student contributed greater than 50% of the content in the publication and is the "primary author", ie. the student was responsible primarily for the planning, execution and preparation of the work for publication
- The student has approval to include the publication in their thesis in lieu of a Chapter from their supervisor and Postgraduate Coordinator.
- The publication is not subject to any obligations or contractual agreements with a third party that would constrain its inclusion in the thesis

Please indicate whether this thesis contains published material or not.

☐ *This thesis contains no publications, either published or submitted for publication (if this box is checked, you may delete all the material on page 2)*

☒ *Some of the work described in this thesis has been published and it has been documented in the relevant Chapters with acknowledgement (if this box is checked, you may delete all the material on page 2)*

☐ *This thesis has publications (either published or submitted for publication) incorporated into it in lieu of a chapter and the details are presented below*

•		
Name **Alberto Ospina Stella**	**Signature**	**Date** **18.03.2020**

Postgraduate Coordinator's Declaration (to be filled in where publications are used in lieu of Chapters)

I declare that:

- the information below is accurate
- where listed publication(s) have been used in lieu of Chapter(s), their use complies with the Thesis Examination Procedure
- the minimum requirements for the format of the thesis have been met.

PGC's Name	**PGC's Signature**	**Date (dd/mm/yy)**

COPYRIGHT STATEMENT

Signed …….....

Date ……18.03.2020…….....

AUTHENTICITY STATEMENT

‘I certify that the Library deposit digital copy is a direct equivalent of the final officially approved version of my thesis.’

Signed …….....

Date ……18.03.2020…….....

Acknowledgements:

The work described in this thesis was performed at The Kirby Institute (University of New South Wales, Australia). The last four years would not have been possible without numerous people, who have helped or supported me in various ways through this enriching but challenging time.

Firstly, I would like to sincerely thank my primary supervisor A/Prof Stuart Turville, for his continuous, genuine, determined and inexhaustible guidance and support during my candidature. His expertise in the field of HIV and myeloid immune cells has been an invaluable resource to me during this project, and I dare to say that I now share his passion for these fascinating topics. I must also thank Stuart for always being available to meet with me to discuss experiments, literature, my writing, or any other issue related to or affecting my candidature. I would also like to thank my co-supervisor Dr. Anu Aggarwal, who I am extremely grateful to for sharing her laboratory expertise with me, for being always available and willing to answer my questions, for her patience and kindness, for her interest in my candidature and wellbeing, and for being a role-model for great lab scientists.

To the members of the HIV-Biology team, past and present, I am incredibly grateful for your support and friendship both in and outside work. In particular I need to thank Andrew Wong and Samantha McAllery, who were there for me from the beginning. I must also thank a large number of other people from Kirby Level-5, including; Mee Ling, Chantelle, Michelle, Kristin, Vera, Vennila, Annett, Katherine, Christina and Hannah from the IVPP program (in the order that I met them), as well as Auda, Roshana, the "Alex's", Arun, Nick, Liz, Hui and Anurag (from VISP) and Tanya, Maria, Andrey and Alison (from VHCRP), all of whom were always friendly and there for me in one way or another when I needed them. I also thank the head of IVPP (now also director of the Kirby Institute) Professor Anthony Kelleher for welcoming me into his program, always offering sound advice and good feedback, as well as for always showing interest for my candidature.

To my friends outside the Kirby (both in Australia and overseas), thank you for always being there for me through these last 4 years. I don't think I could have made it through without your encouragement and support, as well as all the fun and/or memorable times shared as part of our friendship. Although too numerous to list them all, I feel compelled to write some names, for you are a very important part of my life. Thank you; Leonel, Oriana, Sabrina, Aida (and everyone else from our medicine group), Adam, Raimonda, Olly, Sophia, David R., David M., Rikki, Mary, Honza, Nick (and all my other Sydney friends), Alejandro, Sonia, Edylu, Ramiro (from home), all my amazing Berlin friends (special mention to Karina, Benny and Talitha), my dear Bayern friends (Isabella, Jens, Mark), and my good friends from school (especially Michelle).

Last but certainly not least, I want to thank my family, who have been my inspiration, motivation and main pillar of support over the last 4 years (despite the distance), as well as before. With my deepest sincerity, I thank my parents, who have given me unconditional love, a very happy childhood, and the best education I could possibly have hoped for. I would not be where I am if it were not for their support.

Abstract:

HIV has evolved elaborate mechanisms to manipulate the host cell's actin cytoskeleton. This supports specific steps of the viral life cycle but also leads to cell-type specific changes in leukocyte shape and behaviour that promote overall spread of the infection. In particular, actin manipulation is important for direct cell-cell transfer of HIV (CCTH), which is now recognized as a highly efficient mode of viral spread. This study aimed to further resolve the molecular players and mechanisms involved in this process.

Through the use of CRISPR–Cas9-mediated gene editing, herein we systematically interrogated the loss-of-function phenotype of over 50 cytoskeletal regulators, in both HIV-donor and target cells during CCTH. This was then combined with a portfolio of complementary assays ranging from live cell microscopy through to the ultrastructural resolution of focused ion beam scanning electron microscopy. This approach identified several core actin regulators to be required on both sides of viral transfer, including the Rho-GTPases Cdc42/Rac1 (signalling proteins), upstream of the Arp2/3 complex (actin nucleator), and Profilin (which indirectly supports F-actin elongation, e.g. via Formins). In infected myeloid cells, Cdc42-Arp2/3 and Formins collaborated to form distinct "HIV-Filopodia", which were shown to be important for CCTH.

The overall findings of this work support that, while HIV uses diverse strategies to influence numerous cytoskeletal targets, there is a high tolerance for the individual loss of many manipulated regulators in the context of CCTH. However, core regulators that secure the cellular ability to mediate F-actin polymerization remain essential to this process, in particular via their contribution to cortical F-actin membrane protrusions that facilitate intercellular contacts and later maturation of the virological synapse. To conclude, we have mapped a landscape of complex interactions between HIV and the actin cytoskeleton. This not only builds on our understanding of F-actin regulation in cells of our immune system but will also facilitate the continued development of host-directed therapeutics for lentiviral and/or other pathogenic infections.

Publications and conference proceedings

Publications

Ospina Stella, A & Turville, S. All-round manipulation of the actin cytoskeleton by HIV. Viruses **2018**, 10, 63; https://doi.org/10.3390/v10020063

Publications in preparation

Ospina Stella, A., Aggarwal, A., Fichter, C., and Turville, S. A systematic reverse genetics CRISPR screen identifies actin nucleators downstream of Rho-GTPases as key actin regulators on both sides of cell-cell HIV transfer.

Aggarwal, A. and Ospina Stella, A., Henry, C., Narayan, K., and Turville, S. HIV corrupts the Cdc42-IQGAP1 axis of actin regulation to hijack cellular filopodia that promote cell-cell viral spread.

Conference proceedings

Ospina Stella, A., Aggarwal, A., and Turville, S. (2017) Resolving the intersection of HIV and F-actin in the context of cell-cell viral spread. *Australasian HIV&AIDS Conference, Adelaide, South Australia, Australia.* (Oral presentation)

Ospina Stella, A., Aggarwal, A., Narayan, K., and Turville, S. (2018) Resolving the intersection of HIV and the actin cytoskeleton. *22nd International AIDS Conference (AIDS 2018), Amsterdam, Netherlands.* (Poster presentation)

Ospina Stella, A., Aggarwal, A., and Turville, S. (2018) Manipulation of the actin cytoskeleton by HIV. *13th Annual Australian Centre for HIV and Hepatitis Virology Research Workshop, Yarra Valley, Victoria, Australia.* (Awarded oral presentation)

Ospina Stella, A., Aggarwal, A., Narayan, K., and Turville, S. (2019) HIV cell-cell transmission and the role of the actin cytoskeleton. *14th Annual Australian Centre for HIV and Hepatitis Virology Research Workshop, Canungra, Queensland, Australia.* (Awarded oral presentation)

Table of Contents:

List of Figures:

List of Tables:

List of supplementary videos:

The following supplementary video files (fluorescence-microscopy) have been attached to this thesis:

Supplementary videos S1 and S2:

Live imaging of U937 cells (productively infected with HIV-iGFP, see Table 2.7) coincubated with TZM-bl target cells for observation of virological synapse formation. Experimental and acquisition conditions were as described in section 2.2.12.2. Still images from these representative time series are shown and described in Figure 3.13.

Supplementary video S3:

Live imaging of U937 cells (productively infected with SPLN7-IRESeGFP, see Table 2.7) coincubated with TZM-bl target cells for observation of conjugate and syncytia formation. Experimental and acquisition conditions were as described in section 2.2.12.2, except for the use of SPLN7-IRESeGFP to infect donor cells, and that target cells have been labelled with red cytoplasmic dye (see section 2.2.9). The events observed in this video and their biological interpretation are described and discussed in section 3.5.5.

Supplementary video S4:

Live imaging of U937 cells expressing a constitutively active variant of the formin Dia2 (see 6.3.1) and productively infected with HIV-iGFP (see Table 2.7), coincubated with TZM-bl target cells. Experimental and acquisition conditions were as described in section 2.2.12.2. Still images from these time series are shown and described in Figure 6.13 and section 6.4.2.3.

List of abbreviations:

AIDS	Acquired Immune Deficiency Syndrome
ART	Antiretroviral Therapy
BiFC	Bimolecular Fluorescence Complementation
CCTH	Cell-Cell Transfer of HIV
CD4TC	CD4+ T-cells
CRISPR	Clustered Regularly Interspaced Short Palindromic Repeats
CSK	C-terminal Src kinase
CytoD	Cytochalasin D
DC	Dendritic Cells
Dia	Diaphanous-related Formin
DMEM	Dulbecco's Modified Eagle Medium
DNA	Deoxyribonucleic acid
EFV	Efavirenz
EIAV	Equine Infectious Anaemia Virus
Env	HIV-1 Envelope glycoprotein
FCS	Foetal Calf Serum
FIB-SEM	Focussed Ion Beam - Scanning Electron Microscopy
FRET	Fluorescence Resonance Energy Transfer
FW	FACS-Wash buffer
Gag	p55 Gag (main structural protein of HIV-1)
GFP	Green Fluorescent Protein
gRNA	CRISPR guide-RNA
HCK	Hematopoietic cell kinase
HEK	Human Embryonic Kidney cells
HIV	Human Immunodeficiency Virus

HF	HIV-Filopodia
hpi	hours post infection
IAD	Inhibitors of Actin Dynamics
ICAM	Intercellular Adhesion Molecule
iDC	immature Dendritic Cells
IRES	Internal Ribosomal Entry Site
IS	Immunological Synapse
ITR	Infection Transfer Rate
LB	Luria-Bertani (e.g. medium or agar)
LCV2	LentiCRISPR v2 (Addgene plasmid #52961)
mDC	mature Dendritic Cells
mL	millilitre
MOI	Multiplicity Of Infection
Mφ	Macrophages
NPF	Nucleation Promoting Factor
ORF	Open Reading Frame
PBMC	Peripheral Blood Mononuclear Cells
PBS	Phosphate-buffered Saline
PCR	Polymerase Chain Reaction
PEI	Polyethyleneimine
PIP2	Phosphatidylinositol 4,5-bisphosphate
PM	Plasma Membrane
PMC	Primary Myeloid Cells
PuroR	Puromycin Resistance
RF10	RPMI-medium supplemented with 10% foetal calf serum
RNA	Ribonucleic acid
RPMI	Roswell Park Memorial Institute 1640 medium

shRNA	short hairpin Ribonucleic Acid
SIV	Simian Immunodeficiency Virus
$TCID_{50}$	Median Tissue Culture Infectious Dose
VC	C-terminal fragment of Venus fluorescent protein
VCC	Virus Containing Compartments
VLP	Virus-like Particle
VN	N-terminal fragment of Venus fluorescent protein
Vpx	Viral Protein X (accessory protein of SIV and HIV-2)
VS	Virological Synapse
VSVg	Vesicular Stomatitis Virus Glycoprotein

Chapter 1. Literature Review

1.1 HIV virology and pathogenesis

1.1.1 Introduction to HIV

The human immunodeficiency virus (HIV) is a retrovirus and the etiological agent of the acquired immunodeficiency syndrome (AIDS). HIV is believed to have originated from simian immunodeficiency viruses (SIV) after zoonotic transmission and subsequent evolutionary adaptations to the new host [1]. HIV first gained public attention in 1981 with the first media report marking the start of the AIDS epidemic [2], although earlier cases have now been confirmed, with estimates of HIV entering the human population early in the 20th century (reviewed in [3]). The virus was first isolated and given different names by two independent groups in 1983 [4,5]. In 1986, it was renamed to HIV by the international committee on the nomenclature of viruses [6]. There are 2 types of HIV known as HIV-1 and HIV-2, with the latter being less infectious and largely confined to West Africa [7]. Throughout this work, HIV refers to HIV-1 unless otherwise specified.

1.1.2 Epidemiology and burden of disease

By end of 2017, ~37 million people worldwide were estimated to be living with HIV (UNAIDS fact sheet 2018). Despite steadily increasing access to antiretroviral therapy, ~2 million new infections and ~1 million associated deaths occurred in 2017. In 2015 alone, global spending associated with HIV/AIDS treatment, prevention and care reached 48 billion US$, accumulating to at least 500 billion $ for the period 2000-2015 [8]. The human burden of disease is unequally distributed, with the large majority of HIV infected people residing in developing countries [9].

1.1.3 Disease progression and treatment

The course of HIV infection is characterized by a short yet acute symptomatic phase, followed by a clinical latency phase of variable length, which in most cases progresses to life-threatening AIDS if untreated. Three to six weeks following primary infection, acute HIV presents clinically as a mononucleosis-like syndrome with symptoms of variable intensity, which can often go unnoticed or misdiagnosed [10,11]. Symptoms are concurrent with aggressive viral replication [12,13] and significant declines in CD4+ T-cell (CD4TC) levels in peripheral blood [14]. With symptoms resolving within 1-2 weeks, the acute phase is followed by a clinical latency or asymptomatic stage, which can last from several weeks to decades [10,15]. This phase is associated with a precipitous decline in plasma viremia and a

temporary stabilization of CD4TC numbers, which are at least in part believed to be a consequence of activation of both humoral and cellular immune responses [16]. At this stage, virtually all patients have developed HIV-specific antibodies, a process termed seroconversion [17]. Despite absence of symptoms, continual and slowly increasing viral replication occurs during the clinical latency stage [18]. Without treatment, most patients eventually exit the steady state and progress to AIDS, with their blood CD4TC counts dropping below 200 cells/μL [19]. Full-blown AIDS is characterized by progressive failure of the immune system, which renders individuals highly susceptible to pathogens, opportunistic infections and neoplastic malignancies, thus resulting in premature death.

A decisive change in the history of the HIV pandemic was achieved by introduction of "combination antiretroviral therapy" [20], which was historically also referred to as "highly active antiretroviral therapy" or now simply "antiretroviral therapy" (ART). This potent treatment typically combines reverse transcriptase inhibitors with other inhibitor classes, and is highly effective in reducing plasma viral loads, preventing occurrence of AIDS symptoms, remarkably increasing the life expectancy in HIV+ individuals [21] and significantly reducing the probability of transmitting HIV to others [22]. However, while access to ART dramatically improves the theoretical prognosis of diagnosed HIV+ patients, in reality, a multitude of factors undermine the effectiveness of current treatment options to eliminate the risk that HIV poses on both individuals and populations. A high proportion of undiagnosed infections [23], limited accessibility to treatment due to high costs [24], issues in regime adherence and compliance [25], toxicity of long-term treatment [26], as well as viral escape mutations leading to pharmacological resistance [27] all result in major impediments to eliminate HIV via ART. As of 2019, no effective preventive vaccine has been approved and sterilising/functional cures are hard to achieve, given that the virus invariably integrates its genome into long-lived cells, such as memory CD4TC, forming a latent reservoir [28]. While the extent and implications of the reservoir are still not fully understood [29], long half-live estimates suggest that multiple decades of antiretroviral therapy are likely required before the virus can be cleared from an infected individual by natural decay of the reservoir [30].

1.1.4 Classification

HIV is an enveloped, single-stranded RNA virus. It belongs to the family of *Retroviridae*, subfamily *Orthoretrovirinae* and the genus *Lentivirus* [31]. The defining feature of retroviruses is their ability to insert a copy of the viral genome into the host's genome. This requires conversion of the viral RNA to DNA through a process termed reverse transcription, which is mediated by a reverse transcriptase enzyme encoded and delivered by the virus. A unique feature of lentiviruses is their ability to integrate the reverse transcribed DNA into the

genome of non-dividing cells [32]. This exceptional ability has turned them into valuable tools for gene delivery [33].

1.1.5 Viral genome and structure

The genome of HIV is approximately 10-kb in size, and consists of two copies of single-stranded RNA of positive polarity, comprising only 9 genes which successfully encode all viral proteins [34,35]. Three major genes, *gag, pol* and *env* encode large polyproteins, from which all structural components and 3 essential enzymes are derived . The additional genes (*tat*, *rev*, *vif*, *vpr*, *vpu*, and *nef*) encode proteins with the same names. Tat and Rev are essential regulatory elements for viral gene expression, whereas Nef, Vpr, Vif and Vpu are accessory proteins.

1.1.5.1 HIV-Gag and its role in viral assembly and budding

Gag encodes a 55 kDa protein (i.e. Pr55gag or henceforth simply "Gag") which directs the process of virion assembly. Gag is post-translationally myristoylated at the N-terminus [36], which together with a highly basic protein region allows targeting to membrane domains enriched with the lipid phosphatidylinositol 4,5-bisphosphate (PIP2) [37]. Gag oligomerization is triggered by binding viral RNA via the nucleocapsid domain [38]. Multimerization of Gag complexes at the plasma membrane (PM) drives lattice formation and assembly of budding viral particles. While Gag alone can mediate binding to the PM, packaging of the viral RNA, concentration of Env and formation of spherical particles [39], the final steps of budding require host proteins. Gag binds and recruits the cellular proteins TSG101 and Alix via its p6 domain [40,41]. These in turn recruit additional components of the cellular ESCRT machinery, which is essential for coordinating membrane abscission of budding viral particles [42]. The released immature viral particle is composed of an inner protein shell made of ~2,500 copies of Gag, enclosed within a lipid bilayer envelope derived from the cellular PM [43]. During and/or shortly after the abscission, Gag is sequentially cleaved by HIV-Protease to produce the Matrix (p17 or MA), Capsid (p24), Nucleocapsid (p7 or NC), and p6 proteins [44]. These abundant proteins assemble to form the corresponding viral structures, which stabilize the virion, package the genetic material and form the viral core. These changes mediate maturation of the virion into its final infectious form. An overview of the mature viral particle structure and its components is shown in the figure below.

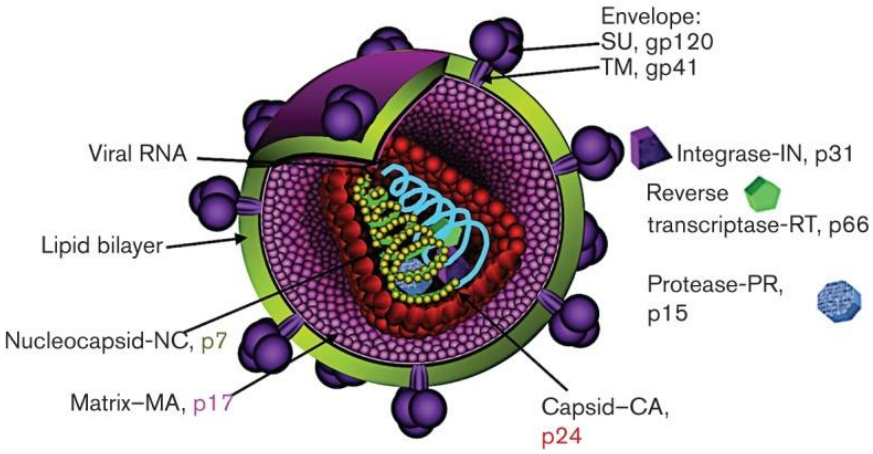

Figure 1.1: Mature virion structure. HIV is roughly spherical with a diameter of ~120 nm. The viral genome is enclosed by a conical fullerene core constituted of Capsid protein (red circles). The core contains the viral RNA (bound to Nucleocapsid), as well as the reverse transcriptase, protease and integrase enzymes. The core is surrounded by an outer shell constituted of Matrix proteins, which in turn is surrounded by the viral envelope (green ring). The glycoprotein Env is the only surface-exposed viral protein and corresponds to a homotrimer of gp120 and gp41 heterodimers. Except for Vpr (not shown), most accessory proteins are not actively incorporated into the virion. Image was reproduced from [45], in agreement with its open access licensing conditions.

1.1.5.2 The role of *Pol*

Pol supplies the enzymatic tools for viral reproduction including; 1) the reverse transcriptase (RT), which converts the RNA genome to a DNA template, 2) integrase, which incorporates that template into the host cell genome, and 3) the protease which cleaves precursor polyproteins and thus mediates viral maturation [44]. The *pol* gene products are produced and incorporated into the virion through the synthesis of Gag-Pol, a polyprotein resulting of a programmed -1 ribosomal frameshifting event [46]. In infected cells, this generates Gag and Gag-Pol in an estimated ratio of ~20:1, a number which is conserved among retroviruses [47]. The *pol*-derived proteins are released by protease-mediated cleavage of Gag-Pol during viral maturation.

1.1.5.3 The Envelope glycoprotein

Env encodes gp160, a precursor protein which provides the components for the trimeric envelope glycoprotein complex of HIV-1 (Env). The biosynthesis, trafficking, and incorporation of Env is reviewed in [48]. Briefly, gp160 is targeted to the ER, where it forms homotrimers and core glycosylation occurs. These are then transported to the Golgi network, where they are cleaved by cellular proteins into the gp120/gp41 components and additional glycan modification ensues. Gp120 provides the interface for interaction with cellular receptors and gp41 the transmembrane component and the membrane fusion machinery. The

mature Env glycoprotein is composed of a homotrimer of gp120-gp41 heterodimers [49]. The exact mechanism of Env incorporation into the budding particle is not yet understood, however it is known to involve the cytoplasmic tail of Env and its association with Matrix [50]. Only few Env trimers (~14 on average) are incorporated per virion, as revealed by cryo-electron tomography [51].

1.1.5.4 Accessory proteins

HIV accessory proteins are known to mediate a myriad of different functions. Most of these are associated with; i) enhanced virion infectivity (e.g. by counteracting cellular restriction factors [52], ii) modulation of host gene expression [53], and iii) enhanced viral persistence, replication and dissemination [54]. Overall, accessory proteins are dispensable for HIV particle formation *in vitro* but are important for pathogenesis *in vivo* [55].

1.1.6 Viral life cycle

The HIV-1 life cycle is illustrated in Figure 1.2. Viral entry begins with attachment of the virion to the cell-surface, which is in part mediated by binding of gp120 to the cellular CD4 receptor. This triggers conformational changes in Env, which, among other things, expose co-receptor binding sites in gp120 and hydrophobic fusion peptides in gp41 [56,57]. The cascade of conformational changes ultimately allows gp41 to mediate fusion of the viral envelope with the host cell membrane via a complex but well understood process (reviewed in [58]). Upon fusion, the viral core is released into the cytoplasm immediately below the plasma membrane. Complex spatiotemporal events involving actin remodelling facilitate transport of the core through the cellular actin cortex (see 1.5.6). In parallel, the capsid shell begins to dissociate in a multistep process termed uncoating. Although this process is not fully understood, it is known to be coordinated by cellular proteins and to affect reverse transcription and transport to the nucleus (reviewed in [59]). Released RT enzyme mediates reverse transcription of the viral single stranded RNA genome into double stranded cDNA in the cytoplasm. This process is exceptionally error-prone due to the lack of exonucleolytic proofreading activity of the RT enzyme, which has an average error rate of ~1/1700 per incorporated nucleotide [60]. The resulting sequence diversity in progeny virus is considered to be the determinant factor allowing viral immune escape and development of resistance against monotherapy treatments. The DNA genome is subsequently imported into the nucleus, in association with numerous viral and cellular proteins which together form a nucleoprotein complex known as the pre-integration complex [61]. Once in the nucleus, the viral DNA genome is stably inserted into the host genome by action of the viral integrase [62]. Integration does not occur at a specific site, but genome-wide sequencing analyses revealed a preference for integration into gene-

encoding regions [63]. The permanently integrated viral genome is known as "provirus" and serves as the template for the transcription of viral genes required for productive replication [64]. Infected cells can be in a latently infected or productively infected state. The former are characterized by the lack of viral gene expression, but can transition to productive infection following different stimuli [65]. In productively infected cells, the provirus is transcribed by the cell machinery, resulting in translation of viral proteins in the cytoplasm (and the endoplasmic reticulum). This in turn leads to production of new viral particles, as described in sections 1.1.5.1-3). Persistence of HIV in long-lived cells such as latently infected memory CD4TC constitutes the latent HIV reservoir, which is now considered the most critical barrier to curing HIV infection.

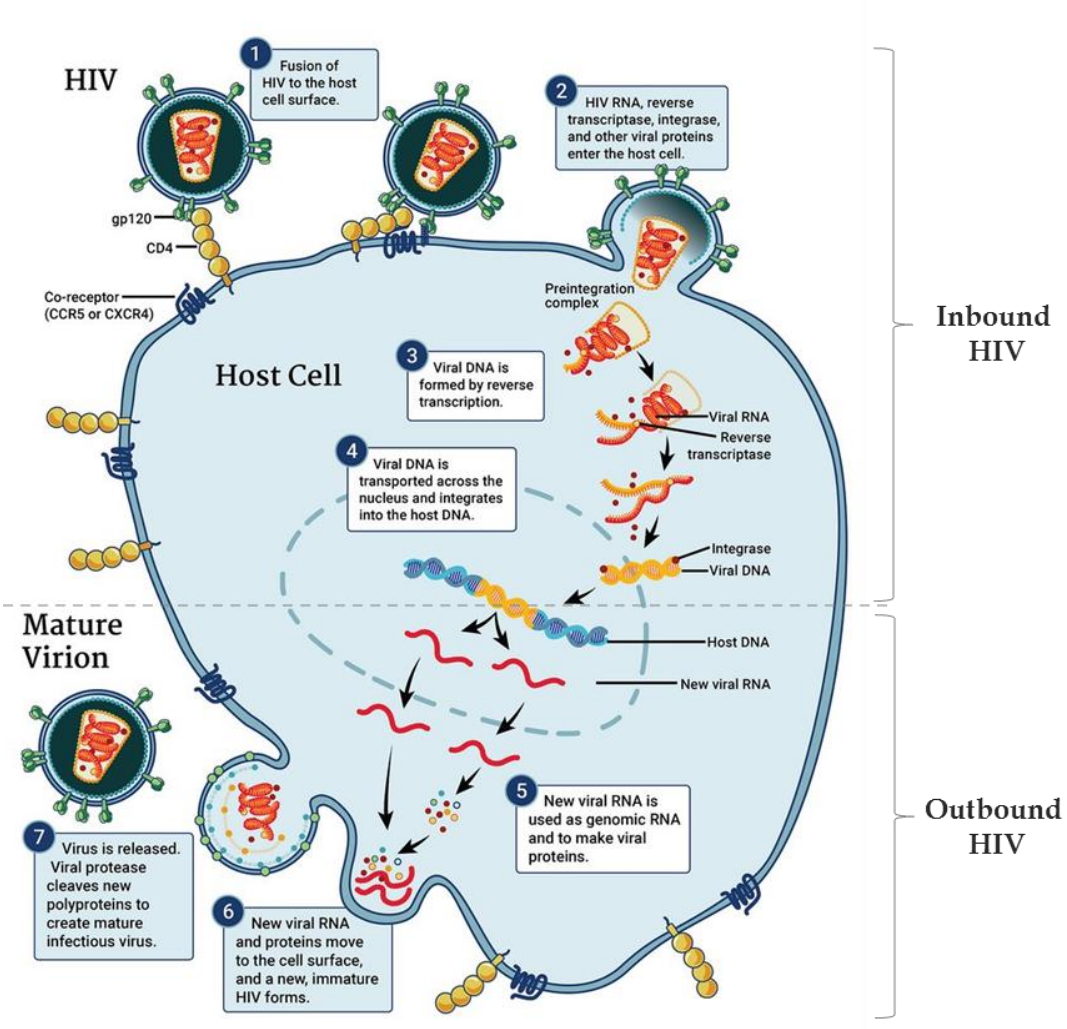

Figure 1.2: Overview of the HIV life cycle. This image was adopted and modified from the "National Institute of Allergy and Infectious Diseases" website (https://www.niaid.nih.gov/diseases-conditions/hiv-replication-cycle) in agreement with its licensing conditions (CC BY 2.0). The only modifications are shown in grey and correspond to the delineation of "inbound" and "outbound" HIV, as defined below.

1.1.7 Inbound vs. outbound HIV

For the purpose of this work, it is important to distinguish between events occurring in cells which are already productively infected, and those in uninfected cells upon challenge with virus. We define "inbound virus" as any naturally occurring infectious particle that originated from an infected cell and which, after an extracellular phase of variable length, is in the process of moving from the plasma membrane (PM) to the nucleus of a different cell. This includes mature virions bound to target cells, and the intermediates which result after membrane fusion and during uncoating, reverse transcription, nuclear transport and genome integration. In contrast, we define "outbound virus" as the collection of viral components which are produced de novo in an infected cell, and which are in the process of exiting this cell in the form of initially immature HIV particles. This includes viral proteins and RNA during their transport to the PM, particle assembly and budding, up to the point of abscission. Note that these definitions were recently published by the author of this thesis in [66]. A graphic overview of the life cycle steps corresponding to inbound and outbound HIV is shown above (Fig. 1.2).

1.1.8 HIV tropism

HIV can infect cells that express the CD4 protein, along with either of the chemokine receptors CCR5 or CXCR4. CD4 is therefore the primary HIV receptor and CCR5/CXCR4 are considered the classical HIV co-receptors [67]. The cellular surface concentration of these proteins plays an important role in susceptibility to viral infection. Thus, mononuclear cells of the immune system such as CD4+ T-cells (CD4TC), macrophages (Mφ) and dendritic cells (DC) are the major cellular targets for HIV infection *in vivo* [68-70]. The ability of viral variants to use either coreceptor usually determines the tropism. Strains that use CCR5 for viral entry are termed R5 viruses, whereas strains that use CXCR4 are known as X4 viruses [71]. However, dual-tropic R5X4 viruses have also been isolated [72]. Generally speaking, R5 viruses dominate in clinical samples and are able to infect Mφ and primary CD4TC, whereas the susceptibility of DC is affected by their maturation stage [73]. Most transmitted/founder strains (i.e. those which typically establish primary infection) are R5-tropic [74]. In contrast, X4 variants emerge only in ~50% of HIV patients and are associated with increased pathogenicity and more aggressive disease progression [75]. Of note, alternative receptors such as C-type lectins have been described, but these receptors alone simply aid viral attachment and cannot lead to direct infection unless CD4 and CCR5 or CXCR4 are present [76].

1.2 Viral spread

1.2.1 Cell-free vs. cell-cell HIV spread

A crucial, yet unresolved, issue in HIV pathogenesis is the dominant mechanism by which the virus spreads between and/or within individuals. Both free virions and different types of infected cells coexist in the blood and tissues of HIV-infected individuals throughout the course of infection. The same is true for the bodily fluids clinically associated with HIV-transmission, such as semen [77], genital secretions [78] and maternal milk [79]. Given the high plasma viral loads present during AIDS, HIV spread was initially thought to be mediated by dissemination of free viral particles, which could travel long distances within the organism. However, it was recognized early that the virus can also spread from HIV-infected cells via direct cell-cell contacts [80-83]. Since then, a vast amount of evidence has accumulated and revealed cell-cell transfer of HIV (CCTH) to be a highly efficient mechanism of viral spread.

1.2.2 Viral transfer *in cis* vs. *in trans*

Two major modes of CCTH have been proposed. CCTH "*in cis*" occurs when the viral particles being transferred also originated *de novo* in the donor cell (i.e. via assembly of cytosolic viral components at the PM, which leads to viral budding). By definition, this requires the donor cell to be productively infected. In contrast, CCTH "*in trans*" is mediated by cells which, without themselves becoming productively infected, can capture extracellular mature HIV particles and deliver them to target cells (reviewed in [84]). Both *in cis* and *in trans* CCTH can occur either immediately after viral production/capture, or after storage of extracellular virions in membrane-invaginated or intracellular compartments for variable periods of time. These concepts are further expanded in sections 1.3.1-1.3.3.

1.2.3 Evidence of cell-mediated HIV transfer

In vitro, cell-cell transfer of HIV has been observed between many different cell types. For CCTH *in cis* this includes; from T-cells to T-cells [85-88], immature DC to T-cells [89,90], macrophages to T cells [83,91], T-cells to epithelia [82], monocytes to epithelia [80,92], T-cells to placental trophoblasts [93], T-cells to astrocytes [94], plasmacytoid DC to thymocytes [95], among others. It should be however noted that HIV transfer in some of these contexts (e.g. epithelial target cells) did not require CD4-dependent viral fusion and/or did not lead to productive infection of the recipients. For CCTH *in trans*, observations include viral transfer from; mature DC to T-cells [81], immature DC to T-cells [96], Langerhans cells to T-cells [92], macrophages to T-cells [97], and even epithelial cells to T-cells [98,99]. Most of these *in vitro* studies showed that adding infected (or HIV-pulsed) donor cells led to a dramatic

increase in target cell infection, compared to adding equivalent amounts of cell-free virus alone. Trans-well systems that allow free virus diffusion were also used to demonstrate that direct contact between donor and target cells was required [86-88]. A key study by Sourisseau et al. also emphasized the importance of stable cell-cell contacts for HIV transfer, by showing that target cell infection was dramatically impaired upon gentle shaking of cocultures, despite unaffected free virus release [86].

Numerous observations from animal models also directly or indirectly support an important role of CCTH for HIV transmission *in vivo.* Exposure of simian animal models to cells infected with SIV via the intrarectal [100], intravaginal [101-103] or intravenous [101,104] route all led to systemic and persistent infection. Doses as low as two infected cells could serve as infectious inoculum via the intravenous route [104]. Data from humanized mice models also supports a role for cell-mediated HIV transmission *in vivo*. Two studies showed that HIV-infected cells administered intravaginally could cross the mucosal epithelium and be found first in vaginal tissue and later in lymph nodes [105,106]. Di Fabio et al. showed that this resulted in systemic infection of the animals [106], which could also be achieved by intravenous injection of HIV-infected cells [107]. The latter study used intravital imaging to show that HIV-infected cells could arrest migration of uninfected T-cells and lead to formation of Env-dependent cell-cell conjugates in the spleen. On the other hand, impeding egress of infected T-cells (but not free virus) from the lymph node highly limited the ability of a local infection to spread systemically in humanized mice [108].

Analysis of human tissue also supports occurrence of CCTH both *ex vivo* and *in vivo.* Two studies using foreskin explant models showed that infected mononuclear cells can transmit HIV to inner foreskin cells within 1 hour The virus was then captured by Langerhans cells in the epidermis, which migrated to deeper tissue and formed conjugates with CD4TC, to which they transmitted the virus *in trans* [92,109]. Furthermore, multi-copy infected cells have been found in lymphoid tissue of HIV+ individuals at relatively high frequency [110-112], which is consistent with a cell-cell mode of transmission [113]. Spatial segregation and enrichment of different viral quasi-species within distinct micro-anatomical regions of lymphoid tissue has also been reported [114,115]. This suggests that viral replication in lymphoid tissue occurs, at least in part, via cell-cell contacts within local cell clusters and not by free virus diffusion [107]. Mathematical modelling based on real patient data also predicts an important role of CCTH in HIV pathogenesis. In this context, Zhang et al. concluded that while both cell-cell and cell-free virus are required for establishing the initial infection, CCTH becomes increasingly more important as the infection progresses [116].

Finally, it should be noted that the ability to spread cell-to-cell is not a unique feature of HIV. The potential of viruses to spread via cell-cell contacts was recognized even long before HIV was discovered [117,118]. Since then, an ever-increasing number of viruses (and mechanisms) have been found to mediate cell-cell infection transfer, which is now widely recognized as a highly efficient mode of viral spread. Indeed, some viruses seem to have evolved to rely almost entirely on cell-cell infection mechanisms (e.g. varicella-zoster virus [119] and the retrovirus HTLV-1 [120]), with their cell-free virus forms being nearly absent or uninfectious. For extensive reviews on cell-cell transfer of other non-HIV viruses we refer to [121,122].

1.2.4 Efficiency of cell-mediated HIV transfer

The relative efficiency of CCTH compared to free virus has been primarily studied *in vitro*, with the former being more efficient in virtually every study which directly compared both. However, the reported extent of this difference varies considerably between studies. Transfer of HIV material from T-cell to B-cell lines was 2-fold more efficient than when delivered by free viral particles *in vitro* [123], although it should be noted that B-cells are not believed to be natural targets of infection *in vivo*. Others observed a ~10-fold increase for CCTH from Mφ to T-cells [83,91,124]. While this is consistent with the findings of [86], who also observed a 10-fold higher efficiency of CCTH in Jurkat and primary T-cells, other studies observed even larger differences in homotypic T-cell systems. Hubner et al. found a 20-fold difference for CCTH from Jurkat to MT4 T-cells [125], whereas others reported 10^2 -10^3 higher efficiency of CCTH between H9 T-cells [126]. Chen et al studied CCTH from Jurkat cells to primary CD4TC and observed cell-associated transfer of virus by Jurkat cells to be up to 18,000-fold more efficient than uptake of cell-free virus [127]. Clearly, a multitude of reasons can account for the discrepancies in these observations. On one hand, there are experimental-associated factors such as the use of different cell-types, viral strains, experimental setups, coculture conditions, different readout strategies, etc. On the other hand, biological factors such as cellular origin and state likely also affect the inclination of donor cells to transfer virus, or of target-cells to become infected by cell-cell or cell-free mechanisms. In agreement, CCTH from DC could be dramatically increased in the presence of cytokines, antigen or CD40-stimulation [128], whereas resting cell activation notably increased target cell permissivity to HIV infection. Two studies showed that resting PBMCs were susceptible to CCTH but not free virus infection. Resting cell activation increased CCTH and rendered target cells partially permissive to free HIV infection [83,129].

Several studies have also suggested a higher efficiency of CCTH *in vivo*. Intra-rectal exposure to SIV-infected lymphocytes (but not equivalent amounts of cell-free virus) resulted in acute

systemic infection of rhesus monkeys [100]. Intravaginal exposure to SIV-infected cells (but not their free virus supernatant), in amounts within the range of that observed in the semen of HIV+ patients, induced systemic and persistent infection in macaques [103]. Similar observations were made by Khanna et al. in humanized mice [105]. In contrast, other studies reported that cell-free virus was also able to initiate infection via the intravaginal [101,104,130,131], intrarectal [132] or intravenous [101,104,133] routes. Overall, the indisputably higher efficiency of CCTH *in vitro*, the theoretical advantages of CCTH (see 1.3.5), and the tendentially higher ability of infected cells to initiate systemic infection in animal models have led to a well-accepted view in the field that CCTH is likely to be the predominant mode of viral spread also *in vivo* [121,134-136]. This, however, remains to be formally demonstrated.

1.2.5 Role of myeloid cells in spreading the infection (*in vivo*)

Given their immediate relevance to the work conducted in this thesis, this section reviews the most important aspects of myeloid immune cells that are natural targets of HIV (i.e. DC, Mφ and monocytes) and what is known about their contribution to HIV spread *in vivo*. The mechanisms by which these cells mediate CCTH *in vitro* are discussed in later section 1.3.

1.2.5.1 Role of dendritic cells

Dendritic cells are professional antigen presenting cells, and as such play a pivotal role in communication of the adaptive immune response [137]. They are found in the skin and in most sub-epithelial mucosae, scavenging for invading pathogens. Note that while different subsets of dendritic cells exist, and their interactions with HIV may vary, this is beyond the scope of this thesis. Here, the term "DC" is generally used and may refer to either some or all dendritic cell subtypes of myeloid origin, unless otherwise specified. Distinctions between immature (iDC) and mature (mDC) dendritic cells is made, where relevant. Upon pathogen sensing, these can be captured, internalized and processed by DC to mediate antigen presentation on the DC surface. This is concomitant with a DC maturation process, which involves morphological, phenotypic and functional changes [138]. Maturing DC then migrate to secondary lymphoid organs, where they peregrinate to find cells with T-cell receptors matching the presented non-self antigen. The natural sentinel function of DC therefore has the potential to be exploited by HIV at multiple levels. First, DC are abundant at the mucosa and epidermis of anogenital tissue, such as vagina and rectum [90]. Second, the membrane projections of some DC can extend through the epithelium and even into the lumen [90,139]. Therefore, DC are not only enriched at the primary sites of inter-host HIV transmission, but they likely also represent the first immune cell type to encounter incoming virus, whether in

cell-free or cell-associated form. Third, DC have the ability to migrate and transport internalized pathogens to lymph nodes, where they can engage with T-cells in thousands of contacts per hour [140]. In addition, DC *in vitro* can mediate potent CCTH to CD4TC, both *in trans* and *in* cis [81,96,128,141,142]. DC therefore represent an exceptional vehicle opportunity for the virus to rapidly reach the lymphoid tissue and replicate there, provided the virus can infect the DC or escape degradation. Indeed, accumulating evidence suggests that HIV has evolved mechanisms to hijack DC and use them to disseminate during the earliest stages of infection. While this theory is supported by findings from animal models (which can be analysed days/hours after initial viral exposure), it has proven difficult to assess in humans, given the challenge of obtaining such early clinical samples. Nevertheless, a consensus in the field has emerged that immunodeficiency viruses can be quickly and directly carried by DC from the initial site of infection to the lymphoid tissue, where massive amounts of tightly packed HIV target cells are located, thus likely allowing CCTH to occur efficiently *in vivo* [96,143-147]. This is supported by the observations of [148], who showed that SIV rapidly enters the vaginal mucosa and associates primarily with intraepithelial DC but not T-cells or Mφ. As soon as 18h after exposure, SIV-carrying DC could be detected in the lymph nodes draining the tissue [148]. Somewhat similarly, Spira et al. observed DC to be the first SIV-infected cell type in the vaginal epithelium after viral exposure. SIV-infected cells then sequentially appeared in the draining ileal lymph nodes and finally in the blood [149]. Subcutaneous injection of HIV-pulsed DC also led to rapid appearance of detectable viral RNA in the associated draining lymph nodes of a murine mouse model [150]. Since the kinetics and localization of SIV-infected cells in these *in vivo* studies, correlated well with the typical migration pattern of DC from epithelia to lymphoid tissue [150], this strongly supports a role of DC in disseminating the early HIV infection events.

However, a major unresolved and highly debated issue remains whether DC *in vivo* spread the infection *in cis* or *in trans* (see also section 1.3.3). Many authors have discarded a potential role of the *in cis* mechanism in HIV pathogenesis due to; i) the fact that DC are remarkably difficult to infect *in vitro*, and ii) the very low frequencies at which infected DC have been observed *in vivo*. As for the first point, monocyte derived DC (the most frequently used DC model) express low levels of CD4 and moderate levels of the CCR5 and CXCR4, as well as other Env-binding receptors (e.g. the C-type lectin receptor DC-SIGN) [151]. While all of these in theory open avenues for HIV infection, immature DC *in vitro* have been reported to support only low levels of infection (notably more susceptible to R5-tropic compared to X4-tropic virus), whereas mature DC are refractory to HIV-infection [146,152]. The general resistance of myeloid cells to HIV has been largely associated to the presence of various restriction factors (reviewed in [147]), most prominently including SAMHD1. This cellular

enzyme strongly limits inbound HIV infection by (among other mechanisms) depleting the pool of nucleotides required for viral reverse transcription (discussed in further detail in chapter 7.3.1). However, recent studies have revealed that resting CD4TC are also protected by SAMHD1 (reviewed in [153]). Indeed, these cells are remarkably difficult to infect *in vitro*, yet their critical importance for HIV pathogenesis *in vivo* is well defined. Poor propensity to infection *in vitro* (especially of monocultures) is therefore not a compelling reason to exclude important roles *in vivo*. In any case, productive infection of DC has been reported both *in vitro* [89,90,128,141,154-156] and *in vivo* [149,157-164]. And although the latter may occur at rather low frequencies, it can presently not be excluded that small numbers of infected DC play a major role in early dissemination of HIV from mucosal to lymphoid tissue, in a manner similar to how small numbers of DC (potentially as little as 1) can effectively communicate the adaptive immune response between these sites [141,153,165]. This theory fits particularly well with two well-documented but poorly understood *in vivo* phenomena, i.e.; i) that HIV infection is often initiated by a single viral quasispecies, and ii) that R5-tropic variants are "selected" during the earliest stages of infection, despite the fact that both R5 and X4 variants may be present in infectious bodily fluids [166]. These observations would be consistent with the postulate that a rare DC productive-infection event is required for disseminating the infection. This is because immature DC are preferentially infected by R5 compared to X4 tropic virus, with productive infection being required for viral transfer *in cis*, whereas CCTH *in trans* is independent of viral tropism [152,167]. Alternatively, the R5 selection phenomenon may be explained by an increased ability of DC to mediate CCTH of R5 compared to X4 tropic virus [168,169]. An immediately recent study has also challenged the view that infected DC do not play a role in HIV pathogenesis. Bertram et al. showed for the first time that CD11+ DC cells are not only frequent but also enriched in the epidermis of anogenital tissue. These DC express high levels of CCR5, preferentially interact with HIV (*in situ*), support higher levels of both HIV uptake and productive infection (*ex vivo*), and are highly efficient at transmitting the virus (*in cis*) to CD4TC, compared to DC from other tissues [90]. These findings therefore strongly suggest a critical role of DC for sexual transmission of HIV.

1.2.5.2 Role of macrophages

Macrophages (Mφ) are mononuclear phagocytes that are present in virtually all tissues of the human body. Macrophages arise by differentiation of monocytes or by self-renewing proliferation at their resident tissue [170], where they serve important housekeeping functions. These primarily include patrolling for invading pathogens and removal of any foreign substances by phagocytosis and subsequent digestion. Since they also have the ability to

mediate antigen presentation, Mφ are important components of both innate and adaptive immune responses [171]. It is now well-accepted that Mφ play an important role in HIV pathogenesis [70,172-174], although the specifics of their contribution are far from fully understood. Unlike DC, macrophages are not believed to participate in early stages of the HIV infection. In fact, transmitter-founder viruses replicate poorly in Mφ, compared to other HIV target cells [175,176]. Still, the potential of Mφ to be infected by HIV was recognized over three decades ago [177], and since then numerous studies have confirmed the presence of infected macrophages in HIV+ human subjects. This includes in liver [178], brain [179,180], gut [181,182] and lung [183] tissue. Productive infection of Mφ is thought to occur by at least three possible routes; i) by Env-CD4 dependent viral entry, ii) by ingestion of infected T-cells or their debris, and iii) by differentiation of infected monocytes (reviewed in [173]).

By far the most important contribution proposed for Mφ in HIV spread/pathogenesis is their ability to serve as viral reservoirs. This is because infected macrophages do not succumb to cytopathic effects, which is likely a combined consequence of host restriction factors (reviewed in [173]) and viral manipulation which actively extends the lifespan of infected Mφ [184]. Thus, infected Mφ may be able to survive for years and/or be maintained by self-renewing proliferation [170], while sustaining low levels of viral replication [185]. In addition, Abreu et al also showed the presence of SIV latently infected Mφ in macaques [186], which adds another layer of complexity to the Mφ reservoir. Recent evidence from human patients indeed confirms that infected macrophages can persist in the organism even after prolonged antiretroviral treatment [182,187-189]. Observations from animal models also suggest that Mφ harbour functional virus that can be reactivated upon treatment interruption [186,190]. Extensive viral replication in Mφ was observed when macaques were depleted of CD4TC [191], suggesting that Mφ may play an important role in advanced stages of AIDS. In addition, Mφ can mediate CCTH both *in cis* and *in trans* (see 1.3.2.3), which may contribute to viral spread in (or to) non-lymphoid tissues [91]. Overall, Mφ seem to be a fundamental component of the HIV reservoir *in vivo* [174], yet their contribution to HIV pathogenesis is only beginning to emerge.

1.2.5.3 Role of monocytes

Monocytes are the myeloid progenitor cells for macrophages and dendritic cells. They are produced in the bone marrow and typically circulate in the blood for less than a week before entering various tissues, where they differentiate into Mφ or DC [192]. Like their progeny, monocytes contribute to both the innate and adaptive immune system thanks to their ability to mediate phagocytosis, antigen presentation and cytokine production. Monocytes show low susceptibility to HIV infection *in vitro*. This is associated with expression of several host

restriction factors (e.g. APOBEC3G), yet susceptibility increases notably as monocytes mature towards the Mφ phenotype (reviewed in [193]). Still, numerous studies have reported the presence of HIV-infected monocytes *in vivo* [194-200], albeit at low frequencies (<1%) [194]. Most of these observations suggest a latent infection state in circulating monocytes, but low levels of viral replication have also been reported [197,198]. Interestingly, a specific subset of monocytes (CD16+) is preferentially infected by HIV both *in vitro* and *in vivo* [199], and this population expands considerably in untreated HIV+ patients [201].

The contribution of infected monocytes to HIV spread/pathogenesis has historically received little attention, yet potentially important roles for this cell population are now appreciated. First, monocytes likely contribute to the establishment of HIV reservoirs. Indeed, infected monocytes continue to be detected in HIV+ patients even after prolonged antiretroviral therapy [196,197,202-204], and infectious virus can be obtained from these cells [186,203,204]. Second, the ability of monocytes to cross the blood brain barrier is believed to be determinant for the ability of HIV to reach the brain [205]. Infected Mφ in other non-lymphoid tissues may similarly arise from the extravasation and tissue colonization by HIV+ monocytes, which support productive infection once differentiated. This has led to propose a role of monocytes as "trojan horses" that disseminate the infection to different tissues [204,205]. Third, although the ability of monocytes to mediate CCTH directly (i.e. in their undifferentiated form) is largely understudied, the available evidence suggests that they can transfer virus both *in cis* [80,89,206] and *in trans* [207]. This could play an important role in sexual HIV transmission, given the presence of infected monocytes in semen [207]. In summary, monocytes are natural HIV target cells *in vivo*, where they contribute to HIV pathogenesis [70] and establishment of viral reservoirs [174]. However, the mechanisms that lead to HIV-infection of circulating monocytes (especially during ART) remain obscure and controversial.

Overall, myeloid cells are largely refractory to HIV infection *in vitro* but numerous studies have confirmed that infected macrophages, monocytes and dendritic cells can and do exist *in vivo*, albeit at notably low frequencies. Despite this, abundant evidence suggests that these cells play pivotal roles in HIV spread and pathogenesis. The remarkable ability of DC to mediate highly efficient CCTH, both *in trans* and *in cis*, may be critical for early dissemination of the infection to target CD4TC, either locally at mucosal entry sites and/or after viral transport to the lymphoid tissue. In contrast, the abilities of monocytes and long-lived Mφ to sustain latent and/or productive infection (without succumbing to cytopathic effects) may be determinant for driving the establishment of viral reservoirs, as well as low levels of free viral replication and/or cell-cell HIV spread in both lymphoid and non-lymphoid tissues, even in the presence of antiretroviral drugs. The substantial benefits (for the virus) of infecting

myeloid cells *in vivo* have led to the postulate that these cells represent "quality rather than quantity HIV substrates" [153], and recent evidence has substantially reinforced this notion.

1.2.6 Role of CD4+ T-cells in spreading the infection (*in vivo*)

CD4TC play an indisputable, central and well-documented role in HIV pathogenesis. However, since this thesis specifically focused on the spread of outbound HIV from myeloid cells, this section will only briefly summarize the most general and key aspects of T-cell–mediated infection spread. CD4TC are both the primary HIV-target cells and primary virus producing cells during acute and chronic infection [68]. Over 99 % of viral particles *in vivo* are produced by recently infected and short-lived CD4TC [143,208]. Their continued depletion in untreated chronic infections is the determinant factor for the immunodeficiency symptoms which characterize AIDS. The majority of infected CD4TC at all stages of infection are found within secondary lymphoid tissue, where most of the viral replication and HIV-associated CD4TC-death occur [209]. This is thought to be at least in part a consequence of the high density of HIV target cells within these tissues, which allows efficient (but potentially lethal) CCTH to occur [210,211]. The mechanisms by which productively infected CD4TC mediate efficient CCTH, in particular via virological synapses, have been extensively studied *in vitro (*see 1.3.2), and accumulating evidence increasingly supports its long-inferred but formally unconfirmed role *in vivo* ([108,212] and see 1.2.3). Importantly, a recent study has also demonstrated that CCTH between T-cells promotes latent infection of resting CD4TC to a greater extent than cell-free virus [211]. Given their remarkably long half-lives and potential of reactivation and proliferation, latently infected resting memory CD4TC constitute the best studied and most important component of the latent HIV reservoir [213], and therefore the major obstacle towards HIV cure approaches.

1.3 Mechanisms of HIV cell-cell transmission

By definition, the process of CCTH involves direct cell-cell contacts between HIV donor and target cells. Since immune cells strongly depend on intercellular contacts to mediate immune surveillance and orchestrate highly complex immune responses [214], the virus has likely evolved to take advantage of this vitally important feature of the immune system in order to facilitate viral spread, while simultaneously avoiding and/or disrupting immune defences. This involves passively exploiting naturally occurring leukocyte interactions, as well as actively inducing non-physiological cell-cell contacts by manipulating cellular behaviour. Numerous HIV-relevant contact variants have been described so far. These can be grouped as either; i) long-range or "remote" contacts (i.e. via membrane protrusions on the donor and/or target cell, which can span several μm and typically involve small contact surface areas), or

ii) short-range "intimate" contacts (which involve close apposition of donor and target cell bodies, typically with extensive interaction of their plasma membranes, leading to a narrow intercellular or "synaptic" space over a significant surface area). Intimate contacts include the so-called HIV "synapses", which are typically considered the most efficient mechanisms of CCTH [84]. However, accumulating evidence also suggests an important role of remote contacts, such as those mediated by filopodia and nanotubes, in facilitating CCTH. The most relevant of these different structures (to this thesis) are introduced below.

1.3.1 The infectious synapse and HIV transfer "*in trans*"

CCTH "*in trans*" occurs when cells that are not productively infected capture extracellular HIV particles and deliver them in an infectious form to target cells. When this occurs via intimate cell-cell contacts and between cells that could normally participate in "immunological synapses" [215], the resulting structure is referred to as an "infectious synapse" [136]. While all antigen presenting cells can serve as HIV donor/carrier cells [216], the best studied infectious synapse variant is the one forming between HIV-pulsed DC and CD4TC. Since this thesis focuses on CCTH "*in cis*", only the canonical infectious synapse will be briefly introduced here. It should be noted that the term "infectious synapse" is sometimes interchangeably used with "virological synapse". However, as many others, we reserve the latter term for structures that mediate CCTH "*in cis*".

The potential of DC to mediate potent CCTH *in trans* (at least *in vitro*) was recognized early. Cameron et al. described how mature DC "amplified the cytopathic effects of small amounts of virus" and "formed clusters with T-cells that are driven to replicate HIV", without detectable infection of the DC themselves [81]. For uninfected DC to mediate CCTH, they must first capture infectious HIV particles. Rather than via CD4, this is believed to occur via other surface receptors such as the C-type lectin receptor DC-SIGN (which can interact with Env) [217] and the I-type lectin Siglec-1 (which binds host-cell-derived glycosphingolipids on the viral membrane) [218]. Although it was initially believed that CCTH *in trans* involved internalization and later release of HIV [219], recent studies have shown that DC and Mφ rather store viral particles in deep membrane invagination pockets, which are still connected to the extracellular space [220,221]. These pockets are now referred to as "virus containing compartments" (VCC) [222]. The membrane of VCC is enriched with tetraspanins proteins, in particular CD81 and CD9 [223]. Live imaging microscopy has shown that VCC rapidly polarize towards the infectious synapse upon contact with a target T-cell [219,220]. Conversely, CD4, CCR5 and CXCR4 polarize on the target cell side, which likely enhances the likelihood of infection events [219]. Indeed, target cell infection was dependent on Env-CD4 mediated viral fusion and not endocytosis [221].

At the ultrastructural level, infectious synapse formation is characterized by the extensive interaction of specialized membrane protrusions extending from both donor and target cells. This can involve extensive "embracement" of the target T-cell by large membrane sheets of the DC, although this phenotype is more prominent for mDC than iDC [221,224,225]. Within the synaptic space, filopodial extensions have been observed to extend from both cells and interdigitate, as well as from the target cell to penetrate into the VCC of the DC [221,224]. These intimate contacts allow active release of HIV from VCC, as well as "viral surfing" along the T-cell membrane projections. Importantly, the presence of HIV does not increase conjugate formation, which is independent of Env-CD4 interactions but requires interactions between ICAM-1 and LFA-1 [226]. Antigen presentation was not required for infectious synapse formation, although it did significantly enhance target-cell infection, perhaps due to CD4TC activation [219]. CCTH via infectious synapses is also enhanced upon DC activation or maturation [219,227-229]. Altogether, these observations strongly suggest that HIV exploits naturally occurring DC-CD4TC contacts, rather than actively inducing them. However, once these contacts are formed, HIV clearly manipulates cellular behaviour on both sides of the infectious synapse to facilitate viral spread. This is further expanded in section 1.5.10, where the role of the actin cytoskeleton for infectious synapses is addressed.

1.3.2 The virological synapse and HIV transfer "*in cis*"

CCTH "*in cis*" requires productive infection of the donor cell and involves expression of viral proteins leading to assembly of a *de novo* viral pool. HIV transfer to the target cell can occur immediately upon viral budding or after remaining associated with the producer cell for variable periods of time (depending on the donor cell involved). Virological synapses are specialized intimate cell-cell contacts that mediate CCTH "*in cis"*. The virological synapse (VS) can be defined as an organized multi-molecular structure that forms in a cytoskeleton-dependent manner at the contact area between a retrovirus-infected cell and an uninfected target cell, with concomitant polarization of viral effector and receptor molecules to the donor-target cell interface, and which mediates direct cell-cell viral particle and infection transfer in the absence of donor-target cell fusion [85,125,134,230-232]. The hallmark of the HIV-VS is co-polarization of Env and CD4 to the donor and target cell sides of the synapse respectively [85], although many other molecules are now known to be involved. While various cell types have been reported to engage in VS, here we will concentrate on those formed by T-cells, DC and Mφ, as these are the best studied and likely the most relevant *in vivo*.

1.3.2.1 The homotypic T-cell synapse

The VS that forms between a HIV-infected and an uninfected CD4TC is by far the best characterized VS variant. At the ultrastructural level, it is characterized by intimate contacts mediated by short membrane protrusions (on both donor and target cell) that extensively wrap around each other to form an adhesive ring that nearly encloses the synaptic space [85,224]. VS forming between primary CD4TC are however tighter than those involving T-cell lines [87,224]. HIV virions at the VS can be found either clustered at the periphery of the contact zone, "surfing" along short filopodia within the synapse, or accumulating in button-like structures at the center of the VS [85,87,125,224]. The exact mechanism by which the T-Cell VS forms is not fully elucidated, but it has been studied extensively and is now known to involve the following steps: **i)** Adhesion: Binding of surface Env and CD4 at the site of contact is believed to lend the forces for initial donor-target cell adhesion and is indispensable for triggering VS formation. Disruption of this interaction impairs conjugate formation and completely inhibits donor-target cell polarization [85]. Interactions between intercellular adhesion molecules (primarily ICAM1) and the integrin LFA1 further stabilize the initial adhesion [233,234]. **ii)** Signalling and cytoskeletal remodelling: Both Env-CD4 and ICAM1-LFA1 binding initiate complex signalling pathways that trigger cytoskeletal remodelling events that are essential for both conjugate stabilization and the recruitment of diverse molecules on both sides of the VS. These events are described in further detail in section 1.5.10. **iii)** Polarization of viral and cellular components**:** On the donor cell side, Env and Gag [85,235], ICAM1 and ICAM3 [233,236], tetraspanins [232,234], lipid rafts [237] and even mitochondria [238] polarize to the VS. On the target cell side, CD4, CXCR4/CCR5, LFA1, F-actin and Talin become enriched at the VS [85,233,239]. **iv)** Viral transfer: Within minutes of conjugate formation, Env polarizes to the donor-cell side of the conjugate and is then followed by Gag [235]. Both can accumulate to form button-like structures, which are characteristic of the T-cell VS [125,235]. Gag oligomerization results in polarized viral assembly, budding, and transfer across the synaptic space to the target cell [85,87,125,235]. Electron and fluorescence microscopy studies have confirmed sites of particle assembly at the donor-cell membrane, as well as mature and immature virions at the synaptic space of the VS [82,125,212,224]. However, few viral entry events have been captured by electron microscopy at the target-cell [212], despite abundant evidence of viral material and infection transfer in CCTH assays. **v)** Further evolution: Whether typical synapses undergo a final resolution step is unclear, but contacts of multiple hours have been reported [125,127]. In addition, simultaneous contacts between a donor cell and multiple target cells have been observed, leading to the concept of "polysynapses" [224,234]. While HIV transfer across the VS between T-cells is highly efficient *in vitro* (see 1.2.4), its contribution to HIV spread and

pathogenesis in humans remains to be confirmed. A study by Murooka et al used multiphoton intravital microscopy in HIV-infected humanized mice and observed migrating infected T-cells to engage in polarized tethering contacts with resident lymph node cells [108], thus supporting the occurrence of VS *in vivo*.

1.3.2.2 Dendritic cell to T-cell synapse

Compared to the infectious synapse and the T-cell VS, relatively little is known about the VS that form between productively infected myeloid cells and target CD4TC. While some studies have researched the potential of DC to mediate CCTH *in cis*, very few have directly attempted to resolve the ultrastructural or mechanistic features of the DC-VS. Here we review the available knowledge, in particular by highlighting the differences/parallels with the DC infectious synapse. The mechanisms by which HIV is transferred *in cis* and *in trans* are fundamentally different, because in one case the virus is produced "*de novo*" from within infected DC, whereas in the other mature extracellular virions are simply captured and passed on. Studies have shown that *in trans* HIV is stored in VCC that are enriched with tetraspanins molecules [221,223,240], whereas egress of *in cis* HIV primarily occurs at the PM [156]. Direct cell-cell contacts are required for DC-mediated CCTH *in cis* and *in trans*, with initial conjugate formation primarily depending on ICAM-LFA interactions in both cases [226,241]. However, progression to the synapse state (i.e. polarization of HIV-Gag to the donor-target interface) is dependent on Env for the VS but not the infectious synapse [156,226], whereas the inverse is true for DC-SIGN [242]. For the VS, synapse progression involves both relocation of VCC [240] and polarization of immature Gag and viral budding towards the CD4TC [156].

Although the infectious synapse (with mature DC) has been studied at much higher imaging resolution [221], the available evidence suggests some similar ultrastructural features for the VS. In both cases, DC-CD4TC clusters are characterized by tightly-attached actin-dependent contacts and extensive membrane interactions between both cells, with T-cells often appearing to be engulfed by DC sheet-like projections [128,156,221,241]. Enrichment of intracellular Gag, membrane-budding HIV and mature virions occur at the VS [89,156,241], whereas only the latter is observed at the infectious synapse [221]. Interestingly, binding of mature HIV at the proximal target cell membrane has been observed to be followed by the apparent accumulation of virus at the distal face of the CD4TC in both types of synapses [89,219]. Of note, a VS involving an infected DC may have been observed *in vivo* by intravital imaging of lymphoid tissue in HIV-infected humanized mice [212].

1.3.2.3 Macrophage to T-cell synapse

Contrary to the initial belief that HIV in infected macrophages buds within intracellular vacuoles, it is now known that budding in Mφ occurs at the PM, but within deep membrane invaginated VCC that remain connected to the surface [243,244]. These compartments, which are enriched with the Tetraspanins CD81, CD9, and CD53 [245], are believed to allow storage of infectious virions for long periods of time. In agreement, suppression of viral transcription in infected cells abolished new viral synthesis, but Mφ were still able to pass "archived" virus to target cells for up to 6 weeks [246]. The architecture of these VCC has been studied at high resolution, and the term "HIV-assembly and holding compartments" has been proposed [222] to emphasize that HIV is produced and transferred *in cis*.

Although Mφ-VS are poorly understood compared to other types of HIV synapses, they show some parallels to both the T-cell VS and the DC infectious synapse. Gag, Env and ICAM1 concentrate on the donor cell, and co-polarize with CD4, CXCR4/CCR5 and LFA-1 on the target cell at the cell-cell contact interface [91,247]. These studies also showed that contacts between infected Mφ and target CD4TC can be transient and that CCTH is rapid, with polarization of surface molecules and transfer of viral material occurring within minutes/hours [83,91,247], and leading (in part) to productive target cell infection. At the ultrastructural level, the synapse was characterized by tight adhesive junctions between both cells, with VCC on the macrophage polarized to the interface and viral particles found in the synaptic space [248]. Interestingly, although target cell infection requires Env-CD4 interactions, conjugate formation and polarization of Gag by Mφ can occur even in the absence of Env [248], which is an important difference to the T-Cell VS. Of note, macrophages can also mediate CCTH *in trans* [97,246,249], however this is beyond the scope of this review.

1.3.3 Dendritic cell mediated HIV transfer (*in cis* vs. *in trans*)

Apparently conflicting observations led to initial controversy regarding the mechanism by which DC mediate CCTH. While many argued that DC primarily capture HIV particles and pass them to target cells *in trans*, others reported efficient CCTH *in cis*. The main argument against the latter mechanism was that infection of DC is an extremely rare event. However, it is now recognized that DC susceptibility to infection depends on multiple factors including their activation and maturation status. Immature DC are permissive to HIV productive infection but viral synthesis in these cells can be arrested at one or more post-entry steps [152,250]. Yet when infected DC are coincubated with CD4TC, extensive (*in cis*) viral transfer and replication is observed, suggesting that even limiting numbers of infected DCs can mediate robust HIV transfer if CD4TC are present [128,141,152,167]. In addition,

activation of infected iDC by cross-linking of CD40 molecules or by the presence of antigen-specific CD4TC also drastically increased their ability to mediate CCTH *in cis* [167,241,251]. In contrast, mature DC are resistant to HIV infection [73,152,227] for multiple reasons including upregulation of various restriction factors upon maturation (reviewed in [84,252,253].

The original controversy regarding CCTH *in cis* vs. *in trans* was addressed and resolved by Turville et al., who elegantly showed that these are not interdependent or mutually exclusive processes but rather separated in two kinetically distinct phases when the donor DC are permissive to HIV infection [96]. When either mature or immature DC are exposed to infectious HIV and then coincubated with CD4TC, a first phase of CCTH is observed, which corresponds to delivery of captured viral inoculum to the target cells *in trans*. Although mature DC mediate this type of transfer very efficiently, this mechanism only provides CCTH in a short-term period (up to 48h) because of viral degradation within DC. Once this finite pool of extracellular virus is exhausted, CCTH from mDC is terminated [96]. In contrast, the *in trans* CCTH phase of iDC is shorter and less efficient (due to faster degradation of the virus) but is followed by a second and durable phase of viral transfer that begins after 48-72h. This phase is entirely dependent on productive infection of immature DC and subsequent *de novo* production of HIV (i.e. CCTH *in cis*) [96]. Since these observations have been recapitulated in independent studies [90,254], it is now clear that: i) the long-term ability of DC to transfer virus to CD4TC is dependent on their ability to become productively infected, ii) mature DC do not support CCTH *in cis* [96] unless they originate from already infected immature DC [169], and iii) CCTH *in cis* and *in trans* represent distinct, dissociable, not exclusive and not interdependent processes that involve different cellular and viral mechanisms [69,96,146,227,255,256], despite certain parallels between the virological and infectious synapses.

1.3.4 HIV-Filopodia

Previous work from our research group led to the identification of unique structures where HIV buds are embedded at the tip of cortical F-actin protrusions. These structures, which were termed “HIV-Filopodia” (HF), are of direct and high relevance to the work presented in this thesis. The following section therefore summarizes these previous findings, as published in [89]. Primary monocyte-derived iDC display a prominent uropod at the cell rear and lamellipodia at the leading edge when in pure culture. However, when these iDC are mixed with autologous CD4TC (both uninfected), their cortical F-actin phenotype switches to displaying abundant, long (~10 μm) and dynamic filopodia that mediate contacts between both cell types. Interestingly, when iDC are productively infected with HIV in this context, more

than 90% of these filopodia are found to be capped with budding viral particles at their tips (hence, HIV-Filopodia). Characterization by a combination of electron microscopy and biochemical approaches confirmed that these particles indeed correspond to immature budding virions [89]. Other studies reported similar structures in HIV-infected cells *in vivo* [212] and MLV-infected cells *in vitro* [257]. Immunofluorescence staining confirmed the presence of Env at the tips of HF, as well as highly dense F-actin content within the shaft [89]. Live imaging suggested that the budding reaction might be arrested or dramatically delayed at the filopodial tip. Interestingly, HIV infection did not alter the length, apparent morphology or dynamics of filopodia, but it did increase filopodial frequency in a Nef-dependent manner.

In terms of functional relevance, HF were observed to probe the cellular microenvironment with rapid arc-like movements. When this resulted in contacts with neighbouring CD4TC, filopodia switched to slower "scanning" dynamics. HF on infected iDC were found to mediate ~500 contacts per hour (on average) with potential HIV target cells. Filopodial activity often preceded tethering and subsequent pulling of T-cells closer to the iDC membrane. This cell-cell contacts eventually matured into stable conjugates where the target T-cells became nearly engulfed in extensive sheet-like iDC membrane projections [89]. The resulting VS structures resembled previously described infectious synapse arrangements [221], where mature donor DC are HIV-loaded but not productively infected. In our setting (with productively infected donor cells), both immature and mature viral particles could be observed at the synaptic space, and Env-dependent transfer of Gag to the T-cell membrane could be confirmed. One of the main aims of this thesis was to investigate the mechanisms by which HIV manipulates the actin cytoskeleton to produce HF, and further define their contribution to CCTH. This is discussed in detail in Chapter 6.

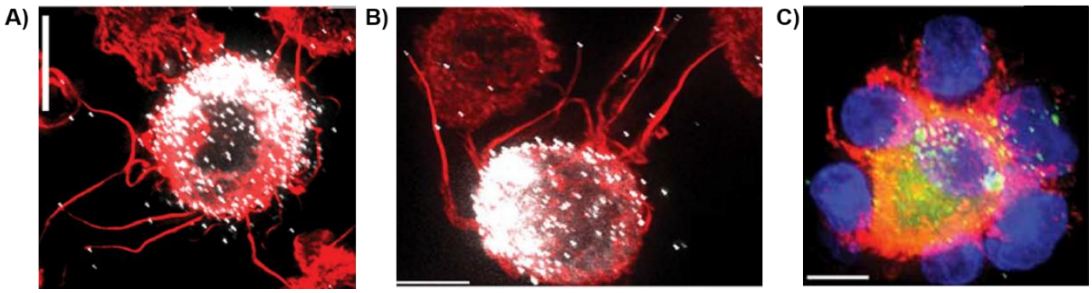

Figure 1.3: HIV-Filopodia. F-actin is shown in red and HIV-Gag in white or green. A) U937 cell infected with HIV-iGFP. B) Infected immature dendritic cell in early contacts with CD4TC. C) Infected DC in mature contacts with multiple target cells. Images are reproduced from [89] with the authors permission and in agreement with its open access licensing conditions.

1.3.5 Advantages of direct cell-cell viral transfer

Although determining their contribution might prove difficult in some cases, CCTH offers a number of theoretical advantages compared to cell-free viral infection. Many of these are given by the ability of infected cells to release large amounts of virus directly onto a relevant target cell, which minimizes the time and distance that extracellular virus needs to travel. This is beneficial given; i) the short half-life of cell-free viral particles [258,259], ii) the poor infectivity of single virions [260], iii) their rapid dissociation from target cell membranes [261], iv) exposure to innate and adaptive immune responses in blood and the extracellular milieu, iv) high concentration of HIV receptors and coreceptors on the target cell side of the VS [134], v) potentially higher Env content in virions originating from the VS (due to strong Env polarization), and vi) higher local MOI at the VS, which increases the probability of target cell infection and is believed to explain the partial resistance of CCTH to antiretroviral drugs and neutralizing antibodies (extensively reviewed in [84]). Other advantages include the potential of activating the target cell (thus increasing its susceptibility to infection and promoting its proliferation [128,226,241,262], as well as the ability of infected leukocytes to carry virus over long distances and into specific tissues ([108] and see 1.2.5). Together with the dramatically higher efficiency of CCTH *in vitro* (and partially *in vivo*), these advantages support the now well-accepted view in the field that cell-mediated HIV transmission is likely to be essential for HIV pathogenesis *in vivo* (see 1.2.3-4).

1.4 The actin cytoskeleton

Actin is the most abundant protein in eukaryotic cells [263] and is extraordinarily conserved throughout evolution [264]. Actin monomers can assemble into polymers that form long "microfilaments", which together with microtubules and intermediate filaments constitute the eukaryotic cytoskeleton. In this thesis, the term cytoskeleton always refers to the actin component, unless otherwise specified. In most cells, actin filaments form complex networks, which are under constant partial remodelling [265]. The dynamic turnover of actin filaments is essential for a wide range of cellular processes, including: maintenance of cellular architecture [266], driving cell motility [267] and cell migration [268], transport of intracellular cargo [269], cell adhesion and cell-cell contacts [270], cell polarization [271], cell division [272], mechanosensing [273], cell self-defence [274], and an ever-increasing number of other functions, including recently recognized roles within the nucleus [275]. In human leukocytes, actin accounts for over 10% of the total protein content [276]. Within all cell types, actin continuously cycles between two states.

1.4.1 The actin monomer (G-actin)

The actin monomer is a 42 kDa protein of ~375 amino acids which folds into a globular structure and is therefore referred to as "G-actin". Structural studies revealed that the globule is composed of four subdomains which form two pseudo-symmetric lobes separated by a deep cleft, where the ATP binding site resides [277]. The cleft also binds magnesium (Mg2+), which is essential for the enzymatic ability of the protein to hydrolyse ATP [278]. Most free G-actin in the cell is bound to ATP, whereas ATP hydrolysis to ADP occurs gradually from actin polymers [279]. There are six isoforms of actin in mammals [280]. The isoforms are encoded by homologous genes in different chromosomes and share a highly conserved amino acid sequence and protein structure [281]. Expression of the three α-Actin isoforms (α-skeletal, α-cardiac and α-vascular) is strongly restricted to specific tissues, whereas β- and γ-actins are more ubiquitously expressed [282]. While we note that β-Actin is the predominant isoform in leukocytes, the term "actin" is used in this work to globally refer to any isoform(s) present in the cell types discussed. G-actin is the basic unit required to build actin filaments.

1.4.2 The actin filament (F-actin)

Filamentous actin (F-actin) refers to linear homopolymers of G-actin bound by non-covalent protein interactions. Actin filaments (microfilaments) are linear and double stranded [283]. The filament is approximately 7-9 nm in diameter and can reach lengths in the μm range. The canonical actin filament is considered to have a helical repeat every 37 nm, with a rotation of 166° around the helical axis, and a constant rise of 27.3 Å per subunit [284-287]. However, extensive research on the properties of the filament has concluded that F-actin is flexible and dynamic, so that it can exist in multiple structural states that may moderately vary from the values indicated above. This is partly due to the ability of monomers to rotate up to 10° from their ideal positions within the filament [288]. F-actin is considered to have structural polarity because all monomers within a filament are oriented in the same direction [289]. The end where the cleft is exposed is conventionally called the "(-)" or "pointed" end, whereas the opposite end where the cleft is covered by an adjacent monomer is called the "(+)" or "barbed" end" (Fig. 1.4). The (+) end is the energetically favourable end for (ATP-bound) monomer addition and thus represents the fast-growing side of the filament. In contrast, the (-) end typically shrinks by dissociation of ADP-bound actin monomers. In the absence of intervening actin-regulatory proteins (e.g. purified actin *in vitro*), this can result in a phenomenon now referred to as "actin treadmilling", which represents a dynamic equilibrium between polymerization at the (+) end and depolymerization at the (-) end (first described in [290]). However, if growth at the (+) end is interrupted, the filament gradually "ages" due to ATP hydrolysis and subsequent inorganic phosphate release from the (-) end, which destabilizes the

filament and results in depolymerisation from (-) to (+) [278]. *In vitro*, F-actin polymerisation rates are strongly dependent on G-actin concentration, and filaments can converge to create linear arrays, two-dimensional networks and three-dimensional gels (reviewed in [291]).

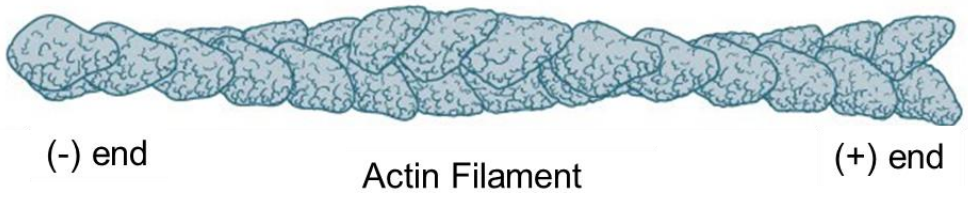

Figure 1.4: Schematic representation of an actin filament (F-actin). Image adopted from [287], in agreement with its licensing conditions (CC-BY-NC 4.0). Link to resource: https://www.mechanobio.info/cytoskeleton-dynamics/what-is-the-cytoskeleton/what-are-actin-filaments/

1.4.3 F-Actin nucleation

While elongation of pre-existing actin filaments is energetically favourable, spontaneous polymerization of F-actin from a pure G-actin pool is inefficient both *in vitro* and *in vivo*. This is because initial filament "nucleation" involves the energetically unfavourable formation of unstable intermediates [292]. These include first an actin dimer and then a trimer or "nucleus", which is the minimal arrangement that displays the lateral and longitudinal contacts of a filament, which can then be elongated [293]. Since cells require the ability to seed actin filaments at variable G-actin concentrations, evolution has provided a select group of proteins with different nucleation-mechanisms and kinetics. These cellular factors are known as "actin nucleators". They can initiate F-Actin polymerisation from a pool of actin monomers and can also mediate rapid filament growth at the barbed end [294]. Different actin nucleators allow cells to build architecturally diverse actin structures (reviewed in [295]). The two major classes of cellular actin nucleators are the Arp2/3 complex and Formins, which are introduced below. A third class of actin nucleators known as "tandem-monomer-binding nucleators" also exists [296] but is beyond the scope of this review.

1.4.3.1 The Arp2/3 complex

The Arp2/3 complex is highly conserved among eukaryotes as a major component of the actin cytoskeleton and is involved in numerous critical cellular functions [297]. It is the most abundant actin nucleator in eukaryotic cells [298,299]. The hallmark feature of Arp2/3 is its ability to initiate formation of a new branch filament from an existing mother filament at an angle of 70 degrees. The resulting branched actin networks are essential for formation of the actin cortex and most types of membrane protrusions [295]. The Arp2/3 complex is composed of 7 different subunits, two of which (Arp2 and Arp3) emulate an actin dimer [300]. Still, the complex displays little activity by itself and requires additional factors to efficiently mediate actin nucleation. These "nucleation promoting factors" (NPFs) are proteins that directly bind

to Arp2/3 and stimulate its activity by; i) increasing initial association of the complex with the side of pre-existing F-actin filaments and ii) delivery of the third actin monomer, which completes the actin trimer or "nucleus" [300,301]. Unlike the Arp2/3 complex, which remains associated with the pointed end of the daughter filament, NPFs are thought to dissociate after the start of polymerization, and thus can be recycled to promote iterative rounds of nucleation [302]. NPF's are subdivided in type-I and type-II proteins. Most type-I NPFs belong to the WAS or WAVE families. WAS NPFs (e.g. WASP and N-WASP) have a characteristic VCA domain at their C-terminus, which enables binding to both Arp2/3 and G-actin [297]. They are typically autoinhibited in the cytosol and their activation is tightly regulated by direct binding of Rho-GTPases, PIP2 and/or phosphorylation. In contrast, WAVE NPFs (Wave1-3) are not autoinhibited, but instead form part of an obligate multi-protein complex known as the WAVE regulatory complex. Its activation occurs downstream of Rac1 but seems to also require additional signals [303]. Type II NPFs so far comprise only Cortactin and its leukocyte-specific homologue HCLS1 [302]. Since Arp2/3-actin nucleation is involved in a myriad of cellular functions, it is the individual features and regulation of NPFs that allows cells to spatiotemporally regulate Arp2/3 activity to mediate highly diverse outcomes. This has been best studied in the context of building distinct cellular protrusions and driving different aspects of cell motility [295,304].

1.4.3.2 Formins

Formins are the second-best studied class of actin nucleators. They are characterized by the presence of a formin homology 2 domain (FH2), which is highly conserved among eukaryotes. There are at least 15 different formins in humans [305]. These large (>100 kDa) multidomain proteins act downstream of Rho-GTPases [306] to mediate a broad variety of cellular functions, including cytokinesis, cell polarity, filopodium formation, cell-adhesion and endocytosis (reviewed in [307]). Most of these functions require Formins' ability to regulate both actin and microtubule cytoskeletal dynamics [308,309]. Importantly, formins drive polymerization of unbranched linear actin filaments, as required for formation of filopodia, stress fibers, actin cables, among other structures (reviewed in [294]). This can involve F-actin nucleation and/or subsequent elongation. The nucleation mechanism of formins is complex and not fully understood but is believed to involve the stabilization of actin dimers [310]. Formins also serve as potent elongation factors. This involves i) association with barbed ends via dimeric FH2 domains, ii) the use of long "rope-like" FH1 domains to recruit and deliver Profilin-bound actin monomers to the barbed end, and iii) processive movement or "stepping" along the filament to stay associated with the barbed end, which it simultaneously protects from capping proteins [294,311]. Filament elongation by formins is dramatically accelerated

in the presence of Profilin-bound G-actin, whereas this form of actin is not compatible with Arp2/3 nucleation [311,312]. Therefore, by sequestering G-actin in a formin-accessible but Arp2/3-inaccessible form, Profilin regulates cellular F-actin homeostasis and allows Formins to compete with the much more abundant nucleator Arp2/3 [299,313].

1.4.4 F-actin remodelling by cellular proteins

The ability to rapidly reorganize the actin cytoskeleton is essential for numerous key cellular processes and therefore is a fundamental aspect of eukaryotic life [314]. But since F-actin turnover by treadmilling is far too slow and unspecific to meet these requirements, how do cells mediate reorganization of their most abundant protein network? The answer is partly given by the highly promiscuous nature of Actin, which is capable of interacting with one of the largest numbers of protein partners known to date [263,315,316]. This myriad of cellular actin-binding proteins (Fig. 1.5-A), together with their upstream regulators, mediate and coordinate actin "remodelling", which involves elongation, stabilization, architectural organization and turnover of microfilaments. Therefore, it is the combination (and concentration) of active regulators at any given time and subcellular location that determine the functional outcome actin remodelling [295]. And while it is now understood that dynamic and spatiotemporal regulation of the actin cytoskeleton is critical for the correct functioning of nearly all cell types, various inherent factors make this an exceptionally complex system for biologists to study. These include: i) the large and ever-increasing number of known actin binding proteins (Fig. 1.5-A), ii) closely related homologous genes with different functions [317,318], iii) large signalling nodes capable of connecting numerous pathways [319], iv) partially redundant regulators and pathways [320], iv) tissue-specific expression of cytoskeletal regulators [321], v) interplay of biochemical and biomechanical regulatory mechanisms [322], vi) responsiveness to a wide range of both intracellular and extracellular cues, and vii) diversity and complexity of cellular F-actin structures [323], just to name a few. Therefore, it is beyond the scope of this thesis to review all mechanisms of actin regulation. Rather, we provide a brief summary of the most important actin binding protein classes and how they affect actin remodelling (see Table 1.1), as well as a simplified schematic overview of their interaction for regulation of cellular actin dynamics (Fig. 1.6). Other specific actin regulators that are of relevance to this study are later introduced in sections 1.5.9 and 4.4. of this thesis.

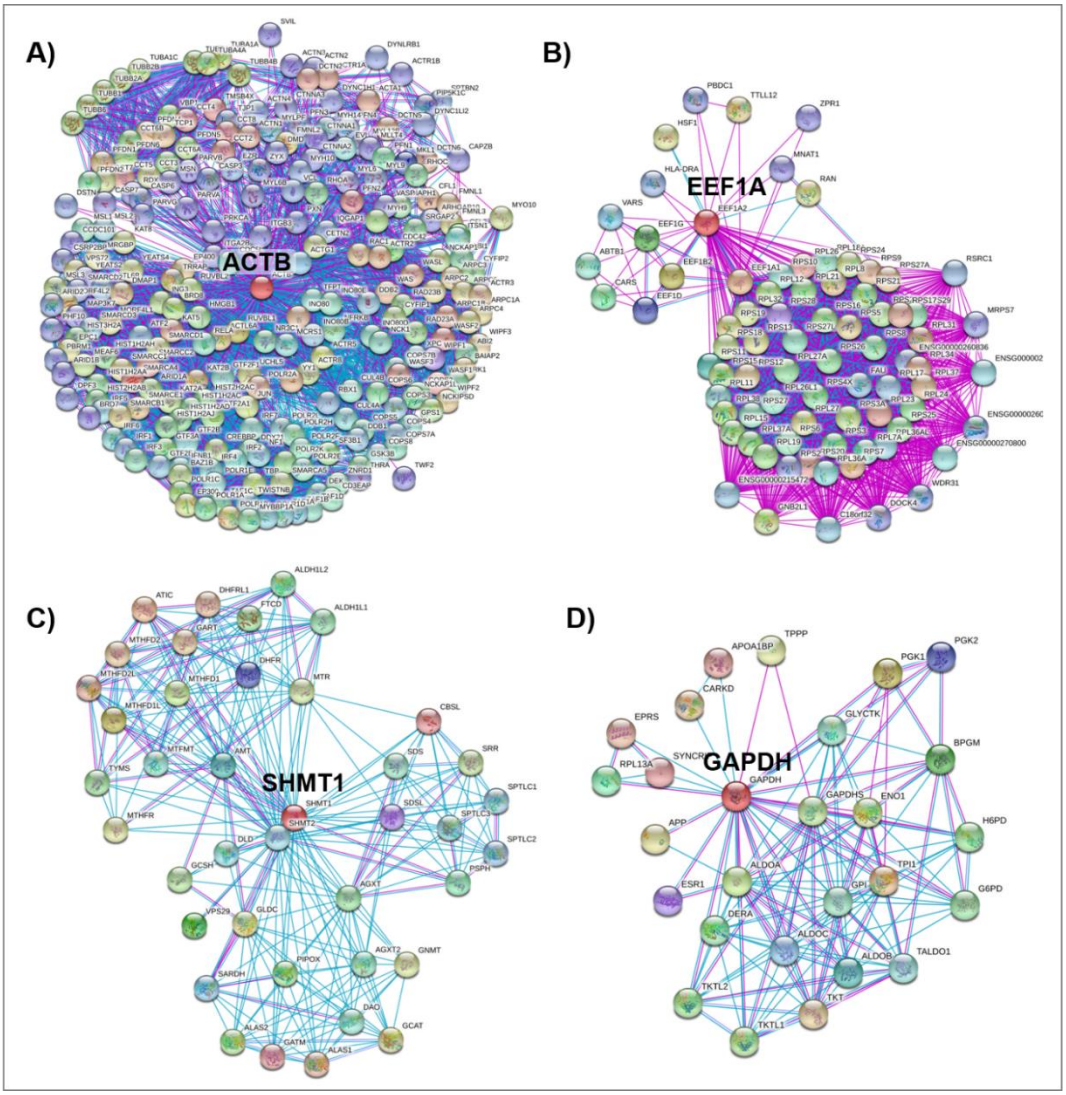

Figure 1.5: Promiscuity of Actin protein. Graphic representation of functional association networks generated using the online STRING database [324] for various query proteins (human). The nodes represent proteins and the edges indicate predicted associations. To bias the networks towards protein-protein interaction associations, "high-confidence" settings (i.e. score > 0.7) and only two types of evidence (purple line = experimental evidence and blue line = database evidence) were selected. The number of direct (first shell) interaction partners was set to 250 for each network alike. A) Interactome for human β-Actin. Note that only 1 of the 6 human Actin isoforms is considered here. For comparison, we also include the equivalently generated interactomes for; B) Eukaryotic translation elongation factor EEF1a, which is the second most abundant cellular protein in mammals, is predominantly found bound to F-Actin and is highly evolutionary conserved across eukaryotes [325]. C) Serine hydroxymethyltransferase (SHMT), one of the most highly conserved proteins in both eukaryotes and prokaryotes [326]. D) GAPDH, a ubiquitous, abundant and evolutionary conserved protein that is often used alongside β-Actin as housekeeping gene reference in biomedical research [327]. A-D) Clearly, neither the abundant expression of Actin, nor its subcellular distribution, nor its central role to life, nor its evolutionary conservation can by themselves explain the extraordinary number of protein interaction partners showcased by Actin. Note: this figure was inspired by the analysis of α-Actin interactions performed by Povarova et al. in [263].

Class	Function	Examples
G-actin binding proteins	Regulate the size, compartmentalization and dynamics of the G-actin pool in cells, by preventing uncontrolled monomer polymerization and/or regulating their incorporation into growing filaments. Reviewed in [328].	Profilins, β-Thymosins, WASP/WAVE families, Cofilin, etc.
Actin nucleators	Nucleation of new actin filaments from G-actin or the side of pre-existing filaments. Filament elongation. Reviewed in [302].	Formins, Arp2/3, Spire, APC
Nucleation promoting factors (NPF)	Assist the Arp2/3 complex by delivering actin monomers and providing mechanistic support for actin nucleation. Reviewed in [297].	WASP family, WAVE family, Cortactins, etc.
F-actin elongators (other)	Mediate linear filament elongation from the (+) end, independently of Arp2/3. Reviewed in [294].	Formins, Ena/Vasp
Rho-GTPases	Small GTP-binding proteins that can act as molecular switches and orchestrate many actin-dependent processes including cell morphology and migration [329]. Rho-GTPases are considered "master regulators of the cytoskeleton" [330] as they are critical regulators of Formins and the Arp2/3 complex.	RhoA, Rac1 and Cdc42 (canonical Rho-GTPases)
Membrane-cytoskeleton linkers	Proteins associated with the inner leaflet of the PM, which can bind both surface-proteins and F-actin directly [331]. They mediate anchorage, docking and movement of membrane proteins, while also serving as scaffolding proteins to facilitate signal transduction.	Filamin-A, Ezrin, Moesin, Dystrophin, etc.
Capping proteins	Control of filament length by protecting and stabilizing its ends. Barbed end cappers block addition of new monomers, whereas pointed end cappers reduce depolymerization from the (-) end. Reviewed in [332].	CAPZA, CAPZB, CAPG, Tropomodulin, β-actinin, etc.
Cross-linking proteins	Interconnect actin filaments to form F-actin bundles or networks. Typically have more than one actin binding site. Reviewed in [333]	Fascin, Filamins, α-Actinin, Fimbrin, Spectrin, Villin, etc.
Membrane-cytoskeletal linkers	Connect the cytoskeleton and the PM by directly binding F-actin and membrane elements or surface proteins. Reviewed in [334].	Filamin-A, Ezrin, Moesin, Dystrophin, etc.
Filament severing proteins	Filament degradation. Can directly reduce F-actin content or indirectly increase it (e.g. by generation of new (+) ends and replenishing G-actin pools). Reviewed in [335].	Cofilin and Gelsolin families

Table 1.1: Major actin binding protein classes and examples.

Figure 1.6: Cellular regulation of actin dynamics. Illustration reproduced courtesy of Cell Signaling Technology, Inc. (www.cellsignal.com) with the owner's explicit permission (master copy only). To see this image, follow the link to the original resource: https://www.cellsignal.com/contents/science-cst-pathways-adhesion-ecm-cytoskeleton/regulation-of-actin-dynamics/pathways-actin

1.4.5 Generation of force and membrane protrusion

Protrusion of the plasma membrane is essential for a wide range of biological processes across all kingdoms of life. Most notably, it is required for all known types of active cell movement in eukaryotic cells. In humans, leukocytes represent a notorious example of the importance of membrane protrusion for specialized cellular functions, as it is required for; i) dynamic changes in cell morphology, ii) cell migration and chemotaxis, iii) scanning of the microenvironment, iv) transient and stable intercellular contacts, v) transendothelial migration and vi) capture and phagocytosis of pathogens, all of which are distinctive features of immune cells. It is now well accepted that the actin cytoskeleton is the predominant force-generating system in the cell, with actin polymerisation producing most of the force involved in membrane protrusion. This has been intensively studied in the fields of biophysics and

biomechanics, and thus it is not our intention to provide a detailed description of how these forces are generated. Rather, we refer to excellent previous reviews in these areas [332,336-339], and simply summarize some of the key aspects of this topic that are of relevance to later sections of this work. In cells, cortical microfilaments often have their (+) ends facing the PM. This is in part due to the ability of many cytoskeletal regulators (including actin nucleators), to bind PIP2 at the inner membrane leaflet, as well as the convenient angles resulting from branched F-actin nucleation by Arp2/3. During F-actin polymerisation, "the binding energy from subunit addition is converted into physical force with high thermodynamic efficiency" [332]. ATP hydrolysis also releases considerable energy, most of which is translated into a protrusive force [336]. Thus, elongation of actin filaments produces forces in the piconewton range [340,341]. The polarity of the actin filament naturally provides directionality to the "actin polymerisation motor" [336]. Bundling and/or parallel elongation of filaments locally increases protrusive forces [332]. When filaments linked to the cortical actin network begin to grow with their (+) ends opposing the PM, the above described forces lead to bending and protrusion of the membrane. The main opposing force to protrusion is membrane tension, which is dependent on both intracellular tensile forces and extracellular pressures [342].

1.4.6 The actin cortex

Cellular protrusions arise from remodelling of cortical F-actin. The actin cortex is a thin and highly cross-linked F-actin network found immediately below the PM of animal cells. The cortex thickness ranges between ~100-500 nm in most cell types [343] and is about ~230 nm in Jurkat T-cells [344]. The gap between the cortex and the membrane is as small as ~10 nm [344], and the cortex is physically connected to the PM by "membrane linker proteins" (for examples see Table 1.1), which simultaneously bind membrane components and F-actin filaments. The actin cortex participates in various cellular functions, most notably cell-shape changes and cell migration, but also cell division [343]. While the biomechanical properties of the cortex (including viscoelasticity, stiffness and cortical tension) are essential to its functions, they are beyond the scope of this work. We refer to an excellent review by [345]. Rather, we here focus on the molecular composition of this specialized actin layer. Biro et al. developed a method to purify cortical structures and provided the first detailed proteomics analysis of the actin cortex. Over 150 actin binding and regulatory proteins were identified, many of which were enriched in this compartment. Importantly, this included; the actin nucleators Arp2/3 and Dia Formins, F-actin capping proteins (e.g. CAPZA and CAPZB), turnover stimulating proteins such as Cofilin, numerous actin cross-linkers, membrane-cytoskeleton linkers, Profilin, and myosin II motors [346]. A related study confirmed that the majority of cortical F-actin was generated by Arp2/3 and Dia formins alone [347]. The exact

organization of microfilaments in the actin cortex is not only mechanistically difficult to study, but also strongly dependent on cell-type and cellular context [345]. Generally speaking, however, cortical actin filaments are organized in a densely cross-linked meshwork, with most filaments running parallel to the PM, whereas others are aligned perpendicularly [348]. Importantly, the actin cortex can undergo extensive remodelling within fractions of seconds [343]. Selective reorganization of the cortex by activated actin regulators, while preserving the inner cellular actin cytoskeleton structure is possible due to at least two phenomena; i) subcellular localization of actin remodelling proteins (often targeted to the PM), and ii) the protective action of Tropomyosins. Tropomyosins (at least ten different isoforms in mammals) are α-helical coiled-coil proteins that form polymers along each side of the actin filament and thereby control the interaction of F-actin with other proteins, mainly by steric hindrance [349]. For instance, Tropomyosins protect microfilaments from Arp2/3 nucleation and Cofilin severing activity. Therefore, since Tropomyosins are found in most cellular compartments but are relatively scarce near the PM, their presence/absence allows spatial regulation of cellular actin dynamics and confines the activity of many of the proteins shown in Table 1.1 to the actin cortex [350,351]. In summary, the actin cortex is a thin layer of actin, myosin, and actin-binding proteins forming a dynamic and contractile network below the PM, that is essential for maintenance/alteration of cellular shape, as well as many biomechanical properties of cells.

1.4.7 Cortical F-actin structures

Actin-rich membrane protrusions arising from remodelling of the actin cortex are of key importance for immune cells, which are highly motile and engage in abundant intercellular contacts [352,353]. The architecture and biogenesis of many of these cortical F-actin cellular structures have been studied extensively [295,297,308,323], and yet the fundamental mechanisms that lead to their formation remain controversial and/or only partially resolved. In this thesis we discuss only the two best studied cortical F-actin structures that are present in leukocytes (filopodia and lamellipodia), given their importance for communication of the immune response and their direct relevance to later sections of this work. A brief overview of other (physiological) cortical F-actin structures is provided in Table 1.2.

1.4.7.1 Filopodia

Filopodia are thin, finger-like plasma membrane protrusions with an F-Actin rich core. They are typically 1-10μm in length and 0.1–0.3 μm in diameter but can extend well beyond these limits [354]. Filopodia have been described as “sticky fingers” [355], tentacles [356] or antennae [357], due to the multiple cellular functions that they can perform. The best studied functions ascribed to filopodia include; directed cell migration, probing of the

microenvironment and mediating adhesion (cell-cell or to the extracellular matrix) (reviewed in [354]). Filopodia are most often observed protruding from the leading edge of migrating cells. Their internal structure consists of densely packed, long and parallel actin filaments (with their barbed ends facing towards the tip) bundled together by cross-linking proteins such as Fascin or Fimbrin [323,358,359]. Ultrastructural studies have revealed that filopodial microfilaments are often embedded in or connected to the branched actin network of the lamellipodia from which they originate [358]. While filopodia are relatively stiff structures due to crosslinking of F-actin into bundles, they are far from static in nature. Filopodia are dynamic structures that can bend, buckle, oscillate, extend, retract, perform sweeping motions and rotate around their base or their axis, all of which is dependent on actin dynamics (reviewed in [360]). Filopodia extend by active actin polymerisation at the tips, and they retract primarily by retrograde flow [361], although depolymerisation at the base may also be involved [362]. Importantly, filopodial retraction can pull objects towards the cell (or vice versa) and generate traction forces in the piconewton to nanonewton ranges [363].

Numerous actin binding proteins have been associated with filopodial structures. However, filopodia are found in numerous cell types and in organisms as distant as amoeba, sea urchins and humans [354]. Filopodia from different cellular contexts often significantly vary in their structure, behaviour and molecular composition [364]. Great caution should therefore be exercised when attempting to define core filopodial regulators. Indeed, abundant contradictory observations in the field now suggest that filopodia can be formed by alternative regulators and/or mechanisms in different contexts (even within a species) [365]. For instance, both Rho-GTPases Cdc42 and Rif can induce filopodium formation in mammals. The Cdc42 pathway involves recruitment of IRSp53 and N-WASP, with subsequent activation of the Arp2/3 complex to mediate initial membrane protrusion (reviewed in [354]). In contrast, Rif acts by interacting with Dia Formins and mediating their relocation to the PM [366,367]. Overall, two main models of filopodial biogenesis have been proposed. These have been extensively reviewed elsewhere [354,364,368] and will therefore only be briefly introduced here. In the convergent elongation model [358], filopodia are formed by reorganization and subsequent elongation of pre-existing actin filaments from the branched cortical F-Actin network. At a minimum, this model would require i) Arp2/3 (for the branched networks), ii) spontaneous or assisted convergence of multiple barbed ends (a role of Fascin has been proposed), and iii) linear elongation of filaments in the presence of anti-capping activity (both Ena/VASP proteins and Formins have been suggested). In contrast, the *de novo* filament nucleation model proposes that microfilaments in filopodia are not reorganized from pre-existing structures, but rather nucleated and elongated by formins directly at the PM. This would require local enrichment of formins at discrete regions of the membrane, to polymerize

multiple parallel filaments and thus provide the force required to protrude the membrane and give birth to filopodia. The observation of large multiprotein complexes at the tips of filopodia [358] is however consistent with both models, and both formins [366,369,370] and Ena/VASP proteins [371] have been reported to be enriched at filopodial tips. Therefore, non-exclusive hybrid models have also been proposed [354,365]. Importantly, filopodia have been observed in HIV target cells such as dendritic cells, T-cells, and macrophages [89,372,373].

1.4.7.2 Lamellipodia

Lamellipodia are thin, sheet-like, actin-rich membrane protrusions found at the leading edge of motile cells, including leukocytes [374,375]. Lamellipodia, which are sometimes also described as "sheets" or "veils", are thin (0.1–0.2 μm) and typically extend 2-3 μm beyond the leading edge [295,353,374]. Ultrastructural studies have revealed that lamellipodia are filled with a distinctive and extensively branched mesh of F-actin [376]. In this dendritic actin networks (~70° angles), free filament barbed ends are abundant and predominantly point towards the membrane, whereas free pointed ends are scarce, due to association of most pointed ends with Arp2/3 complexes at network branch points [377]. Filament density is highest at the leading edge and decreases towards the cell interior [353]. Lamellipodia are highly dynamic structures and likely do not exist in a stable form but rather continuously protrude and retract [378]. Its primary functions are cell motility and mechanosensing. The essential role of lamellipodia in cell migration has been extensively studied and reviewed elsewhere [353,375,379,380]. Briefly, lamellipodia extend at the leading edge driven by prominent branched F-actin polymerisation and form adhesive contacts with the substratum via transmembrane receptors, which are linked to the cytoskeleton. Previous adhesive contacts at the cell rear are then disassembled, and the cell contracts in an actomyosin (Myosin-II) dependent manner, which pushes the cell body "forward" by traction towards the adhesive contacts at the leading edge. Cell migration along the substrate (also known as cell crawling) occurs by cyclic repetition of this process. However, lamellipodia are also thought to be important for other types of cell migration *in vivo* [353].

Compared to filopodia, the actin regulators and mechanisms involved in lamellipodial formation are well defined. Rac1, a small Rho-GTPase, is considered the master regulator of lamellipodia in mammalian cells [353]. Rac1 mediates potent Arp2/3 complex stimulation via activation of the NPFs Wave2 and N-WASP, which it binds directly. These can be targeted to the PM by interactions with PIP2 [381], which is thought to be important for lamellipodia. Dendritic actin network formation and lamellipodial protrusion are both critically dependent on polymerisation of branched F-actin by Arp2/3 downstream of Rac1. In agreement, suppression of either Rac1 [382,383], Wave2 [384] or Arp2/3 [385,386] severely impairs

lamellipodia formation, whereas Rac1 expression/activation is sufficient to induce lamellipodia [387]. Other key actin regulators in lamellipodia include capping proteins, Cofilin and Profilin. Capping proteins block elongation of free barbed ends and thus funnel actin monomers into Arp2/3 nucleation events from the side of pre-existing filaments, thus highly increasing network branching [388]. Cofilin (see 1.5.9.1) mediates disassembly of actin filaments at the proximal end of lamellipodia and is therefore essential for ensuring F-actin turnover and monomer recycling in these dynamic and rapidly changing structures [389]. Profilin promotes the exchange of ADP for ATP in actin monomers, thus preparing them for new rounds of polymerisation [390]. In summary, the dendritic nucleation model of lamellipodium formation [391] is widely accepted and relies on branched F-actin polymerisation mediated by Arp2/3 and NPFs downstream of Rac1, which generates the protrusive force required for spreading of lamellipodia. Cooperation with proteins that mediate dynamic remodelling and turnover of the resulting dendritic actin network allows for repetitive cycles of protrusion and retraction [295,376].

1.4.7.3 Other cortical F-actin structures

In Table 1.2 below, we briefly introduce other physiological cortical F-actin structures that protrude from the PM and that are present in leukocytes. Despite some parallels, the structures presented below are well-defined (in terms of their actin arrangement and regulation) and represent clearly distinguishable entities from each other and from filopodia and lamellipodia.

Structure	Description	Refs.
Microspikes	Short filopodia-like structures that are almost completely embedded in the actin cortex and/or the leading edge. Their assembly is thought to require Cdc42, N-WASP and Profilin. Microspikes likely contribute to cell adhesion at the leading edge.	[354,392,393]
Microvilli	Microvilli are short (~1 µm) finger-like membrane extensions. Unlike filopodia, microvilli are remarkably stable, and their structure is well defined. They contain parallel linear actin filaments cross-linked and bundled by proteins like Villin or Fimbrin. (+) ends at the tip are capped, (-) ends are anchored to the actin cortex and filaments are laterally linked to the membrane. Typically found at apical epithelial cells, the main function of microvilli is to increase the exposed membrane surface area. Microvilli have been found on T-cells and macrophages, and they contribute to leukocyte migration.	[394-396]
Lamella	The lamellum is located behind the lamellipodium and serves as its broader supporting structure. Lamella are wider (up to ~10 µm wide) and more stable than lamellipodia. They primarily consist of linear actin bundles, Tropomyosin and Myosin-II.	[397,398]
Membrane ruffles	Lamellipodia-like structures that lift upwards and curl backwards to the cell. Believed to form upon inefficient lamellipodia adhesion. Like lamellipodia, membrane ruffles are strongly Rac1-dependent. Membrane ruffling plays an important role in macropinocytosis.	[374,399,400]

Podosomes	Podosomes are conical actin-rich PM protrusions that play important roles in cell adhesion, matrix degradation and tissue infiltration. Typically ~0.5-1 μm in diameter and ~0.5 μm deep, they display a distinct architecture characterized by a dense core of F-actin and actin binding proteins, surrounded by a ring of integrins and adaptor proteins. Podosome markers include: WASP, Cortactin, Arp2/3 and Tsk5 (core), as well as Talin, Vinculin and Paxillin (ring). Podosomes primarily form on cells of the monocytic lineage (e.g. Mφ, DC and osteoclasts).	[401-403]
Blebs	Blebs are bag-like protrusions of cell membrane that result from cytoplasmic filling upon actomyosin cellular contraction at regions of missing or weakened actin cortex. While initially devoid of underlying actin structures, bleb expansion is followed by reconstitution of the actin cortex (F-actin and membrane-cytoskeletal linkers) and then myosin-dependent retraction to deflate the bleb. Blebbing plays important roles in migration of many cell types. Key actin regulators include RhoA, ROCK, Ezrin and Myosin-II.	[404-406]

Table 1.2: Other cortical F-actin structures.

1.5 Manipulation of the actin cytoskeleton by HIV

NOTE: This section is heavily based on our recent publication [66], where the author of this thesis reviewed the available knowledge in terms of manipulation of the actin cytoskeleton by HIV. The reader should therefore be aware that large passages (and figures) have been reproduced from [66] with few changes and without the use of quotation marks. This is an open access article published under the creative commons attribution license (CC BY 4.0), and thus inclusion of this material in this thesis is in compliance with its licensing conditions.

1.5.1 How pathogens exploit the host's cytoskeleton

Actin is the most abundant protein in human cells and is essential for a wide range of cellular processes [263], including many that are required for the life cycle of intracellular pathogens (e.g. endocytosis, transport of cargo, membrane protrusions, etc.). Actin filaments build complex and dynamic three-dimensional networks within the cell and, in particular, the dense F-actin cortex below the PM represents a barrier for cell-invading pathogens. These are therefore obliged to navigate through and interact with the host cell's actin cytoskeleton in order to establish and sustain intracellular infection. The key importance of this ability is emphasized by the fact that elaborate mechanisms to manipulate cellular actin networks have convergently evolved across incredibly diverse pathogen families, including most human viruses (reviewed in [407-412], and numerous species of bacteria [412-417]. These mechanisms have been extensively studied and reviewed elsewhere and are therefore beyond the scope of this thesis. Still, here we highlight some of the major common themes to provide relevant perspective for this work.

Most cytoskeletal manipulation strategies involve pathogen-encoded proteins that are by themselves capable of altering cytoskeletal dynamics. This can occur by directly interfering with the cytoskeletal remodelling machinery, or indirectly by manipulating upstream regulatory events. Some pathogens encode proteins that "mimic" cellular regulators and can therefore "usurp" cytoskeletal regulatory or remodelling functions [417,418], whereas others go as far as encoding their own actin nucleators [419]. It is therefore increasingly clear that pathogens have evolved abilities to manipulate the full spectrum of host actin regulatory pathways [414]. Some commonly manipulated regulators include Rho-GTPases [412,420], tyrosine kinases [421], nucleation promoting factors [422] and the Arp2/3 complex [418]. Some common functional outcomes of actin cytoskeleton manipulation include; i) enhanced pathogen uptake/internalization [423,424], ii) formation of pathogen-associated membrane protrusions [425,426], iii) intracellular motility [269,415,427], and iv) cell-cell infection spread [415,424,428].

1.5.2 Strategies of HIV-mediated actin manipulation

Unlike with other pathogens, none of the HIV gene products seems to be specifically dedicated to the task of cytoskeletal deregulation, and none are known to mimic cellular cytoskeletal components. Instead, HIV manipulates actin dynamics indirectly by leveraging many of its essential components to exercise control over a wide range of cytoskeletal regulators and pathways. This multi-strategy and multi-target approach makes manipulation of cellular actin networks by HIV particularly complex to study. Observations from the literature report that the virus can "exploit", "neutralize" or "hijack" cytoskeletal proteins (definitions further below), by promoting protein activation/inactivation, modulation of gene expression, changes in cellular localization and even altering cellular protein function (Fig. 1.7). Some host proteins are even manipulated by multiple strategies, depending on the stage of the viral life cycle. Far from being random in nature, these manipulation events are spatiotemporally regulated, and their coordinated implementation results in cell-type specific changes in cellular behaviour to promote defined outcomes which are overall favourable for HIV infection. Most notably, these include impairment of immune cell functions and improvement of viral outcomes, both in terms of cell-free virus and cell-cell spread (see Fig. 1.7 and section 1.5.11).

Subversion of the host actin cytoskeleton is essential for both establishing and spreading the infection by HIV. Virtually all known stages of the viral life cycle have been reported to be dependent on actin to lower or greater extent, including viral entry [429-431], reverse transcription [432], nuclear migration [433-435], transport of viral components to the membrane [436-438], assembly [239,257,439], budding [440-442] and cell-cell transfer (see 1.5.8 & 1.5.10). Of note, the microtubule network has also been identified to play several roles

during HIV infection; however, this extends beyond the scope of this thesis (for more detail we refer to [239,443-445]).

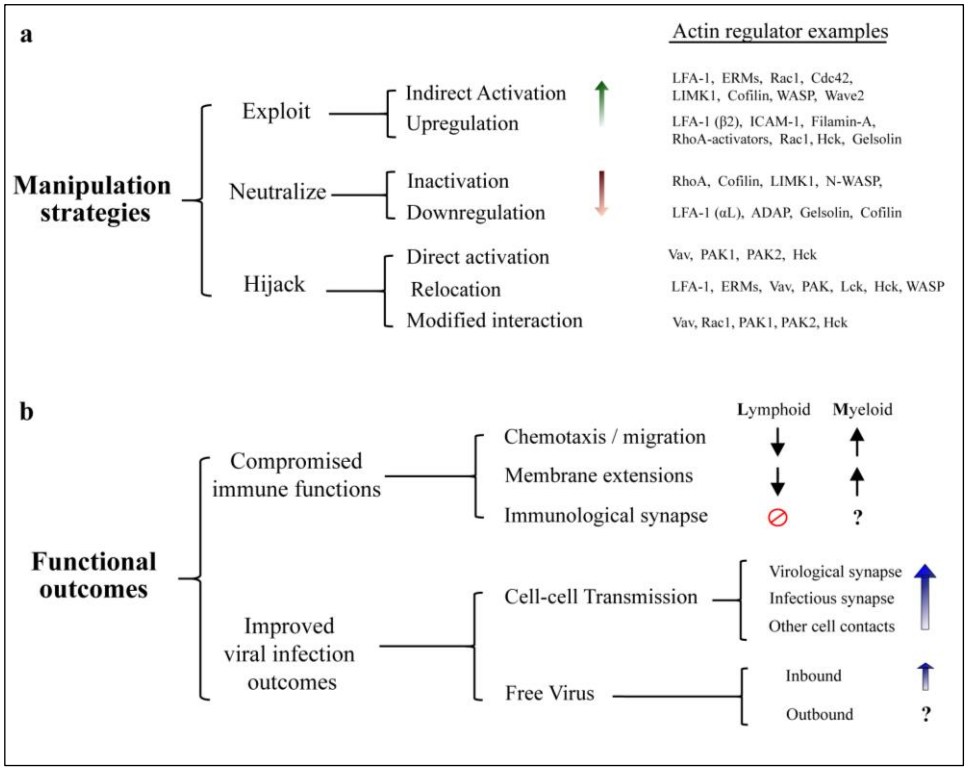

Figure 1.7: Manipulation of the actin cytoskeleton by HIV. **A**) Actin regulators subjected to modulation by HIV. Mechanistically diverse strategies enable the virus to alter cellular cytoskeletal functions. Manipulation of host factors can be either direct, when mediated by physical interaction with viral proteins, or indirect, when requiring upstream cellular factors. Exploitation mechanisms increase native protein activity by upregulation of gene expression, or indirect activation within a cellular pathway. Neutralization of host factors is achieved by downregulation of gene expression or protein inactivation. Hijacking alters the functional outcome of host protein activity, either by overriding regulatory mechanisms (i.e., direct protein activation), changing protein subcellular localization, and/or modifying protein interaction partners. Select examples of actin regulators corresponding to each strategy are provided. Importantly, some host factors can be manipulated by multiple strategies at diverse stages of the viral life cycle, as well as differentially in infected and uninfected cells. **B**) Functional consequences of actin-dependent changes induced by HIV. Normal immunological functions are compromised upon HIV infection, partly due to actin-remodelling changes orchestrated by viral proteins. CD4+ lymphocytes display severe impairment of chemotaxis and immunological synapse formation. Myeloid cells display aberrant enhancement of actin dependent structures, which alters cell motility and tissue distribution. Concurrent changes in actin remodelling in both cell types also promote viral spread via actin-dependent cell-cell contacts and support infection by inbound cell-free virus. Note: this image was created by the author of this thesis and was published in [66] under an open access license (CC-BY-4.0).

1.5.3 Actin manipulation by inbound vs. outbound HIV

The concepts of inbound and outbound virus were introduced in section 1.1.7. An important difference between the two is that manipulation of the cytoskeleton by inbound virus can only rely on viral factors that are incorporated in the virion (mainly proteolytically cleaved mature products of Gag and Gag-Pol, alongside Vpr, Env and Nef), and is limited by the relatively low abundance of these proteins, compared to the large pool of host cytoskeletal proteins in the target cell. In contrast, during outbound virus production, viral RNA and proteins (including all accessory proteins) are present at high concentrations in the cytosol and therefore have direct access to cytoskeletal components, most of which are purely intracellular. A third scenario is given by soluble viral proteins such as Tat, Env and Nef, which are known to be present extracellularly, as well as inside uninfected cells both *in vitro* and *in vivo* [446-448]. Thus, these soluble factors can induce cytoskeletal changes in a broad range of cells, including cell types that are not typically infected by HIV.

1.5.4 Actin in HIV virions

The presence of actin in enveloped viruses was recognized over four decades ago [449], yet a functional role within the virions (if any) remains unresolved. In 1996, Ott et al. reported the presence of actin within HIV produced in T-cells, exceeding 10% of the molar abundance of Gag within the virion [450]. Gag alone was shown to be sufficient for actin incorporation into the particle [451]. Several groups have since confirmed that both actin and numerous host cytoskeletal proteins are incorporated within HIV virions [452-454]. A conserved set of host proteins shared by virions produced in T-cells and Mφ was identified by Linde et al., with about half corresponding to actin isoforms [454]. Both the mechanisms by which cytoskeletal proteins get incorporated and their potential roles within viral particles remain mostly controversial [455,456], with few exceptions. Nevertheless, it is well accepted that identification of these host factors can provide important information regarding potential viral–host protein interactions, the microenvironment of viral assembly and the cellular origin of virions. A recent study has challenged the view of active packaging of actin into HIV particles. Stauffer et al. reported the load of actin within virions to be lower than previously described and postulated that this parameter is affected by the concentration of actin in the cell of origin. Thus, actin in virions might be simply due to the pinching of cytosolic pools during budding [457]. Further interpretation is currently limited by the technical complexity of specifically measuring actin concentrations at different subcellular regions, i.e., at HIV budding sites.

1.5.5 Physical interaction between Gag and F-actin

In addition to their ability to manipulate actin regulators, some HIV proteins might be able to associate with actin filaments directly [432,458-460]. The structural protein Gag represents the best understood example in this respect. Early studies showed that Gag co-sediments with the cytoskeletal cellular fraction and that this association could be disturbed by actin- but not microtubule-depolymerizing drugs, thus suggesting a direct physical interaction between HIV-Gag and microfilaments [461]. Soon after, the nucleocapsid domain of Gag (NC) was observed to be the one required for its association with F-actin. Absence of NC, but not matrix or capsid, abrogated co-fractionation of Gag with the cytoskeleton, whereas recombinant NC was able to bind polymerized F-actin in a dose-dependent manner *in vitro*. Furthermore, Gag could be coimmunoprecipitated with actin but not tubulin. Based on these observations, a direct physical interaction between HIV-Gag and F-actin via Gag's NC-domain was concluded [462]. Immunogold labelling and electron microscopy also showed that actin significantly colocalizes with NC within the virion. Even after detergent and protease treatment, about half of the virion-associated actin content remained in stable complex with NC [451]. A physical association between HIV-Gag and actin (<5 nm) was confirmed by fluorescence resonance energy transfer (FRET), albeit in fixed and adherent cell lines [463]. Overall, convincing evidence supports physical association between HIV-Gag and F-actin, although whether or not this interaction plays any function role in the viral life cycle is still unknown.

1.5.6 Role of Actin for HIV Entry

Inhibitors of actin dynamics (IAD) are small molecule drugs that interact with G- or F-actin and interfere with normal actin remodelling [464]. Several observations following the use of IAD indicated an essential role of actin remodelling for inbound HIV. IAD have been shown to dramatically decrease HIV infection in T-cells, by arresting viral entry at a pre-fusion step [429,465-467]. A seminal study revealed that Env induces actin-dependent concentration of CD4 and CXCR4 receptors, which become copolarized on the target cell surface [429]. This is thought to increase the density of viral receptors in the vicinity of membrane-bound HIV virions and thereby promote viral entry. In contrast, treatment of virions with the IAD "Cytochalasin D" did not reduce their infectivity [429], indicating that only actin changes in the target cell are required. Subsequent studies identified many of the cytoskeletal regulators involved in this process and confirmed that actin remodelling is required for viral entry both before and after membrane fusion. Unlike for other stages of the viral life cycle, sufficient evidence exists to provide a relatively complete and unambiguous model. Figure 1.8 summarizes our updated view of the molecular mechanisms involved in actin regulation

around HIV entry into T-cells (as previously proposed by *[468,469]*). The mechanisms by which HIV manipulates cellular proteins to orchestrate these events in T-cells we have reviewed in great detail in [66] and some are briefly discussed in section 1.5.9.

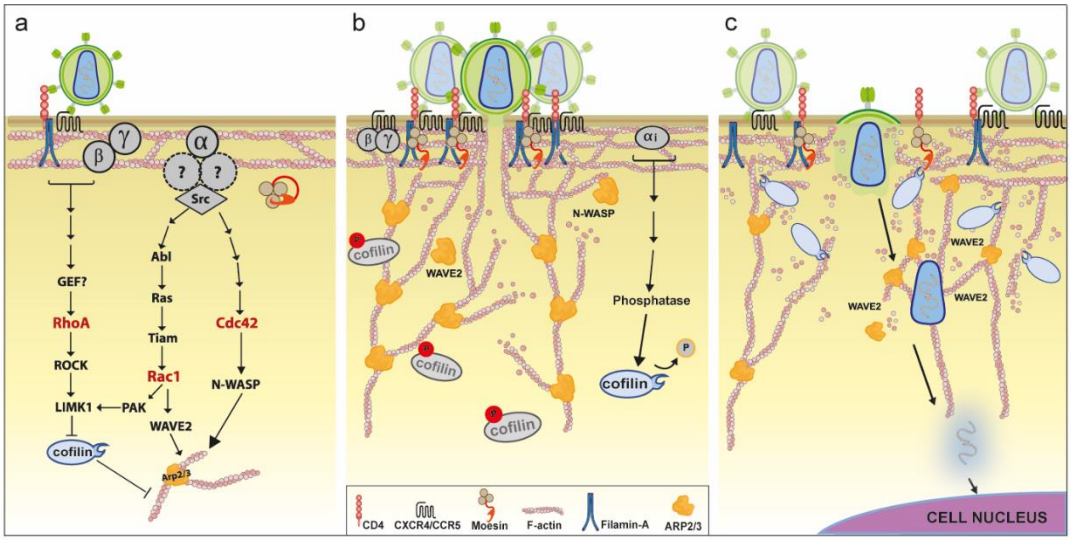

Figure 1.8. Model of manipulated actin dynamics during inbound HIV infection in T-cells. A) Early signaling events: Binding of Env to CD4 and coreceptor molecules (CXCR4/CCR5) initiates signaling via the receptor-coupled G-protein. $G\alpha_i/G\alpha_q$ signaling via Src activates both Rac1 [430,470,471] and Cdc42 [472,473], which in turn activate downstream nucleation-promoting factors (NPFs) that stimulate actin polymerization activity by the Arp2/3 complex. Env binding to CD4 also triggers RhoA activation in a Filamin-A-dependent manner [474], and results in Moesin activating phosphorylation [475]. Both RhoA and Rac1 lead to Cofilin inactivation via phosphorylation by LIMK1 [474,476]. Rho-GTPases are shown in red. **B) Receptor capping:** Stimulation of Arp2/3 by active NPFs and simultaneous inhibition of Cofilin leads to increased cortical F-actin polymerization. This results in aggregation of CD4 and CXCR4 receptors, which requires linking of these molecules to actin filaments by Filamin-A and Moesin [474,475]. Enhanced colocalization of these receptors near Env promotes viral entry, with actin polymerization participating in fusion-pore formation and expansion [430,471]. Delayed Env-CXCR4 signaling via $G\alpha_i$ leads to Cofilin activating dephosphorylation by a currently undefined mechanism [476]. **C) Intracellular transport:** After virus–cell fusion, transport of HIV to the nucleus is limited by the dense cortical F-actin network. Cofilin activation results in local F-actin depolymerization that allows passage of the viral core through the actin cortex. This is supported by observations that Cofilin silencing in primary T-cells leads to aberrant accumulation of cortical actin and reduces HIV integration without affecting viral entry or reverse transcription [476], whereas Cofilin activation by different stimuli increased nuclear translocation and HIV infection levels [435,477]. Transport of the pre-integration complex towards the nucleus is thought to involve Arp2/3-mediated actin polymerization [434,478]. Note: this image was created by the author of this thesis and was published in [66] under an open access license (CCBY4.0).

1.5.7 Role of Actin for free HIV egress

Compared to inbound HIV infection, the role of actin filaments towards release of outbound free virus particles remains controversial. Studies using IAD have so far reported inconsistent effects on viral release. The actin polymerization inhibitor Cytochalasin D either reduced or

had no effect on HIV release [123,239,441,442,479]. While this might be explained by differences in cell lines and experimental conditions, no unified conclusion can be drawn from these observations. In contrast, complete depolymerization of F-actin by the potent marine toxin Mycalolide-B decreased HIV release in a dose-dependent manner, with viral proteins failing to reach the PM [437]. In addition, several studies have observed prominent association of HIV budding sites with F-actin. Using atomic force microscopy, aster-shaped NC-dependent actin structures were visualized to emanate from HIV buds during viral assembly and disappear upon viral release [257]. Cryo-electron tomography confirmed the presence of actin filaments near budding sites, and revealed occasional and direct physical contacts with nascent particles [257,457,480]. Others however argue against a functional role of these actin filaments in viral budding, given that; i) the absence of NC did not reduce actin content near budding sites [457], and ii) real-time tracking of single-virus buds revealed no F-actin recruitment during viral assembly [481]. This study also showed that budding-initiation and Gag assembly were not affected in the presence of IAD, despite confirmed disruption of the cortical F-actin network [481]. However, since the latter studies did not measure supernatant viral contents, a role for actin in the actual egress of HIV virions cannot be excluded. Indeed, studies looking at particle production upon interference with prominent actin regulators do suggest a role of actin dynamics in HIV budding ([440,482] and section 1.5.9).

1.5.8 Role of Actin for cell-cell transfer of HIV

Compared to its effects on free virus release, generalized disruption of actin dynamics by IAD leads to a more consistent impairment of CCTH. Treatment with Cytochalasin D or Latrunculin B reduced infection of target T-cells (20-80% decrease) in various coculture systems [123,125,127,239,483]. Despite the potential limitations of such approaches (e.g. may also affect inbound/outbound free HIV), this has led to the well accepted view that CCTH is strongly dependent on actin remodelling [85,239,407,484,485]. In part this is expected, given the known requirement of actin filaments for generation of membrane protrusions and anchoring of adhesion molecules, both of which are important for cell-cell interactions [486,487]. However, the actin cytoskeleton also plays other more specific roles in CCTH that go beyond simply supporting formation of intercellular contacts. Actin remodelling has been repeatedly shown to be essential for the recruitment of diverse viral and cellular factors to the donor-target cell interface of HIV synapses [85,226,233,239]. This most notably includes Gag and Env on the donor cell, and CD4 and CXCR4/CCR5 on the target cell, but many other molecules are also recruited in an actin-dependent manner. However, since many of these observations come from the use of IAD that broadly impair actin remodelling, it has remained challenging to dissect the specific cytoskeletal pathways or regulatory events that

facilitate/drive CCTH. Furthermore, while new studies have begun to shed light on various molecular players involved in this process, it has become increasingly evident that different cell-types/pairs have different cytoskeletal requirements for mediating CCTH. For these reasons, no unified model can yet be provided for actin (de)regulation during CCTH, and the accumulating evidence of HIV-manipulated actin regulators must still be discussed individually, or in the context of specific CCTH-structures. This will continue to be addressed in the following sections 1.5.9 and 1.5.10.

1.5.9 Actin regulators and pathways manipulated by HIV

While HIV can directly associate with F-actin, the most striking manipulation of the cytoskeleton occurs by reprogramming the expression, activity and interactions of actin-regulatory proteins upstream of microfilaments (Fig. 1.7). Figure 1.9 emphasizes that manipulation is mechanistically diverse and not limited to a particular class of proteins, but rather extends throughout all layers of the cytoskeleton. While in [66] we reviewed a large number of cytoskeletal regulators, here we have only included those that are relevant to the results presented in this thesis. The role of various of these proteins as therapeutic targets for HIV treatment is partially discussed in [488].

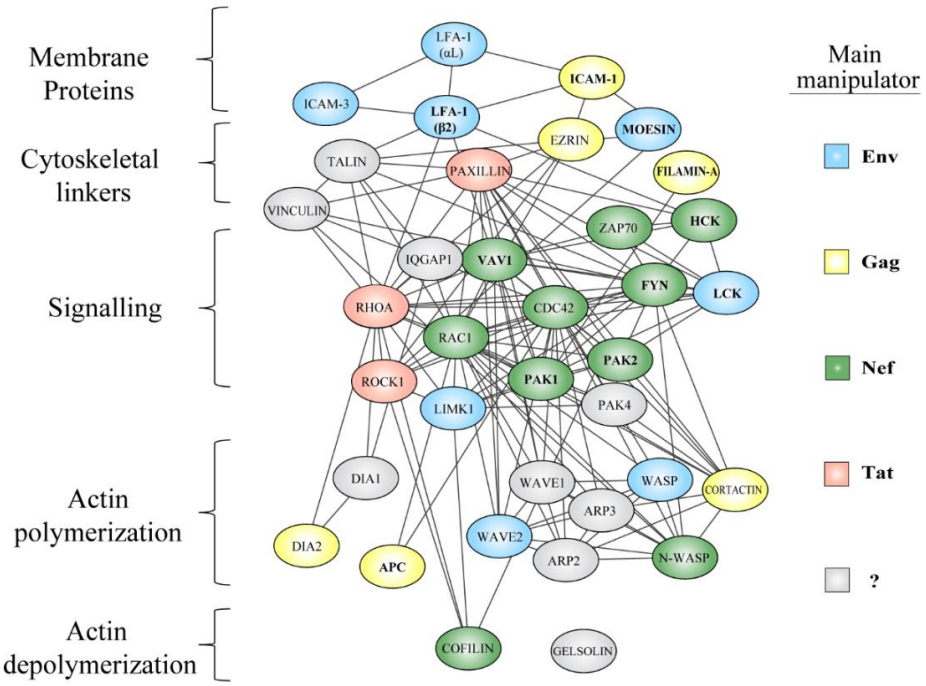

Figure 1.9: Functional protein interaction network of actin regulators manipulated by HIV. Subversion of the actin cytoskeleton occurs throughout all layers of the actin cytoskeleton, including surface proteins, their linkers to actin filaments, diverse signaling nodes, their effectors, and proteins that directly mediate actin remodelling. Color coding of host factors indicates the main viral protein involved in their deregulation; Nef = green, Gag = yellow, Tat = pink, Env = blue, presently undefined = grey. So far, only proteins shown in bold have been experimentally

confirmed to physically interact with the indicated viral proteins (i.e., direct manipulation). Network data was obtained from the STRING database [489], as described in [66] where this figure was published by the author of this thesis under an open access license (CCBY4.0).

1.5.9.1 Exploitation of Actin Regulators and Pathways by HIV

While some HIV proteins can physically engage cellular actin regulators and directly activate them, a greater number of host factors seems to be taken advantage of indirectly. Their ability to promote specific changes in the actin cytoskeleton can be exploited by HIV, even in the absence of direct physical interaction, by increasing total protein abundance or native protein activity within cellular pathways. We consider host factors to be "exploited" by HIV whenever this increase occurs by mechanisms that do not affect endogenous protein function or subcellular localization. Based on the available knowledge, this so far includes; i) upregulation of gene expression; and ii) indirect protein activation (i.e., downstream of host factors that are directly activated by HIV proteins). Here we only discuss select examples that are relevant to this thesis' results (i.e. Rac1, Cdc42, Arp2/3, Dia formins and Cofilin), and address how each factor is exploited by inbound or outbound HIV.

Rac1 is a Rho-GTPase known to regulate several actin polymerization pathways, which in healthy cells allow formation of membrane ruffles and lamellipodia. Rac1 has been shown to play a determinant role for inbound HIV infection. Harmon et al. elegantly showed that HIV triggers Rac1 activation via Env to promote actin polymerization events that support viral entry (see Fig. 1.8-A). This is dependent on the Env-CCR5 interaction, which signals over a defined $G\alpha q$ cascade and results in activation of the tyrosine kinase Abl [430,470]. Abl then phosphorylates Ras, allowing it to stimulate Tiam1, which is a potent activator of Rac1 [430,490]. Both Rac1 and Abl activate WAVE2 to prompt actin polymerization by the Arp2/3 complex [430]. Since disruption of any of these proteins resulted in decreased HIV entry and arrested fusion at the hemi-fusion stage, the authors conclude that this signalling pathway ultimately leads to actin remodelling changes that facilitate HIV fusion-pore formation and enlargement (Fig. 1.8-B) [430,471,491]. In agreement, interfering with Rac1 function reduced viral fusion, leading to decreased inbound infection rates [492,493]. While these mechanisms were elucidated mainly in adherent cell lines, other studies support Env-dependent activation of Rac1 in primary T-cells and monocytes *ex vivo*, as well as brain macrophages *in vivo* [491]. Of note, soluble Tat is also able to activate Rac1, although the corresponding mechanisms are less well understood [494-496].

On the other hand, HIV-infected cells also display dramatic Rac1 activation, and this is mainly mediated by Nef. Nef expression increased Rac1 activity in a wide range of cell types, including podocytes [497,498], T-cells [499], monocytes [491,500] and DC [501]. The

mechanism of Nef-mediated Rac1 activation is currently controversial but most likely involves direct binding of Nef to the leukocyte-enriched GDP-exchange factor Vav [66]. In terms of outbound virus, silencing of Rac1 led to decreased viral production in T-cells, but only for Nef-encoding virus [482]. In agreement, constitutively active Rac1 boosted free-virus release [502]. It is worth noting that while most Rac1 activation in infected cells is mediated by Nef, the presence of Gag alone also led to strong Rac1 activation and actin polymerization in Jurkat cells [482]. In conclusion, Env-triggered Rac1 signalling and potent Nef-induced Rac1 activation mediate actin remodelling changes that promote both inbound and outbound viral spread, respectively. The fact that Nef, Env, Gag and Tat all independently lead to Rac1 activation in human cells, emphasizes layers of redundancy that enable activation, and in turn highlight this protein as a critical regulator in HIV infection.

Cdc42 is a Rho-GTPase well known for its physiological role in promoting long and actin-rich membrane protrusions such as filopodia [503]. The role of Cdc42 for inbound HIV has been studied by Swaine et al. and recently reviewed in [472]. Briefly, novel Cdc42-specific inhibitors have revealed that, as for Rac1, Env-triggered Cdc42 signalling mediates actin-remodelling changes that facilitate viral entry. The authors conclude that the Cdc42-NWASP-Arp2/3 pathway may be equally or more important than the Rac1 pathway described above [472]. Recent studies have confirmed this hypothesis, by showing that Env-signalling through CD4 and CCR5 leads to activation of both Rac1 and Cdc42 in primary CD4TC when these are exposed to either cell-free [473] or cell-transmitted HIV [262]. In terms of outbound HIV, Cdc42 seems to play a negligible role in free-virus-release [482], despite being incorporated into virions produced in both T-cells and Mφ [454,504]. In contrast, Cdc42 seems to play an important role for outbound CCTH (*in trans*) via infectious synapses (reviewed in section 1.5.11). As with Rac1, Nef has been shown to activate Cdc42 in various cell types [491,498,501,502], which is likely required for some Nef-mediated cytoskeletal effects [502,505]. Overall, the Rho-GTPases Rac1 and Cdc42 are two of the cytoskeletal regulators most potently and diversely manipulated by HIV, despite a clear lack of evidence to suggest direct interaction with viral proteins [66]. Figure 1.9 highlights that these regulators represent signalling nodes of actin regulation, where multiple HIV-manipulated cytoskeletal pathways converge. In particular, signalling to the Arp2/3 complex and subsequent actin polymerization events seem to be crucial for mediating both viral entry and egress.

Arp2/3. Several studies have revealed a critical role for the Arp2/3 complex and its associated NPFs at multiple stages of the HIV life cycle. The role of Arp2/3 downstream of Rac1 and Cdc42 in free-virus entry was discussed above. In addition to these effects, Komano et al. showed that inhibition of Arp2/3 significantly reduced inbound HIV infection and replication

in 293T and H9 cells. Since membrane-fusion was not affected, and VSVg-pseudotyping could overcome the observed restriction, the authors suggest Arp2/3 might be involved in intracellular transport of the viral core through the actin cortex [478]. These observations were recently confirmed and expanded by Spear et al., who used various methods to inhibit Arp2/3 activity in primary CD4TC [434]. Interfering with Arp2/3 and/or Wave2 in this context strongly reduced inbound HIV infection, despite only moderately reduced entry and unimpaired reverse transcription. Given a dramatic decrease in 2-LTR circles (a correlate for nuclear entry [506]), the authors concluded Arp2/3 and Wave2 to be essential cofactors for HIV nuclear migration (Fig. 1.8-C) [434].

Several lines of evidence also suggest a role of Arp2/3 for outbound HIV. On one hand, Thomas et al. reported Arp2/3 activity to be involved in free-virus production and this could be mapped to the Rac1-IRSp53-Wave2-Arp2/3 actin polymerization pathway. Interfering with any of these regulators was associated with reduced membrane-targeting of outbound Gag and impaired viral release in CD4TC [482]. On the other hand, Arp2/3 could play an important role for CCTH from DC via infectious synapses (i.e. *in trans*) downstream of Cdc42 ([507] and see 1.5.11). In agreement, four of the seven Arp2/3 subunits were identified by a shRNA-screen as factors that promote CCTH *in trans*. The authors confirmed that interfering with Arp2/3 activity reduced transfer of virus from HIV-pulsed (uninfected) iDC to CD4TC, and that this was accompanied by loss of actin-rich "dendrites" [508]. Altogether, these observations implicate Arp2/3 activity in both cell-free and cell-cell spread of HIV, likely downstream of HIV-activated Rac1 and Cdc42. Importantly, however, the role of Arp2/3 for CCTH *in cis* remains largely unexplored.

Formins. The potential implication of formins in HIV-manipulation of the cytoskeleton has only been recently recognized and suggest specific involvement of the diaphanous-related formin (Dia) family in this context. Silencing of Dia1 or its main upstream regulator RhoA did not reduce free-virus production from infected Jurkat cells [482], but it impaired infectious synapse progression by reducing actin-dependent HIV polarization and transfer of viral particles (*in trans*) from HIV-pulsed DC [507]. Similarly, while silencing of Dia2 did not reduce free virus release, this formin was previously identified in our lab as an important regulator in HIV-Filopodia [89], and these observations have been expanded as part of this thesis (see Chapter 6). Finally, a recent study revealed potentially critical roles of Dia for inbound HIV [509]. Interfering with Dia1 or Dia2 dramatically reduced inbound HIV infection in various cell lines and was associated with impaired intracellular transport of viral cores and their uncoating. [509]. Overall, Dia formins play an unexpected key role for inbound HIV, and likely participate in CCTH, whereas they seem dispensable for free virus release.

Cofilin is a highly homologous protein in eukaryotes and participates in numerous cellular processes [510]. Many of these functions involve Cofilin's ability to accelerate actin disassembly by two mechanisms; i) severing of microfilaments; and ii) enhancing depolymerization rates from both ends [511,512]. Cofilin is a key regulator of the actin cortex, which represents both a barrier and an ally for HIV spread [468]. Thus, manipulation of Cofilin by HIV is temporally regulated and involves both exploitation and neutralization at different stages of the viral life cycle [468]. These events were reviewed in great detail in [66] and were summarized in Figure 1.8. Increased levels of active Cofilin were also detected in the resting T-cell population of HIV+ patients [513], implying increased susceptibility to infection. In terms of outbound HIV, Cofilin was consistently incorporated into virions produced by myeloid and lymphoid cells [454,504], reaching up to 10% of the molar abundance of Gag [450], indicating its presence at HIV assembly sites and thus a potential role in viral budding. However, potential contributions of Cofilin to CCTH have been largely unexplored.

1.5.9.2 Neutralization of Actin Regulators by HIV

Carefully orchestrated manipulation of the actin cytoskeleton by HIV requires not only activation but also neutralization of actin regulators, sometimes even in a spatiotemporally coordinated manner, as exemplified by the Cofilin example above. We define "neutralization" as any manipulation that results in a decrease of target protein activity. Neutralization mechanisms therefore include protein inactivation (direct or indirect), downmodulation, degradation and repression of gene expression, all of which are employed by HIV for cytoskeletal manipulation (Fig. 1.7). Table 1.3 below briefly summarizes select examples of actin regulators that are inactivated by Nef. These are discussed in much greater detail in our review [66]. Note that while these regulators may be neutralized in HIV-infected T-cells (i.e. outbound HIV), their activation downstream of Env-initiated signalling is important for inbound HIV infection (Fig. 1.8).

Regulator	Normal function	Neutralization by HIV-Nef
RhoA	Rho-GTPase known for regulating stress-fiber formation	HIV infection leads to RhoA inhibition in a Nef-dependent manner [497,514]. Inhibition of RhoA may be beneficial for outbound HIV, given that RhoA activation inhibits free virus release in various cell types, including macrophages and T-cells [66,479,515,516].
Cofilin	F-actin turnover by filament severing & depolymerization from both ends	Potent Nef-mediated neutralization of Cofilin activity has been observed in T-cells [517,518], and this is a strongly conserved feature of Nef [519]. Potential mechanisms are discussed in detail in [66]. For the functional consequences, see section 15.11.1.

N-WASP	Nucleation promoting factor for Arp2/3 complex, downstream of Rac1 and Cdc42	Nef-mediated inhibition of N-WASP prevents normal actin remodelling associated with immunological synapse formation in T-cells (i.e. cell-spreading, cell-cell contacts, actin-ring formation, and T-cell receptor signalling [520]. For more details see 1.5.11.1

Table 1.3: Examples of actin regulators neutralized by HIV

1.5.9.3 Actin Regulators Hijacked by HIV

Some of the best understood examples of cytoskeletal manipulation are given by cases where regulators of actin dynamics are directly engaged by viral factors via protein–protein interactions. We consider such host factors to be hijacked by HIV whenever their activation results as a direct consequence of physical interaction with a viral protein. Importantly, this allows the virus to override cellular regulatory pathways, by promoting downstream events even in the absence of upstream activating signals, or despite the presence of inhibitory cues. In addition, our definition of hijacking includes manipulation events where the functional outcome of host protein activity is altered, for example, by modification of host protein interaction partners, and/or deliberate alteration of protein subcellular localization. Since most (if not all) of the cytoskeletal exploitation and neutralization events likely occur downstream of HIV-hijacked host factors, resolving the molecular mechanisms by which the virus engages these proteins is of essential importance to the field. Here we discuss only one of the best understood examples of HIV-hijacked proteins, which is the hematopoietic cell kinase (Hck). Other prominent examples such as the Rac1/Cdc42-activator Vav and the serine/threonine-kinase PAK, were discussed in depth in our recently published review [66]

Hck is a member of the Src family and is expressed selectively and at high levels in phagocytic cells, including monocytes, Mφ and DC [521,522], where it regulates various inherent functions of these cells that involve actin polymerization [523]. Manipulation of Hck by HIV is dependent on Nef, and thus mainly affects infected cells. Nef binds Hck directly and with much higher affinity than other SH3-bearing kinases [524,525]. This dramatically increases Hck activity by inducing its autophosphorylation and by releasing the catalytic region via displacement of the SH3 domain [521,526]. In Mφ, HIV infection was shown to increase already high levels of Hck expression and activity. This correlated with increased virus production, whereas Hck silencing strongly impaired viral release [527]. In agreement, disruption of the Nef:Hck interaction was shown to impair viral replication [524,528]. Furthermore, Hck was found within virions produced by Mφ and Hck-expressing HEK cells. Incorporation was dependent on Nef's PxxP domain, suggesting that loading into the virus occurs by direct binding to Nef [529]. Expression of Hck in producer cells also increased particle infectivity [529], whereas Hck silencing decreased it at the entry level [530].

Importantly, Nef reprograms Mφ migration via Hck by inducing dramatic cytoskeletal changes [522]. Nef increased the number, size, F-actin content and lifespan of podosome structures (see Table 1.2) on the surface of infected Mφ in a Hck-dependent manner. This is likely a consequence of strong WASP activation by Hck, given massive accumulation of phosphorylated WASP on these structures, which was dependent on Nef:Hck interactions and Hck-mediated WASP phosphorylation [522]. Nef also increased adhesion, matrix degradation and mesenchymal migration, while inhibiting ameboid migration of infected macrophages. In *nef*-transgenic mice, this results in Mφ tissue accumulation that mimics that of HIV+ patients [522]. A similar *in vivo* study showed that Hck is required for rapid onset of Nef-induced AIDS-like disease. Both Hck-knockout mice and those with mutations in the Hck-SH3 domain displayed prolonged latency periods and delayed appearance of symptoms [531]. Altogether, Hck is subject to profound and multifaceted manipulation by HIV that includes upregulation, strong direct activation and virion incorporation. This enhances Hck actin remodelling and promotes outbound HIV spread by increasing both virion release and infectivity.

1.5.10 Actin manipulation at virological and infectious synapses

As mentioned before, the mechanisms by which HIV manipulates the actin cytoskeleton to facilitate CCTH remain incompletely understood. Here, we briefly provide an overview of the known role of actin filaments and/or regulators for formation of HIV-synapses. Still, it should be noted that in most cases one can only speak of parallel/sequential events, the functional interrelation of which remains to be resolved.

The **homotypic T-cell VS** is by far the most studied and best understood example in terms of its actin regulation. Initial conjugate formation by infected donor cells is dependent on both Env and actin remodelling, as it can be impaired by Env-antibodies or IAD [85,239]. Env likely induces the activation of LFA-1 on the target-cell side [532,533], increasing its ligand affinity and leading to binding of ICAM-1 on the donor-cell side, which provides the initial adhesive force for conjugate formation [233]. Env-CD4/CXCR4 and LFA-1 signalling then leads to actin remodelling and actin-dependent polarization of these same molecules on the target-cell side, likely by a similar mechanism as described in (Fig. 1.8-B) and additionally supported by simultaneous polarization of Env on the opposing cell [239]. Despite this initial concentration of actin at the VS, F-actin is eventually cleared from the center of this structure as the synapse matures. This process, which involves abnormal T-cell receptor signalling triggered by Env via Src [534], has been proposed to help the incoming virions overcome the cortical actin barrier (analogously to Fig. 1.8-C). The focal adhesion protein Talin may also be involved, as it colocalizes with LFA-1 and actin, often forming a “ring-like structure” at the VS [85]. On the donor cell side, several cellular and viral components also polarize in an

actin-dependent manner. This includes Env and Gag [85,234,239], as well as phosphorylated Ezrin [535], tetraspanins which are thought to prevent donor-target cell fusion [536] [537], the microtubule organization center [538,539], and mitochondria [238]. This remarkable donor-cell polarization likely involves the TCR-related signalling protein ZAP70, which is phosphorylated in donor T-cells within minutes of mixing with uninfected target cells. This is dependent on Env and the TCR-Lck-ZAP70 phosphorylation pathway [262]. Although not cytoskeletal proteins per se, these signalling proteins are known to be help coordinate cortical F-actin remodelling upon TCR activation [540]. Since absence of any of these proteins impaired actin-dependent recruitment of Gag, Env and the MTOC to the VS, as well as CCHT between T-cells [262,538], they are now considered important regulators of the T-cell VS. However, since they are only expressed in lymphoid cells, other mechanisms/regulators must be involved in other cell types (e.g. myeloid cells).

The **DC infectious synapse** relies on the actin cytoskeleton at multiple levels. First, actin-dependent processes (including macropinocytosis and formation of VCC) are important for the uptake of mature HIV particles by uninfected DC, which serve as donor cells for CCTH *in trans* [541]. Second, actin remodelling is required for stable conjugate formation between HIV-pulsed DC and target T-cells, as IAD can potently disrupt this process [226,541]. IAD also impaired polarization of F-actin and trafficking of HIV on the DC surface towards the target cell, as well as target T-cell infection [221,507,541]. These studies also confirmed that CCTH *in trans* from HIV-pulsed DC relies on extensive F-actin-rich "sheet-like" membrane projections on the donor cell that either fully engulf (mDC) or more loosely interact (iDC) with the target cell, as shown by electron tomography and ion-abrasion electron microscopy [221,507]. While such thin-walled membrane projections are common in uninfected mDC, they seem to be actively induced by the virus in iDC in an Env-dependent manner. Two studies [225,507] observed the following sequential events of actin deregulation when iDC are pulsed with mature HIV particles; i) rapid activation of Src (likely via DC-SIGN signalling upon binding of Env), ii) activation of Cdc42 and its downstream effector PAK1, iii) increased complexing of WASP with Arp2/3 and F-actin, iv) increased complexing of the formin Dia2 with F-actin, and v) increase in sheet-like membrane extensions on the cell surface. Importantly, mature HIV was found over the entire length of these structures, and directional transfer of virions was observed in a rapid and linear manner towards target cells [507]. Thus, the authors concluded that these structures are essential for CCTH at the infectious synapse. In agreement, interfering with Cdc42 activity reduced the number of these structures, and although it did not reduce conjugate formation, it reduced the speed of viral movement along their surface and moderately decreased HIV-transfer to target cells *in trans* [507].

Compared to the T-cell VS or the DC infectious synapse, very little is known about the process of actin (de)regulation at the DC-VS (i.e. CCTH *in cis*). One of the major limitations of studying this process has been the inability of imaging not only assembling particles but also fragile F-actin structures in fixed samples [156]. With the ability of labelling HIV in live cells, came the first glimpses of HIV's association with a dynamic network of cortical F-actin filopodia [89,156]. Yet compared to other cell types (see 1.3.4), very little was known about the landscape of F-actin regulator interactions and mechanisms that can coordinate filopodia formation in myeloid cells. This unknown landscape, and the question of how HIV would manipulate it, were key motivating drives of this study and its aims as described in section 1.6.

1.5.11 Other functional consequences of actin manipulation in HIV-target cells

Given the tropism of HIV, manipulation of the actin cytoskeleton by this lentivirus inevitably affects the host's immune system at various levels. Altered regulation of actin dynamics is therefore not only key for promoting spread of the infection, but also simultaneously compromises normal immunological functions. Three decades of research have increased our understanding of how HIV reprograms actin dynamics in these cells to promote specific changes in cellular behaviour. Here we discuss the functional consequences of global actin cellular changes induced by HIV and highlight the striking differences in morphology and motility observed between infected T-cells and myeloid antigen presenting cells (Fig. 1.10).

1.5.11.1 T-Cells

HIV infection and expression of viral proteins in CD4TC is associated with compromised immune functions [542]. This is, in part, due to dramatic deregulation of actin remodelling, which severely impairs cell motility. Nef plays a major role in this process, and expression of this viral protein alone is sufficient to impair chemotaxis, cell movement and transendothelial migration both *in vitro* and *in vivo* [543-546]. This is associated with the observed impairment of membrane protrusions [545], which is likely explained by strong aberrant activation of Rac1/Cd42 [547], and simultaneous neutralization of Cofilin via PAKs [517]. Nef also interferes with chemokine receptor signalling involved in cell migration [520,543]. In addition, Tat mediates important cytoskeletal changes, mainly by modulation of host gene expression. Tat consistently downregulates multiple actin regulatory genes including Cofilin and Gelsolin [548], whereas it increases RhoA activity by upregulating several of its upstream activators [549]. Together, these changes lead to an aberrant increase in F-actin content that in T-cells translates into impaired chemotaxis and cell migration [549,550]. Interruption of chemotaxis likely increases local HIV spread within lymphoid tissue, as observed in AIDS.

HIV-1 also disrupts effective communication of the immune response from infected T-cells by blocking formation of the "immunological synapse" (IS) [551,552], which is a highly organized multimolecular structure that forms in a cytoskeleton-dependent manner at the junction between T-cells and antigen presenting cells during antigen presentation (reviewed in [215]). Although it was initially hypothesized that the VS represents a corrupted form of the IS, abundant research has shown that these structures importantly differ in their structure and regulation, despite some parallels [553]. Since the IS is beyond the experimental scope of this thesis, it will only be briefly addressed here to emphasize how HIV-infection impairs T-cell immune function by deregulation of the actin cytoskeleton. Most detrimental effects to the IS are mediated by Nef [554]. By a still unknown mechanism, Nef inhibits N-WASP phosphorylation early upon TCR-signalling, as well as its later recruitment to the IS and the associated F-actin remodelling changes which are required for cell-spreading, cell-cell contacts, actin-ring formation and IS function [520]. In addition, Nef can bind to Lck directly [555], and induces intracellular accumulation of TCR and Lck in endocytic compartments [556]. This not only explains their decreased accumulation at the IS [556,557], but also the reduced phosphorylation of their associated downstream signalling proteins Zap70 and Lat [520]. While TCR-signalling components are not cytoskeletal regulators per se, they are known to trigger actin remodelling upon TCR activation [540]. Therefore, Nef employs diverse mechanisms to impair actin remodelling events required for IS formation [558].

1.5.11.2 Myeloid cells

In strong contrast to T-cells, infected myeloid cells tend to display aberrant enhancement of actin-rich membrane protrusions. This can result in increased cell motility, altered cell-matrix adhesion or intercellular contacts, shifts in tissue distribution, and other changes that compromise normal immune function while promoting viral spread (Fig. 1.10). In macrophages, HIV increases the number and size of actin-rich podosomes, which correlates with strongly enhanced mesenchymal migration and tissue infiltration. This requires Hck manipulation by Nef, whereas impairment of Cofilin regulation was not observed [522]. In addition, Tat impairs Mφ phagocytosis by preventing recruitment of Cdc42 to the phagocytic cup [559]. In monocytes, Tat induces integrin expression [560,561], and increased adhesion to the extracellular matrix and endothelium [560,562,563], as well as transendothelial migration [563,564]. Soluble Tat also induced thin actin-rich membrane protrusions [560], and promoted chemotaxis of monocytes, neutrophils and Mφ [550,563,565]. Note that increased tissue infiltration and impaired phagocytosis in both Mφ and monocytes have been observed in HIV+ patients *in vivo*, and this is associated with various aspects of disease [70]. In DC, both outbound Nef and inbound Env induce actin remodelling changes that promote formation

of HIV-filopodia and thicker membrane extensions, respectively. While structurally different, both types of actin-rich membrane protrusions increase intercellular contacts with T-cells, and facilitate cell-cell viral transfer either *in cis* or *in trans*, respectively [89,507]. Exogenous Nef also triggers DC ruffle and uropod formation [501], whereas soluble Env induces DC chemotaxis and migration by a specific actin polymerization pathway [566,567]. Altogether, HIV can manipulate actin dynamics to promote tissue infiltration of infected monocytes/Mφ and enhance migration of both infected and uninfected DC. These actin-dependent changes likely reinforce the role of myeloid cells as potentially essential components of the viral reservoir in different organs, and in viral dissemination via direct cell-cell contacts.

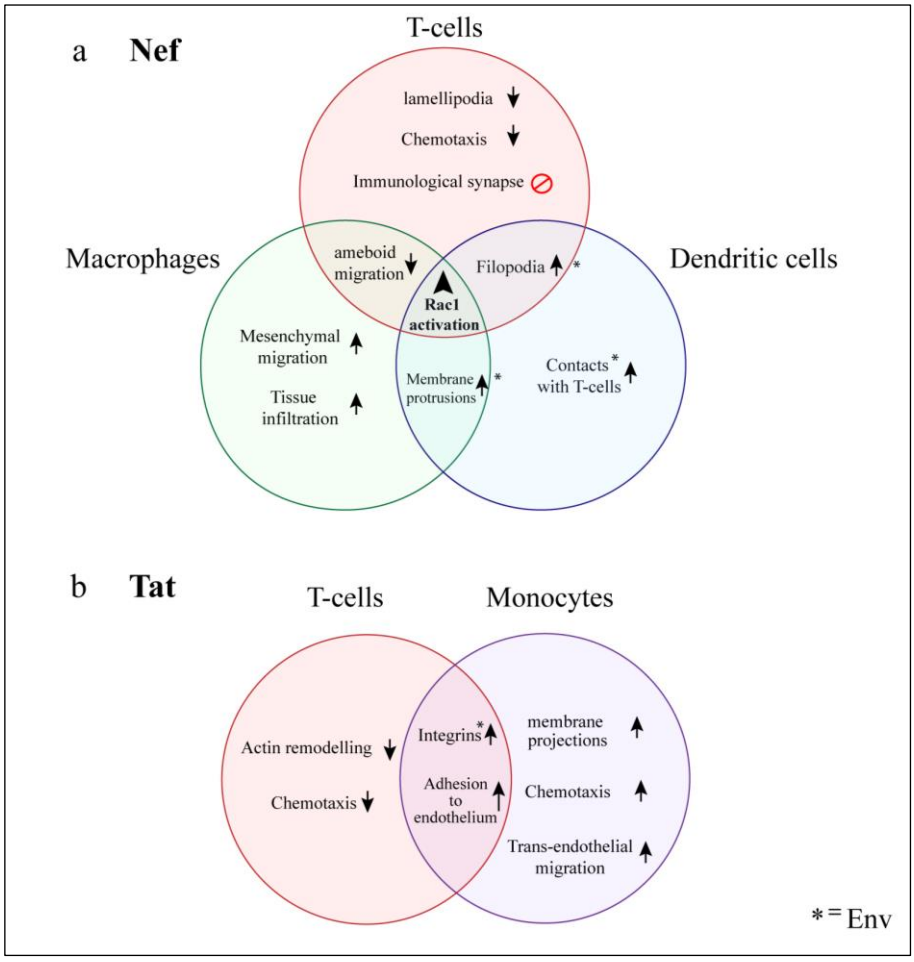

Figure 1.10: Actin-related changes in cellular behavior induced by HIV. Coordinated manipulation of actin regulators results in global and cell-type specific changes in cellular morphology and motility that contribute to viral spread, impairment of immune function and HIV comorbidities. Many of these changes can be mapped to specific HIV accessory proteins, which act as master regulators of the cytoskeleton. Nef and Tat are expressed in HIV-infected cells but are also present extracellularly in serum and, thus, can affect both infected and uninfected cells. **A) Nef** leads to Rac1 activation in a wide range of cell types. In T-cells, this is associated with inactivation of Cofilin and severe cytoskeletal disorganization, which impairs cell migration and immunological synapse formation. In myeloid cells, Nef enhances formation of several membrane protrusions which promote cell motility and contacts with uninfected cells; **B) Tat** modulates the expression of numerous genes involved in actin regulation. In

T-cells, Tat interferes with chemotaxis and F-actin remodelling, whereas in monocytes it increases cell motility, chemotaxis and phagocytosis. Tat also induces expression of adhesion molecules and promotes leukocyte binding to the endothelium. Upward arrows represent enhancement of biological processes or increases in number of structures, whereas downward arrows represent impairment of processes. * = Effects also induced by HIV envelope glycoprotein (Env). Note: this image was created by the author of this thesis and was published in [66] under an open access license (CCBY4.0).

1.6 Overview and aims

This literature review has provided a summary of basic HIV-1 virology, the cellular actin cytoskeleton, various actin-dependent mechanisms that facilitate cell-cell transfer of HIV (CCTH), and the diverse strategies that HIV employs to manipulate the host cell's actin machinery, as well as the functional consequences of this manipulation. Since this revealed that cytoskeletal manipulation in HIV-infected myeloid cells leads to augmentation of their cortical F-actin structures (see 1.5.11), these cells represent a unique opportunity to dissect the complex intersection of HIV and F-actin regulatory pathways, e.g. by exploiting the power of high-resolution imaging techniques. Indeed, similar F-actin augmentation phenotypes elicited by other pathogens have been instrumental to our understanding not only of host-pathogen interactions [418], but also of the workings of our own cytoskeleton [422,568], which is essential for numerous cellular functions and directly relevant to a wide range of human diseases. Furthermore, it is evident that the process of CCTH from infected myeloid cells to target CD4TC is underexplored, compared to the equivalent process between infected and uninfected T-cells (see 1.3 & 1.5.10). Understanding the former process could substantially contribute to our ability to design and implement effective strategies to block HIV transmission, given; i) the much higher efficiency of cell-cell viral transfer mechanisms compared to infection by cell-free virus (see 1.2.4 & 1.3.5), and ii) the potentially critical role of myeloid cells in both acute and chronic phases of lentiviral infections (see 1.2.5). The overall aim of this thesis was therefore to advance our understanding of the interactions between HIV and the human cellular actin cytoskeleton, in particular in the context of CCTH from infected myeloid cells. Each chapter pursued the following specific aims:

Chapter 3: To identify and validate a relevant model to study the HIV-Actin interaction in the myeloid cell context, and to establish a robust *in vitro* assay that allows reliable quantification of actin-dependent CCTH and the effect of different cytoskeleton-impairing treatments in this process.

Chapters 4 & 5: To identify key actin regulators involved in CCTH, by using a reverse genetics approach (involving the revolutionary CRISPR-Cas9 gene-editing technique) to

systematically interrogate their contribution to this process, both at the donor (Chapter 4) and target (Chapter 5) cell sides of viral transfer.

Chapter 6: to determine the mechanisms by which the above identified cellular actin regulators support CCTH. In particular, and based on the findings from chapter 4, this thesis aimed to resolve the molecular mechanism leading to HIV-Filopodia formation.

Chapter 7: To use a combination of the above-mentioned approaches to evaluate the corresponding phenotypes in directly HIV-relevant primary myeloid cells, such as dendritic cells and macrophages.

Note that the above provides a general overview of the aims of this study. The specific aims of each chapter are discussed in further detail within the relevant chapters.

Chapter 2. Materials and Methods

2.1 Materials

2.1.1 Solutions, buffers and chemicals

The following solutions and buffers were used for the experimental component of this thesis. The comprehensive list below includes composition, concentrations and abbreviations for each reagent. Where supplier information is not provided, the solutions were prepared in-house.

2.1.1.1 Phosphate-buffered Saline (PBS)

PBS (at the salt concentrations specified below) provides a suitable aqueous buffer system for short term keeping of mammalian cells in culture, while maintaining physiological pH range, cell tonicity and viability. For the purpose of this thesis it was primarily used for washing steps in cell culture and as a diluent for other reagents or solutions. The buffer's composition was extracted from the manufacturer's website (Gibco, Life Technologies #14190250). The use of the term "PBS" in this thesis always corresponds to the concentrations shown below.

2.67 mM Potassium Chloride (KCl)
1.47 mM Potassium Phosphate monobasic (KH_2PO_4)
138 mM Sodium Chloride (NaCl)
8.06 mM Sodium Phosphate dibasic (Na_2HPO_4-$7H_2O$)
No Calcium, no Magnesium
Dissolved in H_2O

2.1.1.2 FACS-Wash buffer (FW)

FW buffer was used to prevent the aggregation of cells while held in suspension and for some antibody staining procedures. EDTA prevents cell clumping by chelating the calcium ions required by many intercellular adhesion molecules. The presence of human serum helps decrease non-specific binding of antibodies.

1mM Ethylenediaminetetraacetic acid (EDTA)
1% Human AB serum (Sigma Aldrich #H6914)
Diluted in PBS

2.1.1.3 MACS buffer

MACS buffer was used to prevent the aggregation of human blood cells, while held in non-culture suspension (i.e. during washing steps and other processing steps during experimental setup). For magnetic-activated cell sorting (MACS), buffer was always used ice-cold.

2mM EDTA
1% Human AB serum
Diluted in PBS

2.1.1.4 Tris-EDTA buffer (TE)

TE-buffer was used to dissolve/elute precious DNA samples such as primers, synthetic gene blocks and transfection-grade DNA. The Tris buffer system at pH=8.0 improves DNA solubility and stability, whereas EDTA chelates Mg2+ cations that are often required for DNA-degrading enzyme activity. A 1x TE-buffer solution has the following final concentrations:

10 mM Tris
pH = 8.0
1 mM EDTA
Dissolved in molecular grade H_2O

2.1.1.5 Tris-acetate-EDTA Buffer (TAE)

TAE buffer (1x) was used for agarose electrophoresis of nucleic acids. Buffer was obtained as a 50x solution from UNSW Upper Campus Stores and diluted to a 1x working solution for use as required. The final composition for the 1x solution is shown:

40 mM Tris
20 mM acetic acid
1 mM EDTA
Dissolved in H_2O

2.1.1.6 Trypsin-EDTA

A 10x Trypsin-EDTA (0.5%) solution was obtained from Life Technologies Australia (Thermo Fisher Scientific #15400054). For cell culture, a 1x Trypsin solution was generated by diluting 1:10 in PBS and storing at 4ºC for up to a month.

2.1.1.7 X-gal

X-gal (5-bromo-4-chloro-3-indolyl-β-D-galactopyranoside) is an organic indoxyl glycoside used to test for the presence/activity of β-galactosidase (LacZ enzyme). The enzyme catalyses hydrolysis of this compound to yield galactose and an insoluble blue compound. X-gal powder was purchased from Thermo Fisher Scientific (#15520034), dissolved in dimethylformamide (Sigma-Aldrich #227056) to 50 mg/mL, and stored at -20°C in the dark.

2.1.1.8 TZM-bl developing solution

The solution was used to reveal the presence of the presence of LTR-driven β-galactosidase expression in TZM-bl cells (see 2.2.6.3). Solution was always prepared fresh before use.

4.2 μM potassium ferrocyanide (Sigma-Aldrich)
4.2 μM potassium ferricyanide (Sigma-Aldrich)
420 μg/mL X-gal
Dissolved in PBS

2.1.1.9 Polyethyleneimine (PEI) transfection reagent

Master stocks (50x) of polyethyleneimine (PEI) were prepared by dissolving powder (Polysciences #9002-98-6) in molecular grade distilled water to a concentration of 50 mg/mL and stored at -80 ºC. To make up 1x working stocks (1mg/mL), the master stock was diluted 50-fold in molecular grade distilled water, pH-neutralized by titration with a 1M sodium hydroxide solution (until pH=7). The 1x PEI solution was filter sterilized (0.22 μm), aliquoted in single-use tubes and stored at -80 ºC.

2.1.2 Media and supplements

2.1.2.1 Lysogeny Broth (LB medium)

LB (also known as Luria-Bertani) medium is a nutrient-rich medium suitable for growth of many bacterial species, including common lab-adapted *E.Coli* strains. LB medium sterilized by autoclaving was obtained from UNSW Upper Campus Stores. Unless otherwise specified, LB-medium for work described in this thesis contained Ampicillin (Sigma-Aldrich #A0166) at a final concentration of 100μg/mL (LB-Amp) and was stored at and stored at 4ºC. Antibiotic was added to cold medium, post-autoclaving.

1% (w/v) bacto-tryptone
0.5% (w/v) Yeast Extract
0.5% (w/v) sodium chloride (NaCl)
100 μg/ml Ampicillin

2.1.2.2 LB-Agar

LB-Agar (1.5% w/v, final agar concentration) was obtained from UNSW Upper Campus Stores. Semi-solid agar plates in 10 cm plastic petri dishes were prepared by melting LB-Agar by microwaving and allowing the liquid to cool down to 55ºC before mixing with antibiotics and dispensing 15 mL per dish. Unless otherwise specified, LB-Agar for work described in this thesis contained Ampicillin (Sigma-Aldrich #A0166) at a final concentration of 100μg/mL and was stored at 4 ºC.

2.1.2.3 RPMI medium

Roswell Park Memorial Institute 1640 medium (RPMI) was obtained from Gibco, Thermo Fisher Scientific, and mainly used to culture suspension cells of human hematopoietic lineage. The exact media formulation can be found at the manufacturer's website (Gibco #21870-076). Unless otherwise stated, RPMI medium used in this thesis was always supplemented with foetal calf serum and L-glutamine to final concentration of 10% and 2 mM respectively (this medium is henceforth referred to as RF10). For culture of primary human blood cells, 10%

(v/v) human serum was used instead of foetal calf serum (RH10 medium) and supplemented with cytokines as required.

2.1.2.4 DMEM medium

Dulbecco's Modified Eagle Medium (DMEM) was obtained from Gibco, ThermoFisher Scientific and used for culture of adherent human cell-lines, unless otherwise specified. DMEM uses a sodium bicarbonate buffer system and among other things contains phenol red, sodium pyruvate, L-glutamine and a "high glucose" concentration (25 mM). The exact media formulation can be found at the manufacturer's website (Gibco #11965-092). Unless otherwise stated, DMEM used in this thesis was always supplemented with foetal calf serum to a final concentration of 10% (v/v) (henceforth referred to as D10 medium).

2.1.2.5 L-glutamine

L-Glutamine for media supplementation was obtained from Thermo Fisher Scientific (#A2916801) at 200 mM stock concentration. It was aliquoted in 5ml tubes upon receipt and stored at -20ºC until use.

2.1.2.6 Foetal Calf Serum (FCS)

Foetal calf serum (FCS) for this project was obtained from Sigma Aldrich (#F9423). Purchased bottles were stored at -30ºC in temperature-monitored biomedical freezers. 50 ml aliquots were generated by thawing a bottle overnight at 4ºC followed by heat inactivation in a pre-heated water bath at 56ºC for 30 minutes and dispensing into 50 ml falcon tubes. Aliquots were stored at -30ºC until use.

2.1.2.7 Human AB serum

Human AB serum for this project was obtained from Sigma Aldrich (#H6914). Bottles were thawed upon arrival and aliquoted (5ml) into 15 ml falcon tubes, which were stored at -30ºC in a temperature-monitored biomedical freezer.

2.1.2.8 Cytokines

The following cytokines were used for generation of monocyte-derived DC and macrophages.

Cytokine name	Provider and Catalogue #	Details
GM-CSF	Biosource Invitrogen (#PHC2013)	Master stocks prepared at 10^7 IU//mL and stored at -80ºC. Working stocks prepared by diluting master stock 1:10 in PBS with 0.1% (w/v) Human Serum Albumin (ThermoFisher #12055-091)

Interleukin 4 (IL-4)	Biosource Invitrogen (#CTP0041)	Master stocks prepared by resuspending 1 mg powder (2.9x10^7 IU/mg) in 1 mL sterile molecular grade water at ambient temperature for 5 mins. 50 µL aliquots were dispensed and stored at -80°C . Working stocks were prepared by adding 1.4mls of 1xPBS with 0.1% human serum albumin to 50 µL master stock, dispensed as 100 µL and stored at -80°C . When used, working stocks were thawed and kept at 4°C for up to a month.

Table 2.1: Cytokines used in this study.

2.1.2.9 Antibiotics

The following antibiotics were obtained from Sigma Aldrich and resuspended/stored as per manufacturer's instructions. Unless otherwise stated, antibiotics in this thesis were used at the final concentrations shown below.

Antibiotic name	Manufacturer and Catalogue number	For selection of	Final concentration
Ampicillin	Sigma Aldrich #A0166	bacterial cells	100 µg/mL
Blasticidine	Sigma Aldrich #15205	mammalian cells	10 µg/mL
Hygromycin	Sigma Aldrich #H0654	mammalian cells	350 µg/mL
Puromycin	Sigma Aldrich #P8833	mammalian cells	0.5 - 2 µg/mL

Table 2.2: Antibiotics used in this study

2.1.3 Antiretrovirals

The following antiretrovirals were obtained from the indicated providers, resuspended following the manufacturer's indications and stored as single-use aliquots at -80ºC in temperature monitored biomedical freezers. The final concentrations used for each application are indicated in the relevant sections.

Drug name	Provider and Catalogue number	Details
BMS-378806	Selleckchem #S2632	Selectively inhibits the binding of HIV-1 gp120 to the CD4 receptor.
Efavirenz	AIDS reagents #12732	Non-nucleoside HIV reverse transcriptase inhibitor (NNRTI)
Enfurvitide (T-20)	Sigma Aldrich #P8833	Small peptide which binds to HIV-gp41. Prevents structural changes necessary for viral/cell fusion with CD4+ cell membranes (fusion inhibitor)
Raltegravir	AIDS reagents #11680	HIV-1 integrase inhibitor

Table 2.3: Antiretroviral drugs used in this study.

2.1.4 Other reagents

The following reagents were obtained from the indicated providers, resuspended in DMSO to the stock concentrations shown below and stored at -20ºC. The final working concentrations for each application are indicated in the relevant sections.

Reagent name	Provider and Catalog number	Stock concentration	Details
Cytochalasin D	Sigma #C8273	1 mM	Potent inhibitor of actin polymerization (binds F-actin)
Latrunculin A	Sigma #L5163	2 mM	Potent inhibitor of actin polymerization (binds G-actin with 1:1 stoichiometry)
Phalloidin	ThermoFisher Scientific (#A22287)	165 µM	Membrane impermeable drug that binds F-actin and stabilizes it. Conjugated to Alexa-647 fluorophore, it was used for staining of F-actin in fixed samples.
CellTracker™ Deep Red Dye	ThermoFisher Scientific (#C34565)	added 20 µl DMSO per vial upon use	Cell-permeable and non-toxic fluorescent dye (630/650 nm) that is retained within living cells. Dye is transferred to daughter cells but not to adjacent cells in a population.

Table 2.4: Other reagents used in this study.

2.1.5 Enzymes

2.1.5.1 Restriction enzymes

Restriction enzymes were used to cleave purified DNA at/near sequence-specific restriction sites. Unless otherwise specified, restriction enzymes were obtained from New England BioLabs (Ipswitch, USA) as high-fidelity versions and used with the compatible "CutSmart® Buffer". Enzymes were used at 10 units/µg DNA for complete plasmid digestion (i.e. for plasmid cloning) or at 1 unit / µg DNA for analytical purposes (i.e. bacterial clone verification). The BsmbI (Eps3I) enzyme was obtained from Thermo Fisher Scientific (#FD0454) and used with the supplied compatible fast-digest buffer, as indicated in the relevant sections.

2.1.5.2 PCR enzymes

The Velocity DNA polymerase (Bioline#21098) was used for high-fidelity PCR amplification of DNA sequences. The enzyme possesses a 3'–5' proofreading exonuclease activity leading to a low estimated error rate of 4.4 x 10^-7 base pairs. Enzyme-related PCR conditions were selected according to the manufacturer's instructions.

2.1.5.3 Other enzymes

Enzyme name	Manufacturer and Catalogue number	Details	Purpose
Fast Alkaline Phosphatase	Thermofisher Scientific (#EF0651)	(1 unit/µL)	dephosphorylation of digested vector ends
T4 Polynucleotide Kinase	New England BioLabs (#M0201S)	(10 units/µL)	phosphorylation of 5'-ends on annealed DNA oligo-pairs.
T4 DNA-Ligase	Promega (#M1794)	Used with 2X Rapid Ligation Buffer (Promega #C671B)	Ligation of DNA fragments with cohesive ends.

Table 2.5: Enzymes used in this study.

2.1.6 Plasmids

2.1.6.1 Lentiviral expression vectors and other non-viral plasmids

The following plasmids obtained from third parties were used in this study. Plasmids generated from these parental vectors are described in the relevant sections of this thesis.

Name	Source and catalogue#	Type	Key features
pMD2.G	Addgene #12259	non-lentiviral plasmid	Encodes the vesicular stomatitis virus glycoprotein (VSVg) envelope, commonly used for pseudotyping of viral particles.
pVpx	Prof. Nathaniel Landau **(NYU)**		CMV-based vector containing codon-optimized Vpx (SIVmac239 variant) fused to a myc-his tag.
pLVX Actin-mCherry	Clontech #631078	lentiviral expression vector	Encodes human β-actin fused to mCherry under the control of a CMV promoter and confers puromycin resistance. The actin-mCherry ORF is exactly flanked by unique ApaI-XbaI sites.
pLKO hygro	Addgene #24150		Has cloning sites for expression of genes under U6 or hPGK promoter. Confers hygromycin resistance.
psPAX2	Addgene #12260	2nd generation lentiviral backbone	Encodes all structural and enzymatic proteins required for generation of lentiviral particles.
psPvpxD	[569]		psPAX2-derivative containing a Vpx packaging motif.
LentiCRISPRv2 (LCV2)	Addgene #52961	Lentiviral expression vectors for CRISPR-Cas9	Encodes both CRISPR components spCas9 and guideRNA (gRNA) in a one-vector system. Confers puromycin resistance. The gRNA must first be cloned into the vector using BsmbI sites.
LentiCas9 Blast	Addgene #52962		Encodes a human codon-optimized S. pyogenes Cas9 protein and confers blasticidin resistance. 3rd generation lentiviral backbone.
LentiGuide-Puro (LGP)	Addgene #52963		Has a BsmbI-flanked site designed to clone-in CRISPR guide-RNAs under the control a U6 promoter and followed by a critical scaffold sequence. Confers puromycin resistance.

Table 2.6: Lentiviral expression vectors and other non-viral plasmids used in this study.

2.1.6.2 HIV plasmids

All HIV plasmid constructs used in this study are based on the CXCR4-tropic NL4-3 HIV-clone [570], unless otherwise indicated. The complete sequence for the source pNL4-3 plasmid used in this study can be found in the NCBI database using the GenBank accession number "AF324493.2". For the rationale behind selection of the viral strain, see 3.4.1.2. The table below describes the key features of the different constructs.

Name	Description	Source
HIV-IRESeGFP	HIV (NL4-3) encoding eGFP followed by an IRES element in between the Env and Nef open reading frames.	Courtesy of Dr Paul Cameron (Doherty Institute, Melbourne)
HIV-iGFP	HIV (NL4-3) carrying eGFP between the Matrix and Capsid domains of Gag	[89,571]
HIV-iVN-Gag	HIV (NL4-3) carrying the N-terminal fragment of Venus fluorescent protein (residues 1-173) flanked by two poly-Alanine linkers (6xA) between the Matrix and Capsid domains of Gag.	this study
HIV-iVN-Gag IRESmOrange ("HIV-BiFC")	HIV-iVN Gag expressing mOrange followed by an IRES element in between the Env and Nef open reading frames.	this study
Spln7-IRESeGFP	HIV-IRESeGFP where the NL4-3 envelope has been replaced with the dual-tropic Spln7 envelope, which is described in [572] and section 3.5.5.	this study

Table 2.7: HIV plasmids used in this study.

2.1.7 Primers and oligos

The following DNA oligos were used in this study. All DNA oligos were obtained from Integrated DNA Technologies, Inc. (IDT, Iowa, United States).

2.1.7.1 General cloning primers

Primer Name	Sequence (5'-3')	Purpose
pLKO.1 MCS Fwd	CCGGTCACACGCGTTAGTTCGAAC ACGCTAGCAAATCTAGAACGGG	Introduce a multiple cloning site (MCS) in the EcoRI-AgeI region of the pLKO vector
pLKO.1 MCS Rvs	AATTCCCGTTCTAGATTTGCTAGCG TGTTCGAACTAACGCGTGTGA	
mCherry Fwd	TCCTAAACGCGTACAGCAGAGATC CAGTTTATCG	Produce a mCherry ORF amplicon (including the upstream CMV promoter), all flanked with MluI-XbaI.
mCherry Rvs	CATTGATTATCTAGAGTCGCGGCCG CTC	
pLVX MCS Fwd	CATAGGATCCTTGCGGCCGCTAT	Introduce a multiple cloning site (MCS) in the ApaI-XbaI region of the pLVX vector
pLVX MCS Rvs	CTAGATAGCGGCCGCAAGGATCCT ATGGGCC	
Dia1 Fwd	ATAGCGGCCGCATG GAG CCG CCC GGC GGG A	Produce a Dia1 ORF amplicon (truncated to lack the C-terminal

Dia1 Rvs DeltaDAD	GCGTCTAGACTGCATTCATGTCTATGAGTTGCTCTCTCTTCTGCTGCTTCTCTAGC	DAD domain) flanked with NotI-XbaI
Dia2 Fwd	ATAGGGCCCATGGAGCAGCCCGGGGCGG	Produce a Dia2 ORF amplicon (truncated to lack the C-terminal DAD domain) flanked with NotI-XbaI
Dia2 Rvs DeltaDAD	CCTGCGGCCGCTTAACCCTCTTTGTTTATATCAATGAGTTGTTTC	
β-Actin Fwd	TATGCGGCCGCGATGGATGATGATATCG	Produce a β-Actin ORF amplicon flanked with NotI-XbaI.
β-Actin Rvs	GGCTCTAGACTAGAAGCATTTGC	
α-Tubulin Fwd	AATGCGGCCGCGATGCGTGAGTGCATCTCCATCC	Produce an α-Tubulin ORF amplicon flanked with NotI-XbaI.
α-Tubulin Rvs	CGCGTCTAGATTAGTATTCCTCTCCTTCTTCCTCACCCTC	

Table 2.8: General cloning primers used in this study.

2.1.7.2 CRISPR gRNA sequences

For gRNA design strategy, parameters and cloning procedure see sections 2.2.7.1-3.

Target gene (protein name)	NCBI gene ID	gRNA Specificity score	gRNA Sequence (5'-3')
ARP2 (ACTR2)	10097	89	GTGGTGTGCGACAACGGCAC
Angiomotin	154796	95	AGTTCCGGTTCTCGTCTGAG
APC	324	91	CCCGGCTTCCATAAGAACGG
BCR	613	99	AACTTCGAGCGGATCCGCAA
BRK1	55845	82	TTCACCAGGACTGGGCTAAC
CAP1	10487	70	AAGGACTGTCTGCATACCCA
CapG	822	85	GCCATTGTGCAGCACTAGGT
CAPZA1	829	45	AATGACAATCTCCTCAGGGA
CAPZB	832	83	AGCTTTCTCAGCCGAGCTGA
CCR5	1234	82	TCACTATGCTGCCGCCCAGT
CD4	920	83	GGAGGCAAAGGTCTCGAAGC
Cdc42	998	38	ACAGTCGGTACATATTCCGA
Cofilin 1	1072	84	GCGTAAGTCTTCAACGCCAG
Control gRNA #1	N/A	91	GCGGTTCCGGGAGCACATTT
Control gRNA #2	N/A	99	GTAGGCGCGCCGCTCTCTAC
Coronin1	11151	96	TGGCCGGCTGTCCAAACACG
Cortactin	2017	89	ATCGGCCCCCGCGTCATCCT
Csk	1445	92	AGTGCCGTGGAAGTTGTACT
Dia1	1729	84	CTCTTGATAGGGCATGCGGA
Diaph2	1730	92	GAACCGGGCCGCCAATGAAG
Diaph3	81624	93	GGGAAAGCAAGATGCCGCGC
Ezrin	7430	89	TGTGGCATGCGGAACACCGT
FHOD1	29109	92	TGGGTGTCCACCCGCCTCAT
Filamin-A	2316	97	GCTGCGGCTTATCGCGCTGT

FMNL1	752	84	GCCGAAAGGTAGCAGCTGAT
Gelsolin	2934	82	GTATGACCTCCACTACTGGC
HCK	3055	94	TGTCGCCCGCGTTGACTCTC
HCK gRNA #2	3055	93	ATGTATTGCCTCCGACCTGG
HCK gRNA#3	3055	92	ACACTGTCCTGTGTACGTGC
HCLS1	3059	88	AAACCGACCTCCATAGCCAT
ICAM-1 (CD54)	3383	85	GCTATTCAAACTGCCCTGAT
ICAM-3 (CD50)	3385	95	GCTGGACGGAGTTCCGGCCG
ITGAL (CD11a)	3683	97	GCTGCGTCGTCGTAGTTTTT
ITGAM (CD11b)	3684	92	GCCGTAGGTTGGATCCAAAC
ITGB1	3688	93	AATGTAACCAACCGTAGCAA
ITGB2 (CD18)	3689	89	GTAAAGCGTCACTTTTTGTG
LIMK1	3984	94	TCTCATAGTACTGGTGCGAC
mCherry	N/A	95	GGCCACGAGTTCGAGATCGA
ENAH + EVL	55740 + 51466	43	AGCATCTCGCCACTGGTGGA
Moesin	4478	92	CTTAGACTGGACAGCATACG
N-WASP	8976	88	CAGCAGATCGGAACTGTATG
PAK1	5058	97	GATGTAGCCACGTCCCGAGT
PAK2	5062	99	TTTCGTATGATCCGGTCGCG
Profilin-1	5216	89	GACGAACGTTTTCCCGGGGA
Rac1	5879	65	TGGTTGTGTAACTGATCAGT
Rac2	5880	94	AGGAGGACTACGACCGTCTC
RhoA	387	89	AATCACCAGTTTCTTCCGGA
Rif	54509	94	CTTGCTGCCAACGGTCACGC
ROCK1	6093	83	CGGACACAGCTGTAAGATTG
Syk	6850	83	TCTTTTTCGGCAACATCACC
Talin-1	7094	92	ACTACTACATGCTCCGAAAT
VASP	7408	75	CTATTGCTGGAGCCAAACTC
VAV1	7409	91	GGCGCAGGTTGACCTCACGC
Vinculin	7414	92	CCTGGTGATAATGCACGAGG
WASF2	10163	99	TGAGAGGGTCGACCGACTAC
WASP	7454	94	GCTTTTGGATCAAATCCGGC
ZAP70	7535	90	CACGGAAGAGATGATGCGCG

Table 2.9: CRISPR gRNA sequences used in this study (full CRISPR panel).

Note that the used software considers any gRNA with a score above 50 to have "high specificity" and those with scores between 50 and 25 to have "medium specificity". In this study we aimed for scores >80 (or as high as possible) for extra stringency. In the table above, three gRNAs (CAPZA1, Cdc42 and ENAH) have only medium specificity scores. The rationale for their acceptance is described below.

CAPZA1 gRNA: the lower specificity score in this gRNA is only caused by a 1bp mismatch with the CAPZA2 gene. Therefore, this gRNA was intentionally selected above other options, due to its convenient potential ability to target both proteins with the same gRNA.

Cdc42 gRNA: Introduction of all 5 exons from Cdc42 into the gRNA design tools delivered gRNA options with scores < 50, with only 2 exceptions. However, these gRNAs genes sat in the last 36 bp of the last exon. CRISPR-induced indels at this region would only result in loss of the last 12 amino acids of the protein (best case scenario), out of 191 total residues. This would in all likelihood produce a protein that can still mediate many/most of Cdc42 functions, and therefore these gRNAs are not suitable for loss of function approaches. We systematically assessed all other possible gRNAs and selected the best option in our opinion (shown in table above). Note that while the MIT specificity score for this gRNA is 38, its CFD specificity score is 95 (these algorithms use two different off-target models).

ENAH gRNA: the lower specificity score in this gRNA is only caused by a 1 bp mismatch in the EVL gene (close homologue of ENAH, and third member of the ENA/VASP family). Therefore, this gRNA was intentionally selected, due to its convenient ability to target both closely-related proteins with the same gRNA. Since the 1 bp mismatch is at the furthest possible position from the PAM sequence, this gRNA is likely to target both sites effectively.

2.1.7.3 Short hairpin RNA (shRNA) oligo sequences

Target gene protein name	Source & Sequence identifier	Sequence (5'-3')
Arp2 (shRNA1)	obtained from [573]	GTGGGTAAATCTGAGTTTA
Arp2 (shRNA2)		CTGTGTTACGTGGGATATA
Arp3 (shRNA1)		GAAGAGAGCGAAAGTGATT
Arp3 (shRNA2)		GAGCAAGTGATCTTTAAATA
Diaph2 (shRNA1)	*SC-35192-SHA	GCATCAATGGAACAACAAATT
Diaph2 (shRNA2)	*SC-35192-SHB	GGAACGTGACATCAAGAAATT
Diaph2 (shRNA3)	*SC-35192-SHC	GGAATCCAGTGGTAAATCATT
Rac1 (shRNA1)	#TRCN0000004873	CCCTACTGTCTTTGACAATTA
Rac1 (shRNA2)	#TRCN0000004871	CGCAAACAGATGTGTTCTTAA
IQGAP1 (shRNA1)	#TRCN0000047483	GCCCACATTGTGCCTTTATTT
IQGAP1 (shRNA2)	#TRCN0000047487	GCATCCACTTACCAGGATATA

Table 2.10: Short hairpin RNA sequences used in this study.

* These sequences were directly obtained from Santa Cruz Biotechnology Inc (SC)
# These sequences were obtained from The RNAi Consortium (TRC) database

2.1.7.4 Surveyor primers

Surveyor primer sequences were obtained directly from the gRNA design tool used. These primers allow amplification of the human genomic region containing the gRNA target sites

shown in Table 2.9. Settings were selected so that all surveyor primers have a melting temperature of ~60°C and so that amplicon sizes are within the 300-750 bp range. The tool's algorithms automatically exclude primers that anneal to repetitive sequences or that bind at multiple regions in the genome. In the table below, horizontal half arrows indicate forward primers (→) and reverse primers (←).

Surveyor Primers	Sequence (5'-3')	Amplicon size
Arp2 →	CGGGAAGACGCAAGAGGAAG	404 bp
Arp2 ←	CGGTCAGTAGGCTCCATGTC	
Cdc42 →	TTGCTCTGAGTGCCTGAACC	474 bp
Cdc42 ←	AGTTTTGCCTCCCAGCACTT	
Cofilin →	CACTAGTGACCACTCGGGA	536 bp
Cofilin ←	CAGTGAGGAGTCTTTTGTTACAACC	
CSK →	AGCAGAGGAGAGAGGATGCA	553 bp
CSK ←	GAGTTTGGTACCCGCCTTCA	
Dia2 →	CCCGAGGTGCTTTCTCAGTT	520 bp
Dia2 ←	GGTTTGCGCCCACAAGTTAG	
Dia3 →	GACCCCGGGAGTAAAACCTG	422 bp
Dia3 ←	GACCCGGTCGTTGTCAATCT	
HCK →	CAGAGGTGGCAAGGATGGAG	582 bp
HCK ←	GAGGCCTGAGATGCTCACTC	
N-WASP →	ACCCCTTTAGTGTCGGGTTTC	727 bp
N-WASP ←	GCCTTAATGCGTGGTAGCAG	
PAK2 →	CACCCGCAGTAGTGACAGAG	490 bp
PAK2 ←	TTTGAATGACAGCAAGGCGC	
Profilin →	CAACTGAGGGACCCACTCAC	494 bp
Profilin ←	TAAAAATCTAGCGGGGCGGG	
Rac1 →	GGTACCAATGTGTATGTGGTGA	785 bp
Rac1 ←	CCTCACAGACAGTTAAAGTTTGC	
RhoA →	AGGTGGATCGGCGTACTAGA	443 bp
RhoA ←	AGATGGCAGGATGAGAATGGA	
Vav →	GTCCTTCTGTGTCAGCTGCT	400 bp
Vav ←	ATGAACCACAGTAGAGGCGC	
Wave2 →	GCAGTCATCTGCATATAGCCCA	328 bp
Wave2 ←	GCTCAGCAGAGCCTGCAAAT	

Table 2.11: Surveyor sequencing primers used in this study.

2.1.8 Antibodies

The following primary antibodies were obtained from the indicated companies.

Target protein	Provider and Catalogue number	Type	Details
Dia2	Bethyl laboratories #A300-079A	rabbit anti-human polyclonal antibody (whole IgG)	unconjugated primary antibody
Arp2	SantaCruz #sc-15389 (H-84)	rabbit anti-human polyclonal antibody (IgG1)	
Arp3	Abcam #AB49671	mouse anti-human monoclonal antibody (IgG2b)	
HCK	BD Biosciences #610277 (Clone 18)	mouse anti-human monoclonal antibody (IgG1)	
IQGAP1	SantaCruz #sc-376021 (C-9)	mouse anti-human monoclonal antibody (IgG1)	
N-WASP	SantaCruz #sc-100964 (93-W)	mouse anti-human monoclonal antibody (IgG2b)	
Profilin	Abcam #ab50667	rabbit anti-human polyclonal antibody (IgG1)	
ICAM-1	BD # 347977 (LB-2)	mouse anti-human monoclonal antibody (IgG2b)	PE/Alexa647-conjugated primary antibody
CD4	Biolegend #317422 (OKT4)		

Table 2.12: Primary antibodies used in this study.

When required, the secondary antibodies Alexa647-conjugated goat anti-mouse (ThermoFisher #A-21235) or Alexa633-conjugated goat anti-rabbit (ThermoFisher #A-21071) were used at a final 1:400 dilution of supplied concentration for detection of primary antibodies bound to their epitopes.

2.1.9 Cell lines

The main cell lines used in this study are outlined in the table below. For cell culture conditions, see 2.2.1.1. For details on other cell lines generated during this study from these parental cell lines, see Table 4.1 and sections 6.3-6.4.

Name	Source and catalogue number	Details
U937	ATCC®* CRL-1593.2™	Human pro-monocytic cell line (suspension cells), originally isolated from the histiocytic lymphoma of a 37-year old male [574].
Jurkat	ATCC®* TIB-152™	Transformed T-cell line (suspension cells) originally derived from the peripheral blood of a 14-year-old boy with acute lymphoblastic leukaemia [575]. Initially referred to as JM.
TZM-bl	AIDS Reagent Program (NIH) #8129	TZM-bl (originally referred to as JC53BL-13) is derived from the parental epithelial HeLa cell line "JC.53" (adherent cells), which was engineered to stably express CD4 and CCR5 at high levels [576]. TZM-bl cells harbours separately integrated copies of the luciferase and ß-galactosidase genes under the control of the HIV-1 LTR promoter [577].

HEK293T	ATCC®* CRL-3216	HEK 293 cells (adherent) are human embryonic kidney (HEK) cells originally obtained from foetal tissue and transfected with sheared adenovirus 5 DNA [578]. HEK293T cells (originally referred to as 293/tsA1609neo) were obtained by stable transfection of the HEK 293 with a plasmid encoding the SV40 large T antigen [579].

Table 2.13: Common cell lines used in this study.
*ATCC = American Type Culture Collection

2.1.10 Software

The following software versions were used for data analysis and processing in this thesis:

Software name and version	Company details	Purpose
GraphPad Prism 8	GraphPad Software Inc.	For generation of all graphs in this thesis and to perform all statistical analysis (unless otherwise specified).
FloJo_V10.1	Treestar Inc. / FlowJo LLC	For analysis of flow cytometry data and generation of FACS plots.
Adobe Illustrator CC2019	Adobe Inc.	For arrangement of figures and original design of illustrations/schematics.
SoftWorx 6.5.2	Applied Precision Inc.	For processing and analysis of Delta Vision images and movies.
IN CELL Developer Toolbox v1.9.3	GE Healthcare	For automatic analysis of high-content microscopy data
ImageJ 1.8.0	NIH (open source)	For software-assisted quantitative image analysis including event counts and length measurements.

Table 2.14: Software versions used in this study

2.1.11 Equipment

The following instruments were used in this thesis. More detail related to specific applications is provided in the relevant sections.

Instrument name, model & (manufacturer)	Type	Purpose
Allegra X15R (Beckman Coulter)	Benchtop centrifuge	All centrifugation steps unless otherwise specified.
APT line C 150 E2 (Binder GmbH)	cell culture incubator	Culture of human cell lines and primary blood cells
C1000 Touch (Bio-Rad)	Thermocycler	All PCR applications and incubation of samples in PCR-tubes.
CLARIOstar (BMG Labtech GmbH)	Polychromatic plate reader	DNA quantification and absorbance/fluorescence measurements
Coulter AcT diff (Beckman Coulter)	Haematology analyser	Automatic counting of blood cell populations

Cytell Cell imaging system (GE Healthcare)	high content microscope	Automated and fast imaging of numerous fields of view per well with different fluorescent channels.
DeltaVision Elite (GE Healthcare)	high resolution fluorescence microscope	Olympus IX-70 microscope with 60 x 1.42 NA oil immersion lens and Evolve 512 back-thinned EM-CCD camera (512*512).
Gel Doc XR (Bio-Rad)	Gel imaging system	Visualization of stained-DNA in agarose gels
Heratherm (ThermoFisher)	incubator	Incubation of bacterial cells on petri-dishes
OM25 (Ratek)	bacterial shaking incubator	Incubation of liquid bacterial cultures

Table 2.15: Large equipment used in this study.

2.2 METHODS

2.2.1 Cell line culture

2.2.1.1 Cell line culture conditions

All cells used in this thesis were cultured at 37°C with 5% CO_2 in a humidified incubator except during handling, which occurred in in a Class II Biological Safety Cabinet (BSCII) under sterile conditions.

Suspension cells (U937, Jurkat and derivatives thereof) were cultured in RF10 medium at cell densities between 10^5 and 2x10^6 cells/mL, unless otherwise stated. Suspension cells were passaged by removing 90% of culture volume (after mixing and cell resuspension) and replacing with fresh medium. Cells were discarded after reaching passage numbers p>40.

Adherent cell lines were passaged by removing medium, washing with PBS and incubating for 3 mins (293Ts) or 5 mins (TZM-bl) at 37ºC with 1X Trypsin-EDTA. The cell monolayer was then dissociated by vigorous pipetting up and down. The single-cell suspension was then centrifuged at 400xg for 3 minutes and the cell pellet was resuspended in fresh medium. A fraction of this suspension (usually 1:10) was then seeded into a new flask with fresh medium.

HEK293T cells were regularly cultured in D10 medium at confluence levels between ~10-70% without ever allowing full confluence to occur (flasks were allowed to reach ~85% confluence when destined for transfection). Cells were discarded after reaching passage numbers p>25. TZM-bl cells for viral titrations were cultured in either D10 or RF10 medium (see below) at confluence levels between ~10-70% without allowing full confluence to occur. The original line was cultured in D10 medium and used for viral titrations only. For all other experiments, a RF10-adapted cell line was used. This line was generated by expanding TZM-bl cells (p3) in RF10 medium (5 passages over 15 days), and large-scale freezing (20 vials at

5 million cells/vial). This line was generated to allow coculture with suspension cells in RF10 medium. TZM-bl cells were discarded after reaching an accumulated passage number p>21.

2.2.1.2 Cryopreservation and thawing of cells

Cell line seed-stocks were generated for long-term cryopreservation storage as follows. A single-cell suspension was generated, medium was removed, and cells were then gently resuspended at 5 x 10^6 cells/mL in cold freezing medium (90% FCS and 10% dimethyl sulfoxide). 1 mL aliquots were quickly transferred to cryovials (5 million cells/vial) and moved to a CoolCell® alcohol-free controlled freezing rate container (Biocision#BCS-405), which was then placed at a -80^{o}C freezer for up to a month. For long-term storage, cells were moved to liquid nitrogen vapour phase tanks.

When required, frozen cell stocks were rapidly thawed by successively adding pre-warmed (37^{o}C) fresh medium and removing the thawed volume into a 15mL falcon tube. The tube was gently spun at 1000 rpm for 4 minutes, the supernatant was discarded, and the cell pellet was gently resuspended in fresh pre-warmed medium, moved to an adequate flask and placed in a cell-culture incubator.

2.2.1.3 Single-cell sorting and clonal expansion of suspension cell lines

For obtaining clonal cell populations (all derived from a single ancestor cell), the culture was resuspended thoroughly to the single-cell level in MACS buffer. Single cell sorting was performed with help of experienced operators at the UNSW Flow cytometry core facility under sterile conditions. Single cells were sorted into the wells of a round-bottom 96-well plate (Corning #CLS3799) containing 150µL of conditioned medium. Conditioned medium was produced by seeding a culture of the wildtype cell line at 2x10^5 cells/mL and removing all cells 3 days later by centrifugation and subsequent sterile filtration of the supernatant through a 0.2 µm filter. This was then mixed with an equal volume of fresh medium containing a Penicillin-Streptomycin solution (ThermoFisher #15070063) for a final antibiotic concentration of 50 units/mL. Single-cell sorted plates were incubated for at least 14 days without disruption, and then inspected every 2 days for colony evaluation. For wildtype cells, recovery rates were typically above 50%. When wells contained colonies visible by eye, and a noticeable colour-change occurred in the medium (pink to orange), the well content was moved to the well of a 24-well plate. Cells were then inspected by microscopy and clones with good apparent viability were subsequently expanded and cell seed stocks were generated.

2.2.2 Primary cell culture

All cells used in this thesis were cultured at 37°C with 5% CO_2 in a humidified incubator except during handling, which occurred in a sterile Class II Biological Safety Cabinet (BSCII).

2.2.2.1 Isolation of Peripheral Blood Mononuclear Cells (PBMCs) from whole blood

Whole human blood was obtained from healthy volunteers and processed on the same day. Blood was first transferred into conical centrifuge tubes (BD 50 mL Falcon tubes) and diluted up to 1:2 with PBS so that tube volume is ~35 mL. 15 mL Ficoll-Paque (GE Healthcare, Sweden) were then carefully underlayed. PBMCs were separated by Ficoll gradient centrifugation at 700 x *g* in a swing bucket rotor for 20 min at RT with slow acceleration and no brakes. The PBMCs were collected at the plasma-Ficoll interface using a sterile plastic transfer pipette (cells from up to three falcon tubes were pooled into a new tube). PBMCs were then washed twice with PBS by centrifugation at 400 x *g* for 10 min at RT (with brakes on). Cell pellet was gently resuspended in between washes by flicking the tube. Finally, all pooled cells from a single donor were resuspended to the single-cell level in 10 mL ice-cold MACS buffer. A 50 µL aliquot was taken for counting with a haematology analyser (Beckman Coulter, COULTER® AcT diff™) and the concentration of PBMCs was recorded. Of note, the author underwent formal quality assessment by the Australian Immunovirology Research Network (IVRN) for isolation and cryopreservation of PBMCs and passed with confirmed fractionation recoveries>70%, post-thaw recoveries>80% and PBMC viabilities>95%.

2.2.2.2 Isolation of CD14+ monocytes from PBMCs

CD14+ cells were isolated from PBMCs by Magnetic-Activated Cell Sorting (MACS) using ice-cold MACS buffer for all steps. PBMCs were centrifuged immediately after isolation at 400 x *g* for 5 min at 4ºC. Supernatant was discarded by one quick inversion, and the pellet was resuspended in the remaining liquid drops. CD14 magnetic labelling microbeads (Miltenyi #130-050-201) were then added at 5µL per 10^7 PBMCs and tube was gently mixed by flicking. Then, 10 µL MACS buffer were added per 10^7 PBMCs and the tube was mixed again. The cell-bead suspension was incubated at 4ºC for 30 minutes, with gentle flicking at 10 and 20 minutes. Cells were then washed three times with 20mL MACS buffer, interspaced by centrifugation 400 x *g* for 5 min at 4ºC. The Quadro-MACS magnetic stand was set-up and the LS column beads (Miltenyi #130-041-306) primed with 3mL MACS buffer. The PBMCs were run through the column and washed three times with 3mL MACS buffer (negative fraction). The column-bound CD14+ cells were released by pipetting 5mL MACS buffer into the column and firmly pushing the plunger into the column (after removing the

magnet). This flushing step was repeated once to ensure all the monocytes were retrieved. Monocyte purity using this procedure is regularly above 97%.

2.2.2.3 Generation of Monocyte Derived Dendritic Cells

Monocyte-derived dendritic cells (hereafter just "DC") were generated by culturing freshly purified CD14+ monocytes at 1 x 10^6/mL in RH10 medium supplemented with GM-CSF and IL-4 (both at final concentration of 1000U/mL, see Table 2.1). These cells were incubated for at least 3 days before their use in experiments. Cells were monitored by light microscopy and morphological changes associated with immature dendritic cell phenotype were confirmed. Medium was refreshed every 3 days by replacing half of the well volume with fresh RH10 medium containing GM-CSF and IL-4 as indicated above.

2.2.2.4 Generation of Monocyte Derived Macrophages

Monocyte-derived macrophages were generated by allowing freshly purified CD14+ monocytes to adhere to tissue-culture treated surfaces in serum-free RPMI medium. After 30 minutes, an equal volume of RH20 (RPMI medium with L-glutamine and 20% human serum) was added. Differentiation was allowed to occur for at least 6 days before experiments, and macrophage-like phenotype was confirmed by light microscopy. Unless otherwise stated, monocytes were seeded at 7x10^4 cells per well of a 96-well plate when intended for macrophage differentiation. Medium was refreshed every ~4 days by replacing half of the well volume with fresh RH10 medium.

2.2.3 Assessment of cell viability

The viability and/or metabolic activity of cell populations was assessed by one or more of the following methods (specified where relevant) following the manufacturer's instructions.

Method	Rationale	Procedure
Trypan Blue exclusion	Used to determine the number of viable cells present in a cell suspension. Cells with compromised cell membranes (e.g. dead or damaged cells) allow entry of trypan blue dye, whereas live healthy cells do not. Dye inclusion/exclusion can be easily determined by light microscopy.	A cell suspension is mixed with an equal volume of 0.4% trypan blue dye (Sigma #T8154). 15uL are then transferred to a haemocytometer and cells are counted by light microscopy. The percentage of viable cells is given by [100 x #dye negative cells / #dye positive cells].
fixable Live/Dead stain	The fluorescent dye covalently binds to amine groups in proteins. Only cells with compromised cell membrane allow entry of the dye, which results in more intense staining due to the larger number of intracellular proteins. Dead/damaged cells (bright staining) can be easily distinguished from live cells (faint staining) by flow cytometry.	Cells at 10^4-10^6 / ml are mixed with 1 µL/mL near-infrared fluorescent dye (ThermoFisher Scientific #L34975) in protein free buffer and incubated for 30 minutes. Cells are then washed once with PBS, fixed with 4% paraformaldehyde and analysed by flow cytometry.

Alamar Blue	Resazurin is a non-toxic, cell-permeable and non-fluorescent compound that is reduced by cellular esterases in living cells to fluorescent resorufin. A linear response is observed between the number of metabolically active cells and the resorufin signal, but this can also be affected by cell health. Since this method can detect changes in cell proliferation, viability and metabolic activity it is considered a general indicator of cell health and growth.	Alamar blue (ThermoFisher Scientific, #DAL1100) is added directly (10% of well volume) to living cells in a microwell plate (well duplicates per treatment). Plate is incubated at 37ºC for 2 hours and fluorescence signal is then measured with a suitable plate reader (560 nm excitation / 590 nm emission). The raw signal can be compared across treatments or normalized to an untreated/control group.

Table 2.16: Methods to assess cell viability.

2.2.4 Plasmid engineering

2.2.4.1 PCR Amplification of sequences of interest

The directional cloning of DNA sequences into vector plasmids was facilitated by PCR. Forward and reverse primers were designed with regions complementary to the ends of the target sequence (typically 20-25 bp long and GC content 40-60%). Upstream of the complementary region, the required restriction sites (matching the destination vector and orientation) were included, as well as 3 extra nucleotides at the 5' end to allow for optimal cutting. Primer pairs were checked with the IDT Oligo analyser software for melting temperatures, predicted hairpin structures and to exclude homodimer/heterodimer issues. The Velocity PCR platform (Bioline# BIO-21098) was used for all PCRs in this study following manufacturer's instructions, unless otherwise specified. Briefly, 50µL reactions were prepared in molecular grade water with the following final concentrations: 1x supplied buffer, 0.5mM dNTPs and 0.4 µM of each primer, as well as 1 µL template and 0.5 µL enzyme. For plasmid templates, 10 ng DNA were used, whereas for human genomic DNA 200 ng DNA or direct cell lysates were used.

Amplification occurred in an automated thermocycler (Bio-Rad "C1000-Touch"). Initial denaturation (98ºC for 2 minutes) was followed by (18-25) repetitive cycles comprised of successive denaturation (98ºC for 30 seconds), annealing (case-specific temperatures for 30 seconds) and elongation (72ºC for 20 seconds per kilobase). A final extension period (72ºC for 2 minutes) was allowed before moving DNA to 4ºC for same day processing or otherwise to -20ºC. Annealing temperatures were calculated based on the primer pair used (5ºC below the lowest melting temperature of the primer pair). When primers had non-complementary regions (e.g. overhangs with restriction sites), the melting temperatures for the complementary region only were considered for the first 3 cycles. For later cycles, full complementarity was assumed, and annealing temperatures were adjusted accordingly.

The obtained PCR products were purified using a commercial column-based kit (Promega #A9281) and eluted in 35µL molecular grade water. 2µL were then analysed by gel electrophoresis to confirm the expected amplicon size and the absence of unspecific products. A negative control (no template) was always included for each primer pair.

2.2.4.2 Restriction digests and DNA Gel electrophoresis

Plasmid and/or linear DNA were digested with the restriction enzymes required to produce complementary sticky overhangs. For cloning purposes, 2µg DNA were digested in compatible buffer with 20 units enzyme, unless otherwise specified. For analytical purposes 1 unit per µg DNA was used. Samples were incubated in a temperature block at the optimal enzyme temperature for at least 1 hour.

To confirm DNA digestion, products were loaded into a gel (1% agarose in TAE buffer) pre-stained with SYBR Safe reagent (Thermo Fisher Scientific #S33102) next to a DNA size-ladder control (NewEngland Biolabs #N3232L), and separated by electrophoresis (typically 90V for 45 mins) in a tank with 1xTAE buffer. Where intended for further cloning, gels were initially visualised on a transilluminator using long wavelength UV light and the desired DNA bands were excised with disposable X-tracta Gel cutters (Promega #A2121). The DNA was then purified from the Gel bands using a commercial column-based kit (Promega #A9281) and eluted in 30µL molecular grade water. When intended for analytical purposes (or after band excision), gels were visualised within a Gel Doc™ XR (BioRad #1708195) to confirm the expected sizes of digested vector and/or insert.

2.2.4.3 Vector-insert DNA Ligation

Unless otherwise specified, 20µL ligation reactions were prepared in microfuge tubes by combining ~100 ng digested backbone plasmid (the fragment containing the bacterial origin of replication) with insert DNA (a shorter sequence of interest with compatible sticky ends) at a 1:5 molar ratio. 10 µL of 2x LigaFast buffer (Promega # C6711) and 1µL of T4 DNA ligase (Promega # M1804) were used per reaction. Ligations were incubated at room temperature for 15 minutes and either used directly for transformation into competent cells or stored at -20ºC until needed.

2.2.4.4 Bacterial Transformation and verification of colonies

For propagation, plasmids were transformed into chemically competent Stbl2 cells (MAX Efficiency™ Stbl2™, ThermoFisher Scientific #10268019). This Escherichia coli strain was selected due to their high transformation efficiency and unique genotype, specifically engineered for cloning direct repeat and retroviral sequences such as those contained in the

HIV genome. Transformations were performed according to manufacturer's instructions, with few deviations to conserve reagents. Briefly, 2µL ligation product were added to 20µL of competent bacteria (thawed on ice). The mixture was incubated on ice for 30 minutes in 14ml round-bottomed polypropylene tubes (Greiner Bio-One). Cells were then heat-shocked by placing the bottom of the tubes into a 42ºC water bath for exactly 25 second. Tubes were incubated again on ice for 5 minutes and then 200µL of SOC medium (supplied with Stbl2s) were added and tubes were moved to a shaking incubator (200 rotations/minute) and incubated for 90 minutes at 30ºC (this lower temperature aims to further reduce the probability of plasmid recombination). 100µL of the shaking culture were then plated on a pre-warmed LB-Amp agar plate containing ampicillin at 100 µg/mL, and plates were incubated overnight. Once visible, single colonies were transferred into 5mL of LB-Amp medium and grown overnight in a shaking incubator at 30ºC. For cryopreservation, glycerol stocks were prepared by adding 800µL of bacterial culture to 200µL of sterile 50% (v/v) Glycerol in 2ml cryovials, followed by vortexing for 10 seconds before moving vials into temperature-monitored -80ºC biomedical freezers. The rest of the overnight culture was used for verification of ligation product. DNA was extracted using a commercial miniprep kit (see further below) and 1µg DNA was digested and checked by gel electrophoresis to meet the following criteria: i) band pattern confirms introduction of expected restriction sites, ii) sum of estimated band sizes adds up to the expected plasmids size, iii) restriction pattern clearly different from parental vector control. For restriction-verified clones, 30 ng of undigested DNA were set apart for Sanger sequencing with a primer specifically designed to evaluate the cloning region of interest. Only clones confirmed to exactly match the expected sequence of interest (100% base pair alignment) were used for experiments.

2.2.5 Plasmid DNA isolation from bacterial cultures

The concentration and purity of all DNA preparations were measured with the CLARIOstar® plate reader (BMG Labtech). Only sterile DNA preps with desirable values (c>500 ng/µL and A260/280 = [1.8–2.0]) were used for transfections. For large scale transfections, microgram amounts of endotoxin-free plasmid DNA were obtained by using the QIAGEN Plasmid Plus Maxi Kit (Qiagen #12963) with ~0.7g of bacterial pellet as starting material. To generate this pellet, a frozen master glycerol stock of transformed Stbl2 bacteria was scratched and inoculated into 5mL LB-Amp medium and incubated for 16 h at 30°C with shaking (then tube was moved to the fridge). At the end of the day, 300µL or 500µL (high-copy or low-copy plasmids respectively) were transferred into 130mL or 250mL of LB-Amp medium and incubated for additional 16 h. The culture was then centrifuged in 50 mL falcon tubes at 5000 x g for 10 minutes at 4°C, and pellets were then combined into a pre-weighed tube. The pellet

mass was determined, and excess was removed until m <0.8g. The pellet was then processed exactly as per manufacturer's instructions. The isolated DNA was eluted in 400µL sterile TE-buffer, then aliquoted and stored at -80°C.

For lower scale transfections (<10 million 293T cells), pure DNA was obtained by generating 20mL bacterial cultures from glycerol stocks as described above, followed by processing (split into 2 columns) with a commercial DNA extraction kit (Promega #A1470) following manufacturer's instructions. After bacterial lysis, samples were moved to a clean room, and the rest of the protocol was carried out inside a BSCII hood with sterile kit components specifically reserved for this purpose. DNA was eluted in sterile molecular grade water (30µL per column), pooled together and stored at -80°C.

For plasmid engineering purposes, DNA was isolated from 5ml glycerol-scratched cultures grown at 30°C for 24h. Bacterial pellets were obtained by centrifugation at 5000 x g for 10 minutes at 4°C and processed with the Wizard® Plus SV Miniprep kit (Promega #A1470) following manufacturer's instructions. Such DNA was stored at -20°C until further use.

2.2.6 Generation of viral and VLP stocks

2.2.6.1 Transfection of HEK-293T Cells

Plasmid DNA was diluted in tissue culture grade 0.9% (w/v) sodium chloride solution (Sigma Aldrich #S8776) to a final volume of 440 µL and a final DNA mass of 10 µg for one 10cm-dish transfection. The plasmid ratios used are outlined in Table 2.16 below. To the diluted plasmid, 60 µL of 1xPEI reagent were added dropwise and then vortexed for 10 seconds and incubated at room temperature for at least 30 minutes. Meanwhile, HEK 293T cells at 75-85% confluence were washed with PBS, trypsinized and resuspended in fresh D10 medium at 8 million cells/mL. Per transfection, 1 mL cells (8 million) were added dropwise to the 500µL DNA-PEI mixture and this was incubated for 5 minutes at room temperature. The 1.5mL cell suspension was then added dropwise to a 10 cm tissue-culture treated dish with 8mL pre-laid D10 medium. The medium was carefully replaced with 8mL fresh D10 at 18 h post transfection. At 72 h post transfection the supernatant was harvested by careful aspiration and cleared from cells and debris by centrifugation at 3000 x *g* for 15 mins at 4°C. The supernatant containing the lentiviral particles was aliquoted and frozen as single-use vials at -80°C. Note that pre-warmed D10 medium (37°C) was used throughout all steps of this protocol.

Preparations	Packaging plasmid	HIV / lentiviral plasmid	Envelope plasmid	Vpx plasmid
HIV stocks * (VSVg+)	-	HIV plasmid (8 µg)	VSVg (2µg)	-
HIV stocks * (VSVg-)	-	HIV plasmid (10 µg)	-	-
HIV for primary cells * (VSVg+, Vpx+)	psPvpxD (3.52 µg)	HIV plasmid (3.52 µg)	VSVg (1.76µg)	pVpx (1.19 µg)
virus-like particles (VLPs)	psPAX2 (4 µg)	lentiviral plasmid (4 µg)	VSVg (2µg)	-
VLPs for primary cells	psPvpxD (3.52 µg)	lentiviral plasmid (3.52 µg)	VSVg (1.76µg)	pVpx (1.19 µg)

Table 2.17: Transfection reaction plasmid ratios and amounts.

* = full-length, replication-competent and infectious HIV
HIV-plasmid examples: NL4-3_IRESeGFP, NL4-3_iGFP, NL4-3_iVN-Gag
Lentiviral-plasmid examples: LCV2, pLVX and pLKO derivatives

2.2.6.2 Concentration of Lentiviral supernatant by ultracentrifugation

When higher lentiviral titres were required (specified in the relevant sections), six 10cm-dish transfections were set up. At 72 h post-transfection, 50 ml supernatant were collected and pre-cleared as above, then filtered through a 0.22 µm filter using a 50 mL plastic syringe. 38 mL were then transferred to a sterile polyallomer tubes (Beckman Coulter #326823), which were carefully placed into sealable buckets and centrifuged at 27000 x g for 90 mins at 4°C, with slow acceleration and no brake (Beckman Coulter, Optima XPN-100 ultracentrifuge with SW 41Ti Rotor). After the spin, the supernatant was removed by careful aspiration, and the pellet was gently resuspended in 400 µL of serum-free RPMI, until no visible aggregates remain. The concentrated VLPs were aliquoted as single-use tubes and immediately frozen at -80°C.

2.2.6.3 Determination of functional viral titer ($TCID_{50}$)

The Median Tissue Culture Infectious Dose ($TCID_{50}$) is a commonly used method to quantify viral titers. To determine the $TCID_{50}$ of HIV-1 viral preparations, a titration was performed on the indicator cell line TZM-bl, and the β-gal reporter readout was used. TZM-bl were seeded at 5 x 10^3 cells/well in a 96 well plate (100 µL/well) and incubated overnight (37°C, 5% CO_2) to allow adherence to tissue-culture substrate and regeneration of surface receptors. Border-wells had no cells and were filled with 200µL cells to reduce evaporation. Viral supernatant (25 µL) was added to 5 wells in the first row with cells (wells B2-B6), generating a 1:5 dilution. After thorough mixing, 25 µL of these wells were transferred into the lower

row, and this process was repeated to generate a 1:5 dilution series with 9 steps and 5 technical replicates per dilution. These parameters were adopted from [580], who optimized and validated the luciferase TZM-bl assay for specificity, accuracy, precision, linearity, range and robustness in compliance with good clinical laboratory practice guidelines. The plate was then incubated for 4-5 days until the no-virus control row displayed a confluent cell sheath. Infected cells were visualized by replacing all medium with 50 µL TZM-bl developing solution (see 2.1.1.8) and incubating at 37°C for 1 h. In infected cells, β-galactosidase cleaves X-gal to yield an intensely blue and insoluble product. The solution was then replaced with 1x PBS and the plate was inspected by light microscopy and the dilution row was identified were no positive wells are detected (positive wells have 4 blue cells or more). Then, the number of positive wells per row were counted upwards until finding the first row where all wells are positive. The $TCID_{50}$ was then calculated by the Spearman & Karber algorithm, as described in "Virology Methods Manual" (Hierholzer & Killington 1996), p.374.

2.2.7 CRISPR-Cas9-mediated gene knockout

2.2.7.1 Design of CRISPR gRNAs

Guide RNA (gRNA) sequences for target genes were designed using the following protocol:

1) The entire gene sequence (for the target protein of interest) was extracted from the NIH GenBank database, including annotation of protein coding sequences (exons). The latest reference human genome annotation at the time (GRCh38 primary assembly) was used in all cases. GenBank gene IDs are provided in Table 2.9.

2) The first exon that is common to all target-protein isoforms was copied and submitted to the CRISPR-Cas9 guideRNA design software CRISPOR ([581] and see further below) and the "NGG" PAM sequence parameter (for SpCas9) was selected.

3) The gRNA with the highest specificity score was selected, that also fulfilled the following requirements; 1) efficiency and out-of-frame scores should be above 30, 2) gRNA should have no less than 4 mismatches with any known human exon (except the intended target gene). Where specificity scores were all high, preference was given to gRNAs with higher out-of-frame scores.

4) Where all obtained gRNA options had a specificity score below 80, the following common coding exons were sequentially entered into the software, until gRNAs with better scores were obtained or until 60% of the protein ORF had been explored (gRNAs should ideally sit closer to the N-terminus, to ensure that frameshifts result in true loss of function).

Of note, gRNA-design software options (including their intrinsic algorithms) are continuously improved and updated. As a consequence, some software platforms are no longer available, and re-running a sequence on the same software on subsequent years can provide different results (e.g. in terms of gRNA scores). In this study, we originally (2015-2016) used the guideRNA design tool from the Feng Zhang lab (crispr.mit.edu). Since this online resource was closed in 2017, we migrated to the CRISPOR software (crispor.tefor.net, [581]), as encouraged by the Zhang group. Since then, this platform has undergone considerable changes. For instance, while originally only 1 value was predicted for specificity, efficiency and out-of-frame scores, now 2 values are provided for each (based on two different algorithms). In Table 2.9, we provide the specificity scores that were obtained by the available software option at the time of gRNA design (2015-2018). Please note that reintroducing these sequences on CRISPOR at later times might produce slightly different values.

2.2.7.2 Design of non-targeting CRISPR control gRNAs

Non-targeting gRNA sequences, which in theory lack the ability to target Cas9 to any genomic region, are often used as negative controls in CRISPR-Cas9 experiments. The number and position of tolerable mismatches between the 20mer gRNA sequence and the target DNA sequence is highly context dependent [582,583]. However, it is generally accepted that the greater the number of mismatches, the lower the chance of off-target editing. Since generating (balanced) 20-mer nucleotide sequences with more than 4 mismatches to every region of the human genome is often not feasible, most gRNAs designed with current software have at least a few off-target sites with 4 mismatches or less. Non-targeting control gRNAs sequences in this thesis, which have been intensively curated by bioinformatic approaches to ensure low sequence similarity to the species genome of interest, were obtained from the human GeCKOv2 CRISPR library [584]. These were selected from the library to ensure no less than 4 mismatches to any known human genomic region.

2.2.7.3 Cloning of gRNAs into CRISPR vectors

For each gRNA, two single-strand DNA oligos were ordered from IDT-Technologies as indicated by the Zhang lab protocols [584]. Annealing of these oligos produces a short double stranded DNA sequence (gRNA site), with overhangs compatible with those generated in the LCV2 and LGP plasmids after digestion with BsmbI (recognizes asymmetric DNA sequences and cleaves outside the recognition site).

Oligo 1	5'-CACCG(G) + 20bp gRNA sequence -3'
Oligo 2	5'-AAAC + 20bp complementary to gRNA sequence +C(C) -3'

The (G) and (C) in Oligos 1 and 2 were added only if G was not the first base of the gRNA. This is because a G at this position is known to enhance transcription from the U6 promoter.

The complete oligo design and cloning protocol can be found under: http://genome-engineering.org/gecko/wp-content/uploads/2013/12/lentiCRISPRv2-and-lentiGuide-oligo-cloning-protocol.pdf. Cloning was performed exactly as indicated in this resource from the Zhang lab. Briefly, 5 µg LCV2 plasmid were digested with FastDigest BsmbI (Esp3I, ThermoFisher #FD5404) in the provided buffer (1x) supplemented with DTT to a final concentration of 1mM. 3 units of fast alkaline phosphatase (ThermoFisher Scientific #EF0651) were also added to dephosphorylate the ends of cut plasmid DNA. Final reaction volume was 60µL and tubes were incubated at 37°C for 3 h in a thermocycler. The digested DNA was then separated by gel electrophoresis (as described in 2.2.4.2). The larger band (cut vector) was excised, when presence of a smaller 2 kb band (filler) confirmed efficient DNA digestion. The backbone DNA was extracted from the excised gel band by using a commercial kit (Promega #A9281) following manufacturer's instructions.

In parallel, oligos 1 and 2 were phosphorylated and annealed in a 10 µL reaction with 100 pmol of each oligo, 1x T4 Ligation Buffer (NewEngland BioLabs #B0202S) and 0.5µL T4 Polynucleotide Kinase (NewEngland BioLabs #M0201S). Hybridization occurred in a thermocycler as follows: 37°C for 30 min, 95°C for 5 min and then temperature ramp-down at 5°C/min until reaching 25°C. A ligation reaction was set up (5µL Rapid Ligation Buffer, 50ng digested plasmid, 1µL of a 1:200 dilution of the annealed insert, 1µL T4 DNA ligase and water to a final volume of 11 µL) and this transformed into Stbl2 cells as described in 2.2.4.4.

2.2.7.4 Transduction of mammalian cells with lentiviral CRISPR vectors

Virus-like particles (VLPs) pseudotyped with VSVg and containing any LCV2gRNA lentiviral vector variant (CRISPR VLPs) were produced as described in section 2.2.6. A detailed description of the optimized procedure for the lentiviral delivery (transduction) of human cells with CRISPR VLPs (including the rationale and implications of this strategy) is provided in chapter 4 (see 4.3.5). Briefly, cells were transduced at a MOI of 0.5 and puromycin selection (1 µg/mL) was started at 48h post-transduction. Cells were maintained in selection medium for at least 7 days before they were used for experiments.

2.2.8 Short hairpin RNA (shRNA)-mediated gene knockdown

Cells were transduced with lentivirus stocks expressing respective shRNA at a MOI of 1 and transduced cells were selected by passaging in RF10 medium containing either puromycin or hygromycin for 2 weeks. For double knock down cells, transduced cells stably expressing

single gene knockdowns were transduced with lentivirus carrying the shRNA for the second target and then cultured in double-selection medium.

2.2.9 Cellular staining with cytoplasmic dyes

Suspension cells or freshly trypsinized adherent cells were resuspended to 10^6 cells/mL in serum free RPMI medium (pre-warmed to 37°C). Either 1 μL (suspension cells) or 2 μL (adherent cells) of CellTracker™ Deep red dye were added per million cells and immediately mixed by vigorous pipetting. The cell suspension was incubated at 37°C in a water bath for 45 minutes and then the staining solution was removed and replaced with fresh full medium.

2.2.10 Flow cytometry analysis

Unless otherwise stated, flow cytometry analysis of fixed cells (stained or expressing fluorescent proteins, or both) was conducted with help of a BD-LSRII flow cytometer. For staining of surface proteins with fluorophore-conjugated antibodies, 10^5 cells were resuspended in 50 μL PBS and mixed with 2 μL antibody, followed by 30 minutes incubation at room temperature and washed once with PBS prior to fixation. Samples were always fixed in 4% (w/v) paraformaldehyde for 10 minutes to ensure biological inactivation. Samples were resuspended in FW buffer for loading on the instrument. Note that non-fluorescent/mock-stained, single-color and pure-population tubes were included in every experiment for compensation and gating purposes. The same instrument settings and gating strategy were used in replicate experiments. Flow cytometry data was analyzed using FlowJo version 10.1.

2.2.11 HIV cell-cell viral transfer assay

A detailed description of the optimization procedure (including assay design considerations, controls, characterization and readout validation) for the cell-cell HIV transfer assay used in this thesis is provided in Chapter 3 (see 3.4). The section below describes the step by step technical procedure and Figure 3.1 provides a schematic overview of this method.

U937 cells were infected with VSVg-pseudotyped HIV-IRESeGFP virus at a MOI=1 to produce the donor cell population (cells were mixed with the virus and then spinoculated at 1200 g for 90 minutes at 32°C). At 48 hpi, donors were washed twice with PBS to remove any free virus, then counted and infection rate was measured by flow cytometry. Both cell concentration and infection rate were normalized so that it is constant across all donor group conditions (5x10^5 cells/mL at 30-40% infection). Target cells were labelled with a cytoplasmic far-red fluorescent dye as described on 2.2.9. When TZM-bl cells were used as targets, 10^4 cells were seeded 18h prior to start of coculture in flat-bottom 96-well plates (a RPMI-adapted cell line was used, see 2.2.1.1). When Jurkat cells were used as targets, 4x10^4

cells were seeded on the same day on U-bottom 96-well plates. Donor cells were then added at defined donor:target ratios (specified in the relevant sections, but typically between [0.125-0.5]) and the plate was centrifuged at 1500 rpm for 5 minutes at ambient temperature to bring donor and target cells together in a synchronized fashion. Note that only infected U937 cells are considered HIV donors for donor:target ratio calculations. A stop reaction (BMS-378806 at a final concentration of 10 μM) was added at 12h from start of coincubation to prevent any viral fusion beyond this point, and the coculture was allowed to continue for additional 36 h (up to 48 h total). The number and proportion of DeepRed+/GFP+ double positive cells (productively infected target cells) was determined as outlined below.

For the TZM-bl system, a RF10-adapted TZM-bl line was used (see 2.2.1.1) to best allow coculture with suspension cells. Endpoint readout occurred via high-content fluorescence microscopy (Cytell® GE Healthcare), after removing donor cells by two PBS wash steps and staining the nuclei of live target cells with NucBlue dye (ThermoFisher #R37605) for cell enumeration. At least 60% of the well area was acquired in multiple fields of view. Obtained images were batch-analyzed with the INCELL Developer Toolbox software based on fluorescence intensity and size. The proportion of productively infected target cells was calculated as the number of DeepRed+|GFP+ double positive cells, divided by the total number of nuclei.

For the Jurkat system, the mixed cell population was washed once with PBS, resuspended in 1x Trypsin solution and incubated at 37°C for 5 minutes to completely dissociate any cell conjugates prior to fixing with 4% paraformaldehyde for 10 minutes. The proportion of productively infected target cells was assessed by flow cytometry as the percentage of Red+|GFP+ double positive events within the Jurkat-cell gate population.

2.2.12 Fluorescence microscopy

Unless otherwise stated, cells used for fluorescence microscopy experiments were infected with HIV-iGFP virus. Since in this virus the fluorescent protein sits within the Gag-polyprotein, GFP signal within cells can be used as a surrogate for visualization of Gag trafficking and localization. After budding and maturation, GFP is released by activity of the HIV protease, but virions remain fluorescent as several thousand GFP molecules remain entrapped within the viral particle.

2.2.12.1 Immunofluorescence imaging

For fixed cell imaging, samples were essentially prepared as described in [89]. Briefly, 5 x 105 cells were infected (where required) with HIV-iGFP at a MOI=0.1 for 48 hours under

standard culture conditions. Cells were then cytospun on glass coverslips (22 x 60 mm #1.5 coverslips, VWR international #48393-221) pre-coated with CellTak reagent (Corning #354240). Samples were fixed with 4% formaldehyde (20 minutes) and then quenched with 50 mM NH_4Cl for 3 minutes. Cells were permeabilized with 0.05% (v/v) Triton™ X-100 (Sigma Aldrich #T8787) for 1 minute at and then stained with the relevant primary antibody in presence of 5% (v/v) species-appropriate serum, followed by a fluorescently labelled secondary antibody. For additional staining of actin filaments (F-actin), cells were also treated with Alexa647-conjugated phalloidin (Thermofisher Scientific #A22287). Coverslips were mounted on slides using Prolong Gold antifade mountant with DAPI (Thermofisher Scientific #P36931). These were visualized with a 100 x 1.4 NA oil immersion lens in the DeltaVision Elite microscope combined with a Photometrics CoolSnap QE camera. Images were acquired as 50 to 60 optical sections (0.15-0.20 µm thickness), then deconvoluted and volume projections generated using the SoftWorx 7.0 software. Immunostaining images presented here correspond to Z-series volume projections, unless otherwise stated.

2.2.12.2 Live cell imaging

Live cell imaging was performed using the DeltaVision Elite microscope with a 60 x 1.42 NA oil immersion lens and coupled to an Evolve512 back-thinned EM-CCD camera (512x512, gain = 10). U937 cells infected for 48 h were added to the wells of a 96-well glass-bottom plate (Greiner Bio-One #655892) in a final volume of 100 µL RF10 medium. When U937 cells were imaged alone, 25 x 10^4 cells were seeded per well. For imaging of cocultures, 12 x 10^4 U937 cells (30% infection rate) were added to wells where 8 x10^3 TZM-bl target cells had been seeded 24 h prior in RF10 medium. Before start of imaging, plates were gently centrifuged at 300 rpm to bring cells in contact with the glass surface. Plates when then placed on the pre-heated (37°C) microscope. For image acquisition, the FITC and DIC channels were imaged at 90 second frame-intervals for at least 3 hours. Time lapse movies were generated using SoftWorx 7.0 and are presented as overlays of both channels. For a schematic summary of the live imaging procedure, see Figure 3.11.

2.2.12.3 Single-particle virion counts

For counting of virus particles, 15 µL of supernatant were loaded in wells of a glass-bottom 384-well SensoPlate™ (Greiner Bio-One #781892) pre-coated with poly-L-lysine according to manufacturer's instructions (Sigma Aldrich #P8920). Virions were forced to meet the coated glass-surface by spinning the plate at 2500 x g for 40 minutes at 15°C . The plate was then fixed with 4% (w/v) paraformaldehyde for 20 minutes at room temperature. Fluorescent virus particles (HIV-iGFP) were then imaged using DeltaVision Elite microscope (60x

objective and EM-CCD camera as described above) FITC channel with optimized settings (10% transmission, 0.1ms exposure time and a gain of 10). At least five fields of view per well and condition were acquired. Viral particles were then enumerated by software-assisted counting with help of the 2D/3D particle tracker plugin in the MOSAIC suite of ImageJ.

2.2.13 Statistical analysis

All statistical analysis was performed in GraphPad Prism software version 8.0, unless otherwise specified. Tests to determine statistical significance were not performed in sample sizes lower than three biological replicates per group. For all tests used, differences between groups were considered statistically significant where the obtained p-value is lower than 0.05 and this was visually indicated on all figures with asterisks as follows: * = $p<0.05$, ** = $p<0.01$ and *** = $p < 0.001$. Datasets were first tested for normal distribution by Shapiro-Wilk normality test and QQ-plot analysis.

For normally distributed data, comparison of two groups occurred via a two-tailed, unpaired, parametric Student's T-test with Welch's correction to account for potentially unequal variances. In contrast, two-group comparisons of data that is not normally distributed were done with a two-tailed Mann-Whitney test.

When more than two groups were compared, unpaired one-way analysis of variance (ANOVA) parametric test was used for normally distributed data, whereas the non-parametric Krustal-Wallis test was otherwise used. In both cases, multiple testing was corrected for by using either the Dunnett's test for multiple comparisons (if all groups are compared to a control group) or the Bonferroni correction (if selected pairs of means are compared).

Of note, the statistical test used in each case and the corresponding number of replicate experiments (independent experiments) is specified in the relevant sections.

Chapter 3. Development and characterization of a new and specific *in vitro* system to study cell-cell transfer of HIV

3.1 Introduction

The main aim of this work is to advance our understanding of the process by which HIV is directly transferred from infected myeloid cells to uninfected target T-cells in an actin-dependent manner via cell-cell contacts (i.e. CCTH *in cis*). To this end, it was important to adopt or establish an assay specifically designed to study this process and how it is affected by different variables or treatments. An extensive analysis of the available literature revealed that a wide variety of methodological approaches and model systems have been previously used to study CCTH. These methodological discrepancies somewhat limit our ability to reconcile and compare observations across independent studies. In addition, experimental procedures are not always described in sufficient detail to allow understanding of the rationale behind the choice of assay parameters and conditions. In this section we briefly introduce some of the previous approaches and consider both their advantages and limitations in the context of this study's aims. It should be noted that it is not our intention to criticize previous studies. We acknowledge that all experimental approaches have inherent limitations and recognize that, despite these, the data and knowledge obtained can often greatly advance our understanding. If we observe previous approaches through a scrutinous lens here, it is only with the intention of contributing to the continuous refinement of the methodology used in the field. Table 3.1 summarizes some of the better described coculture-based HIV transfer assays reported to date and highlights some representative examples and recurrent elements from the literature, without aiming to provide a complete list. An independent review addressing additional examples, including non-coculture approaches, is provided by [585], who emphasized the benefits of more systematic research in the field.

Most assays in the literature have used T-cell lines as donor cells and either transformed or primary T-cells as targets (homotypic T-cell systems). Fewer studies have looked at myeloid cells as HIV donors and in most cases this corresponded to HIV-pulsed (uninfected) dendritic cells, which mediate CCTH "*in trans*" (see 1.3.1-3). By far the most common viral strain used has been NL4-3 (and variants thereof), although some studies have used BaL or LAI (see Table 3.1). Coculture conditions varied widely, with coculture times ranging between 3 hours and 7 days in the presence or absence of antiretroviral drugs such as RT or protease-inhibitors. Donor:target ratios (when reported) where often in the range between 0.25 – 1.0. In terms of readout strategy, varied approaches have been used. These include; i) qPCR to detect *de novo* HIV DNA synthesis, ii) p24 staining and flow cytometry to detect the presence of HIV-Gag

in the target cell population, iii) luciferase readouts via LTR reporters to assess productive infection of target cells, and iv) measurement of p24 accumulation in the supernatant as an indicator of viral replication.

Reference	Donor cells	Target cells	Viral strain	Coculture conditions	Readout	Free virus controls
[239]	Jurkat	A3.01	LAI	D:T = 1 t ≤6h	qPCR (detects *de novo* viral DNA)	cell-free fraction
[87]		A301.R5	BaL & NL4-3	D:T = 1 t = 12h		cell-free fraction trans-well shaking
[88]	A3.01-CCR5	A3.01-CCR5	JR-FL	D:T = 1 t = 2-7 days	intracellular p24 staining + FC	cell-free fraction trans-well
[586]	U937	CEM-GFP	NL4-3	D:T = 2:1 t = 16h (ART+)		trans-well
[587]	Jurkat	primary CD4+ T-cells	NL4-3-iGFP	t = 3h	FC readout (GFP+)	several suggested but not shown
[483]		CEM cells	NL4-3	t = 24h (ART+)	Luciferase	cell-free fraction
[588]		TZM-bl	HIV IIIB	Donors removed at t = 24h		none reported
[86]	Jurkat / primary CD4+ cells		NL4-3	t ≤ 48h	intracellular p24 staining + FC	shaking trans-well ART
[440]	transfected HeLa	Jurkat	NL4-3	t = 2h		shaking of cocultures
[91]	infected macrophages	primary CD4+ T-cells	BaL	t ≤ 12h		cell-free fraction
[589]	HIV-pulsed iDC	primary CD4+ T-cells	NL43-BAL	D:T = 0.5 t = 72h	p24 in supernatant by ELISA	none reported
[226]			NL43-RenilaLuc	t = 48h (ART+)	Luciferase	

Table 3.1. Overview of coculture-based HIV transfer assays previously used in the literature. Only a reduced selection of representative examples from a large number of analysed references is shown. ART+ = coculture in the presence of antiretroviral drugs, D:T = donor-target ratio, FC = flow cytometry, shaking = shaking of cocultures to prevent cell-cell contacts, t = coincubation time.

Most studies in Table 3.1 reported the use of at least one control to ensure that the majority of target cell infection occurred by CCTH and not via cell-free virus. However, only few studies to date have evaluated the role of actin-remodelling for CCTH in their systems. While each approach has its advantages and disadvantages, no single assay from the literature seemed to meet all requirements for our intended purpose. A robust viral transfer assay, in the specific

context of this thesis, should ideally be; i) specifically designed to assess CCTH, ii) optimized to use myeloid cells as HIV donors, iii) have a well-defined and relevant readout, iv) quantitative and ideally linear, v) limited to a single round of viral transfer (i.e. from donor to target cells), vi) include sufficient controls, vii) be compatible with imaging approaches (for further characterization), and viii) have a confirmed role of actin-remodelling.

While donor cells and coculture conditions can be easily adapted between protocols, the choices of the readout strategy and timing are of fundamental importance. Several previous studies have used either short coculture times (e.g. 3-6 h) followed by immediate analysis, or coincubation for longer periods but in the presence of antiretroviral drugs. The readout often occurred by detection of Gag in target cells via intracellular antibody staining and flow cytometry. While these approaches allow measuring "transfer of HIV material", they do not always allow to distinguish between this scenario and actual target cell infection. This is important because, as with cell-free HIV, a large proportion of the virus delivered by CCTH (e.g. at the VS) may be uninfectious. Furthermore, the VS is believed to be a "hot spot" for exocytic and endocytic activity [231], which is supported by redistribution of secretory organelles on donor cells towards the site of virus particle release at the VS [590], as well as by substantial endocytic activity in target cells [125,587,591]. Whilst prior studies suggested that HIV may fuse within endosomes [592], recent studies have challenged this hypothesis [467,593] and concluded that fusion proceeds primarily at the PM of recipient targets. Thus, although a considerable and directional cytoplasmic exchange occurs at the VS from donor cells to target cells, bulk-uptake of HIV particles can involve dead-end pathways that primarily result in lysosomal degradation of incoming virions, and therefore "HIV material transfer" must not necessarily correlate with "transfer of infection".

Other assays used a luciferase readout to assess CCTH. While this can more accurately reflect infection transfer, it has some limitations (see 3.4.1.1). qPCR readout, which indicates successful reverse transcription in target cells, is also likely a better surrogate for infection transfer than measuring Gag-transfer alone. However, since it requires lysis of the cell population, it is not compatible with imaging approaches and the produced data is better suited for relative comparisons than absolute quantifications. Accumulation of free-virus in the coculture supernatant has also sometimes been used to assess CCTH. However, the prolonged coculture periods involved can potentially introduce confounding factors, such as multiple rounds of viral transfer and/or unexpected changes in the cell population (e.g. total number of cells, or donor:target ratios). Overall, we decided to aim for an approach which would combine the strengths of previous studies with new strategies and appropriate controls, in order to establish a relevant system that best allows to undertake the specific aims of this study.

3.2 Aims

Given the complexity of the interaction between HIV and the actin cytoskeleton (see 1.5.2) and its cell-type specific manifestations (see 1.5.11), it is paramount to select appropriate models and methods for the study of this biological paradigm. Therefore, and based on the specific interest of this work on the role of actin regulation in the context of CCTH from myeloid cells, this chapter had two primary aims:

1) To select a relevant, representative and practical (myeloid) cell-model system to study the interaction between HIV and cellular actin, as well as to validate said interaction.

2) To establish and characterize a suitable assay to specifically evaluate the effect of different variables on the ability of infected cells to mediate CCTH.

3.3 Identifying a relevant model to study the intersection between HIV and the actin cytoskeleton

A good model to study the link between HIV and the actin cytoskeleton should be; i) relevant (i.e. human cells of hematopoietic lineage), ii) versatile (e.g. genetically malleable and/or compatible with various experimental techniques), iii) representative of the cell population of interest (in our case, DC and Mφ), and iv) ideally validated for its HIV-Actin interaction. Here, we introduce the U937 cell line and address how it meets all the above-mentioned criteria. U937 is a human pro-monocytic cell line of myeloid hematopoietic lineage, originally isolated from the histiocytic lymphoma of a 37-year old male [574]. It is the most frequently used monocytic line [594], and widely recognized as valid experimental model to study the behaviour of monocytes and macrophages. Previous studies with this cell line have allowed to resolve key mechanistic aspects of their biology, including; differentiation [594], endothelial attachment [595] and apoptosis [596]. U937 cells exhibit many fundamental characteristics of monocytes (including morphology, phagocytic ability and cytokine production), and can be differentiated to Mφ or DC simply by exposure to different stimuli (reviewed in [594]). From a HIV point of view, use of U937 provided the first visualization of direct CCTH, via a structure that is now known as the virological synapse [80,597]. Similarly, HIV-Filopodia (see 1.3.4) in U937 cells were shown to morphologically and mechanistically resemble those in primary DC [89]. To a certain extent, these long actin-rich membrane projections capped with immature HIV buds confirm an intersection of viral pathways with the F-actin cytoskeleton in myeloid cells. A physical interaction between HIV-Gag and cellular actin was also formally confirmed in U937 cells as part of this work (see 3.5.1). Furthermore, data from our lab has confirmed the incorporation of various actin

isoforms and abundant cytoskeletal regulators within virions produced in U937 cells (unpublished), and importantly this protein footprint closely matches that reported for HIV produced in primary human macrophages [504].

U937 cells are thus a useful model to study the intersection of HIV and F-Actin in myeloid cells. Despite (or perhaps because of) their early differentiation stage, they allow the combined study of biological mechanisms in monocytes, macrophages and dendritic cells, all of which can be infected by HIV (both *in vitro* and *in vivo*) and are believed to play important roles in HIV pathogenesis (see 1.2.5). In terms of cytoskeletal regulation, U937 cells share the expression pattern of lineage-restricted factors that are enriched in primary myeloid cells [321,598]. Furthermore, their natural susceptibility to lentiviral infection (mainly due to the lack of several restriction factors) allows easier genetic manipulation, compared to primary leukocytes. For these reasons, we selected the U937 cell line as our main model to study the manipulation of the actin cytoskeleton by outbound HIV. Of note, prior to starting this work, the identity of our U937 cell line was confirmed by STR microsatellite profiling and database authentication by a NATA accredited third-party institution (Garvan Institute, Sydney, Australia).

3.4 Methodological approach

3.4.1 Viral transfer-assay general considerations

3.4.1.1 Choice of Readout

While other studies have measured mainly "physical transfer" of HIV-Gag from donor to target cells (see Table 3.1), our interest was to look at productive infection of target cells (i.e. integration of functional viral genomes and *de novo* expression of viral proteins). Despite its relative simplicity and high-throughput compatibility, we decided against a luciferase-reporter approach given that; i) it requires lysis of the cell population, thus making it impossible to determine the absolute infection rate of the target-cell population, ii) it cannot distinguish between infection transfer and donor-target cell fusion and iii) high cost of luciferase-substrate reagents. Instead, we decided to use a fluorescence approach given that; i) it can provide information at the single-cell level (i.e. morphology and signal intensity of infected target-cells), ii) it allows cells to be imaged while alive and at multiple timepoints, iii) it provides absolute quantitative information such as the number of cells (total vs. infected) and iv) simpler, more accurate and negligible cost compared to other approaches. While some HIV-permissive target cell lines with LTR-driven fluorescent reporters exist, we preferred to encode the fluorescent protein within the viral genome, as this approach has a much lower baseline signal in uninfected cells and it also allows the use of various target cell types.

3.4.1.2 Choice of viral strain

Previous studies with fluorescent virus have used variants where GFP is directly fused to Gag at a 1:1 stoichiometry (e.g. HIV-iGFP). While this construct can be extremely useful in some contexts, it is not ideal for the specific aims of our study. Firstly, because it allows detection of non-infectious "Gag-transfer" between cells, since every HIV-iGFP virion contains ~2400 copies of GFP [43]. Secondly, the Gag-GFP fusion may interfere with Gag kinetics, membrane transport and budding dynamics in ways that have not yet been assessed for CCTH. Instead, we decided to encode GFP via an IRES element in the viral genome (i.e. HIV-IRESeGFP, see Table 2.7), so that it is expressed as an independent protein that is not actively packaged into budding virions. Thus, IRESeGFP virus essentially resembles wildtype virus at the protein level, and only productively infected cells become GFP-positive in this context. Importantly, constructs with and without IRESeGFP displayed equivalent viral titers.

For the choice of the viral envelope/tropism, we had to compromise between relevance, performance, versatility and consistency with previous literature. While founder strains are most relevant, they tend to replicate poorly in culture compared to laboratory isolates, and few mechanistic studies have used such strains in the past (none in the HIV-Actin field, to our knowledge). In terms of performance, the focus was on efficient infection of target cells (e.g. T-cells) after transfer from infected donor cells. We tested two R5-tropic (AD8 and BaL), one X4-tropic (NL4-3) and one dual-tropic strain (SPLN7). Compared to NL4-3, both R5-tropic variants performed poorly in infecting Jurkat T-cells, when virus was transferred *in cis* from U937 cells (not shown). This was somewhat expected due to low/undetectable levels of CCR5 in most CD4+ T-cell lines [321]. In contrast, SPLN7 displayed highly efficient transfer to target cells. However, this was accompanied with dramatic cytopathic effects, including large syncytia formation and abundant cell death (see 3.5.5). Therefore, we selected NL4-3, which also has two added benefits for this study. First, it is by far the most commonly used viral strain both in the context of CCTH and HIV-Actin research (see Table 3.1 and [66]), thus enhancing comparability of our results with the existing literature. Second, our lab specializes in viral genome engineering and possesses a large collection of HIV mutants, most of which correspond to the NL4-3 background. For the above-mentioned reasons, we decided to use NL4-3-IRESeGFP (hereafter referred to as HIV-IRESeGFP) as the main viral strain in this study.

3.4.1.3 Choice of target cells

Previous studies have used a wide variety of HIV-permissive cells as recipients for cell-cell viral transfer (see Table 3.1). This included adherent cells (TZM-bl), T-cell lines (Jurkat,

CEM and A3.01) and primary CD4TC. While each system has its own advantages and disadvantages, this variety makes it harder to compare results from different studies in the field. Also, the reasons for the target-cell type selection (and the associated limitations) are not always discussed in the literature. For this study, we selected two target-cell models, which are briefly introduced below.

Jurkats (see Table 2.1.9) represent one of the best characterized T-cell lines and their use has allowed fundamental insights into multiple aspects of T-cell biology, including TCR signalling [599] and viral infection [600]. Of immediate relevance to this study, Jurkats have been established by the team of Claire Jolly (and others) as a recognized model to study the molecular mechanisms leading to CCTH between T-cells [85,231,233,239,539]. Furthermore, many derivatives of the Jurkat cell line exist, including mutants of the cytoskeletal and HIV context. Thus, this cell line is well suited to serve as a model for target T-cells in the context of CCTH and HIV-Actin.

TZM-bl (see 2.1.9) are HeLa cells engineered to express high levels of HIV receptors and coreceptors, as well as LacZ and Luciferase reporter genes upon HIV infection. They are highly permissive to infection with most HIV and SIV isolates, and reporter gene expression is induced by the viral protein Tat. TZM-bls have been widely used in the study of HIV infection and have been fundamental to our understanding of viral entry, in particular viral fusion [601] and receptor-concentration requirements [602]. Furthermore, robust assays have been previously developed with these cells to allow simple and quantitative analysis of cell-free HIV viral titers and antibody neutralization at high throughput [580,603]. While their epithelial origin makes them less directly relevant models to study HIV infection, they present important technical advantages over T-cell lines in the context of studying cell-cell viral transfer. These include; i) TZM-bl are surface-bound so that conjugates/VS formed with these cells become confined to a static X-Y-Z location (which substantially facilitates real-time live imaging), ii) they are morphologically distinguishable from U937 cells, which eliminates the need to use fluorescent markers to discern between both populations in live imaging experiments (thus reducing phototoxicity), iii) Their high levels of HIV-receptor/coreceptor expression make them ideal to induce VS formation in infected donor cells, and iv) the adherent nature of TZM-bl and its multiple readout options (e.g. LacZ, luciferase and impedance) makes these cells compatible with high-throughput instrument platforms, such as those used in industrial drug screenings.

3.4.2 Optimization of assay parameters

The HIV viral transfer assay protocol used in this thesis is described in full technical detail in section 2.2.11 and is summarized in Figure 3.1 below. In this section we provide brief insight into the rationale behind the choice of the various assay parameters.

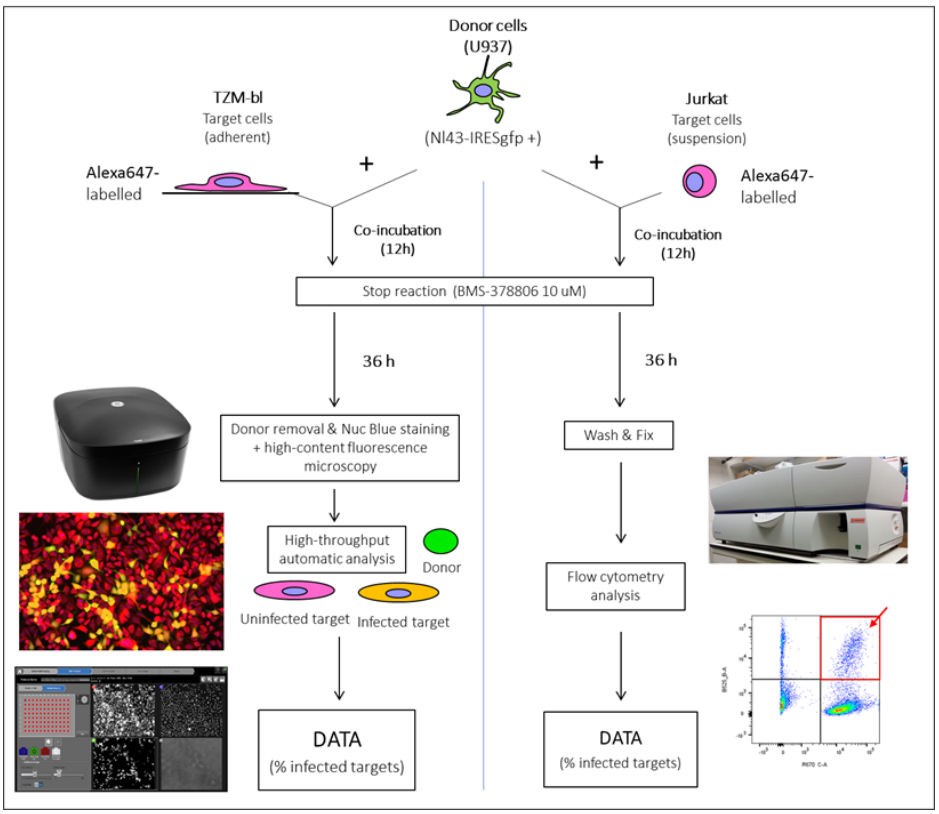

Figure 3.1: Overview of the HIV transfer assay used in this study.

3.4.2.1 Infection of U937 donor cells

Controlling the donor:target cell ratio is critical for any assay that measures CCTH "*in cis*". When only a fraction of the donor cell population is infected, the "donor infection rate" is an important parameter that directly affects CCTH. Ideally it should be high enough to reduce steric hindrance constraints of uninfected donor cells (e.g. by blocking productive donor:target contacts). Obtaining high infection rates in U937 cells was surprisingly challenging and required extensive testing and optimization at the beginning of this study. This included testing the effects of; MOI, VSVg-pseudotyping, spinoculation, Vpx incorporation, use of poly-cations and cell-cycle synchronization, among others (not shown). The optimized conditions correspond to mixing U937 cells with VSVg-pseudotyped HIV-IRESeGFP virus at a MOI =1, followed by spinoculation at 1200g for 90 mins at 32°C and further incubation at 37°C for 48h. This typically resulted in infection rates between 30-50 %, as assessed by both fluorescence microscopy and flow cytometry.

3.4.2.2 Infected donor cell preparation and normalization

Infected donor cells were washed prior to start of the coculture to remove any cell-free virus (see 3.4.2.7). To ensure that the exact same amount of infected donor cells per donor condition are added to the recipient cells, cells were counted after washing and using a stringent method (cells were counted in a haemocytometer in a 0.32% trypan blue solution to ensure only live cells are counted, and counts were repeated if outside the range of 40-150 cells per haemocytometer corner-square, or if corner-square counts variated by more than 10%). After counting, donor cell concentrations were normalized to 5x10^5 cells/mL, the infection rates were determined by flow cytometry, and these were normalized to a constant value for all groups by adding uninfected control U937 cells as required. Thus, in any given experiment, the number of infected donor cells, the total number of donors, the total number of targets, and the final cell densities were identical across all groups to be compared.

3.4.2.3 Labelling of target cells

To be able to resolve target cells and unequivocally distinguish them from donor cells by endpoint flow cytometry or high-content microscopy, Jurkat or TZM-bl cells were labelled with the fluorescent cytoplasmic dye "CellTracker™ Deep Red" (ThermoFisher #C34565). For staining protocol conditions see 2.2.9. Initial testing confirmed that the obtained fluorescent signal was durable, homogeneous, passed linearly to daughter cells but not horizontally to bystander cells, and had no impact on cell viability or proliferation, as indicated by the manufacturer (not shown). Note that while labelling of TZM-bl target cells is required for the automatic, software-driven, endpoint analysis described in section 2.2.11, it is not required (and best avoided) for live imaging experiments, as explained in section 3.5.4.

3.4.2.4 Target cell density

Preliminary testing revealed that the percentage of target cell infection increased linearly with the number of infected donor cells added. However, as long as donor:target cell ratios were maintained constant, the total number of target cells per well had no obvious effect on viral transfer efficiency (not shown). This parameter was therefore selected based on maximisation of donor-target cell contacts, while ensuring that space and metabolic conditions remain suitable for cells to remain viable until the time of readout. For suspension cocultures (Jurkat target cells), 4x10^4 target cells were mixed with donor cells in the wells of U-bottom 96-well plates, followed by pelleting at 1500 rpm for 10 mins. This allows formation of a 3D cell mass that arguably emulates some aspects of lymphoid tissue environment (which is where cell-cell transfer is most likely to play a role *in vivo*). For adherent target cells, 10^4 TZM-bl cells were seeded in flat-bottom wells 24h before the start of the experiment. This allows regeneration

of surface-proteins and enough space for cells to grow and reach confluence by 48h, which helps limit the loss of target cells during donor-removal wash steps.

3.4.2.5 Stop reaction and duration of coculture

A stop reaction was included to limit the assay to a single round of viral transfer (i.e. to prevent newly infected target cells to serve as donor cells). This is important because this study focuses on viral transfer from myeloid donor cells, and because only the original donor cells have been exposed to specific treatments (e.g. shRNA or CRISPR). Furthermore, a stop reaction allows for a short-term viral transfer window, which poses several advantages over long-term cocultures, including; i) it limits the amount of cell-free HIV accumulation in the coculture supernatant (thus likely reducing its contribution to total viral transfer), ii) it minimizes the effects of (donor and target) cell proliferation on changing the coculture conditions (e.g. donor:target ratio), iii) it reduces the window for impaired viral transfer (e.g by knockout cells) to be rescued by treatment-resistant donor cells in the same population (e.g. wildtype-like in-frame CRISPR mutants, see Fig. 4.5).

An ideal stop reaction will prevent any new infection of target cells, while still allowing previous transfer events (i.e. cells where HIV has fused) to result in productive infection and expression of viral proteins and GFP for the intended readout. To this end, we used the gp120-CD4 interaction inhibitor BMS-378806 (Selleckchem #S2632) at the non-toxic final concentration of 10 µM. A time course series was performed by adding this stop reaction to the U937:TZM-bl cocultures at various time points. Total viral transfer increased over time in a somewhat linear fashion until at least 15h (Fig. 3.2-A). A standard coincubation time of 12h was selected for all CCTH experiments. Interestingly, however, adding the stop reaction from the beginning of the coculture (t = 0h) did not completely reduce the readout to 0%. This was confirmed across multiple experiments, which revealed that "only" a ~93% or ~97% reduction of the viral transfer readout in TZM-bl and Jurkat target cells, respectively (Fig. 3.2-B). This difference may be explained by the higher resolution of flow cytometry over high content microscopy to discern "real" GFP+|Red+ double positive events from superimposed single positive cells. On the other hand, some residual target cell infection is consistent with numerous previous observations that CCTH can occur (at least at low levels) in the presence of antiretroviral drugs (reviewed in [84]). In any case, this confirmed the ability of our assay to exclude most (albeit not all) potential confounding events such as donor:target conjugates, unspecific cytoplasmic exchange and/or drug-resistant CCTH.

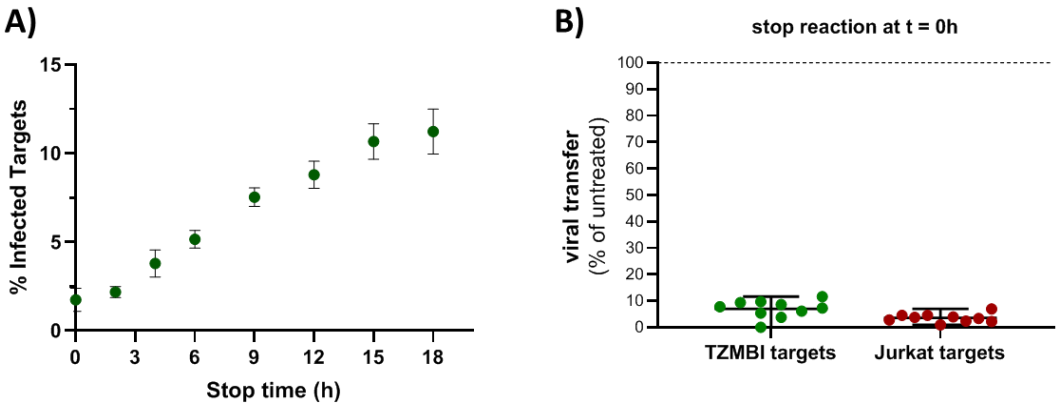

Figure 3.2: Stop reaction for viral transfer assay. A) Time course, representative of one experiment**. B)** Stop reaction from the start of coculture for 10 experiments. Additional details for this figure are described in the paragraph above.

3.4.2.6 Assay linearity

As expected, a proportional increase in target cell infection was observed with increasing donor:target cell ratios for both TZM-bl and Jurkat target cells (Fig. 3.3 A-B). Importantly, pooling raw data from multiple experiments revealed considerable variation in the observed absolute percentage of infected target cells, as indicated by the error bars (standard deviation) in Figure 3.3A-B. This therefore suggests a high inter-assay variability. However, when individual experiments were considered, a low intra-assay variability was observed, as indicated by the small variation between technical replicates (Fig. 3.3-C). Furthermore, linear regression of data from individual experiments revealed exceptionally strong linear correlations between the donor:target ratio and the observed percentage of infected target cells. This is indicated by the correlation coefficient value "R", which ranges from -1 to +1, with R= ±1 indicating a perfectly linear correlation and 0 indicating absolute lack of correlation [604]. For individual experiments, R was always > 0.95 (Fig. 3.3-D), whereas for pooled experiments R was always > 0.85 (Fig. 3.3 A-B). Together, this suggests that while there is considerable inter-assay variability in the total magnitude of infection transfer (even at identical D:T ratios), the assay can accurately detect subtle changes in CCTH and offer valid quantitative information, especially when comparing multiple donor groups within the same experiment. Therefore, an internal normalization control (e.g. untreated) was included in every experiment.

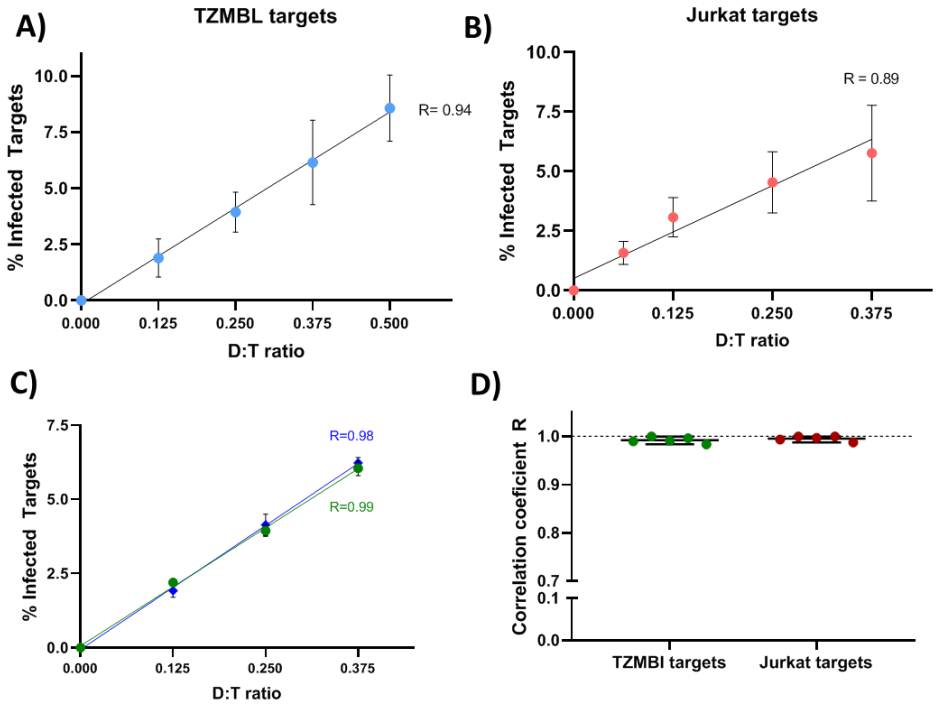

Figure 3.3: Readout of viral transfer assay with U937 donor cells and **A)** TZM-bl or **B)** Jurkat target cells at increasing donor:target ratios (D:T), with stop reaction at t=12h and total coincubation of 48h. Datapoints indicate the means and error bars the standard deviation of five independent experiments. C) Two wildtype U937 cell lines kept in culture by 2 independent investigators (blue = passage 8, green = passage 27) were run against each other in the same experiment (error bars indicate standard deviation of duplicates for each group). D) Correlation coefficient "R" obtained by linear regression of individual experiments (N=5).

3.4.2.7 Free virus controls

CCTH is "difficult" to quantify in coculture systems because of concurrent infection of target cells with cell-free virus [88,585]. Therefore, to ensure that the infection transfer observed in our assays is primarily cell-mediated, we have incorporated multiple controls to account for the role of free virus in our system. In this context, we need to distinguish between the initial "cell-free inoculum" (VSVg-pseudotyped HIV particles used for the infection of donor cells) and the cell-free virus produced *de novo* (i.e. that which is produced and released by the infected donor cells during the co-culture, hereafter always referred to as "free virus").

Effective removal of cell-free inoculum could be achieved by vigorously washing infected donor cells twice in warm PBS, as this virtually abolished the infectivity of the cell-free donor fraction when this was added to target cells 1h after washing (Fig 3.4-A). On the other hand, culturing donor and target cells separately and then adding the cell-free fraction of the donors (i.e. the free virus) to the target cells reduced target cell infection by at least 1 order of magnitude compared to direct cocultures (Fig. 3.4-B). The relative contribution of free virus to total viral transfer is discussed more in detail in section 3.4.3. To exclude the possibility

that the equivalent free-virus infection was lower due to instability of cell-free virus during the 12h collection window, we used a trans-well system to prevent donor-target cell contacts, while allowing for free virus diffusion in real time. This did not increase target cell infection compared to the "equivalent free-virus" control (Fig. 3.4-C). Finally, we also considered the possibility that part of the observed viral transfer in cocultures could be due to bystander uninfected U937 cells delivering free virus to target cells *"in trans"* rather than by "CCTH *in cis*" (see 1.2.2) mediated directly by infected donor cells. To this end, we tested whether adding equivalent amounts of uninfected donor cells together with the "equivalent free-virus" condition would increase target cell infection. No evident increase was observed under these conditions (Fig. 3.4-D), suggesting that U937 cells do not mediate CCTH *in trans*. This is supported by our high-resolution 3D-imaging in Chapter 6 (see 6.4.3-4), which revealed that infected U937 lack the extracellular virus-containing compartments (VCC) that allow primary DC and Mφ to mediate CCTH *in trans*. Thus, U937 cells represent a good model to specifically study CCTH *in cis* from myeloid cells, which is a primary aim of this study.

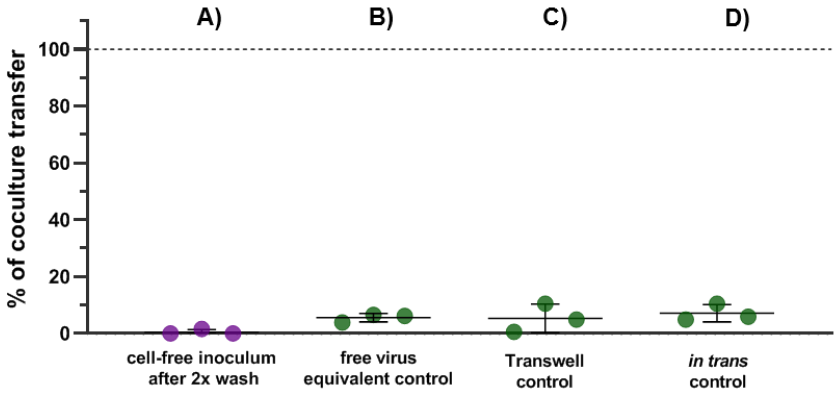

Figure 3.4: Free-virus controls. Infected U937 donor cells were washed twice with PBS at 48 hpi and processed as described in 3.4.2.2. Washed donors were then either added directly to target TZM-bl cells (coculture), or as indicated below. **A) Control for removal of the initial HIV-VSVg+ inoculum.** One hour after washing, an equivalent volume of cell-free fraction (compared to the amount of donor cells used for cocultures) was added to the target cells. **B) Free virus equivalent control.** An equivalent amount of donor cells (compared to coculture) was incubated for 12h in the absence of target cells, and then the cell-free fraction was collected and added to target cells. **C) Trans-well control.** Donor cells were added to the upper chamber of a trans-well to physically separate them from target cells in the lower chamber via a polycarbonate membrane with a pore size of a 0.4 µm (Corning #3401). **D) *In trans* control.** Same as B) but an equivalent amount of uninfected U937 cells was added simultaneously with the free virus. **A-D)** A stop reaction was added 12h after coculture start or free virus introduction. Target cell infection rates were measured 36h later and compared to that of the coculture condition. Data indicates the mean and range of three experiments.

3.4.3 Bimolecular fluorescence complementation (BiFC)

BiFC is a technique that allows direct visualization of protein interactions within living cells or organisms (Reviewed in [605]). The biochemical principle of the assay is summarized in Figure 3.5 below.

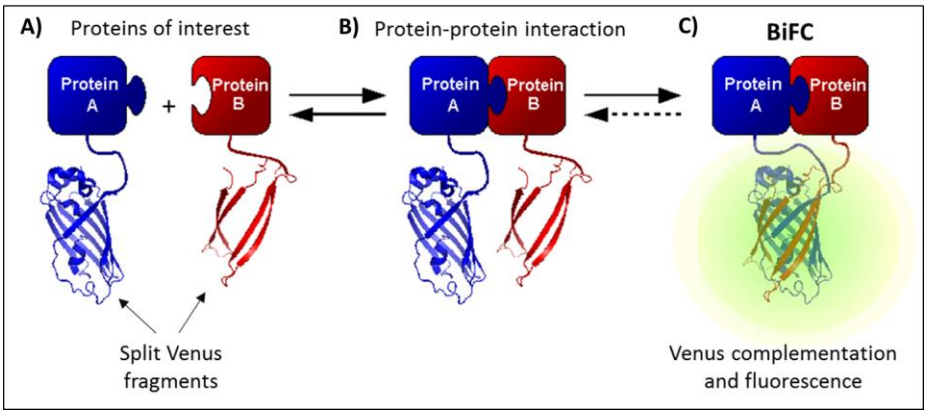

Figure 3.5: Schematic representation of the Bimolecular Fluorescence Complementation technique (BiFC). A) To test putative protein-protein interactions, the proteins of interest are each fused to the non-fluorescent complementary fragments of a fluorescent protein (most commonly Venus / YFP). **B)** Close physical association between the proteins of interest facilitates an interaction between the fragments leading to **C)** formation of a BiFC complex. Image was modified from https://commons.wikimedia.org/wiki/File:BiFC_(details).png, in compliance with its licensing conditions.

In this work, the BiFC approach was used to explore the physical interaction of HIV-Gag with cellular actin. To this end, the sequences encoding the N-terminal fragment (amino acid residues 1-173 = "VN") or the C-terminal fragment (amino acid residues 155-238 = "VC") of the Venus protein (each flanked by two 6xAlanine linkers) were used to replace the GFP sequence between the matrix and capsid domains of Gag in the full-length viral plasmid NL43-iGFP (HIV-iGFP). The replacement was achieved by ligation of an XbaI/MluI flanked VN- or VC-PCR into a XbaI + MluI digested HIV-iGFP backbone, resulting in the HIV-iVN-Gag and HIV-iVC-Gag plasmids respectively. The template for the PCRs was purchased in form of "gBlock® Gene Fragments" (Integrated DNA Technologies Inc.), based on the sequences kindly provided by the authors of [606]. To be able to distinguish infected cells independently of their BiFC Venus signal, an additional variant was generated by moving the IRES-mOrange reporter site from NL43-IRESmOrange into HIV-iVN-Gag using the BamHI/XhoI sites to create HIV-iVN-Gag_IRESmOrange, hereafter referred to as "HIV-BiFC". Thus, in our experiments, the VN-Gag fusion protein is always expressed in cells in the context of HIV infection.

In contrast, the sequence encoding the C-terminal fragment of Venus (amino acid residues 155-238 = "VC") was used to tag the N-terminal region of proteins of interest in the lentiviral vector pLVX. This was achieved in two steps. First, the Actin-mCherry region of the pLVX-Actin-mCherry plasmid (Clontech) was replaced by a Gene block (using EcoRI/XbaI) containing the VC-fragment flanked by two 6xAlanine linkers and followed by a short multiple cloning site. This created the "pLVX-VC-wildcard vector", which then allows cloning of any open reading frame (ORF) for expression of N-terminally VC-tagged proteins

by using the NotI/XbaI cloning sites. Both the human sequences for β-Actin (ActB) and α-Tubulin open reading frames were cloned into this vector to produce the plasmids "pLVX-VC-Actin" and "pLVX-VC-Tubulin". Thus, in our experiments, the VC-Actin / VC-Tubulin fusion proteins are expressed in cells from otherwise identical lentiviral constructs, under the control of a CMV promoter. U937 cells were transduced at low MOI's to avoid integration of multiple copies into the genome. Transduced cells were enriched by puromycin selection (2 μg/mL) for at least 7 days before use in experiments.

Fluorescence microscopy: For epifluorescence imaging of BiFC, cells expressing VC-proteins and growing in glass-bottom 96 well plates were observed directly without any fixation, labelling or permeabilization steps at 48 hours after infection with VN-Gag expressing virus. This live imaging was performed with the DeltaVision ELITE microscope as described in 2.2.12.2.

Flow cytometry analysis: cells expressing VC-Actin / VC-Tubulin were infected with NL43-IRESmOrange-iVN-Gag (HIV-BiFC). At 48 hpi, cells were washed once with PBS then fixed (4% paraformaldehyde for 10 minutes) and resuspended in FW-buffer. A minimum of 5x10^4 events were acquired on a BD-LSRII flow cytometer and analysed with FlowJo software.

3.5 Results

3.5.1 Physical association between HIV-Gag and F-Actin

The literature reports a considerable amount of evidence suggesting that HIV-Gag can physically interact with F-actin (see 1.5.5). However, the approaches used in previous studies have not allowed confirmation of this hypothesis in intact and/or living cells, nor in cells of relevant lineage or in the context of HIV infection. Thus, to further explore the possibility of a Gag-Actin interaction in living infected cells of human hematopoietic lineage, we decided to use the bimolecular fluorescence complementation technique (BiFC), as elegantly done by Chen and colleagues for equine infectious anaemia virus (EIAV) [606]. Using this and other methods, Chen et al. revealed an intimate and specific association between EIAV-Gag and actin in simian fibroblasts (COS-7) and equine dermal cells [606]. Based on their strategy, we generated a similar set of constructs for the HIV-Gag and human β-Actin protein pair. For an overview of the BiFC technique and a detailed description of the generation of these constructs, see 3.4.3. Briefly, the N-terminal region of the fluorescent Venus protein (VN) was cloned within the HIV-Gag sequence of a full-length HIV plasmid, and the C-terminal region of Venus (VC) was fused to human β-Actin in a lentiviral expression vector. Thus, in our experiments the VN-Gag fusion protein was expressed in the context of cellular HIV infection. Since we decided to express the VN-fragment within the large Gag polyprotein sequence, as

opposed to a conventional N- or C-terminal fusion approach, it was important to first test the ability of this protein to form fluorescence complexes. To this end, we co-transfected 293T cells with plasmids expressing VN-Gag and VC-Gag and assessed the resulting BiFC signal by fluorescence microscopy. We could readily observe bright fluorescence at the expected excitation/emission spectra in HEK 293T cells (Fig. 3.6-A), thus confirming the feasibility of our approach.

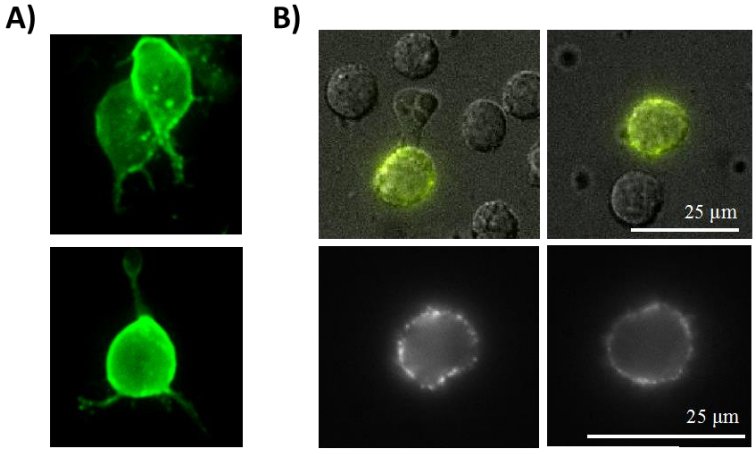

Figure 3.6: BiFC fluorescence of cells expressing VN-Gag + VC-Gag. A) 293T cells co-transfected with plasmids encoding iVN-Gag and iVC-Gag (Olympus Inverted fluorescence microscope, FITC-channel). **B)** U937 cells coinfected with HIV-iVN-Gag and HIV-iVC-Gag. Four different and representative cells with enriched and punctuate signal at the membrane are shown (DeltaVision Elite microscope, FITC channel).

When U937 cells were coinfected with VN-Gag and VC-Gag virus, we observed bright yellow fluorescence, albeit at low cell frequencies. These low frequencies were due to reduced viral titers, which were significantly lower for iVN-tagged compared to iGFP-tagged virus (~10-fold, $^{**}p<0.01$, N = 4 different viral batches, data not shown). The signal on these cells showed a punctuate pattern at the membrane and was stronger than in the cytoplasm (Fig. 3.6-B), as expected for visualization of Gag oligomers. Together, the above-mentioned observations confirmed that, even when expressed within Gag, the Venus fragments could complement to produce a fluorescent complex and that this complementation was favoured in the context of Gag-Gag associations. We then infected U937 cells that stably express VC-Actin with HIV-iVN-Gag. Under these conditions we observed occurrence of bright Venus fluorescence. Unlike with VN/VC-Gag coinfection, fluorescence in these cells was rather diffuse and homogenous in the cytoplasm, with no apparent membrane enrichment (Figure 3.7-A). As a specificity control, we replaced the β-Actin ORF in pLVX-VC-Actin for the α-Tubulin ORF and observed little to no signal by fluorescence microscopy under otherwise identical experimental conditions.

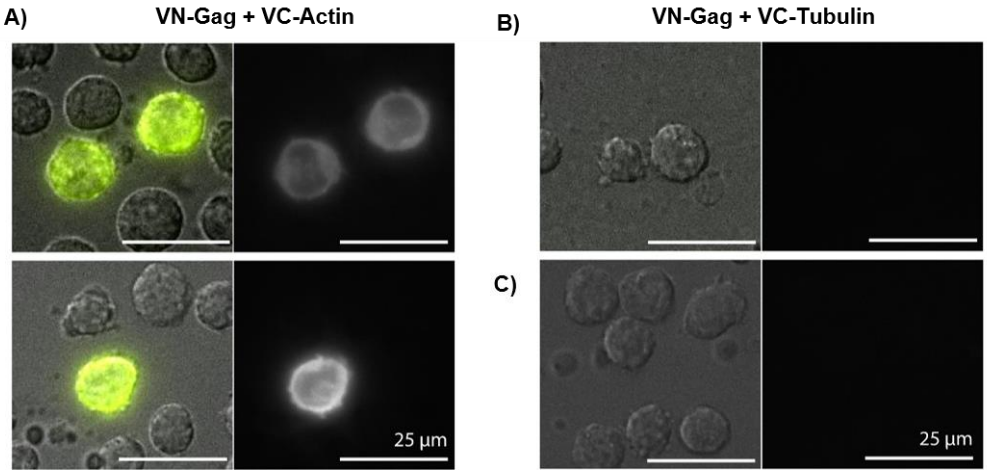

Figure 3.7: BiFC analysis by fluorescence microscopy of **A)** VC-Actin or **B)** VC-Tubulin expressing cells infected with VN-Gag HIV. The signal for VC-Tubulin/VN-Gag pair is not readily visible at the exposure conditions used (constant for all images). **C)** No-fluorescence control (VC-Actin + VC-Gag). **A-C)** Right panels = FITC channel, left panel = overlay of DIC and FITC channels.

To assess which percentage of VC-actin expressing cells led to detectable BiFC signal upon infection with HIV-iVN-Gag, it was necessary to distinguish between infected and uninfected cells. To this end, an additional IRES-mOrange element was added to the HIV-iVN-Gag virus, so that any infected cell would display orange fluorescence, independently of BiFC occurrence. When VC-Actin cells were infected with this HIV-IRESmOrange-iVN-Gag virus (HIV-BiFC), virtually all infected cells (mOrange+) were also BiFC positive (Venus+), as revealed by flow cytometry analysis. In contrast, a significantly lower number (~25% vs. ~95%) of BiFC+ cells was detected upon infection of VC-Tubulin cells (Fig. 3.8-A, $p<0.05$). Appropriate compensation controls (i.e. non-fluorescent control and single-colour samples) were included to exclude any overlap between the mOrange and Venus readouts. Similarly, when the Venus fluorescence intensity of infected cells was compared, the VC-Actin/VN-Gag pair exhibited a significantly stronger BiFC signal (> 6-fold) compared to the VC-Tubulin/VN-Gag pair (Fig. 3.8-B, $p<0.05$). No fluorescence was observed by either microscopy or flow cytometry when VN-Gag or VC-proteins were expressed alone, or when VN-VN or VC-VC pairs where expressed (Fig. 3.7-C). The fact that we observe a clear above-background signal for VC-Tubulin (when VN-Gag is present) indicates that the VC-ORF is being correctly expressed. Together, these observations confirmed that in HIV-infected cells, there is an intimate and specific physical association between HIV-Gag and F-actin.

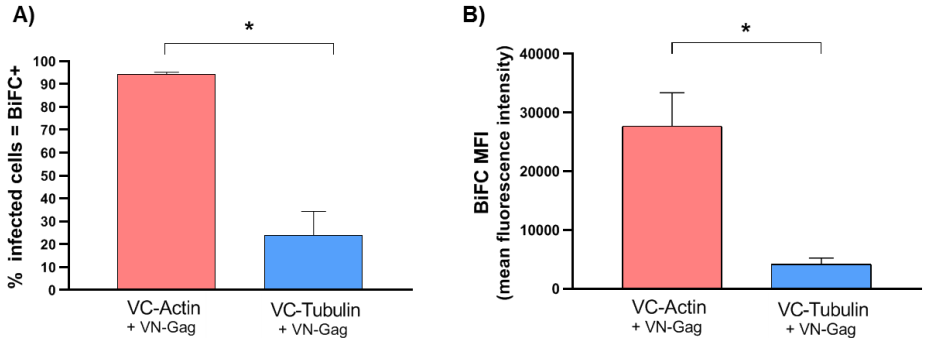

Figure 3.8: BiFC analysis by Flow Cytometry. U937 cells transduced to stably express either VC-Actin or VC-Tubulin were infected with VN-Gag expressing virus at a MOI = 0.2. **A)** Percentage of HIV infected cells that display any BiFC signal. **B)** Mean fluorescence intensities compared for both BiFC pairs. Data indicates the mean and standard error of 4 independent experiments. * = $p < 0.05$ by Mann-Whitney test.

3.5.2 Role of actin remodelling in cell-cell HIV transfer and free virus release

Several previous studies have reported a key role of actin-remodelling in CCTH after assessing the effects of multiple inhibitors of actin dynamics (IAD) on this process (see 1.5.8). However, careful interpretation of these observations and their related experimental procedures is required to understand which steps are affected by such treatments. Since actin remodelling is essential for target cell infection by free HIV, CCTH is expected to be reduced in settings where target cells are pre-treated with IAD [85], or where these drugs are added directly to cocultures [483]. Only few studies to date have looked at the effect of IAD specifically on donor cells, perhaps because of associated technical difficulties. First, IAD are small and often membrane-permeable molecules that bind to actin in a reversible manner, so that their effects are rapidly reversed after washing [239]. Second, reliable detection of HIV transfer requires coincubation for several hours thus limiting the drug effect window if donor cells are pre-treated. Third, treatment with some IAD may impair free virus release (see 1.5.7), which further complicates assessment of their effect on CCTH. Still, it has been shown in a homotypic T-cell system that short-term pre-treatment of donor cells with Cytochalasin D or Latrunculin A can impair Gag/Env polarization (donor cell), as well as HIV particle transfer to target cells [239]. We therefore decided to test also in our system, whether specific treatment of donor cells with IAD could selectively affect HIV transfer from myeloid cells and whether this was due to decreases in CCTH, free virus release, or both.

Donor cells were pre-treated for 1 hour with either Cytochalasin D or Latrunculin A (5 μM final concentration), followed by two washing steps with PBS before mixing with target cells. Donor cell viability was not impaired by these treatments, as confirmed by both LIVE/DEAD™ staining and Alamar Blue assay (see 2.2.3) 24h after treatment (not shown). For these viral transfer experiments, we reduced the coculture time to 6 hours, to try to account

for the rapid drug reversibility, but the stop reaction and readout times remained unchanged at 12h and 48h respectively. In this setting, Cytochalasin D treatment mildly reduced total viral transfer (~30% lower, $p<0.05$) compared to both the mock-treated and DMSO controls (Fig. 3.9-A). In contrast, free virus release was unimpaired for the Cytochalasin D group (compared to the mock-treated control), whereas Latrunculin A and DMSO seemed to slightly increase particle release (Fig. 3.9-B). Although effects were rather weak (likely due to rapid drug reversibility) these results suggests that disruption of the actin cytoskeleton was able to impair cell-cell transfer without reducing free virus release.

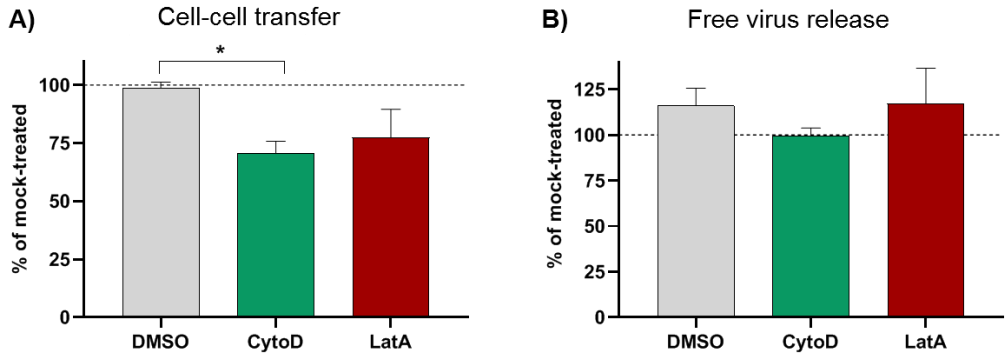

Figure 3.9: Pre-treatment of donor U937 cells with actin inhibitors. Cytochalasin D (CytoD) and Latrunculin A (LatA) were used at a final concentration of 5 μM. Cells were drug-treated for 1h then washed twice with PBS. **A)** Infected donor cells were mixed with target cells immediately after washing. Stop reaction was added 6 hours after start of coculture. **B)** Donor cells were cultured in the absence of target cells, and the cell-free fraction was collected at 6 hours and viral particles in the supernatant were counted as indicated in 2.2.12.3. **A-B)** Data indicates the mean and standard error of 4 independent experiments. * = $p < 0.05$ by Krustal-Wallis test with Dunnett's correction.

3.5.3 Relative contribution of cell-free virus

To evaluate the relative contribution of free virus in our viral transfer assay system, we seeded an amount of infected donor cells equivalent to that used in cocultures and the resulting cell-free fraction was collected at 12h and added to target cell wells (i.e. "equivalent free-virus infection" as described in 3.4.2.7). The resulting proportion of infected target cells was dramatically lower compared to when donor cells were directly cocultured with target cells (Fig. 3.10-A). As expected, a similar linear decrease was observed for both cell-cell and free virus for decreasing donor:target cell ratios or decreasing number of separately-seeded donor cells respectively. The relative contribution of free virus was found to be always lower than 10% in all experiments where this was assessed (Fig. 3.10-B). This confirmed that, as expected from the literature (see 1.2.4), CCTH is more efficient than infection by cell-free virus in our system.

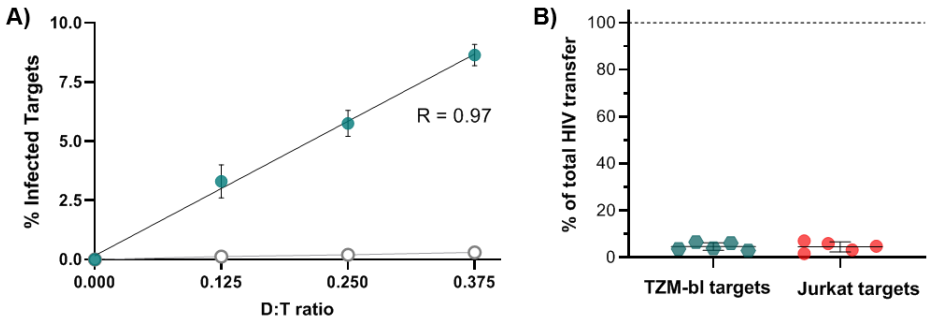

Figure 3.10: Relative contribution of cell-free virus. Viral transfer assay with HIV-infected U937 donor cells and TZM-bl or Jurkat target cells, including equivalent free virus control collected from donor cells cultured separately from target cells and added to target cells after 12h as described in 3.4.2.7. **A)** Representative experiment with TZM-bl target cells at increasing donor:target cell ratios (D:T). Full circles indicate total viral transfer and empty circles equivalent free virus infection. **B)** Relative contribution of free virus to total viral transfer at equivalent D:T = 0.25. Datapoints indicate the values from 5 independent experiments for each target cell type.

3.5.4 Visualization of viral synapses

Since our viral-transfer assay was designed to study CCTH, it was important to confirm that virological synapses can form in our system. To this end, we resorted to live imaging via high-resolution fluorescence microscopy. In contrast to our standard assay, donor cells were infected with HIV-iGFP, which encodes a copy of GFP within the Gag polyprotein. Since the fluorescent protein is only cleaved by the HIV protease after virion release and maturation, this construct is suitable for tracking HIV-Gag dynamics within the infected donor cell [571]. For live imaging, we used the U937:TZM-bl system, given its multiple advantages in this context (see 3.1.3). Live imaging conditions are described in detail in methods section 2.2.12.2 and summarized in Figure 3.11 below. Since live imaging time series are analysed manually by the investigator (in a software-assisted and frame-by-frame manner) and TZM-bl cells are easily morphologically distinguishable from U937 cells at this high magnification, this eliminates the need of using additional fluorescent dyes to identify target cells. This is highly beneficial for live imaging because (in contrast to endpoint analysis as described in 2.2.11) cells must remain viable despite being exposed to fluorescence-inducing light every few seconds for up to 3 hours (due to multiple fields of view being acquired per well). Thus, adding an additional fluorescence channel would at least double the total exposure to phototoxic light, which could compromise cell viability.

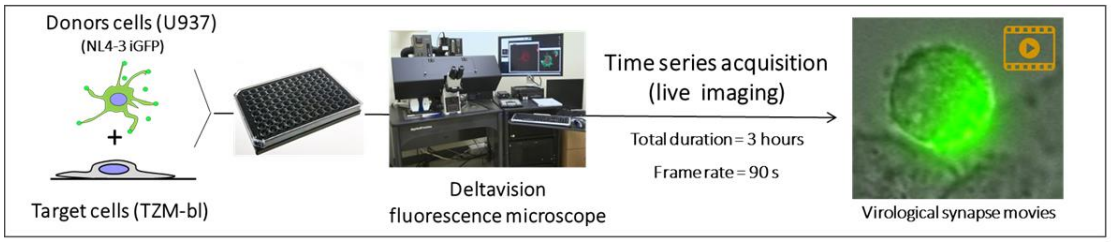

Figure 3.11: Summary of live imaging experiments. U937 cells were infected with HIV-iGFP virus and then washed and counted at 48 hpi. U937 cells at 30% infection rate were added to TZM-bl targets in a glass-bottom 96-well plate. Plates were imaged on a pre-heated DeltaVision microscope (37°C). Time series was created by acquiring brightfield and FITC channels, using autofocus function, at a 90 second frame rate for a total duration of 3 hours.

Live imaging of U937:TZM-bl cocultures revealed that more than half of infected donor cells formed conjugates with at least one target cell during the lapse of the 3-hour movies. In this setting, we defined conjugates as cell-cell contact interactions that lasted for at least 5 consecutive frames (~8 mins). However, conjugates were often long lived and sometimes lasted for the entire duration of the movie. Analysis of over 100 cells from multiple experiments also revealed that >35% of donor cells showed polarization of the Gag-iGFP signal towards target cells at some point during the imaged period. Polarization herein was defined as visible enrichment of GFP signal within the proximal third of the cell, while in direct contact with a target cell. Around 25% of infected cells were also observed to form virological synapses (Fig. 3.12), considered here as conjugates that display Gag polarization over at least 3 consecutive frames (~5 mins), although many VS lasted for over 30 mins.

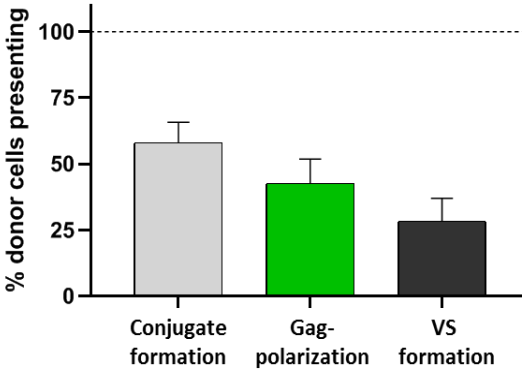

Figure 3.12: Observed frequencies of viral synapse formation. Donor cells (U937 infected with HIV-iGFP virus) were mixed with target TZM-bl cells and imaged in real time for 3h. Shown is the observed percentage of infected donor cells that engage in conjugate formation, display Gag polarization and form viral synapses. Data indicates the mean and standard deviation of 3 independent experiments. At least 10 fields of view and over 30 infected cells were analysed per experiment.

Early conjugate formation was often preceded/characterized by extensive filopodial activity at the contact site (Fig. 3.13-A and supplementary Video S1, attached to this thesis). In contrast, synapse progression was often preceded by retraction of filopodia and extensive apparent cytoskeletal rearrangement, with most cells rounding up during peak Gag-polarization. Note

that by "cell rounding" we mean loss of membrane protrusions and not necessarily a true circular shape of the cell body (although this was also often observed). Figure 3.13 shows two representative time series and figure 3.14 shows a panel of representative synapses at the time of peak Gag-polarization.

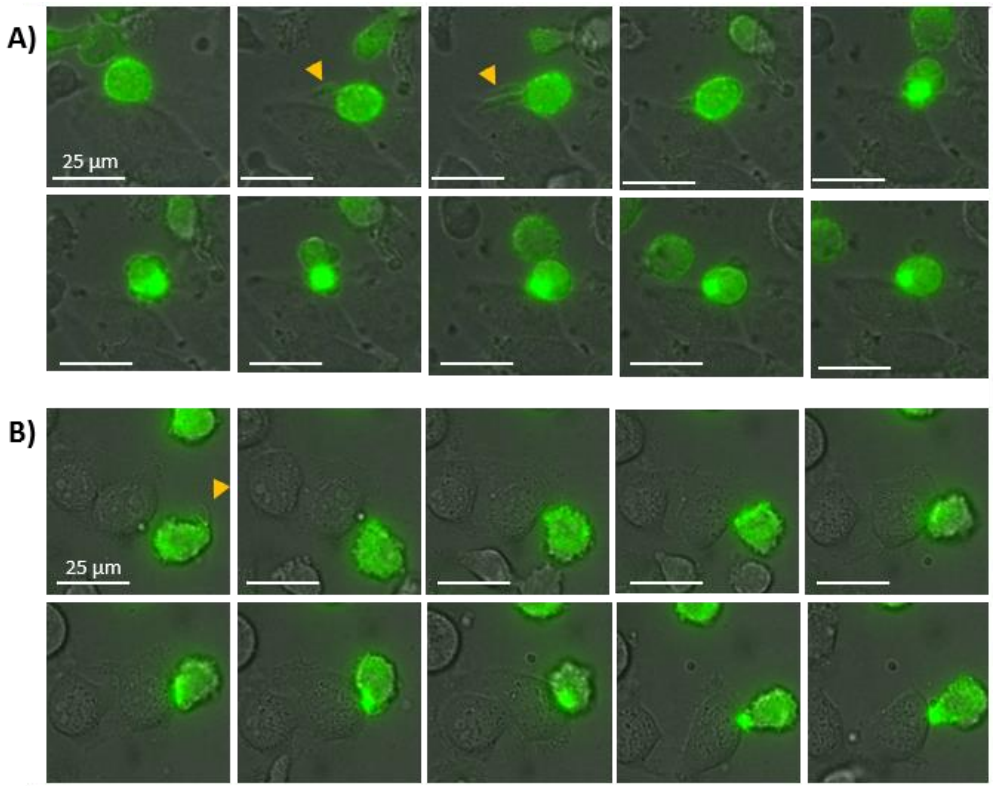

Figure 3.13: Representative time series examples of viral synapse formation. Infected U937 donor cells tend to be highly motile and display pronounced membrane projections (yellow arrows). Upon formation of intimate contacts with TZM-bl target cells, donor cells often polarize Gag towards the target cell, and this can progress into a viral synapse with a distinctive Gag-button and donor-cell "rounding". For complete time series see supplementary Videos S1 and S2 (attached to this thesis).

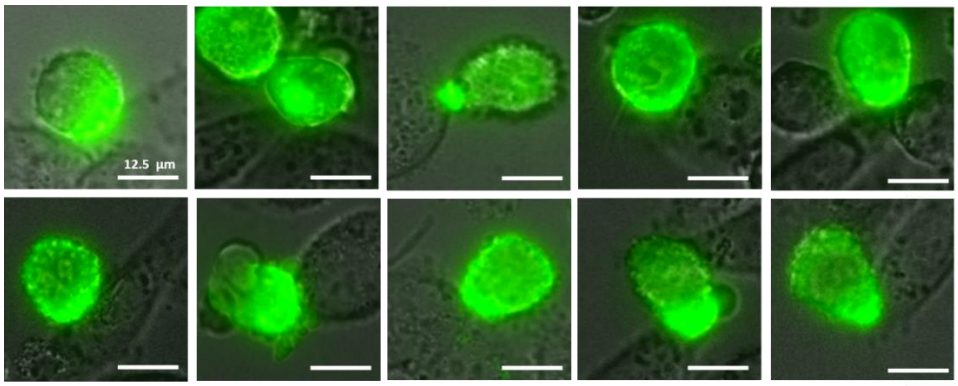

Figure 3.14: Representative images of virological synapses from different time series at frame of peak Gag-iGFP polarization. Scale bar = 12.5 µm.

3.5.5 The Spln7 envelope highly increases cell-cell infection and target cell death

CCTH is believed to be most efficient within lymphoid tissue, given the large number of potential target cells and their compact organization at high cellular densities. The solid nature of this tissue environment also allows spatial segregation of HIV quasi-species *in vivo* (see 1.2.3), and thus the isolation of HIV variants that proliferate extensively in this tissue. Here we tested the CCTH potential of a HIV variant (Macs1-SPLN) isolated post-mortem from the spleen of an AIDS patient with aggressive disease progression [607]. To be able to directly compare this variant to our viral strain, we replaced the envelope of our NL4-3-IRES-GFP viral vector with the gp160 coding region of the Macs1-SPLN Clone7 (obtained from [572]) to create SPLN7-IRES-GFP. Thus, both viral variants differ only in their envelope ORF. We found that U937 cells infected with SPLN7-virus led to a significantly higher transfer of infection (~3-fold, $p < 0.05$) compared to NL4-3 envelope, if donor and target cells were cocultured together, but not when the equivalent amount of cell-free donor virus was added to the targets (Fig. 3.15-A). The average relative contribution of free virus compared to total viral transfer was similarly low (< 5%) for both viral variants.

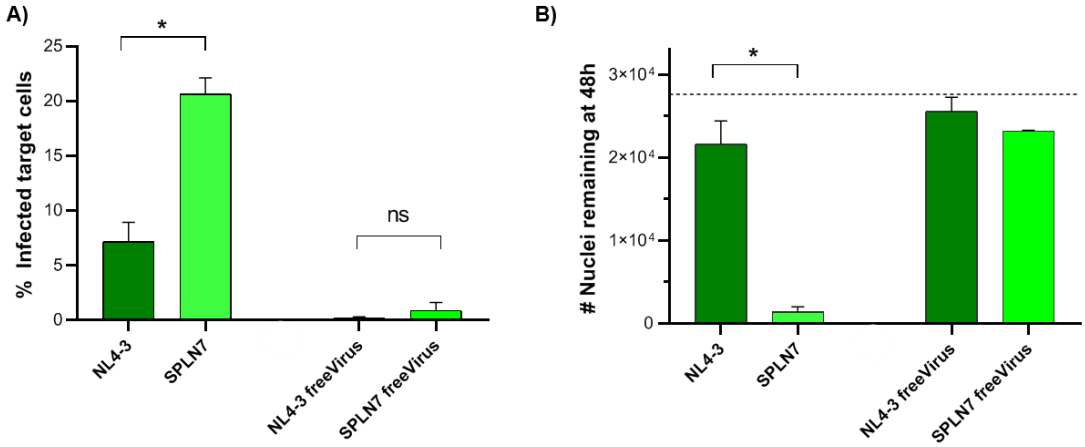

Figure 3.15. Viral transfer of spleen-derived HIV envelope variant SPLN7. U937 cells were infected with NL43-IRES-GFP or SPLN7-IRES-GFP and added to Alexa647-labelled target TZM-bl cells. Coculture conditions and readout were as outlined in 2.2.11. An equivalent amount of donor cells was seeded without targets and the cell-free fraction was collected at 12h and added to equivalent target cells for the free-virus controls. **A)** Percentage of infected target cells. **B)** Number of cell nuclei remaining per well of a 96-well plate (after PBS washes for donor cell removal). The dotted line indicates the average observed number of nuclei in the absence of donor cells or free virus. Data indicates the mean and standard error of three independent experiments. * = $p < 0.05$ by unpaired two-sided student t-test with Welch's correction. NS = not statistically significant

Visual inspection of cocultures from SPLN7-donors also revealed the presence of large syncytia and extensive cell death, which we predict would be from syncytia formation. Nuclei counts by high content microscopy (after donor-cell removal wash steps) confirmed that there was a dramatic and significant reduction in the number of target cells present at the end of the

coculture period (~15-fold reduction compared to NL4-3, $p < 0.05$), when SPLN7 infected cells (but not free virus) were used as donor cells (Fig. 3.15-B). Live imaging of SPLN7 cocultures (U937 donor cells infected with SPLN7-IRESeGFP) allowed visualization of frequent donor:target cell fusion and rapid subsequent fusion with adjacent target cells in a chain-like fashion (see supplementary video S3). To confirm that the increase in CCTH observed for SPLN7 was not solely due to donor:target cell fusion, we performed a similar experiment, where the proportion of infected target cells at 48h was assessed by flow cytometry, using stringent gating to only consider normal-sized TZM-bl cells. This analysis revealed similar results to those shown in Fig. 3.15-A (data not shown). Together, these observations strongly suggest that the SPLN7 HIV envelope has an enhanced viral-transfer capacity that is dependent on cell-cell contacts. Furthermore, use of SPLN7 dramatically increased cell-cell fusion, syncytia formation and target cell death. These findings emphasize the importance of using experimental settings and readouts that allow absolute quantification of target cell infection. In the above example, the decimated number of TZM-bl target cells for the SPLN7 condition would likely result in a lower luciferase signal than for NL4-3 (Fig. 3.15-B: ~300 vs. ~1400 infected target cells per well respectively). This would incorrectly predict a lower CCTH potential of this strain. Finally, we also performed pilot experiments with Spln7-infected donor U937 cells and Jurkat cells as targets. In this setting we observed some evidence for both increased viral transfer and syncytia formation for Spln7-infected donor cells compared to the NL43-infected controls, although the difference between both groups was smaller and more variable than in the TZM-bl setting (not shown). Overall, Spln7 was discontinued as an envelope-candidate for robust CCTH analysis, due to its high toxicity in the TZM-bl setting and because the modest increase of viral transfer in the Jurkat setting did not justify the additional layers of complexity which are introduced in the analysis by the occurrence of syncytia.

3.6 Discussion

The overall aim of this thesis is to further resolve the intersection of HIV and F-actin in the context of cell-cell viral spread. This chapter aimed to define, refine and validate the methodology that would be used over large sections of this thesis to specifically study the complex process of direct CCTH. Therefore, it was important to consider each aspect of our methodological approach to ensure; i) that the selected experimental conditions allow the process of interest (actin-dependent CCTH *in cis*) to occur at high levels and with minimal interference of confounding factors (e.g. free virus infection), ii) a well-defined readout, and iii) the ability to reliably detect and quantify (even small) changes in CCTH upon perturbation of the system (e.g. by treatments that affect the actin cytoskeleton).

Before optimizing the CCTH assay-parameters, we first validated one of the principal premises of this work, which is that there is a physical interaction of Gag with F-actin in HIV-infected myeloid cells. To this end, we used a BiFC approach, as previously described by Chen et al. for an equine lentivirus [606]. This involved fusing complementary fragments of the Venus fluorescent protein to each HIV-Gag and Actin. Indeed, using this approach we could confirm that in U937 cells, these proteins come in close enough proximity to allow Venus fragment complementation and therefore fluorescence. Furthermore, this interaction was specific to Gag-Actin, as indicated by the much brighter fluorescence of this BiFC pair compared to Gag-Tubulin, even when Actin and Tubulin were expressed at similar levels and under identical conditions.

Of note, previous literature had suggested and convincingly supported a Gag-Actin interaction (see 1.5.5 and [451,461-463,608]). Despite the important contributions of these early studies to the field, the methodology used in each case had some noteworthy limitations. First, many used cell-fractionation approaches to study HIV–F-Actin interactions [461,462,608]. This involves cell lysis and detection of Gag in the "cytoskeletal" (detergent insoluble) fraction. Since the cellular context is completely disrupted in this scenario, and proteins may no longer be in their native conformations or may aggregate with reduced specificity, this approach bears the risk of potential artefacts. Second, most of the previous studies have independently expressed Gag via transfection or other non-lentiviral methods [451,462,463,608]. The studied interaction would thus occur in the absence of other viral proteins (and their associated cytoskeletal changes), and Gag expression levels may be very different from those associated with HIV infection. In addition, some studies partly used cells of non-human origin for their observations, including insect cell lines [451], and murine [608] or simian [463] fibroblasts.

Other studies succeeded in assessing Gag-Actin interactions by imaging approaches in unlysed cells [463,608,609]. While this approach is more "natural" than cell-fractionation, the fixation and membrane-permeabilization steps used still prevent visualization of interactions in living cells (and in real time). As an example of the above-mentioned limitations, we comment on the most recent of these studies by Poole et al. [463], although it should be noted here that it is not our intention to present this study in a critical light (we simply aim to highlight the methodological aspects which were open for refinement in subsequent studies). Their elegant use of the highly sensitive technique of fluorescence resonance energy transfer (FRET), which can detect protein interactions with distances up to a maximum of 100 Å, suggested a highly intimate Gag-Actin physical association. However, the fixed cells used in this study were transfected with Gag-Pol in a non-lentiviral context. The FRET partners corresponded to indirectly detected Gag (anti-p24 primary + secondary antibody) and labelled-

phalloidin, rather than Gag and Actin themselves. Furthermore, these experiments were performed with human epithelial or simian fibroblast cells (HeLa and COS, respectively), which are not of HIV-relevant lineages.

Overall, our BiFC results presented here complement, refine and expand previous observations that support an intimate physical interaction between HIV-Gag and Actin. Importantly, our study is the first to confirm this interaction in intact and living cells of human hematopoietic/myeloid lineage and in the context of cellular HIV infection using a highly sensitive method. However, from our observations alone (bright but diffuse cytoplasmic signal without apparent membrane enrichment) we are unable to conclude whether association of Gag occurs preferentially with F-actin vs. G-actin, or for Gag-monomers vs. Gag-oligomers. Our interpretation of the earlier cofractionation and the more recent FRET data agrees with those authors that an interaction with F-actin seems more likely. It should also be noted that neither our study nor the others mentioned above have yet proven a direct protein-protein interaction between Gag and Actin. At this time, it cannot be excluded that their interaction is mediated by a third unidentified protein or as part of a of a larger complex. This seems possible given the unrivalled promiscuity of cellular Actin (see Figure 1.5) and the fact that HIV-Gag shows very low homology to all classical actin-binding domains [462]. One way to exclude this possibility could be to perform BiFC or FRET with highly purified recombinant proteins *in vitro*.

Having confirmed that Gag associates with cellular Actin in HIV-infected myeloid cells, we continued with the second major aim of this chapter, which was to establish and characterise a robust assay to specifically study CCTH (*in cis*) from this cell type. We first reviewed previous CCTH assays from the literature, focusing on their strengths and limitations. Based on this, we selected and optimized the various experimental parameters, until we obtained a system that met the desired requirements for this study. The resulting CCTH assay uses infected U937 cells as HIV-donors and either Jurkat T-cells or adherent TZM-bl cells as targets. The U937:Jurkat system is more biologically relevant (i.e. HIV transfer from myeloid donor cells to target CD4TC in a dense 3D environment), whereas the use of adherent TZM-bl target cells provides important technical advantages. In both cases, the readout corresponds to productive target cell infection (measured by detection of viral-encoded *de novo* GFP expression by flow cytometry or high content microscopy), which allows quantification of both the absolute and relative number of productively infected target cells in a mixed population, without requiring cell lysis or indirect viral detection steps. Importantly, infection transfer in our system displays a strongly linear dependency correlation with the number of infected donor cells added (within individual experiments). This was expected and also

consistent with observations from previous studies [88,127]. Therefore, we expect the assay to be able to detect even minor changes in CCTH performance when donor or target cells within an experiment are subjected to different treatments. To account for the observed inter-experiment variability, an internal normalization control group (e.g. untreated) was included in every experiment of the following chapters.

We also observed cell-mediated HIV transfer to be at least one order of magnitude more efficient than infection by cell-free virus under otherwise identical conditions. Cell-free infection was assessed by; i) adding equivalent amounts of free virus (collected from donor cells in the absence of targets), and ii) the use of trans-well chambers to physically separate donor and target cells within the same well. In both cases, the relative contribution of the cell-free infection mechanism was comparable and always below 10% of the total viral transfer. Importantly, a higher efficiency of cell-mediated vs. free-virus infection has been reported in every *in vitro* study (to our knowledge) that has directly compared both mechanisms. However, the magnitude of the reported efficiency differences varies considerably. While some studies with homotypic T-cell systems have reported fold changes in the 10^2-10^4 range [126,127], our findings are consistent with those of [83,86,87,91,124], all of which observed a ~10 fold higher efficiency of CCTH compared to free virus. Importantly, the latter three studies used infected myeloid cells (macrophages) as HIV donors and therefore are of particular relevance to this study. However, while the nature of the involved cell types likely plays a critical role in determining the efficiency of CCTH, a multitude of other reasons could also account for the discrepancies reported in the literature (see section 1.2.4).

Besides the obvious role of different experimental conditions, the choice of readout plays a critical role. For instance, Chen et. al calculate an efficiency fold-difference of either 92 or 18,000 in the same system, depending on how their readout is interpreted. Other studies also used endpoint readouts that require lysis of the cell population. Examples include qPCR detection of *de novo* synthesized viral DNA [87,91,239] or luciferase-based assays with target cells encoding a compatible LTR-induced reporter [94,226,483,588]. One disadvantage of these approaches is that they only allow relative quantification of target cell "infection" over a baseline signal. Unfortunately, this limits the possibility of comparing the obtained data to that of other studies and impedes assessing the kinetics of CCTH in absolute terms (e.g. percentage of infected target cells or infection transfer efficiency).

Readout approaches that allow absolute quantification of infected targets at the single-cell level are therefore preferable. However, because HIV can enter cells by multiple ways (some of which result in viral degradation and/or do not lead to viral infection), we consider the distinction between "viral particle transfer" and "infection transfer" of essential importance.

In some studies, assessment of CCTH was limited to detection of physical transfer of viral material (e.g. Gag) from donor to target cells. This was because cells were analysed after only short coculture periods [587], or due to the presence of antiretrovirals in the coculture [586]. The drawback of not accurately distinguishing between the two scenarios is also shared by approaches that rely on Gag detection (i.e. via Gag-GFP fusion protein or p24 intracellular staining). This is evidenced by the FACS plots in [86,88,127], where positive events in the target-cell gate appear as gradual smears rather than two distinct populations. Groot et al. also reported that part of their readout Gag signal was due to extracellular virus adhered to target-cells. Indeed, some of the above-mentioned studies confirmed that a large fraction of the observed "HIV transfer" did not lead to productive target cell infection, even if cells were incubated under favourable conditions [91,586]. In contrast, our assay is "blind" to viral particle transfer without subsequent infection because the GFP reporter encoded in HIV-IRESeGFP is not actively packaged into virions. Indeed, fusion of these particles (even at high concentrations) in the presence of antiretroviral drugs did not increase target cell fluorescence (not shown). In summary, our CCTH system presents some advantages over alternative methods previously used in the literature, in particular the ability to distinguish between productive "infection transfer" and "transfer of viral material", which may or may not lead to target cell infection.

As a proof of concept for our study, we were also able to confirm involvement of the F-actin cytoskeleton in CCTH. Pre-treatment of donor cells with Cytochalasin D reduced cell-mediated viral transfer to target cells, without impairing free virus particle release. The effect was moderate (~30% reduction) but statistically significant. While Jolly et al. reported a stronger effect of ~70% reduction [239], our results are in line with those of [123,125,127], who observed 20-50% reductions with Cytochalasin D in their CCTH systems. In any case, the magnitude of these observed effects is likely underestimated, given the rapid drug-effect reversibility after washing [239,610]. Therefore, we predicted actin remodelling to play a significant role for outbound CCTH "*in cis*" from myeloid cells, and this was later confirmed in Chapters 4, 6 and 7. Importantly, the drug pre-treatment used here did not impair cell viability or cell-free HIV release. This observation therefore adds to a long list of conflicting reports on whether actin-remodelling plays an important role for HIV budding (see 1.5.7). Our interpretation of this controversy is that, while perturbation of the actin cytoskeleton may be able to impair free virus release under certain conditions, the contribution of the actin cytoskeleton for cell-mediated HIV transfer is always greater than for free HIV budding. Therefore, and since the contribution of free virus to total HIV transfer is minimal (at least *in vitro*), we expect any changes in HIV transfer upon cytoskeletal modulation to be predominantly related to the cell-mediated component.

The virological synapse (VS) is believed to be the major cell-cell contact structure enabling CCTH (see 1.3.2). Using live imaging fluorescence microscopy, we confirmed formation of VS to occur in our system, as indicated by strong and sustained Gag-iGFP polarization on the donor cell towards the donor-target cell interface. One limitation of our live imaging approach is that it reduces the possibility to label or stain many different viral and cellular components to determine their participation at the VS. However, this aspect has been extensively assessed in previous studies ([85,87,233,539] and see 1.32). Our approach instead allows to study kinetic and dynamic aspects of VS-formation in real time. We observed VS formation to be invariably preceded by formation of stable donor-target cell conjugates. The initial and early phases of cell-cell contact often involved long membrane protrusions on the infected donor cell. In some cases, conjugate progression was associated with prominent morphological changes on the donor cell, which are indicative of cytoskeletal remodelling. Donor cells typically appeared roundest at the time of peak Gag-polarization. At this time, we often observed distinct Gag "buttons", which were reminiscent in shape, size and dynamics to those previously described in [125] for homotypic T-cell systems (including primary CD4TC). Hubner et al. confirmed that these VS events involved; i) HIV budding at the donor cell side, ii) "Gag-transfer" to target cells, and iii) preferential productive infection of target cells when they were previously engaged in VS [125]. In line with previous reports, we observed VS contacts in our system to last from ~10 minutes to over an hour [125,127].

To evaluate the efficiency of CCTH in our setting and to be able to compare it to other systems, we decided to estimate the "infection transfer rate" (ITR) as indicated in Figure 3.16 below. An ITR of 100% would mean that (on average) every infected donor cell is able to transfer HIV infection to a new target cell every hour. Using this formula, we estimated an ITR of ~ 1.5 % for our U937:Jurkat system. When replacing U937 by Jurkats as donor cells, we obtained an ITR ~1.6 (not shown).

$$\text{Infection transfer rate } \textit{(\% per hour)} = \frac{\text{\% Target cell infection}}{\text{\% Donor cell infection} \times \text{D:T ratio} \times \text{\#hours}} \times 100$$

Figure 3.16: Formula for calculation of "infection transfer rate" (ITR)

From all the CCTH assays in the literature, the one reported in ([125], Figure 4A) represents (to the best of our knowledge) the most directly comparable system to our approach, given their use of a similar readout and methodology. They cocultured infected Jurkat cells with fluorescently labelled MT4 target cells for 48h and (like us) used a viral construct that limits the readout to productively infected target cells. Based on the information provided by the authors, we could estimate ITRs in the range of 1-2% for this study [125]. Therefore, we

conclude that the efficiency of HIV "infection transfer" in our experiments (myeloid U937 to Jurkat T-cells) is roughly comparable to that in homotypic T-cell line systems. As expected, studies which used "Gag transfer" readouts showed much higher ITRs (i.e. 15-40%) [86,127,587]. This once again emphasizes the importance of correctly distinguishing between particle transfer and infection transfer. In summary, we propose ITR as a useful parameter to compare CCTH data from different experimental systems, provided similar readouts are used and enough information is reported.

Despite our attempts to establish a CCTH assay as robust as possible, our approach is not without limitations. For instance, it should be noted that, although valuable tools in basic science and biomedical research, cell lines do not always necessarily reflect the behaviour of primary cells *in vivo*. The implications of this for this study are discussed in depth in chapter 7. Another potential limitation of this study is the use of the NL4-3 viral strain. The rationale for choosing this strain was described in detail in section 3.4.1.2. However, one could argue that the use of an X4-tropic strain is inadequate for studying viral transfer from myeloid cells because these are poorly infected with this virus *in vitro*, and because primary X4-tropic viruses that can infect myeloid cells are rare [572,611]. That said, X4-infection of myeloid cells *in vitro* can be easily circumvented by using VSVg-pseudotyped virus. Furthermore, we consider that the tropism of the viral envelope should have little impact on the interaction of outbound HIV with the actin cytoskeleton (which is the main focus of this study). This is because tropism-defining sequence variability is mostly limited to the extracellular portion of Env revealed post CD4-binding, whereas interaction with the actin cytoskeleton occurs only via the relatively small intracellular region. Both regions are likely subject to completely different evolutionary pressures. High variability of the extracellular region is essential for immune escape and increasing cell-target range, whereas mutations that disrupt interaction with cytosolic proteins are likely counterproductive. In agreement, when we compared the NL4-3 and AD8 envelope sequences we found 85% of amino acid differences to be within gp120 (purely extracellular), whereas the intracellular region of gp41 has a 95% sequence similarity for both strains. Furthermore, the intracellular region of gp41 is evolutionarily well conserved at the physicochemical, structural and protein sequence levels (compared to gp120), even across different HIV clades [612]. We therefore hypothesize that the mechanisms of actin manipulation by outbound HIV should be relatively well evolutionarily conserved.

3.7 Chapter acknowledgements

All experiments and data analysis in this chapter were performed by the author of this thesis. Note that the personal pronoun “we” is used throughout this thesis to reflect common scientific practice and to avoid the tedious use of the personal pronoun “I”. The reader is invited to think of “we” as the author and the reader as the former guides the latter through this thesis, or as the author and his supervisory team, given the important contributions of the latter to the guidance of this work.

We sincerely thank the lab of Ronald C. Montelaro for providing the *in silico* sequences for the VN- and VC-fragments as used in [606].

Chapter 4. A systematic and literature-based screen using CRISPR to identify actin regulators involved in outbound cell-cell HIV spread

4.1 Introduction

Manipulation of the actin cytoskeleton by HIV is complex. HIV uses a multi-strategy and multi-target approach to influence the host's actin cytoskeleton in a temporally regulated and cell-type specific manner (see 1.5.2). Furthermore, the prerequisites and mechanisms for cytoskeletal manipulation are fundamentally different in HIV-infected donor cells (outbound HIV) and uninfected target cells (inbound HIV) (see 1.5.3). While the role of actin remodelling has been relatively well mapped for inbound HIV infection (see 1.5.6), the role of F-actin for outbound free virus budding remains controversial. In contrast outbound CCTH is known to depend on actin remodelling on both the donor and target cell sides (see 1.5.8 & 1.5.10), however the molecular events involved remain poorly understood. Despite considerable efforts in the field to mechanistically resolve these pathways of cytoskeletal manipulation, integrating the different observations from the literature into a unified view or model has remained elusive, mainly due to profound differences in the experimental systems used. This spans the use of different model systems (non-human vs. human cell lines of various lineages vs. primary leukocytes), experimental conditions (viral strains, coculture parameters, etc.) variables (RNA silencing, drug treatment, mutants) and readouts (particle release into the supernatant vs. particle transfer between cells vs. *de novo* productive infection of target cells). A more systematic approach could therefore be beneficial to overcome these issues, especially if it allows to assess the role of multiple actin regulators (in parallel) using standardized methods, suitable models, well defined readouts, and sufficient controls.

4.2 Aims

The overall aim of this work is to advance our understanding of the complex interactions between HIV and the cellular actin cytoskeleton. Therefore, both literature- and experimental-based approaches are within the scope of this project. From a literature point of view, many cytoskeletal regulators have been implicated at punctual steps of the HIV life cycle. However, their role at other stages of infection (e.g. inbound vs. outbound or cell-free vs. cell-cell) remains unexplored. Similarly, the role of additional and perhaps more relevant regulators (e.g. structurally or functionally related genes that are lineage-restricted to HIV target cells) remains uncharted or has not been reported. Therefore, the main aims of this chapter included:

1) To critically evaluate the literature on the F-actin cytoskeleton, in order to identify regulatory genes which may play important roles in CCTH, but whose role in this process has

not been previously considered/reported. Then, both incompletely assessed and unexplored genes would be combined to create a comprehensive panel of candidate genes that can be used to further dissect the intersection between HIV and cellular actin.

2) To employ a systematic experimental approach and the methods outlined in Chapter 3 to formally test the role of each candidate in the above-mentioned panel at the myeloid donor-cell side of the HIV cell-cell transfer process.

4.3 Materials and methods

4.3.1 CRISPR based gene editing and benchmarking of existing platforms

The DNA-editing ability of CRISPR/Cas systems has recently revolutionized life sciences and medical research. This powerful technique allows efficient modification of cellular genomes. In its simplest form, CRISPR-editing requires only two components, namely a RNA-guided DNA-endonuclease called Cas (CRISPR associated protein) and a short RNA polynucleotide (guide RNA or gRNA), which dictates the specificity of the complex by targeting the Cas protein to the DNA sequence of interest [613]. CRISPR-Cas9 is by far the most widely used CRISPR system in biology research. However, numerous strategies and a myriad of reagents now exist to express or deliver Cas9 and the associated gRNA to the cells of interest. For this work, we decided to deliver both components into our cells via transduction with lentiviral vectors, given the following advantages; i) viral vectors are the most common CRISPR-Cas9 delivery vectors, especially for *in vivo* work [614], ii) lentiviral transduction allows permanent expression of selection markers, which is ideal for establishing clonal cell lines, iii) our model cell lines are easily transducible with these vectors, and iv) our lab is experienced in both lentiviral vector engineering and efficient delivery of lentiviral constructs to primary HIV-target cells, by exploiting the ability of the SIV-Vpx accessory protein to overcome antiviral restriction factors.

Concretely, we decided to use the lentiviral constructs recommended by Feng Zhang's lab, which was one of the first to describe genome editing in human cell cultures using CRISPR-Cas9 [615]. The Zhang lab not only offers optimized lentiviral vectors, but also a wide and comprehensive set of resources (Available under: https://www.addgene.org/crispr/zhang/ and https://zlab.bio/guide-design-resources) for genome engineering applications tailored to the use of their CRISPR plasmids. For this project, we tested the third-generation vectors lentiCRISPRv2 (one vector system) and the LentiGuide-Puro plus Lenti-Cas9-Blast in combination (two vector system). LentiCRISPRv2 (LCV2) allows expression of Cas9, guide RNA and puromycin resistance from the same plasmid. In contrast, the combination approach relies on LentiGuide-Puro (LGP) delivering the gRNA and puromycin resistance, whereas

lentiCas9-Blast is required for Cas9 expression and warrants blasticidine resistance. In both cases, expression of a human-codon optimized Cas9 protein is controlled by an EF1a promoter and the gRNA is controlled by a U6 promoter [584]. For more information on these plasmids see section 2.1.6.1.

4.3.2 Proof of concept for chosen CRISPR strategy

Prior to commencing our screen, it was important to first test the feasibility of lentiviral CRISPR delivery in our model cell system. While detection of endogenous proteins (and their depletion) by either immunolabelling or biochemical assays is feasible, these methods rely on indirect quantitation, and as such are susceptible to artefacts and false negative/positive issues. Therefore, we decided to choose a readout that allowed direct and unambiguous detection of CRISPR-mediated loss of function phenotype. To this end, we generated a U937 cell line that stably expresses the visible fluorescence reporter mCherry. This allowed direct assessment of phenotype changes, without labelling steps and at a single-cell level by flow cytometry. To ensure compatibility with our CRISPR plasmids, mCherry had to be expressed from a plasmid without puromycin or blasticidine resistance. The mCherry ORF (including the upstream CMV promoter) was amplified by PCR from the vector pLVX-mCherry-N1 (Clontech) with primers designed to introduce the flanking restriction sites MluI and XbaI. This was then cloned into a variant of the lentiviral vector "pLKO.1 hygro" (Addgene #24150) which contained a multiple cloning site between the original AgeI-EcoRI sites. U937 cells were transduced with "pLKO.1 hygro mCherry" at medium MOI to ensure integration of more than one copy in the genome (there are 2 copies of endogenous genes per cell and our model should ideally reflect this). Transduced cells were then selected in the presence of hygromycin at 350 μg/mL for at least 7 days and bright homogeneous mCherry expression was confirmed by fluorescence microscopy.

We then transduced U937-mCherry cells with the LCV2 or LGP vectors encoding a mCherry-gRNA (or empty vector control) and selected with puromycin for at least 7 days (2 μg/mL). For the two-vector system approach, cells were further transduced with lentiCas9-Blast and selected for at least 7 days in blasticidine containing medium (10 μg/mL). Cells cultured in triple-antibiotic medium were found to display abnormally enlarged cell bodies and poor viability (Fig. 4.1-A,C). In contrast, cells sequentially selected for 1 week with each antibiotic led to viable cells with normal cell morphology. To assess changes in mCherry expression, cells were first stained with LIVE/DEAD Alexa647 stain (see 2.2.3) to exclude dead cells from analysis. In the absence of a mCherry-targeting gRNA, over 99% of cells were found to be positive for mCherry expression. In contrast, cells expressing mCherry-targeting gRNA showed variable levels of mCherry expression (Fig. 4.1-B). For the two vector CRISPR

approach, we tested multiple combinations of VLP concentrations for each construct (only the most successful Cas9 cell line is shown as an example). For LCV2 we did a simple dilution series of VLP concentration. We found that while both approaches led to loss of mCherry expression, the one-vector system (LCV2) had a more predictable dose-dependent effect and achieved higher levels of knockout frequency, including up to 95% mCherry depletion (Fig. 4.1-D). Cell viability was above 90% across all conditions, when cells were sequentially transduced and selected. Based on these optimization process, we confirmed the feasibility of CRISPR gene edition in our system and selected the lentiCRISPRv2 (LCV2) one-vector system for lentiviral delivery and expression of the CRISPR-Cas9 components.

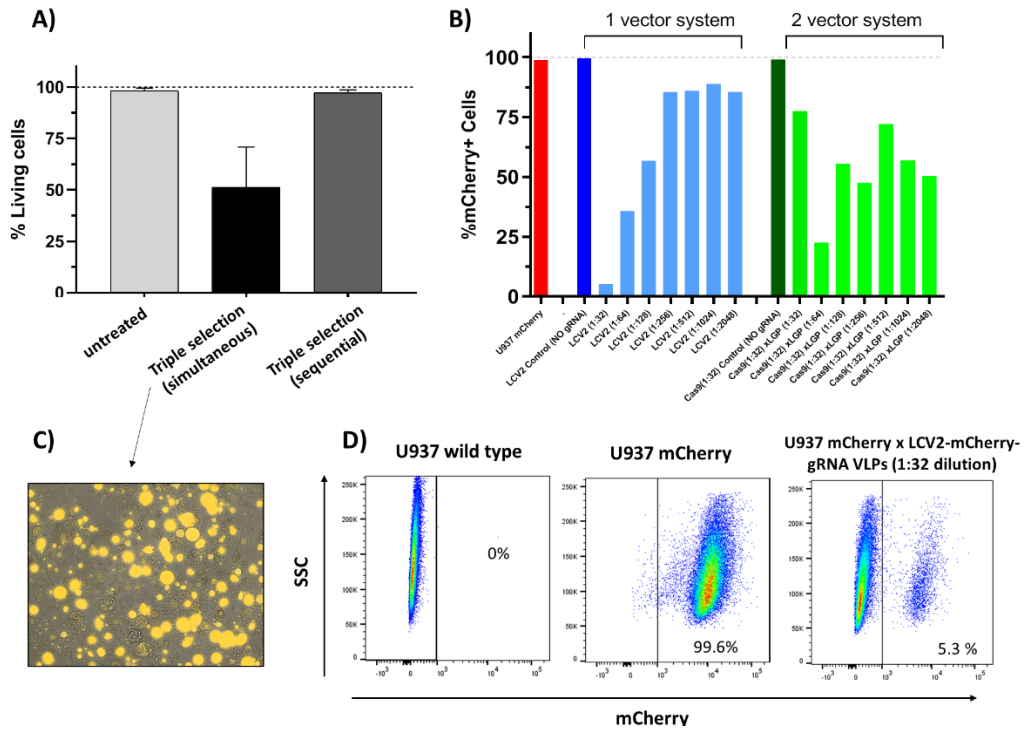

Figure 4.1: CRISPR-mediated disruption of mCherry expression (proof of concept). U937mCherry cells were transduced with lentiCRISPRv2 (LCV2) alone or LentiGuide-Puro (LGP) and lentiCas9-Blast VLPs. **A)** Cell viability of triple transduced cells at day 21, when grown in the absence of antibiotics (untreated), in the presence of hygromycin, puromycin and blasticidine (triple selection) or after sequential selection with each antibiotic for a week. **B)** U937 mCherry cells were sequentially transduced with lentiviral particles at the indicated dilutions, with antibiotic selection lasting for 7 days each. LCV2 and LGP plasmids contained mCherry-targeting guide RNA unless otherwise indicated. Cells were then stained with LIVE/DEAD Alexa647 dye and the percentage of living cells that are mCherry positive was assessed by flow cytometry. **C)** Fluorescence microscopy image of cells in triple selection medium reveals abundant cell death and abnormally enlarged cell bodies. **D)** FACS plots showing the negative and positive control for mCherry detection, as well as the condition where the highest mCherry depletion rate was achieved.

4.3.3 Titration of lentiviral CRISPR particles

For optimal comparison of CRISPR-modified cell lines, these should be transduced with identical MOIs for all gRNA conditions. We therefore performed a formal titration of our LCV2-gRNA VLP batches. The functional titration protocol was modified from [616] and carried out as follows: 15x10^3 U937 cells were seeded in 50 µL RF10 medium in the wells of a 96-well plate. A dilution series of LCV2 VLPs was added to the cells as 50 µL in quadruplicate. Cells were incubated for 48h and then 15 µL of each well were transferred to a new 96-well plate so that final well volume is 100 µL and so that each VLP dilution has two duplicates in plain RF10 medium and two duplicates in RF10 medium containing 1 µg/mL puromycin. 72h after replating, 10 µL Alamar Blue solution were added to each well and plates were incubated for 2h at 37°C. The amount of resorufin produced is directly proportional to the number (and metabolic activity) of cells in culture (see 2.2.3). For each VLP dilution, the Alamar Blue signal for puromycin containing wells was divided by that of matching wells without puromycin. This value was interpreted as the MOI, as suggested in [616]. For a MOI = 0.5, the VLP dilution was selected that led to closest of 50% survival of transduced cells in the presence of puromycin selection. The titer could vary considerably between different LCV2-gRNA batches (Fig. 4.2), thus emphasizing the importance of the titration step. Of note, all LCV2 VLPs were produced under identical conditions (see 2.2.6) and each aliquot was used only once after thawing.

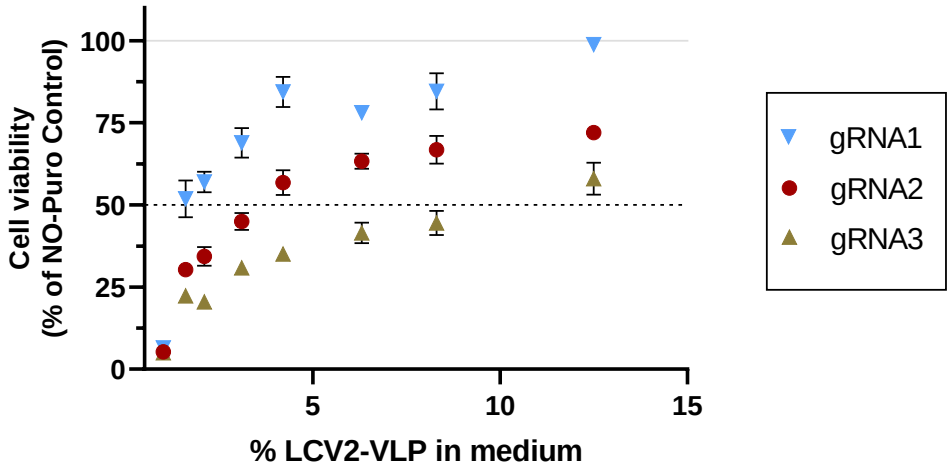

Figure 4.2: Functional titration of LCV2-gRNA CRISPR VLPs. U937 cells were transduced with a dilution series of CRISPR VLPs as described above. The titration results for three different LCV2-gRNA batches are shown. The dotted line indicates 50% survival of transduced cells in selection medium, compared to transduced cells in non-selection medium.

4.3.4 Depletion of endogenous target proteins via CRISPR

To confirm that we could also achieve CRISPR-mediated disruption of endogenous genes, we tested the ability of our LCV2 lentiviral approach to knock-out the CD4 gene in U937 and

Jurkat cells. To this end, cells were transduced with LCV2 CD4-gRNA and non-targeting control gRNA at a MOI = 0.5. At 48h post-transduction, puromycin selection was started (1 µg/mL). Cells were kept in culture at concentrations between 10^5-10^6 cells/mL for 13 days. CD4 phenotyping was performed by staining with a CD4 antibody directly conjugated to Alexa647 (Biosearch#17422) and flow cytometry analysis, at multiple time points after transduction. This revealed that when cells were transduced with LCV2 CD4-gRNA, the percentage of CD4+ cells in the population decreased over time, dropping below 50% from day 11 after transduction (Fig. 4.3-A). In contrast, cells transduced with LCV2 CTRLgRNA#1 retained normal CD4 expression. Note that the slight drop of both groups at day 3 is expected, given the start of puromycin selection at day 2, which results in some cell death.

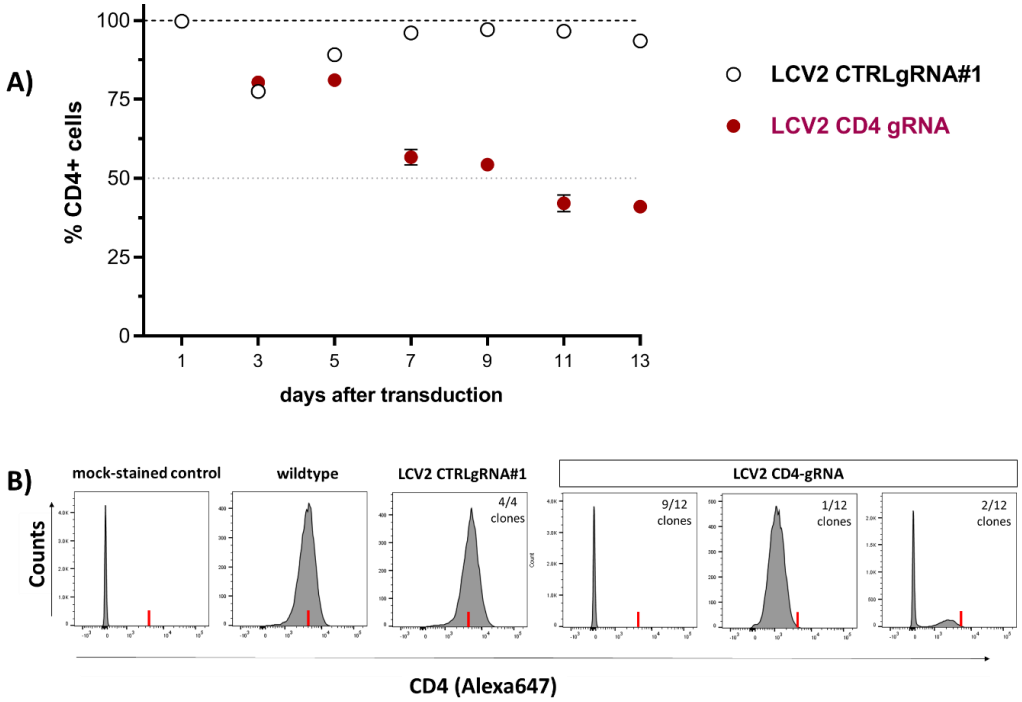

Figure 4.3: Depletion of endogenous CD4 by CRISPR-gene editing. A) U937 cells were transduced with the indicated CRISPR VLPs at a MOI=0.5 and monitored for CD4 expression over time. Puromycin selection (1 µg/mL) began at 48h post-transduction. B) CD4 phenotyping of U937 clones after single-cell sort and clonal expansion. Mock-stained control underwent same procedure as other samples but without adding the anti-CD4 Alexa647 antibody. The red line indicates the mean fluorescence intensity of the wildtype control group.

To further test whether we could isolate and grow homozygous knockout clones (CD4 -/-), we repeated the experiment and single-cell sorted at day 7 into a U-bottom 96-well plate with pre-conditioned medium as described in 2.2.1.3. Clones took 2-3 weeks to grow and were puromycin resistant. Of the phenotyped clones, 75% (9/12) completely lacked any detectable CD4 expression, which strongly suggests a CD4 -/- genotype (Fig. 4.3-B). On the other hand, intermediate expression (1/12 clones) is suggestive of a hemizygous condition (CD4 +/-), whereas bimodal expression (2/12 clones) likely indicates that these populations were not

clonal. Altogether, these observations confirmed the feasibility of fully knocking-out endogenous genes at high frequency in the U937 cell line via LCV2 lentiviral delivery of Cas9 and a single gene-targeting guideRNA.

4.3.5 Standardised procedure for CRISPR delivery

A standard procedure was adopted to minimize the sources of variability between different U937 CRISPR groups used for viral transfer experiments. U937 wildtype cells were seeded at 10^5 cells/well (500µL) in 48-well plates. Cells were then transduced with previously tittered LCV2-gRNA VLPs at a MOI=0.5. Puromycin selection (1 µg/mL) was started at day 2 after transduction (except for untransduced control). Transduced cells were kept under antibiotic selection for additional 10 days, following a structured passaging strategy (Fig. 4.4) to maintain cell concentrations within ~10^5-10^6 /ml and cell densities within ~10^5-10^5.7 /cm^2. For experiments, cells were switched to RF10 medium and infected at day 12 post-transduction. Thus, all groups compared within an experiment are derived from the same parental wildtype cell line and share identical passage number and culture history conditions.

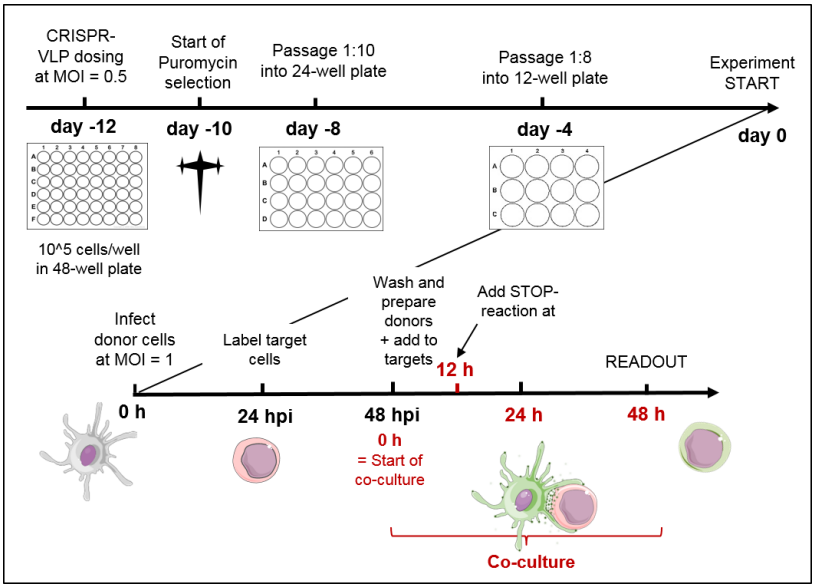

Figure 4.4: Standardised procedure for CRISPR delivery and viral transfer assay timeline.

The duration of puromycin selection was decided after consideration of two factors. On one hand, there is the "heterogeneous CRISPR effect" (see Fig. 4.5). This dictates that when cells are bulk-treated with CRISPR lentivirus and antibiotic selected, most surviving cells will have both gene copies edited, but this only results in loss of protein expression within a subset of the population. A (variable) proportion of cells is always expected to retain the wildtype phenotype, due to the occurrence of in-frame mutations. Therefore, should the loss of the targeted gene result in a fitness cost, it is expected that the wildtype-phenotype cells will gradually out-grow mutant-phenotype cells over time. Thus, bulk-treated cells should not be

kept in culture for prolonged periods of time. On the other hand, protein depletion is a gradual process that depends on each protein's turnover within the cells, so that a certain time is required between gene-edition and loss of protein. While the half-life of different proteins in human blood cells can vary widely (i.e. from ~10 to >1000 h) [617], here we assume a practical "maximum half-life" of ~24h (i.e. one cell cycle). This is because the protein pool is expected to be halved after each cell division (from the point of biallelic gene disruption). Assuming this maximal half-life, any protein pool would be depleted beyond 99% within 7 days of gene disruption. However, some additional time is required to allow for Cas9 expression, multiple rounds of gene-editing and repair, as well as cell recovery from puromycin selection.

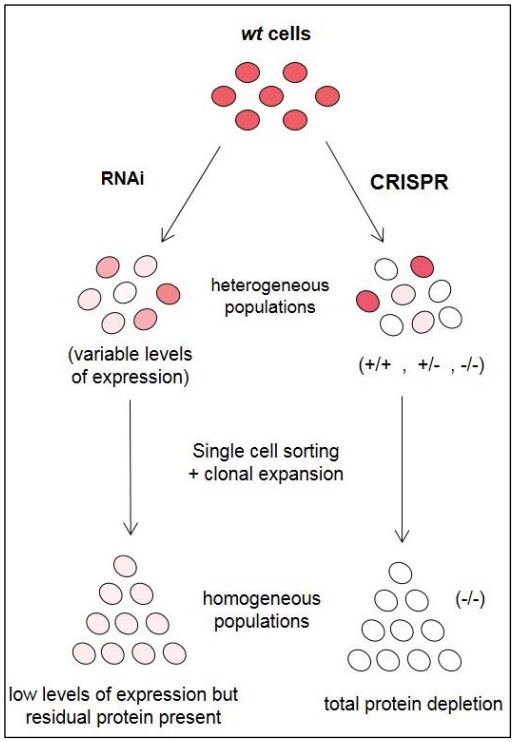

Figure 4.5: The heterogeneous CRISPR effect. (See paragraph above for details).

4.3.6 Generation and verification of clonal CRISPR cell lines

Clonal CRISPR cell lines were generated by single cell sorting at day 7 after bulk-treating the parental cell population with LCV2-VLPs (with puromycin selection starting 48h post transduction). Single-cell sorting was performed as described in section 2.2.1.3, into plates with medium contained puromycin at 1 μg/mL, and clones were allowed to grow under for 2-3 weeks. Retrieved clones were phenotyped by either antigen-staining (for antibodies used in this study see Table 2.12) or genomic DNA sequencing as described further below.

For surface antigen staining, monoclonal antibodies directly conjugated to fluorophores were used (all primary antibodies used in this study are outlined in Table 2.12. 10^5-10^6 cells

were first washed in PBS, and then 2µL antibody were added to the cells in 50µL PBS and mixed. Cells were incubated with the antibody for 30 minutes at ambient temperature in the dark, then the staining solution was removed, and cells were washed once with PBS before fixing for 10 minutes with 4% (w/v) paraformaldehyde and resuspending in FW buffer. For intracellular antigen staining, cells were first washed in cold PBS, then fixed in 200µL Cytofix Buffer (BD Biosciences #554655), for 20 minutes at 4ºC in the dark. Cells were washed once with FW buffer and permeabilized by adding 200µL cold Phosflow Permeabilization Buffer III (BD Biosciences #558050) for 2 minutes at 4ºC in the dark. Cells were then washed and resuspended in 50µL FW buffer containing a primary unconjugated antibody and incubated for 30 minutes at 4ºC in the dark. Wells were washed twice and then resuspended in 50µL FW buffer containing a fluorescently labelled secondary antibody (see 2.1.8) at 1:400 dilution. Plate was incubated at room temp. for 20 minutes in the dark then washed twice and resuspended in FW buffer for flow cytometry analysis. Positive controls (stained wildtype cells) and negative controls (cells naturally lacking antigen and/or unstained control) were included in every antibody phenotyping experiment.

For genomic DNA sequencing, a pair of target-specific surveyor primers (see Table 2.11) was used to PCR-amplify the genomic region targeted by the gRNA (300-800bp amplicons). Genomic DNA extraction from CRISPR-edited cells was performed as described in [618]. Briefly, ~10^6 cells were pelleted at 500×g for 3 minutes. The supernatant was removed, and the cell pellet was resuspended in 100µL QuickExtract solution (Lucigen #QE09050), then transferred to PCR-tubes and incubated in a thermocycler for 15 minutes at 68°C , followed by 8 mins at 95°C and then held at 4°C until use. Of this cell-lysate solution, 2µL were used as template for genomic PCRs. The PCR was otherwise set up as described in section 2.2.4.1. The PCR-DNA was purified with a commercial spin column kit (Promega #A9281) and 5µL were used to visualize the PCR product by electrophoresis on a 2% agarose gel with a 100bp DNA-ladder. Where correct amplicon size was confirmed, a sequencing reaction was set up with either the forward or reverse surveyor primer. To this end, 30ng of genomic DNA were mixed with 3.2 pmol primer in a volume < 5µL and analyzed by Sanger sequencing at a NATA-accredited core facility. Only high-quality DNA sequence traces were used to confirm frameshift mutations. Sequencing data was analyzed using Sequence Scanner Software v2.0. Note that in the context of this work, the term homozygous knockout (-/-) refers to cellular clones where both gene copies have been edited in a way that results in loss of native protein expression due to introduction of frameshifts or premature stop codons in the protein coding sequence.

4.3.7 Clonal CRISPR cell lines generated in this study

Parental cell line	Genotype/ Phenotype	Test method	Phenotype/genotype verification
U937 and Jurkat	CD4 -/-	Immunofluorescence staining	Surface staining with Alexa647-conjugated CD4 monoclonal antibody (Biolegend #317422) and analysis by flow cytometry as described in 2.2.10. Confirmed >98% signal reduction compared to wildtype controls.
U937	ICAM1 -/-	Immunofluorescence staining	Surface staining with PE-conjugated ICAM1 monoclonal antibody (BD # 347977) and analysis by flow cytometry as described in 2.2.10. Confirmed >95% of signal reduction compared to wildtype control.
U937	Dia2 -/-	Genomic DNA sequencing	A 1 bp deletion at the position #17 of Dia2-gRNA (5'-GAACCGGGCCGCCAATGAAG-3'), resulting in a frameshift within exon 1 that leads to >95% loss of native protein sequence.
U937	Wave2 -/-	Genomic DNA sequencing	3 point-mutations and a 1 bp deletion at position #17 of Wave2-gRNA (5'-TGAGAGGGTCGACCGACTAC-3'), resulting in a frameshift within exon 2 that leads to >74% loss of native protein sequence.
U937	Cofilin -/-	Genomic DNA sequencing	A 1 bp deletion at position #18 of Cofilin1-gRNA (5'-GCGTAAGTCTTCAACGCCAG-3'), resulting in a frameshift within exon 1 that leads to >80% loss of native protein sequence.
U937	Cdc42 -/-	Genomic DNA sequencing	A 1 bp deletion at position #17 of Cdc42-gRNA (5'-ACAGTCGGTACATATTCCGA-3'), resulting in a frameshift within exon 1 that leads to >84% loss of native protein sequence.

Table 4.1: Clonal CRISPR cell lines generated in this study.

Note that the frequently observed mutations at or near position 17 (of the gRNA target sequence) are consistent with accumulating observations that SpCas9 (as encoded in the LCV2 vector) preferentially cuts the target DNA 3-bp upstream of the PAM recognition sequence "NGG" [619], which sits immediately after the 20-bp sequence recognized by the gRNA.

4.4 Design of CRISPR panel

The design of our CRISPR panel was based on the primary aim of this chapter, which is to systematically dissect the network of actin regulatory and remodelling proteins which enable CCTH. This includes both the further characterisation of previously reported HIV-manipulated genes, as well as exploration of other regulators that may not have been previously considered. The rationale for the inclusion of these genetic targets in our panel and their potential relevance to this work is briefly discussed in the subsections below. Note that a full list of all CRISPR targets and gRNAs used in this study is provided in Table 2.9 (see section 2.1.7.2).

4.4.1 Known HIV-manipulated actin regulators

In our published review [66], we discussed many cytoskeletal regulators whose manipulation by HIV is known to have a functional consequence for the HIV life cycle or HIV pathogenesis. However, while the role of some of these proteins is prominent and/or well-defined at specific stages of the viral life cycle, their potential involvement at other stages of viral replication (in particular CCTH) has not been reported. For example, the key role of many actin regulators (e.g. RhoA, Moesin, Cofilin, etc.) for inbound virus is now well understood, yet whether these proteins have a functional relevance for outbound HIV remains unknown. However, since actin dynamics and/or actin structures have been associated with almost every stage of viral replication [66], cellular actin regulators involved in one step of the viral life cycle are likely to be able to affect other steps to a certain extent. We therefore decided to include gRNAs against all genes reviewed in [66], in order to formally assess their role in CCTH with methods specifically designed for this purpose.

4.4.2 Novel gene candidates

During our extensive review of the literature, we also identified other actin regulatory proteins that have few or no reported associations with HIV, but which we hypothesize may be important unexplored targets of HIV manipulation and/or of critical importance to the viral life cycle. These novel hypotheses are based on those regulators playing important cellular roles in actin cytoskeleton regulation and/or remodelling, as well as meeting at least two of the following criteria: i) gene is evolutionarily and/or functionally related to a well-known HIV-manipulated gene, ii) expression of this gene is restricted to and/or enriched in cells of hematopoietic lineage, iii) protein found by ourselves and/or others to be incorporated within HIV virions, and iv) protein known to bind both F-actin and HIV components directly. Various examples are introduced below.

Rac2 is a closely related Rac1 homologue (92% protein sequence identity) [620] and it is the hematopoietic-specific Rac subfamily member. While both Rac1 and Rac3 are expressed ubiquitously, Rac2 expression is strongly and selectively enriched in cells of the hematopoietic lineage [321,598,621]. The functional differences between Rac1 and Rac2 are not well characterized, but similar and partly redundant functions are expected [499,621]. Importantly however, Rac2 is not an essential gene. Rac2−/− mice develop normally and are fertile [622], whereas Rac1 -/- mice embryos die pre-gastrulation [623]. In the context of HIV, Rac2 was found alongside Rac1 in virions produced from both macrophages and T-cells [454,504]. It has also been shown that both Rac1 and Rac2 can interchangeably be recruited to Nef-induced multiprotein complexes, which dysregulate cellular cytoskeletal functions

[499]. Importantly, most commercial kits used to measure "Rac1 activation" are not able to distinguish between Rac1 and Rac2. Therefore, the strong "Rac1" hyperactivation often reported in the literature may in reality be a sum of strong Rac1 and Rac2 activation, especially in cells of hematopoietic lineage. However, no studies have specifically looked at the role of Rac2 for HIV infection. We therefore decided to include a Rac2 gRNA in our CRISPR panel and hypothesized that Rac2 could play an equal or more important role than Rac1 in HIV infection and/or cytoskeletal manipulation. If this were the case, Rac2 would represent an excellent alternative to Rac1 as pharmacological target, given its lineage-restricted expression and dramatically more dispensable nature *in vivo*.

Rif is a lesser known member of the Rho-GTPase family that can nevertheless coordinate a vast range of actin remodelling events in the cell [624]. Unlike the ubiquitous RhoA/Cdc42/Rac1, Rif displays a more restricted expression pattern and is highly enriched in leukocytes [321,598]. Importantly, Rif can interact with the formins Dia1 and Dia2 and induce filopodia formation via pathways fundamentally different from those used by Cdc42 [366,367]. Like Cdc42/Rac1, Rif was upregulated upon Nef expression in podocytes [498]. Altogether, this suggests that Rif may play an important role in cytoskeletal remodelling in HIV infected cells, in particular HIV-Filopodia formation and CCTH. Since Rif -/- mice are viable and have normal leukocyte counts [625], Rif could be an excellent alternative pharmacological target to Rac1/Cdc42, if it was found to play similar or more important roles for HIV infection.

Syk. The prominent role of ZAP70 for CCTH at the donor side of the T-cell VS was addressed in section 1.5.10. However, ZAP70 is virtually only expressed in T-cells. Syk is a functionally related family member, which is abundantly expressed in myeloid cells [321,598]. Thus, Syk is a good alternative candidate for mediating ZAP70's functions in HIV-infected myeloid cells. In agreement, Syk was able to replace ZAP70 in the Nef-assembled multi-kinase complexes in promonocytic TF1 cells [626]. Furthermore, Syk can phosphorylate and activate Vav1 [627], which is an important activator of Rac1 and Cdc42. We hypothesized Syk could play a critical role for CCTH from myeloid cells.

Cortactin and its hematopoietic homologue HCLS1, represent the only type-II NPFs for the Arp2/3 complex known in mammals [302]. So far, known associations between Cortactins and HIV are limited to coincidental findings of omic-oriented studies. On one hand, substantial amounts of HS1 were found in virions produced in H9 cells, reaching up to 1% of the molar abundance of Gag [452]. On the other hand, Cortactin activating-phosphorylation was found to be increased in HIV infected monocytes [491]. The interplay between cortactin and HIV has not been specifically investigated. However, given the multifaceted role of this actin

regulator in many cellular functions [628], a more prominent role of cortactin in HIV infection cannot be excluded. Indeed, several features make Cortactin an attractive candidate for HIV manipulation. Not only is it involved in regulation of cell adhesion and migration (reviewed in [629]), but it also localizes to the actin cortex, where it regulates actin dynamics by interacting with the Arp2/3 complex [630]. Furthermore, while virtually all NPFs have proline-rich domains which allow them to interact with SH3-bearing proteins, cortactins themselves also have a C-terminal SH3 domain [302], which in theory puts them at risk of direct manipulation by Nef. Furthermore, Cortactins can bind PIP2 [631] and thus are likely to colocalize with Gag at the PM, where they could serve as a bridge between the virus and Arp2/3 and/or F-actin. Indeed, another proteomics study identified Cortactin as a potential interaction partner of outbound Gag [632]. HCLS1 is also recruited to the IS, where it is important for F-actin accumulation [633], and thus it may play a similar role at the VS. Of note, HS1 expression is strongly restricted to cells of hematopoietic origin [321,598].

ITGAM. The prominent role of the integrin LFA1 for HIV infection is well established (reviewed in [84]). ITGAL encodes the α-chain of LFA-1, whereas ITGAM encodes an alternative α-chain which combines with the β2-chain to form the integrin MAC-1. Both ITGAL and ITGAM have been found on the surface of HIV virions [504,634], yet the role of MAC-1 for CCTH has not been explored so far. MAC-1 and LFA-1 have related functions, but since ITGAM is strongly enriched in myeloid cells [321,598], it is of particular relevance to this study.

Coronins can interact with both F-actin and microtubules and exhibit moderate ability to regulate cytoskeletal changes. Coronin-1 forms homotrimers that bind both F-actin and the PM, and thus can link the cytoskeleton to the PM [635]. To our knowledge, no previous studies have specifically looked at a possible interaction of Coronin with HIV. However, it was coincidentally found in two omic studies. Coronin1 was upregulated (both mRNA and protein) in PBMCs from HIV+ patients [636], and it was found within virions produced by T-cells [454]. Coronin1 also assembles at the IS, where it can influence F-actin and Arp2/3 polarization [637,638]. Since coronins comprise a unique class of actin regulators, they may represent a previously unexplored link of HIV to the cytoskeleton. We decided to target Coronin1A in our panel, given its leukocyte-restricted expression [638].

Angiomotin is a protein best known for its important roles in angiogenesis. However, Angiomotin has been recently shown to play a role for outbound free HIV. Angiomotin depletion impaired HIV particle production by arresting budding virions at the PM, whereas its overexpression enhanced both particle release and infectivity [639]. Angiomotin is also now known to directly bind F-actin [640] and Gag [639] and thus it may represent an important

link between HIV and the cytoskeleton. Of note, the role of Angiomotin for CCTH transfer has not been explored.

Capping proteins tightly bind free barbed ends to potently block addition of further monomers [641]. In addition, they can also bind barbed end occupied by formins and promote formin dissociation [642]. Thus, capping proteins antagonize filament elongating proteins such as formins or ENA/VASP by multiple mechanisms [512]. Since no previous study has evaluated a potential functional interaction of capping proteins with HIV, it was worthwhile to represent this protein class in our panel. We selected CAPZA1, CAPZB and CapG as CRISPR targets in our panel, given their abundant and leukocyte-restricted expression [598], and because we and others have found these proteins within virions produced by HIV infected myeloid cells (unpublished and [504]). Of note, these proteins were also found to be upregulated upon Vpr expression in macrophages [643].

CAP-1. Despite its misleading name, CAP-1 (Adenylyl cyclase-associated protein 1) does not functionally interact with adenylate cyclase in humans. Instead, CAP1 is a multidomain protein believed to serve as a unique bridge for linking diverse signals to the actin cytoskeleton [644]. While the involved mechanisms are poorly understood, CAP1's abilities to modulate the actin cytoskeleton are conserved from yeast to mammals and may represent a unique but powerful arm of cytoskeletal regulation [645]. CAP-1 can directly bind G-actin [646], as well as various key cytoskeletal regulators, including Cofilin and Profilin [645]. To our knowledge, no previous studies have specifically evaluated the role of CAP1 in HIV infection. However, cellular CAP1 protein was found within the cores of HIV virions produced in THP1 cells [647], and CAP1 expression was upregulated both at the transcriptional and protein level in PBMCs from HIV+ patients [636]. Furthermore, CAP1 expression is strongly enriched in leukocytes [598]. We therefore decided to target CAP1 in our panel, to explore the possibility that HIV manipulates this protein to hijack its versatile actin-cytoskeleton regulatory abilities.

4.4.3 Other strategic gRNAs

In addition to those discussed above, we also included some additional gRNAs with strategic purposes. This included negative controls and other gRNAs that either offer unique opportunities to simultaneously target multiple actin-regulatory genes or that can serve as functional controls.

Non-targeting control gRNAs. Negative controls are important in every experiment that assesses phenotypic changes as a result of different treatments. For CRISPR-Cas9 experiments, ideal controls are given by gRNAs that behave identically to other treatment gRNAs, except for the fact that they do not lead to Cas9-mediated editing anywhere in the

genome. In the case of our selected CRISPR strategy, all gRNAs are expressed from the same lentiviral vector LCV2, so that only the target sequence specificity region (i.e. the ~20mer bp upstream of the PAM sequence) is variable. Thus, gRNA expression, loading into Cas9 and gRNA functionality are therefore expected to be similar, due to identical U6 promoter, scaffold sequences and Cas9 protein respectively. For more details on non-targeting control gRNA sequences, see section 2.2.7.2. In this study we used two such control gRNAs for a total of ~60 gRNAs in our CRISPR panel (i.e. ratio of 1:30). For comparison, the GeCKOv2 CRISPR library recommended by the Zhang lab has a less stringent ratio of 1:60. [584]).

ICAM-1 and ICAM-3. Although not cytoskeletal proteins per se, intercellular adhesion molecules (ICAMs) are connected both physically and functionally to the actin cytoskeleton [648,649]. Upon binding of their cognate ligands, their signalling can trigger extensive actin remodelling and thereby dictate obvious changes in cell morphology and behaviour. Given their roles in mediating intercellular contacts, these proteins can play obvious roles for CCTH. Since ICAM-1 is known to be required for both virological synapse and infectious synapse formation (see sections 1.3.1-1.3.2), it was included here as a positive control for our CCTH assay. ICAM-3 was included as a specificity control for ICAM-1, but also because of its leukocyte-specific expression (whereas ICAM-1 is ubiquitously expressed) [321,598].

ITGB1 encodes the integrin β1 chain, which (like β2) can give birth to many integrins. Both ITGB1 and ITGB2 were found in virions produced by infected Mφ [504] and interacted with gp160 trimers during Env biosynthesis [650]. Since integrins are obligate α:β heterodimers (α chains are unique but β-chains are shared), targeting ITGB1 or ITGB2 by CRISPR allowed the unique opportunity to knock out entire integrin subfamilies with single gRNAs, and thereby assess their combined role in CCTH.

Csk is a leukocyte-restricted kinase that phosphorylates and inactivates Src-family protein kinases such as SRC, HCK, FYN, LCK and LYN [598,651]. Thus, knocking out CSK allowed the unique opportunity to simultaneously activate these kinases and test how this affects CCTH. Furthermore, CSK was among the top 10% upregulated proteins in HIV infected T-cells [652], suggesting it may play an important role for outbound HIV.

Profilin is the most abundant G-actin binding protein. It is considered the main "gatekeeper" of actin monomers, and as such plays important roles in numerous cellular processes that involve the actin cytoskeleton [653,654]. It is also a key regulator of F-actin network homeostasis, by favouring formin-mediated filament elongation over Arp2/3 activity, which allows both pathways to compete despite the dramatically higher abundance of Arp2/3 complex molecules in the cell [299,313]. Profilin binds to formins (via their FH1 domains) on barbed ends and feeds them actin-monomers. Since this is the rate-limiting step for formin-

mediated filament growth, the presence of Profilin dramatically increases the speed and rate of elongation, whereas formin activity in the absence of Profilin is slow and inefficient [311,312]. Therefore, since all human formins have FH1 domains, CRISPR targeting of Profilin offers a unique opportunity to paralyse most formin activity in the cell with a single gRNA and offers a simple solution to the issue of formin genetic redundancy. In this study we targeted Profilin-1, which is prominently enriched in the hematopoietic lineage, whereas the other 3 isoforms are highly tissue restricted and absent in leukocytes [598,653].

FMNL1 and **FHOD1** were included in our CRISPR panel as intended specificity controls for the diaphanous-related formins (Dia1-3), which are the primary suspects of manipulation by HIV in the formin family (see 1.5.9.1). To our knowledge, no association between these non-diaphanous formins and HIV has been reported. However, FMNL1 is important for actin dependent MTOC polarization at the IS [573], and could therefore also play a role at the VS.

ENA/VASP proteins and formins are the only two known linear F-actin elongator families [294]. ENA/VASP can bind F-actin, G-actin and Profilin, and they have filament elongating, bundling, anti-capping and anti-branching properties [655]. Unlike formins, ENA/VASP cannot nucleate actin filaments, but they can elongate filaments created by either formins or Arp2/3 [656]. Thus, ENA/VASP play an important role in filopodial elongation in various cell types and have been often found at the tips of filopodia [657,658]. We included ENA/VASP in our panel as functional controls to formins. While no interaction between HIV and these proteins has been reported to date, their potential involvement in HIV-Filopodia formation is plausible. Of note, the gRNA for ENA was designed so that it would also target the very closely related EVL gene.

BRCK1. The role of Wave2 for outbound HIV was discussed in section 1.5.9.1, and given its relative enrichment in leukocytes, this protein in an important candidate in our panel. However, Wave2 does not act alone but rather is part of an obligate multi-protein "WAVE complex". Since two other Wave isoforms exist (Wave1 and Wave3), loss of Wave2 does not necessarily abrogate all WAVE complex activity. In contrast, loss of non-redundant subunits results in degradation of the entire complex and all its components [659,660]. We therefore decided to target BRK1, as in theory this offered a unique opportunity to simultaneously deplete all subunits of the WAVE complex and thus completely shut down its activity.

4.5 Results

4.5.1 Exploring the role of actin regulators for outbound cell-cell HIV transfer

To interrogate the role of diverse actin regulators in outbound viral transfer, donor cells were individually transduced with LCV2-gRNAs and puromycin-selected, following a standardized procedure to minimize sources of variability between groups (see 4.3.5). CRISPR-treated cells were infected with NL43-IRESeGFP for 48h and donors were then washed to remove free virus, stringently counted and infection-rate normalized as described in 3.4.2.1-2. Preparation of multiple donor groups on the day of coculture-start involved considerable effort and thus represented the rate-limiting step of viral transfer experiments. A maximum of 10 groups could be reasonably processed within one day. Therefore, the panel of 60 target genes was divided into more manageable groups of functionally related proteins, i.e.; surface proteins, cytoskeletal-membrane linkers, Rho-GTPases, other signaling proteins, Arp2/3 activity related, formin-related, and other F-actin binding proteins. Donor cells were added to both TZM-bl and Jurkat target cells, as described in 2.2.11 and Figure 3.1. This has the added benefit of evaluating cell-cell transfer in two different settings (2D vs. 3D cocultures) and with two well-characterized target cell types commonly used in the literature. An untransduced-control group (for data normalization) and a non-targeting control guideRNA group were included in every experiment. Two independent experiments for each of the target genes were performed as part of the CRISPR screen. It is important to remark that the purpose of this screen was to identify candidate genes that may be involved in CCTH ("hits"), but not yet to provide statistical confirmation of their role in this process. Selection criteria for hits and the hit validation process (incl. statistical analysis) are discussed in later sections of this chapter (see 4.5.4), whereas lead characterization is addressed in Chapter 6. It should also be noted here that the efficacy of each gRNA treatment in achieving the intended target protein depletion was not validated for the entire CRISPR panel because, as typical for most genetic screens, this would be prohibitively expensive. Thus, the CRISPR screen data presented in the following sections 4.5.1.1-3 is expected to contain at least some false negative results. This limitation is discussed in much greater detail in section 4.6.

4.5.1.1 Role of membrane-associated proteins

In this section, we consider the target genes from our panel that encode membrane-associated proteins. The results from these viral transfer experiments revealed that the control-gRNA group showed the smallest deviation from the wildtype (i.e. the untransduced control, which is set at 100% for data normalization purposes). From the surface proteins (Fig. 4.6-A), the ICAM1-gRNA treated group showed the largest reduction in viral transfer (77% from wt), as

expected given that this gRNA was included as a positive control. However, transfer was notably lower to Jurkat target cells, compared to TZM-bl cells, thus suggesting a differential role of ICAM1 in both systems. In contrast, both gRNAs targeting the α-chains of the LFA-1 and MAC-1 integrins (ITGAL and ITGAM respectively), resulted in a moderate increase (~20%) of target cell infection. No appreciable difference was observed for the other members of this group. Among the membrane-cytoskeletal linkers, Filamin-A, Ezrin- and Moesin-gRNAs all led to a moderate decrease in viral transfer (Fig. 4.6-B), reaching 25% for Moesin. While these effects are rather small, the similar decrease for these 3 functionally related proteins suggests their true involvement and potential redundancy in the process of CCTH. For the Talin, Vinculin and Angiomotin groups the deviation from the wildtype was minimal for Jurkat targets and inconsistent for TZM-bl targets.

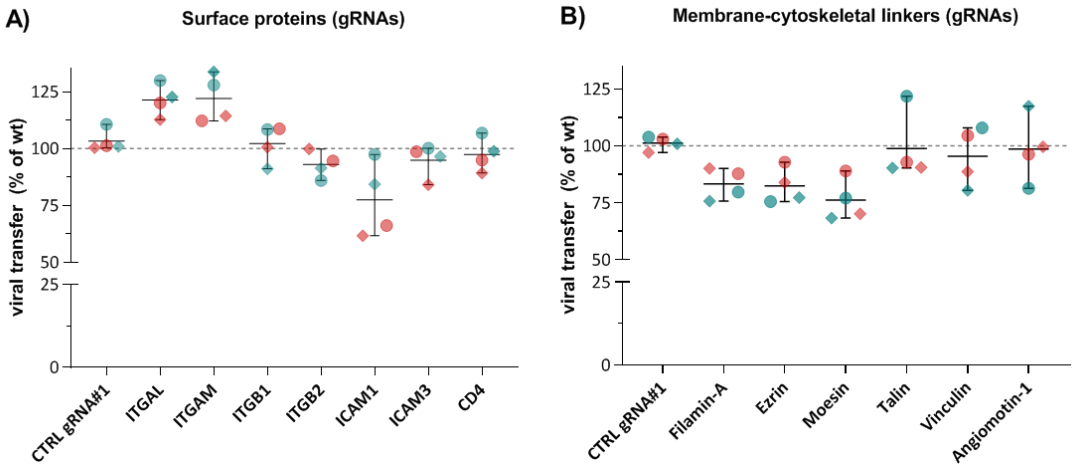

Figure 4.6: Exploring the role of membrane-associated proteins on the donor cell side of CCTH. U937 cells were transduced with the CRISPR lentiviral vector LCV2, encoding Cas9 and the individual gRNAs shown. At day 12 post-transduction, cells were HIV infected for 48h and then cocultured with Jurkat (red symbols) and TZM-bl (blue symbols) target cells (for a detailed description of experimental procedures see 2.2.11). Viral transfer was stopped after 12h by adding the gp120-CD4 inhibitor BMS-378806 at 10 µM. The percentage of infected Jurkat and TZM-bl cells at 48h from start of coculture was assessed by flow cytometry and high content microscopy respectively. Data from each experiment was normalized to the internal untransduced-control group (wildtype) represented by the dashed line at 100%. Shown is the mean and range for each gRNA-treated group. Different symbol shapes indicate 2 independent experiments.

4.5.1.2 Role of signalling proteins

Rho-GTPases are considered master regulators of the cytoskeleton, whereas many other signaling proteins serve upstream or downstream of these to coordinate translation of extracellular or regulatory stimuli into actin remodelling events. The majority of signaling proteins in our panel showed either a minimal or no effect for HIV transfer upon single-gRNA treatment (Fig. 4.7). All Rac1, Rac2, ZAP70, SYK, ROCK1, LIMK1, Vav1, BCR, PAK1 and HCK showed negligible (+/-5%) and/or inconsistent (above and below 100%) deviations from

the wildtype normalization control. In contrast, gRNAs against RhoA and CSK led to slight but consistent increases in CCTH (13% and 17% respectively). From all signaling proteins in the panel, the Cdc42-gRNA showed the strongest reduction effect (~75% from wt) and a small variation (+/- 3.5% STD), thus suggesting a potential role of Cdc42 for outbound CCTH

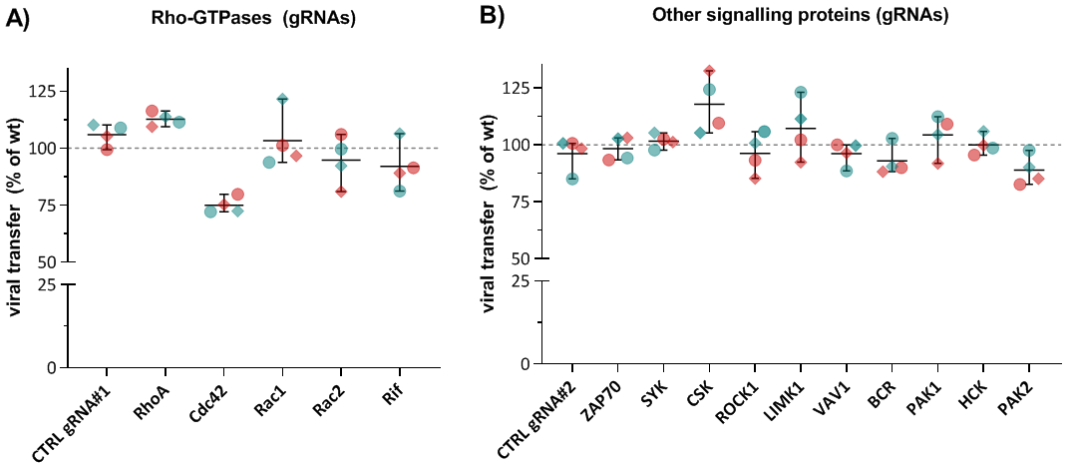

Figure 4.7: Exploring the role of cytoskeleton-regulatory signalling proteins on the donor cell side of CCTH. U937 cells were CRISPR-treated for 12 days with the gRNAs shown. A HIV cell-cell viral transfer assay was performed as described in Figure 4.6 (see 2.2.11 for full description of experimental procedures). Red symbols = Jurkat target cells, blue symbols = TZM-bl target cells. Data from each experiment was normalized to the untransduced wildtype control represented by the dashed line at 100%. Shown is the mean and range for each gRNA-treated group for 2 independent experiments (different symbol shapes). **A)** Rho-GTPases and **B)** other signalling proteins.

4.5.1.3 Role of actin-polymerizing and other actin-binding proteins

Within the group of proteins related to Arp2/3 activity (Fig. 4.8-A), CRISPR treatment against the essential core subunit Arp2 of the Arp2/3 complex led to the strongest reduction in viral transfer (65% of wt control). Furthermore, the gRNAs against the type-I nucleation promoting factors Wave2, WASP and N-WASP all led to appreciable reduction (>10%) in viral transfer, reaching 20% below wildtype for N-WASP gRNA. In contrast, no effect was observed for gRNAs against the type-II NPFs Cortactin and HCLS1. Within the formin-related group (Fig. 4.8-B), gRNAs against all 3 diaphanous-related formins (Dia1-3) resulted in mild but similar reductions in viral transfer (10-15%), whereas Profilin-gRNA led to 20% reduction. Targeting the non-diaphanous formin FHOD1 led to a mild but consistent increase in viral transfer (~15%). In contrast, gRNAs against the ENA/VASP proteins had no apparent impact on viral transfer. As for the rest of actin-binding proteins in our panel (Fig. 4.8-C), gRNAs targeting the F-actin capping proteins CAPZA1, CAPZB, CapG all led to a mild but similar increase (~10-15%) in viral transfer compared to the wildtype control. A similar effect was observed for CAP1-gRNA. Conversely, APC and Cofilin gRNA treatment had a comparable effect but in the opposite direction (~12.5% reduction).

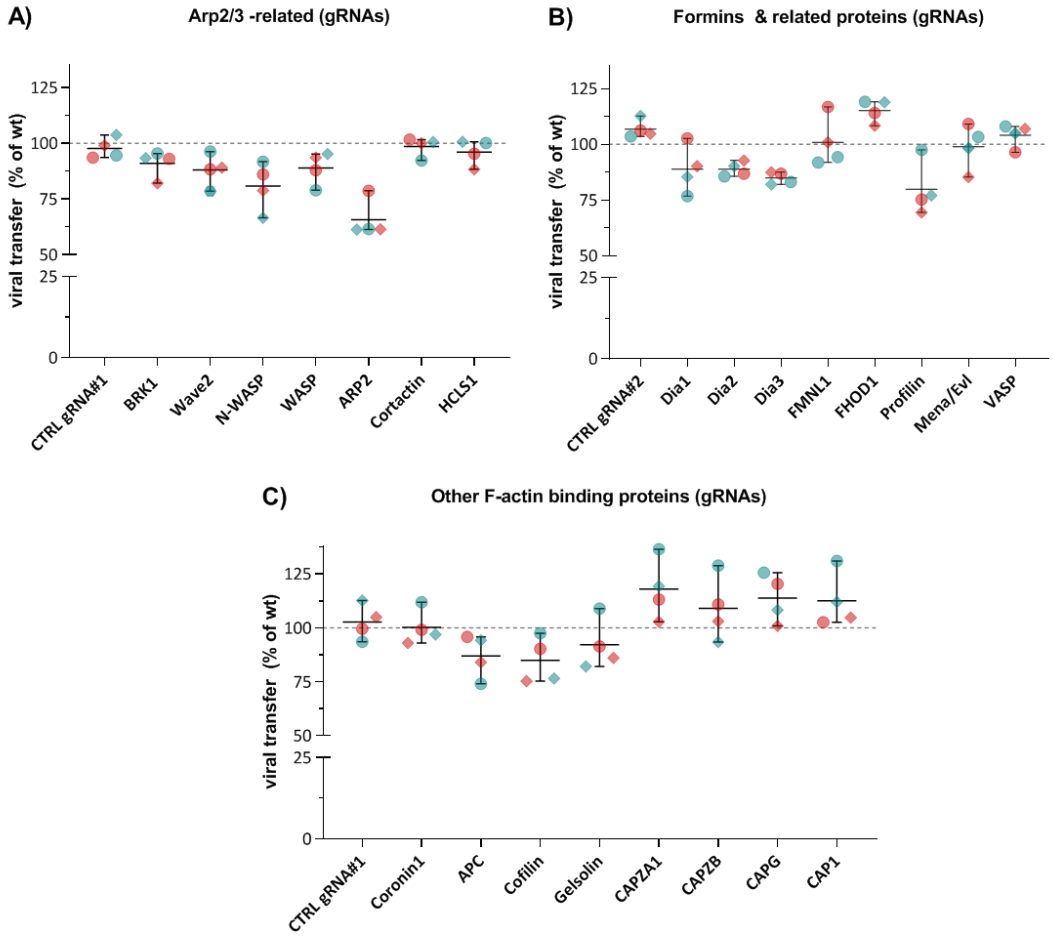

Figure 4.8: Exploring the role of actin polymerizing and other actin-binding proteins for outbound CCTH. U937 cells were CRISPR-treated for 12 days with the gRNAs shown. A HIV cell-cell viral transfer assay was performed as described in 2.2.11 or the figures above. Red symbols = Jurkat target cells, blue symbols = TZM-bl target cells. Data from each experiment was normalized to the untransduced wildtype control (dashed line at 100%). Shown is the mean and range for each gRNA-treated group for 2 independent experiments (different symbol shapes). **A)** Arp2/3 related proteins, **B)** Formin-related proteins and **C)** other F-actin binding proteins.

4.5.2 Cell-viability assessment of CRISPR-treated groups

Since CRISPR treatment can achieve total target-protein depletion in individual cells, knockout of essential or "fitness" genes can compromise cellular health or viability. However, tolerance for loss of most genes is strongly cell-type context dependent [661]. Therefore, to control for the possibility that potential changes in viral transfer in our experiments could be due to such reduced viability of CRISPR-treated U937 donor cells, these were also assessed for their overall fitness via the Alamar Blue assay. This assay uses the reductive potential of living cells as a combined indicator for cellular viability, metabolic state and proliferation of cell populations (see 2.2.3). Note that the exact same CRISPR-treated cell populations were

used for viral transfer experiments and cell viability assessment. Therefore, the cell viability data shown here is directly linked to the viral transfer assay data shown above. The normalized Alamar Blue readout showed stronger deviations from the wildtype, but also larger inter- and intra-experiment variability compared to the CCTH data (error bars in Fig. 4.9 and not shown, respectively). Importantly however, no gRNA treatment resulted in reduced viability compared to the wildtype when either 3x or even 1x standard deviations from the control gRNA were taken as threshold. Interestingly, gRNAs against some specific groups of proteins seemed to result in increased Alamar blue signal. For the β2 integrin subunits and the type-I NPFs in the panel, this surpassed the 3 x standard deviation mark. However, the variability was quite high in these cases, and the trend was not mirrored in the HIV transfer data. Overall, these results suggest that the bulk CRISPR-treated cell populations used for viral transfer assays did not have a compromised cell viability at the time of experiment.

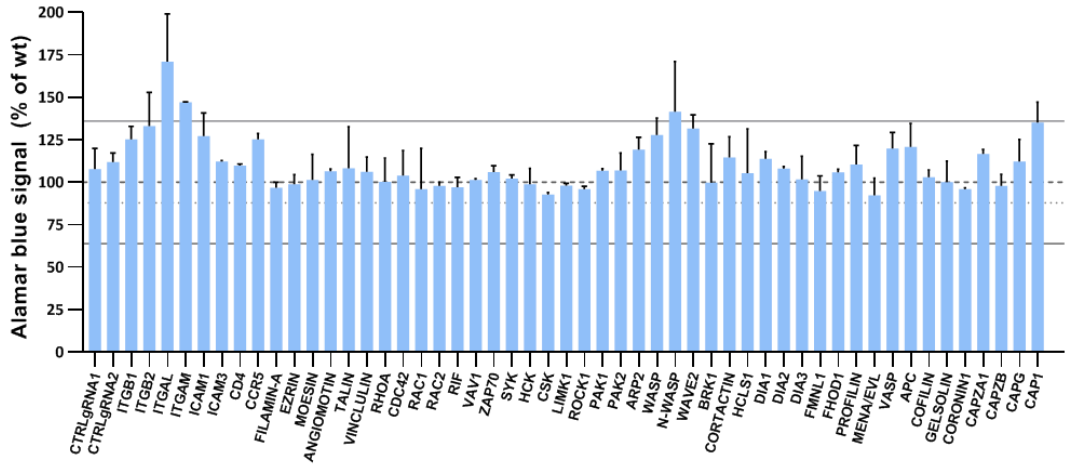

Figure 4.9: Cell viability assessment of CRISPR bulk-treated U937 groups by Alamar Blue assay. 3 x 10^5 CRISPR-treated U937 cells were seeded in duplicate in 96-well plates with a randomized plate design and incubated for 18h. Alamar blue assay was then performed as described in section 2.2.3. Data from each experiment was normalized to its internal untransduced-control group (i.e. wildtype represented by the dashed line at 100%). Data indicates the mean and standard deviation (STD) for 2 independent experiments. Solid lines at ~65% and 135% indicate 3 x STD of the Control gRNA#2 group from the normalization control. The dotted line indicates 1 x STD below the wt.

4.5.3 Criteria and analysis for hit selection

For the first layer of our wide genetic screen we performed two biological replicates, in a similar manner to other recent HIV/Ebola screening efforts [508,662]. While the above approach does not provide a robust base for statistical analysis, this approach does allow to confidently identify "hits" among the tested candidate genes. Indeed, Hart et al. evaluated multiple whole-genome CRISPR screen studies and found that "there are rapidly diminishing returns for additional gRNAs per gene and more than two replicates" [663]. Among other things, this means that while additional replicates will increase sensitivity (i.e. detect more hits

with weaker effects), they are unlikely to change the list of genes that most deviate from the controls. Such "top hits" are likely to play a role in the process in question but require further validation to increase result confidence. Unfortunately, the details of the hit selection process are often not or only poorly reported. Since most of the effects observed in our screen were rather weak, we used stringent criteria to recognize only hits that are likely to play a real role in outbound CCTH. We decided to continue only with the Jurkat-target data, as this system showed higher precision and lower inter-experimental variability compared to the TZM-bl system, as well as being a more biologically relevant model. Figure 4.10 displays the normalized viral transfer data to Jurkat target cells for all functional groups next to each other.

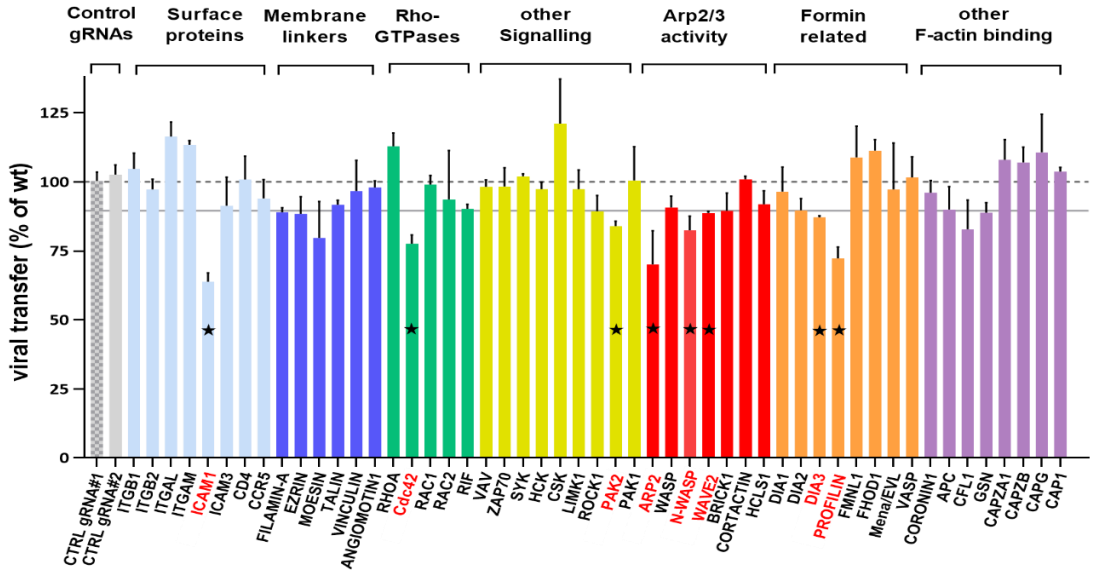

Figure 4.10: Summary of CRISPR screen to explore the role of cytoskeletal regulators on the donor cell side of HIV cell-cell transfer. U937 cells were CRISPR-treated with the gRNAs against the genes shown for 12 days. Donor cells were then HIV infected and cocultured with Jurkat target cells for 12h. For a detailed description of experimental procedures see 2.2.11. Data from each experiment was normalized to its internal untransduced-control group (wildtype), which is represented by the dashed line at 100%. Data indicates the mean and standard deviation (STD) of two independent experiments. The checked column for CTRLgRNA#1 represents the pooled data for that group from all datasets depicted in this figure. The solid line at 89.5% indicates 3 x STD from the pooled CTRLgRNA#1values below the normalization value. Treatments for which both mean and STD fall below this threshold are highlighted with red font and a black star.

The data distribution was tested for normality by both QQ-plot analysis and Shapiro-Wilk test, and a normal distribution was confirmed. We therefore decided to take a three-time standard deviation (3 x STD) from the non-targeting control-gRNA group as a threshold for hit selection. For normally distributed data, this corresponds to a confidence level of > 99%. While there were gRNA treatments both above and below this threshold, from here on we concentrate only on genes whose absence led to a reduction of HIV transfer (i.e. where treatment-mean + STD was below the threshold: 100 – 3 x STD = 89.5% of wildtype transfer).

The hits from our CRISPR screen therefore included the genes ICAM-1, Cdc42, PAK2, Arp2, N-WASP, Wave2, Dia3 and Profilin-1 (see highlighted genes in Fig. 4.10).

4.5.4 Hit validation by protein depletion in clonal cell lines

To validate the hits from our screen, we pursued two strategies. Firstly, an increased number of replicates to allow for formal statistical comparisons, and secondly a higher treatment penetration (i.e. a purer population of protein-depleted cells). Therefore, we decided to perform additional experiments with clonal knockout cell lines (-/-), where possible. These were generated and phenotyped as described in section 4.3.6 and are listed in Table 4.1. These conditions were expected to reveal stronger effects compared to the screen, by removing the residual wildtype cells that remain in the bulk-treated population due to the "heterogeneous CRISPR effect" (see Fig. 4.5) and that retain unimpaired viral transfer. Note that for some genes we could not retrieve full-knockout clones after single-cell sorting (possibly due to lethal effect or high fitness cost of homozygous mutations). Therefore, for Arp2, N-WASP and PAK2 we repeated experiments with bulk CRISPR-treated cells. We could also not obtain Dia3 -/- cells, but we decided to continue with Dia2 -/- cells instead, given that; i) both formins are very closely related, ii) both showed similar reduction effects on the CRISRP screen (Diaph2 just missed the threshold by 0.25%), and iii) our lab has previously shown an important role of Diaph2 for elongation of HIV-Filopodia. Profilin -/- clones could be obtained, however these cells displayed aberrantly enlarged cell morphology, associated with cell-division defects (see 6.4.1). Therefore, Profilin-gRNA bulk-treated cells were used for hit validation in this chapter. We also decided to pursue clonal Cofilin knockout cells, despite this gRNA treatment having missed the screen hit threshold (due to high variation), given the known prominent role of this protein at other stages of the HIV life cycle (see Figure 1.8) but its largely unknown contribution to CCTH. Control gRNA-treated cells were also single cell sorted and clonally expanded, however due to the non-targeting nature of these gRNAs, clones cannot be phenotyped other than by confirmation of permanently acquired puromycin resistance, which indicates genomic integration of the LCV2 vector. Hits were considered to be validated when a statistically significant reduction of viral transfer could be detected compared to the control gRNA group.

Within the panel of clonal knockout cells (-/-), a statistically significant reduction in HIV-transfer was observed for all groups except Dia2. ICAM1, Cdc42, Wave2 and Cofilin knockout cells (-/-) displayed ~49.8 ± 11%, 57.8% ± 18.2%, 68.8 ± 12, and 65.6 ± 9.5% of wildtype viral transfer respectively (Fig. 4.11-A, * = $p < 0.05$). In contrast, when cells were bulk-treated with CRISPR gRNAs and used as HIV donors, only the Arp2-gRNA and Profilin-

gRNA groups reached a statistically significant reduction in viral transfer (Figure 4.11-B, ~65 ± 9.3% and 73.1 ± 3.7% of wt transfer respectively, * = p <0.05).

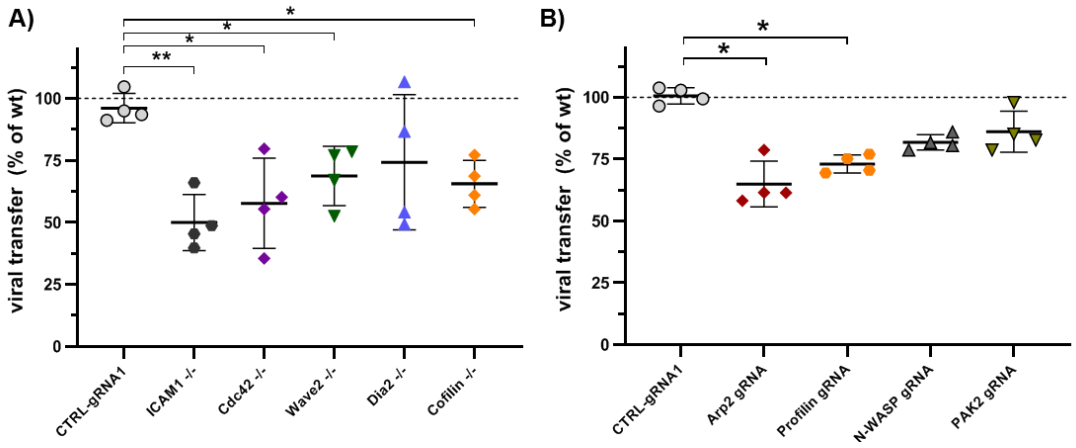

Figure 4.11: Hit validation strategy. CRISPR-treated U937 cells were used as used as donors in HIV viral transfer assays with Jurkat targets at a D:T ratio = 0.25. For a detailed description of experimental procedures see 2.2.11. Data from each experiment was normalized to its internal untransduced-control group (wildtype), represented by the dashed line at 100%. Data indicates the values, mean and standard deviation of 4 independent experiments. All treatment groups were compared to the corresponding control gRNA. **A)** Clonal knockout (-/-) U937 cell lines were used as donor cells and compared to clonally expanded Ctrl-gRNA cells. Normal distribution of data was confirmed as described in 2.2.13. * = $p < 0.05$ by unpaired one-way ANOVA with Dunnett's test for multiple comparisons. **B)** Where -/- clones could not be obtained, experiments were repeated with gRNA bulk-treated cell populations. * = $p < 0.05$ by Krustal-Wallis test with Dunnett's correction.

Of note, a stronger variation was observed between independent experiment replicates with -/- clones compared to gRNA bulk-treated cells (Fig. 4.11-A vs. B). This could be in part due to the standardized CRISPR dosing procedure used for bulk-treated cells (see 4.3.5), which was specifically conceived to reduce sources of variation. Alternatively, it could be related to phenotypic instabilities of -/- cells resulting from the stress associated with the clonal selection procedure (i.e. equivalent to high passage numbers due to regrowth of the population from a single cell).

4.6 Discussion

This chapter aimed to identify actin regulators that play important roles in cell-cell transfer of outbound HIV from infected myeloid cells. To this end, we first performed an in-depth assessment of the literature and rationally designed a panel of candidate genes likely to be manipulated by HIV in leukocytes. This was based on; i) previous direct evidence, ii) circumstantial evidence (i.e. hits from omics studies) and iii) inference of plausible implication. We then exploited the power of CRISPR-Cas9 to individually target these genes for inactivation in U937 cells and used these genetically modified cells as HIV-donors in our well-characterized CCTH assay to formally test their performance in this context. Within the

earlier results section, we already discussed the considerations, implications and systematic nature of our methodological approach in great detail. In this section, we focus on the potential biological implications of our observations and some of the limitations of our approach.

Functional reverse genetic screens are routinely used to interrogate the role of numerous genes in a biological process of interest. Given the large number of targeting constructs used (e.g. shRNAs or CRISPR gRNAs), which can range from dozens/hundreds in curated custom libraries to >10^5 in genome-wide libraries [664], the individual efficacy of the targeting constructs is not validated upfront, as this would significantly increase the cost and reduce the throughput of the approach. Instead, the ability of the constructs to target the intended sequence is typically validated after the screen and only for the "hits" of interest. This of course conveys an important limitation to these approaches, which is the risk for potential false-negative results, since it cannot be excluded that some constructs may be non-functional or have reduced activity. For CRISPR gRNAs this could be due to undesired secondary structures, inefficient guiding of the Cas9 to the genomic target site, inefficient transcription from the U6 promoter or poor choice of targeted sequence. However, the efficiency of gRNAs designed and curated by experienced and software-assisted investigators can be expected to be higher than that of those mass-produced by algorithms, simply because of the higher number of factors considered during their individual design for the specific intended application. In agreement, we did observe evidence of frequent on-target Cas9-editing for every gRNA in our panel for which this was assessed by genomic sequencing with surveyor primers (i.e. Arp2, Cdc42, Cofilin, CSK, Dia2, Dia3, HCK, ICAM1, N-WASP, PAK2, Profilin, Rac1, RhoA, Vav and Wave2). Thus, we will concentrate most of our discussion on results involving these actin regulators. For other target genes in our panel, their participation in CCTH may be considered unlikely but cannot be excluded based on the lack of observed effects in our system alone (i.e. "absence of evidence is not evidence of absence" [665]).

Another limitation of our CRISPR approach is that the extent of protein depletion (both at the population level and per cell) is variable and unknown for each LCV2 bulk-treated donor cell group. This is in part due to the CRISPR heterogeneous effect (see Fig. 4.5). For our CCTH assay, this means that strong deviations from the control group may either be a consequence of moderate effects in many cells, or strong effects in a fraction of cells. Conversely, smaller deviations from the control may be due to the sum of weak effects in many cells, or strong effects in few cells. Care should therefore be taken when interpreting the magnitude of the observed effects in our polyclonal CRISRP screen data. The relative contribution of different actin regulators to CCTH is best compared in the context of clonal homozygous knockout cell lines (-/-), as conducted in the hit validation part of our study (see Table 4.1 and Figure 4.11).

It should be noted that verification at the DNA level was most commonly used in this study (due to its higher throughput and more cost-effective nature compared to protein immunodetection methods, especially when screening large numbers of clones). Where possible, we are continuing to confirm functional knockouts at the protein level for additional controls and stringency. This will be particularly important for the final panel of regulators that are of mechanistic interest (see also Chapter 6), as their phenotypes provide a significant and key contribution to how F-actin is regulated within our immune system.

From the surface proteins tested in our panel, only depletion of ICAM1 led to a clear impairment of outbound CCTH, even at the polyclonal level. This was then confirmed by generation of ICAM1 -/- cells, which displayed a ~50% reduction in their ability to infect target Jurkat T-cells. Since ICAM1 was included as a positive control (see 4.4.3), this confirmed that our CCTH assay can detect impairment of viral transfer upon CRISPR-targeting of relevant genes. Interestingly, this CCTH reduction was not observed when TZM-bl cells were used as targets, which is consistent with the prominent role of ICAM-1 as ligand for the integrin receptor LFA-1 (present on leukocytic but not epithelial cell lines [321]). Indeed, the mechanisms by which ICAM-1 enhances outbound HIV infection (both free virus and CCTH) in a LFA-1 dependent manner have been previously reviewed in great detail [666]. Our observations are therefore consistent with previous reports that disrupting ICAM-1 interaction with LFA-1 reduced CCTH both *in cis* [233] and *in trans* [226,241,589,667]. On the other hand, ICAM3 gRNA had virtually no effect on CCTH in our system. This is consistent with the findings of Jolly et al. [233], who found that ICAM-3 is enriched at the T-cell VS but does not significantly contribute to viral transfer. This suggests that ICAM-1 may be the dominant ICAM that mediates CCTH from both T-cell and myeloid cells, despite the fact that ICAM-3 is more abundantly and more selectively expressed in leukocytes [598].

Interestingly, we observed a slight increase in CCTH when the α integrin chains ITGAL or ITGAM were targeted by CRISPR in U937 donor cells. Since both LFA-1 and MAC-1 (i.e. the integrins involving these chains) are known to be present on the surface of HIV, our results would suggest that they are not critical for virion infectivity and/or CCTH. One possible explanation for the observed increase in target cell infection could be that the lack of LFA1 or MAC1 reduces "sequestration" of ICAM-1+ virions on the donor cell surface. However, if this were the case, we would expect to see a similar effect upon depletion of ITGB2 (common β2 integrin chain for LFA1 and MAC1). We instead did not observe an effect for ITGB2-gRNA in our system, and this is in line with the findings of [668], who found that ITGB2 siRNA did not affect viral assembly, release or infectivity from producer macrophages. We also did not observe any effect for ITGB1-gRNA. This would suggest that neither β1 nor β2

integrins play a critical role for outbound HIV. As expected, CD4-depletion did not have any effect on outbound CCTH, which is unsurprising given that infected cells downregulate CD4.

Within the group of membrane-cytoskeletal linkers, only Filamin-A, Ezrin and Moesin gRNAs tendentially decreased viral transfer. A role for Filamin-A in free-virus release has been previously described [438]. Since free HIV only plays a negligible role in our system, our results suggest that Filamin-A may also contribute to CCTH. The observed reduction of CCTH upon Ezrin or Moesin depletion is consistent with reports that they are incorporated at very high levels in virions [450,454,504], which suggests they are actively recruited to HIV budding sites. Indeed, Ezrin recruitment was observed at the T-cell VS and other VS-like contacts [535,669]. Overall, our findings support an at least moderate effect of Filamin-A and ERM proteins for outbound CCTH, but further studies will be required to assess the involved mechanisms.

Among the Rho-GTPases, Cdc42-gRNA led to the only clear impairment of CCTH in our initial CRISPR screen. An important role of Cdc42 was confirmed by generation of clonal Cdc42 -/- cells, which displayed at significant reduction in their ability to mediate viral transfer. Further characterization of these cells (see later section 6.4.5) confirmed a functional effect of Cdc42 knockout, as these cells completely lacked filopodia on their surface (Cdc42 is an important regulator of filopodia, see 1.4.7.1). The mechanisms by which Cdc42 contributes to outbound CCTH were further explored in Chapter 6. A mild impairment of CCTH to Jurkat cells was also observed upon Rif-gRNA treatment. While this did not reach our hit-threshold level, we do not exclude a potential role for this regulator in outbound HIV. In contrast, RhoA-gRNA consistently increased CCTH (mild effect in polyclonal screen). This is compatible with our view in [66] that RhoA is selectively "neutralized" in infected cells because of potential counterproductive effects for outbound HIV. Furthermore, we observed no effect of Rac1-gRNA treatment for CCTH from U937 cells, despite confirming a high efficiency of this gRNA at the DNA-editing level. This strongly suggests that Rac1 does not play a role for outbound CCTH from myeloid cells, and this was later confirmed by shRNA knockdown of Rac1 (see Chapter 6, Fig. 6.16). Overall, these results support our hypothesis that Nef-mediated hyperactivation of Rac1 is tailored towards directing actin remodelling changes in T-cells, whereas analogous manipulation of Cdc42 is instead required for improved viral outcomes in myeloid cells. This is supported by the fact that most Rac1-HIV effects have been observed in T-cells, whereas most Cdc42-HIV effects have been reported in the context of DC (see 1.5.9 and 1.5.11).

PAK2 is an effector protein for both Cdc42 and Rac1. We observed a mild reduction in CCTH upon depletion of PAK2, but we were not able to isolate PAK2 -/- cellular clones.

Nevertheless, our results suggest that although PAK2 is directly manipulated or "hijacked" by HIV (reviewed in [66]), this cannot overcome the requirement for upstream signaling from Cdc42, at least for outbound CCTH. Most gRNAs against the other signaling proteins in our panel had no appreciable effect, including those for Vav1 and HCK. This was highly surprising because both proteins are known to be directly manipulated by HIV (as we reviewed in [66]). Vav1 is an important physiological activator of Rac1/Cdc42. Nef binds to Vav1 and recruits it to multiprotein complexes where it activates Rac1, Cdc42 and PAK2 [66]. However, our results suggest that Cdc42 activity, as required in infected myeloid cells, may be independent of Vav1. Hck is expressed selectively and at high levels in myeloid cells, including Mφ, DC and monocytes [521,598]. Nef binds HCK with high affinity leading to its hyperactivation (see 1.5.9.3). In Mφ, this has been shown to enhance virus production [527], particle infectivity [529], cytoskeletal changes, cellular adhesion and migration [522]. Therefore, and because U937 cells express one of the highest reported HCK levels among cell lines [321], we expected to see a dramatic effect of HCK in our assay. Surprisingly, however, HCK-gRNA treatment did not have any effect on CCTH from U937 cells. This was despite confirmed genomic editing at the HCK-gRNA target site. To explore this further, we designed two additional gRNAs and repeated viral transfer experiments using three HCK-gRNAs (either simultaneously or separately) in both U937 and primary Mφ. No effect was observed under any of these conditions (not shown). Our results therefore unexpectedly suggest that HCK is entirely dispensable for outbound HIV in myeloid cells, at least *in vitro*. This however contrasts with observations in mice, which concluded that the Nef-HCK interaction is important for HIV pathogenesis (see 1.5.9.2). One way to reconciliate these observations could be that the advantage of HCK manipulation by HIV is only revealed in the more complex *in vivo* setting. This is consistent with the data and hypothesis of Verollet et al., who proposed that Nef:HCK enhances HIV pathogenicity *in vivo* by increasing Mφ migration and tissue infiltration, whereas HCK was dispensable for HIV particle production *in vitro* [522].

Arp2/3 represents the most abundant actin nucleator within mammalian cells. However, the Arp2/3 complex by itself is inactive, and thus requires assistance from one of many possible nucleation promoting factors (NPFs, see 1.4.3.1). Our CRISPR screen revealed a clear impairment of CCTH upon Arp2-gRNA treatment, whereas milder effects were observed for gRNAs against N-WASP, WASP and Wave2 (i.e. type-I NPFs). In contrast, gRNAs against Cortactin and HCLS1 (type-II NPFs) had no appreciable effect. Our results therefore indicate that Arp2/3 activity (likely via type-I NPFs) plays an important role in CCTH from infected myeloid cells. The weak but similar decreases observed for type-I NPFs could suggest either partial redundancy of these proteins in our context, or distinct small additive effects. A somewhat similar phenomenon was observed for formins, which constitute the second most

abundant class of actin nucleators in the cell. CRISPR targeting of Profilin, which is required by all human formins for rapid filament elongation, led to a clear impairment of outbound CCTH. Individual targeting of the diaphanous formins Dia1-Dia3 observed weak but similar decreases in CCTH. In contrast, targeting the non-diaphanous formins FML1 or FHOD1, or proteins from the ENA/VASP family (which also elongate F-actin in cooperation with Profilin [670]) did not impair CCTH in our system. Together, our results therefore suggest that Profilin is important for CCTH because it is required for efficient formin but not ENA/VASP activity in this context. We propose that this formin activity is specific to the family of Dia formins (with potential partial redundancy across family members) and that it involves F-actin elongation rather than nucleation. This is because Profilin is known to stimulate the former and inhibit the latter mechanism (reviewed in [671]). Another observation from our CRISPR screen further support this hypothesis. Targeting F-actin capping proteins such as CAPZA, CAPZB and CAPG for degradation all tendentially increased viral transfer to target cells. This is consistent with the idea that formin activity promotes CCTH, because capping proteins primarily antagonize formin-mediated filament elongation (by binding to and stabilizing free barbed ends). In contrast, ENA/VASP proteins can elongate filaments even in the presence of capping proteins due to their potent anti-capping activity [672], whereas the Arp2/3 complex mediates filament branching from the side of pre-existing elements and therefore does not require free-barbed ends for its activity. Of note, some of the molecular mechanisms by which Arp2/3 and Formins conceivably contribute to outbound HIV infection were already discussed in 1.5.9.1, whereas others (resulting from experimental work in this thesis) are further discussed in later Chapter 6.

A potential role of Cofilin as an important factor for outbound CCTH is highlighted by the observation that clonal Cofilin -/- cells displayed a significant reduction in their ability to mediate target cell infection. A previous study reported that silencing of Cofilin in HeLa cells impaired outbound free virus release [440]. This is consistent with the fact that Cofilin is incorporated at high levels in virions, where it can reach up to 10% of the molar abundance of Gag [450,454,504], thus suggesting its abundant presence at HIV-budding sites. However, given the magnitude of the effect observed in our system, where the contribution of free HIV is minimal, we conclude that Cofilin is also likely to play a role in CCTH. It is interesting, however, that Cofilin would be required for outbound viral spread, because elaborate and evolutionarily conserved mechanisms exist to neutralize Cofilin via Nef and Tat in infected cells (reviewed in [66]). In this study, we propose that indiscriminate Cofilin-inactivation may selectively occur in T-cells but not myeloid cells. This is supported by several observations. First, Cofilin inactivation and its associated cell-crippling effects (e.g. impaired cell migration, chemotaxis and membrane protrusions) have so far only been reported in T-cells (see 1.5.11).

HIV-infected myeloid cells rather display enhancement of actin-rich membrane protrusions and cellular motility (Fig. 1.5.10), both of which require Cofilin activity. In agreement, Cofilin inactivation was not detected in infected Mφ, despite clear occurrence of other Nef-mediated actin effects [522]. Together, these observations support that Cofilin may be differentially manipulated by outbound HIV in lymphoid and myeloid cells, and that it contributes to outbound viral spread, at least in the latter cell type. Further experiments will be required to characterize exactly how Cofilin depletion impairs CCTH.

To recapitulate, our CRISPR screen identified numerous actin regulators whose activity may influence outbound CCTH. A reduction in viral transfer beyond the confidence threshold (i.e. "hits") was observed for gRNAs against ICAM1, Cdc42, Wave2, Cofilin, Arp2, PAK2, Dia3/2, Profilin and N-WASP. For the first four, we could validate a significant role in CCTH by generation of -/- cell lines, where the template for protein production has been destroyed. The stronger reduction effects observed for these clonal cell lines are expected due to the lack of residual wildtype or hemizygous cells, which would still be present in the LCV2 bulk-treated populations (see Fig. 4.5). In contrast, we were not able to obtain -/- cell clones for Arp2, PAK2 or N-WASP. This could be due to lethality or high fitness cost associated with homozygous mutations of these genes in U937 cells. In agreement, germline mutations (-/-) of these genes lead to early embryonic lethality in mice [673-675], and both Arp2 and PAK2 were identified as "fitness genes" in a genome-wide CRISPR screen [661]. Importantly, however, cell viability was not affected by any of these gRNA treatments (Fig 4.9).

When evaluating the functional interconnection of our hits in the context of actin dynamics, we primarily observe pathways of cortical F-actin regulation. Cdc42 is one of the master regulators of the cytoskeleton and is best known for its ability to trigger filopodia formation. This can occur via the Cdc42→N-WASP→ Arp2/3 pathway or via Cdc42-mediated activation of Dia formins (see 1.4.7.1 and Fig. 4.12). In contrast, high Arp2/3 and Cofilin activity is a hallmark feature of dynamic lamellipodia. In this context, Arp2/3 is usually activated downstream of Rac1 via the type-I NPFs WASP, N-WASP and/or WAVE (see 1.4.7.2). Most of the above-mentioned proteins have been found by ourselves and others within virions produced in infected leukocytes (unpublished and [454,504]). This not only confirms their presence at HIV-budding sites, but also suggests their direct or indirect interaction with viral proteins. Altogether, our CRISPR-screen data suggests an important role of cortical F-actin structures (in particular filopodia and/or lamellipodia) for CCTH from infected myeloid cells, and this was further explored in detail in Chapter 6. Furthermore, the observation that many of our hits correspond to functionally related proteins within specific pathways, can be

interpreted as an additional layer of validation for both the specificity of the gRNA treatments and the functional relevance of the hits identified in this chapter.

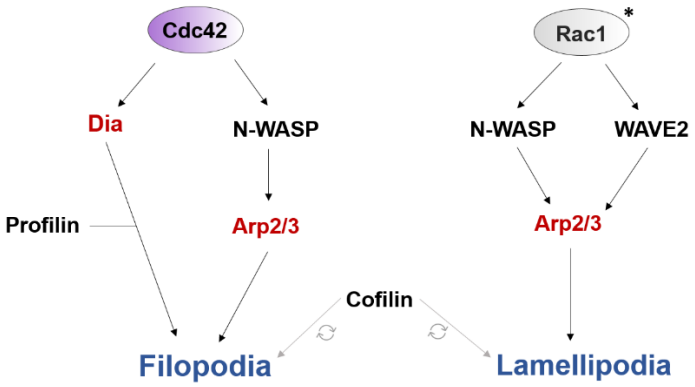

Figure 4.12. Summary of cortical F-actin regulation in leukocytes. Only "hits" from the CRISPR screen in this chapter are shown (except for Rac1*). Actin nucleators are shown in red. Circular arrows indicate structure turnover.

4.7 Chapter acknowledgements

All experiments and data analysis in this chapter were performed by the author of this thesis. Note that the personal pronoun "we" is used throughout this thesis to reflect common scientific practice and to avoid the tedious use of the personal pronoun "I". The reader is invited to think of "we" as the author and his supervisory team, given the important contributions of the latter to the guidance of this work.

Chapter 5. Exploring the role of actin regulators for inbound HIV infection

5.1 Introduction and aims

One of the main aims of this work was to increase our understanding of the process by which HIV infection can be efficiently transferred between different cell types, with emphasis on viral egress from the donor cell side (i.e. outbound CCTH). However, the resources assembled for this purpose can also be easily applied to study the opposing side of the equation, which is the infection of target cells via intercellular contacts (i.e. inbound CCTH). This could prove beneficial to the field, because most previous studies have focused on either the donor or the target cell independently. Therefore, the role of actin dynamics on each side of the virological synapse (VS) has rarely been assessed in parallel or within the same CCTH system. While it is clear that actin remodelling is required at both sides of the VS (see 1.5.10), this process is better understood and seems to play a more determinant role at the recipient cell side. This may be because cell-free inbound HIV also relies on actin-mediated events to enter and infect the target cell (see 1.5.6), whereas actin dynamics may be dispensable for outbound free virus release (see 1.5.7). In any case, the hypothetical models available for actin manipulation during inbound HIV infection are based on numerous and often independent observations, which have been integrated from studies using widely different model systems and experimental conditions. They may therefore not accurately represent a consensus series of events taking place in each cell type. Furthermore, while there is some overlap in the actin-dependent steps occurring during inbound free HIV and cell-mediated infection, it is presently unclear whether these are coordinated by fundamentally similar or different manipulation mechanisms. Since our resources were specifically designed to study actin-dependent CCTH, they represent unique opportunities to fill these gaps and to expand the current knowledge in this field. Firstly, they allow us to study the role of specific actin regulators at both sides of the VS by using the same experimental model, reagents and conditions. Secondly, we can assess and compare (in parallel) the role of many cytoskeletal proteins for inbound HIV within the same system. Finally, our CRISPR panel includes many actin regulators that have not previously been assessed for their potential role for inbound HIV. We expect all these factors to greatly contribute to our ability to corroborate, complement and/or refine current hypothetical models regarding the role of actin dynamics for CCTH and for inbound HIV in general.

This chapter therefore has two primary experimental aims:

1) To harness the resources already assembled in Chapters 3 and 4 to systematically interrogate the role of actin regulators for inbound HIV, while clearly distinguishing between free virus and cell-mediated infection.

2) To identify new cytoskeletal regulators involved in actin-dependent cell-cell HIV transfer (target-cell side), while also validating previous findings from the literature in parallel.

5.2 Materials and Methods

5.2.1 Overview of approach

The methodology to approach these aims experimentally was mostly established and discussed in previous chapters. A summarized index of these resources and the relevant linked sections is presented below.

Approach	Summary	Chapter / section
Donor cells	wildtype U937 (promonocytic cell line)	3.3
Target cells	CRISPR-treated Jurkats (T-cell line)	3.4.1.3
CRISPR reagents	LentiCRISPRv2 (LCV2) (lentiviral vector encoding all required CRISPR components)	4.3.1-4.3.4
CRISPR treatment	Standardized procedure for CRISPR bulk-treatment of cell populations	4.3.5
CRISPR gRNA panel	Lists all gene targets in the panel and the rationale for their inclusion	2.1.7.2 and 4.4 respectively
HIV transfer assay	assay optimized to quantitatively detect changes in cell-cell HIV transfer upon different treatments	Adapted from 2.2.11. See 3.4, Fig. 3.1 and details below

Table 5.1: Overview of methodological approach used in Chapter 5.

All procedures were performed as described in the above-mentioned sections, unless otherwise specified. Only few changes in experimental conditions were required to adapt the protocol for assessing the role of actin regulators for inbound HIV. Unlike the experiments performed in Chapter 4, donor cells in this chapter always correspond to wildtype U937 cells (HIV+). A single donor group was prepared in each experiment and added to the different target-cell variants as required. Since CD4TC are the most biologically relevant targets of HIV infection and given our intention to mechanistically dissect the role of actin regulation for inbound HIV, we decided to use only the Jurkat target cell system in this chapter. Thus, for all experiments presented here, only the target cell populations (Jurkat cells) were CRISPR treated, whereas the myeloid donor cells have a wildtype phenotype.

5.2.2 Summary of protocol adapted for study of inbound CCTH

Twelve days before the start of coculture, wildtype Jurkat cells were transduced with LCV2-VLPs (MOI =0.5) to generate single-gRNA CRISPR-treated populations. Standardised selection and passaging conditions were applied as described in 4.3.5. 48h before start of coculture, wildtype U937 cells were infected with HIV-IRESeGFP as described in 3.4.2.1-2. On the day of the experiment, the various target cell populations (Jurkat) were counted and normalized to 10^6 c/mL prior to staining with CellTracker Deep Red dye at 1µM (see 3.4.2.3). For each group, 4 x 10^4 target cells per well were seeded either on U-bottom 96-well plates (for cocultures) or flat-bottom plates (free virus controls). Immediately prior to start of coculture, infected donor U937 cells were washed twice with PBS and donor cell infection rate was adjusted to 30-40%. Donor cells were added to target cells at a donor:target ratio of 0.25 (final well volume = 200 µL). Plates were centrifuged at 1500 rpm for 5 mins to bring donor and target cells together in a synchronized fashion. At 12 h from the start of coculture, well contents were moved to 24-well plates containing stop reaction so that well volume = 300 µL and BMS-378806 = 10 µM. Readout occurred at 48 h post initial exposure of target cells to HIV (i.e. 36 h after stop reaction). Cells were first resuspended in 1xTrypsin solution and incubated at 37°C for 5 minutes to completely dissociate any cell conjugates. Cells were then fixed and analysed by flow cytometry. The proportion of productively infected target cells in each sample was calculated based on the number of Red+|GFP+ double positive cells within the Jurkat-cell gate (Red+) population.

5.2.3 Inbound free virus controls

Additional controls were included to the inbound viral transfer assay, in order to better resolve which stages of the viral life cycle are affected upon knockout of the various actin regulators.

Free HIV control: In our coculture system, we expect at least ~90% of target cell infection to be a consequence of CCTH under wildtype conditions (see 3.5.3). However, the actin regulatory pathways required for infection of target cells may overlap for cell-free and cell-cell delivered HIV. Therefore, it is important to have a "free virus only" control. When compared to the coculture readout, this control allows to resolve whether treatment-induced changes in the target cell population impact both infection mechanisms equally or whether one of them is preferentially affected.

Pseudotyped HIV control: Since actin structures and processes have been associated with almost every stage of the inbound HIV life cycle [66], changes in target cell infection upon CRISPR treatment could initially be the result of CD4/chemokine receptor mediated attachment, entry and fusion steps. To help resolve viral blocks pre and post the plasma

membrane using cell free virus, we included a VSVg-pseudotyped HIV control ("HIV-VSVg+"). The use of VSVg, would enable entry across the endosomal membrane, as VSVg fusion is triggered through a lowering of pH. Therefore, if infection impairment can be rescued by VSVg pseudotyping, there is high probability that entry mediated through CD4/chemokine receptor attachment and latter fusion are interrupted. In contrast, where VSVg-pseudotyping does not rescue inbound HIV infection, a common post-entry event, that is independent of the route of viral entry is affected.

For selecting the MOIs and experimental conditions for infection with free inbound virus controls, the infectivity of cell-free HIV stocks (single round of infection) was first tested as indicated in Figure 5.1 below. Note that these viral stocks were titrated on TZM-bl cells as described in 2.2.6.3. A strongly linear relationship was observed between the MOI used and the percentage of infected target cells. Jurkat cells were extremely permissive to VSVg-pseudotyped virus (Fig. 3.1-B), with MOIs as low as 0.05 eliciting ~ 20% infection rates. This suggests Jurkat cells are about 40-fold more permissive to infection with this type of virus compared to U937 cells. In contrast, infection of Jurkat cells with non-pseudotyped cell-free HIV was inefficient (Fig. 3.1-B). While infection rates can be increased by spinoculation, this poses at least two problems in our system. First, spinoculation increased target cell infection but disrupted the linear dose-dependent effect (not shown), which would complicate interpretation of results when comparing multiple treatments. Second, spinoculation can induce short-term changes in the actin cytoskeleton [477] that could interfere with CRISPR-induced effects. Overall however, the strong linear dose-dependent effect suggests that this simple assay can detect even subtle changes in target cell permissiveness to infection by cell-free HIV. Therefore, the exact MOI values are not as important as maintaining constant doses across experiments. We selected a MOI = 0.05 for VSVg-pseudotyped virus and a MOI = 1 for non-pseudotyped HIV. Culture conditions for free virus controls in CCTH experiments were as indicated in Figure 3.1 below.

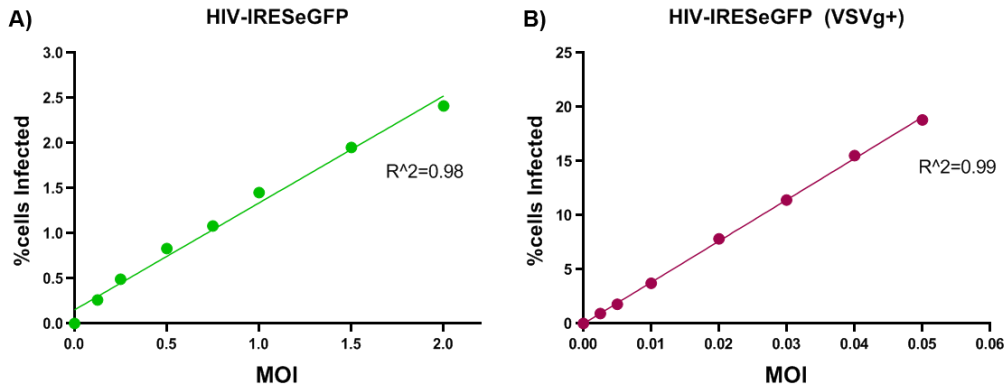

Figure 5.1: Dilution series of cell-free HIV stocks in Jurkat target cells. Cell-free HIV-IRESeGFP stocks were produced in HEK 293T cells as indicated in section 2.2.6.1 and titrated on TZM-bl cells as

described in section 2.2.6.3. Experiment conditions were chosen to emulate those in CCTH experiments. Jurkat cells transduced with LCV2 CTRL-gRNA were labelled with CellTracker DeepRed (1 µM) at day 12 post-transduction. 4 x 10^4 cells were seeded per well in flat bottom 96-well plates. Virus was added directly at the indicated MOIs and mixed with cells. Well volumes were adjusted to 250 µL with RF10 medium. At 12h, BMS-378806 was added to a final concentration of 10 µM. Readout occurred 36h later by flow cytometry.

5.2.4 Normalization control

Importantly, inbound HIV infection data was normalized to the HCK gRNA treated group, rather than the untreated wildtype group. This was because, unlike with U937 cells, transduction of Jurkats with LCV2-gRNA lentivirus led to an appreciable change in cellular behavior compared to the wildtype. This was characterized by lower metabolic activity and slower cell proliferation (delayed medium exhaustion and lower Alamar blue readouts). Preliminary testing (not shown) confirmed this could also result in differences in HIV infectivity, with wt cells being more permissive to infection than cells transduced with LCV2 (regardless of the gRNA sequence). This was later also confirmed during the screen (Fig. 5.2-A). Therefore, untreated cells did not represent an ideal normalization control. Instead, we selected HCK gRNA treatment as a normalization control group for these experiments. HCK is a non-essential tyrosine kinase with expression restricted to the myeloid lineage and not T-cells [321,598]. In agreement, previous studies found only negligible levels of HCK in Jurkat cells [676]. Therefore, HCK-gRNA treated Jurkat cells should share all phenotypic changes associated with LCV2 transduction (i.e. expression of Cas9, gRNA, puromycin N-acetyltransferase, etc.), but should not have phenotypic changes associated with genetic-editing of the HCK locus.

5.3 Results

5.3.1 Role of actin regulators for inbound HIV infection

Compared to experiments with multiple donor groups performed in Chapter 4, HIV transfer experiments with various target cell conditions are considerably less labor-intensive. This is because only one group of donor cells needs to be prepared following the procedure outlined in section 3.4.2.2, whereas the different target cell groups (uninfected) do not require such time-consuming processing. Up to 30 CRISPR groups could be reasonably set up for cocultures within one day for inbound HIV experiments. The panel of 60 target genes was therefore divided in 2 halves, and each half was run in two independent experiments through the viral transfer assay. However, normalized data for the entire panel is presented here together for easier visualization purposes. Three linked data sets were generated in every experiment for each target cell variant (i.e. cell-cell transfer data, free inbound HIV and free

HIV-VSVg+ data) (Fig. 5.2_A-C). Data is described below in the context of cytoskeletal regulator classes, for easier comparison of functionally related genes.

Surface proteins: CD4 is the most important cellular factor for HIV entry known to date. Therefore, a CD4 gRNA was included in the CRISPR panel to serve as positive control for impaired inbound HIV infection. As expected, depletion of CD4 resulted in the strongest reduction of inbound HIV infection for the entire panel. Infection rates decreased by ~80% for Env-dependent HIV, whether it was delivered by cell-cell or cell-free mechanisms (Fig. 5.2_A-B). In contrast, infection was fully rescued when inbound virus was pseudotyped with the VSVg envelope (Fig. 5.2-C). No striking change in HIV infection was observed for Jurkat target cells treated with gRNAs against ITGAL, ITGAM, ICAM-1 or ICAM-3. ITGB1 gRNA treatment led to a notable increase in target cell infection (~1.5 fold) for cell-cell delivered virus (Fig. 5.2-A), whereas the effect was weaker for cell-free virus and not observed for HIV-VSVg+ (Fig. 5.2_B-C). Similarly, ITGB2 and CCR5 gRNA treatments mildly but consistently increased target cell infection (~18% on average) for non-pseudotyped virus (Fig. 5.2_A-B).

Membrane cytoskeleton linkers: CRISPR treatment with gRNAs against the membrane-cytoskeleton linker proteins Filamin-A, Ezrin, Moesin, Talin, Vinculin and Angiomotin did not result in any clear change in target cell infection (Fig. 5.2_A-C). Deviations from the control groups were small, and often in opposing directions for cell-cell and cell-free virus, suggesting these correspond to stochastic variability rather than meaningful effects. The only potentially relevant observation in this group was a mild (~12%) reduction of inbound CCTH for Talin gRNA treated target cells, consistent with a previously proposed role of Talin at the T-cell VS [85].

Rho-GTPases: As expected, depletion of some Rho-GTPases notably affected inbound HIV infection in Jurkat cells. CRISPR targeting of Rac1 led to a clear and consistent reduction of infection for all cell-cell, cell-free and VSVg delivered HIV (~50%, 23% and 19% reductions respectively), with the strongest effect observed in the CCTH context. Treatment with RhoA gRNA also led to a moderate but consistent infection impairment for cell-cell and VSVg delivered virus (~22% and 12% reduction). gRNA treatments against Rac2 or Rif did not seem to have any effect on inbound HIV infection. In contrast, Cdc42 gRNA treatment led to a clear increase of CCTH (~35%, Fig.5.2-A) but had no effect on free virus infection.

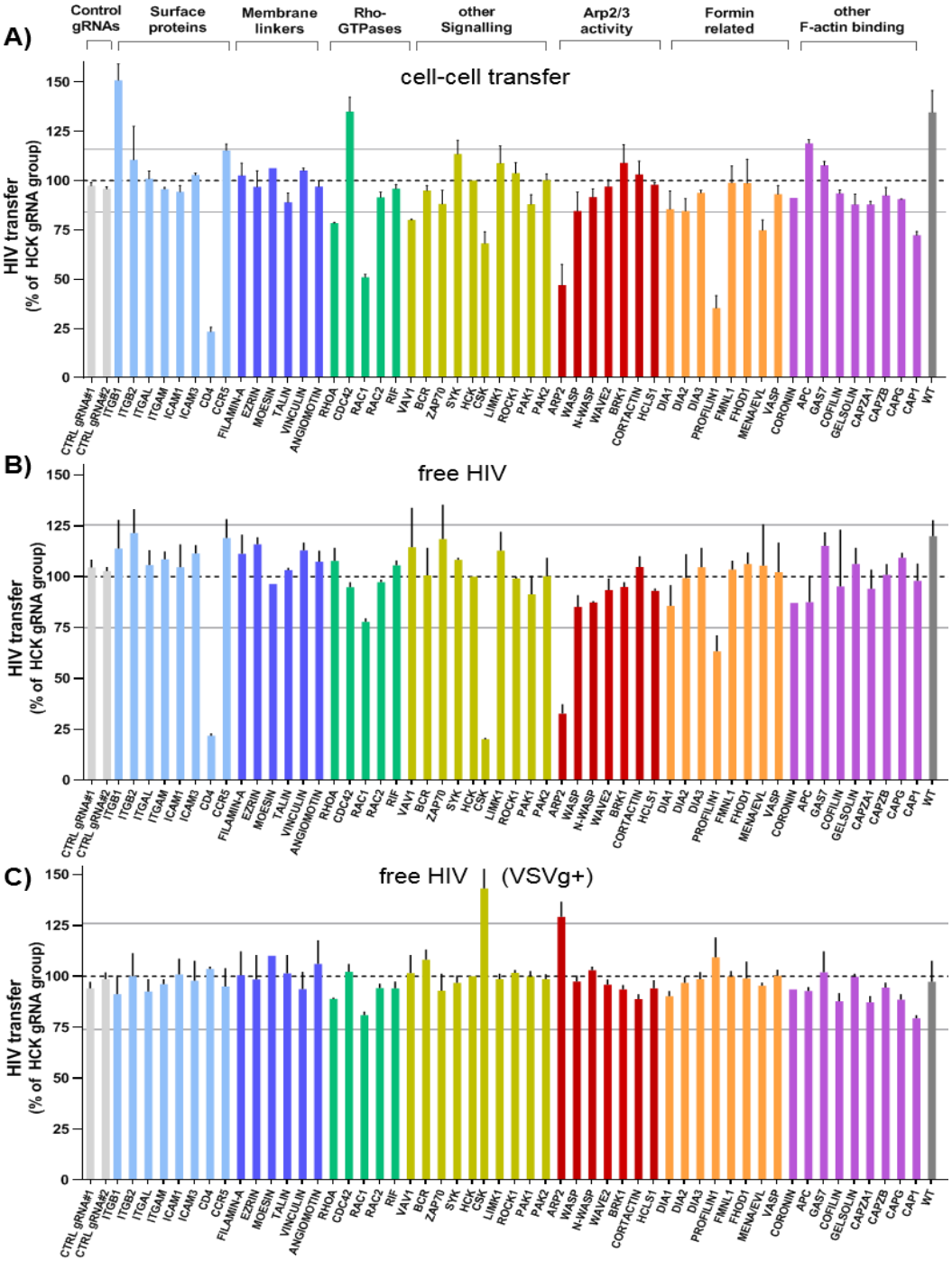

Figure 5.2: Summary of CRISPR screen to dissect the role of actin regulators for inbound HIV infection. Jurkat cells were CRISPR-treated with gRNAs against the indicated genes and used at day 12 post transduction as target cells for cell-cell or cell-free HIV-IRESeGFP infection. Infection was limited to a single round by adding the stop reaction BMS-378806 (10 µM) at 12h. The percentage of infected target cells was assessed at 48h by flow cytometry. For a full and detailed description of experimental procedures see section 5.2.2. Data from each experiment was normalized to an internal control treatment (HCK-gRNA group, see 5.2.4), which is represented by the dashed line at 100%. Columns indicate the mean and error bars the standard error of 2 independent experiments. The solid horizontal lines indicate 5x standard deviations of control gRNA groups from the normalization control. A) Target cells were cocultured with wildtype U937 cells previously infected with HIV. B) Target cells were mixed with cell-free HIV, or C) VSVg-pseudotyped cell-free HIV.

Other signalling proteins: The greatest fold-changes within this group were obtained by targeting the C-terminal Src kinase (Csk). Csk depletion led to a clear reduction of Env-dependent infection. Reductions of ~32% and ~80% were observed for cell-cell and cell-free HIV infection respectively, with the latter reaching values comparable to those of CD4 gRNA treatment (Fig. 5.2_A-B). In contrast, infection by VSVg-pseudotyped virus was increased ~1.4 fold in these cells, resulting in the strongest change for any treatment for this type of infection (Fig. 5.2-C). This was confirmed to be statistically significant and also occurring in U937 cells (Fig. 5.3). Vav1-gRNA treatment of target cells reduced inbound CCTH by ~20%, (Fig. 5.2-A). For the rest of the gRNAs in this group, only weak effects in either direction were observed in the Env-dependent context, whereas HIV-VSVg+ infection remained virtually unchanged.

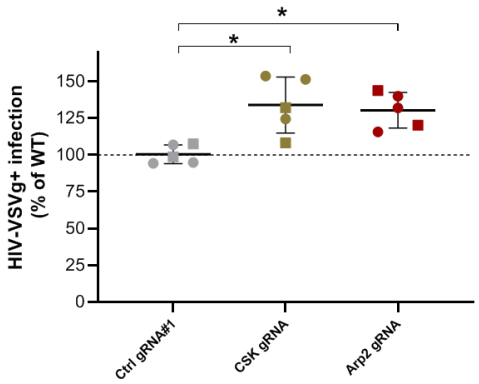

Figure 5.3: Role of CSK and Arp2 for inbound HIV-VSVg+ infection. Experimental procedure was identical to that described in Figure 5.2-B. Data shows the mean and standard deviation of 5 independent experiments. Different symbol shapes indicate different cell types (circles = Jurkat and squares = U937). * = $p < 0.05$ by Mann Whitney test.

Actin polymerizing factors: The strongest effects within this group were observed for Arp2-gRNA treatment. As for Csk, targeting of Arp2 led to a strong reduction of Env-dependent infection (Fig. 5.2_A-B) and a clear increase (~1.3 fold) of HIV-VSVg+ infection (Fig. 5.2-C and Fig. 5.3). The impairment was more pronounced for cell-free HIV compared to cell-cell delivered virus (~67% and 53% reductions respectively). All three changes fell outside the 5 x STD confidence range. Targeting the type-I NPFs WASP, N-WASP and Wave2 also seemed to decrease Env-dependent infection, although the effects were weaker than for Arp2-gRNA. Targeting of the type-II NPF Cortactin may have slightly impaired HIV-VSVg+ infection (~12% reduction) but had no effect on Env-dependent virus. Dia1-gRNA slightly impaired inbound HIV infection via all 3 mechanisms (~15 % reduction on average). Tendentially, targeting of Dia formins led to lower infection values compared to the non-diaphanous formins FMNL1 and FHOD1 or the VASP filament elongator, although effects were rather weak. However, gRNA treatment against the formin-cooperator Profilin importantly decreased inbound infection by CCTH and cell-free virus (~65% and 37% reduction respectively),

whereas infection was rescued when virus was pseudotyped with VSVg. Co-depletion of Mena and EVL seemed to impair inbound CCTH (~26% decrease) but had no effect on infection by cell-free virus.

Other actin binding proteins: Mixed and mostly moderate effects were observed for gRNAs in this group. Targeting of CAP1 notably reduced inbound infection by cell-cell and VSVg-pseudotyped virus (~28% and ~21% reduction respectively) but had no effect on free HIV. APC-gRNA seemed to enhance inbound CCTH (~20% increase) but, if anything, decreased infection by cell-free virus. No substantial infection impairment was observed in cells treated with Cofilin or Gelsolin gRNA. CRISPR targeting of capping proteins may have tendentially reduced cell-mediated and VSVg-dependent infection, but these effects were rather weak (~6-13% reductions).

5.3.2 CRISPR treatments did not compromise target cell viability

As commented on section 4.5.2, complete loss of cellular proteins after CRISPR treatment can potentially compromise cellular health or viability depending on the associated protein function and cell-type. For CRISPR gRNA bulk-treated cells, this can reflect on the viability of the cell population. Therefore, to exclude that inbound infection impairment was due to unspecific detrimental effects associated with some gRNA treatments, we also assessed the overall fitness of our CRISPR treated Jurkat populations. Since the same cells were used for inbound HIV and cell-viability experiments, these represent linked datasets. Given the high inter- and intra-experiment variability previously observed for the Alamar Blue assay (see Fig. 4.9), we decided to include an additional method to evaluate cellular health in this chapter (i.e. Trypan Blue cell viability assay, see 2.2.3).

The Alamar Blue method revealed that most LCV2-treated groups had a similar signal to the normalization and reference controls within each experiment (Fig. 5.4-A). However, in some cases (ITGB1, ITGB2, ITGAM, ICAM-1 and LIMK-1 gRNAs) treatment seemed to result in impaired cell health in at least one of the experiments (standard deviations ranging between 33-53% indicate high inter-experiment variability). In other cases (ITGAL, Filamin-A, Ezrin, Angiomotin, ROCK1 and WASP gRNAs) the Alamar blue signal was higher (>1.25 fold) than the average control signal. Importantly, however, these changes did not in any way correlate with changes observed for the inbound HIV infection data. Except perhaps for Rac1 (87% of control Alamar Blue signal), none of the gRNA treatments that reduced inbound HIV infection were observed to impair cell viability. The untreated wildtype control was the only group to show a correlation between increased Alamar Blue signal (~1.25 fold) and increased inbound HIV infection (1.34-fold for cell-cell and 1.2-fold for cell-free virus).

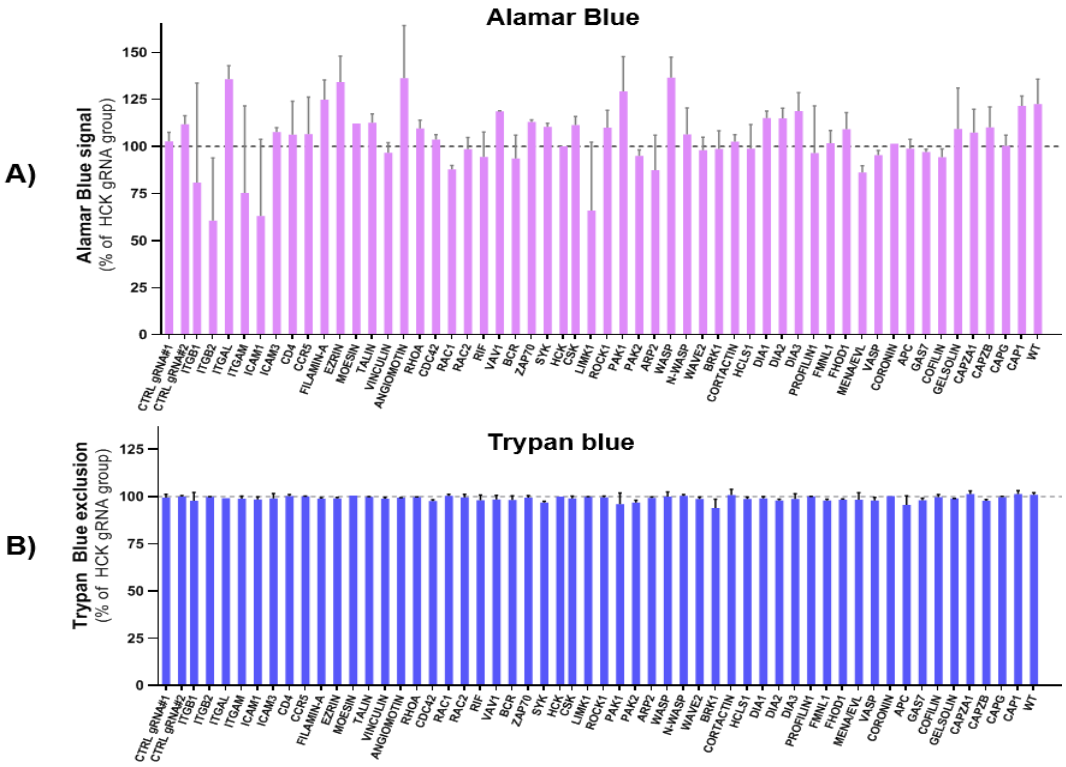

Figure 5.4: Cell viability assessment of CRISPR bulk-treated Jurkat cells. A) Alamar blue assay. 3 x 10^4 cells were seeded in duplicate in 96-well plates with a randomized plate design and incubated for 18h before start of Alamar blue assay. **B) Trypan blue exclusion method.** During counting of target cell groups in Trypan blue containing solution, the number of Trypan-Blue positive and negative cells was recorded. The proportion of viable cells was calculated as % = [#TrypanBlue-neg / Total#Cells] x 100. **A-B)** Data from each experiment was normalized to the internal control group (HCK-gRNA), which is represented by the dashed line at 100% (see 5.2.4 for rationale). Data indicates the mean and standard deviation for 2 independent experiments.

On the other hand, the linked Trypan blue data showed virtually no deviation from the control groups. Cell viability (as assessed with this method) for all target cell populations was within +/-5% of the normalization control, the non-targeting control gRNA and the untransduced wildtype control groups (Fig. 5.4-B). Together, both datasets suggest that i) CRISPR treatment did not compromise cellular viability in any of the gRNA-treated groups, ii) while there may be differences in metabolic state and/or proliferation between treated groups, these did not correlate with the observed changes in inbound HIV infection, and iii) transduction of Jurkat cells with LCV2 gRNA lentivirus and continued antibiotic selection moderately decreases cell metabolism/proliferation and permissiveness to HIV infection (compared to untransduced wildtype cells) in a way that persists after cell viability recovers to wildtype levels.

5.3.3 Analysis for hit selection

For general considerations about hit selection criteria in wide CRISPR screens, see section 4.5.3. Normality testing could not confirm normal distribution for any of the 3 datasets in

Figure 5.2. Therefore, we decided to increase the confidence range for hit selection to 5 x standard deviations (5xSTD) of the averaged control gRNA groups for each dataset. Figure 5.5 shows the 10 gRNA treatments that fell outside this range. To further narrow down this list, we excluded genes whose CRISPR-targeting only increased inbound HIV infection (i.e. ITGB1, Cdc42 and APC). The final hit list thus comprised the Rho-GTPases RhoA and Rac1, the tyrosine kinase Csk, the Arp2 subunit of the Arp2/3 complex, the formin-cooperator Profilin and the multifunctional CAP1 protein. CD4 was used as a positive control.

gRNA treatment	Cell-cell HIV	cell-free HIV	HIV-VSVg+
ITGB1	↑	↑	
CD4	↓	↓	
RHOA	↓		↓
CDC42	↑		
RAC1	↓	↓	↓
CSK	↓	↓	↑
ARP2	↓	↓	↑
PROFILIN	↓	↓	
APC	↑		
CAP1	↓		↓

Figure 5.5: Hits from inbound HIV CRISPR screen. The list shows all gRNA treatments that caused mean target cell infection to fall outside of the 5xSTD confidence range in at least one of the three datasets (green = increase in target cell infection and red = decrease). Where the trend appears to be maintained across other datasets (but does not exit the confidence range), only the direction of the change is shown in a colourless box.

5.3.4 Hit validation strategy

To validate our hits, we used a similar strategy to that described in the previous chapter (see 4.5.4). However, given; i) the large number of hits, ii) relatively strong effects even with bulk gRNA treatment, iii) that outbound and not inbound CCTH is the primary focus of this work, and iv) the time and cost associated with generation of pure clonal knockout cell lines, we used CRISPR gRNA bulk-treated Jurkat cells for the validation process. Additional inbound CCTH experiments were performed to obtain a sufficient number of replicates for statistical analysis. Hits were considered to be validated when a statistically significant reduction of viral transfer could be detected compared to the control gRNA group, after accounting for multiple testing.

The results from the additional experiments were consistent with that observed in the CRISPR panel screen. As expected, Jurkat cells treated with CD4-gRNA showed the strongest impairment in CCTH (Fig. 5.6). In contrast, the non-targeting control gRNA and the targeting HCLS1-gRNA control had virtually no effect on target cell infection (Fig. 5.6). A consistent

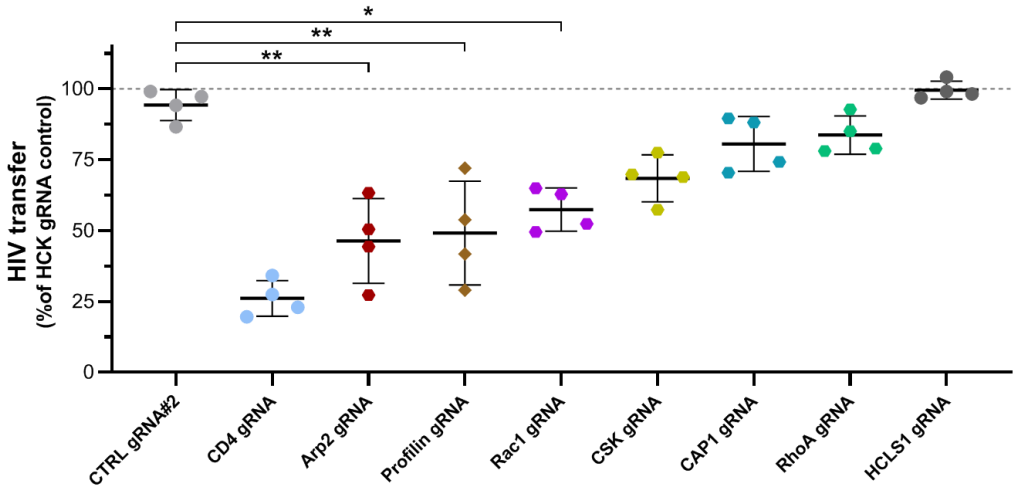

Figure 5.6: Impairment of cell-cell HIV transfer by CRISPR treatment of target cells. Wildtype U937 cells infected with HIV-IRESeGFP were used as donor cells in HIV-transfer assays and mixed with the indicated CRISPR-treated target cells. CRISPR gRNA bulk-treated cell populations were used as target cells. For a full and detailed description of experimental procedures see section 5.2.2. The percentage of infected target cells was normalized to an internal control treatment within each experiment (HCK-gRNA group), represented by the dashed line at 100%. Shown are the values, mean and standard deviation from 4 independent experiments. CD4-gRNA was included as a positive control, and HCLS1-gRNA as additional (targeting) negative control. All non-control treatment groups were compared to the non-targeting Control gRNA#2. Hits are arranged in order, according to the strength of the observed effects, for easier visualization purposes. * = $p < 0.05$ and ** = $p<0.01$ by Krustal-Wallis test with Dunnett's correction.

impairment of CCTH was observed when Jurkat target cells had been treated with gRNAs against Arp2 (53.6 ± 15% reduction compared to the HCK normalization control), Profilin (51 ± 18.3% reduction), Rac1 (42.6% ± 7.6% reduction), CSK (31.6 ± 8.3% impairment). Targeting of CAP1 or RhoA also moderately decreased inbound viral transfer (19.4 ± 9% and 16.3±6.7% reductions respectively). When these groups were compared to the non-targeting control gRNA, and multiple testing was accounted for, only Arp2 ($p < 0.01$), Profilin ($p < 0.01$) and Rac1 ($p < 0.05$) gRNA treatments observed statistical significance. This suggests that these three actin regulators play a non-redundant role for inbound HIV during entry or early post-entry steps. Indeed, Rac1 and Arp2/3 have been previously reported to play an important role for inbound infection with free HIV (see discussion below). In contrast, a role for Profilin during inbound HIV infection has not been previously described for either cell-free or cell-cell infection. We therefore attempted to generate Profilin -/- Jurkat clones to characterize this phenotype furhter. However, as with U937 cells, the Profilin -/- genotype resulted in aberrant and enlarged cell morphologies when cells were clonally expanded. Preliminary experiments supported an important role for Profilin in cytokinesis. This is further discussed in later section 6.4.1.

5.3.5 CSK-gRNA treated cells downregulate CD4

While the effect of CSK depletion on CCTH was moderate, the strong impairment of free HIV infection in these cells was intriguing, as it was comparable to that observed upon CD4-depletion. Preliminary characterisation experiments allowed us to determine the cause of their refractitivty to HIV infection. Since Csk directly regulates all Src family kinases, including Lck, which is involved in CD4 recycling, we speculated that depletion of CSK may indireclty affect CD4 surface levels. To test this hypothesis, we clonally expanded CSK-gRNA treated Jurkat cells and performed surface CD4 antibody staining. Cells were compared to validated CD4 -/- Jurkat cells and clonally expanded Control-gRNA Jurkat cells either stained with the same procedure (positive control) or mock stained (i.e. identical procedure except no CD4 antibody added). Indeed, we found that while all wildtype and control gRNA cell clones had detectable CD4 on their surface, ~60% of CSK clones essentially lacked CD4 on the cell surface, mimicking the phenotype of CD4 -/- cells. Representative examples are shown in Figure 5.7 below. This data must be however be treated as preliminary until; i) the phenotyping experiment is repeated with a new batch of CSK-gRNA treated cells (to ensure reproducibility of this observation), and ii) the phenotype can be reproduced with alternative CSK-gRNAs in order to exclude a potential off-target effect on the CD4 gene.

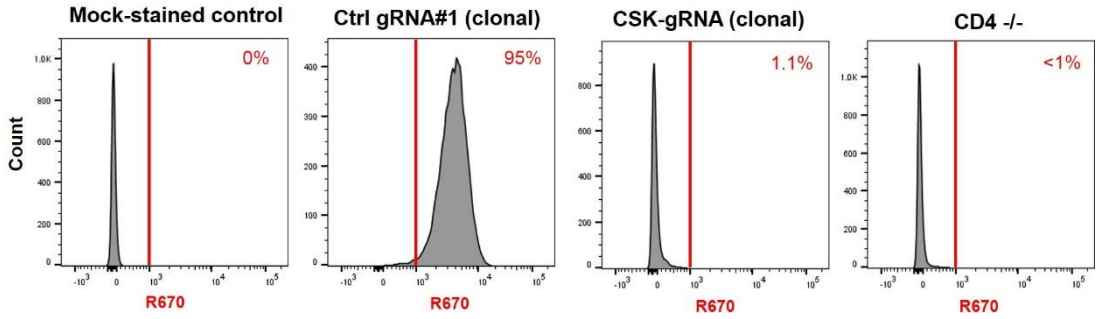

Figure 5.7: CSK-gRNA treated cells lack surface CD4 molecules. Clonally expanded Jurkat cells with different genotypes were surface stained with a monoclonal antibody against human CD4 directly conjugated to Alexa647 fluorophore for 30 minutes (no permeabilization step). Cells were fixed and analyzed by flow cytometry. The cell and signal gates were set based on the mock stained control (identical staining procedure except no antibody added). Shown are FACS histogram plots with signal intensity on the x-axis and event frequency on the y-axis. Data is representative of various clones for each cell-type in one experiment.

5.4 Discussion

This chapter aimed to identify actin regulators that are required for infection of target cells by inbound HIV. A major question was to what extent these requirements overlap for cell-transferred vs. cell-free HIV. Furthermore, we were interested in comparing the cytoskeletal mechanisms involved on both sides of CCTH, i.e. donor and target cells within the same experimental system. To answer these questions, we harnessed our CRISRP-VLP panel and

the CCTH assay established previously in this work. The latter was adapted for use with genetically modified target/recipient cells (see 5.2.2.). Target T-cells (Jurkat) were first CRISPR-treated to deplete specific actin regulators, and then exposed to either HIV-infected myeloid cells or cell-free HIV. A VSVg-pseudotyped free virus control was also included to help determine if HIV-specific entry steps were affected by the treatment. As with the previous chapter, most technical considerations were discussed within the earlier methods and results sections. Given the similar methodology, the major limitations of our experimental approach remain those exposed in section 4.6. It is also noteworthy that since our panel was designed primarily for myeloid cells, some of the targeted genes (e.g. HCK, ITGAM or Syk) are already expressed at low levels (if at all) in T-cell lineages. Thus, their influence may not be observed in Jurkat cells. However, for other regulators/pathways that overlap between myeloid and lymphoid cell types, it is important that phenotypes are observed in each relevant cellular setting, given the fundamental differences in HIV-actin manipulation outlined in 1.5.11. Below we discuss our findings in terms of their potential biological relevance.

Given the numerous observations from the CRISRP screen in this chapter, we will focus our discussion to those effects strong enough to exceed the 5x standard deviation confidence range below the value of the control group. The strongest infection-impairing effects were observed for gRNAs against CD4, Profilin, Arp2 and Rac1. Targeting these regulators for depletion notably reduced both cell-mediated and cell-free HIV (Env-dependent) infection. A strong effect was evidently expected upon depletion of CD4, given it is the primary HIV-entry receptor and as positive control in our screen. Depletion of Rac1 or Arp2 both notably reduced inbound infection by free HIV at an early stage (i.e. HIV Env-dependent). This is consistent with previous observations that Arp2/3 activity downstream of Rac1 is required for HIV-receptor/coreceptor concentration at the PM and subsequent fusion of virions with the PM (see Fig. 1.8 and [430,434,478]). Our results expand these observations for the first time to the CCTH setting (target-cell side). Given the strong effects observed in this context, we propose a combined mechanism where Rac1/Arp2/3 are required for both; i) actin-dependent polarization of HIV receptors at the VS, and ii) fusion of cell-transferred individual virions with the target cell. In addition, Rac1 depletion may also impair X4-HIV infection by associated conformational changes in the CXCR4 receptor, as reported in [677]. Interestingly, VSVg-pseudotyping only partially rescued infection in Rac1-depleted cells, whereas it significantly increased infection in Arp2-depleted cells (both Jurkat and U937). The latter contrasts with the findings of [478], which showed that VSVg-pseudotyping could rescue (but not increase) HIV infection in Arp2/3-inhibited 293T cells, and those of [434] who observed infection was still impaired in Arp3-depleted primary T-cells even upon VSVg-pseudotyping.

The discrepancies for these observations are presently not clear but could be related to the use of different cell types in each study.

Depletion of RhoA also moderately decreased inbound CCTH in our system. This could be a consequence of either inactivating the RhoA-Dia1 axis or reducing RhoA-mediated Cofilin repression (see Fig. 1.8), which would result in an aberrant decrease or increase of cortical F-actin, respectively. However, we favour the earlier hypothesis, because Dia1-gRNA had a similar effect to RhoA-gRNA, whereas targeting ROCK or LIMK1 had no effect. We did also not observe a reduction of inbound HIV infection upon Cofilin-gRNA treatment, despite confirmed CRISPR activity. This does not conflict with the model proposed in Figure 1.8, because previous studies have confirmed that Cofilin activation by inbound HIV is a specific requirement of primary resting CD4TC but not activated or transformed T-cells (e.g. Jurkat). This is likely due to largely inactive Cofilin pools, a relatively static actin cortex and low levels of endocytosis in resting T-cells [467,469,476,678]. Our observations are therefore consistent with those of previous reports.

Targeting Profilin1 for depletion strongly reduced inbound HIV infection. This was observed for both cell-free and cell-transferred virus but was more prominent in the latter context. While direct manipulation of Profilin by HIV cannot be excluded at this point, we consider an indirect contribution to F-actin-dependent HIV infection more likely. This is because Profilin's main roles as "guardian" and "gatekeeper" of the actin monomer are to replenish ATP-Actin (so that it can be again used for polymerization) and to facilitate F-actin elongation by formins and Ena/VASP proteins [313,328]. Indeed, gRNAs against the diaphanous formins (Dia), Ena/Evl or VASP also mildly reduced CCTH inbound infection, with the sum of their effects matching that of Profilin-gRNA. This could suggest that these proteins play a partially redundant role in HIV infection, which requires cooperation with Profilin (i.e. linear F-actin elongation). To our knowledge, no previous evidence has implicated Ena/Vasp with inbound HIV, whereas a recent study proposed a critical role of Dia formins in this context. Delaney et al. reported siRNA knockdown of Dia1 or Dia2 to reduce HIV infection, even when the inbound virus was VSVg-pseudotyped. Mechanistic experiments suggested an important role of Dia for HIV uncoating [509]. However, our observations strongly contrast with these findings. Targeting of Dia1 or Dia2 via CRISPR did not reduce VSVg-pseudotyped HIV infection of U937 or Jurkat cells in our hands. This was confirmed in Dia2 -/- and Dia2 shRNA-knockdown U937 cell lines, which could be infected at normal levels with HIV-VSVg+ (not shown). While we cannot explain these discrepancies, we highlight that the effect observed by Delaney et al. was independent of the ability of Dia to interact with the actin

cytoskeleton [509]. It can therefore at least be agreed that individual Dia formins are mostly dispensable for actin-manipulation by inbound HIV.

While our data suggests that Profilin's contribution may be related to its ability to assist linear F-actin elongators, Profilin depletion may also more generically impair HIV infection by reducing overall actin polymerisation levels (including Arp2/3-related activity). This is because Profilin promotes the exchange of ADP for ATP in actin monomers, which is essential for actin turnover. Indeed, our CRISPR screen also identified the functionally related G-actin-binding protein "CAP1" as likely to play a role for inbound CCTH. Like Profilin, CAP1 can bind actin monomers in a 1:1 ratio and mediate their recharging with ATP. And while it can also mediate a wide range of other cytoskeletal changes [644], this Profilin-like activity has been proposed to be CAP1's most important function [645]. Based on these observations, we hypothesize that depletion of Profilin or CAP1 may impair inbound HIV infection (at least in part) by decreasing the pool of available ATP-bound actin monomers, and thus limiting the dynamic cortical F-actin remodelling events that are required for HIV entry.

Our preliminary observations with CSK-gRNA treated cells suggest that their reduced susceptibility to inbound HIV infection may be indirect due to a loss of CD4 surface expression in CSK depleted cells. While this requires further investigation, we envision at least two mechanisms that may contribute to this phenotype. Firstly, of the CSK target proteins, only Lck is known to directly bind CD4 and this interaction is critical for regulating CD4 internalization [679]. Thus, since CSK constitutively inhibits Lck, removal of CSK may result in strong Lck deregulation and its subsequent uncoupling from CD4, thus exposing endocytosis motifs and leading to reduced CD4 surface levels by endocytosis. This is consistent with the findings of Schmedt et al., who observed CSK inactivation to reduce CD4 levels in living mice and suggested that "CSK is involved in regulating CD4 surface expression" at the protein level [680]. Secondly, constitutive activation of CSK-target proteins may lead to chronic T-cell activation (e.g. via TCR-tyrosine phosphorylation by Lck), which has been observed *in vivo* to result in complete CD4 cell-surface depletion [681].

On the other hand, bulk-treatment with CSK-gRNA significantly increased susceptibility to infection with VSVg-pseudotyped HIV. Since this type of infection does not require CD4 expression, and this phenotype was not observed in CD4 -/- Jurkat cells, this is likely a consequence of losing CSK, but not CD4. This would suggest that constitutive activation of Src-family kinases is beneficial for inbound HIV infection at a post-entry step. This is consistent with previous observations that HIV increases Src-family kinase activity in Jurkat cells as early as 30 minutes after exposure [682] and that inhibitors against these kinases impair inbound HIV infection (post-entry) in primary CD4TC [683]. One potential mechanism could

again involve T-cell activation, which can increase endocytosis rates [467,678] and thus may increase VSVg-mediated entry levels upon removal of CSK.

5.5 Chapter acknowledgements

All experiments and data analysis in this chapter were performed by the author of this thesis. Note that the personal pronoun “we” is used throughout this thesis to reflect common scientific practice and to avoid the tedious use of the personal pronoun “I”. The reader is invited to think of “we” as the author and his supervisory team, given the important contributions of the latter to the guidance of this work.

Chapter 6. "HIV exploits cellular actin nucleators and corrupts the Cdc42-IQGAP1 axis of actin regulation"

6.1 Introduction

In the previous chapters we identified cellular cytoskeletal regulators that are likely to contribute to actin-dependent cell-cell transfer of HIV (CCTH). The master regulators of F-actin cellular protrusions Cdc42 and Rac1 (Rho-GTPases), the main actin nucleators (Arp2/3 complex and formins) and the formin-cooperator Profilin were found to play important roles for both inbound and outbound HIV infection and spread. These and other identified regulators were found to converge in pathways associated with cortical F-actin remodelling and formation of filopodia and/or lamellipodia (see Fig. 4.12). These previous observations were made with functional assays that measured the effect of specific CRISPR-gRNA treatments at the level of entire cell populations. In this chapter, we used a broad range of additional methods, including high-resolution imaging techniques, to further characterize the role of these regulators in the complex landscape of HIV-mediated actin manipulation at the single-cell level. Since directed changes in F-actin remodelling/regulation often result in altered cell morphology, the ability to "zoom in" on individual cells to directly assess the functional consequences of these changes is an invaluable resource in the study of F-actin manipulation by intracellular pathogens. Such approaches have previously contributed greatly to our understanding of both molecular pathogenesis mechanisms and the functioning of our own cytoskeleton [418,422,568]. As with most studies involving observation of biological processes, the higher the resolution, the more informative the result. Therefore, not only did we push the imaging abilities of our in-house (PC3 facility) fluorescence microscopy instruments to the limit, but we also collaborated with international groups that have consolidated expertise on high-end imaging techniques such as focused ion beam scanning electron microscopy (FIB-SEM). Both of these efforts allowed to evaluate HIV-actin changes not only at the single-cell but also at the single-virion level. In addition, we also resorted to mass-spectrometry and immunolabelling techniques to extend the resolution of our study towards the single-molecule level. By combining these powerful approaches with genetic manipulation of both cells and virus, we set to further dissect the intricate and pluriaxial intersection of HIV with the host's F-actin cytoskeleton

6.2 Aims

The primary aims of this chapter can be summarized as follows:

1) To exploit the genetic manipulation strategies described in sections 2.2.7 and 2.2.8, including, where possible, the use of pure knockout cellular clones, to determine the contribution of specific actin regulators to HIV-induced cytoskeletal changes, as well as their role for cell-cell viral spread.

2) To harness the power of high-resolution imaging techniques to evaluate the spatial correlation of outbound HIV with cortical F-actin networks and structures such as filopodia and lamellipodia.

3) To further resolve and define the molecular pathways leading to formation of actin-dependent structures that support cell-cell transfer of HIV, such as HIV-Filopodia and/or virological synapses.

6.3 Methods

6.3.1 Generation of CA-Dia2 cell lines

A constitutively active version of the formin Dia2 (CA-Dia2) was cloned into the lentiviral expression vector pLVX under the control of a CMV promoter. Constitutive activation was achieved by exclusion of the C-terminal autoregulatory domain (DAD) which corresponds to residues 1051-1081. Forward and reverse primers were designed to amplify the sequence coding the first 1050 residues of Dia2 from MGC human cDNA template (Dharmacon) and to introduce the relevant restriction sites. For pLVX_CA-Dia2, this sequence was cloned using ApaI/NotI into a modified pLVX-mCherry-Actin (Clontech) which harbors a multiple cloning site between the original ApaI/XbaI sites. For pLVX_CA-Dia2-mCherry, the sequence was cloned into pLVX-mCherry-N1 (Clontech) using the XhoI/ApaI sites. The resulting plasmids were sequence-verified to confirm that the entire Dia2-ORF minus the DAD domain was introduced without mutations or frameshifts at the desired location. VSVg-pseudotyped lentiviral particles were generated as described in 2.2.6, and cells were transduced at a MOI=0.5 and selected in puromycin containing medium (2 μg/mL) for at least 14 days.

6.3.2 IQGAP1-targeting sequences

The following DNA sequences were used to disrupt IQGAP1 expression by either shRNA-mediated knockdown or CRISPR-Cas9-mediated gene editing. All oligos were obtained from IDT technologies Inc. CRISPR gRNAs were cloned into LCV2 vector (see 2.2.7.3) and shRNAs were cloned into pLKO.1 vector (Addgene#8453). For LCV2-treated cells, the surveyor primers in Table 6.1 were used as indicated in 4.3.6 to monitor changes at the gRNA-target locus.

Sequence name	Source	Sequence (5'-3')
IQGAP1_gRNA1	This study. Designed with: http://crispor.tefor.net gRNA-design tool as described in section 2.2.7.	TGGGGTCTACCTTGCCAAAC
IQGAP1_gRNA2		GTGGATGGAAGCATGCCTAG
IQGAP1_Surveyor-Fwd		CCTCTCTCCTTTGGTGCAGG
IQGAP1_Surveyor-Rvs		GAGGCGGGCTTTCCAGATAA
IQGAP1_shRNA1	Broad Institute. (TRCN0000047483)	GCCCACATTGTGCCTTTATTT
IQGAP1_shRNA2	Broad Institute. (TRCN0000047487)	GCATCCACTTACCAGGATATA

Table 6.1: Oligonucleotide sequences used to target IQGAP1 DNA or mRNA.

6.3.4 HIV-Gag mutant panel

HIV-mutant	Mutation description	Effect of mutation	Source
Δp6	deletion of p6 domain in Gag	Inability to recruit the cellular abscission machinery, which is known to interact with actin cytoskeletal regulators [684,685]	[89]
ΔNC	The nucleocapsid domain was replaced with an LZ domain from the GCN4 protein (yeast).	The LZ-domain preserves the ability to oligomerize. The missing NC domain is thought to be critical for the association of HIV-Gag with F-actin (see 1.5.5).	[89]
Capsid-P99A	point mutation(s) in Capsid domain of Gag. Known as Gag "curvature mutants"	Failure to induce Gag-curvature at the membrane [686,687]. Impaired viral budding [688].	[686,688]
Capsid-E75A/E76A			

Table 6.2: HIV Gag-mutant panel used in this study

6.4 Results

6.4.1 Profilin depletion results in clear defects in cytokinesis

In this study we identified Profilin1 as a key actin regulator that is important for both inbound and outbound CCTH. These experiments involved Profilin-gRNA bulk-treated cells, which appeared normal by light microscopy and had unimpaired cell viability (Alamar blue and trypan blue assays). To identify a phenotype associated with Profilin depletion, we single-cell sorted these cells, expanded them and phenotyped them as described in 4.3.6 to obtain Profilin -/- clones. A striking phenotype of these cells was readily apparent by light microscopy, even at low magnifications. Clonally expanded Profilin knockout cells were characterized by the abundant presence of notably enlarged cells, which often spanned several diameters of a normal cell (Fig. 6.1-A). This was repeatedly observed across numerous cellular clones for both U937 and Jurkat cell lines. To investigate this phenotype further, cells were live stained with NucBlue® (nuclear dye) and imaged at high magnification. This revealed that enlarged cells typically contained multiple distinct nuclei within the cell body (Fig. 6.1-B). This

observation is consistent with previous studies, which have suggested a role for Profilin in cytokinesis (see discussion, 6.5.1). Due to their extreme phenotype, we decided not to pursue further experiments with Profilin knockout cells, as these will likely have a highly abnormal cell behaviour. Future studies to assess the role of Profilin for HIV infection would therefore benefit from shRNA-mediated knockdown approaches rather than complete protein depletion. In any case, the critical role of Profilin for many cellular functions [653] makes it an unlikely target for medical therapies in any disease context. Since our results obtained in Chapter 4 suggest that Profilin's contribution to outbound CCTH is related to its cooperation with diaphanous formins (Dia), we turned our attention to this protein class instead.

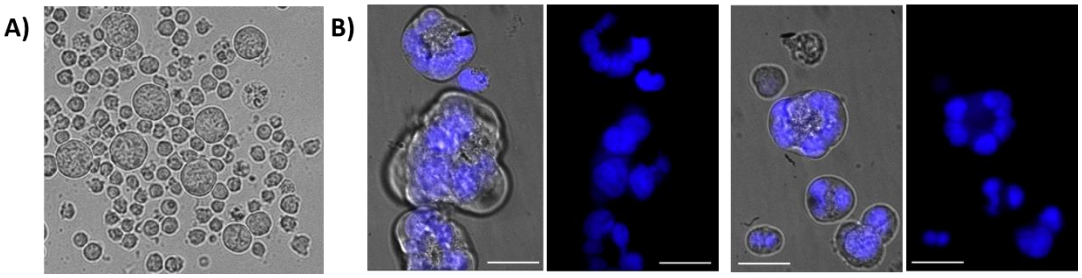

Figure 6.1: Profilin-depleted cells show cytokinesis defects. U937 cells were treated with LCV2-Profilin-gRNA, then single cell sorted and clonally expanded for 3 weeks before phenotyping. Cell aggregates were dissociated by resuspension 30 minutes before imaging. A) Representative image of a culture with enlarged cells. B) Cells were stained with NucBlue® nuclear dye for 30 mins then imaged at high magnification (60x) with a DeltaVision Elite microscope. Scale bar = 25 μm.

6.4.2 The role of diaphanous formin activity for cell-mediated HIV spread

6.4.2.1 Dia2 activation increased cell-cell transfer of HIV but not free virus release

The mild but similar effect of gRNA bulk-treatment when individually targeting Dia1, Dia2 and Dia3 (Fig. 4.8-B), together with the stronger effect of Profilin-gRNA, suggested that there may be functional redundancy among Dia formins in the context of HIV transfer. Therefore, we decided to test the effect of constitutive formin activation on CCTH, as this would increase viral transfer independently of isoform redundancy. A constitutively active version of Dia2 (i.e. CA-Dia2, which lacks the autoregulatory DAD domain) was cloned into the lentiviral expression vector pLVX under the control of a full-CMV promoter as described in 6.3.1. When HIV transfer experiments were repeated with donor cells expressing CA-Dia2, we observed a statistically significant increase in target cell infection whether Jurkat or TZM-bl cells were used as targets (Fig. 6.2-A, 36.4 ± 6.5% and 55 ± 12.7% increase respectively). Similar results were obtained when a CA-Dia1 variant was used (not shown). In contrast, there was no obvious differences in free virus release between CA-Dia2 and wt infected cells (Fig. 6.2-B). These results confirm that Dia2 activity can positively influence cell-mediated transfer of HIV from myeloid cells.

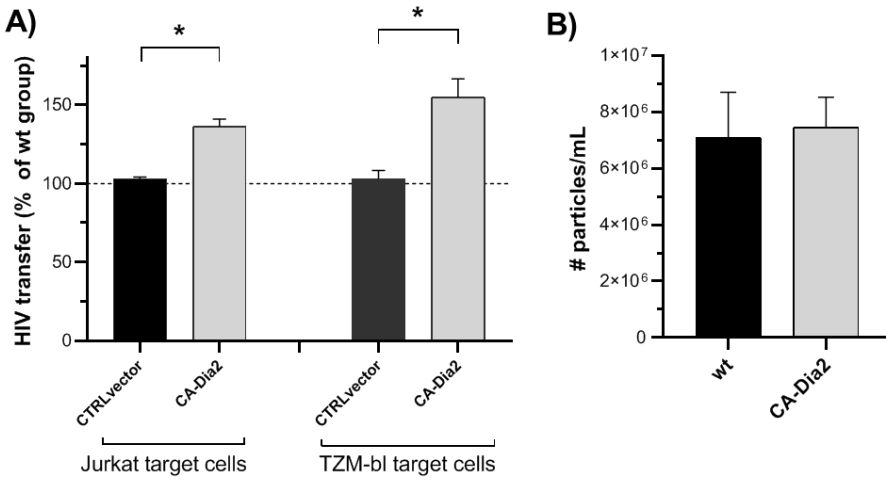

Figure 6.2: Effect of constitutively active Dia2 for outbound HIV. U937 cells were transduced with pLVX-CA-Dia2 which expresses a constitutively active version of the formin Dia2 (CA-Dia2). Cells were infected with HIV-IRESeGFP and used as HIV donors in viral transfer experiments as described in 2.2.11. **A)** The percentage of infected target cells (HIV transfer data) was normalized to that of the wildtype control in every experiment. Equivalent lentiviral vector without CA-Dia2 was used as control. Data indicates the mean and standard error of 4 independent experiments. Statistical significance was assessed via Mann-Whitney test (* = $p < 0.05$). **B)** Wildtype and CA-Dia2 expressing cells were infected with HIV-iGFP for 48h. Donor cells were then washed to remove free virus and seeded under identical conditions to those used in viral transfer assays but in the absence of target cells. The cell-free fraction was collected 12h later and the number of viral particles per sample was determined by single particle counts as described in 2.2.12.3.

6.4.2.2 Constitutively active Dia2 leads to straight filopodia uncoupled from HIV

To investigate how CA-Dia2 increases CCTH, we first resorted to high resolution fluorescence microscopy. A CA-Dia2-mCherry fusion construct was combined with fluorescent phalloidin staining to assess the interplay of HIV, F-actin and CA-Dia2 in infected cells. Initial experiments revealed that both infected and uninfected CA-Dia2 cells often displayed long straight filopodia. These appeared more rigid than wildtype filopodia when observed by live imaging. Enrichment of mCherry signal was also often observed at the filopodial tips (Fig. 6.3-A). Strikingly, however, filopodia in CA-Dia2 infected cells were not decorated with HIV buds at their tips (Fig. 6.3-C), which is in strong contrast to that observed in wt cells. This exclusion of HIV from filopodial tips was found to be statistically significant (Fig. 6.3-D).

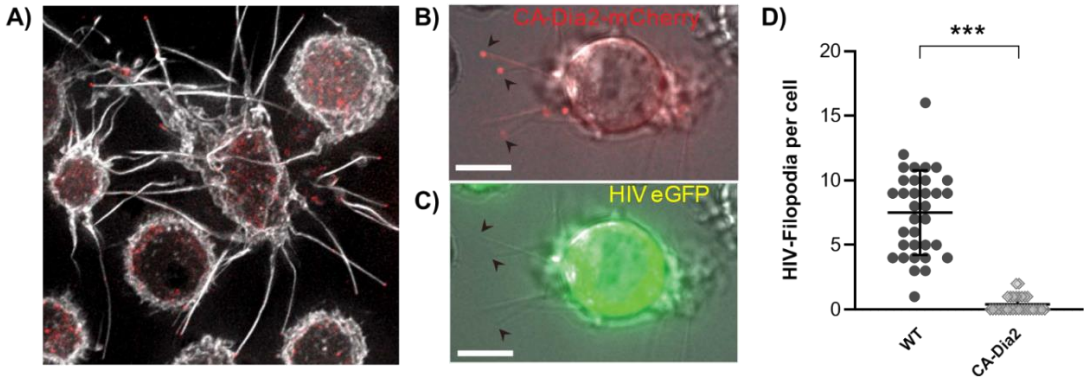

Figure 6.3: Filopodia in CA-Dia2 cells. U937 cells were transduced with pLVX CA-Dia2-mCherry and infected with HIV-iGFP. A) Phalloidin stained CA-Dia2 U937 cells (white = F-actin, red = CA-Dia2). Note enrichment of mCherry signal at filopodial tips. B) mCherry signal of a CA-Dia2 HIV-infected cell. C) GFP signal of the same cell. D) Quantification of HIV-positive filopodia per cell in live cell cultures. At least 30 cells from three independent experiments were analysed per condition. *** = $p<0.001$ by Mann-Whitney test.

6.4.2.3 Constitutively active Dia2 increases infected donor-cell adhesion

Wildtype HIV-Filopodia are highly motile and mediate scanning and repositioning of target cells that likely depend on Env-CD4 interactions [89]. Since CA-Dia2 filopodia are more rigid and do not have HIV at their tips, they are unlikely to facilitate viral transfer by this mechanism. To visualize the interaction of HIV-infected CA-Dia2 cells with target cells we used live imaging approaches as described in section 2.2.12.2. Our intention was to assess changes in conjugate and virological synapse formation compared to the wildtype. These experiments are typically set up at lower cell densities than viral transfer assays for better visualization but also to evaluate the ability of donor cells to find, engage and maintain association with target cells. However, at these cell densities we could not observe almost any interaction between infected donor and target cells. This was because infected CA-Dia2 cells seemed to be anchored to the cell culture substrate and did not move around the culture. Interestingly, this atypically enhanced adhesion was only observed for infected but not uninfected CA-Dia2 cells. Figure 6.4 and supplementary video S4 show a representative time series. All U937 cells in these experiments are puromycin resistant and therefore express the pLVX_CA-Dia2 construct. An infected donor cell (HIV-iGFP+) is found near the centre of the field of view, and despite abundant filopodial activity it's X-Y position remains virtually unchanged for the entire duration of the movie, never reaching the target cells below it. In contrast, uninfected donor cells (also CA-Dia2) are able to move around, often entering or exiting the field of view. Even when these experiments were repeated at higher cell densities, similar observations were made (although more evident in the example below). These qualitative observations suggested that in the context of HIV infection, Dia2 activity may somehow increase cell-adhesion.

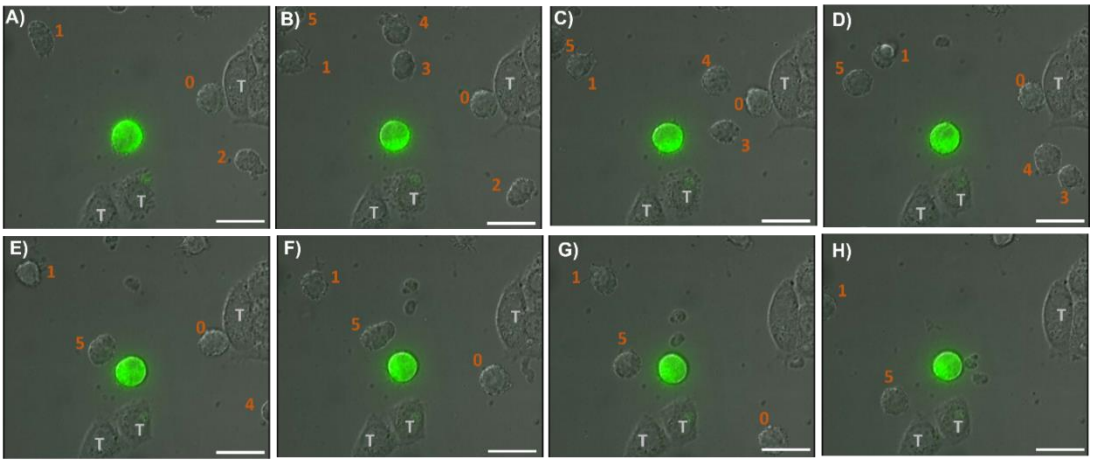

Figure 6.4: Representative time series of CA-Dia2 U937 cells in coculture. U937 cells were transduced with pLVX_CA-Dia2 and selected with puromycin for over 14 days to ensure all cells express the lentiviral construct. Cells were then infected with HIV-iGFP for 48h, washed to remove free virus and incubated with TZM-bl cells. Cells marked as "T" correspond to TZM-bl cells. Uninfected U937 cells of interest are numbered 0-6 to facilitate visual tracking through different frames. Scale bar = 25 μm. For complete time series see supplementary video S4 (attached to this thesis).

To test this hypothesis, we used available datasets from the viral transfer assays with TZM-bl target cells. Instead of looking at the number of Red+|GFP+ double positive cells (productively infected target cells), we looked at the number of Red-|GFP+ cells. These correspond to infected donor cells that remained attached to the surface of the target cells after the two washing steps that remove most donor cells at the end of the coculture period. Indeed, about 5-fold more wash-resistant donors were found at the end of cocultures with TZM-bl target cells when donor cells expressed CA-Dia2 compared to wt cells (Fig. 6.5). While this approach does not provide information about uninfected donor cells (since these are non-fluorescent), it confirms that U937 CA-Dia2 infected with HIV adhere more strongly to TZM-bl target cells compared to infected U937 wildtype cells.

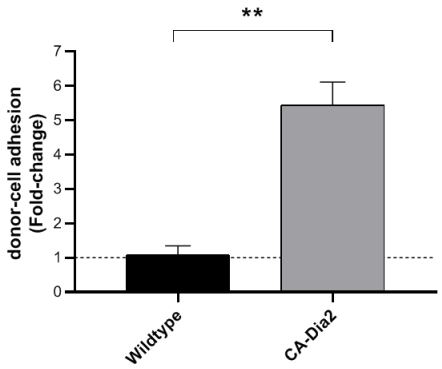

Figure 6.5: Enhanced donor-cell adhesion in CA-Dia2 cells. HIV transfer assay with TZM-bl target cells was conducted as described in 2.2.11. Donor cell adhesion to target cells was estimated as follows. At the end of the coculture (confluent target-cell sheath), the number of Red-|GFP+ cells (infected donor cells) remaining after two PBS washes was normalized to that of the BMS-378806 (10 μM) control group, where Env-CD4 interactions are inhibited from the start. Data indicates the mean and standard deviation of 4 experiments. ** = $p < 0.01$ by Mann-Whitney test.

6.4.3 HIV exploits Arp2/3 to seed Filopodia that aid cell-cell viral spread

Two main pathways are thought to initiate filopodia formation in healthy mammalian cells. Both are regulated by Rho-GTPases and lead to the activation of actin nucleators (see 1.4.7.1). One is dependent on Dia2/Dia3 downstream of either Rif or Cdc42, whereas the other is dependent on the Cdc42-WASP/N-WASP-Arp2/3 pathway [354,368]. Since many of these regulators were identified as hits in chapter 4 (e.g. Dia2/Dia3, Cdc42, N-WASP and Arp2), this further supports an important role for filopodia in CCTH. Previous studies from our lab showed that >80% depletion of Dia2 protein expression by shRNA led to a significant reduction in the length of HIV-Filopodia but did not result in their disappearance. In fact, Dia2 knockdown cells have more (albeit shorter) filopodia per cell [89]. Since we could recapitulate these observations with our clonal Dia2 -/- cells, this suggests that other actin regulators must be responsible for seeding of the initial HIV-Filopodia structure, whereas Dia2's main role is likely filopodial elongation. We therefore turned our attention to the Arp2/3 complex to explore; i) whether it plays a role in HIV-Filopodia formation, and ii) whether this is related to the impairment of CCTH observed in Arp2-depleted cells.

6.4.3.1 Arp2/3 is present along the base, shaft and tip of HIV-Filopodia

Filopodia formation is thought to occur from underlying cortical branched F-actin networks (see 1.4.7.1). Therefore, the presence of Arp2/3 at the filopodial base is expected. However, if Arp2/3 plays a more active role in initial filopodial protrusion, it should also be present within the shaft or towards the tip. To evaluate this, we performed immunofluorescent staining in HIV-infected U937 cells with antibodies directed against Arp2 and Arp3 as described in section 2.2.12.1. When we examined the footprint of Arp2/3 along the filopodia, we observed that the base, the shaft and the tip were all positive for Arp2/3 antigen (Fig. 6.6-B). As a control, we also stained infected CA-Dia2 U937 cells with the same procedure and in this case observed Arp2/3 signal at the base and proximal section of the shaft, but not on filopodial tips (Fig. 6.6-C). Formal measurement of the distance from the tip of filopodia to the first detectable Arp2/3 signal confirmed a significantly greater distance in CA-Dia2 cells compared to wildtype cells (Fig. 6.6-D, 6.9 vs. 1.8μm). These observations support the hypothesis that Arp2/3 plays an important role in formation of wildtype HIV-Filopodia.

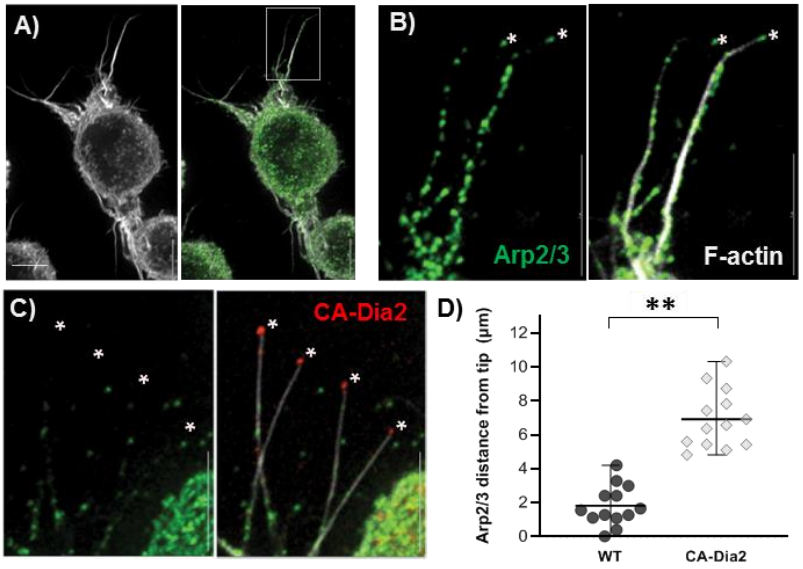

Figure 6.6: Immunofluorescence staining of HIV-Filopodia. U937 cells were infected with HIV-iGFP for 48h and staining was performed as described in 2.2.12.1. Asterisks highlight the terminal ends of filopodia. A) Wildtype infected cell stained for F-actin (white) and Arp2/3 (green). B) Magnification of the highlighted region in A. C) CA-Dia2-mCherry infected cell (magnified to see filopodial tips). D) Distance from filopodial tip to first detectable Arp2/3 signal. ** = $p < 0.01$ by non-parametric Mann-Whitney test.

6.4.3.2 Both Arp2/3 and formin actin nucleators are required for HIV-Filopodia

In chapters 4 and 5 we observed a strong effect of LCV2-Arp2-gRNA in reducing both outbound and inbound CCTH, which suggests a strong CRISPR treatment penetration. However, despite extensive phenotyping we were unfortunately not able to establish Arp2 -/- knockout cell lines after clonal expansion, likely due to an essential role of this protein for cell survival or proliferation (see 6.5.1). We therefore decided to instead pursue partial protein depletion by shRNA knockdown. Two shRNAs for each Arp2 and Arp3 (see Table 2.1.7.3) were cloned into the pLKO.1 vector (Addgene#8453) and delivery occurred by lentiviral transduction. Transduced cells were selected in antibiotic-containing medium for at least 2 weeks before experiments. Despite confirmed ~80% total target protein depletion (see below), Arp2/3-knockdown cells infected with HIV still displayed filopodia on their cell surface. While there could be multiple explanations for this (see discussion), one possibility is that Arp2/3 could play a catalytical rather than structural role in filopodia formation. In this case, the remaining Arp2/3 pool could still potentially "seed" nascent filopodia, which would be then elongated by formins such as Dia2. To test this hypothesis, we attempted simultaneous depletion of Arp2/3 and Dia2. We re-transduced Arp2/3 knockdown cells (puromycin resistant) with pLKO.1-Dia2-shRNA (hygromycin resistance) and selected cells in the presence of both antibiotics for 2 weeks. Effective knockdown of Dia2, Arp2 and Arp3 was confirmed at the protein level by western blot (see Supplementary Figure 1), which revealed

target protein depletion rates of >95%, >85% an >75 respectively, compared to wildtype cells. Fluorescence microscopy of these Arp2/3-Dia2 double knockdown cells (F-actin stained with fluorescent phalloidin) revealed a clear lack of filopodia (whether long or short) in virtually all cells. These cells were however not round but rather displayed what appeared to be "veil-like" protrusions on the cell surface (Fig. 6.8-C). To further characterize these structures, we engaged in collaboration with the lab of Dr. Siriam Subramaniam at the National Cancer Institute (Bethesda, USA). Samples (HIV-iGFP infected U937 cells) were prepared and imaged in our lab on gridded coverslips before fixing with Karnovsky's fixative and shipping to the National Cancer Institute where they were imaged at the indicated grid positions with "correlative Focussed Ion Beam Scanning Electron Microscopy" (FIB-SEM), roughly as described in [689]. This advanced technique, which allows reconstructed 3D-imaging of entire cells and sub-cellular features at high resolutions (~10 nm) is described in Figure 6.7 below.

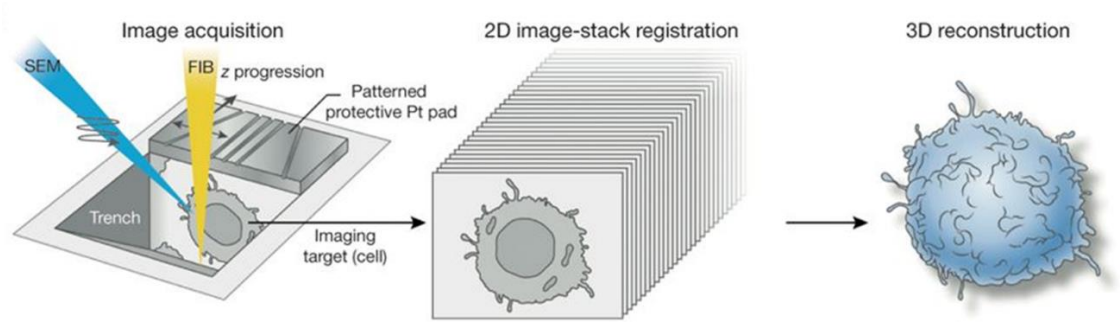

Figure 6.7: Overview of Focussed Ion Beam - Scanning Electron Microscopy (FIB-SEM). Image adopted from [690] with the author's consent. This technique uses a focused ion beam (FIB) to sequentially ablate the surface of fixed and resin-embedded biological samples with nanometer precision. Combination of sequential "milling" with alternating scanning electron microscopy (SEM) of the exposed surface leads to serial image stack acquisition of large volumes in an automated way. The resulting stack of images can be processed to yield correlated 3D models of entire cell volumes, which allow examination of cell topology and individual z-slices, as well as visualization of sub-cellular features at high resolution (~10 nm) in either 2D or 3D formats.

FIB-SEM high resolution 3D models confirmed our previous observations from fluorescence microscopy. Wildtype U937 cells displayed long and thin filopodia protruding from the cell surface (Fig. 6.8-A). At this higher resolution we could also confirm that these structures were thicker at the base and essentially unbranched (Fig. 6.8-G). In contrast, Dia2-depleted cells had more abundant but shorter filopodia (Fig. 6.8-E), and branching was occasionally observed (Fig. 6.11-A). Interestingly, Arp2/3-Dia2 co-depleted cells showed complete absence of filopodia, which instead were replaced by a large network of lamellipodial structures (Fig. 6.8-F). These were ultrastructurally distinguishable from "blebs" (see Table 1.2) when observed with FIB-SEM and were more reminiscent of lamellipodia (Dr. Kedar Narayan, personal communication). In any case, the strong phalloidin staining of these structures confirms that they are primarily F-actin dependent and consistent with protrusions

where the PM is still intimately associated with the F-actin cytoskeleton (Fig. 6.8-C). Together, these results indicate that both Arp2/3 and Dia2 are required for formation of long HIV-Filopodia as observed in HIV-infected wildtype U937 cells and dendritic cells.

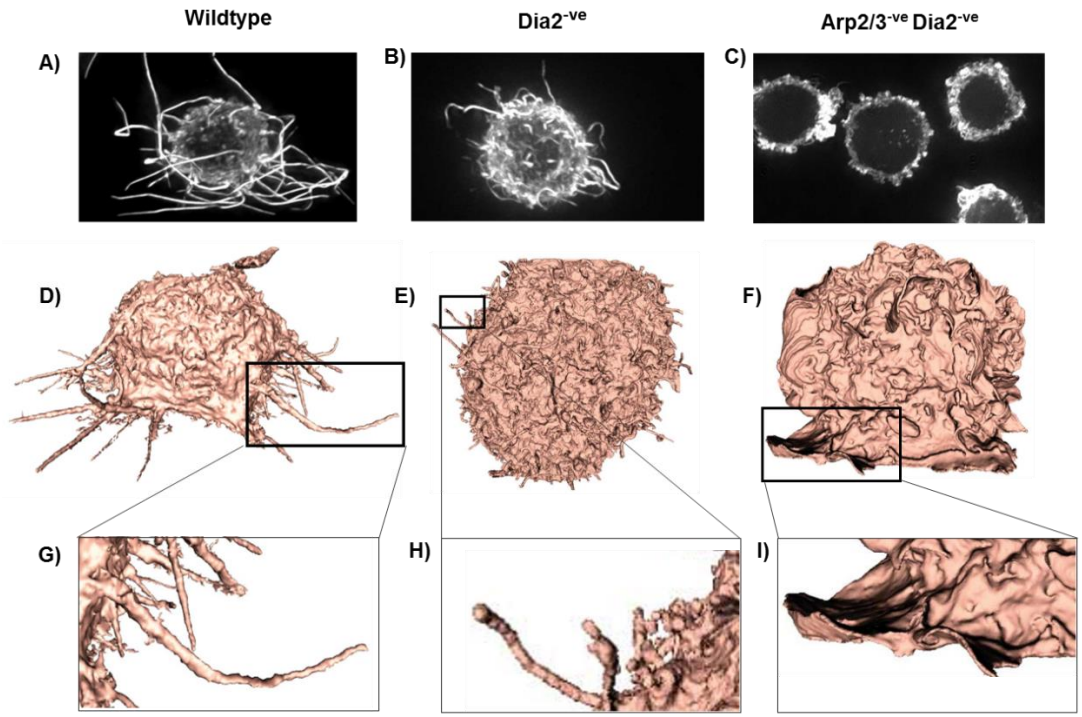

Figure 6.8: Topology of HIV-infected U937 cells depleted of actin nucleators. U937 wildtype cells, Dia2^{-ve} cells (depleted of the formin Dia2) and Arp2/3^{-ve} Dia2^{-ve} (co-depleted of both Arp2/3 and Dia2) were infected with HIV-iGFP and imaged post-fixation at high resolution. Representative images are shown for each cell-type with: **A-C)** High resolution fluorescence microscopy. Cells were fixed with 4% paraformaldehyde and stained with fluorescent phalloidin, then 50 optical Z-sections (~0.15 μm) were acquired with a DeltaVision Elite microscope. Images were deconvoluted and volume projected using SoftWorx software. **D-F)** FIB-SEM microscopy. **G-I)** Magnification of highlighted regions. A,D,G = Wildtype. B,E,H = Dia2^{-ve}. C,F,I = Arp2/3^{-ve} Dia2^{-ve}.

6.4.3.3 Lack of filopodia impaired cell-cell HIV transfer but not free virus release

To assess the role of HIV-Filopodia in cell-mediated viral spread, we repeated cell-cell viral transfer experiments with our Arp2/3-Dia2 co-depleted cells. Interestingly, HIV transfer from double knockdown U937 to Jurkat target cells was significantly reduced (39 ± 5% of average wildtype transfer), whereas transfer to TZM-bl target cells was unimpaired (Figure 6.9-A). This strongly suggests that the disruption in viral transfer is not due to a reduction in free virus release or particle infectivity, as this would be expected to affect both target cell types similarly or to show a stronger effect for TZM-bl targets, which are more permissive to this type of infection. In agreement, particle release from U937 double knockdown cells was only slightly lower (Fig. 6.9-B, ~18 ± 8.4% reduction) compared to the wildtype and this difference did not reach statistical significance.

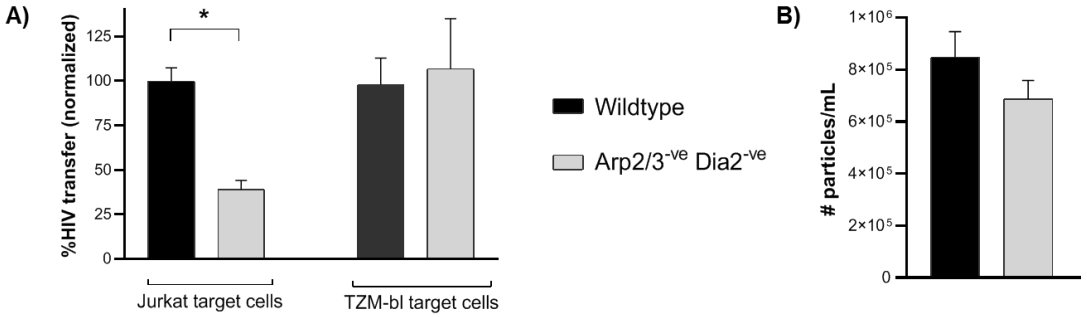

Figure 6.9: Outbound HIV transfer from Arp2/3-Dia2 double knockdown cells. A) Viral transfer assay was performed as described in 2.2.11. The percentage of infected target cells from each experiment was normalized to the inter-experiment average of the wildtype control group (i.e. "type-I normalization" as per [691]). **B)** Cells were infected with HIV-iGFP for 48h, then washed and infection-rate normalized. Cells were incubated for 12h and the cell-free fraction was collected. The number of viral particles per sample was determined by single particle counts as described in section 2.2.12.3. A-B) Data indicates the mean and standard error of 3 independent experiments. Data normally distributed. * = $p < 0.05$ by two-sided student t-test with Welch's correction.

We then evaluated the potential of cells depleted of Arp2/3-Dia2 to form stable donor:target conjugates and virological synapses (VS). When VS formation was visualized and quantified as indicated in 3.5.4, we did not observe any obvious differences in terms of VS frequency (Fig. 6.10-A) or morphology (not shown) between double knockdown cells and wildtype. Arp2/3-Dia2 depleted cells were able to form VS, characterized by strong polarization of the iGFP-signal (Gag) towards the target cell and by frequent formation of button-like structures. We also decided to test whether depletion of actin nucleators affected the HIV-Actin interaction in Arp2/3-Dia2 co-depleted cells. This could be assessed with the bimolecular fluorescence complementation (BiFC) platform established in chapter 3 (see 3.4.3 & 3.5.1). Since double knockdown cells were already puromycin- and hygromycin-resistant, we switched the PuroR region in the pLVX-VC-Actin vector for a blasticidine resistance gene. Multiple experiments confirmed that the VC-Actin:VN-Gag BiFC signal was not reduced when cells were co-depleted of Arp2/3-Dia2. Together, these observations suggest that although HIV-Filopodia can play an important role in cell-mediated viral transfer, the intersection between HIV and the actin cytoskeleton is preserved even after severe (~90%) cellular depletion of actin nucleators (Arp2/3 and Dia2), as is the ability to form virological synapses and to release free virus.

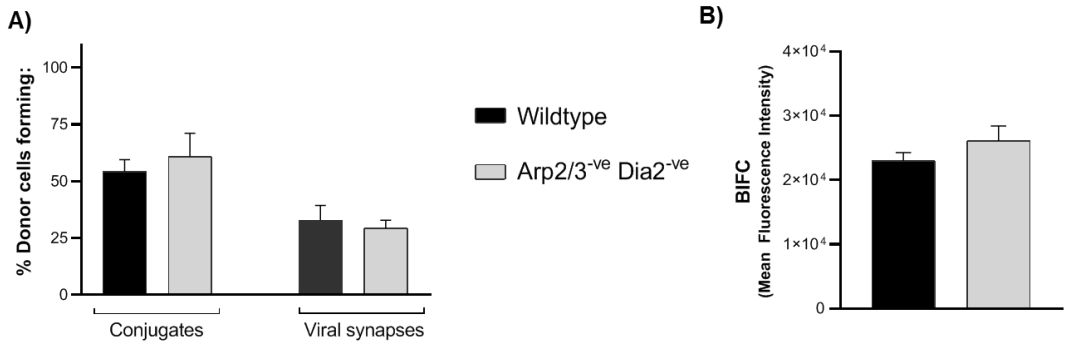

Figure 6.10: Further characterization of Arp2/3-Dia2 double knockdown cells. A) Observed frequencies of conjugate and viral synapse formation. Cells were infected with HIV-iGFP for 48h, then added to TZM-bl target cells. Experiment procedure, live imaging conditions and data analysis was performed as described in 3.5.4. Data indicates the mean and standard deviation from 2 independent experiments with at least 30 cells analysed per condition and experiment. **B) BiFC analysis by Flow Cytometry.** Cells were transduced with a pLVX-VC-actin and selected (10 μg/mL Blasticidine) for at least 14 days before experiments. Cells were then infected with HIV-iVN-Gag-IRESmOrange for 48h and the mean fluorescence intensity (Venus) per infected cell (Orange+) was determined by flow cytometry. Data indicates the mean and standard error of 4 independent experiments.

6.4.4 The correlation of HIV assembly and membrane curvature

We know from previous experiments that the HIV-Actin interaction occurs at least at two levels. The first is at the membrane/cortical F-actin level, as indicated by embedment of immature HIV virions at the tips of filopodia in infected myeloid cells and T-cells [89]. The second is at the cytoplasm, as indicated by the homogeneous BiFC signal presented in chapter 3 (see 3.5.1), which may involve interaction of Gag with F-actin, G-actin, or both. In the previous section we showed that the second type of interaction is preserved in Arp2/3-Dia2 co-depleted cells. However, given the collapse of the filopodial network in this cell type, we were interested in the potential uncoupling of HIV and F-actin at the membrane level. To evaluate this, we used the already available FIB-SEM data and mapped the location of HIV buds on the cell surface of cell types with different cortical F-actin structures (i.e. filopodia and lamellipodia). The procedure used for this purpose is described in Figure 6.11. We compared Arp2/3-Dia2 co-depleted cells to Dia2-depleted cells because the long (and fragile) filopodia in wildtype cells were often compromised/damaged during the sample preparation process, as revealed by the 3D models.

This analysis revealed that, in Dia2-depleted cells, HIV buds were primarily associated with filopodial structures (Fig. 6.11-A). Most budding virions were found at the tips of filopodia (strong positive membrane curvature), followed by the sides of the filopodial shaft (neutral curvature) (Fig. 6.11-B). In contrast, few virions were found at regions of negative curvature on the cell surface, even though a much larger area of the cell is covered by this feature, compared to filopodial tips. Indeed, normalization of counts to the total surface area per

structure, revealed a dramatic enrichment of virions to filopodial tips (Fig. 6.11-C). This is consistent with our previous qualitative observations from wildtype cells [89]. In Arp2/3-Dia2 co-depleted cells, virions were primarily found in areas of neutral and positive curvature within lamellipodia (Fig. 6.11_D-E). HIV at filopodial tips outscored lamellipodial ridges by ~5-fold, when surface area was considered (Fig. 6.11-F). Altogether, these observations indicate that; i) the location of the budding reaction on the PM is not randomly distributed, and ii) the virus may preferentially bud in regions with higher membrane curvature. Importantly, the structures enumerated as "viral buds" for this analysis can be unequivocally distinguished from other spherical surface structures (e.g. microvesicles). While this is not evident in the reconstructed 3D models (e.g. Figure 6.11), the raw FIB-SEM datasets are composed of stacks of hundreds of electron microscopy images with resolutions as high as 5 nm, which allows resolving the budding particles in all three planes. Real HIV buds are distinguishable due to the dark stain provided by the viral capsid underneath the membrane, whereas vesicles typically appear "empty" (Dr. Kedar Narayan, personal communication). Furthermore, the size of the observed structures is consistent with that of HIV virions (i.e. 80-120 nm across), and these were virtually not observed by FIB-SEM in uninfected U937 control cells.

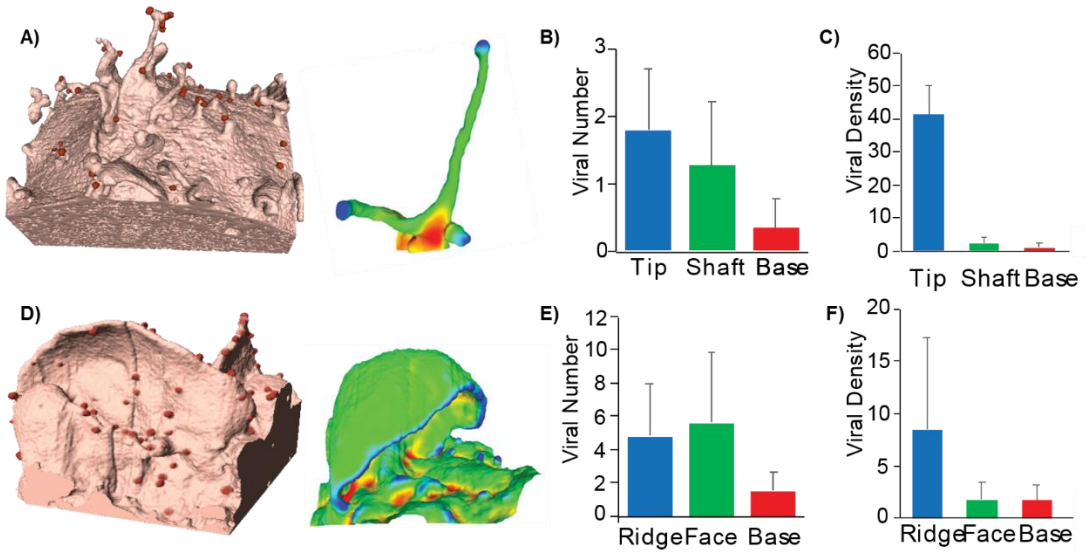

Figure 6.11: The location of the HIV assembly reaction. The 3D cell models obtained by FIB-SEM for Dia2-depleted cells (A-C) and Arp2/3-Dia2 co-depleted cells (D-F) were subjected to segmentation using Amira (ThermoFisher Inc) or 3D-Slicer [692]. Sub-volumes of lamellipodia and filopodia were extracted from these data, and fiducials were placed at the locations of budding virions. The number and location of individual virions as well as the surface area of lamellipodia and filopodia could be quantified with the XimagePAQ extension for Amira. This extension was also used to calculate mean curvature of lamellipodia and filopodia. Areas with negative curvatures (pseudo-coloured in red) were named "base", those with positive curvature (blue) as "ridge" or "tip", and neutral curvature (green) as "face" or "shaft", depending on the structure. A) & D) Representative sections of 3D models with HIV buds highlighted in red. B & E) Average number of buds per structure. C & F) Viral density calculated as the sum of counts for each structure normalized to their total surface area occupied per cell.

This preferential enrichment could be explained by at least two mechanisms. On one hand, HIV budding could simply be facilitated by areas of pre-existing positive curvature. Alternatively, curvature may be a consequence of cortical F-actin polymerisation associated with outbound HIV assembly. Our observations with CA-Dia2 cells argue against the first scenario (see discussion, 6.5.2). To explore the second hypothesis, we utilized a panel of HIV-Gag mutants (Table 6.2), which either do not bend the membrane (P99A and E75A/E76A), do not interact with F-actin (ΔNC) or do not allow particle release (Δp6). Surprisingly, deletion of the nucleocapsid domain, which is thought to mediate the Gag–F-actin interaction, had no obvious effects on the shape of cortical F-actin structures in infected cells, nor did it affect localization of Gag to the tips of filopodia (Fig. 6.12-A). The same was observed for the Δp6 mutant, which showed no differences to wildtype virus in these respects. In strong contrast, infection of Dia2-depleted cells with the HIV curvature mutants P99A and E75A/E76A led to a complete collapse of short HIV-Filopodia, which were instead replaced by an extensive network of lamellipodia, similar to that observed in Arp2/3-Dia2 co-depleted cells (Fig. 6.12 C-D). Quantification of filopodial frequencies confirmed a dramatic and statistically significant difference for these mutants compared to wildtype virus (Fig. 6.12-A). However, since Gag curvature mutants largely prevent formation of typical HIV-buds, we are unable to determine by FIB-SEM whether "flat" Gag-oligomers still preferentially accumulate at the ridges of lamellipodia in these cells. The biological relevance of these observations is discussed further below in section 6.5.2.

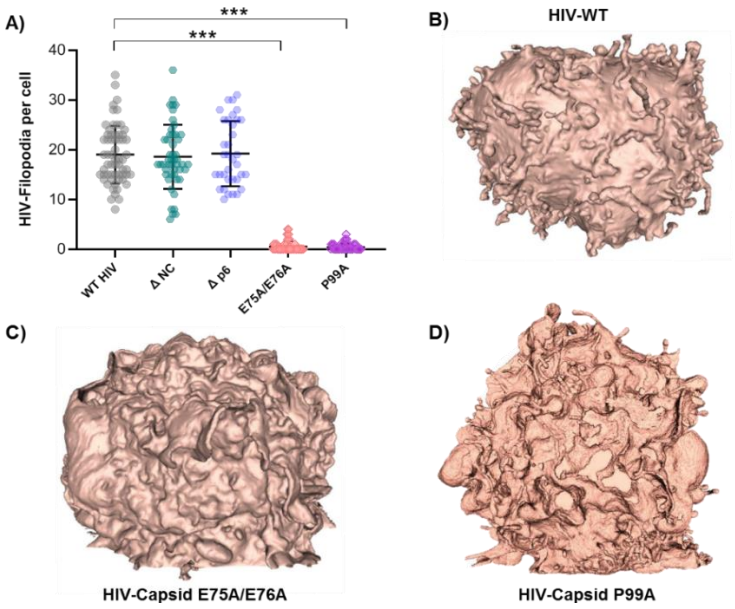

Figure 6.12: The effect of HIV-Gag mutants on cortical F-actin. Dia2-depleted U937 cells were infected with the HIV variants shown in Table 6.2 and incubated for 48h. A) Quantification of HIV-positive filopodia per cell in live cell cultures. At least 40 cells from three experiments were analysed per condition. ***p<0.001 by Krustal Wallis test with Dunnett's correction. B-D) Representative FIB-SEM 3D models of cells infected with the indicated HIV variants.

6.4.5 Corruption of Arp2/3 activity by HIV occurs via Cdc42

Abundant evidence suggests that the nucleocapsid domain is required for the association of HIV-Gag with actin filaments (see 1.5.5). The fact that ΔNC virus can form HIV-filopodia suggests that the viral corruption of the actin cytoskeleton that leads to these structures is mediated indirectly (i.e. via manipulation of cellular actin regulators), rather than by direct Gag-F-actin interactions. Given the results presented above, the most logical candidate for such manipulation would be the Arp2/3 complex. However, despite the prominent role of Arp2/3 activity at multiple stages of the viral life cycle, no direct physical association has been reported between Arp2/3 and viral proteins. Rather, the virus seems to exert control over Arp2/3 and its unique actin polymerisation abilities by indirect manipulation via Rho-GTPases (see section 1.5.9.1). Several lines of evidence point towards a key role of Cdc42 in the context of HIV-filopodia and cell-mediated HIV spread. These include; i) Cdc42's known ability to regulate filopodia formation in various cell types (see 1.4.7.1), ii) activation of Cdc42 in HIV infected cells (see 1.5.9.1), iii) our identification of Cdc42 as a factor important for CCTH (see 4.5.4), and iv) our observations that HIV-Filopodia play a role in CCTH (Fig. 6.9). We therefore decided to further characterize the role of Cdc42 in HIV-Filopodia formation. Cdc42 -/- U937 cells were generated and phenotyped as described in 4.3.6-4.3.7. When these cells were stained with fluorescent phalloidin (to visualize F-actin) and imaged by high-resolution fluorescence microscopy, we observed a clear lack of filopodia, and instead an abundant network of lamellipodia, as previously observed for Arp2/3-Dia2 double knockdown cells, and cells infected with curvature mutant virus. While this phenotype was present in both infected and uninfected Cdc42 -/- cells (Fig. 6.13-B), it was much more evident in the context of HIV infection, when compared to wildtype cells that display abundant HIV-Filopodia.

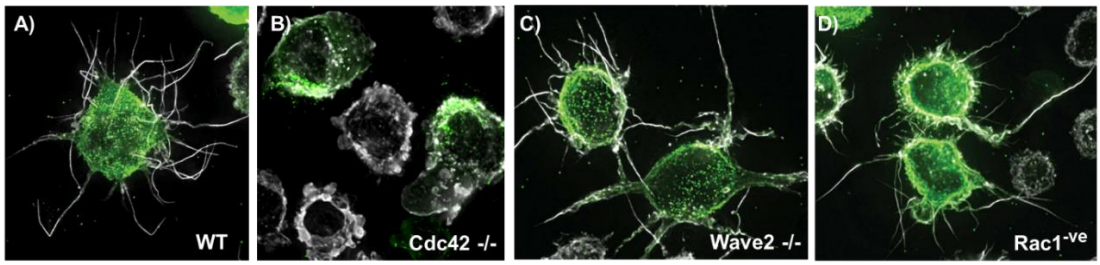

Figure 6.13: Cortical F-actin in HIV+ cells depleted of cytoskeletal regulators. U937 cells were infected with HIV-iGFP (green), incubated for 48h, then fixed and stained with fluorescent phalloidin (white). Images correspond to high resolution fluorescence microscopy with a DeltaVision Elite microscope. 50 optical Z-sections (~0.15 μm) were acquired, then deconvoluted and volume projected using SoftWorx software. A) Wildtype, B) Cdc42-/-, C) Wave2 -/- and D) Rac1-shRNA cells.

The ideal control in this case would have been to use Rac1-null cells, yet we were not able to obtain pure Rac1 -/- clones. As a surrogate, we used Wave2 -/- knockout cells (see Table 4.1) because Rac1-mediated activation of the Arp2/3 is mainly dependent on the WAVE complex

[297]. Interestingly, we observed Wave2-/- cells to display much thicker and longer HIV-Filopodia than those typically found in wildtype cells (Fig. 6.13-C). This was evident from the fact that these thicker filopodia could be readily observed at low magnifications (e.g. 10x objectives in Cytell and even standard light microscopes), whereas imaging of thin wildtype filopodia requires higher magnification and special imaging conditions. Furthermore, this enhanced phenotype seemed to predominantly affect HIV-infected cells. Indeed, formal quantification of thick filopodia (defined here as those visible with 10x objective magnification) revealed a statistically significant increase in both frequency (Fig. 6.14-A, ~2-fold) and length (Fig. 6.14-B, 33% longer) in Wave2 -/- cells compared to wildtype cells (when both cell types were infected). In Wave2 -/- cells, thick filopodia were also 3.3-fold more frequent in infected vs. uninfected cells (Fig. 6.14-A, $p < 0.05$), whereas a significant length increase (~2-fold) was observed for both wildtype and Wave2 -/- cells in the context of HIV infection (Fig. 6.14-B).

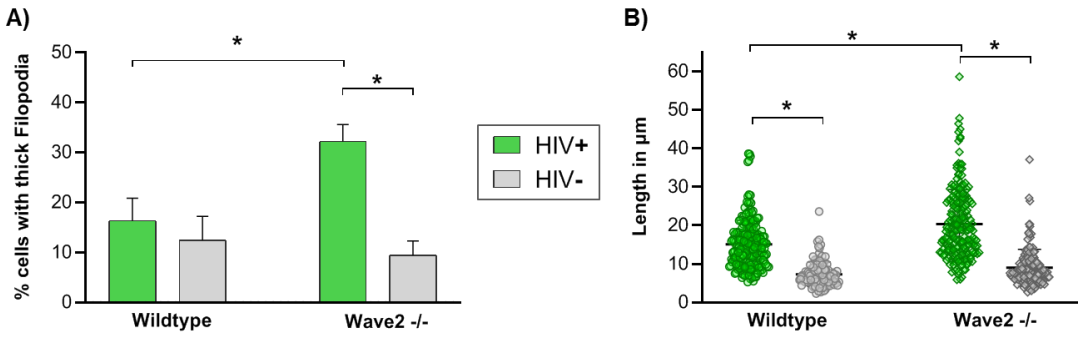

Figure 6.14: Quantification of thick filopodia in Wave2-depleted cells. U937 cells were infected with HIV-IRESeGFP and incubated for 48h. Live cultures were then imaged using a Cytell microscope (10x objective). Data was obtained by manual analysis of images with ImageJ software as specified below. At least 60 cells from 4 independent experiments were analysed per condition. HIV-infected cells were easily distinguishable by their GFP+ signal. A) Frequency of thick filopodia. Cells from multiple fields of view per experiment were manually scored using the Cell Counter plugin as either having (+) or lacking (-) at least one thick filopodium (binary score). Proportions for each condition were calculated as % = [100 x (sum of (+))/total]. B) The length of thick filopodia in (+) cells was determined by manual outlining from the base to the tip, followed by applying the "measure function" of ImageJ. The average values from each experiment (N=4) were used for statistical comparisons with the non-parametric Mann-Whitney test (* = $p < 0.05$).

Since Rac1 -/- clones could not be obtained by CRISPR, at a later point we also generated a Rac1-knockdown cell line by transducing U937 cells with pLKO.1 lentivirus encoding 2 different Rac1 shRNAs (see Table 2.10). High resolution microscopy of these cells confirmed occurrence of the thick filopodia phenotype that specifically affected HIV-infected cells (Fig. 6.13-D), mimicking the phenotype of Wave2 -/- cells (Fig. 6.13-C) and thus confirming a functional correlation of these phenotypes. Together, our observations in this section suggest that HIV manipulation of the actin cytoskeleton stimulates a normal pathway of filopodial

formation and that this is further enhanced when the Rac1-Wave2-Arp2/3 pathway is interrupted (Fig. 6.15). We therefore propose a key role of Cdc42 in HIV-Filopodia formation given that; i) Rac1 and Cdc42 compete for Arp2/3 activation in HIV infected cells, and ii) we observed complete lack of filopodia in infected Cdc42 -/- cells. This is discussed in further detail in later section 6.5.3.

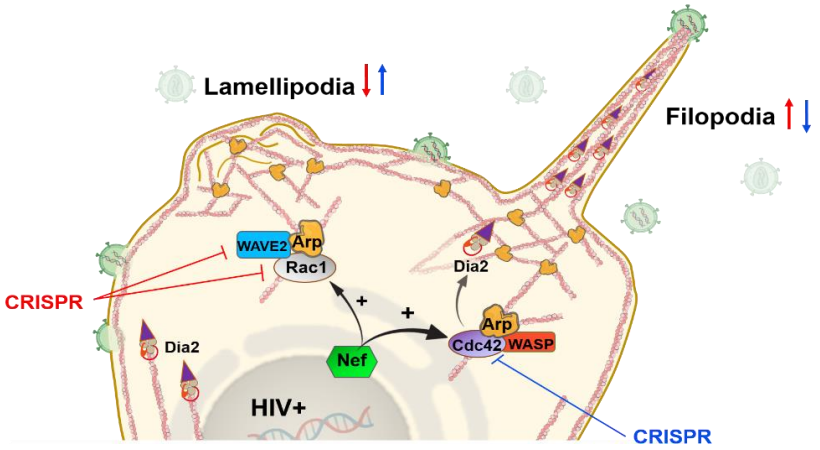

Figure 6.15: Model of cortical F-actin dysregulation in HIV-infected myeloid cells. Rac1 is an important regulator of lamellipodia, whereas Cdc42 is known to promote the building of filopodia. Since both Rac1 and Cdc42 are potently activated in HIV-infected cells (likely via Nef), these pathways are likely to compete for downstream Arp2/3 activation. Interfering with the Rac1-Wave2 signalling arm could therefore enhance/exacerbate filopodia formation, whereas impairing Cdc42 could favour lamellipodial structures. This would be consistent with our experimental observations in Fig. 6.13-6.14.

6.4.6 IQGAP1 as potential coordinator of cytoskeletal manipulation by HIV

Since we could confirm an important role of Cdc42 (upstream of the Arp2/3 complex) for HIV-Filopodia formation and CCTH, we decided to further map the interaction of HIV with this central node of actin regulation. Cdc42 is however known to interact with dozens of proteins [489], consistently with its role as master signalling node. To narrow our scope, we focused on proteins that have been described as downstream effectors of Cdc42 [693] and that meet the criteria previously used for design of our CRISPR panel (see 4.4.2). The resulting list included seven proteins already tested in chapter 4 (i.e. PAK1-2, Dia1-2,WASP, N-WASP and WAVE), as well as the adaptor proteins IQGAP1 and IQGAP2. IQGAPs are large (195 kDa) and highly conserved scaffolding proteins which can interact with a multitude of different cellular proteins [694]. IQGAPs play important roles in coordinating, integrating and transducing cellular signalling events, by serving as versatile and dynamic platforms that allow spatiotemporal regulation of protein-protein interactions [695,696]. IQGAP1 is expressed ubiquitously but is dramatically enriched in leukocytes, whereas expression of IQGAP2 and IQGAP3 is more tissue restricted [697,698]. We therefore concentrated on IQGAP1 for this thesis. Importantly, IQGAP1 can bind F-actin and a large number of actin regulators. By

modulating their function, IQGAP1 plays major (but poorly resolved) roles in coordination of cellular events that require the actin cytoskeleton (reviewed in [699,700]). No previous studies have specifically assessed the role of IQGAP1 in HIV infection. Reports include only limited and coincidental evidence, such as IQGAP1 being found within virions produced by infected macrophages [504] and in cytoplasmic ribonucleoprotein complexes containing various HIV proteins, Staufen1 and >200 other host proteins [701]. Interestingly however, IQGAP1 is manipulated by various other intracellular pathogens, which exploit its ability to coordinate cytoskeletal changes and/or interact with the cellular abscission machinery (reviewed in [699]). Therefore, IQGAP1 could play an important role for HIV-mediated manipulation of the actin cytoskeleton and viral spread. To test this hypothesis, we designed two CRISPR gRNAs (see 6.3.2) against early exons of IQGAP1 that code for the N-terminal Calponin-homology domain, which allows interaction with F-actin and other cytoskeletal proteins [702]. Cas9-induced frameshift mutations near these regions would result in loss of >95% of the native protein sequence. However, despite repeated attempts, we were not able to establish IQGAP1 -/- cell lines, possibly due to essential roles of IQGAP1 for cytokinesis [703,704]. We therefore resorted to shRNA-mediated depletion of IQGAP1. U937 were transduced with pLKO.1 lentiviral vectors encoding two IQGAP1 shRNA sequences (see 6.3.2), and then selected in the presence of puromycin for at least 2 weeks before experiments.

In using these cells, we observed several lines of evidence supporting a role of IQGAP1 at the intersection of HIV and F-actin regulation, with important consequences for cell-cell viral spread. Firstly, IQGAP1-knockdown cells displayed shorter filopodia (compared to the wildtype), reminiscent of those observed in Dia2-depleted cells (Fig. 6.16-A). Secondly, our lab could confirm by mass spectrometry the presence of IQGAP1 in virions produced in HIV-infected U937 cells, along with numerous IQGAP1 binding partners, including cytoskeletal regulators such as Cdc42 and Rac1 (Unpublished, Dr. Anu Aggarwal personal communication and Fig. 6.16-B). Thirdly, IQGAP1-depleted cells were notably impaired in their ability to mediate outbound HIV spread and mimicked the behaviour of Cdc42-null cells in this respect. Both IQGAP1-knockdown and Cdc42 -/- U937 cells displayed significantly reduced levels of CCTH, compared to both wildtype and Rac1-knockdown control cells (Fig. 6.16-C, >60% and >40% reduction, respectively, $p < 0.01$). In contrast, CCTH from Rac1-knockdown cells was not significantly lower than for the wildtype (Fig. 6.16-C). A similar trend was observed in experiments where infected U937 donor cells were serially diluted into populations of primary CD4+ target cells as previously described in [89] (Fig. 6.16-D). Although partly still preliminary data, these observations collectively support the hypothesis that IQGAP1 is required downstream of HIV-manipulated Cdc42 to coordinate cytoskeletal events that aid outbound viral spread.

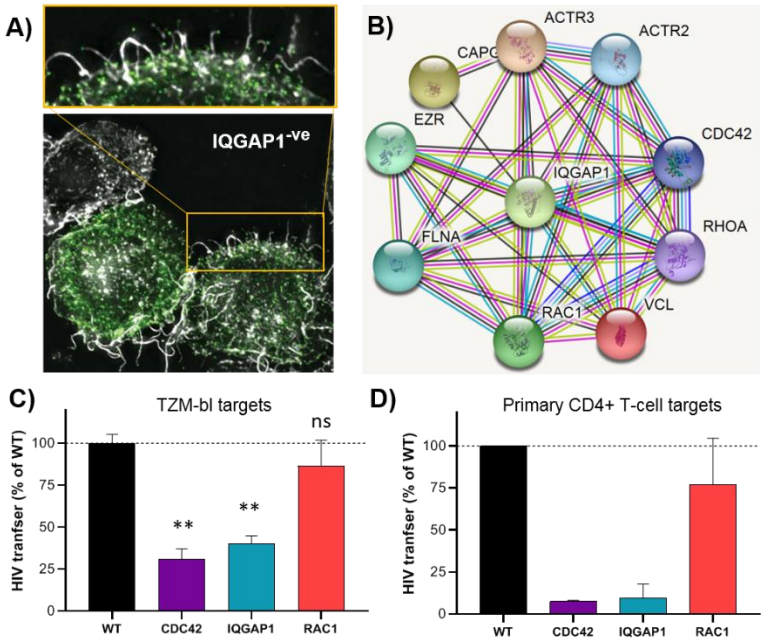

Figure 6.16: The roles of IQGAP1 for outbound HIV. A) Immunofluorescence microscopy of IQGAP1-knockdown U937 cells infected with HIV-iGFP (green) and stained with fluorescent phalloidin (white). Imaging conditions were as described in 2.2.12.1. A representative image containing two infected cells and one uninfected cell is shown. **B)** Viral proteome analysis by mass spectrometry was used to assess the footprint of cytoskeletal proteins enriched in close vicinity of the HIV budding reaction in infected U937 cells. Shown is the node of identified cytoskeletal regulators that are known to associate with IQGAP. Virion preparation, concentration and purification were performed roughly as described in [504]. Virions were lysed, and protein contents were separated by SDS-PAGE. Gel slices were digested with trypsin and peptides were separated by nano-liquid chromatography (Dionex UltiMate 3000 HPLC and autosampler system) and subsequently ionized as described in [705]. Mass spectrometry (MS/MS) was performed by the UNSW core facility (using a Q Exactive Plus mass spectrometer, Thermo Scientific), who also guided and assisted with data analysis. The protein interaction network diagram was generated using the STRING web-database [489]. **C)** HIV transfer assay from infected U937 donor cells to TZM-bl target cells. The percentage of infected target cells from each of three experiments was normalized to the inter-experiment average of the wildtype control group (i.e. "type-I normalization" as per [691]. Normal distribution of data was confirmed as described in 2.2.13. Each group was compared to the wildtype control using ANOVA test with Dunnett's correction for multiple testing (** = $p < 0.01$). **D)** Primary CD4+ T-cells labelled with CellTracker® fluorescent dye were used as target cells. Infected U937 donor groups were prepared as described in 3.4.2.1-2 and added to 10^5 target cells at a donor:target ratio of 0.01 in round bottom 96-well plates. Viral transfer was stopped at 12h with BMS-378806 at 10 µM. The proportion of infected target cells was determined at 96h by high content microscopy. Data was normalized to the wildtype control and is representative of one experiment with target cells from three independent blood donors.

A)

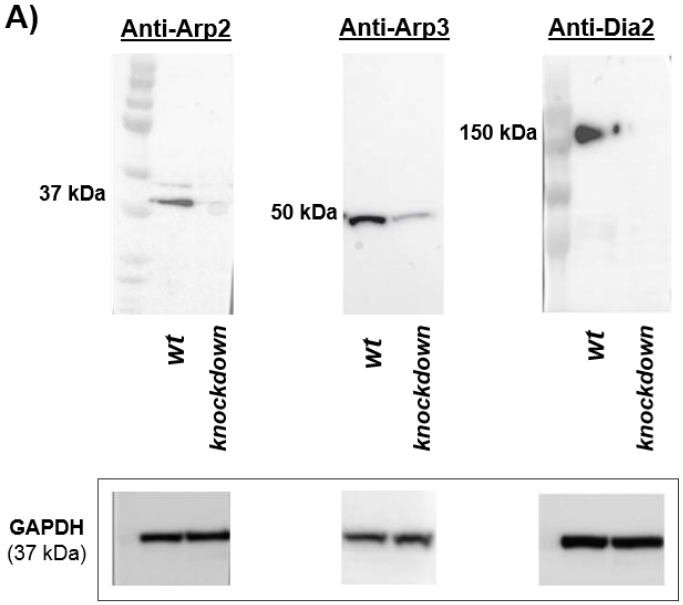

B)

Cell line (U937)	% Residual protein	% knockdown
Arp2/3 + Dia2 shRNA	13.0 (Arp2)	87
	22.7 (Arp3)	77.3
	1.8 (Dia2)	98.2

Supplementary Figure 6.1: Verification of multiple knockdown at the protein level for U937 Arp2/3-Dia2 co-depleted cells. U937 were transduced with the lentiviral expression vector pLKO.1 encoding shRNAs against Arp2 and Arp3 (see Table 2.7.1.3), as well as puromycin resistance. After 2 weeks of incubation in puromycin-containing medium, cells were re-transduced with pKLO.1 encoding shRNA against Dia2 and hygromycin resistance. Cells were incubated for additional 2 weeks in hygromycin containing medium, before phenotyping by western blot with the following antibodies: anti-Arp2 rabbit polyclonal (Santa Cruz #SC-15389), anti-Arp3 mouse monoclonal (Abcam #AB49671), anti-Diaph2 rabbit polyclonal (Bethyl laboratories #A300-079A). U937 wildtype cells were used as normalization control. Matching secondary antibodies (anti-rabbit or anti-mouse) coupled to horse radish peroxidase were obtained from GE Life Sciences. Protein bands on a polyvinylidene fluoride membrane (previously separated by SDS-PAGE, where identical amounts of total protein lysate were loaded) were developed using Clarity HRP Chemiluminescent Kit (BioRad, CA, USA). Images were obtained using a GBox-Chemi XX6 (Syngene, Cambridge, UK). **A)** Representative images of the western blot experiment with relevant bands highlighted with the expected band size, and the corresponding GAPDH loading controls in the box below. B) Densitometry quantification of band intensity. Percentage of residual protein was calculated by dividing the intensity of the knockdown condition band by that of the corresponding band from the wildtype sample x 100. Percentage of knockdown was calculated as 100 - % residual protein.

6.5 Discussion

6.5.1 Genetic deletion of core actin regulators

CRISPR-based approaches inactivate cellular factors at the genomic DNA level. When successful, this corruption of their genetic "source code" allows for complete target-protein depletion, which is typically not possible with RNA-based techniques. However, when the targeted gene is required for critical cellular functions, homozygous knockout mutations (-/-) can potentially result in cellular death or proliferation defects. This has hindered researchers from obtaining "true knockout" models (e.g. null-mice or -/- cell lines) for a long list of genes. This in turn prevents us from gaining full understanding of their biological functions, because specific gene functions can often still be mediated by residual levels of protein after incomplete knockdown [706]. Our observations in this study suggest that the actin regulators Arp2, Rac1, PAK2 and N-WASP may play non-redundant critical roles for cell survival and/or proliferation, since we were not able to obtain -/- cell lines for these genes. This is in good agreement with previous observations from the literature. Firstly, -/- germline mutations for any of these genes leads to early embryonic lethality in mice [623,673-675,707]). Secondly, a genome-wide CRISPR screen associated these genes with proliferation defects in human cell lines [661]. It should be however noted that conditional knockout mice and/or validated knockout cell lines exist for some of these genes. This suggests that these are cellular "fitness genes" rather than "essential genes", as defined by Hart et al. [661]. In any case, a reduced ability to grow or survive under adverse conditions is sufficient to explain why -/- cell lines could not be obtained via clonal expansion. Although Profilin is also listed as a fitness gene [661], we were able to retrieve Profilin -/- cellular clones. However, these cells displayed aberrantly enlarged morphology, and cell size roughly correlated with increasing numbers of multiple distinct nuclei within the cell body, which is strongly indicative of cytokinesis defects. This is consistent with previous observations. In yeast, Profilin is essential for cytokinesis due to its requirement for assembly of the medial contractile F-actin ring [708], which is also required for cell division in most eukaryotic cells. Profilin depletion also impaired cytokinesis in amoeba [709], worms [710], and mice [711]. However, Profilin depletion by siRNA-mediated knockdown in human endothelial cells did not lead to cytokinesis defects, which led the authors to conclude that this regulator "is not essential for cytokinesis" in human cells [712]. Our findings contrast with this view and suggest that complete loss of Profilin can indeed impair cytokinesis, although low levels of Profilin are likely sufficient to maintain normal cell division. We speculate that Profilin's role in cytokinesis is one of the main reasons for its high evolutionary conservation across the eukaryotic kingdom [653].

6.5.2 The role of membrane curvature for the HIV-budding reaction

Through our FIB-SEM experiments, we studied the spatial segregation of HIV budding on the cell surface and readily observed HIV-buds to be enriched to areas where F-actin structures bend the membrane into strong positive curvature (e.g. the tips of filopodia or the ridges of lamellipodia). This preferential enrichment could be explained by at least two non-exclusive mechanisms; 1) HIV-assembly may be facilitated by positive membrane curvature on pre-existing F-actin structures (e.g. due to lower energetic constraints to bend the membrane outwards), or 2) HIV assembly could itself induce positive membrane curvature (beyond simply that of the HIV-bud) by recruitment and/or activation of cellular proteins which mediate cortical F-actin polymerisation and PM protrusion. Our observations with constitutively active Dia2 (CA-Dia2) argue against the first model. If strong positive membrane curvature would be sufficient to concentrate the budding reaction to filopodial tips, then the abundant filopodia in HIV-infected U937 CA-Dia2 cells should be decorated with viral buds. We instead observed these structures to be completely uncoupled from HIV, with no detectable buds at the tips. As for the second mechanism, we showed that the NC domain (which mediates the Gag–F-actin interaction, see 1.5.5) was not required for localization of HIV-buds to the tips of filopodia. In contrast, mutations in Gag that prevent bending of the membrane (curvature mutants) led to a collapse of Arp2/3-dependent short HIV-Filopodia. To test whether this effect was specific to these structures or more generally affected all pathways of filopodial formation, we infected U937 CA-Dia2 cells with curvature mutant virus and observed that filopodia could still form under these conditions (not shown). Overall, our observations suggest that positive membrane curvature cannot explain the dramatic enrichment of HIV-buds at the tips of filopodia. Rather, this seems to be related to an intersection of outbound HIV with cellular Arp2/3 pathways. This is highly consistent with observations from numerous other intracellular pathogens, which are known to exploit the unique ability of the Arp2/3 complex to promote formation of specialized cortical F-actin membrane protrusions that facilitate cell-cell infection spread [418,713,714]. Importantly, nascent buds have also been observed at the tips of filopodia-like structures for other types of viruses [715-719]. However, since most of these observations come from electron microscopy studies in fixed samples, it is not possible to conclude whether viral release occurs more or less efficiently at this position. While FIB-SEM imaging has the same limitation, our live imaging data suggests that HIV-budding is arrested at the tips of HIV-Filopodia. This, which is further discussed in section 6.5.5, is compatible with the observation that cells infected with the Δp6 HIV mutant (associated with a well-known defect in viral release) can still form HIV-Filopodia.

6.5.3 Biogenesis of HIV-Filopodia

Our observations suggest that HIV-Filopodia (see 1.3.4) play an important role for CCTH from infected myeloid cells. This is because; i) various filopodial regulators were identified during our outbound CCTH CRISPR screen in Chapter 4 (see Fig. 4.12), and ii) we could confirm that two independent cell types that completely lack filopodia (i.e. Cdc42 knockout and Arp2/3-Dia2 double knockdown cells) show significantly reduced CCTH. One important aim of this work was therefore to elucidate the mechanisms by which actin manipulation by outbound virus allows formation of HIV-Filopodia (HF). In Table 6.3 below, we summarize the results from our experimental efforts, which aimed to mechanistically resolve this pathway.

Experimental approach	HIV-Filopodia phenotype
Cdc42 knockout	complete lack of filopodia (replaced by extensive lamellipodial network)
(Arp2/3 + Dia2) knockdown	
HIV-Gag Curvature mutants	
Arp2/3 immunostaining	Arp2/3 present at the base, shaft and tips of wt HIV-Filopodia
IQGAP1 knockdown	shorter filopodia
Dia2 knockdown	
CA-Dia2 expression	long straight filopodia with CA-Dia2 at the tips (uncoupled from HIV)

Table 6.3. Summary of filopodial phenotypes observed.

The pathways and models that are believed to contribute to filopodia formation in other settings were introduced in 1.4.7.1. The two major signalling regulators of filopodia are the Rho-GTPases Cdc42 and Rif. Since we observed HIV-infected Cdc42 -/- cells to completely lack HF, this strongly suggests that these filopodia are entirely dependent on Cdc42 (but not Rif) signalling. This is consistent with the fact that HF frequency is positively influenced by Nef [89], which is known to activate Cdc42 (see 1.5.9.1). Since Cdc42 can promote filopodia by at least two different pathways, i.e. Cdc42-WASP/N-WASP-Arp2/3 [354] and/or Cdc42-Dia2 [503], we decided to investigate both routes. In our setting, depletion of either Arp2/3 or Dia2 alone did not eliminate HF. Despite confirmed >80% total target protein depletion, Arp2/3-knockdown cells infected with HIV still displayed HF on their surface. This could either mean that Arp2/3 is not essential for the building of filopodia, or that even residual amounts of Arp2/3 are sufficient to initiate filopodia formation. Further exploration of the first scenario is prevented by our inability to obtain cells completely lacking Arp2/3 (see 6.5.1). The second scenario seems however likely, considering the sheer abundance of Arp2/3 complexes per cell, which can reach micromolar concentrations [298]. This is consistent with previous calculations that even 95% depletion of Arp2/3 can still (in theory) provide enough building material for thousands of filopodia per cell [364]. In addition, >80% depletion of

Arp2/3 implies a loss of most actin nucleator activity in the cell (Arp2/3 is thought to outnumber formins at by at least one order of magnitude). The resulting F-actin imbalance is likely to be compensated by funnelling excess G-actin into the remaining active Arp2/3 molecules and formin pathways, which would actively rescue filopodia formation. Nevertheless, Arp2/3-depletion was able to reduce filopodial abundance in other systems [720-722], which suggests that this regulator can indeed play a critical role for filopodia initiation. On the other hand, depletion of Dia2 alone led to more abundant but shorter HF, as previously reported [89]. Since we could now recapitulate these observations in Dia2 -/- cells, this further confirmed that Dia2 is required for HIV-Filopodia elongation but not for their initiation. This is consistent with observations from Dia2 (or homologues) in other systems, which showed that; i) overexpression or activation leads to long filopodia [369,723,724], ii) Dia formins are recruited late during filopodia initiation [358,722,723], and iii) Dia2 was located at the tips of some types of filopodia [366,722,725,726].

To test whether Arp2/3 and Dia2 work cooperatively to build HF, we attempted their simultaneous depletion. Cells co-depleted for both actin nucleators completely lacked HIV-Filopodia on their surface, and instead displayed an extensive network of lamellipodia/veils. Since this implies that both Arp2/3 and Dia2 are required for HF (with the Formin being mainly responsible for their elongation), biogenesis of HF more closely aligns with the "convergent elongation model" than with "*de novo* nucleation model" of filopodia formation. The former argues that filopodia are formed by reorganization and subsequent elongation of pre-existing actin filaments from Arp2/3-dependent branched actin networks, whereas the latter proposes that filaments are nucleated and elongated by formins directly at the PM (see 1.4.7.1). Our observations are also consistent with those of Young et al., who showed that filopodia induced by transfection of Dia2 in Jurkat cells are dependent on Arp2/3 activity [365]. Furthermore, our results argue against an independent role of formins (i.e. *de novo* nucleation model) in HIV-Filopodia. Firstly, constitutively active Dia2 induced long filopodia, but these were uncoupled from HIV-buds. Secondly, we found Arp2/3 along the base, shaft and even tips of wildtype HF, which is consistent with previous observations that Arp2/3 can be present in the shaft or tip of some types of filopodia [722,727]. The higher frequency of HF in Dia2-depleted cells is also interesting and may be explained by funnelling of the "released" G-actin pool into the Cdc42-Arp2/3 pathway, which is constantly activated in HIV+ cells. Analogous shifts of actin pools between formin and Arp2/3 dependent structures have been previously described [299,313]. Overall, our findings suggest that both Arp2/3 and formin activity in cooperation are required for normal HF formation.

Interestingly, depletion of the adaptor protein IQGAP1 also led to filopodial shortening. IQGAP1 is not normally considered a filopodial regulator, but some evidence does suggest it may play a role in the assembly or maintenance of these structures. IQGAP1 was identified by immunostaining in filopodia of non-human cells [728,729]. In human MCF-7 epithelial cells, overexpression of IQGAP1 induced filopodia in a Cdc42-dependent manner, whereas a dominant-negative version impaired their formation [730]. Based on our experimental data and previous literature, we envision several mechanisms by which IQGAP1 could contribute to HIV-Filopodia. First, IQGAP1 can bind Cdc42, stabilize its active state, and target it to the PM [730]. Second, IQGAP1's scaffolding ability allows it to bind numerous cytoskeletal regulators and recruit them into large multiprotein complexes. IQGAP1 not only facilitates complexes that include Cdc42 and Arp2/3 [731] but can also bring Arp2/3 and formins together, which has been proposed to spatially link these different types of actin nucleators to promote cooperative actin structure assembly (reviewed in [732]). We therefore propose that IQGAP1 could recruit Dia2 to sites of Arp2/3-initiated filopodial assembly, which would bring it in contact with its activator Cdc42. This is consistent with our observation that IQGAP1-depletion allows Arp2/3-dependent short filopodia formation but prevents their Dia2-dependent elongation. Alternatively, the same phenotype may be related to IQGAP1's ability to bundle and cross-link actin-filaments [728,733]. This is because the force produced by individual linear actin filaments is insufficient to push the membrane over long distances, given that non-bundled filaments "bend rather than push" [341,358,734]. Thus, if one would assume that IQGAP1 contributes to filament-bundling in HF, its absence could also explain shorter filopodia. In agreement, mutations of Fascin (canonical F-actin-bundling protein in filopodia) can lead to shorter and fewer filopodia [735].

One complicating factor in the study of HF, is that uninfected U937 and iDCs also display morphologically analogous structures on their cell surface (see 1.3.4), although at lower frequencies and of course with absence of viral components. This raises the conundrum of whether HF are built through a unique and independent mechanism enabled by the virus, or whether outbound HIV simply hijacks and enhances a pre-existing cellular F-actin regulatory pathway to embed itself at the tips of "regular" filopodia. All our observations in this respect consistently support the latter scenario. First, virtually all filopodia on HIV-infected cells are decorated with HIV buds. Second, F-actin regulator depletion (e.g. Cdc42 knockout and Arp2/3-Dia2 double knockdown) that abolished HF formation also led to identical outcomes in uninfected cells. Third, Gag curvature mutants led to a collapse of all filopodia, suggesting that these Gag variants can act as dominant negative factors for both HF and non-HIV filopodia. The latter in turn implies that there is a physical or functional intersection between both pathways. Our curvature-mutant data also strongly suggests that Gag-induced membrane

curvature is important for HIV-Filopodia formation. This is consistent with accumulating observations, which support that membrane curvature can directly affect cortical F-actin remodelling, including stimulation of Cdc42-NWASP-Arp2/3-mediated actin polymerization [736-739]. While the exact nature of this regulation is not yet fully understood, it is thought to involve interaction of Cdc42 with BAR-domain proteins (which alter membrane curvature), as well as the membrane phospholipid phosphatidylinositol 4,5-bisphosphate (PIP2). Indeed, PIP2 is a critical regulator of actin cytoskeleton organization and dynamics [740,741], which has been proposed to coordinate HIV-mediated actin manipulation events, in particular by inbound virus [742]. PIP2 is also a determinant factor in targeting outbound Gag to the PM and this plays a role for HIV-budding [37,743]. Importantly, many actin regulatory proteins can directly bind PIP2, including most of the regulators identified as relevant for HF formation and/or CCTH in this thesis (e.g. Cdc42 and N-WASP [744], IQGAP1 [745], Dia formins [746], Profilin and Cofilin [742], among others). PIP2 binding not only affects their subcellular distribution by targeting them to the PM, but also directly modulates their activity.

We speculate that, in uninfected myeloid cells, small pools of Cdc42, IQGAP1, Dia2, Profilin and Arp2/3 (e.g. via N-WASP or IRSp53) congregate at the PM due to their interactions with PIP2. Increases in positive membrane curvature (e.g. via BAR-domain proteins, Arp2/3-mediated cortical actin polymerisation, or both) likely contribute to filopodia initiation downstream of Cdc42 signalling events. Filopodial growth would then occur by convergent linear elongation of filament free barbed ends by formins, such as Dia2 (potentially recruited by IQGAP1 and activated by Cdc42), likely in cooperation with Profilin. This theory would be highly consistent with the "clustering-outgrowth model" of filopodia formation proposed by Lee et al., who used a cell-free *in vitro* system to study the biogenesis of filopodia [722]. In this study, a minimal set of cytoskeletal proteins (isolated from frog egg extracts) was sufficient to allow formation of filopodia-like structures from lipid-bilayers in a PIP2-dependent manner. Real-time fluorescence microscopy with labelled proteins revealed that the F-BAR protein Toca-1 was recruited first, which "broke" the membrane symmetry. This was followed by recruitment of N-WASP and then Arp2/3, which was concomitant with nucleation of an initial actin structure in a small patch. The F-actin elongating proteins VASP and Dia were recruited only after the initial actin polymerization and were responsible for filopodial elongation. Importantly, filopodia formation was strongly dependent on the presence of PIP2 and Cdc42 and could be most efficiently disrupted by simultaneous inhibition of Arp2/3 and Dia formins [722].

Assuming a similar model of filopodia formation in uninfected human myeloid cells, HIV-infection could be expected to hijack and/or potentiate these structures at multiple levels. This

is because; i) Gag is produced in large amounts and targeted to PIP2-rich regions at the PM, where it likely colocalizes with filopodial regulators, ii) Gag is known to induce coalescence of specific membrane microdomains [686], which would lead to local increases of PIP2 density and therefore of PIP2-binding actin regulators, iii) Gag oligomerization increases membrane curvature, which likely lowers the energy barrier for filopodia formation, iv) curvature, PIP2 and Nef can all lead to Cdc42 activation, and v) Gag may recruit IQGAP1 either directly or via TSG101/Alix (see 8.4). In Figure 6.17 below, we present a hypothetical model of HIV-filopodia formation, primarily based on our experimental observations and complemented with previous reports from the literature, as discussed in this chapter.

6.5.4 Unique features of HIV-Filopodia

Importantly, the actin regulators involved in HF formation and CCTH from infected myeloid cells (i.e. CCTH *in cis*) as described in this thesis, have been previously also reported to be critical for the formation of other F-actin-rich membrane protrusions that contribute to CCTH *in trans* (see section 1.5.10), but which have not yet received a formal name. However, despite the overlap of actin regulators involved in each case, the structures described by Nikolic et al. and in this study are fundamentally different in terms of their ultrastructure, their physical association with HIV, the mechanisms of HIV-mediated manipulation involved, and the way in which they promote CCTH. While the structures described by Nikolic et al. resembled filopodia in transmission electron microscopy images, more complex ultrastructural analysis via both electron tomography and ion-abrasion electron microscopy revealed that they in reality correspond to "thin-walled" "sheet-like" projections [221,507]. For simplicity we will refer to these structures as HIV-Sheets (HS). This high-resolution imaging also allowed to confirm the presence of fully extracellular virions that are associated with the surface of HS. In strong contrast, our 3D FIB-SEM data presented here confirms our previous electron microscopy observations [89], that our structures correspond to genuine filopodia as defined in section 1.4.7.1, and that the virions associated with the shaft and tip of HF correspond to immature HIV-buds that have not yet undergone abscission from the host cell membrane.

Furthermore, although Cdc42 and Arp2/3 are required for both HS and HF formation, manipulation of these actin regulators by the virus is entirely different, in part because it occurs at opposing sides of the host cell membrane. HS form upon exposure of DC to extracellular virions in an Env-dependent manner. Since this occurs within minutes [507], it is clear that it does not involve productive infection or *de novo* expression of viral proteins. Rather, it is believed to be a consequence of Src signalling upon binding of Env to DC-SIGN on the DC membrane [225]. In strong contrast, HF-formation is entirely dependent on cellular expression of immature Gag and is potentiated by expression of Nef but is completely independent of the

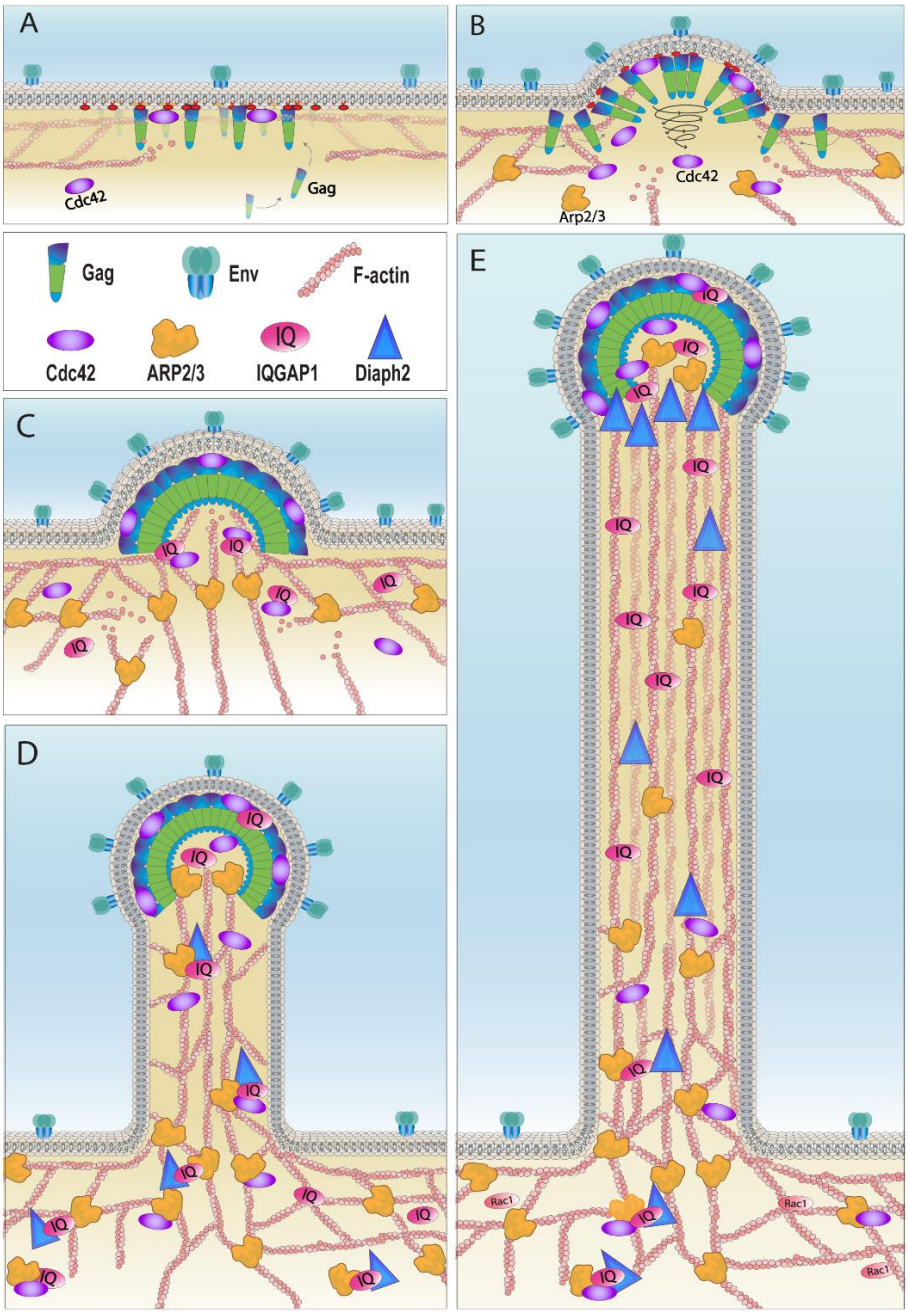

Figure 6.17: Model for HIV-Filopodia formation. A) HIV-Gag is targeted to PIP2-rich cellular membrane regions (shown in red), where it accumulates. B) Gag oligomerization locally increases positive membrane curvature and PIP2 density. Both curvature and PIP2 activate Cdc42 via mechanisms that are not yet fully understood. C) Active Cdc42 in turn leads to activation of the Arp2/3 complex, which initiates branched F-actin polymerisation. The scaffolding protein IQGAP1 is also recruited by binding to active Cdc42 and PIP2 . D) Growing actin filaments further bend the membrane and push the nascent viral bud away from the cell's surface, seeding a short Arp2/3-dependent filopodium. IQGAP1 facilitates assembly of multiprotein complexes that spatially link formins to the Arp2/3 complex and active Cdc42. E) Activation of the formin Dia2 (e.g. via Cdc42) results in rapid formin-mediated elongation of free F-actin barbed ends, which leads to formation of long linear actin filaments. This process is dramatically accelerated in the presence of Profilin (not illustrated). IQGAP1's actin-bundling ability may also contribute to stabilisation and parallel arrangement of actin filaments within the filopodial shaft. The filopodial tip is composed of an immature viral bud harbouring all proteins shown in the figure legend.

presence of Env, or the activation of Src as previously shown in [89]. Last but not least, since HS form in uninfected cells they can only mediate CCTH *in trans*, whereas the viral transfer associated with HF, as observed in this study, occurs exclusively *in cis*. This is because U937 cells do not form VCC or HS (as evidenced by our FIB-SEM data) and are unable to mediate CCTH *in trans* (as shown in Fig. 3.4). In any case, the fact that HIV exploits common actin regulators for facilitating CCTH *in cis* and *in trans* is overall positive for the biomedical research field, because it means that potential intervention strategies targeting these regulators (further discussed in section 8.4) would likely counteract both modes of HIV spread.

6.5.5 HIV-Filopodia and cell-mediated HIV transfer

Regardless of how they are built, another question is how exactly HF contribute to outbound CCTH *in cis*. Previous work from our lab extensively characterized HF dynamics and found that these structures are used to scan the cellular microenvironment. Infected U937 and primary DC used filopodia to engage with neighbouring CD4TC in hundreds of contacts per hour [89]. This often involved repositioning and pulling of the target cell, leading to stable intercellular contacts with tight membrane apposition and a narrow synaptic space through which virions can be transferred. This is consistent with our observations in chapter 3, where prominent filopodial activity was often observed prior to formation of virological synapses, with intense polarization of Gag towards the target cell (see 3.5.4 and supplementary video S1). Another interesting observation is that immature HIV-buds remain associated with filopodial tips, as revealed by real-time tracking of HF via live-imaging. This suggests that viral budding is arrested or significantly delayed at this position, which could also explain the observed enrichment of viral buds at HF-tips observed in this work (i.e. viral abscission would render many filopodia HIV-negative, whereas the sheer majority of filopodia are observed to be HIV-positive). Although this might reduce free virus budding, it could provide important advantages for CCTH. By stably positioning HIV-buds at the leading edge of F-actin protrusions, the first line of cell-cell contact is effectively biased in favour of the virus. Since HF-tips are Env+, this could provide additional and specific adhesive forces when contacting suitable CD4+ target cells. Furthermore, Env-CD4 binding could trigger signalling through the filopodial shaft [747] to initiate pulling of the target cell towards the infected cell's body. This is supported by other studies which showed that filopodium retraction is controlled by adhesion of its tip [748]. Since retraction force is dependent on the number of receptor-ligand interactions and enhanced by receptor clustering, the Env-CD4 pair would provide an ideal catch mechanism in this context. Overall, we propose that HF primarily serve as "search and catch" organs (for productive target cells) that facilitate long-range intercellular contacts which can evolve into closer range contacts such as VS, rather than as structures that facilitate

free virus budding as proposed for other viruses [717]. In agreement, Arp2/3-Dia2 co-depleted cells (which lack HF) displayed reduced CCTH to target T-cells but no impairment in free virus release. Still, HF are not indispensable for the occurrence of VS, since Arp2/3-Dia2 co-depleted cells could still form VS with TZM-bl cells.

6.5.6 Challenges and limitations

Here, we discuss some of the challenges associated with current experimental approaches in this chapter. One such important limitation is that shRNA-mediated knockdown cannot entirely deplete target proteins of interest (Fig. 4.5). Residual protein activity can therefore lead to potentially false negative observations or confounding intermediate phenotypes. For instance, a more critical role of IQGAP1 in HF formation (beyond supporting formin-mediated elongation) can presently not be excluded and would require IQGAP1 -/- cells for verification. Similarly, it is currently not possible to conclude whether the F-actin-rich lamellipodia-like structures in Arp2/3-Dia2 co-depleted cells require Arp2/3-mediated nucleation. Given the difficulty of obtaining true knockout cell lines for some regulators, alternative methods such as inducible expression of dominant-negative factors could be considered. Another limitation of this study is that we have only assessed the impact of actin-regulator depletion on free-HIV release for a limited subset of treatments so far. It is therefore possible that part of the observed reduction in target-cell infection upon coculture with CRISPR-treated donor cells might be due to impaired virion release. Multiple observations however argue against this idea. First, we could confirm that cell-free virus only plays a negligible role in our system, and this was consistent with previous reports (see 3.5.3 and 3.4.2.7). Second, for the conditions where this was assessed, changes in the amount of released free virus did not always correlate with changes in CCTH (e.g. Rac1 knockdown cells had notably reduced free virus release, as also previously reported in [482], but displayed unimpaired CCTH, whereas the inverse was true for Arp2/3-Dia2 co-depleted cells). Alternatively, specific treatments may reduce free-virus infectivity, which would likely affect both mechanisms of transmission. Unfortunately, however, this is an inherent limitation of the CCTH-study field. Genuine cell-cell HIV transmission in this context is “difficult to assess” because cell-mediated HIV infection also requires replication-competent virus that is “cell-free” at the synaptic cleft for a brief period of time [88]. Still, formal characterization of the ability of key cell types to produce abundant and infectious virus is also of interest to our group and will continue to be pursued. We would however expect that partial defects in free-particle infectivity could be largely compensated by CCTH, given the multiple advantages of this system (see 1.3.6). This is consistent with observations that CCTH can efficiently mediate target-cell infection, despite the fact that the vast majority of free HIV virions are uninfectious [126]. Finally, one last important limitation

of this study is that, even when carefully selected and relevant models are used, cell lines do not always adequately reflect the biology or behaviour of cells *in vivo*. Validation experiments with primary cells should therefore always be performed, where methodologically possible. Yet the systems currently available to us for gene editing still require significant optimisation to achieve this latter goal, at least in primary myeloid cells. This is discussed in further depth in the following chapter.

6.5.7 Ongoing and future work

Despite the advances presented in this work, many questions remain about how HIV manipulates the actin cytoskeleton to mediate efficient CCTH. For instance, it remains to be explored how constitutive activation of the formin Dia2 may selectively increase the adhesive potential of HIV-infected cells. The role of formins in regulating intercellular adhesions is only beginning to emerge [749], and while this is known to involve association with E-cadherins at epithelial cell junctions [750], little is known about the mechanisms involved in other cellular contexts, or how this may be manipulated by pathogens. Other interesting aspects for future study are the potential contributions of Cdc42/IQGAP1 for CCTH, beyond their role in HIV-Filopodia formation (e.g. at the virological synapse). For instance, our observations that peak-Gag polarization at the VS is associated with prominent donor-cell rounding suggest that Cdc42 may be specifically inactivated as the synapse matures. This could be important for mass viral release, given previous observations that; i) an F-actin depleted zone is observed at the center of the VS, where Gag/Env accumulation is strongest [553], and ii) Cdc42, IQGAP1 and TSG101 are all recruited to the midbody of daughter cells, where changes in Cdc42 activity are required for actin ring maturation, F-actin clearance from the midbody and the final step of daughter cell abscission, which requires Cdc42 inactivation [751-753]. Thus, Cdc42 inactivation at the VS may support/trigger viral abscission events, similar to its role in late stage cytokinesis. Furthermore, the numerous and versatile functions of IQGAP1 as scaffolding protein and coordinator of cytoskeletal remodelling make it an attractive candidate for orchestrating actin manipulation at the VS. Indeed, preliminary live imaging observations suggest that IQGAP1-mCherry is recruited together with Gag-iGFP early during VS-formation, whereas it is actively excluded/depleted from the Gag-button in mature synapses (not shown). This may be related to Cdc42 inactivation and also raises the exciting possibility that HIV-Gag may interact with IQGAP1 either directly or via TSG101/Alix (discussed in 8.4).

It is also presently unclear which NPF is used by Arp2/3 downstream of Cdc42 to initiate HIV-Filopodia and mediate CCTH. Data from our outbound HIV CRISPR-screen highlights N-WASP as the primary suspect, but also suggests that other type-I NPFs may be interchangeably

used. This is consistent with previous observations that N-WASP gain-of-function can potently enhance Cdc42-Arp2/3 dependent filopodia [754], whereas individual depletion of WASP, N-WASP or WAVE had limited effect in this context [675,754,755]. Given the confirmed role of membrane curvature, Cdc42 and Arp2/3 in HF formation, a potential role of BAR-domain proteins is currently of great interest to our group. For instance, IRSp53 not only selectively binds PIP2-rich membranes and increases membrane curvature via its I-BAR domain [756], but can also induce filopodia in a Cdc42-, N-WASP- and Arp2/3-dependent manner [757]. On the other hand, the F-BAR protein PACSIN2 can induce filopodia formation [758], and has been recently shown to be recruited by HIV-Gag and contribute to CCTH [759]. Both proteins also contain SH3 domains, which allows them to interact with other actin regulators [759,760] and potentially Nef. Thus, it is tempting to speculate that these or related proteins could provide the membrane deformation required for filopodia initiation in uninfected myeloid cells, whereas HIV-Gag could take over this physiological pathway by either usurping or hijacking these proteins at PIP2-rich membrane regions. Future studies in our lab will therefore aim to deplete IRSp53, PACSIN2 and other BAR-domain proteins to assess their requirement for filopodia in uninfected vs. HIV-infected cells.

We also aim to further explore our hypothesis that outbound HIV hijacks the filopodial machinery predominantly by targeting of Gag to PIP2. This model is consistent with observations that: i) expression of Gag alone is sufficient for HF formation [89], and ii) the Gag-NC domain (believed to mediate the interaction with F-actin) is entirely dispensable for HF formation. Unfortunately, Gag's ability to bind PIP2 is also required for its targeting to (and stable association with) the PM, given the role of PIP2 for exposing the myristate moiety [761]. This will likely hinder the use of PIP2-Gag mutants for future HF studies. Alternative approaches could include overexpression of enzymes that hydrolyse/synthesize PIP2, or expression of actin regulator mutants that lack PIP2 binding ability (e.g. Cdc42 R186Q-R187Q [744]) in regulator-null backgrounds, such as Cdc42 -/- U937 cells.

6.6 Chapter acknowledgements

The author acknowledges that the results as presented and described in this chapter were only possible thanks to the valuable contribution of several collaborators both within and without our research group. Concretely, I thank my co-supervisor Dr. Anupriya Aggarwal, who I collaborated extensively with during this project. Her substantial contributions to this chapter included the generation of shRNA constructs for the knockdown of cellular proteins, the confirmation of Arp2/3 and Dia2 depletion at the protein level by western blot, immunofluorescence-staining of Arp2/3 complexes, and fluorescence microscopy imaging of

fixed samples at a high-enough resolution to allow phenotyping of individual HIV-Filopodia (as previously described in [89]). She also prepared the virus-lysate protein samples for mass spectrometry analysis, which was then performed by the "UNSW bioanalytical mass spectrometry facility", which is acknowledged here (mass spectrometry data not shown but briefly discussed). I also acknowledge the substantial contribution of Dr. Kedar Narayan from the National Cancer Institute (Bethesda, USA), who provided all the technical expertise regarding FIB-SEM imaging and, together with his team, performed all the laboratory work and the *in silico* processing of data associated with this technique. Ms. Catherine Henry from the Massachusetts Institute of Technology (USA) is also thanked for her contribution in the segmentation analysis and quantification of structures on the FIB-SEM data. Finally, I also acknowledge the important role of my supervisor Assoc. Prof. Stuart Turville in facilitating these rewarding collaborations and obtaining the necessary funding for this project. A manuscript containing many of the results presented in this chapter is currently in preparation, and the contribution of all the above-mentioned researchers will be acknowledged with authorship, as appropriate.

Chapter 7. Approaches for validating findings in primary cells

7.1 Introduction and aims

Cell lines are valuable tools for biomedical research and have played an indisputable historical role in elucidation of numerous biological and cellular processes. Cell lines continue to be widely used in modern academic research [762,763], where they serve as practical models for biological systems of higher complexity. However, their use has also extended to various areas of direct practical application including biotechnology [764,765], as well as drug and vaccine development [766,767]. Despite their numerous advantages, the use of cell lines as models for medical research is associated with several limitations (reviewed in [768]). Briefly this include; i) the genetic and phenotypic differences (compared to *in vivo* cells) that are associated with the original cell line establishment events (e.g. cell transformation and/or commitment to an immature pre-differentiated stage), ii) further changes resulting from long term serial passaging and lab adaptation, iii) contamination with other cell types, iv) cell line misidentification and v) contamination with mycoplasma. While the latter issues (iii-v) can be effectively circumvented by adoption of rigorous and appropriate guidelines [769], the main problem remains in that cell lines do not always adequately represent the behaviour of primary cells *in vivo*. Since it is unlikely that we will ever be able to fully map the extent of these differences, findings obtained from cell line models alone always bear the risk of being undermined by false negative or false positive observations. Therefore, there is a growing consensus that studies involving cell line model systems should be designed carefully to minimize this risk and that key findings need to be confirmed and validated by corresponding experiments involving primary cells.

The broad methodological aim of this thesis was therefore to use relevant cell line models to conduct initial medium-scale screening studies to identify "hits", followed by mechanistic characterization of top "leads", and ultimately concluding with a validation phase where the transferability of these findings is assessed in cells of primary origin. However, due to technical difficulties, this validation phase could not be conducted to its originally intended full extent. Since we predominantly used the LentiCRISPRv2 (LCV2) platform (see 2.1.6.1 and 4.3.1-4) to genetically modify HIV donor and target cell lines in the screening and follow-up phases of this work, it was our first and preferred choice to use this same system to manipulate primary cells. This approach would have the following advantages; i) LCV2 CRISPR strategy previously optimized and validated in a myeloid cell model (U937), ii) all guide-RNAs already cloned into LCV2 plasmid and constructs are sequence-verified, iii) consistency of all elements in the lentiviral vector used (e.g. promoters, ORFs, spacers, etc.),

and iv) LCV2 is explicitly recommended by the Feng Zhang lab as the preferred resource for transduction of primary cells [584,770].

However, a major barrier to our results validation approach was the finding that treatment of primary myeloid cells with LCV2-VLPs did not result in productive lentiviral transduction and therefore lacked subsequent expression of the delivered genes. This strongly contrasted with that observed for other lentiviral vectors, for which effective transduction rates of nearly 100% and high gene expression could be achieved under identical conditions to those used for LCV2. The series of experiments and controls that ultimately led to this conclusion are described further below. Overall, the **aims** of this chapter were adjusted to address this unexpected barrier, and they can be summarized as follows:

1) To identify the cause of the limited transduction efficiency of primary myeloid cells with LCV2 lentivirus and, where possible, optimize and/or troubleshoot this process to overcome this limitation.

2) To evaluate the feasibility of CRISPR-Cas9 genomic editing under these optimized conditions to determine whether it is sufficient to allow validation of findings (from cell line model system) in primary cells. Where this is not the case, devise and validate alternative strategies for eliciting the phenotypes required in primary myeloid cells.

3) Attempt validation of previous results by using effectively CRISPR-treated primary myeloid cells.

7.2 Materials and Methods

7.2.1 LCV2-mOrange cloning procedure

The puromycin N-acetyltransferase (PuroR) gene within the LCV2 vector was replaced with a sequence encoding mOrange. The strategy used was designed to make the vector as versatile as possible while maintaining DNA sequence changes to a minimum. The stop codon of PuroR is directly followed by a MluI restriction site, which is the only practical available site in the vicinity to mediate its replacement. However, LCV2 also contains a second MluI site upstream of the CMV promoter. We therefore removed this MluI site by replacing the PvuI-SpeI region with a nearly identical sequence where ACGCGT was changed to ACGCGC (sequence obtained as GBlock from IDT Technologies Inc). Then, the BamHI-MluI region (PuroR and part of the P2A element) were replaced by an identical sequence where the PuroR coding sequence was replaced exactly by an mOrange coding sequence. A single bp change (silent mutation) was also included to introduce a unique XhoI site that allows replacement of

mOrange by any other sequence by using XhoI-MluI. Finally, the 2 kb filler between the BsmbI sites was replaced by the non-targeting Control gRNA#1 as indicated in section 2.2.7.3.

7.2.2 Lentiviral vectors used

The following lentiviral plasmids were used in this chapter.

Plasmid name	Size	5'LTR-3'LTR size	Reporter	Promoter	Source / References
PPT-GFP	7.4 kb	3.9 kb	eGFP	hPGK (511 bp)	Modified from Addgene #12252
pLKO-GFP	8.2 kb	4.6 kb	eGFP	hPGK (582 bp)	Addgene #14748
Empty-mOrange	10 kb	5.1 kb	mOrange	Ubiquitin (1211 bp)	Modified from "FG11F-U-GFP" (obtained from Calimmune Pty Ltd)
pLVX-mCherry	8.8 kb	5.7 kb	mCherry	CMV (508bp)	Clontech #632562
LCV2-mOrange (with gRNA)	13.1 kb	8.3 kb	mOrange	EF-1a core (212 bp)	Modified from Addgene #52961 as described in 7.2.1.
LCV2-Puro (with gRNA)	13 kb	8.2 kb	PuroR *	EF-1a core (212 bp)	Modified from Addgene #52961
LentiGuide Puro (with gRNA)	8.3 kb	4.8 kb	PuroR *	EF-1a IntronA (1.2 kb)	Modified from Addgene #52963
LentiCas9Blast	12.8 kb	8.1 kb	BlastR **	EF-1a core (212 bp)	Addgene #52962
NL43-IRESeGFP	16.1 kb	10.5 kb	eGFP	N/A. IRES-sequence from Env transcript	Courtesy of Dr Paul Cameron (Doherty Institute, Melbourne)

Table 7.1 Overview of lentiviral vectors used in Chapter 7.
* PuroR = Puromycin N-acetyltransferase, **BlastR = Blasticidin-S deaminase

7.2.3 Viral transfer assays with primary myeloid cells as HIV donors

The assay was modified and optimized from section 2.2.11 to ensure the feasibility of replacing U937 by primary myeloid cells. Where not specified, procedure was performed exactly as described in section 2.2.11. Primary cells were obtained as described in section 2.2.2 and seeded at 7x10^5 cells/well in flat-bottom 96 well-plates. Since macrophages become so strongly adhered to the cell culture surface that they cannot be detached without compromising normal cell behaviour (and/or Env molecules on the PM), a different donor-cell preparation procedure was used for this cell type.

Immature Dendritic cells as HIV donors: Where required, cells were transduced with the specified CRISPR VLPs (VSVg+, Vpx+) at day 1 of differentiation. VLPs packaging Vpx protein *in trans* were produced as described in section 2.2.7.3. Medium was refreshed at days

3 and 7 before infection. At day 7, cells were infected with HIV-IRESeGFP (VSVg+, Vpx+) by adding viral supernatant at a MOI=0.2. At 72 hpi, cells were extensively washed and prepared as described in 3.4.2.2, with the exception that each donor group was processed individually to avoid loss of cells due to strong adhesion to plastic surfaces after washing and counting. Donor cells were then added to 4x10^4 target Jurkat cells (labelled with CellTracker® Deep Red dye) at the indicated donor:target cell ratios in round-bottom 96-well plates. Stop reaction occurred exactly 12h after start of coincubation for each donor group by introducing the inhibitor BMS-378806 at 10µM. Cocultures were incubated for additional 36h and then cells were processed for flow cytometry analysis as follows: 1) washed once with PBS, 2) resuspended in 1 x Trypsin solution and incubated at 37°C for 5 minutes, 3) fixed with 4% paraformaldehyde for 10 minutes, and iv) resuspended in FW-buffer.

Macrophages as HIV donors: Where required, cells were transduced with the specified CRISPR VLPs (VSVg+, Vpx+) at day 3 of differentiation. Medium was refreshed at days 5, 8 and 11 before infection. At day 11, cells were infected with HIV-IRESeGFP (VSVg+, Vpx+) at a MOI = 0.2. At 72 hpi, cells were vigorously washed twice with PBS to remove free virus. NucBlue® dye was added according to the manufacturer's instructions to label cell nuclei. The entire content of each well was live-imaged using the "InCell 2500HS" high content microscopy platform (GE Healthcare). The number of cells (total and infected) was then enumerated with help of the IN Carta® image analysis software provided by the manufacturer based on fluorescence intensity and size (nuclei = DAPI+, and infected cells = GFP+). Then, the number of required target cells was calculated to obtain the desired donor:target ratios. Target Jurkat cells (labelled with CellTracker® dye) were then added to each donor well to start the cocultures. At 12 hours, target cells were physically separated from adherent donor cells by vigorous pipetting and transferred to 48-well plates containing the stop reaction BMS-378806 at final concentration of 10µM. Successful separation of donor and target cells by this method was confirmed by high content microscopy (>90% target cell recovery and <3% donor cell carry-over). Retrieved target cells were then incubated for additional 36h and analysed by flow cytometry as indicated above.

7.3 Results

7.3.1 Lentiviral infection can be notably enhanced by VSVg and Vpx *in trans*.

Primary myeloid cells (PMC) are well known to be refractory to HIV infection *in vitro*, and this is primarily due to expression of the myeloid-cell-specific HIV-1 restriction factor SAMHD1 [771]. SAMHD1 limits HIV-1 replication by hydrolysing the intracellular pool of

deoxynucleoside triphosphates (dNTPs) and reducing their concentration below the limits required for reverse transcription of the viral genome [772]. However, SAMHD1 does not restrict replication of HIV-2 in myeloid cells, and this is due to the antagonistic effect of Vpx. Vpx is an accessory protein encoded by HIV-2 and some variants of the primate lentivirus SIV, but not HIV-1 [771]. Vpx directly binds SAMHD1 and targets it for ubiquitin-proteasome-dependent degradation in the nucleus[773]. Recently, HIV-1-derived lentiviral vector systems have been developed, which can incorporate and deliver Vpx and thereby highly enhance the efficiency of transduction/infection in myeloid cells [569,774,775]. Furthermore, VSVg-pseudotyping of viral particles is long known to overcome HIV membrane restrictions and greatly increase infectivity in a wide range of cell types. VSVg mediates these effects by targeting HIV entry to an endocytic pathway [776], and this is highly efficient in cells with phagocytic activity such as most myeloid cells. Therefore, we decided to combine both approaches and incorporate both Vpx and VSVg "*in trans*" into our lentiviral preparations for any experiments with PMC. This system is described in section 2.2.6.1 and has been previously optimized in our lab for use in primary Mφ and DC [569]. Of note, VSVg and Vpx are only present in the initial lentiviral inoculum, since they are not encoded within the integrated lentiviral genome. For viral transfer experiments, we produced HIV-IRESeGFP (VSVg+, Vpx+) and tested its ability to productively infect our primary donor cells. Figure 7.1 shows that the combination of VSVg-pseudotyping and Vpx incorporation dramatically enhanced viral particle infectivity against macrophages (Mφ) and immature dendritic cells (iDC) *in vitro*. Saturating infection rates of at least ~60% were observed even at the lowest MOIs used. In contrast, individual incorporation of only Vpx or VSVg into the HIV-IRESeGFP viral particles (which contain HIV-Envelope) was not sufficient to elicit viral infection, even at higher MOIs (Fig. 7.1). Based on these experiments we selected a MOI = 0.2 to infect PMC (with VSVg+ Vpx+ virus) for CCTH experiments.

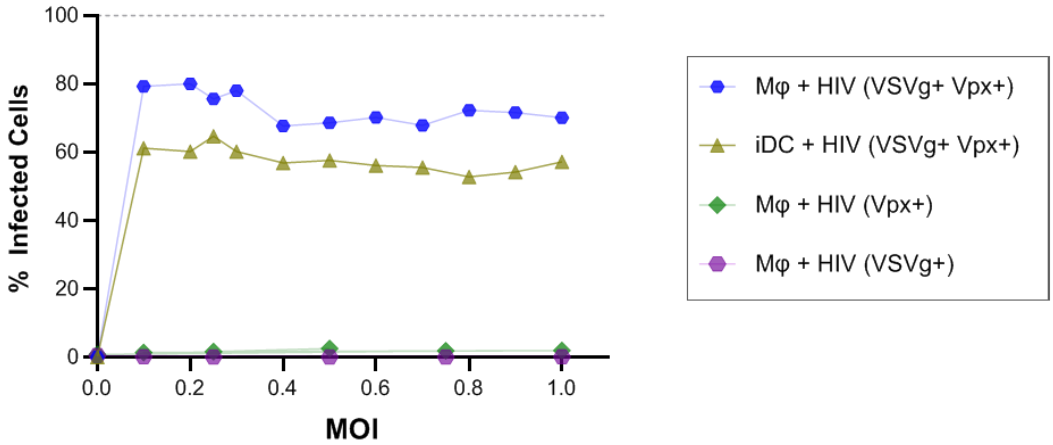

Figure 7.1: Effect of incorporating Vpx and VSVg in virions for infection of primary myeloid cells. HIV-IRESeGFP virus was produced by transfection of HEK293T cells with full length viral DNA

plasmid and the packaging plasmid psPvpxD as described in section 2.2.6.1. Where indicated, producer cells were co-transfected with non-lentiviral plasmids expressing Vpx or VSVg, which get incorporated into viral particles "*in trans*". Viral batches were first titrated on TZM-bl cells (see 2.2.6.3) to determine the number of infectious particles per mL. Virus was then added to primary human myeloid cells at day 6 of differentiation at the indicated MOIs and cells were incubated for 72h. Readout occurred by high content microscopy after live-staining with NucBlue dye. The total number of cells (nuclei) and infected cells (GFP+) per field of view was enumerated on the DAPI and FITC channels respectively. At least 3x10^4 cells were acquired per well. Shown is the percentage of GFP+ Macrophages (Mφ) or immature dendritic cells (iDC) at 72 hpi. The "Vpx only" and "VSV only" conditions are shown only for Mφ but are representative of that observed for both cell types.

7.3.2 Puromycin resistant primary myeloid cells could not be obtained through LCV2 transduction

For primary cells, the Zhang lab recommends attempting transduction with LCV2 lentivirus and subsequent puromycin selection to enrich cells that express the delivered genes [584,770]. Use of antibiotics for positive selection of primary Mφ or iDCs is relatively rare in the literature. However, we found some studies that reported successful use of puromycin in this context at concentrations between 5 - 7.5 µg /mL [777,778]. To identify the minimal lethal concentration to use for selection purposes in PMC obtained with our protocols, we first performed puromycin toxicity curves on these cells. Data from two blood donors suggested that a concentration of at least 10 µg/mL for 72h was required to completely kill untransduced cells (Fig. 7.2).

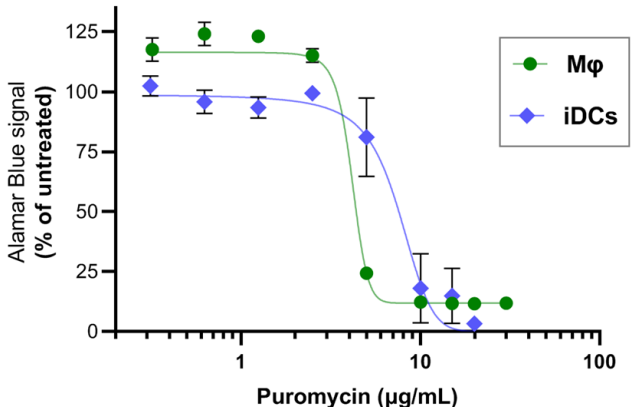

Figure 7.2: Puromycin titration on primary myeloid cells. Monocytes were isolated from PBMCs, seeded at 10^5 cells/well in 96-well plates and differentiated into Mφ and iDC as described in section 2.2.2. At day 6 of differentiation, an equal volume of medium containing 2x of final puromycin concentration was added to each well to create the puromycin dilution series shown (in duplicate). Cells were incubated with the antibiotic for 72h and then 10% of the well volume was added as Alamar Blue reagent. Plates were incubated for additional 24h and fluorescence (560/590 nm) was measured using a Clariostar® plate reader. Relative fluorescence intensities were normalized to the average untreated control wells (0 µg/mL puromycin) for each cell type. Data is representative of 2 independent experiments with cells from different blood donors.

However, when we transduced primary cells with LCV2 VLPs (VSVg+, Vpx+) for 72h and then selected with puromycin containing media (10 μg/mL), we could not detect any increase in survival compared to the untransduced control. In fact, higher VLP concentrations seemed to rather further reduce cell viability (Fig. 7.3 A-B). In contrast, the same VLPs were capable of conferring puromycin resistance to U937 cells, even at high dilutions (Fig. 7.3-C). This was quite surprising for two reasons. Firstly, the permanently acquired puromycin resistance in U937 cells confirms expression from an integrated lentiviral genome, which in turn confirms that these VLPs can package and deliver the LCV2 plasmid. Secondly, we know that our lentiviral system (VSVg+, Vpx+) is very capable of achieving high transduction rates when using other lentiviral constructs in PMC. In any case, since puromycin selection of primary blood cells is not common practice in the field and potentially has nuisances of its own (e.g. toxicity from death of bystander cells), we decided to pursue alternative strategies to validate LCV2 activity in PMC.

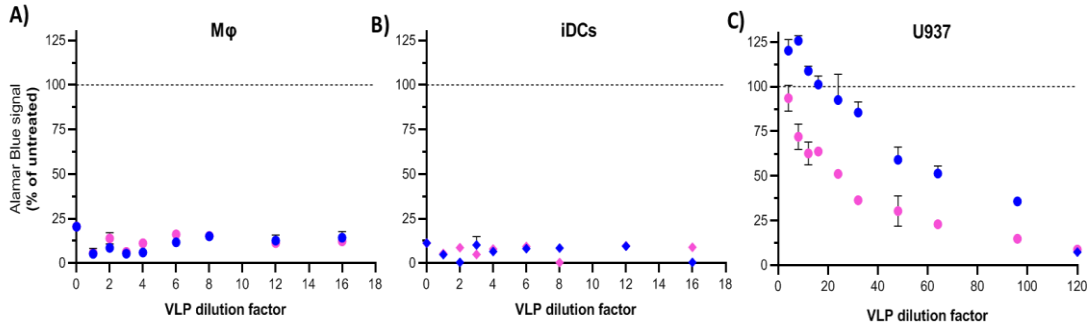

Figure 7.3: Transduction of primary myeloid cells with LCV2 gRNA vectors and subsequent puromycin selection. A) Macrophages (Mφ) and B) immature dendritic cells (iDCs) were obtained as described in section 2.2.2. At day 6 of differentiation, primary cells or C) U937 cells were transduced by lentiviral delivery (VSVg+, Vpx+) of LCV2, which encodes a puromycin resistance marker. Transduced cells were incubated for 72 h before an equal volume of (2x) selection medium was added to reach a final puromycin concentration of 10 μg/mL. Cells were incubated in selection medium for additional 72h and then cell viability of all wells was measured by Alamar Blue assay (see 2.2.3). Relative fluorescence intensities were normalized to the average signal of untreated control wells (untransduced and without puromycin) for each cell type (represented by dashed line at 100%). Data of 2 independent experiments with different LCV2 gRNA VLPs is shown for each cell type (pink = LCV2 CD4 gRNA and blue = LCV2 ICAM1 gRNA).

7.3.3 LCV2 transduction leads to poor expression levels in both primary myeloid cells and cell lines

Binary readouts such as drug-resistance provide only limited information on gene expression levels per cell. We therefore decided to switch to a fluorescence reporter approach to evaluate whether transduction with LCV2 leads to different (and perhaps insufficient) levels of gene expression in primary cells vs. cell lines. The plasmid LCV2-eGFP, in which the PuroR coding sequence is replaced by GFP, was obtained from the Addgene plasmid repository

(Addgene #82416). Of note, LCV2 encodes both Cas9 and PuroR within a single ORF, where both sequences are separated by a P2A element ("self-cleaving" 2A peptide from porcine teschovirus-1). The cleavage occurs at the poly-peptide level, during or after translation [779], so that the resulting proteins are produced at a 1:1 ratio. Therefore, measuring the expression level of the PuroR locus is a good indicator of Cas9 expression from LCV2 vectors.

Transduction of primary or transformed myeloid cells with LCV2-GFP VLPs (VSVg+, Vpx+) resulted in similar transduction rates (Figure 7.4-A) and fluorescence intensities (Fig. 7.4-B) across all cell types, as assessed by GFP fluorescence. This would suggest that LCV2 integration and expression occurs at similar levels in PMC and U937 cells. However, trans-

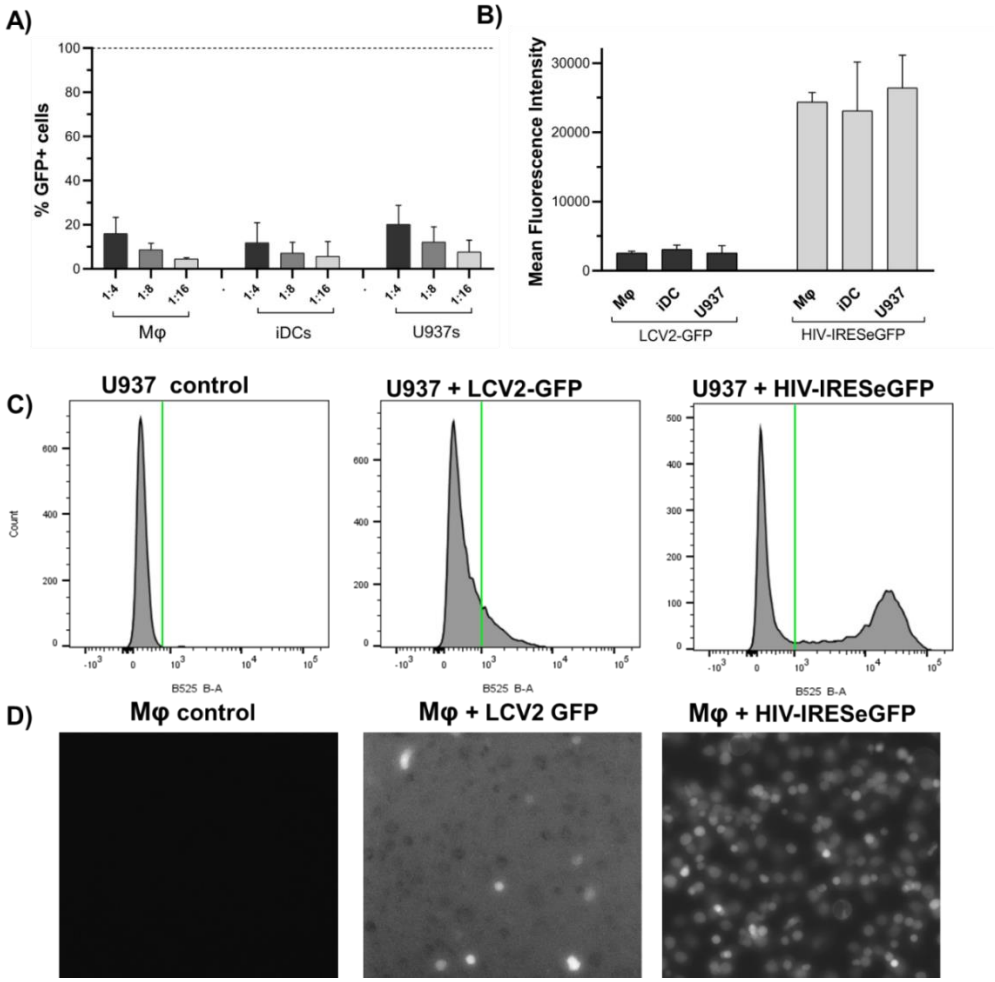

Figure 7.4: LCV2 Cas9-ORF expression in primary myeloid cells and U937 cells. Macrophages (Mφ) and immature dendritic cells (iDCs) were used at day 7 of differentiation. **A)** Cells were transduced with LCV2-GFP VLPs (VSVg+, Vpx+) at the indicated concentrations (e.g. 1:8 = 12.5% VLP in medium). Readout occurred 72h later by flow cytometry. **B)** The mean signal intensity of GFP+ cells is shown for LCV2-transduced cells (1:8) and compared to that of cells infected with HIV-IRESeGFP virus at a MOI = 0.2 (VSVg+, Vpx+). **C**) The histogram distributions of signal intensities are shown only for U937 cells but are representative of all 3 cell types. **D)** Cells were imaged with the Cytell® imaging platform. Images were acquired under identical exposure conditions (however the software automatically adjusts the gamma for better visualization). Images are shown only for Mφ, but results are representative of all 3 cell types.

duction rates with LCV2-GFP were suspiciously low in U937 cells, even at VLP concentrations much higher than normally used for experiments. The fluorescence intensity of LCV2-GFP+ cells was also much weaker than expected post lentiviral transduction. On one hand, their mean signal intensity was only ~10% of that observed in cells infected with HIV-IRESeGFP (Fig. 7.4-B). On the other hand, only a mild "peak shift" was observed by flow cytometry, as opposed to the expected "peak separation" (Fig. 7.4-C). Furthermore, LCV2-GFP+ cells could only be visualized by fluorescence microscopy when using high exposure times to enable detection, which resulted in a low signal-to-background ratio (Fig. 7.4-D). Altogether, this confirmed that both PMC and U937 display similarly low levels of GFP after "transduction" with LCV2-GFP.

Since we have previously shown that ~100% transduction rates can easily be achieved with LCV2-Puro in U937 cells, we could not explain the limited transduction efficiency of LCV2-GFP. Furthermore, the undisturbed growth of LCV2-transduced U937 cells in selection media containing puromycin up to 5 μg/mL (not shown) suggests that the Cas9-PuroR ORF must be expressed at relatively high levels. Since the LCV2-GFP version obtained from Addgene has several sequence differences to our LCV2-Puro vector (in addition to replacement of PuroR by GFP), and did not originate from the Zhang CRISPR group, we suspected this plasmid may not accurately represent the performance of our LCV2 vector. Therefore, we decided to create our own LCV2 fluorescence-reporter version, by exactly replacing the PuroR coding sequence of our LCV2 vector (Zhang lab version) with the coding sequence for mOrange. The detailed cloning procedure is described in section 7.2.1. To our surprise, LCV2mOrange mostly recapitulated that observed with LCV2-GFP. The signal intensities of cells transduced with either vector were comparable across the different cell types, and both transduction efficiency and signal intensity were lower than expected in U937 cells (not shown). However, slightly higher transduction rates could be achieved with LCV2-mOrange in primary cells. Therefore, and because this vector more accurately represents the LCV2-Puro version used in this study, we continued all further optimization experiments using LCV2-mOrange.

7.3.4 Optimizing primary cell transduction with LCV2

By combining the results described above with our observations from Chapter 4, we concluded that expression of the Cas9-PuroR ORF at the low levels observed in U937 cells is sufficient for both efficient puromycin-resistance and Cas9-mediated gene editing, at least in cell lines. Since we show that PMC transduced with LCV2 show similar levels of Cas9/GFP expression compared to U937 cells, this should be in theory also enough to allow Cas9-mediated genome editing in these cells. Therefore, the remaining barrier for using our CRISPR strategy for experiments with primary cells was to increase transduction rates enough to ensure sufficient

representation of the loss of function phenotype at the cell population level. To overcome this barrier, we optimized the transduction conditions. However, the weak fluorescent signal of LCV2 compromised our ability to accurately measure changes in transduction rates (i.e. low signal to noise ratio by microscopy and lack of peak separation by flow cytometry as in Fig. 7.4). Therefore, we also included other lentiviral vectors designed to express high levels of fluorescent proteins in these experiments. This served two purposes; i) to simplify the transduction optimization process, and ii) to compare the performance of LCV2 to other vectors delivered by the exact same platform. A complete list of the lentiviral vectors used in this chapter, including detailed technical information, was provided in Table 7.1. Briefly, we used PPT-GFP and pLKO-GFP (both of which express GFP from a human PGK promoter), pLVX-mCherry (CMV promoter), Empty-mOrange (ubiquitin promoter) and LCV2-mOrange (EF-1a core promoter). Transfection of these plasmids in HEK 293T cells revealed clear differences in expression levels, as could be expected (Fig. 7.5). Importantly, we could confirm that both LCV2-GFP and LCV2-mOrange correctly express the Cas9-fluorescent-protein ORF, as indicated by the clear above-background signal in transfected 293T cells, albeit weaker compared to the other plasmids.

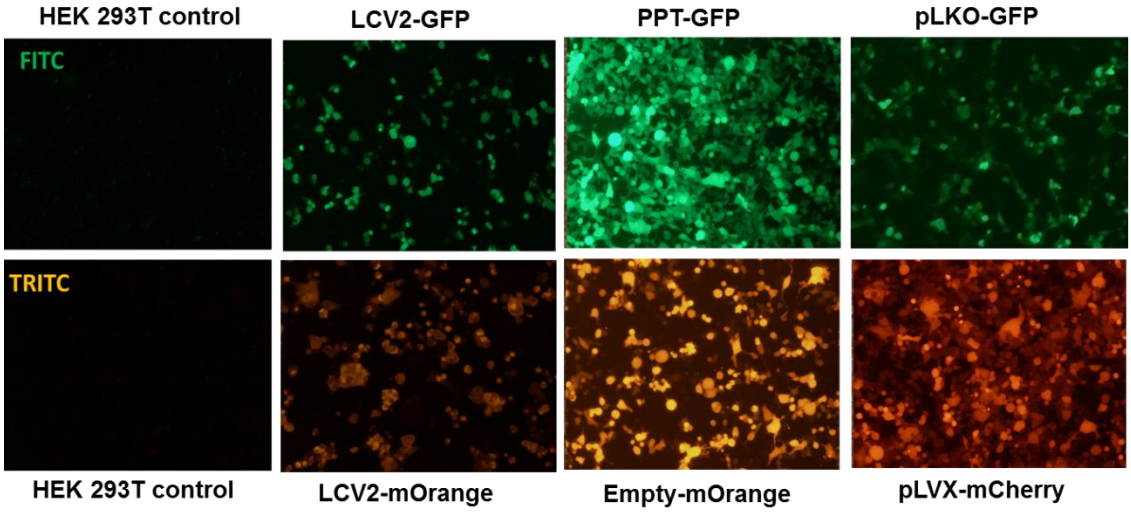

Figure 7.5: Comparative fluorescence reporter expression in HEK 293T cells. Cells were transfected side by side with equal amounts of each plasmid as described in section 2.2.6.1. Fluorescence was assessed by microscopy (IX53 Olympus microscope) at 72 h post-transfection. The same exposure conditions were used for all FITC/TRITC images. Representative images are shown for each condition.

For optimization of the lentiviral transduction protocol in primary cells, we tested the effect of several parameters including; increasing MOIs, concentration of VLPs by ultracentrifugation, spinoculation and duration of exposure to VLPs. Only a brief summary of the most relevant observations from this trouble-shooting process are commented here. The final optimized transduction protocol was used to obtain the results is described in Figure 7.6. When PMC

were transduced with the various VLPs (VSVg+, Vpx+), we found that LCV2 was outperformed by all other tested lentiviral vectors, both in terms of transduction efficiency and expression levels.

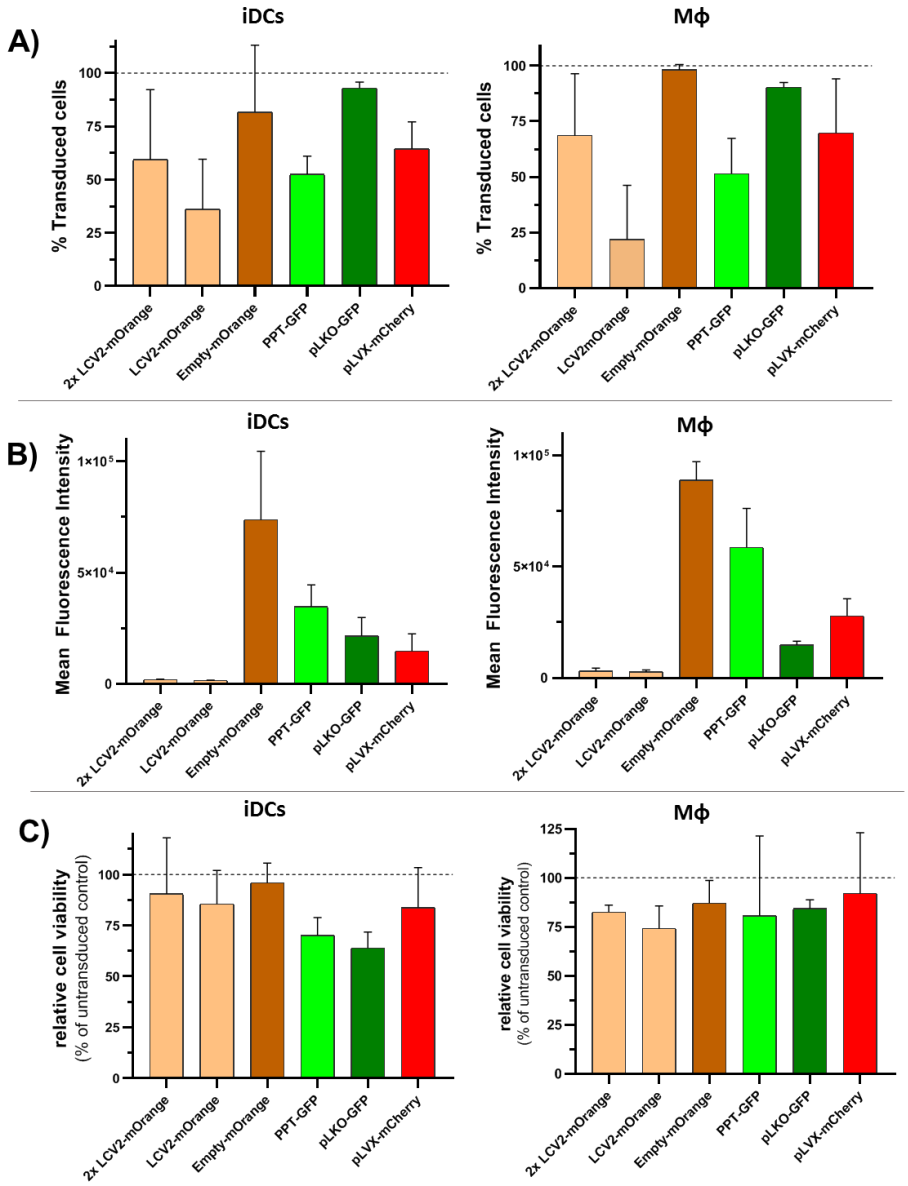

Figure 7.6: Transduction of primary myeloid cells with lentiviral fluorescent reporter vectors. Macrophages (Mφ) and immature dendritic cells (iDCs) were obtained as described in section 2.2.2. Transduction occurred by adding 12.5% (or 2x = 25%) of well volume as VLP supernatant (VSVg+, Vpx+). Medium was refreshed after 24h, and readout occurred by flow cytometry at 72h. Mφ and iDC cell gates were defined based on the forward-scatter and side-scatter distribution of untransduced controls. Fluorescence+ sub-gates were set to exclude fluorescence levels present in untransduced negative controls. Data represents the mean and standard deviation of at least 2 independent experiments per condition. **A)** Percentage of fluorescent cells in the transduced cell population. **B)** Mean fluorescence intensity of cells within the corresponding fluorescence gates. **C)** Cell viability (relative to the untreated control) was estimated as [% events within cell gate for transduced sample / % events in cell gate of untransduced control] x 100.

PLKO-GFP and Empty-mOrange showed the highest efficiency, consistently allowing up to ~90% transduction rates (Fig. 7.6-A). pLVX-mCherry and PPT-GFP were also efficient, allowing ~67% and ~50% transduction respectively. In contrast, the same amount of LCV2 VLPs could only deliver ~36% and ~22% transduction for iDCs and Mφ respectively. However, care should be taken when interpreting these numbers, given that the low signal intensity of LCV2 vectors makes quantification of relative transduction efficiencies highly threshold dependent. Therefore, absolute fluorescence intensities may be a better way to compare the performance of LCV2 vectors. This strategy revealed that the mean fluorescent intensity of LCV2-transduced cells was at least 5 times and up to 45 times lower than for all other tested conditions (Fig. 7.6-B). The Empty-mOrange vector gave the highest intensity/expression in both iDCs and Mφ, followed by PPT-GFP (Fig. 7.6-B). As observed before in U937 cells, a peak shift rather than peak separation was observed upon LCV2 transduction of PMC (Fig. 7.8). In contrast, all other transduction conditions resulted in strong shifts in mean fluorescence intensity (Fig. 7.6-B) and clear peak separation (Fig. 7.8). As expected, transduction of primary cells with the above VLPs had an impact on cell viability. Compared to the untransduced controls, the relative cell viability of transduced cell populations ranged between ~64-96% and ~74-92% for iDCs and Mφ respectively (Fig. 7.6-C). These levels were considered acceptable for primary cells.

In terms of the optimization process, we found that increasing the amount of LCV2-VLPs increased the percentage of transduced cells in a somewhat proportional manner, whereas the mean fluorescent intensity per cell was only moderately enhanced (Fig. 7.7). No appreciable difference in transduction efficiencies were observed when cells were transduced at days 3 or 7 of differentiation (not shown). Concentration of VLPs by ultracentrifugation (as described in 2.2.6.2) was found to have a variable but tendentially positive effect on transduction efficiency (up to ~2.2-fold), however it also resulted in consistently decreased cell viability, especially for Mφ (Fig. 7.7, up to ~70% reduction compared to untransduced controls).

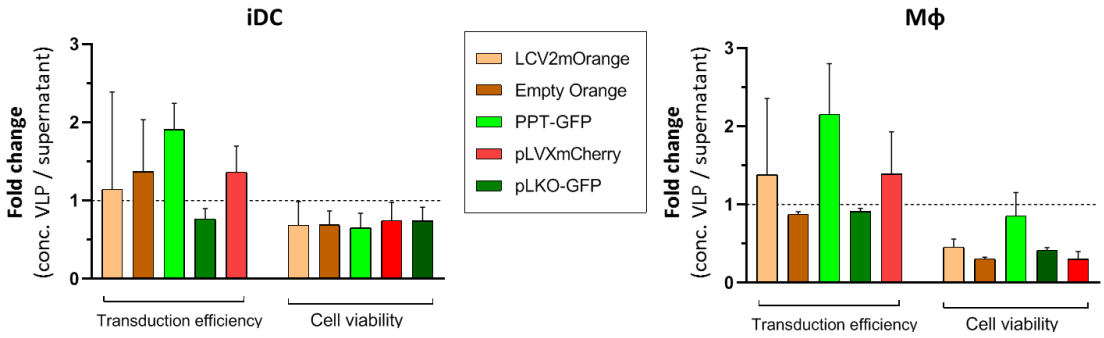

Figure 7.7: Effect of VLP concentration on transduction of primary myeloid cells. Virus like particles (VLPs: VSVg+,Vpx+) were produced in HEK 293T cells as indicated in section 2.2.6. A fraction of VLP supernatant was immediately stored, whereas the rest was first concentrated by

ultracentrifugation as indicated in section 2.2.6.2. Immature dendritic cells (iDCs) and macrophages (Mφ) were transduced with both batches of VLPs and analysed by flow cytometry after 72h. Transduction efficiency and relative cell viability were calculated as described in Figure 7.6-C. The fold-change effect of VLP concentration is shown for each condition (readout for concentrated VLP treatment divided by readout of supernatant VLP treatment). Data indicates the mean and standard deviation of at least 2 independent experiments per condition.

A similar effect (mild enhancement of transduction but decreased cell viability) was observed when VLPs were spinoculated (800 x g for 40 minutes at 32°C) on cells (not shown). Therefore, at least for LCV2, the effect of using these approaches for HIV viral transfer experiments was not beneficial and thus not justified.

7.3.5 Lentiviral delivery of LCV2 does not lead to integration and productive gene expression in primary myeloid cells

The large differences in fluorescence intensities observed between PMC transduced with LCV2 and other lentiviral vectors suggested that perhaps the low levels of fluorescence in LCV2-treated cells were associated with delivery of mOrange as VLP protein cargo, as opposed to *de novo* gene expression. This was supported by the observation that treatment with other VLPs often resulted in bimodal distributions of fluorescence signal intensities (Fig. 7.8-A), whereas LCV2 treatment maintained a normal-like distribution, albeit with an increased mean. For example, for iDCs transduced with Emtpy-mOrange VLPs, nearly all cells fall within the mOrange+ gate, however the frequency distribution of the signal intensities within this gate reveals separation into 2 peaks (Fig. 7.8-A). For pLVX-mCherry treatment, not all cells increase their fluorescence beyond the set threshold, however two peaks are also observed. Since in the previous examples both the higher and lower peaks are shifted towards higher fluorescence (compared to the untransduced control signal peak), we interpret this phenomenon as follows. The higher intensity peak likely corresponds to genuinely transduced cells, where lentiviral integration has occurred, and genes are expressed at high levels. On the other hand, the lower intensity peak may represent cells where high levels of VLP fusion have occurred but post-entry steps (e.g. reverse transcription or integration) have failed. Since only one peak with moderately shifted intensity is observed upon LCV2 treatment (Fig. 7.8-A), we hypothesized that these cells may not actually be effectively transduced. To test this hypothesis, we treated PMC with LCV2 or other VLPs in the presence or absence of the reverse transcriptase inhibitor Efavirenz (EFV). A non-toxic concentration of 10 µM was chosen for these experiments, as this could efficiently and completely block infection of PMC by HIV-IRESeGFP virus. When PMC or U937 cells were treated with pLVX-mCherry in the presence of EFV, the high intensity peak clearly disappeared, leaving only a slightly shifted low intensity peak (Fig. 7.8-B). Importantly, when U937s were treated with LCV2-mOrange in the presence of EFV, the asymmetric tail of the peak protruding beyond the set fluorescence-

threshold disappeared (Fig. 7.8-B) . In contrast, when PMC were treated with LCV2 VLPs, no differences in signal intensities or transduction rates were observed in the presence or absence of EFV (Fig. 7.8-B). Quantitative assessment revealed that in PMC, ~100% of the observed fluorescence signal in the VLP-treated population was resistant to EFV, whereas for other VLPs this averaged to only <10% (Fig. 7.8-D, *p < 0.05). Together, our results suggest that LCV2mOrange VLPs can productively transduce U937 cells, whereas the same treatment is ineffective on PMC. Therefore, the weak increase in fluorescence in these cells is likely due to enrichment of mOrange protein delivered *in trans* by inbound VLP fusion.

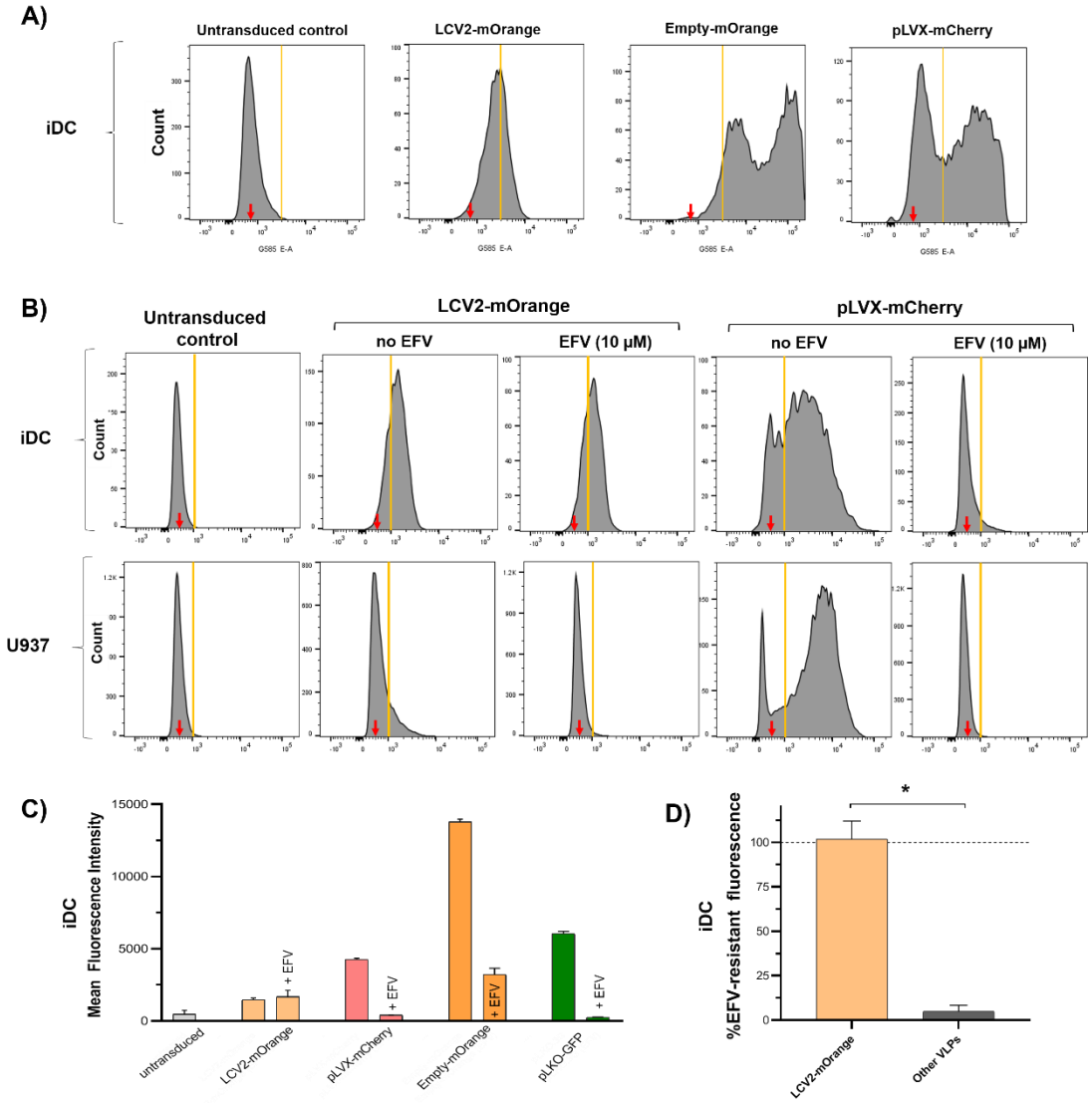

Figure 7.8: Signal intensity distribution upon transduction with various virus-like particles. Immature dendritic cells (iDC) or U937 cells were transduced with VLPs (VSVg+, Vpx+) encoding fluorescent proteins. Readout occurred by flow cytometry at 72h. **A-B)** Shown is the distribution of fluorescence intensities within the cell gate (histogram frequencies). The red arrow indicates the mean fluorescence intensity of the untransduced control. The orange line indicates the lower limit of the fluorescence+ gate. Data is representative of 2 independent experiments. **B-D)** Effect of Efavirenz (EFV, 10µM) treatment on fluorescence intensity distributions. **C)** Changes in absolute mean fluorescence intensity (MFI) values when EFV is added prior to lentiviral transduction (representative

of 2 experiments) **D)** Percentage of EFV-resistant fluorescence (calculated as [100 x MFI in the presence of EFV / MFI without drug]). Data indicates the mean and standard deviation of 4 experiments (* = $p < 0.05$ by Mann-Whitney test).

7.3.6 LCV2 VLPs can deliver CRISPR-Cas9 to primary myeloid cells *in trans*

We concluded above that LCV2-VLPs could deliver low but detectable levels of mOrange to PMC *in trans*. Since mOrange incorporation into the particle most likely occurs in an unspecific manner, it was important to assess whether LCV2-VLPs can also deliver Cas9 and gRNA in functional amounts to these cells. To test this hypothesis, we treated iDC with LCV2-CD4gRNA or LCV2-CTRLgRNA VLPs (VSVg+, Vpx+) and assessed changes in CD4 surface expression. Both untreated and LCV2-Control-gRNA treated iDCs displayed uniform presence of CD4 antigen on their surface (Fig. 7.9-A, 95% and 98% CD4+ cells respectively). In contrast, iDCs treated with LCV2-CD4 VLPs showed variable levels of CD4 across multiple donors, ranging from 92% to ~30%. In the experiment with the strongest depletion, we could even observe a dose-dependent effect of VLP concentration on CD4 expression (Fig. 7.9-B). Although further investigation is required, these preliminary results suggested that CRISPR components can be delivered *in trans* to PMC by LCV2-VLPs, at levels sufficient to elicit Cas9-mediated editing at the gRNA target sequence in the genome. This is consistent with a previous report of successful LCV2-mediated CRISPR in primary Mφ (see discussion). However, it is also important to note that even if LCV2 could productively transduce PMC, slower protein-depletion rates are expected in these cells compared to cell lines. This is because in non-dividing cells protein depletion depends only on protein turnover, whereas in cell lines the pool of remaining protein is halved with every cell division. Proteins with very long half-lives may therefore not represent good targets for CRISPR in primary cells.

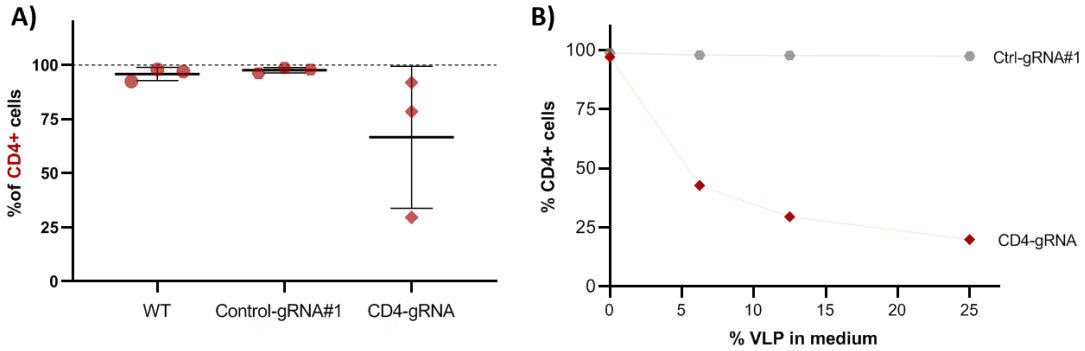

Figure 7.9: Proof of concept CRISPR-Cas9 delivery with LCV2 VLPs in primary myeloid cells. Immature dendritic cells were transduced with LCV2-CD4gRNA or LCV2-CTRLgRNA VLPs (VSVg+, Vpx+). 7 days post-transduction, cells were surface stained with an Alexa647-conjugated CD4 antibody (Biolegend #317422), then fixed and analysed by flow cytometry to assess CD4 surface levels. A) Data indicates the mean and standard deviation of three independent blood donors across 2 experiments. B) A dilution series with one of the donors revealed a dose-dependent response of VLP concentration and CD4 depletion.

7.3.7 Preliminary experiments to validate findings in primary cells (non-integrative approach)

Since our LCV2 delivery system apparently allowed some extent of CRISPR activity in PMC, we decided to attempt validation of the results previously obtained with cell lines in Chapter 4, by repeating similar viral transfer experiments using PMC as HIV donors. Preliminary testing revealed considerable differences between "untransduced" and VLP-treated PMC both in terms of cell-viability and viral transfer. This was particularly a problem for macrophage experiments, where the total number of cells in the coculture is determined by the inalterable number of infected donor cells in the well at the start of the experiment. Therefore, we decided to use LCV2-CtrlgRNA treated cells for the optimization of the CCTH assay conditions and as reference group across experiments. The optimized protocol for the viral transfer assay from primary cells is described in full detail in section 7.2.3. For both types of PMC, we observed a strong linear relationship between donor:target ratios (D:T) and the proportion of infected target cells. Of note, since the number of Mφ per well cannot be adjusted after seeding, the range of D:T ratios tested was limited by the typical macrophage densities and infection rates obtained in 96-well plates. Viral transfer mediated by iDCs was notably more efficient (~5 fold on average) compared to macrophage donor cells (Fig. 7.10-D), however it also showed higher inter-experiment variability. This variability seemed to increase at higher D:T ratios, so we decided to use an intermediate D:T (= 0.065) for experiments where the effect of different treatments is assessed. Since our CRISRP-delivery strategy to PMC requires further optimization, we limited this preliminary round of validation experiments to only the key actin regulators identified in Chapter 4 to play a role for actin-dependent CCTH (i.e. Arp2/3, Cdc42 and Profilin). When PMC were treated with LCV2-VLPs to disrupt these genes, we found that Arp2 gRNA led to a moderate decrease in CCTH in both iDCs and Mφ (~66% and ~77% of control-gRNA transfer respectively) (Fig. 7.10-A). A similar but weaker effect was observed for Cdc42 gRNA treatment, with a slightly higher variability. For both these treatments, the effect was more pronounced in iDCs than in Mφ. In contrast, Profilin-gRNA treatment led to a consistent reduction in CCTH from Mφ (~64% of control and strongest decrease for this cell type), whereas iDC-mediated CCTH was (on average) not affected by this treatment.

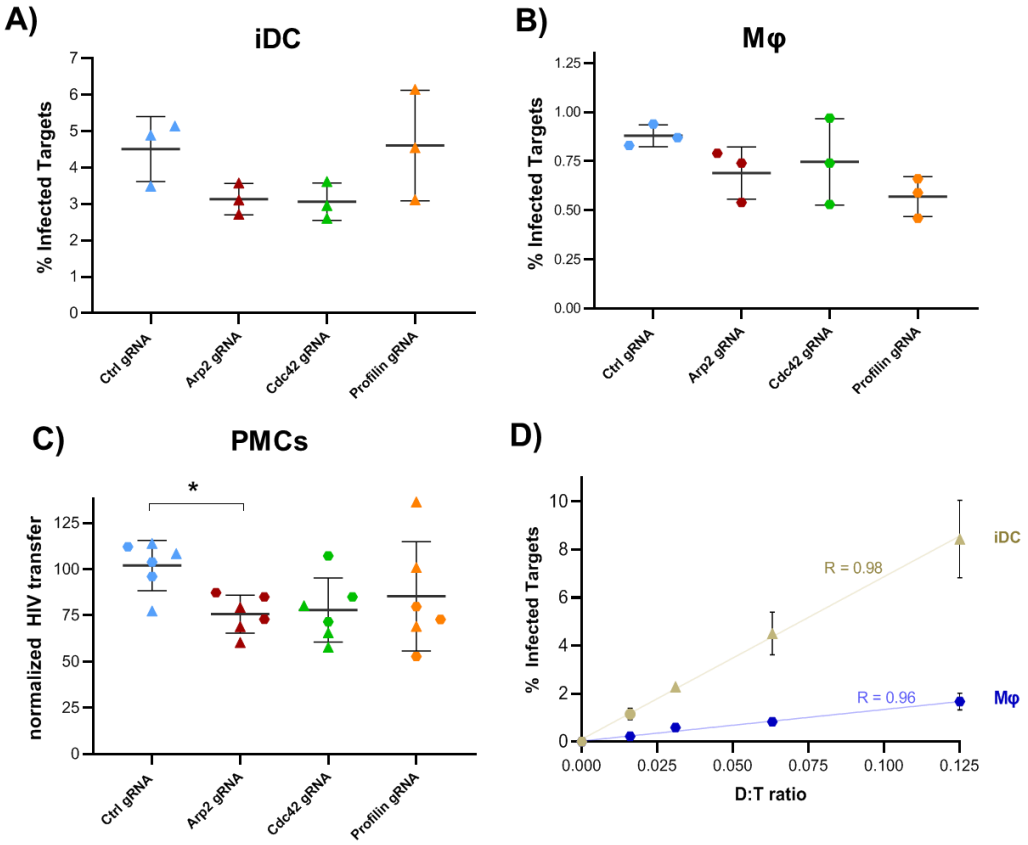

Figure 7.10: HIV transfer from primary myeloid cells. For the full-detailed protocol see section 7.2.3. Briefly, PMC were treated with LCV2-gRNA VLPs (VSVg+, Vpx+) and 7 days later infected with HIV-IRESeGFP (VSVg+, Vpx+) to be used as HIV donor cells in viral transfer assays. At 72 hpi, donor cells were extensively washed to remove free virus and then co-incubated with fluorescently labelled Jurkat target-cells at a donor:target ratio = 0.065. Viral transfer was stopped exactly 12h after start of coincubation by introducing the inhibitor BMS-378806 (10 µM). After additional 36h, cells were washed, trypsinized and fixed. Readout occurred by flow cytometry. **A)** Immature dendritic cell (iDC) and **B)** Macrophage (Mφ) data represents the mean and standard deviation of experiments with primary cells from 3 independent blood donors. **C)** Data from each experiment was normalized to the average of the control-gRNA group for the relevant cell type. Normalized data is shown together for PMC (iDC = triangles, Mφ = hexagons). The effect of each treatment was compared to the control-gRNA group by Mann-Whitney test with Bonferroni correction for multiple testing (* = $p < 0.016$). **D)** PMC treated with LCV2-CtrlgRNA VLPs were co-incubated with target cells at different D:T ratios. Data indicates the mean and standard deviation of 2 independent experiments.

When data was normalized to the inter-experiment average of the control group ("normalization i" as per [691] and PMC data was considered together (Fig. 7.10-C), Arp2 gRNA led to an appreciable reduction in viral transfer with modest variation (75.4 ± 10.2% of control), whereas Cdc42 gRNA had a similar effect but with higher variability (78 ± 17.3% of control). Since Profilin gRNA had a disparate effect in iDC and Mφ, this combined analysis results in high variability for this group (86 ± 29.4 % of control) and thus care should be exercised in interpreting this result. When testing for statistical significance (note that iDC and Mφ experiments were performed on different days and thus can be considered independent

experiments) both the Arp2 gRNA ($p<0.009$) and Cdc42 gRNA ($p<0.026$) groups resulted in a p-value below the significance threshold $\alpha = 0.05$ (for a confidence level of 95%). However, after correcting for multiple testing for extra stringency (by adjusting α with the Bonferroni correction method, so that $p < [\alpha/3 = 0.016] = *$) only the Arp2 gRNA treatment retained statistical significance. These results suggest that Arp2 likely plays a role in outbound CCTH from PMC, whereas the role of Cdc42 will require additional confirmation. However, it should be noted that the level of knockout achieved by each treatment (if any) in these experiments is unknown and/or expected to be low. Therefore, rather than increasing the number of replicates with this "imperfect" CRISPR-delivery method, future experiments to confirm these preliminary results should use alternative approaches with confirmed and efficient ability to reduce target protein levels/activity. Importantly, our research group is currently developing a transient mRNA-based CRISPR delivery system that does not require lentiviral integration and thus is designed to bypass the "transduction block" described in this chapter for PMC.

7.4 Discussion

The original aim of this chapter was to validate our findings from previous chapters in more physiologically relevant models. To do so, we planned to repeat key experiments, but using primary myeloid cells (PMC) obtained from healthy human volunteers. Since most of the methodology used in this work was conceived, established and controlled to specifically address the questions of this study, the ideal scenario would have been to keep the experimental approaches as constant as possible, while replacing cell lines with primary cells. This included not only our optimized cell-cell HIV transfer assay, but also the lentiviral platform used to deliver CRISPR-Cas9 activity to the cells of interest. In terms of lentiviral vectors, the Feng Zhang lab explicitly recommends the LentiCRISPRv2 (LCV2) option for delivery into primary cells [584,770]. Since we could validate the efficient performance of this system in our cell lines, and because our lab is experienced in delivery of lentiviral constructs to primary HIV-target cells, using the LCV2 system was a logical choice. However, to our surprise, we found that LCV2 selectively failed to transduce PMC, whereas these could efficiently be transduced by a wide range of other lentiviral vectors using the exact same lentiviral delivery system and under otherwise identical conditions. Numerous experiments allowed us to conclude that the failure was due to the lack of productive transduction (i.e. lentiviral genome integration and *de novo* gene expression) in PMC.

To understand how we reached this conclusion, it is easiest to review the observations for cell lines and primary cells separately. First, lentiviral delivery and transduction with LCV2 is highly efficient in both U937 and Jurkat cell lines. This is evidenced by the fact that a high

proportion of these cells acquire puromycin resistance even after short-time exposure to low VLP concentrations. This trait is acquired permanently, since the cells continue to grow in puromycin medium even after single-cell sorting and clonal expansion. This is dependent on "productive" transduction (i.e. successful reverse transcription and integration leading to *de novo* gene expression), given that cells exposed to LCV2-VLPs in the presence of the RT-inhibitor Efavirenz do not become puromycin resistant. This therefore means that the LCV2 lentiviral genome is correctly expressed in HEK 293T cells and that it can be successfully packaged into the VLPs produced in these cells. Since cell lines transduced with LCV2 display both puromycin resistance and Cas9 activity (confirmed by genomic sequencing at gRNA target sites), this confirms that the Cas9-PuroR ORF is fully functional in this plasmid. In terms of expression levels however, the vanishingly low fluorescence intensities of U937 cells transduced with either LCV2-GFP or LCV2-mOrange suggest that this ORF is only weakly expressed in these cell lines, whereas transfecting the same plasmids in HEK 293T cells showed robust expression and fluorescence, thus confirming ORF functionality. Such differential expression in these cell lines is possibly related to different performance of the EF1a core promoter, which controls the Cas9 ORF in LCV2. However, it is surprising that this promoter would perform so poorly in U937 cells, given that it is widely recognized as a robust and versatile promoter. This is because EEF1a is one of the most abundantly expressed proteins in all cell-types, including leukocytes [598,780]. A possible explanation for these observations is that the LCV2 vector has a much shorter version of this promoter (EF1a core promoter = 212 bp) which is known to be much weaker than the full-length human EF1a promoter (1200 bp) [781]. In any case, even these low expression levels are clearly sufficient to elicit puromycin resistance and Cas9 activity in U937 cells.

On the other hand, primary cells treated with LCV2-VLPs did not acquire puromycin resistance, even when "transduced" at high MOIs. This was evidenced by the complete lack of Alamar blue signal, regardless of how long the reaction was incubated. This was surprising because these VLPs contained Vpx and VSVg *in trans*, which we showed dramatically enhanced lentiviral infection of PMC with HIV-IRESeGFP under identical conditions (consistent with the findings of [782]). We could exclude that the inefficacy of LCV2 in primary cells was due to the slightly different VLP generation procedure for primary cells (Vpx incorporation requires use of the psPvpxD packaging plasmid), because the very same particles that failed to transduce PMC were highly efficient in cell lines. At this point, we could think of at least two possible explanations. First, transduced PMC may be expressing the puromycin resistance gene, but their death could be a consequence of high levels of danger signals resulting from the death of untransduced bystander cells. Alternatively, the EF1a core promoter may be even more inefficient in PMC than in cell lines and may thus not provide

sufficient expression levels to warrant antibiotic resistance. To test these hypotheses, we transduced PMC with LCV2 variants in which the puromycin resistance gene was replaced by GFP or mOrange. The resulting fluorescence intensity signals were comparable to those observed in U937 cells (i.e. only slight increase over background), as were the apparent transduction efficiencies. We therefore initially concluded that LCV2 must be integrating and expressing at similar levels in both cell types. However, when we blocked lentiviral transduction with the RT-inhibitor Efavirenz, we only observed an effect in U937 (loss of LCV2-mediated fluorescence or antibiotic resistance), whereas the fluorescence profile of LCV2-treated PMC remained unchanged. This strongly suggests that, in PMC, mOrange fluorescence is not obtained by lentiviral integration and subsequent gene expression, but rather by passive delivery of mOrange protein via uptake and/or fusion of the VLPs produced in HEK 293T cells. This lack of integration/gene expression was however specific to the LCV2 context, because VLPs produced with other lentiviral plasmids (under identical conditions) could efficiently transduce PMC and induce strong fluorescence in an Efavirenz-sensitive manner.

The cause for this perplexing selectivity is presently unclear. When comparing LCV2 to the other lentiviral constructs used in this study (see Table 7.1 for an overview), the most striking difference is given by the size of the lentiviral genome (region between the 5' and 3' LTRs). In LCV2, this is nearly twice as large as for the other plasmids, and this is a direct consequence of encoding Cas9 (4.1 kb), which is a 160 kDa protein. Indeed, the large size of the Cas9 gene/protein is currently a limitation of CRISPR for various desirable applications [783]. Our current working hypothesis is that a restriction factor present in PMC (but absent in cell lines) may counteract a post-entry step in transduction of larger viral genomes. We speculate that this could occur before or during reverse transcription, which is when the viral genome (single stranded RNA) is most vulnerable. This restriction factor would have to be different from SAMHD1 and counteracted by a viral accessory protein in HIV-1. This is because; i) delivery of Vpx in LCV2-VLPs cannot overcome this restriction, and ii) HIV-IRESeGFP infection (>2 kb larger genome than LCV2) of PMC occurs with high efficiency (in the presence of Vpx and VSVg). To test this "limiting length" hypothesis we are currently pursuing two approaches. First, we will remove the Cas9 coding sequence from the LCV2-mOrange vector, thus halving the size of its lentiviral genome. We will then test its ability to mediate productive transduction and mOrange expression. Second, we are modifying the Empty-mOrange vector, which showed the highest transduction efficiency and the lowest toxicity in our PMC system. If insertion of Cas9 in this vector (leads to larger genome than LCV2) significantly reduces its ability to integrate/express, our hypothesis will gain support. Conversely, if transduction is not impaired, we will have the means to deliver CRISPR with high efficiency to PMC.

We established above that delivery of LCV2-VLPs did not lead to productive transduction of PMC. We were therefore surprised to find several publications which, at first glance, seemed to suggest having successfully used LCV2 to mediate CRISPR in PMC. To shed light on this issue, we did a systematic literature analysis as follows. A search algorithm was used to identify any publication within the >600 LCV2 references (listed by Addgene) that used the terms "macrophages", "dendritic cells" or "monocytes". Close examination of each of these references revealed that while these terms were often used in the article's title or abstract (and indeed sometimes primary cells were used for part of the experiments), the sections involving LCV2-mediated CRISPR invariably corresponded to myeloid cell lines (e.g. THP-1, RAW264.7, HAP1 or ANA-1) rather than primary cells. The only notable exception (as of September 2019) was the work of Moyes et al. [784]. In this article, the authors report successfully treating human primary Mφ with LCV2-VLPs, and they convincingly show CRISPR-mediated depletion of two different genes in these cells. To achieve this, VLPs were produced with Vpx and VSVg *in trans*, and then concentrated by ultracentrifugation. Mφ were transduced at day 3 or 6 with a MOI=1000 for at least 72h and then further incubated for 6 additional days. Therefore, the only prominent differences with our protocols are the concentration of VLPs and the use of very high MOIs. To monitor "transduction" efficiency, they used a monoclonal antibody to detect EGFRt (truncated epidermal growth factor receptor), which replaces the PuroR sequence in their LCV2 system. Therefore, their readout is analogous to ours but with EGFRt instead of mOrange. Their flow cytometry data is also consistent with our observations in that transduction with LCV2-EGFRt results in mild shifts in signal intensity, rather than distinct population separations. While they did measure the number of integrated copies for other unrelated vectors in this study, they unfortunately did not measure this for LCV2. Based on all the above observations, we hypothesize that EGFRt delivery in their system is by passive protein-delivery via VLP fusion, in the absence of productive transduction. This would readily explain the exorbitant MOIs required for "transduction" with LCV2 in their hands.

Our findings indicate that LCV2-VLPs can deliver low but detectable levels of mOrange protein to PMC *in trans*. It was therefore important to assess whether these VLPs can also deliver Cas9 and gRNA to these cells. This is because Cas9 and mOrange (in LCV2) are translated as a single polypeptide chain and are only separated by a P2A element. This means that both proteins are expressed at a 1:1 ratio. However, cleavage of P2A is believed to occur during or imminently after translation, so that the presence of mOrange within VLPs or target cells does not necessarily imply equimolar presence of Cas9. Still, since mOrange is likely not actively packaged in outbound VLPs, we would expect Cas9 to be also unspecifically incorporated in budding particles to some extent. Furthermore, we speculate that even few

copies of Cas9 should in theory be able to mediate some CRISPR activity. This is because Cas9-mediated effects are cumulative, permanent and directed by sequence-complementarity. This is consistent with the recent findings of Shen et al., who report that even "very low levels of Cas9 expression are sufficient to induce on-target mutagenesis in a short period of time" [785]. It is thus possible that unspecific delivery of CRISPR components by LCV2-VLPs *in trans* could lead to the desired genomic editing and result in target protein depletion and the associated phenotypic changes (as reported in [784]). The guide RNA could be delivered either unspecifically by "cytosolic pinching" of the VLP, or (more likely) complexed to Cas9 through its scaffold sequence. Indeed, we showed that LCV2-CD4-gRNA delivery to primary DC could lead to CD4 depletion in a dose-dependent manner and reach up to 70% reduction, despite the lack of productive lentiviral transduction. This is consistent with the findings of Moyes et al., who showed that they could achieve 40-60% target protein depletion in primary macrophages (PD-L1 or IL-10) using their analogous LCV2 approach [784]. However, we also observed a high inter-donor variability in this respect, with some donors expressing near-wildtype levels of CD4.

Since we could confirm that our non-transducing LCV2-VLPs could mediate CRISPR activity to some extent, and since we were able to deliver protein cargo to enough cells (i.e. > 60% mOrange+ cells with > 75% viability), we decided to attempt validation of our CCHT findings from previous chapters. This should however be considered as preliminary work, given that the proper validation experiments will be performed once an efficient CRISPR platform is optimized for PMC. We first adapted the CCTH assay to use PMC as donor cells. For iDC, the coculture and readout procedures are virtually identical to those used for U937 cells. In contrast, some changes were necessary to account for the strongly adherent nature of Mφ, which impedes their resuspension and reseeding (see section 7.2.3). Both iDCs and Mφ led to a strongly linear increase in target cell infection, in response to raising donor:target ratios. We calculated the infection transfer rate "ITR" (see Fig. 3.16) to be ~6% per hour for iDCs and ~1.2% for Mφ. Therefore, iDCs in our system mediate CCTH (*in cis*) about 5-fold more efficiently than Mφ and U937s, which performed similarly in this context (1.2 vs. 1.6%). When we compare these values to other studies in the literature, we find some discrepancies, which are most likely caused by different experimental conditions. Bertram et al. used a similar system to ours to measure "*in cis* CCTH" from iDCs to JLTR cells, yet their data suggests ITRs of only ~1-2% per hour [90]. This lower transfer efficiency is possibly related to their use of the R5-tropic BaL strain in combination with JLTR cells, which unlike JLTR-R5, do not express significant levels of CCR5. Similar transfer efficiencies (ITR ~ 1%, at best) were observed by Menager et al. for CCTH "*in trans*" from mature DCs to autologous CD4TC [508]. On the other hand, we calculate an ITR of ~16% per hour for Mφ in the work

of Groot et al. [91]. However, their assay measures "p24 transfer" rather than infection transfer, and the authors readily admit that a large portion of this transferred material may not lead to target cell infection. Still, our ITR calculation is entirely consistent with their statement that "each infected MDM is able to "infect" at least one T-cell every 6 hours" [91]. This overall supports the use of ITR as a useful indicator to compare results from different CCTH systems. Unfortunately, the fundamental differences in the experimental systems used by different labs, as well as the lack of reported experimental parameters, currently limit our ability to accurately compare the CCTH potential of different cell types. Our own observations however suggest that infected iDCs may be among the most efficient HIV-donor cells, and this is consistent with the findings reported in [89,90].

To evaluate the role of actin remodelling for CCTH from PMC, we treated both iDCs and Mφ with LCV2-VLPs containing gRNAs against Arp2, Cdc42 and Profilin (i.e. the top leads from our outbound CCTH screen). At least 7 days were allowed for genomic editing and protein depletion to occur before donor cell infection. Our results suggest that both Arp2 and its upstream regulator Cdc42 play a role in CCTH from both types of PMC. In contrast, Profilin seemed to be required for this process in Mφ, whereas its contribution in iDCs remains unclear. Note that the envisioned and/or confirmed mechanistic roles of these actin regulators in outbound CCTH from myeloid cells was discussed in previous chapters. While the results presented here are encouraging and partially validate our findings from the U937 model, this approach has several limitations. First, PMC are not productively transduced in this system, the implications of which are still not fully understood. Second, the rate of protein depletion is unknown for each donor and treatment. This makes it impossible to estimate the real magnitude of each actin regulator's contribution (e.g. small reductions in CCTH may be caused by weak effects in many cells or by strong effects in few cells). Unlike with cell lines, this issue cannot be overcome by generation and expansion of -/- cellular clones. Yet from our observations herein, it is apparent that small quantities of transiently delivered CRISPR-Cas9 may be sufficient to mediate a gene editing outcome.

It may therefore be beneficial, not only for the clinic but also at the basic research level, to express/deliver these components transiently (provided high-enough efficiency can be achieved) rather than by integration and constitutive expression. Successful transient delivery of CRISPR-Cas9 components has been recently reported by other teams working on primary leukocytes (T-cells) through the use of electroporation [786] or nucleofection [787]. Whilst the latter approach indeed looks promising, some studies caution against the use of electroporation based on the occurrence of significant phenotypic changes associated with this technique [788]. Also recently, studies by [789] and [790], have re-engineered lentiviral

particles for the purpose of transient RNA delivery, and the feasibility of this approach for CRISPR-Cas9-mediated gene editing has been confirmed [790]. A transient CRISPR platform based on the constructs of Prel et al. [789] is currently being developed in our laboratory, and preliminary data suggests efficient delivery of RNA into primary resting CD4TC. Once this method is adapted for use in PMC and a high level of CRISPR efficiency can be confirmed in these cells, the CCTH experiments shown in this chapter will be repeated with a larger number of blood donors. Fortunately, this system allows simple gRNA multiplexing, which should notably increase the percentage of knockout cells in each treated population. If, however, the barriers to using CRISPR in PMC cannot be overcome, shRNA-mediated knockdown would be a valid alternative approach, as we could achieve efficient transduction and expression levels with the pLKO lentiviral vector.

Overall, despite the unexpected challenges faced in this chapter, the cause for the limited efficiency of LCV2 lentivirus in PMC could be identified (i.e. lack of productive transduction). We propose that this is a generalized problem that will reproduce in other labs attempting similar approaches. Nevertheless, the protocol for non-integrative delivery of CRISPR components could be optimized here to reach levels high enough to allow at least partial protein depletion. Using this pilot system, we could achieve preliminary validation of our results from previous chapters, in terms of the role that some actin regulation play for outbound CCTH from infected myeloid cells. Further work in our lab is already ongoing to provide a simple and validated strategy to deliver CRISPR to primary leukocytes, and this will be used in future studies for formal validation of our findings in the context of HIV-Actin manipulation.

7.5 Chapter acknowledgements

All experiments and data analysis in this chapter were performed by the author of this thesis. Note that the personal pronoun “we” is used throughout this thesis to reflect common scientific practice.

Chapter 8. General discussion

The overall aim of this thesis was to further resolve the functional and physical intersection of HIV and the cellular actin cytoskeleton. One important aspect of this pathogen-host interaction is the ability of HIV to manipulate cellular actin dynamics to promote F-actin remodelling events that facilitate cell-cell infection transfer, which is believed to be a major and highly efficient mode of viral spread *in vivo*. More concretely, this project aimed to validate the physical interaction of HIV-Gag and F-actin, identify new actin regulators involved in cell-cell transfer of HIV (CCTH), and investigate how these are manipulated by the virus and how this contributes to spread of the infection. Our focus was on infected myeloid cells given their proposed critical role in early dissemination of the infection, but also because HIV-actin manipulation in this lineage results in enhancement of cortical F-actin structures, which offers the unique opportunity to use high-resolution imaging techniques to provide insight into the actin regulators involved. In this chapter we describe and discuss our findings in the light of their contribution and relevance to the field. Note that since methodological approaches and their limitations were extensively discussed within each previous chapter, these aspects will not be addressed again here.

8.1 Key findings

As part of this study, we confirmed a close and specific physical association of HIV-Gag with cellular actin. Our approach demonstrates for the first time that this interaction occurs in living and HIV-infected cells of human hematopoietic lineage. This corroborates that HIV belongs to the long list of intracellular pathogens that can directly interact with the host's actin cytoskeleton [415]. By using a new and improved *in vitro* viral transfer assay, we also confirmed that CCTH is at least one order of magnitude more efficient than infection by cell-free virus, and that pharmacological disruption of actin polymerisation can impair the former mode of transmission without affecting the latter. This fits well with the growing consensus in the field that CCTH is likely to be the predominant mode of viral spread also *in vivo* [121,134-136], and that this mechanism requires specialized intercellular contacts that are strongly dependent on F-actin remodelling (see 1.3 & 1.5.10). Our findings highlight a key role of Rho-GTPases as central nodes where multiple HIV-manipulated actin pathways converge. In uninfected target T-cells, we could confirm a critical role for Rac1 and Arp2/3 in entry of free HIV, but also expanded these observations to CCTH. We also report new potential roles for the G-actin binding proteins Profilin and CAP1 in this context. In infected myeloid donor cells, we identified a group of cortical F-actin regulators as factors that contribute to outbound CCTH (e.g. Cdc42, Arp2, N-WASP, Cofilin, Dia formins and Profilin).

Since many of these are associated with biogenesis of filopodia [354], this suggested an important connection between such structures and viral spread. Indeed, we found that HIV hijacks a myeloid-cell pathway of filopodia formation, which results in positioning and prominent enrichment of HIV-buds at the tips of "HIV-Filopodia", even though these tips cover only a minuscule fraction of the total cell-surface area. Inhibiting HIV-Filopodia at either the signalling or actin nucleator levels (i.e. Cdc42 or Arp2/3-formins, respectively) both significantly reduced the potential of cells to mediate CCTH *in cis*. Importantly, previous studies have reported alternative, sheet-like, Cdc42-dependent membrane extensions to be important for CCTH from HIV-pulsed iDCs (i.e. *in trans*). While these structures are fundamentally different from HIV-Filopodia (see section 6.5.4), this suggests that virus on either side of the plasma membrane can manipulate host Cdc42 F-actin regulatory pathways and that this is important for CCTH from immature dendritic cells both *in cis* and *in trans*.

8.2 New concepts, models and hypotheses

Beyond our experimental findings, some of the contributions of this work are in the form of novel theoretical concepts. We consider that specific terminology is both helpful and necessary to allow navigation of the multiple layers of complexity involved in the discussion of actin-manipulation by HIV, but also other cell-invading pathogens. In this context, our definitions of "outbound" and "inbound" virus [66] provide a simple, intuitive and concise way to specify whether the cytoskeletal manipulation events in question are taking place within infected cells (and therefore with direct access to cytoskeletal elements), or in uninfected cells (which requires signalling through membrane receptors and/or membrane-crossing of active molecules or proteins). This is a fundamentally important aspect for this field of study, and failure to specify which cells (infected vs. uninfected) are manipulated in a particular context strongly limits our ability to interpret otherwise highly relevant *in vivo* data. Furthermore, our introduced formal distinction between "exploitation", "neutralization" and "hijacking" mechanisms [66] further expands, resolves and precises the meaning of what can be understood as cytoskeletal "manipulation" [408,791]. Note that while some of these terms have been previously used in the literature [409,410,417], their connotation was more semantic than scientific, and most often referred to subversion of actin dynamics in general rather than specific regulators. In addition, our definition of "infection transfer rate" (Fig. 3.16) provides a useful and easily calculable parameter, which allows to quantitatively evaluate and compare the efficiency of CCTH from different cell types and/or experimental systems.

In the introductory chapter (and our recently published review article), we also provide an updated view on the molecular mechanisms involved in actin manipulation around HIV entry and nuclear transport (see 1.5.6 and [66]). This expands previous models by [468,469,485],

and incorporates the findings of more recent studies. One of the main conclusions from this updated analysis is that manipulation of the three canonical Rho-GTPases (Rac1, RhoA and Cdc42, rather than Rac1 alone) can facilitate inbound HIV entry and infection, downstream of Env-initiated signalling and likely in a collaborative fashion. Both RhoA and Rac1 contribute to initial Cofilin inactivation, whereas both Rac1 and Cdc42 stimulate Arp2/3 complex activity. Together, this allows the cortical F-actin polymerisation events required for concentration of CD4 and HIV coreceptors to the site of viral entry (see Fig. 1.8).

Based on our experimental observations, we also provide the most detailed hypothetical model to date regarding the biogenesis of filopodia in human myeloid cells, and how this pathway can be corrupted by outbound HIV. We propose that targeting of Gag to PIP2 is crucial to allow its colocalization with cellular filopodial regulators at the plasma membrane. Both Nef and the positive membrane curvature induced by Gag likely activate Cdc42, which is essential for stimulation of Arp2/3 activity and seeding of a short filopodium beneath the nascent HIV-bud. The formin Dia2 is then required for filopodium elongation. Therefore, the biogenesis of HIV-Filopodia is more consistent with the "convergent elongation" [358] or "clustering-outgrowth" [722] models of filopodia formation, than with the "*de novo* nucleation model" [354], also known as "tip nucleation model" [364]. We also found that IQGAP1 is required for HIV-Filopodia elongation and hypothesize that this is due to recruitment of Dia2 to filopodia assembly sites and into multiprotein complexes with Arp2/3 (as proposed in [732,792]) and active Cdc42, which in turn stimulates Dia2 activity in filopodial pathways [503]. Furthermore, colocalization of Gag and cytoskeletal regulators at PIP2-rich membrane regions could also explain how many of these cellular proteins are incorporated into viral particles. Overall, we hypothesize that the ability of outbound HIV-Gag to manipulate the actin cytoskeleton is primarily dictated by its targeting to the same PIP2-rich membrane regions where these cellular proteins concentrate, and not by direct interactions between Gag and F-actin. This is consistent with our observation that virus lacking the nucleocapsid domain still forms normal HIV-Filopodia. Further work in this area is needed to expand our understanding of how HIV misuses PIP2 [742] and lipid rafts [793,794], as this is well understood for inbound but not outbound HIV.

8.3 Other contributions to the field

This work also produced other more tangible contributions to the field. These include; **i)** a rationally designed CRISPR panel with hand-curated gRNAs against over 60 different human cytoskeletal regulators (available upon request as LCV2-plasmid DNA or as titrated and ready to use VLPs) , **ii)** homozygous-knockout leukocyte cell lines for several genes including CD4, ICAM1, Cdc42, Wave2, Dia2, Cofilin and Profilin, **iii)** lentiviral plasmids expressing

constitutively active forms of the formins Dia1 and Dia2, **iv)** a versatile bimolecular fluorescence complementation (BiFC) system, where the VN- and VC-tagged proteins can be replaced in a single step with any ORF of interest, **v)** a robust and well-characterized cell-cell HIV-transfer assay with biologically relevant cell types, and **vi)** a convenient platform for live imaging of virological synapses, which by using real donor and target cells is arguably an upgrade from previous systems based on membrane bilayers and coated surfaces or beads. Importantly, **i-iv)** represent useful resources that can immediately be applied to other areas of medical research where the actin cytoskeleton plays a major role, including but not limited to neurodegenerative [795] or cardiovascular diseases [796] and cancer [797].

8.4 Greater significance

Actin is the most abundant and possibly the most promiscuous protein in mammalian cells, with remodelling of F-actin networks being essential for many cellular processes. Understanding how pathogens manipulate host actin dynamics is a highly active research field, which bears the promise of an entirely new class of drugs in the arms race against antimicrobial resistance. This is because cell-invading pathogens (including many viruses and intracellular bacteria) have evolved elaborate mechanisms to manipulate the cellular actin cytoskeleton, and often depend on specific cellular factors for establishing and/or spreading the infection (see 1.5.1). "Host-directed therapies" therefore aim to interfere with host cell factors or host-pathogen interactions that are required for pathogen replication or persistence [798,799]. One of the main advantages of this approach is that it dramatically reduces the chance of antimicrobial drug resistance, because this would require the pathogen to develop an entirely new mechanism to manipulate (or dispense with) the cellular pathway that it has evolved to require [800,801]. Another important advantage is the possibility to "repurpose" drugs across different areas of therapy [802]. For instance, the need to deregulate central actin regulatory pathways such as those involving Src kinases, Rho-GTPases and/or the Arp2/3 complex is not only evolutionary conserved among many intracellular pathogens [418,803,804], but also a common feature of malignant cancers [805-807]. Drugs intended for use in cancer treatment can therefore be transferred to antimicrobial application pipelines and vice versa. A typical example is Imatinib, a small-molecule tyrosine kinase inhibitor approved for the treatment of leukemia, which has been validated to reduce infection outcomes for several bacteria and viruses both *in vitro* and *in vivo* (reviewed in [800]). While the toxicity of chemotherapeutic agents is an obvious concern, this is alleviated by the much shorter average duration of antimicrobial treatments compared to cancer treatment. Overall, repurposing drugs that are already clinically approved is a promising and economically highly attractive strategy [808].

Advancement of this field however requires a detailed understanding of the involved host-pathogen interactions, as well as the physiological role of the targeted cellular factors *in vivo*.

Interestingly, various of the actin regulators identified in this study (to play key roles for HIV infection) are also highly relevant pharmacological targets in other areas of medical research. Rac1 and Cdc42 are hyperactivated in HIV-infected cells (see 1.5.9), but this is also a common feature of many aggressive cancers [809-813]. Importantly, several FDA-approved Rac1 and Cdc42 inhibitors exist. Ketorolac is a nonsteroidal anti-inflammatory drug used for pain management, but also a selective inhibitor of Rac1 and Cdc42. The effectiveness of ketorolac in breast cancer treatment is supported by preclinical studies in mice and human epidemiological data [814]. Less specific inhibitors have also been shown to have promising anticancer effects. The antidiabetic metformin reduced breast cancer aggressiveness in humans, and this was associated with downregulation of Cdc42 [815]. Statins are among the most widely prescribed drugs worldwide, have pleiotropic beneficial effects and also significantly reduced the risk of cancer [816]. Statins also prevent prenylation of Rho-GTPases and thus reduce their membrane activity. Since Rac1 is important for inbound HIV infection, whereas Cdc42 promotes outbound CCTH (both *in cis* and *in trans*, see 6.5.4) their simultaneous inhibition via any of the above medications could potentially strongly reduce viral spread *in vivo*. Indeed, a previous study found that statins could decrease viral loads and increase CD4+ cell counts in animal models and chronically HIV-1-infected patients [817]. It would therefore be interesting to further explore the potential of repurposing Rac1/Cdc42 inhibitors for the treatment of HIV, or other sexually transmitted infections [420]. Of note, an immediately recent study demonstrates the potential of repurposing statins or developing Cdc42-specific inhibitors to combat infection by intracellular pathogens (e.g. *S. pyogenes*) through a host-directed approach [818].

Similarly, IQGAP1 overexpression is directly associated with tumour malignancy, invasiveness, and poor disease prognosis [819-822]. Accumulating evidence supports that interfering with IQGAP1 can inhibit cancer cell proliferation *in vivo* [823-825]. Furthermore, since IQGAP's ability to coordinate the actin cytoskeleton is manipulated by both bacterial and viral pathogens [699], it represents a seducing target for host-directed therapies. IQGAP1 is bound (directly or indirectly) by the matrix proteins of several viruses including murine leukemia virus [826], African swine fever virus [827], Marburg virus [717,828,829] and Ebola [830], with important consequences for viral assembly, budding and/or pathogenesis. While no direct interaction has yet been reported between IQGAP1 and HIV-Gag, colocalization of these proteins by at least indirect protein interactions is more than likely, given prominently shared binding partners such as TSG101/ALIX [831,832], as occurs with Marburg virus

[828,829]. Hijacking of IQGAP1 may therefore represent a common mechanism of viral egress and thus an attractive pharmacological target for wide-spectrum antiviral activity. No clinically relevant IQGAP1 modulatory drugs are currently known. However, based on our outbound HIV data and the outlined above, we speculate that the simultaneous inhibition of IQGAP1-Cdc42 could synergistically decrease viral spread (of HIV and perhaps other viruses), as well as potentially cancer progression [821].

Beyond their potential therapeutic implications, studying host-pathogen interactions has proven an invaluable resource for basic cell biology research. Not only have these interactions been instrumental to elucidating key cellular processes (such as phagocytosis, membrane trafficking, signal transduction pathways, cell motility, among many others), but they have also revolutionized and "illuminated" our understanding of actin cytoskeleton regulation [418,422,568]. Some prominent examples include identification of; i) the Arp2/3 complex as central actin nucleator in the cell (by studying the actin-based motility of intracellular *L. monocytogenes* [833]), ii) its requirement for additional nucleation promoting factors (NPF) [833], iii) N-WASP as first cellular NPF (actin tails of *S. flexneri* [834]), iv) the role of Rho-GTPases for cytoskeletal regulation (effect of *C. botulinum* toxins [835]), and v) c-Src tyrosine kinases (as cellular counterparts of v-Src from Rous sarcoma virus, [836]). One of the main advantages of studying cytoskeletal regulation by pathogens is that they produce locally focused or exaggerated phenotypes, which facilitates dissection of the involved host pathways [422]. Indeed, here we observed HIV-specific stimulation of Cdc42-dependent filopodial lengths and frequencies. The sophisticated actin manipulation mediated by HIV in leukocytes [66] thus represents a unique opportunity to dissect the pathways of cytoskeletal regulation in our immune system (e.g. filopodia formation). This is of primary importance given that; i) leukocytes express many lineage-restricted cytoskeletal regulators that are absent in other cell types, ii) leukocytes are among the most motile human cells, and iii) the key role of cytoskeletal regulators in many immunological disorders [837]. Overall, there is a strong consensus in the field that further study of pathogen-mediated actin manipulation will continue to accelerate and expand our understanding of the cytoskeleton, with direct and important consequences for numerous medical research fields [414,415,418,419,422,568].

8.5 Conclusions and future perspectives

In conclusion, we have further resolved the intersection of HIV and the actin cytoskeleton by confirming a physical interaction of Gag and Actin, identifying various cytoskeletal regulators involved in CCTH on both sides of the virological synapse (VS), and dissecting the pathway of HIV-Filopodia formation. These findings help the field move away from the early view that actin remodelling "in general" is important for CCTH and, together with the findings of other

recent studies, we continue to map the actin regulatory pathways involved at each step of the viral life cycle, and the nodes where they converge.

This study also emphasizes the role of Rho-GTPases as key coordinators of HIV-actin manipulation, and of the core actin regulators Arp2/3 and Profilin as critical machinery in both HIV-donor and target cells. While these observations clearly confirm the importance of actin dynamics (de)regulation for both inbound and outbound infection, we find that interfering with specific actin regulators (that are known to be manipulated by HIV) often leads to an only mild-to-moderate impairment of infection transfer. Weak effects were often observed for regulators belonging to families of functionally related proteins (e.g. type-I NPFs and Dia formins), whereas stronger effects ensued upon targeting unique or core cytoskeletal regulators where the finer regulators converge (e.g. Arp2/3 and Profilin). Together, this suggests a certain degree of redundancy and/or small additive effects of closely related manipulated actin-regulators. Both scenarios are consistent with the atypical "multi-strategy and multi-target approach" used by HIV to manipulate the actin cytoskeleton [66]. We therefore conclude that, while the effects of individually manipulated regulators might be small, their sum and/or synergy significantly enhances the ability of the virus to spread efficiently *in vitro*. Furthermore, one could speculate that the evolutionarily conserved ability to manipulate the actin cytoskeleton might play an even more critical role *in vivo*, due to its additive effects in different cell types, at different stages of the viral life cycle, and the resulting impairment of the host's immune system.

Despite the advances presented herein, many aspects of the intricate relationship between HIV and the cellular actin cytoskeleton yet remain to be resolved. For instance, further work is required to determine whether Gag interacts with G-actin in addition to F-actin, and to elucidate the functional relevance of either of these interactions. The contribution of actin remodelling for release of free outbound virus remains controversial but relevant, not only for HIV but also other viruses [409,410]. It will also be interesting to define the exact role that newly identified actin regulators (in the HIV field) such as IQGAP1, Profilin and CAP1 play for HIV infection and spread. In particular, their potential involvement in formation of HIV synapses should be further explored, given their importance to CCTH. Furthermore, it is near-certain that the increasing availability and power of high-resolution imaging techniques, such as super-resolution microscopy and FIB-SEM, will accelerate our dissection and understanding of cytoskeletal manipulation by HIV and other pathogens. This knowledge will not only continue to uncover fundamental aspects of cell biology, but also bears the potential to advance the emerging yet highly promising field of host-directed therapeutics [568,838].

9.0 References

1. Sharp, P.M., *et al.* Origins of hiv and the aids pandemic. *Cold Spring Harbor perspectives in medicine* **2011**, *1*, a006841 DOI: 10.1101/cshperspect.a006841.
2. Gottlieb, M.S. Pneumocystis pneumonia--los angeles. 1981. *American journal of public health* **2006**, *96*, 980-981; discussion 982-983 DOI: 10.2105/ajph.96.6.980.
3. Lemey, P., *et al.* The molecular population genetics of hiv-1 group o. *Genetics* **2004**, *167*, 1059-1068 DOI: 10.1534/genetics.104.026666.
4. Barre-Sinoussi, F., *et al.* Isolation of a t-lymphotropic retrovirus from a patient at risk for acquired immune deficiency syndrome (aids). *Science* **1983**, *220*, 868-871 DOI: 10.1126/science.6189183.
5. Gallo, R.C., *et al.* Isolation of human t-cell leukemia virus in acquired immune deficiency syndrome (aids). *Science* **1983**, *220*, 865-867 DOI: 10.1126/science.6601823.
6. Case, K. Nomenclature: Human immunodeficiency virus. *Annals of internal medicine* **1986**, *105*, 133 DOI: 10.7326/0003-4819-105-1-133.
7. Reeves, J.D., *et al.* Human immunodeficiency virus type 2. *The Journal of general virology* **2002**, *83*, 1253-1265 DOI: 10.1099/0022-1317-83-6-1253.
8. Spending on health and hiv/aids: Domestic health spending and development assistance in 188 countries, 1995-2015. *Lancet (London, England)* **2018**, *391*, 1799-1829 DOI: 10.1016/s0140-6736(18)30698-6.
9. Gayle, H.D., *et al.* Global impact of human immunodeficiency virus and aids. *Clinical microbiology reviews* **2001**, *14*, 327-335 DOI: 10.1128/cmr.14.2.327-335.2001.
10. Pantaleo, G., *et al.* The immunopathogenesis of human immunodeficiency virus infection. *The New England journal of medicine* **1993**, *328*, 327-335 DOI: 10.1056/nejm199302043280508.
11. Daar, E.S., *et al.* Clinical presentation and diagnosis of primary hiv-1 infection. *Current opinion in HIV and AIDS* **2008**, *3*, 10-15 DOI: 10.1097/COH.0b013e3282f2e295.
12. Clark, S.J., *et al.* High titers of cytopathic virus in plasma of patients with symptomatic primary hiv-1 infection. *The New England journal of medicine* **1991**, *324*, 954-960 DOI: 10.1056/nejm199104043241404.
13. Tindall, B., *et al.* Primary hiv infection: Host responses and intervention strategies. *Aids* **1991**, *5*, 1-14.
14. Gaines, H., *et al.* Immunological changes in primary hiv-1 infection. *Aids* **1990**, *4*, 995-999 DOI: 10.1097/00002030-199010000-00008.
15. Bacchetti, P., *et al.* Incubation period of aids in san francisco. *Nature* **1989**, *338*, 251-253 DOI: 10.1038/338251a0.
16. Phillips, A.N. Reduction of hiv concentration during acute infection: Independence from a specific immune response. *Science* **1996**, *271*, 497-499 DOI: 10.1126/science.271.5248.497.
17. Cooper, D.A., *et al.* Acute aids retrovirus infection. Definition of a clinical illness associated with seroconversion. *Lancet (London, England)* **1985**, *1*, 537-540 DOI: 10.1016/s0140-6736(85)91205-x.

18. Bonhoeffer, S., *et al.* Human immunodeficiency virus drug therapy and virus load. *Journal of virology* **1997**, *71*, 3275-3278.

19. 1993 revised classification system for hiv infection and expanded surveillance case definition for aids among adolescents and adults. *MMWR. Recommendations and reports : Morbidity and mortality weekly report. Recommendations and reports* **1992**, *41*, 1-19.

20. Ho, D.D. Therapy of hiv infections: Problems and prospects. *Bulletin of the New York Academy of Medicine* **1996**, *73*, 37-45.

21. Yoshimura, K. Current status of hiv/aids in the art era. *Journal of infection and chemotherapy : official journal of the Japan Society of Chemotherapy* **2017**, *23*, 12-16 DOI: 10.1016/j.jiac.2016.10.002.

22. Cohen, M.S., *et al.* Antiretroviral therapy for the prevention of hiv-1 transmission. *The New England journal of medicine* **2016**, *375*, 830-839 DOI: 10.1056/NEJMoa1600693.

23. Ferrer, L., *et al.* Undiagnosed hiv infection in a population of msm from six european cities: Results from the sialon project. *European journal of public health* **2015**, *25*, 494-500 DOI: 10.1093/eurpub/cku139.

24. Mills, E.J., *et al.* A wake-up call for global access to salvage hiv drug regimens. *Lancet (London, England)* **2007**, *370*, 1885-1887 DOI: 10.1016/s0140-6736(07)61790-5.

25. Bangsberg, D.R., *et al.* Provider assessment of adherence to hiv antiretroviral therapy. *Journal of acquired immune deficiency syndromes* **2001**, *26*, 435-442 DOI: 10.1097/00126334-200104150-00005.

26. Stolbach, A., *et al.* A review of the toxicity of hiv medications ii: Interactions with drugs and complementary and alternative medicine products. *Journal of medical toxicology : official journal of the American College of Medical Toxicology* **2015**, *11*, 326-341 DOI: 10.1007/s13181-015-0465-0.

27. Clavel, F., *et al.* Hiv drug resistance. *The New England journal of medicine* **2004**, *350*, 1023-1035 DOI: 10.1056/NEJMra025195.

28. Alexaki, A., *et al.* Cellular reservoirs of hiv-1 and their role in viral persistence. *Current HIV research* **2008**, *6*, 388-400.

29. Vanhamel, J., *et al.* Establishment of latent hiv-1 reservoirs: What do we really know? *Journal of virus eradication* **2019**, *5*, 3-9.

30. Finzi, D., *et al.* Latent infection of cd4+ t cells provides a mechanism for lifelong persistence of hiv-1, even in patients on effective combination therapy. *Nature medicine* **1999**, *5*, 512-517 DOI: 10.1038/8394.

31. Human immunodeficiency virus (hiv). *Transfusion medicine and hemotherapy : offizielles Organ der Deutschen Gesellschaft fur Transfusionsmedizin und Immunhamatologie* **2016**, *43*, 203-222 DOI: 10.1159/000445852.

32. Fassati, A. Hiv infection of non-dividing cells: A divisive problem. *Retrovirology* **2006**, *3*, 74 DOI: 10.1186/1742-4690-3-74.

33. Sakuma, T., *et al.* Lentiviral vectors: Basic to translational. *The Biochemical journal* **2012**, *443*, 603-618 DOI: 10.1042/bj20120146.

34. Frankel, A.D., *et al.* Hiv-1: Fifteen proteins and an rna. *Annual review of biochemistry* **1998**, *67*, 1-25 DOI: 10.1146/annurev.biochem.67.1.1.

35. Li, G., *et al.* An integrated map of hiv genome-wide variation from a population perspective. *Retrovirology* **2015**, *12*, 18 DOI: 10.1186/s12977-015-0148-6.

36. Li, H., *et al.* Myristoylation is required for human immunodeficiency virus type 1 gag-gag multimerization in mammalian cells. *Journal of virology* **2007**, *81*, 12899-12910 DOI: 10.1128/jvi.01280-07.

37. Ono, A., *et al.* Phosphatidylinositol (4,5) bisphosphate regulates hiv-1 gag targeting to the plasma membrane. *Proceedings of the National Academy of Sciences of the United States of America* **2004**, *101*, 14889-14894 DOI: 10.1073/pnas.0405596101.

38. Larson, D.R., *et al.* Direct measurement of gag-gag interaction during retrovirus assembly with fret and fluorescence correlation spectroscopy. *The Journal of cell biology* **2003**, *162*, 1233-1244 DOI: 10.1083/jcb.200303200.

39. Sundquist, W.I., *et al.* Hiv-1 assembly, budding, and maturation. *Cold Spring Harbor perspectives in medicine* **2012**, *2*, a006924 DOI: 10.1101/cshperspect.a006924.

40. Freed, E.O. The hiv-tsg101 interface: Recent advances in a budding field. *Trends in microbiology* **2003**, *11*, 56-59 DOI: 10.1016/s0966-842x(02)00013-6.

41. Strack, B., *et al.* Aip1/alix is a binding partner for hiv-1 p6 and eiav p9 functioning in virus budding. *Cell* **2003**, *114*, 689-699 DOI: 10.1016/s0092-8674(03)00653-6.

42. Usami, Y., *et al.* The escrt pathway and hiv-1 budding. *Biochemical Society transactions* **2009**, *37*, 181-184 DOI: 10.1042/bst0370181.

43. Carlson, L.A., *et al.* Three-dimensional analysis of budding sites and released virus suggests a revised model for hiv-1 morphogenesis. *Cell host & microbe* **2008**, *4*, 592-599 DOI: 10.1016/j.chom.2008.10.013.

44. Adamson, C.S. Protease-mediated maturation of hiv: Inhibitors of protease and the maturation process. *Molecular biology international* **2012**, *2012*, 604261 DOI: 10.1155/2012/604261.

45. Steckbeck, J.D., *et al.* C-terminal tail of human immunodeficiency virus gp41: Functionally rich and structurally enigmatic. *The Journal of general virology* **2013**, *94*, 1-19 DOI: 10.1099/vir.0.046508-0.

46. Jacks, T., *et al.* Characterization of ribosomal frameshifting in hiv-1 gag-pol expression. *Nature* **1988**, *331*, 280-283 DOI: 10.1038/331280a0.

47. Shehu-Xhilaga, M., *et al.* Maintenance of the gag/gag-pol ratio is important for human immunodeficiency virus type 1 rna dimerization and viral infectivity. *Journal of virology* **2001**, *75*, 1834-1841 DOI: 10.1128/jvi.75.4.1834-1841.2001.

48. Checkley, M.A., *et al.* Hiv-1 envelope glycoprotein biosynthesis, trafficking, and incorporation. *Journal of molecular biology* **2011**, *410*, 582-608 DOI: 10.1016/j.jmb.2011.04.042.

49. Merk, A., *et al.* Hiv-1 envelope glycoprotein structure. *Current opinion in structural biology* **2013**, *23*, 268-276 DOI: 10.1016/j.sbi.2013.03.007.

50. Tedbury, P.R., *et al.* Biochemical evidence of a role for matrix trimerization in hiv-1 envelope glycoprotein incorporation. *Proceedings of the National Academy of Sciences of the United States of America* **2016**, *113*, E182-190 DOI: 10.1073/pnas.1516618113.

51. Zhu, P., *et al.* Distribution and three-dimensional structure of aids virus envelope spikes. *Nature* **2006**, *441*, 847-852 DOI: 10.1038/nature04817.

52. Strebel, K. Hiv accessory proteins versus host restriction factors. *Current opinion in virology* **2013**, *3*, 692-699 DOI: 10.1016/j.coviro.2013.08.004.

53. Faust, T.B., *et al.* Making sense of multifunctional proteins: Human immunodeficiency virus type 1 accessory and regulatory proteins and connections to

transcription. *Annual review of virology* **2017**, *4*, 241-260 DOI: 10.1146/annurev-virology-101416-041654.

54. Malim, M.H., *et al.* Hiv-1 accessory proteins--ensuring viral survival in a hostile environment. *Cell host & microbe* **2008**, *3*, 388-398 DOI: 10.1016/j.chom.2008.04.008.

55. Anderson, J.L., *et al.* Recent insights into hiv accessory proteins. *Current infectious disease reports* **2003**, *5*, 439-450.

56. Dimitrov, A.S., *et al.* Conformational changes in hiv-1 gp41 in the course of hiv-1 envelope glycoprotein-mediated fusion and inactivation. *Biochemistry* **2005**, *44*, 12471-12479 DOI: 10.1021/bi051092d.

57. Sullivan, N., *et al.* Cd4-induced conformational changes in the human immunodeficiency virus type 1 gp120 glycoprotein: Consequences for virus entry and neutralization. *Journal of virology* **1998**, *72*, 4694-4703.

58. Gallo, S.A., *et al.* The hiv env-mediated fusion reaction. *Biochimica et biophysica acta* **2003**, *1614*, 36-50 DOI: 10.1016/s0005-2736(03)00161-5.

59. Ambrose, Z., *et al.* Hiv-1 uncoating: Connection to nuclear entry and regulation by host proteins. *Virology* **2014**, *454-455*, 371-379 DOI: 10.1016/j.virol.2014.02.004.

60. Roberts, J.D., *et al.* The accuracy of reverse transcriptase from hiv-1. *Science* **1988**, *242*, 1171-1173 DOI: 10.1126/science.2460925.

61. Jayappa, K.D., *et al.* The hiv-1 passage from cytoplasm to nucleus: The process involving a complex exchange between the components of hiv-1 and cellular machinery to access nucleus and successful integration. *International journal of biochemistry and molecular biology* **2012**, *3*, 70-85.

62. Craigie, R., *et al.* Hiv DNA integration. *Cold Spring Harbor perspectives in medicine* **2012**, *2*, a006890 DOI: 10.1101/cshperspect.a006890.

63. Bushman, F., *et al.* Genome-wide analysis of retroviral DNA integration. *Nature reviews. Microbiology* **2005**, *3*, 848-858 DOI: 10.1038/nrmicro1263.

64. Wu, Y. Hiv-1 gene expression: Lessons from provirus and non-integrated DNA. *Retrovirology* **2004**, *1*, 13 DOI: 10.1186/1742-4690-1-13.

65. Siliciano, R.F., *et al.* Hiv latency. *Cold Spring Harbor perspectives in medicine* **2011**, *1*, a007096 DOI: 10.1101/cshperspect.a007096.

66. Ospina Stella, A., *et al.* All-round manipulation of the actin cytoskeleton by hiv. *Viruses* **2018**, *10*, DOI: 10.3390/v10020063.

67. Coakley, E., *et al.* Assessing chemokine co-receptor usage in hiv. *Current opinion in infectious diseases* **2005**, *18*, 9-15.

68. Schacker, T., *et al.* Productive infection of t cells in lymphoid tissues during primary and early human immunodeficiency virus infection. *The Journal of infectious diseases* **2001**, *183*, 555-562 DOI: 10.1086/318524.

69. Rinaldo, C.R., Jr., *et al.* Virus infection of dendritic cells: Portal for host invasion and host defense. *Trends in microbiology* **2004**, *12*, 337-345 DOI: 10.1016/j.tim.2004.05.003.

70. Campbell, J.H., *et al.* The importance of monocytes and macrophages in hiv pathogenesis, treatment, and cure. *Aids* **2014**, *28*, 2175-2187 DOI: 10.1097/QAD.0000000000000408.

71. Berger, E.A., *et al.* A new classification for hiv-1. *Nature* **1998**, *391*, 240 DOI: 10.1038/34571.

72. Fogel, G.B., *et al.* Identification of dual-tropic hiv-1 using evolved neural networks. *Bio Systems* **2015**, *137*, 12-19 DOI: 10.1016/j.biosystems.2015.09.007.

73. Canque, B., *et al.* The susceptibility to x4 and r5 human immunodeficiency virus-1 strains of dendritic cells derived in vitro from cd34(+) hematopoietic progenitor cells is primarily determined by their maturation stage. *Blood* **1999**, *93*, 3866-3875.

74. Parker, Z.F., *et al.* Transmitted/founder and chronic hiv-1 envelope proteins are distinguished by differential utilization of ccr5. *Journal of virology* **2013**, *87*, 2401-2411 DOI: 10.1128/jvi.02964-12.

75. Weinberger, A.D., *et al.* Persistence and emergence of x4 virus in hiv infection. *Mathematical biosciences and engineering : MBE* **2011**, *8*, 605-626 DOI: 10.3934/mbe.2011.8.605.

76. Pollakis, G., *et al.* Use of (alternative) coreceptors for hiv entry. *Current opinion in HIV and AIDS* **2012**, *7*, 440-449 DOI: 10.1097/COH.0b013e328356e9f3.

77. Houzet, L., *et al.* Origins of hiv-infected leukocytes and virions in semen. *The Journal of infectious diseases* **2014**, *210 Suppl 3*, S622-630 DOI: 10.1093/infdis/jiu328.

78. Politch, J.A., *et al.* Characteristics and quantities of hiv host cells in human genital tract secretions. *The Journal of infectious diseases* **2014**, *210 Suppl 3*, S609-615 DOI: 10.1093/infdis/jiu390.

79. Southern, S.O. Milk-borne transmission of hiv. Characterization of productively infected cells in breast milk and interactions between milk and saliva. *Journal of human virology* **1998**, *1*, 328-337.

80. Bourinbaiar, A.S., *et al.* Transmission of human immunodeficiency virus from monocytes to epithelia. *Journal of acquired immune deficiency syndromes* **1991**, *4*, 56-63.

81. Cameron, P.U., *et al.* Dendritic cells exposed to human immunodeficiency virus type-1 transmit a vigorous cytopathic infection to cd4+ t cells. *Science* **1992**, *257*, 383-387.

82. Pearce-Pratt, R., *et al.* Studies of adhesion of lymphocytic cells: Implications for sexual transmission of human immunodeficiency virus. *Biology of reproduction* **1993**, *48*, 431-445.

83. Carr, J.M., *et al.* Rapid and efficient cell-to-cell transmission of human immunodeficiency virus infection from monocyte-derived macrophages to peripheral blood lymphocytes. *Virology* **1999**, *265*, 319-329 DOI: 10.1006/viro.1999.0047.

84. Bracq, L., *et al.* Mechanisms for cell-to-cell transmission of hiv-1. *Frontiers in immunology* **2018**, *9*, 260 DOI: 10.3389/fimmu.2018.00260.

85. Jolly, C., *et al.* Hiv-1 cell to cell transfer across an env-induced, actin-dependent synapse. *The Journal of experimental medicine* **2004**, *199*, 283-293 DOI: 10.1084/jem.20030648.

86. Sourisseau, M., *et al.* Inefficient human immunodeficiency virus replication in mobile lymphocytes. *Journal of virology* **2007**, *81*, 1000-1012 DOI: 10.1128/jvi.01629-06.

87. Martin, N., *et al.* Virological synapse-mediated spread of human immunodeficiency virus type 1 between t cells is sensitive to entry inhibition. *Journal of virology* **2010**, *84*, 3516-3527 DOI: 10.1128/jvi.02651-09.

88. Abela, I.A., *et al.* Cell-cell transmission enables hiv-1 to evade inhibition by potent cd4bs directed antibodies. *PLoS pathogens* **2012**, *8*, e1002634 DOI: 10.1371/journal.ppat.1002634.

89. Aggarwal, A., *et al.* Mobilization of hiv spread by diaphanous 2 dependent filopodia in infected dendritic cells. *PLoS pathogens* **2012**, *8*, e1002762 DOI: 10.1371/journal.ppat.1002762.

90. Bertram, K.M., *et al.* Identification of hiv transmitting cd11c(+) human epidermal dendritic cells. *Nature communications* **2019**, *10*, 2759 DOI: 10.1038/s41467-019-10697-w.

91. Groot, F., *et al.* Efficient hiv-1 transmission from macrophages to t cells across transient virological synapses. *Blood* **2008**, *111*, 4660-4663 DOI: 10.1182/blood-2007-12-130070.

92. Ganor, Y., *et al.* Within 1 h, hiv-1 uses viral synapses to enter efficiently the inner, but not outer, foreskin mucosa and engages langerhans-t cell conjugates. *Mucosal immunology* **2010**, *3*, 506-522 DOI: 10.1038/mi.2010.32.

93. Arias, R.A., *et al.* Transmission of hiv-1 infection between trophoblast placental cells and t-cells take place via an lfa-1-mediated cell to cell contact. *Virology* **2003**, *307*, 266-277.

94. Luo, X., *et al.* Cell-cell contact viral transfer contributes to hiv infection and persistence in astrocytes. *Journal of neurovirology* **2015**, *21*, 66-80 DOI: 10.1007/s13365-014-0304-0.

95. Evans, V.A., *et al.* Thymic plasmacytoid dendritic cells are susceptible to productive hiv-1 infection and efficiently transfer r5 hiv-1 to thymocytes in vitro. *Retrovirology* **2011**, *8*, 43 DOI: 10.1186/1742-4690-8-43.

96. Turville, S.G., *et al.* Immunodeficiency virus uptake, turnover, and 2-phase transfer in human dendritic cells. *Blood* **2004**, *103*, 2170-2179 DOI: 10.1182/blood-2003-09-3129.

97. Nguyen, D.G., *et al.* Involvement of macrophage mannose receptor in the binding and transmission of hiv by macrophages. *European journal of immunology* **2003**, *33*, 483-493 DOI: 10.1002/immu.200310024.

98. Dorosko, S.M., *et al.* Primary human mammary epithelial cells endocytose hiv-1 and facilitate viral infection of cd4+ t lymphocytes. *Journal of virology* **2010**, *84*, 10533-10542 DOI: 10.1128/jvi.01263-10.

99. Mikulak, J., *et al.* Hiv-1 harboring renal tubular epithelial cell interaction with t cells results in t cell trans-infection. *Virology* **2009**, *385*, 105-114 DOI: 10.1016/j.virol.2008.11.029.

100. Kolodkin-Gal, D., *et al.* Efficiency of cell-free and cell-associated virus in mucosal transmission of human immunodeficiency virus type 1 and simian immunodeficiency virus. *Journal of virology* **2013**, *87*, 13589-13597 DOI: 10.1128/JVI.03108-12.

101. Girard, M., *et al.* Genital infection of female chimpanzees with human immunodeficiency virus type 1. *AIDS research and human retroviruses* **1998**, *14*, 1357-1367 DOI: 10.1089/aid.1998.14.1357.

102. Kaizu, M., *et al.* Repeated intravaginal inoculation with cell-associated simian immunodeficiency virus results in persistent infection of nonhuman primates. *The Journal of infectious diseases* **2006**, *194*, 912-916 DOI: 10.1086/507308.

103. Salle, B., *et al.* Infection of macaques after vaginal exposure to cell-associated simian immunodeficiency virus. *The Journal of infectious diseases* **2010**, *202*, 337-344 DOI: 10.1086/653619.

104. Sodora, D.L., *et al.* Vaginal transmission of siv: Assessing infectivity and hormonal influences in macaques inoculated with cell-free and cell-associated viral stocks. *AIDS research and human retroviruses* **1998**, *14 Suppl 1*, S119-123.

105. Khanna, K.V., *et al.* Vaginal transmission of cell-associated hiv-1 in the mouse is blocked by a topical, membrane-modifying agent. *The Journal of clinical investigation* **2002**, *109*, 205-211 DOI: 10.1172/jci13236.

106. Di Fabio, S., *et al.* Vaginal transmission of hiv-1 in hu-scid mice: A new model for the evaluation of vaginal microbicides. *Aids* **2001**, *15*, 2231-2238 DOI: 10.1097/00002030-200111230-00003.

107. Law, K.M., *et al.* In vivo hiv-1 cell-to-cell transmission promotes multicopy micro-compartmentalized infection. *Cell reports* **2016**, *15*, 2771-2783 DOI: 10.1016/j.celrep.2016.05.059.

108. Murooka, T.T., *et al.* Hiv-infected t cells are migratory vehicles for viral dissemination. *Nature* **2012**, *490*, 283-287 DOI: 10.1038/nature11398.

109. Zhou, Z., *et al.* Hiv-1 efficient entry in inner foreskin is mediated by elevated ccl5/rantes that recruits t cells and fuels conjugate formation with langerhans cells. *PLoS pathogens* **2011**, *7*, e1002100 DOI: 10.1371/journal.ppat.1002100.

110. Gratton, S., *et al.* Highly restricted spread of hiv-1 and multiply infected cells within splenic germinal centers. *Proceedings of the National Academy of Sciences of the United States of America* **2000**, *97*, 14566-14571 DOI: 10.1073/pnas.97.26.14566.

111. Jung, A., *et al.* Recombination: Multiply infected spleen cells in hiv patients. *Nature* **2002**, *418*, 144 DOI: 10.1038/418144a.

112. Josefsson, L., *et al.* Single cell analysis of lymph node tissue from hiv-1 infected patients reveals that the majority of cd4+ t-cells contain one hiv-1 DNA molecule. *PLoS pathogens* **2013**, *9*, e1003432 DOI: 10.1371/journal.ppat.1003432.

113. Del Portillo, A., *et al.* Multiploid inheritance of hiv-1 during cell-to-cell infection. *Journal of virology* **2011**, *85*, 7169-7176 DOI: 10.1128/jvi.00231-11.

114. Delassus, S., *et al.* Nonhomogeneous distribution of human immunodeficiency virus type 1 proviruses in the spleen. *Journal of virology* **1992**, *66*, 5642-5645.

115. Cheynier, R., *et al.* Hiv and t cell expansion in splenic white pulps is accompanied by infiltration of hiv-specific cytotoxic t lymphocytes. *Cell* **1994**, *78*, 373-387 DOI: 10.1016/0092-8674(94)90417-0.

116. Zhang, C., *et al.* Hybrid spreading mechanisms and t cell activation shape the dynamics of hiv-1 infection. *PLoS computational biology* **2015**, *11*, e1004179 DOI: 10.1371/journal.pcbi.1004179.

117. Lodmell, D.L., *et al.* Prevention of cell-to-cell spread of herpes simplex virus by leukocytes. *The Journal of experimental medicine* **1973**, *137*, 706-720 DOI: 10.1084/jem.137.3.706.

118. Iwasaki, Y., *et al.* Cell to cell transmission of virus in the central nervous system. Ii. Experimental rabies in mouse. *Laboratory investigation; a journal of technical methods and pathology* **1975**, *33*, 391-399.

119. Cook, M.L., *et al.* Labile coat: Reason for noninfectious cell-free varicella-zoster virus in culture. *Journal of virology* **1968**, *2*, 1458-1464.

120. Pique, C., *et al.* Pathways of cell-cell transmission of htlv-1. *Frontiers in microbiology* **2012**, *3*, 378 DOI: 10.3389/fmicb.2012.00378.

121. Mothes, W., *et al.* Virus cell-to-cell transmission. *Journal of virology* **2010**, *84*, 8360-8368 DOI: 10.1128/JVI.00443-10.

122. Zhong, P., *et al.* Cell-to-cell transmission of viruses. *Current opinion in virology* **2013**, *3*, 44-50 DOI: 10.1016/j.coviro.2012.11.004.

123. Mazurov, D., *et al.* Quantitative comparison of htlv-1 and hiv-1 cell-to-cell infection with new replication dependent vectors. *PLoS pathogens* **2010**, *6*, e1000788 DOI: 10.1371/journal.ppat.1000788.

124. Duncan, C.J., *et al.* High multiplicity hiv-1 cell-to-cell transmission from macrophages to cd4+ t cells limits antiretroviral efficacy. *Aids* **2013**, *27*, 2201-2206 DOI: 10.1097/QAD.0b013e3283632ec4.

125. Hubner, W., *et al.* Quantitative 3d video microscopy of hiv transfer across t cell virological synapses. *Science* **2009**, *323*, 1743-1747 DOI: 10.1126/science.1167525.

126. Dimitrov, D.S., *et al.* Quantitation of human immunodeficiency virus type 1 infection kinetics. *Journal of virology* **1993**, *67*, 2182-2190.

127. Chen, P., *et al.* Predominant mode of human immunodeficiency virus transfer between t cells is mediated by sustained env-dependent neutralization-resistant virological synapses. *Journal of virology* **2007**, *81*, 12582-12595 DOI: 10.1128/JVI.00381-07.

128. Tsunetsugu-Yokota, Y., *et al.* Monocyte-derived cultured dendritic cells are susceptible to human immunodeficiency virus infection and transmit virus to resting t cells in the process of nominal antigen presentation. *Journal of virology* **1995**, *69*, 4544-4547.

129. Li, P., *et al.* Synthesis of human immunodeficiency virus DNA in a cell-to-cell transmission model. *AIDS research and human retroviruses* **1992**, *8*, 253-259 DOI: 10.1089/aid.1992.8.253.

130. Denton, P.W., *et al.* Antiretroviral pre-exposure prophylaxis prevents vaginal transmission of hiv-1 in humanized blt mice. *PLoS medicine* **2008**, *5*, e16 DOI: 10.1371/journal.pmed.0050016.

131. Stoddart, C.A., *et al.* Superior human leukocyte reconstitution and susceptibility to vaginal hiv transmission in humanized nod-scid il-2rgamma(-/-) (nsg) blt mice. *Virology* **2011**, *417*, 154-160 DOI: 10.1016/j.virol.2011.05.013.

132. Sun, Z., *et al.* Intrarectal transmission, systemic infection, and cd4+ t cell depletion in humanized mice infected with hiv-1. *The Journal of experimental medicine* **2007**, *204*, 705-714 DOI: 10.1084/jem.20062411.

133. Almond, N., *et al.* Protection by attenuated simian immunodeficiency virus in macaques against challenge with virus-infected cells. *Lancet (London, England)* **1995**, *345*, 1342-1344 DOI: 10.1016/s0140-6736(95)92540-6.

134. Jolly, C., *et al.* Retroviral spread by induction of virological synapses. *Traffic* **2004**, *5*, 643-650 DOI: 10.1111/j.1600-0854.2004.00209.x.

135. Sattentau, Q. Avoiding the void: Cell-to-cell spread of human viruses. *Nature reviews. Microbiology* **2008**, *6*, 815-826 DOI: 10.1038/nrmicro1972.

136. Law, K.M., *et al.* Cell-to-cell spread of hiv and viral pathogenesis. *Advances in virus research* **2016**, *95*, 43-85 DOI: 10.1016/bs.aivir.2016.03.001.

137. Rossi, M., *et al.* Human dendritic cells: Potent antigen-presenting cells at the crossroads of innate and adaptive immunity. *Journal of immunology* **2005**, *175*, 1373-1381 DOI: 10.4049/jimmunol.175.3.1373.

138. Dalod, M., *et al.* Dendritic cell maturation: Functional specialization through signaling specificity and transcriptional programming. *The EMBO journal* **2014**, *33*, 1104-1116 DOI: 10.1002/embj.201488027.

139. Rescigno, M., *et al.* Dendritic cells express tight junction proteins and penetrate gut epithelial monolayers to sample bacteria. *Nature immunology* **2001**, *2*, 361-367 DOI: 10.1038/86373.

140. Bousso, P., *et al.* Dynamics of cd8+ t cell priming by dendritic cells in intact lymph nodes. *Nature immunology* **2003**, *4*, 579-585 DOI: 10.1038/ni928.

141. Pope, M., *et al.* Low levels of hiv-1 infection in cutaneous dendritic cells promote extensive viral replication upon binding to memory cd4+ t cells. *The Journal of experimental medicine* **1995**, *182*, 2045-2056 DOI: 10.1084/jem.182.6.2045.

142. Pope, M., *et al.* Dendritic cell-t cell conjugates that migrate from normal human skin are an explosive site of infection for hiv-1. *Advances in experimental medicine and biology* **1995**, *378*, 457-460 DOI: 10.1007/978-1-4615-1971-3_102.

143. Clark, E.A. Hiv: Dendritic cells as embers for the infectious fire. *Current biology : CB* **1996**, *6*, 655-657 DOI: 10.1016/s0960-9822(09)00441-2.

144. Rowland-Jones, S.L. Hiv: The deadly passenger in dendritic cells. *Current biology : CB* **1999**, *9*, R248-250 DOI: 10.1016/s0960-9822(99)80155-9.

145. Frank, I., *et al.* The enigma of dendritic cell-immunodeficiency virus interplay. *Current molecular medicine* **2002**, *2*, 229-248.

146. Wu, L., *et al.* Dendritic-cell interactions with hiv: Infection and viral dissemination. *Nature reviews. Immunology* **2006**, *6*, 859-868 DOI: 10.1038/nri1960.

147. Ahmed, Z., *et al.* The role of human dendritic cells in hiv-1 infection. *The Journal of investigative dermatology* **2015**, *135*, 1225-1233 DOI: 10.1038/jid.2014.490.

148. Hu, J., *et al.* Simian immunodeficiency virus rapidly penetrates the cervicovaginal mucosa after intravaginal inoculation and infects intraepithelial dendritic cells. *Journal of virology* **2000**, *74*, 6087-6095 DOI: 10.1128/jvi.74.13.6087-6095.2000.

149. Spira, A.I., *et al.* Cellular targets of infection and route of viral dissemination after an intravaginal inoculation of simian immunodeficiency virus into rhesus macaques. *The Journal of experimental medicine* **1996**, *183*, 215-225 DOI: 10.1084/jem.183.1.215.

150. Masurier, C., *et al.* Dendritic cells route human immunodeficiency virus to lymph nodes after vaginal or intravenous administration to mice. *Journal of virology* **1998**, *72*, 7822-7829.

151. Manches, O., *et al.* Dendritic cells in progression and pathology of hiv infection. *Trends in immunology* **2014**, *35*, 114-122 DOI: 10.1016/j.it.2013.10.003.

152. Granelli-Piperno, A., *et al.* Immature dendritic cells selectively replicate macrophagetropic (m-tropic) human immunodeficiency virus type 1, while mature cells efficiently transmit both m- and t-tropic virus to t cells. *Journal of virology* **1998**, *72*, 2733-2737.

153. Aggarwal, A., *et al.* Revising the role of myeloid cells in hiv pathogenesis. *Current HIV/AIDS reports* **2013**, *10*, 3-11 DOI: 10.1007/s11904-012-0149-1.

154. Patterson, S., *et al.* Cd4 expression on dendritic cells and their infection by human immunodeficiency virus. *The Journal of general virology* **1995**, *76 (Pt 5)*, 1155-1163 DOI: 10.1099/0022-1317-76-5-1155.

155. Kawamura, T., *et al.* R5 hiv productively infects langerhans cells, and infection levels are regulated by compound ccr5 polymorphisms. *Proceedings of the National Academy of Sciences of the United States of America* **2003**, *100*, 8401-8406 DOI: 10.1073/pnas.1432450100.

156. Turville, S.G., *et al.* Resolution of de novo hiv production and trafficking in immature dendritic cells. *Nature methods* **2008**, *5*, 75-85 DOI: 10.1038/nmeth1137.

157. Donaghy, H., *et al.* Dysfunction and infection of freshly isolated blood myeloid and plasmacytoid dendritic cells in patients infected with hiv-1. *Blood* **2003**, *101*, 4505-4511 DOI: 10.1182/blood-2002-10-3189.

158. Patterson, S., *et al.* Analysis of human immunodeficiency virus type 1 (hiv-1) variants and levels of infection in dendritic and t cells from symptomatic hiv-1-infected patients. *The Journal of general virology* **1998**, *79 (Pt 2)*, 247-257 DOI: 10.1099/0022-1317-79-2-247.

159. Frankel, S.S., *et al.* Replication of hiv-1 in dendritic cell-derived syncytia at the mucosal surface of the adenoid. *Science* **1996**, *272*, 115-117 DOI: 10.1126/science.272.5258.115.

160. Cimarelli, A., *et al.* Quantitation by competitive pcr of hiv-1 proviral DNA in epidermal langerhans cells of hiv-infected patients. *Journal of acquired immune deficiency syndromes* **1994**, *7*, 230-235.

161. Compton, C.C., *et al.* Hiv-infected langerhans cells constitute a significant proportion of the epidermal langerhans cell population throughout the course of hiv disease. *The Journal of investigative dermatology* **1996**, *107*, 822-826 DOI: 10.1111/1523-1747.ep12330574.

162. Henry, M., *et al.* Epidermal langerhans cells of aids patients express hiv-1 regulatory and structural genes. *The Journal of investigative dermatology* **1994**, *103*, 593-596 DOI: 10.1111/1523-1747.ep12396918.

163. Giannetti, A., *et al.* Direct detection of hiv-1 rna in epidermal langerhans cells of hiv-infected patients. *Journal of acquired immune deficiency syndromes* **1993**, *6*, 329-333.

164. Bhoopat, L., *et al.* In vivo identification of langerhans and related dendritic cells infected with hiv-1 subtype e in vaginal mucosa of asymptomatic patients. *Modern pathology : an official journal of the United States and Canadian Academy of Pathology, Inc* **2001**, *14*, 1263-1269 DOI: 10.1038/modpathol.3880472.

165. Tsunetsugu-Yokota, Y., *et al.* Development of human dendritic cells and their role in hiv infection: Antiviral immunity versus hiv transmission. *Frontiers in microbiology* **2013**, *4*, 178 DOI: 10.3389/fmicb.2013.00178.

166. Grivel, J.C., *et al.* Selective transmission of r5 hiv-1 variants: Where is the gatekeeper? *Journal of translational medicine* **2011**, *9 Suppl 1*, S6 DOI: 10.1186/1479-5876-9-s1-s6.

167. Granelli-Piperno, A., *et al.* Virus replication begins in dendritic cells during the transmission of hiv-1 from mature dendritic cells to t cells. *Current biology : CB* **1999**, *9*, 21-29 DOI: 10.1016/s0960-9822(99)80043-8.

168. Yamamoto, T., *et al.* Selective transmission of r5 hiv-1 over x4 hiv-1 at the dendritic cell-t cell infectious synapse is determined by the t cell activation state. *PLoS pathogens* **2009**, *5*, e1000279 DOI: 10.1371/journal.ppat.1000279.

169. Ganesh, L., *et al.* Infection of specific dendritic cells by ccr5-tropic human immunodeficiency virus type 1 promotes cell-mediated transmission of virus resistant to broadly neutralizing antibodies. *Journal of virology* **2004**, *78*, 11980-11987 DOI: 10.1128/jvi.78.21.11980-11987.2004.

170. Roszer, T. Understanding the biology of self-renewing macrophages. *Cells* **2018**, *7*, DOI: 10.3390/cells7080103.

171. Wynn, T.A., *et al.* Macrophage biology in development, homeostasis and disease. *Nature* **2013**, *496*, 445-455 DOI: 10.1038/nature12034.

172. Sattentau, Q.J., *et al.* Macrophages and hiv-1: An unhealthy constellation. *Cell host & microbe* **2016**, *19*, 304-310 DOI: 10.1016/j.chom.2016.02.013.

173. Rodrigues, V., *et al.* Myeloid cell interaction with hiv: A complex relationship. *Frontiers in immunology* **2017**, *8*, 1698 DOI: 10.3389/fimmu.2017.01698.

174. Wong, M.E., *et al.* The hiv reservoir in monocytes and macrophages. *Frontiers in immunology* **2019**, *10*, 1435 DOI: 10.3389/fimmu.2019.01435.

175. Ochsenbauer, C., *et al.* Generation of transmitted/founder hiv-1 infectious molecular clones and characterization of their replication capacity in cd4 t lymphocytes and monocyte-derived macrophages. *Journal of virology* **2012**, *86*, 2715-2728 DOI: 10.1128/jvi.06157-11.

176. Salazar-Gonzalez, J.F., *et al.* Genetic identity, biological phenotype, and evolutionary pathways of transmitted/founder viruses in acute and early hiv-1 infection. *The Journal of experimental medicine* **2009**, *206*, 1273-1289 DOI: 10.1084/jem.20090378.

177. Gartner, S., *et al.* The role of mononuclear phagocytes in htlv-iii/lav infection. *Science* **1986**, *233*, 215-219 DOI: 10.1126/science.3014648.

178. Hufert, F.T., *et al.* Human kupffer cells infected with hiv-1 in vivo. *Journal of acquired immune deficiency syndromes* **1993**, *6*, 772-777.

179. Churchill, M.J., *et al.* Use of laser capture microdissection to detect integrated hiv-1 DNA in macrophages and astrocytes from autopsy brain tissues. *Journal of neurovirology* **2006**, *12*, 146-152 DOI: 10.1080/13550280600748946.

180. Williams, K.C., *et al.* Perivascular macrophages are the primary cell type productively infected by simian immunodeficiency virus in the brains of macaques: Implications for the neuropathogenesis of aids. *The Journal of experimental medicine* **2001**, *193*, 905-915 DOI: 10.1084/jem.193.8.905.

181. Orenstein, J.M. Hiv expression in surgical specimens. *AIDS research and human retroviruses* **2008**, *24*, 947-955 DOI: 10.1089/aid.2008.0265.

182. Zalar, A., *et al.* Macrophage hiv-1 infection in duodenal tissue of patients on long term haart. *Antiviral research* **2010**, *87*, 269-271 DOI: 10.1016/j.antiviral.2010.05.005.

183. Jambo, K.C., *et al.* Small alveolar macrophages are infected preferentially by hiv and exhibit impaired phagocytic function. *Mucosal immunology* **2014**, *7*, 1116-1126 DOI: 10.1038/mi.2013.127.

184. Koppensteiner, H., *et al.* Macrophages and their relevance in human immunodeficiency virus type i infection. *Retrovirology* **2012**, *9*, 82 DOI: 10.1186/1742-4690-9-82.

185. Honeycutt, J.B., *et al.* Macrophages sustain hiv replication in vivo independently of t cells. *The Journal of clinical investigation* **2016**, *126*, 1353-1366 DOI: 10.1172/jci84456.

186. Abreu, C.M., *et al.* Infectious virus persists in cd4(+) t cells and macrophages in antiretroviral therapy-suppressed simian immunodeficiency virus-infected macaques. *Journal of virology* **2019**, *93*, DOI: 10.1128/jvi.00065-19.

187. Cribbs, S.K., *et al.* Healthy hiv-1-infected individuals on highly active antiretroviral therapy harbor hiv-1 in their alveolar macrophages. *AIDS research and human retroviruses* **2015**, *31*, 64-70 DOI: 10.1089/aid.2014.0133.

188. Ganor, Y., *et al.* Hiv-1 reservoirs in urethral macrophages of patients under suppressive antiretroviral therapy. *Nature microbiology* **2019**, *4*, 633-644 DOI: 10.1038/s41564-018-0335-z.

189. Ko, A., *et al.* Macrophages but not astrocytes harbor hiv DNA in the brains of hiv-1-infected aviremic individuals on suppressive antiretroviral therapy. *Journal of neuroimmune pharmacology : the official journal of the Society on NeuroImmune Pharmacology* **2019**, *14*, 110-119 DOI: 10.1007/s11481-018-9809-2.

190. Honeycutt, J.B., *et al.* Hiv persistence in tissue macrophages of humanized myeloid-only mice during antiretroviral therapy. *Nature medicine* **2017**, *23*, 638-643 DOI: 10.1038/nm.4319.

191. Micci, L., *et al.* Cd4 depletion in siv-infected macaques results in macrophage and microglia infection with rapid turnover of infected cells. *PLoS pathogens* **2014**, *10*, e1004467 DOI: 10.1371/journal.ppat.1004467.

192. Geissmann, F., *et al.* Development of monocytes, macrophages, and dendritic cells. *Science* **2010**, *327*, 656-661 DOI: 10.1126/science.1178331.

193. Bergamaschi, A., *et al.* Host hindrance to hiv-1 replication in monocytes and macrophages. *Retrovirology* **2010**, *7*, 31 DOI: 10.1186/1742-4690-7-31.

194. McElrath, M.J., *et al.* Latent hiv-1 infection in enriched populations of blood monocytes and t cells from seropositive patients. *The Journal of clinical investigation* **1991**, *87*, 27-30 DOI: 10.1172/jci114981.

195. Bagasra, O., *et al.* Human immunodeficiency virus type i provirus is demonstrated in peripheral blood monocytes in vivo: A study utilizing an in situ polymerase chain reaction. *AIDS research and human retroviruses* **1993**, *9*, 69-76 DOI: 10.1089/aid.1993.9.69.

196. Lambotte, O., *et al.* Detection of infectious hiv in circulating monocytes from patients on prolonged highly active antiretroviral therapy. *Journal of acquired immune deficiency syndromes* **2000**, *23*, 114-119 DOI: 10.1097/00126334-200002010-00002.

197. Zhu, T., *et al.* Evidence for human immunodeficiency virus type 1 replication in vivo in cd14(+) monocytes and its potential role as a source of virus in patients on highly active antiretroviral therapy. *Journal of virology* **2002**, *76*, 707-716 DOI: 10.1128/jvi.76.2.707-716.2002.

198. Sonza, S., *et al.* Monocytes harbour replication-competent, non-latent hiv-1 in patients on highly active antiretroviral therapy. *Aids* **2001**, *15*, 17-22 DOI: 10.1097/00002030-200101050-00005.

199. Ellery, P.J., *et al.* The cd16+ monocyte subset is more permissive to infection and preferentially harbors hiv-1 in vivo. *Journal of immunology* **2007**, *178*, 6581-6589 DOI: 10.4049/jimmunol.178.10.6581.

200. Williams, D.W., *et al.* Monocytes mediate hiv neuropathogenesis: Mechanisms that contribute to hiv associated neurocognitive disorders. *Current HIV research* **2014**, *12*, 85-96.

201. Thieblemont, N., *et al.* Cd14lowcd16high: A cytokine-producing monocyte subset which expands during human immunodeficiency virus infection. *European journal of immunology* **1995**, *25*, 3418-3424 DOI: 10.1002/eji.1830251232.

202. Crowe, S.M., *et al.* Hiv-1 can be recovered from a variety of cells including peripheral blood monocytes of patients receiving highly active antiretroviral therapy: A further obstacle to eradication. *Journal of leukocyte biology* **2000**, *68*, 345-350.

203. Crowe, S., *et al.* The contribution of monocyte infection and trafficking to viral persistence, and maintenance of the viral reservoir in hiv infection. *Journal of leukocyte biology* **2003**, *74*, 635-641 DOI: 10.1189/jlb.0503204.

204. Wang, T., *et al.* Successful isolation of infectious and high titer human monocyte-derived hiv-1 from two subjects with discontinued therapy. *PloS one* **2013**, *8*, e65071 DOI: 10.1371/journal.pone.0065071.

205. Kim, W.K., *et al.* Monocyte/macrophage traffic in hiv and siv encephalitis. *Journal of leukocyte biology* **2003**, *74*, 650-656 DOI: 10.1189/jlb.0503207.

206. Phillips, D.M., *et al.* Mechanism of monocyte-macrophage-mediated transmission of hiv. *AIDS research and human retroviruses* **1998**, *14 Suppl 1*, S67-70.

207. Barreto-de-Souza, V., *et al.* Monocytes but not lymphocytes carrying hiv-1 on their surface transmit infection to human tissue ex vivo. *Journal of virology* **2016**, *90*, 9833-9840 DOI: 10.1128/JVI.00742-16.

208. Wei, X., *et al.* Viral dynamics in human immunodeficiency virus type 1 infection. *Nature* **1995**, *373*, 117-122 DOI: 10.1038/373117a0.

209. Schacker, T. The role of secondary lymphatic tissue in immune deficiency of hiv infection. *Aids* **2008**, *22 Suppl 3*, S13-18 DOI: 10.1097/01.aids.0000327511.76126.b5.

210. Galloway, N.L., *et al.* Cell-to-cell transmission of hiv-1 is required to trigger pyroptotic death of lymphoid-tissue-derived cd4 t cells. *Cell reports* **2015**, *12*, 1555-1563 DOI: 10.1016/j.celrep.2015.08.011.

211. Agosto, L.M., *et al.* Hiv-1-infected cd4+ t cells facilitate latent infection of resting cd4+ t cells through cell-cell contact. *Cell reports* **2018**, *24*, 2088-2100 DOI: 10.1016/j.celrep.2018.07.079.

212. Ladinsky, M.S., *et al.* Electron tomography of hiv-1 infection in gut-associated lymphoid tissue. *PLoS pathogens* **2014**, *10*, e1003899 DOI: 10.1371/journal.ppat.1003899.

213. Murray, A.J., *et al.* The latent reservoir for hiv-1: How immunologic memory and clonal expansion contribute to hiv-1 persistence. *Journal of immunology* **2016**, *197*, 407-417 DOI: 10.4049/jimmunol.1600343.

214. Davis, D.M. Mechanisms and functions for the duration of intercellular contacts made by lymphocytes. *Nature reviews. Immunology* **2009**, *9*, 543-555 DOI: 10.1038/nri2602.

215. Dustin, M.L. The immunological synapse. *Cancer immunology research* **2014**, *2*, 1023-1033 DOI: 10.1158/2326-6066.CIR-14-0161.

216. Rinaldo, C.R. Hiv-1 trans infection of cd4(+) t cells by professional antigen presenting cells. *Scientifica* **2013**, *2013*, 164203 DOI: 10.1155/2013/164203.

217. Geijtenbeek, T.B., *et al.* Dc-sign: A novel hiv receptor on dcs that mediates hiv-1 transmission. *Current topics in microbiology and immunology* **2003**, *276*, 31-54 DOI: 10.1007/978-3-662-06508-2_2.

218. Gummuluru, S., *et al.* Cd169-dependent cell-associated hiv-1 transmission: A driver of virus dissemination. *The Journal of infectious diseases* **2014**, *210 Suppl 3*, S641-647 DOI: 10.1093/infdis/jiu442.

219. McDonald, D., *et al.* Recruitment of hiv and its receptors to dendritic cell-t cell junctions. *Science* **2003**, *300*, 1295-1297 DOI: 10.1126/science.1084238.

220. Yu, H.J., *et al.* Hiv traffics through a specialized, surface-accessible intracellular compartment during trans-infection of t cells by mature dendritic cells. *PLoS pathogens* **2008**, *4*, e1000134 DOI: 10.1371/journal.ppat.1000134.

221. Felts, R.L., *et al.* 3d visualization of hiv transfer at the virological synapse between dendritic cells and t cells. *Proceedings of the National Academy of Sciences of the United States of America* **2010**, *107*, 13336-13341 DOI: 10.1073/pnas.1003040107.

222. Welsch, S., *et al.* Architecture and regulation of the hiv-1 assembly and holding compartment in macrophages. *Journal of virology* **2011**, *85*, 7922-7927 DOI: 10.1128/jvi.00834-11.

223. Garcia, E., *et al.* Hiv-1 trafficking to the dendritic cell-t-cell infectious synapse uses a pathway of tetraspanin sorting to the immunological synapse. *Traffic* **2005**, *6*, 488-501 DOI: 10.1111/j.1600-0854.2005.00293.x.

224. Do, T., *et al.* Three-dimensional imaging of hiv-1 virological synapses reveals membrane architectures involved in virus transmission. *Journal of virology* **2014**, *88*, 10327-10339 DOI: 10.1128/JVI.00788-14.

225. Shrivastava, A., *et al.* Slit2n inhibits transmission of hiv-1 from dendritic cells to t-cells by modulating novel cytoskeletal elements. *Scientific reports* **2015**, *5*, 16833 DOI: 10.1038/srep16833.

226. Rodriguez-Plata, M.T., *et al.* The infectious synapse formed between mature dendritic cells and cd4(+) t cells is independent of the presence of the hiv-1 envelope glycoprotein. *Retrovirology* **2013**, *10*, 42 DOI: 10.1186/1742-4690-10-42.

227. Dong, C., *et al.* Characterization of human immunodeficiency virus type 1 replication in immature and mature dendritic cells reveals dissociable cis- and trans-infection. *Journal of virology* **2007**, *81*, 11352-11362 DOI: 10.1128/jvi.01081-07.

228. Wang, J.H., *et al.* Functionally distinct transmission of human immunodeficiency virus type 1 mediated by immature and mature dendritic cells. *Journal of virology* **2007**, *81*, 8933-8943 DOI: 10.1128/jvi.00878-07.

229. Izquierdo-Useros, N., *et al.* Maturation of blood-derived dendritic cells enhances human immunodeficiency virus type 1 capture and transmission. *Journal of virology* **2007**, *81*, 7559-7570 DOI: 10.1128/jvi.02572-06.

230. Piguet, V., *et al.* Dangerous liaisons at the virological synapse. *The Journal of clinical investigation* **2004**, *114*, 605-610 DOI: 10.1172/JCI22812.

231. Jolly, C. T cell polarization at the virological synapse. *Viruses* **2010**, *2*, 1261-1278 DOI: 10.3390/v2061261.

232. Haller, C., *et al.* Hiv-1 at the immunological and t-lymphocytic virological synapse. *Biological chemistry* **2008**, *389*, 1253-1260 DOI: 10.1515/BC.2008.143.

233. Jolly, C., *et al.* Adhesion molecule interactions facilitate human immunodeficiency virus type 1-induced virological synapse formation between t cells. *Journal of virology* **2007**, *81*, 13916-13921 DOI: 10.1128/JVI.01585-07.

234. Rudnicka, D., *et al.* Simultaneous cell-to-cell transmission of human immunodeficiency virus to multiple targets through polysynapses. *Journal of virology* **2009**, *83*, 6234-6246 DOI: 10.1128/JVI.00282-09.

235. Wang, L., *et al.* Sequential trafficking of env and gag to hiv-1 t cell virological synapses revealed by live imaging. *Retrovirology* **2019**, *16*, 2 DOI: 10.1186/s12977-019-0464-3.

236. Fais, S., *et al.* Unidirectional budding of hiv-1 at the site of cell-to-cell contact is associated with co-polarization of intercellular adhesion molecules and hiv-1 viral matrix protein. *Aids* **1995**, *9*, 329-335.

237. Jolly, C., *et al.* Human immunodeficiency virus type 1 virological synapse formation in t cells requires lipid raft integrity. *Journal of virology* **2005**, *79*, 12088-12094 DOI: 10.1128/jvi.79.18.12088-12094.2005.

238. Groppelli, E., *et al.* Contact-induced mitochondrial polarization supports hiv-1 virological synapse formation. *Journal of virology* **2015**, *89*, 14-24 DOI: 10.1128/JVI.02425-14.

239. Jolly, C., *et al.* Requirement for an intact t-cell actin and tubulin cytoskeleton for efficient assembly and spread of human immunodeficiency virus type 1. *Journal of virology* **2007**, *81*, 5547-5560 DOI: 10.1128/JVI.01469-06.

240. Garcia, E., *et al.* Hiv-1 replication in dendritic cells occurs through a tetraspanin-containing compartment enriched in ap-3. *Traffic* **2008**, *9*, 200-214 DOI: 10.1111/j.1600-0854.2007.00678.x.

241. Tsunetsugu-Yokota, Y., *et al.* Efficient virus transmission from dendritic cells to cd4+ t cells in response to antigen depends on close contact through adhesion molecules. *Virology* **1997**, *239*, 259-268 DOI: 10.1006/viro.1997.8895.

242. Arrighi, J.F., *et al.* Dc-sign-mediated infectious synapse formation enhances x4 hiv-1 transmission from dendritic cells to t cells. *The Journal of experimental medicine* **2004**, *200*, 1279-1288 DOI: 10.1084/jem.20041356.

243. Welsch, S., *et al.* Hiv-1 buds predominantly at the plasma membrane of primary human macrophages. *PLoS pathogens* **2007**, *3*, e36 DOI: 10.1371/journal.ppat.0030036.

244. Bennett, A.E., *et al.* Ion-abrasion scanning electron microscopy reveals surface-connected tubular conduits in hiv-infected macrophages. *PLoS pathogens* **2009**, *5*, e1000591 DOI: 10.1371/journal.ppat.1000591.

245. Deneka, M., *et al.* In macrophages, hiv-1 assembles into an intracellular plasma membrane domain containing the tetraspanins cd81, cd9, and cd53. *The Journal of cell biology* **2007**, *177*, 329-341 DOI: 10.1083/jcb.200609050.

246. Sharova, N., *et al.* Macrophages archive hiv-1 virions for dissemination in trans. *The EMBO journal* **2005**, *24*, 2481-2489 DOI: 10.1038/sj.emboj.7600707.

247. Duncan, C.J., *et al.* High-multiplicity hiv-1 infection and neutralizing antibody evasion mediated by the macrophage-t cell virological synapse. *Journal of virology* **2014**, *88*, 2025-2034 DOI: 10.1128/jvi.03245-13.

248. Gousset, K., *et al.* Real-time visualization of hiv-1 gag trafficking in infected macrophages. *PLoS pathogens* **2008**, *4*, e1000015 DOI: 10.1371/journal.ppat.1000015.

249. Sewald, X., *et al.* Retroviruses use cd169-mediated trans-infection of permissive lymphocytes to establish infection. *Science* **2015**, *350*, 563-567 DOI: 10.1126/science.aab2749.

250. Bakri, Y., *et al.* The maturation of dendritic cells results in postintegration inhibition of hiv-1 replication. *Journal of immunology* **2001**, *166*, 3780-3788 DOI: 10.4049/jimmunol.166.6.3780.

251. Lore, K., *et al.* Myeloid and plasmacytoid dendritic cells transfer hiv-1 preferentially to antigen-specific cd4+ t cells. *The Journal of experimental medicine* **2005**, *201*, 2023-2033 DOI: 10.1084/jem.20042413.

252. Piguet, V., *et al.* The interaction of hiv with dendritic cells: Outcomes and pathways. *Trends in immunology* **2007**, *28*, 503-510 DOI: 10.1016/j.it.2007.07.010.

253. Blanchet, F.P., *et al.* Tlr-4 engagement of dendritic cells confers a bst-2/tetherin-mediated restriction of hiv-1 infection to cd4+ t cells across the virological synapse. *Retrovirology* **2013**, *10*, 6 DOI: 10.1186/1742-4690-10-6.

254. Burleigh, L., *et al.* Infection of dendritic cells (dcs), not dc-sign-mediated internalization of human immunodeficiency virus, is required for long-term transfer of virus to t cells. *Journal of virology* **2006**, *80*, 2949-2957 DOI: 10.1128/jvi.80.6.2949-2957.2006.

255. Coleman, C.M., *et al.* Cellular and viral mechanisms of hiv-1 transmission mediated by dendritic cells. *Advances in experimental medicine and biology* **2013**, *762*, 109-130 DOI: 10.1007/978-1-4614-4433-6_4.

256. Blauvelt, A., *et al.* Productive infection of dendritic cells by hiv-1 and their ability to capture virus are mediated through separate pathways. *The Journal of clinical investigation* **1997**, *100*, 2043-2053 DOI: 10.1172/jci119737.

257. Gladnikoff, M., *et al.* Retroviral assembly and budding occur through an actin-driven mechanism. *Biophysical journal* **2009**, *97*, 2419-2428 DOI: 10.1016/j.bpj.2009.08.016.

258. Perelson, A.S., *et al.* Hiv-1 dynamics in vivo: Virion clearance rate, infected cell life-span, and viral generation time. *Science* **1996**, *271*, 1582-1586 DOI: 10.1126/science.271.5255.1582.

259. Chuck, A.S., *et al.* Retroviral infection is limited by brownian motion. *Human gene therapy* **1996**, *7*, 1527-1534 DOI: 10.1089/hum.1996.7.13-1527.

260. Layne, S.P., *et al.* Factors underlying spontaneous inactivation and susceptibility to neutralization of human immunodeficiency virus. *Virology* **1992**, *189*, 695-714 DOI: 10.1016/0042-6822(92)90593-e.

261. Platt, E.J., *et al.* Rapid dissociation of hiv-1 from cultured cells severely limits infectivity assays, causes the inactivation ascribed to entry inhibitors, and masks the inherently high level of infectivity of virions. *Journal of virology* **2010**, *84*, 3106-3110 DOI: 10.1128/jvi.01958-09.

262. Len, A.C.L., *et al.* Hiv-1 activates t cell signaling independently of antigen to drive viral spread. *Cell reports* **2017**, *18*, 1062-1074 DOI: 10.1016/j.celrep.2016.12.057.

263. Povarova, O.I., *et al.* Actinous enigma or enigmatic actin: Folding, structure, and functions of the most abundant eukaryotic protein. *Intrinsically disordered proteins* **2014**, *2*, e34500 DOI: 10.4161/idp.34500.

264. Gunning, P.W., *et al.* The evolution of compositionally and functionally distinct actin filaments. *Journal of cell science* **2015**, *128*, 2009-2019 DOI: 10.1242/jcs.165563.

265. Siton-Mendelson, O., *et al.* Functional actin networks under construction: The cooperative action of actin nucleation and elongation factors. *Trends in biochemical sciences* **2017**, *42*, 414-430 DOI: 10.1016/j.tibs.2017.03.002.

266. Pollard, T.D., *et al.* Actin, a central player in cell shape and movement. *Science* **2009**, *326*, 1208-1212 DOI: 10.1126/science.1175862.

267. Ananthakrishnan, R., *et al.* The forces behind cell movement. *International journal of biological sciences* **2007**, *3*, 303-317 DOI: 10.7150/ijbs.3.303.

268. Callan-Jones, A.C., *et al.* Actin flows in cell migration: From locomotion and polarity to trajectories. *Current opinion in cell biology* **2016**, *38*, 12-17 DOI: 10.1016/j.ceb.2016.01.003.

269. Khaitlina, S.Y. Intracellular transport based on actin polymerization. *Biochemistry. Biokhimiia* **2014**, *79*, 917-927 DOI: 10.1134/s0006297914090089.

270. Bachir, A.I., *et al.* Actin-based adhesion modules mediate cell interactions with the extracellular matrix and neighboring cells. *Cold Spring Harbor perspectives in biology* **2017**, *9*, DOI: 10.1101/cshperspect.a023234.

271. Lomakin, A.J., *et al.* Competition for actin between two distinct f-actin networks defines a bistable switch for cell polarization. *Nature cell biology* **2015**, *17*, 1435-1445 DOI: 10.1038/ncb3246.

272. Spira, F., *et al.* Cytokinesis in vertebrate cells initiates by contraction of an equatorial actomyosin network composed of randomly oriented filaments. *eLife* **2017**, *6*, DOI: 10.7554/eLife.30867.

273. Galkin, V.E., *et al.* Actin filaments as tension sensors. *Current biology : CB* **2012**, *22*, R96-101 DOI: 10.1016/j.cub.2011.12.010.

274. Mostowy, S., *et al.* The cytoskeleton in cell-autonomous immunity: Structural determinants of host defence. *Nature reviews. Immunology* **2015**, *15*, 559-573 DOI: 10.1038/nri3877.

275. Kristo, I., *et al.* Actin, actin-binding proteins, and actin-related proteins in the nucleus. *Histochemistry and cell biology* **2016**, *145*, 373-388 DOI: 10.1007/s00418-015-1400-9.

276. Leavitt, J., *et al.* Dissimilar modes of expression of beta- and gamma-actin in normal and leukemic human t lymphocytes. *The Journal of biological chemistry* **1980**, *255*, 4984-4987.

277. Kabsch, W., *et al.* Atomic structure of the actin:Dnase i complex. *Nature* **1990**, *347*, 37-44 DOI: 10.1038/347037a0.

278. Korn, E.D., *et al.* Actin polymerization and atp hydrolysis. *Science* **1987**, *238*, 638-644 DOI: 10.1126/science.3672117.

279. Graceffa, P., *et al.* Crystal structure of monomeric actin in the atp state. Structural basis of nucleotide-dependent actin dynamics. *The Journal of biological chemistry* **2003**, *278*, 34172-34180 DOI: 10.1074/jbc.M303689200.

280. Vandekerckhove, J., *et al.* At least six different actins are expressed in a higher mammal: An analysis based on the amino acid sequence of the amino-terminal tryptic peptide. *Journal of molecular biology* **1978**, *126*, 783-802 DOI: 10.1016/0022-2836(78)90020-7.

281. Herman, I.M. Actin isoforms. *Current opinion in cell biology* **1993**, *5*, 48-55 DOI: 10.1016/s0955-0674(05)80007-9.

282. Garrels, J.I., *et al.* Identification and characterization of multiple forms of actin. *Cell* **1976**, *9*, 793-805 DOI: 10.1016/0092-8674(76)90142-2.

283. Egelman, E.H., *et al.* F-actin is a helix with a random variable twist. *Nature* **1982**, *298*, 131-135 DOI: 10.1038/298131a0.

284. Egelman, E.H. The structure of f-actin. *Journal of muscle research and cell motility* **1985**, *6*, 129-151 DOI: 10.1007/bf00713056.

285. Egelman, E.H. A tale of two polymers: New insights into helical filaments. *Nature reviews. Molecular cell biology* **2003**, *4*, 621-630 DOI: 10.1038/nrm1176.

286. Mechanobio website. Available online:. https://www.mechanobio.info/topics/cytoskeleton-dynamics/actin-nucleation/ (11.11.),

287. Mechanobiology-Institute. What are actin filaments? https://www.mechanobio.info/cytoskeleton-dynamics/what-is-the-cytoskeleton/what-are-actin-filaments/

288. Reisler, E., *et al.* Actin structure and function: What we still do not understand. *The Journal of biological chemistry* **2007**, *282*, 36133-36137 DOI: 10.1074/jbc.R700030200.

289. Moore, P.B., *et al.* Three-dimensional reconstruction of f-actin, thin filaments and decorated thin filaments. *Journal of molecular biology* **1970**, *50*, 279-295 DOI: 10.1016/0022-2836(70)90192-0.

290. Wegner, A. Head to tail polymerization of actin. *Journal of molecular biology* **1976**, *108*, 139-150 DOI: 10.1016/s0022-2836(76)80100-3.

291. Stricker, J., *et al.* Mechanics of the f-actin cytoskeleton. *Journal of biomechanics* **2010**, *43*, 9-14 DOI: 10.1016/j.jbiomech.2009.09.003.

292. Sept, D., *et al.* Thermodynamics and kinetics of actin filament nucleation. *Biophysical journal* **2001**, *81*, 667-674 DOI: 10.1016/s0006-3495(01)75731-1.

293. De La Cruz EM, O.M. Chapter 12.5 actin polymerization is a multistep and dynamic process. In *Lewin's cells*, George Plopper, D.S., Eric Sikorski, Ed. Jones & Bartlett Learning Private Limited: 2015, ISBN 9789380853888.

294. Chesarone, M.A., *et al.* Actin nucleation and elongation factors: Mechanisms and interplay. *Current opinion in cell biology* **2009**, *21*, 28-37 DOI: 10.1016/j.ceb.2008.12.001.

295. Skau, C.T., *et al.* Specification of architecture and function of actin structures by actin nucleation factors. *Annual review of biophysics* **2015**, *44*, 285-310 DOI: 10.1146/annurev-biophys-060414-034308.

296. Mechanobiology-Institute. What are tandem-monomer-binding nucleators? https://www.mechanobio.info/cytoskeleton-dynamics/what-is-the-cytoskeleton/what-are-actin-filaments/what-are-tandem-monomer-binding-nucleators/

297. Rotty, J.D., *et al.* New insights into the regulation and cellular functions of the arp2/3 complex. *Nature reviews. Molecular cell biology* **2013**, *14*, 7-12 DOI: 10.1038/nrm3492.

298. Wu, J.Q., *et al.* Counting cytokinesis proteins globally and locally in fission yeast. *Science* **2005**, *310*, 310-314 DOI: 10.1126/science.1113230.

299. Suarez, C., *et al.* Profilin regulates f-actin network homeostasis by favoring formin over arp2/3 complex. *Developmental cell* **2015**, *32*, 43-53 DOI: 10.1016/j.devcel.2014.10.027.

300. Goley, E.D., *et al.* The arp2/3 complex: An actin nucleator comes of age. *Nature reviews. Molecular cell biology* **2006**, *7*, 713-726 DOI: 10.1038/nrm2026.

301. Mechanobiology-Institute. How does arp2/3-mediate the nucleation of branched filaments? https://www.mechanobio.info/cytoskeleton-dynamics/what-is-the-cytoskeleton/what-are-actin-filaments/how-does-arp23-mediate-the-nucleation-of-branched-filaments/

302. Campellone, K.G., *et al.* A nucleator arms race: Cellular control of actin assembly. *Nature reviews. Molecular cell biology* **2010**, *11*, 237-251 DOI: 10.1038/nrm2867.

303. Lebensohn, A.M., *et al.* Activation of the wave complex by coincident signals controls actin assembly. *Molecular cell* **2009**, *36*, 512-524 DOI: 10.1016/j.molcel.2009.10.024.

304. Oda, A., *et al.* Wasps and waves: From molecular function to physiology in hematopoietic cells. *Seminars in cell & developmental biology* **2013**, *24*, 308-313 DOI: 10.1016/j.semcdb.2013.03.002.

305. Higgs, H.N., *et al.* Phylogenetic analysis of the formin homology 2 domain. *Molecular biology of the cell* **2005**, *16*, 1-13 DOI: 10.1091/mbc.e04-07-0565.

306. Kuhn, S., *et al.* Formins as effector proteins of rho gtpases. *Small GTPases* **2014**, *5*, e29513 DOI: 10.4161/sgtp.29513.

307. Faix, J., *et al.* Staying in shape with formins. *Developmental cell* **2006**, *10*, 693-706 DOI: 10.1016/j.devcel.2006.05.001.

308. Bogdan, S., *et al.* Formin' cellular structures: Physiological roles of diaphanous (dia) in actin dynamics. *Communicative & integrative biology* **2013**, *6*, e27634 DOI: 10.4161/cib.27634.

309. Bartolini, F., *et al.* Formins and microtubules. *Biochimica et biophysica acta* **2010**, *1803*, 164-173 DOI: 10.1016/j.bbamcr.2009.07.006.

310. Pring, M., *et al.* Mechanism of formin-induced nucleation of actin filaments. *Biochemistry* **2003**, *42*, 486-496 DOI: 10.1021/bi026520j.

311. Paul, A.S., *et al.* The role of the fh1 domain and profilin in formin-mediated actin-filament elongation and nucleation. *Current biology : CB* **2008**, *18*, 9-19 DOI: 10.1016/j.cub.2007.11.062.

312. Kovar, D.R., *et al.* Control of the assembly of atp- and adp-actin by formins and profilin. *Cell* **2006**, *124*, 423-435 DOI: 10.1016/j.cell.2005.11.038.

313. Rotty, J.D., *et al.* Profilin-1 serves as a gatekeeper for actin assembly by arp2/3-dependent and -independent pathways. *Developmental cell* **2015**, *32*, 54-67 DOI: 10.1016/j.devcel.2014.10.026.

314. Stossel, T.P., *et al.* Cell surface actin remodeling. *Journal of cell science* **2006**, *119*, 3261-3264 DOI: 10.1242/jcs.02994.

315. Winder, S.J., *et al.* Actin-binding proteins. *Journal of cell science* **2005**, *118*, 651-654 DOI: 10.1242/jcs.01670.

316. Dominguez, R., *et al.* Actin structure and function. *Annual review of biophysics* **2011**, *40*, 169-186 DOI: 10.1146/annurev-biophys-042910-155359.

317. Ampe, C., *et al.* Mammalian actins: Isoform-specific functions and diseases. *Handbook of experimental pharmacology* **2017**, *235*, 1-37 DOI: 10.1007/164_2016_43.

318. Lee, S.H., *et al.* Regulation of actin cytoskeleton dynamics in cells. *Molecules and cells* **2010**, *29*, 311-325 DOI: 10.1007/s10059-010-0053-8.

319. Sit, S.T., *et al.* Rho gtpases and their role in organizing the actin cytoskeleton. *Journal of cell science* **2011**, *124*, 679-683 DOI: 10.1242/jcs.064964.

320. Lee, K., *et al.* Functional hierarchy of redundant actin assembly factors revealed by fine-grained registration of intrinsic image fluctuations. *Cell systems* **2015**, *1*, 37-50 DOI: 10.1016/j.cels.2015.07.001.

321. Ponten, F., *et al.* The human protein atlas--a tool for pathology. *The Journal of pathology* **2008**, *216*, 387-393 DOI: 10.1002/path.2440.

322. Levayer, R., *et al.* Biomechanical regulation of contractility: Spatial control and dynamics. *Trends in cell biology* **2012**, *22*, 61-81 DOI: 10.1016/j.tcb.2011.10.001.

323. Chhabra, E.S., *et al.* The many faces of actin: Matching assembly factors with cellular structures. *Nature cell biology* **2007**, *9*, 1110-1121 DOI: 10.1038/ncb1007-1110.

324. Jensen, L.J., *et al.* String 8--a global view on proteins and their functional interactions in 630 organisms. *Nucleic acids research* **2009**, *37*, D412-416 DOI: 10.1093/nar/gkn760.

325. Abbas, W., *et al.* The eef1a proteins: At the crossroads of oncogenesis, apoptosis, and viral infections. *Frontiers in oncology* **2015**, *5*, 75 DOI: 10.3389/fonc.2015.00075.

326. Rao, N.A., *et al.* Molecular organization, catalytic mechanism and function of serine hydroxymethyltransferase--a potential target for cancer chemotherapy. *The international journal of biochemistry & cell biology* **2000**, *32*, 405-416 DOI: 10.1016/s1357-2725(99)00126-0.

327. Lin, J., *et al.* Histological evidence: Housekeeping genes beta-actin and gapdh are of limited value for normalization of gene expression. *Development genes and evolution* **2012**, *222*, 369-376 DOI: 10.1007/s00427-012-0420-x.

328. Xue, B., *et al.* Guardians of the actin monomer. *European journal of cell biology* **2013**, *92*, 316-332 DOI: 10.1016/j.ejcb.2013.10.012.

329. Murali, A., *et al.* Small rho gtpases in the control of cell shape and mobility. *Cellular and molecular life sciences : CMLS* **2014**, *71*, 1703-1721 DOI: 10.1007/s00018-013-1519-6.

330. de Curtis, I., *et al.* Cell surface dynamics - how rho gtpases orchestrate the interplay between the plasma membrane and the cortical cytoskeleton. *Journal of cell science* **2012**, *125*, 4435-4444 DOI: 10.1242/jcs.108266.

331. Mangeat, P., *et al.* Erm proteins in cell adhesion and membrane dynamics. *Trends in cell biology* **1999**, *9*, 187-192.

332. Pollard, T.D. Actin and actin-binding proteins. *Cold Spring Harbor perspectives in biology* **2016**, *8*, DOI: 10.1101/cshperspect.a018226.

333. Mechanobiology-Institute. Actin crosslinking. https://www.mechanobio.info/cytoskeleton-dynamics/actin-crosslinking/

334. Kapus, A., *et al.* Plasma membrane--cortical cytoskeleton interactions: A cell biology approach with biophysical considerations. *Comprehensive Physiology* **2013**, *3*, 1231-1281 DOI: 10.1002/cphy.c120015.

335. Ono, S. Mechanism of depolymerization and severing of actin filaments and its significance in cytoskeletal dynamics. *International review of cytology* **2007**, *258*, 1-82 DOI: 10.1016/S0074-7696(07)58001-0.

336. Theriot, J.A. The polymerization motor. *Traffic* **2000**, *1*, 19-28.

337. Borisy, G.G., *et al.* Actin machinery: Pushing the envelope. *Current opinion in cell biology* **2000**, *12*, 104-112 DOI: 10.1016/s0955-0674(99)00063-0.

338. Huber, F., *et al.* Emergent complexity of the cytoskeleton: From single filaments to tissue. *Advances in physics* **2013**, *62*, 1-112 DOI: 10.1080/00018732.2013.771509.

339. Svitkina, T. The actin cytoskeleton and actin-based motility. *Cold Spring Harbor perspectives in biology* **2018**, *10*, DOI: 10.1101/cshperspect.a018267.

340. Footer, M.J., *et al.* Direct measurement of force generation by actin filament polymerization using an optical trap. *Proceedings of the National Academy of Sciences of the United States of America* **2007**, *104*, 2181-2186 DOI: 10.1073/pnas.0607052104.

341. Kovar, D.R., *et al.* Insertional assembly of actin filament barbed ends in association with formins produces piconewton forces. *Proceedings of the National Academy of Sciences of the United States of America* **2004**, *101*, 14725-14730 DOI: 10.1073/pnas.0405902101.

342. Mechanobiology-Institute. How does actin filament polymerization generates protrusive force? https://www.mechanobio.info/cytoskeleton-dynamics/what-is-the-cytoskeleton/what-are-actin-filaments/actin-filament-polymerization-generates-protrusive-force/

343. Chugh, P., *et al.* The actin cortex at a glance. *Journal of cell science* **2018**, *131*, DOI: 10.1242/jcs.186254.

344. Clausen, M.P., *et al.* Dissecting the actin cortex density and membrane-cortex distance in living cells by super-resolution microscopy. *Journal of physics D: Applied physics* **2017**, *50*, 064002 DOI: 10.1088/1361-6463/aa52a1.

345. Salbreux, G., *et al.* Actin cortex mechanics and cellular morphogenesis. *Trends in cell biology* **2012**, *22*, 536-545 DOI: 10.1016/j.tcb.2012.07.001.

346. Biro, M., *et al.* Cell cortex composition and homeostasis resolved by integrating proteomics and quantitative imaging. *Cytoskeleton* **2013**, *70*, 741-754 DOI: 10.1002/cm.21142.

347. Bovellan, M., *et al.* Cellular control of cortical actin nucleation. *Current biology : CB* **2014**, *24*, 1628-1635 DOI: 10.1016/j.cub.2014.05.069.

348. Morone, N., *et al.* Three-dimensional reconstruction of the membrane skeleton at the plasma membrane interface by electron tomography. *The Journal of cell biology* **2006**, *174*, 851-862 DOI: 10.1083/jcb.200606007.

349. Gunning, P.W., *et al.* Tropomyosins. *Current biology : CB* **2017**, *27*, R8-r13 DOI: 10.1016/j.cub.2016.11.033.

350. DesMarais, V., *et al.* Spatial regulation of actin dynamics: A tropomyosin-free, actin-rich compartment at the leading edge. *Journal of cell science* **2002**, *115*, 4649-4660 DOI: 10.1242/jcs.00147.

351. Hsiao, J.Y., *et al.* Arp2/3 complex and cofilin modulate binding of tropomyosin to branched actin networks. *Current biology : CB* **2015**, *25*, 1573-1582 DOI: 10.1016/j.cub.2015.04.038.

352. Vicente-Manzanares, M., *et al.* Role of the cytoskeleton during leukocyte responses. *Nature reviews. Immunology* **2004**, *4*, 110-122 DOI: 10.1038/nri1268.

353. Lehtimaki, J., *et al.* Actin filament structures in migrating cells. *Handbook of experimental pharmacology* **2017**, *235*, 123-152 DOI: 10.1007/164_2016_28.

354. Mattila, P.K., *et al.* Filopodia: Molecular architecture and cellular functions. *Nature reviews. Molecular cell biology* **2008**, *9*, 446-454 DOI: 10.1038/nrm2406.

355. Galbraith, C.G., *et al.* Polymerizing actin fibers position integrins primed to probe for adhesion sites. *Science* **2007**, *315*, 992-995 DOI: 10.1126/science.1137904.

356. Kress, H., *et al.* Filopodia act as phagocytic tentacles and pull with discrete steps and a load-dependent velocity. *Proceedings of the National Academy of Sciences of the United States of America* **2007**, *104*, 11633-11638 DOI: 10.1073/pnas.0702449104.

357. You, R., *et al.* Response of filopodia and lamellipodia to surface topography on micropatterned silk fibroin films. *Journal of biomedical materials research. Part A* **2014**, *102*, 4206-4212 DOI: 10.1002/jbm.a.35097.

358. Svitkina, T.M., *et al.* Mechanism of filopodia initiation by reorganization of a dendritic network. *The Journal of cell biology* **2003**, *160*, 409-421 DOI: 10.1083/jcb.200210174.

359. Medalia, O., *et al.* Organization of actin networks in intact filopodia. *Current biology : CB* **2007**, *17*, 79-84 DOI: 10.1016/j.cub.2006.11.022.

360. Leijnse, N., *et al.* An updated look at actin dynamics in filopodia. *Cytoskeleton* **2015**, *72*, 71-79 DOI: 10.1002/cm.21216.

361. Mallavarapu, A., *et al.* Regulated actin cytoskeleton assembly at filopodium tips controls their extension and retraction. *The Journal of cell biology* **1999**, *146*, 1097-1106 DOI: 10.1083/jcb.146.5.1097.

362. Breitsprecher, D., *et al.* Cofilin cooperates with fascin to disassemble filopodial actin filaments. *Journal of cell science* **2011**, *124*, 3305-3318 DOI: 10.1242/jcs.086934.

363. Albuschies, J., *et al.* The role of filopodia in the recognition of nanotopographies. *Scientific reports* **2013**, *3*, 1658 DOI: 10.1038/srep01658.

364. Yang, C., *et al.* Filopodia initiation: Focus on the arp2/3 complex and formins. *Cell adhesion & migration* **2011**, *5*, 402-408 DOI: 10.4161/cam.5.5.16971.

365. Young, L.E., *et al.* Cell type-dependent mechanisms for formin-mediated assembly of filopodia. *Molecular biology of the cell* **2015**, *26*, 4646-4659 DOI: 10.1091/mbc.E15-09-0626.

366. Pellegrin, S., *et al.* The rho family gtpase rif induces filopodia through mdia2. *Current biology : CB* **2005**, *15*, 129-133 DOI: 10.1016/j.cub.2005.01.011.

367. Goh, W.I., *et al.* Rif-mdia1 interaction is involved in filopodium formation independent of cdc42 and rac effectors. *The Journal of biological chemistry* **2011**, *286*, 13681-13694 DOI: 10.1074/jbc.M110.182683.

368. Faix, J., *et al.* Filopodia: Complex models for simple rods. *The international journal of biochemistry & cell biology* **2009**, *41*, 1656-1664 DOI: 10.1016/j.biocel.2009.02.012.

369. Peng, J., *et al.* Disruption of the diaphanous-related formin drf1 gene encoding mdia1 reveals a role for drf3 as an effector for cdc42. *Current biology : CB* **2003**, *13*, 534-545 DOI: 10.1016/s0960-9822(03)00170-2.

370. Young, L.E., *et al.* Roles for ena/vasp proteins in fmnl3-mediated filopodial assembly. *Journal of cell science* **2018**, *131*, DOI: 10.1242/jcs.220814.

371. Drees, F., *et al.* Ena/vasp: Proteins at the tip of the nervous system. *Current opinion in neurobiology* **2008**, *18*, 53-59 DOI: 10.1016/j.conb.2008.05.007.

372. Vonna, L., *et al.* Micromechanics of filopodia mediated capture of pathogens by macrophages. *European biophysics journal : EBJ* **2007**, *36*, 145-151 DOI: 10.1007/s00249-006-0118-y.

373. Hoffmann, A.K., *et al.* Daam1 is a regulator of filopodia formation and phagocytic uptake of borrelia burgdorferi by primary human macrophages. *FASEB journal : official publication of the Federation of American Societies for Experimental Biology* **2014**, *28*, 3075-3089 DOI: 10.1096/fj.13-247049.

374. Abercrombie, M. The croonian lecture, 1978 - the crawling movement of metazoan cells. *Proceedings of the Royal Society of London. Series B, Biological sciences* **1980**, *207*, DOI: 10.1098/rspb.1980.0017.

375. Small, J.V., *et al.* The lamellipodium: Where motility begins. *Trends in cell biology* **2002**, *12*, 112-120.

376. Svitkina, T.M., *et al.* Arp2/3 complex and actin depolymerizing factor/cofilin in dendritic organization and treadmilling of actin filament array in lamellipodia. *The Journal of cell biology* **1999**, *145*, 1009-1026 DOI: 10.1083/jcb.145.5.1009.

377. Svitkina, T.M., *et al.* Progress in protrusion: The tell-tale scar. *Trends in biochemical sciences* **1999**, *24*, 432-436 DOI: 10.1016/s0968-0004(99)01461-9.

378. Heath, J.P., *et al.* On the mechanisms of cortical actin flow and its role in cytoskeletal organisation of fibroblasts. *Symposia of the Society for Experimental Biology* **1993**, *47*, 35-56.

379. Ridley, A.J., *et al.* Cell migration: Integrating signals from front to back. *Science* **2003**, *302*, 1704-1709 DOI: 10.1126/science.1092053.

380. Krause, M., *et al.* Steering cell migration: Lamellipodium dynamics and the regulation of directional persistence. *Nature reviews. Molecular cell biology* **2014**, *15*, 577-590 DOI: 10.1038/nrm3861.

381. Takenawa, T. Phosphoinositide-binding interface proteins involved in shaping cell membranes. *Proceedings of the Japan Academy. Series B, Physical and biological sciences* **2010**, *86*, 509-523 DOI: 10.2183/pjab.86.509.

382. Guo, F., *et al.* Genetic deletion of rac1 gtpase reveals its critical role in actin stress fiber formation and focal adhesion complex assembly. *The Journal of biological chemistry* **2006**, *281*, 18652-18659 DOI: 10.1074/jbc.M603508200.

383. Steffen, A., *et al.* Rac function is crucial for cell migration but is not required for spreading and focal adhesion formation. *Journal of cell science* **2013**, *126*, 4572-4588 DOI: 10.1242/jcs.118232.

384. Yamazaki, D., *et al.* Wave2 is required for directed cell migration and cardiovascular development. *Nature* **2003**, *424*, 452-456 DOI: 10.1038/nature01770.

385. Wu, C., *et al.* Arp2/3 is critical for lamellipodia and response to extracellular matrix cues but is dispensable for chemotaxis. *Cell* **2012**, *148*, 973-987 DOI: 10.1016/j.cell.2011.12.034.

386. Suraneni, P., *et al.* The arp2/3 complex is required for lamellipodia extension and directional fibroblast cell migration. *The Journal of cell biology* **2012**, *197*, 239-251 DOI: 10.1083/jcb.201112113.

387. Wu, Y.I., *et al.* A genetically encoded photoactivatable rac controls the motility of living cells. *Nature* **2009**, *461*, 104-108 DOI: 10.1038/nature08241.

388. Akin, O., *et al.* Capping protein increases the rate of actin-based motility by promoting filament nucleation by the arp2/3 complex. *Cell* **2008**, *133*, 841-851 DOI: 10.1016/j.cell.2008.04.011.

389. Pollard, T.D., *et al.* Cellular motility driven by assembly and disassembly of actin filaments. *Cell* **2003**, *112*, 453-465 DOI: 10.1016/s0092-8674(03)00120-x.

390. Selden, L.A., *et al.* Impact of profilin on actin-bound nucleotide exchange and actin polymerization dynamics. *Biochemistry* **1999**, *38*, 2769-2778 DOI: 10.1021/bi981543c.

391. Mullins, R.D., *et al.* The interaction of arp2/3 complex with actin: Nucleation, high affinity pointed end capping, and formation of branching networks of filaments. *Proceedings of the National Academy of Sciences of the United States of America* **1998**, *95*, 6181-6186 DOI: 10.1073/pnas.95.11.6181.

392. Suetsugu, S., *et al.* The essential role of profilin in the assembly of actin for microspike formation. *The EMBO journal* **1998**, *17*, 6516-6526 DOI: 10.1093/emboj/17.22.6516.

393. Ikeda, W., *et al.* Cooperation of cdc42 small g protein-activating and actin filament-binding activities of frabin in microspike formation. *Oncogene* **2001**, *20*, 3457-3463 DOI: 10.1038/sj.onc.1204463.

394. Sauvanet, C., *et al.* Structure, regulation, and functional diversity of microvilli on the apical domain of epithelial cells. *Annual review of cell and developmental biology* **2015**, *31*, 593-621 DOI: 10.1146/annurev-cellbio-100814-125234.

395. Fath, K.R., *et al.* Microvillus assembly. Not actin alone. *Current biology : CB* **1995**, *5*, 591-593 DOI: 10.1016/s0960-9822(95)00117-5.

396. Singer, II, *et al.* Ccr5, cxcr4, and cd4 are clustered and closely apposed on microvilli of human macrophages and t cells. *Journal of virology* **2001**, *75*, 3779-3790 DOI: 10.1128/jvi.75.8.3779-3790.2001.

397. Ponti, A., *et al.* Two distinct actin networks drive the protrusion of migrating cells. *Science* **2004**, *305*, 1782-1786 DOI: 10.1126/science.1100533.

398. Mechanobiology-Institute. What are lamellipodia and lamella? https://www.mechanobio.info/cytoskeleton-dynamics/what-are-lamellipodia-and-lamella/

399. Borm, B., *et al.* Membrane ruffles in cell migration: Indicators of inefficient lamellipodia adhesion and compartments of actin filament reorganization. *Experimental cell research* **2005**, *302*, 83-95 DOI: 10.1016/j.yexcr.2004.08.034.

400. Swanson, J.A., *et al.* Macropinocytosis. *Trends in cell biology* **1995**, *5*, 424-428.

401. Linder, S., *et al.* Podosomes: Adhesion hot-spots of invasive cells. *Trends in cell biology* **2003**, *13*, 376-385.

402. Linder, S., *et al.* Podosomes at a glance. *Journal of cell science* **2005**, *118*, 2079-2082 DOI: 10.1242/jcs.02390.

403. Burger, K.L., *et al.* The podosome marker protein tks5 regulates macrophage invasive behavior. *Cytoskeleton* **2011**, *68*, 694-711 DOI: 10.1002/cm.20545.

404. Charras, G.T. A short history of blebbing. *Journal of microscopy* **2008**, *231*, 466-478 DOI: 10.1111/j.1365-2818.2008.02059.x.

405. Ikenouchi, J., *et al.* Membrane bleb: A seesaw game of two small gtpases. *Small GTPases* **2017**, *8*, 85-89 DOI: 10.1080/21541248.2016.1199266.

406. Paluch, E.K., *et al.* The role and regulation of blebs in cell migration. *Current opinion in cell biology* **2013**, *25*, 582-590 DOI: 10.1016/j.ceb.2013.05.005.

407. Taylor, M.P., *et al.* Subversion of the actin cytoskeleton during viral infection. *Nature reviews. Microbiology* **2011**, *9*, 427-439 DOI: 10.1038/nrmicro2574.

408. Fackler, O.T., *et al.* Interactions of human retroviruses with the host cell cytoskeleton. *Current opinion in microbiology* **2006**, *9*, 409-415 DOI: 10.1016/j.mib.2006.06.010.

409. Marzook, N.B., *et al.* Viruses that exploit actin-based motility for their replication and spread. *Handbook of experimental pharmacology* **2017**, *235*, 237-261 DOI: 10.1007/164_2016_41.

410. Spear, M., *et al.* Viral exploitation of actin: Force-generation and scaffolding functions in viral infection. *Virologica Sinica* **2014**, *29*, 139-147 DOI: 10.1007/s12250-014-3476-0.

411. Smith, G.A., *et al.* Break ins and break outs: Viral interactions with the cytoskeleton of mammalian cells. *Annual review of cell and developmental biology* **2002**, *18*, 135-161 DOI: 10.1146/annurev.cellbio.18.012502.105920.

412. Stradal, T.E.B., *et al.* Actin dynamics in host-pathogen interaction. *FEBS letters* **2018**, *592*, 3658-3669 DOI: 10.1002/1873-3468.13173.

413. Dramsi, S., *et al.* Intracellular pathogens and the actin cytoskeleton. *Annual review of cell and developmental biology* **1998**, *14*, 137-166 DOI: 10.1146/annurev.cellbio.14.1.137.

414. Choe, J.E., *et al.* Actin-based motility of bacterial pathogens: Mechanistic diversity and its impact on virulence. *Pathogens and disease* **2016**, DOI: 10.1093/femspd/ftw099.

415. Lamason, R.L., *et al.* Actin-based motility and cell-to-cell spread of bacterial pathogens. *Current opinion in microbiology* **2017**, *35*, 48-57 DOI: 10.1016/j.mib.2016.11.007.

416. Kuhn, S., *et al.* Actin: Structure, function, dynamics, and interactions with bacterial toxins. *Current topics in microbiology and immunology* **2017**, *399*, 1-34 DOI: 10.1007/82_2016_45.

417. Colonne, P.M., *et al.* Hijacking host cell highways: Manipulation of the host actin cytoskeleton by obligate intracellular bacterial pathogens. *Frontiers in cellular and infection microbiology* **2016**, *6*, 107 DOI: 10.3389/fcimb.2016.00107.

418. Welch, M.D., *et al.* Arp2/3-mediated actin-based motility: A tail of pathogen abuse. *Cell host & microbe* **2013**, *14*, 242-255 DOI: 10.1016/j.chom.2013.08.011.

419. Bugalhao, J.N., *et al.* Bacterial nucleators: Actin' on actin. *Pathogens and disease* **2015**, *73*, ftv078 DOI: 10.1093/femspd/ftv078.

420. Quintero, C.A., *et al.* Rho gtpases as pathogen targets: Focus on curable sexually transmitted infections. *Small GTPases* **2015**, *6*, 108-118 DOI: 10.4161/21541248.2014.991233.

421. Haqshenas, G., *et al.* Targeting of host cell receptor tyrosine kinases by intracellular pathogens. *Science signaling* **2019**, *12*, DOI: 10.1126/scisignal.aau9894.

422. Haglund, C.M., *et al.* Pathogens and polymers: Microbe-host interactions illuminate the cytoskeleton. *The Journal of cell biology* **2011**, *195*, 7-17 DOI: 10.1083/jcb.201103148.

423. Humphries, A.C., *et al.* The non-canonical roles of clathrin and actin in pathogen internalization, egress and spread. *Nature reviews. Microbiology* **2013**, *11*, 551-560.

424. Burckhardt, C.J., *et al.* Virus movements on the plasma membrane support infection and transmission between cells. *PLoS pathogens* **2009**, *5*, e1000621 DOI: 10.1371/journal.ppat.1000621.

425. Rottner, K., *et al.* Bacteria-host-cell interactions at the plasma membrane: Stories on actin cytoskeleton subversion. *Developmental cell* **2005**, *9*, 3-17 DOI: 10.1016/j.devcel.2005.06.002.

426. Chang, K., *et al.* Filopodia and viruses: An analysis of membrane processes in entry mechanisms. *Frontiers in microbiology* **2016**, *7*, 300 DOI: 10.3389/fmicb.2016.00300.

427. Newsome, T.P., *et al.* Viruses that ride on the coat-tails of actin nucleation. *Seminars in cell & developmental biology* **2015**, *46*, 155-163 DOI: 10.1016/j.semcdb.2015.10.008.

428. Kuehl, C.J., *et al.* Bacterial spread from cell to cell: Beyond actin-based motility. *Trends in microbiology* **2015**, *23*, 558-566 DOI: 10.1016/j.tim.2015.04.010.

429. Iyengar, S., *et al.* Actin-dependent receptor colocalization required for human immunodeficiency virus entry into host cells. *Journal of virology* **1998**, *72*, 5251-5255.

430. Harmon, B., *et al.* Role of abl kinase and the wave2 signaling complex in hiv-1 entry at a post-hemifusion step. *PLoS pathogens* **2010**, *6*, e1000956 DOI: 10.1371/journal.ppat.1000956.

431. Li, Q., *et al.* Single-particle tracking of human immunodeficiency virus type 1 productive entry into human primary macrophages. *ACS nano* **2017**, *11*, 3890-3903 DOI: 10.1021/acsnano.7b00275.

432. Bukrinskaya, A., *et al.* Establishment of a functional human immunodeficiency virus type 1 (hiv-1) reverse transcription complex involves the cytoskeleton. *The Journal of experimental medicine* **1998**, *188*, 2113-2125.

433. Arhel, N., *et al.* Quantitative four-dimensional tracking of cytoplasmic and nuclear hiv-1 complexes. *Nature methods* **2006**, *3*, 817-824 DOI: 10.1038/nmeth928.

434. Spear, M., *et al.* Hiv-1 triggers wave2 phosphorylation in primary cd4 t cells and macrophages, mediating arp2/3-dependent nuclear migration. *The Journal of biological chemistry* **2014**, *289*, 6949-6959 DOI: 10.1074/jbc.M113.492132.

435. Cameron, P.U., *et al.* Establishment of hiv-1 latency in resting cd4+ t cells depends on chemokine-induced changes in the actin cytoskeleton. *Proceedings of the National Academy of Sciences of the United States of America* **2010**, *107*, 16934-16939 DOI: 10.1073/pnas.1002894107.

436. Miyakawa, K., *et al.* The tumour suppressor apc promotes hiv-1 assembly via interaction with gag precursor protein. *Nature communications* **2017**, *8*, 14259 DOI: 10.1038/ncomms14259.

437. Sasaki, H., *et al.* Actin filaments play an essential role for transport of nascent hiv-1 proteins in host cells. *Biochemical and biophysical research communications* **2004**, *316*, 588-593 DOI: 10.1016/j.bbrc.2004.02.088.

438. Cooper, J., *et al.* Filamin a protein interacts with human immunodeficiency virus type 1 gag protein and contributes to productive particle assembly. *The Journal of biological chemistry* **2011**, *286*, 28498-28510 DOI: 10.1074/jbc.M111.239053.

439. Kerviel, A., *et al.* Virus assembly and plasma membrane domains: Which came first? *Virus research* **2013**, *171*, 332-340 DOI: 10.1016/j.virusres.2012.08.014.

440. Wen, X., *et al.* Rock1 and lim kinase modulate retrovirus particle release and cell-cell transmission events. *Journal of virology* **2014**, *88*, 6906-6921 DOI: 10.1128/JVI.00023-14.

441. Sasaki, H., *et al.* Myosin-actin interaction plays an important role in human immunodeficiency virus type 1 release from host cells. *Proceedings of the National Academy of Sciences of the United States of America* **1995**, *92*, 2026-2030.

442. Audoly, G., *et al.* Involvement of a small gtp binding protein in hiv-1 release. *Retrovirology* **2005**, *2*, 48 DOI: 10.1186/1742-4690-2-48.

443. Lehmann, M., *et al.* How hiv-1 takes advantage of the cytoskeleton during replication and cell-to-cell transmission. *Viruses* **2011**, *3*, 1757-1776 DOI: 10.3390/v3091757.

444. Sodeik, B. Unchain my heart, baby let me go--the entry and intracellular transport of hiv. *The Journal of cell biology* **2002**, *159*, 393-395 DOI: 10.1083/jcb.200210024.

445. McDonald, D., *et al.* Visualization of the intracellular behavior of hiv in living cells. *The Journal of cell biology* **2002**, *159*, 441-452 DOI: 10.1083/jcb.200203150.

446. Debaisieux, S., *et al.* The ins and outs of hiv-1 tat. *Traffic* **2012**, *13*, 355-363 DOI: 10.1111/j.1600-0854.2011.01286.x.

447. Olivetta, E., *et al.* The contribution of extracellular nef to hiv-induced pathogenesis. *Current drug targets* **2016**, *17*, 46-53.

448. Oh, S.K., *et al.* Identification of hiv-1 envelope glycoprotein in the serum of aids and arc patients. *Journal of acquired immune deficiency syndromes* **1992**, *5*, 251-256.

449. Wang, E., *et al.* The presence of actin in enveloped viruses. In *Cell motility*, Goldman, R.; Pollard, T.; Rosenbaum, J., Eds. Cold Spring Harbor: 1976; Vol. 1, pp 589-599.

450. Ott, D.E., *et al.* Cytoskeletal proteins inside human immunodeficiency virus type 1 virions. *Journal of virology* **1996**, *70*, 7734-7743.

451. Wilk, T., *et al.* Actin associates with the nucleocapsid domain of the human immunodeficiency virus gag polyprotein. *Journal of virology* **1999**, *73*, 1931-1940.

452. Ott, D.E., *et al.* Actin-binding cellular proteins inside human immunodeficiency virus type 1. *Virology* **2000**, *266*, 42-51 DOI: 10.1006/viro.1999.0075.

453. Katzav, S., *et al.* Vav, a novel human oncogene derived from a locus ubiquitously expressed in hematopoietic cells. *The EMBO journal* **1989**, *8*, 2283-2290.

454. Linde, M.E., *et al.* The conserved set of host proteins incorporated into hiv-1 virions suggests a common egress pathway in multiple cell types. *Journal of proteome research* **2013**, *12*, 2045-2054 DOI: 10.1021/pr300918r.

455. Ott, D.E. Cellular proteins detected in hiv-1. *Reviews in medical virology* **2008**, *18*, 159-175 DOI: 10.1002/rmv.570.

456. Ott, D.E. Potential roles of cellular proteins in hiv-1. *Reviews in medical virology* **2002**, *12*, 359-374 DOI: 10.1002/rmv.367.

457. Stauffer, S., *et al.* The nucleocapsid domain of gag is dispensable for actin incorporation into hiv-1 and for association of viral budding sites with cortical f-actin. *Journal of virology* **2014**, *88*, 7893-7903 DOI: 10.1128/JVI.00428-14.

458. Turlure, F., *et al.* Human cell proteins and human immunodeficiency virus DNA integration. *Frontiers in bioscience : a journal and virtual library* **2004**, *9*, 3187-3208.

459. Kimura, T., *et al.* Rev-dependent association of the intron-containing hiv-1 gag mrna with the nuclear actin bundles and the inhibition of its nucleocytoplasmic transport by

latrunculin-b. *Genes to cells : devoted to molecular & cellular mechanisms* **2000**, *5*, 289-307.

460. Mahmoudi, T., *et al.* The swi/snf chromatin-remodeling complex is a cofactor for tat transactivation of the hiv promoter. *The Journal of biological chemistry* **2006**, *281*, 19960-19968 DOI: 10.1074/jbc.M603336200.

461. Rey, O., *et al.* Hiv-1 gag protein associates with f-actin present in microfilaments. *Virology* **1996**, *220*, 530-534 DOI: 10.1006/viro.1996.0343.

462. Liu, B., *et al.* Interaction of the human immunodeficiency virus type 1 nucleocapsid with actin. *Journal of virology* **1999**, *73*, 2901-2908.

463. Poole, E., *et al.* Hiv-1 gag-rna interaction occurs at a perinuclear/centrosomal site; analysis by confocal microscopy and fret. *Traffic* **2005**, *6*, 741-755 DOI: 10.1111/j.1600-0854.2005.00312.x.

464. Fenteany, G., *et al.* Small-molecule inhibitors of actin dynamics and cell motility. *Current topics in medicinal chemistry* **2003**, *3*, 593-616 DOI: 10.2174/1568026033452348.

465. Gallo, S.A., *et al.* Hiv-1 gp41 six-helix bundle formation occurs rapidly after the engagement of gp120 by cxcr4 in the hiv-1 env-mediated fusion process. *Biochemistry* **2001**, *40*, 12231-12236.

466. Viard, M., *et al.* Role of cholesterol in human immunodeficiency virus type 1 envelope protein-mediated fusion with host cells. *Journal of virology* **2002**, *76*, 11584-11595.

467. Aggarwal, A., *et al.* Hiv infection is influenced by dynamin at 3 independent points in the viral life cycle. *Traffic* **2017**, *18*, 392-410 DOI: 10.1111/tra.12481.

468. Liu, Y., *et al.* Hiv infection of t cells: Actin-in and actin-out. *Science signaling* **2009**, *2*, pe23 DOI: 10.1126/scisignal.266pe23.

469. Spear, M., *et al.* The trinity of the cortical actin in the initiation of hiv-1 infection. *Retrovirology* **2012**, *9*, 45 DOI: 10.1186/1742-4690-9-45.

470. Harmon, B., *et al.* Induction of the galpha(q) signaling cascade by the human immunodeficiency virus envelope is required for virus entry. *Journal of virology* **2008**, *82*, 9191-9205 DOI: 10.1128/JVI.00424-08.

471. Vorster, P.J., *et al.* Lim kinase 1 modulates cortical actin and cxcr4 cycling and is activated by hiv-1 to initiate viral infection. *The Journal of biological chemistry* **2011**, *286*, 12554-12564 DOI: 10.1074/jbc.M110.182238.

472. Swaine, T., *et al.* Cdc42 use in viral cell entry processes by rna viruses. *Viruses* **2015**, *7*, 6526-6536 DOI: 10.3390/v7122955.

473. Lucera, M.B., *et al.* Hiv signaling through cd4 and ccr5 activates rho family gtpases that are required for optimal infection of primary cd4+ t cells. *Retrovirology* **2017**, *14*, 4 DOI: 10.1186/s12977-017-0328-7.

474. Jimenez-Baranda, S., *et al.* Filamin-a regulates actin-dependent clustering of hiv receptors. *Nature cell biology* **2007**, *9*, 838-846 DOI: 10.1038/ncb1610.

475. Barrero-Villar, M., *et al.* Moesin is required for hiv-1-induced cd4-cxcr4 interaction, f-actin redistribution, membrane fusion and viral infection in lymphocytes. *Journal of cell science* **2009**, *122*, 103-113 DOI: 10.1242/jcs.035873.

476. Yoder, A., *et al.* Hiv envelope-cxcr4 signaling activates cofilin to overcome cortical actin restriction in resting cd4 t cells. *Cell* **2008**, *134*, 782-792 DOI: 10.1016/j.cell.2008.06.036.

477. Guo, J., *et al.* Spinoculation triggers dynamic actin and cofilin activity that facilitates hiv-1 infection of transformed and resting cd4 t cells. *Journal of virology* **2011**, *85*, 9824-9833 DOI: 10.1128/JVI.05170-11.

478. Komano, J., *et al.* Inhibiting the arp2/3 complex limits infection of both intracellular mature vaccinia virus and primate lentiviruses. *Molecular biology of the cell* **2004**, *15*, 5197-5207 DOI: 10.1091/mbc.E04-04-0279.

479. Graziano, F., *et al.* Urokinase plasminogen activator inhibits hiv virion release from macrophage-differentiated chronically infected cells via activation of rhoa and pkcepsilon. *PloS one* **2011**, *6*, e23674 DOI: 10.1371/journal.pone.0023674.

480. Carlson, L.A., *et al.* Cryo electron tomography of native hiv-1 budding sites. *PLoS pathogens* **2010**, *6*, e1001173 DOI: 10.1371/journal.ppat.1001173.

481. Rahman, S.A., *et al.* Investigating the role of f-actin in human immunodeficiency virus assembly by live-cell microscopy. *Journal of virology* **2014**, *88*, 7904-7914 DOI: 10.1128/JVI.00431-14.

482. Thomas, A., *et al.* Involvement of the rac1-irsp53-wave2-arp2/3 signaling pathway in hiv-1 gag particle release in cd4 t cells. *Journal of virology* **2015**, *89*, 8162-8181 DOI: 10.1128/JVI.00469-15.

483. Krementsov, D.N., *et al.* Tetraspanins regulate cell-to-cell transmission of hiv-1. *Retrovirology* **2009**, *6*, 64 DOI: 10.1186/1742-4690-6-64.

484. Pearce-Pratt, R., *et al.* Role of the cytoskeleton in cell-to-cell transmission of human immunodeficiency virus. *Journal of virology* **1994**, *68*, 2898-2905.

485. Stolp, B., *et al.* How hiv takes advantage of the cytoskeleton in entry and replication. *Viruses* **2011**, *3*, 293-311 DOI: 10.3390/v3040293.

486. Mege, R.M., *et al.* Regulation of cell-cell junctions by the cytoskeleton. *Current opinion in cell biology* **2006**, *18*, 541-548 DOI: 10.1016/j.ceb.2006.08.004.

487. Ritter, A.T., *et al.* The role of the cytoskeleton at the immunological synapse. *Immunological reviews* **2013**, *256*, 107-117 DOI: 10.1111/imr.12117.

488. Spear, M., *et al.* Novel anti-hiv therapeutics targeting chemokine receptors and actin regulatory pathways. *Immunological reviews* **2013**, *256*, 300-312 DOI: 10.1111/imr.12106.

489. Szklarczyk, D., *et al.* The string database in 2017: Quality-controlled protein-protein association networks, made broadly accessible. *Nucleic acids research* **2017**, *45*, D362-D368 DOI: 10.1093/nar/gkw937.

490. Mertens, A.E., *et al.* Regulation of tiam1-rac signalling. *FEBS letters* **2003**, *546*, 11-16.

491. Woollard, S.M., *et al.* Hiv-1 induces cytoskeletal alterations and rac1 activation during monocyte-blood-brain barrier interactions: Modulatory role of ccr5. *Retrovirology* **2014**, *11*, 20 DOI: 10.1186/1742-4690-11-20.

492. Pontow, S.E., *et al.* Actin cytoskeletal reorganizations and coreceptor-mediated activation of rac during human immunodeficiency virus-induced cell fusion. *Journal of virology* **2004**, *78*, 7138-7147 DOI: 10.1128/JVI.78.13.7138-7147.2004.

493. Pontow, S., *et al.* Antiviral activity of a rac gef inhibitor characterized with a sensitive hiv/siv fusion assay. *Virology* **2007**, *368*, 1-6 DOI: 10.1016/j.virol.2007.06.022.

494. Imamura, J., *et al.* Single particle tracking confirms that multivalent tat protein transduction domain-induced heparan sulfate proteoglycan cross-linkage activates

rac1 for internalization. *The Journal of biological chemistry* **2011**, *286*, 10581-10592 DOI: 10.1074/jbc.M110.187450.

495. Wu, R.F., *et al.* Human immunodeficiency virus type 1 tat regulates endothelial cell actin cytoskeletal dynamics through pak1 activation and oxidant production. *Journal of virology* **2004**, *78*, 779-789.

496. Wu, R.F., *et al.* Hiv-1 tat activates dual nox pathways leading to independent activation of erk and jnk map kinases. *The Journal of biological chemistry* **2007**, *282*, 37412-37419 DOI: 10.1074/jbc.M704481200.

497. Lu, T.C., *et al.* Hiv-1 nef disrupts the podocyte actin cytoskeleton by interacting with diaphanous interacting protein. *The Journal of biological chemistry* **2008**, *283*, 8173-8182 DOI: 10.1074/jbc.M708920200.

498. Tan, R., *et al.* Nef interaction with actin compromises human podocyte actin cytoskeletal integrity. *Experimental and molecular pathology* **2013**, *94*, 51-57 DOI: 10.1016/j.yexmp.2012.06.001.

499. Janardhan, A., *et al.* Hiv-1 nef binds the dock2-elmo1 complex to activate rac and inhibit lymphocyte chemotaxis. *PLoS biology* **2004**, *2*, E6 DOI: 10.1371/journal.pbio.0020006.

500. Chaudhry, A., *et al.* A two-pronged mechanism for hiv-1 nef-mediated endocytosis of immune costimulatory molecules cd80 and cd86. *Cell host & microbe* **2007**, *1*, 37-49 DOI: 10.1016/j.chom.2007.01.001.

501. Quaranta, M.G., *et al.* Hiv-1 nef triggers vav-mediated signaling pathway leading to functional and morphological differentiation of dendritic cells. *FASEB journal : official publication of the Federation of American Societies for Experimental Biology* **2003**, *17*, 2025-2036 DOI: 10.1096/fj.03-0272com.

502. Lu, X., *et al.* Cdc42 and rac1 are implicated in the activation of the nef-associated kinase and replication of hiv-1. *Current biology : CB* **1996**, *6*, 1677-1684.

503. Ridley, A.J. Rho gtpases and actin dynamics in membrane protrusions and vesicle trafficking. *Trends in cell biology* **2006**, *16*, 522-529 DOI: 10.1016/j.tcb.2006.08.006.

504. Chertova, E., *et al.* Proteomic and biochemical analysis of purified human immunodeficiency virus type 1 produced from infected monocyte-derived macrophages. *Journal of virology* **2006**, *80*, 9039-9052 DOI: 10.1128/JVI.01013-06.

505. Fackler, O.T., *et al.* Activation of vav by nef induces cytoskeletal rearrangements and downstream effector functions. *Molecular cell* **1999**, *3*, 729-739.

506. Mandal, D., *et al.* Analysis of 2-ltr circle junctions of viral DNA in infected cells. *Methods in molecular biology* **2009**, *485*, 73-85 DOI: 10.1007/978-1-59745-170-3_6.

507. Nikolic, D.S., *et al.* Hiv-1 activates cdc42 and induces membrane extensions in immature dendritic cells to facilitate cell-to-cell virus propagation. *Blood* **2011**, *118*, 4841-4852 DOI: 10.1182/blood-2010-09-305417.

508. Menager, M.M., *et al.* Actin dynamics regulates dendritic cell-mediated transfer of hiv-1 to t cells. *Cell* **2016**, *164*, 695-709 DOI: 10.1016/j.cell.2015.12.036.

509. Delaney, M.K., *et al.* Distinct functions of diaphanous-related formins regulate hiv-1 uncoating and transport. *Proceedings of the National Academy of Sciences of the United States of America* **2017**, *114*, E6932-E6941 DOI: 10.1073/pnas.1700247114.

510. Kanellos, G., *et al.* Cellular functions of the adf/cofilin family at a glance. *Journal of cell science* **2016**, *129*, 3211-3218 DOI: 10.1242/jcs.187849.

511. Wioland, H., *et al.* Adf/cofilin accelerates actin dynamics by severing filaments and promoting their depolymerization at both ends. *Current biology : CB* **2017**, *27*, 1956-1967 e1957 DOI: 10.1016/j.cub.2017.05.048.

512. Shekhar, S., *et al.* Enhanced depolymerization of actin filaments by adf/cofilin and monomer funneling by capping protein cooperate to accelerate barbed-end growth. *Current biology : CB* **2017**, *27*, 1990-1998 e1995 DOI: 10.1016/j.cub.2017.05.036.

513. Wu, Y., *et al.* Cofilin activation in peripheral cd4 t cells of hiv-1 infected patients: A pilot study. *Retrovirology* **2008**, *5*, 95 DOI: 10.1186/1742-4690-5-95.

514. Meng, W., *et al.* Dip (mdia interacting protein) is a key molecule regulating rho and rac in a src-dependent manner. *The EMBO journal* **2004**, *23*, 760-771 DOI: 10.1038/sj.emboj.7600095.

515. Wang, L., *et al.* Modulation of hiv-1 replication by a novel rhoa effector activity. *Journal of immunology* **2000**, *164*, 5369-5374.

516. Zhang, H., *et al.* Functional interaction between the cytoplasmic leucine-zipper domain of hiv-1 gp41 and p115-rhogef. *Current biology : CB* **1999**, *9*, 1271-1274.

517. Stolp, B., *et al.* Hiv-1 nef interferes with host cell motility by deregulation of cofilin. *Cell host & microbe* **2009**, *6*, 174-186 DOI: 10.1016/j.chom.2009.06.004.

518. Ishaq, M., *et al.* Lim kinase 1 - dependent cofilin 1 pathway and actin dynamics mediate nuclear retinoid receptor function in t lymphocytes. *BMC molecular biology* **2011**, *12*, 41 DOI: 10.1186/1471-2199-12-41.

519. Stolp, B., *et al.* Lentiviral nef proteins utilize pak2-mediated deregulation of cofilin as a general strategy to interfere with actin remodeling. *Journal of virology* **2010**, *84*, 3935-3948 DOI: 10.1128/JVI.02467-09.

520. Haller, C., *et al.* The hiv-1 pathogenicity factor nef interferes with maturation of stimulatory t-lymphocyte contacts by modulation of n-wasp activity. *The Journal of biological chemistry* **2006**, *281*, 19618-19630 DOI: 10.1074/jbc.M513802200.

521. Moarefi, I., *et al.* Activation of the src-family tyrosine kinase hck by sh3 domain displacement. *Nature* **1997**, *385*, 650-653 DOI: 10.1038/385650a0.

522. Verollet, C., *et al.* Hiv-1 reprograms the migration of macrophages. *Blood* **2015**, *125*, 1611-1622 DOI: 10.1182/blood-2014-08-596775.

523. Guiet, R., *et al.* Hematopoietic cell kinase (hck) isoforms and phagocyte duties - from signaling and actin reorganization to migration and phagocytosis. *European journal of cell biology* **2008**, *87*, 527-542 DOI: 10.1016/j.ejcb.2008.03.008.

524. Saksela, K., *et al.* Proline-rich (pxxp) motifs in hiv-1 nef bind to sh3 domains of a subset of src kinases and are required for the enhanced growth of nef+ viruses but not for down-regulation of cd4. *The EMBO journal* **1995**, *14*, 484-491.

525. Lee, C.H., *et al.* A single amino acid in the sh3 domain of hck determines its high affinity and specificity in binding to hiv-1 nef protein. *The EMBO journal* **1995**, *14*, 5006-5015.

526. Lerner, E.C., *et al.* Sh3-dependent stimulation of src-family kinase autophosphorylation without tail release from the sh2 domain in vivo. *Nature structural biology* **2002**, *9*, 365-369 DOI: 10.1038/nsb782.

527. Komuro, I., *et al.* Csf-induced and hiv-1-mediated distinct regulation of hck and c/ebpbeta represent a heterogeneous susceptibility of monocyte-derived macrophages to m-tropic hiv-1 infection. *The Journal of experimental medicine* **2003**, *198*, 443-453 DOI: 10.1084/jem.20022018.

528. Trible, R.P., *et al.* Discovery of a diaminoquinoxaline benzenesulfonamide antagonist of hiv-1 nef function using a yeast-based phenotypic screen. *Retrovirology* **2013**, *10*, 135 DOI: 10.1186/1742-4690-10-135.

529. Cornall, A., *et al.* Hiv-1 infection of t cells and macrophages are differentially modulated by virion-associated hck: A nef-dependent phenomenon. *Viruses* **2013**, *5*, 2235-2252 DOI: 10.3390/v5092235.

530. Tokunaga, K., *et al.* Enhancement of human immunodeficiency virus type 1 infectivity by nef is producer cell-dependent. *The Journal of general virology* **1998**, *79 (Pt 10)*, 2447-2453 DOI: 10.1099/0022-1317-79-10-2447.

531. Hanna, Z., *et al.* The pathogenicity of human immunodeficiency virus (hiv) type 1 nef in cd4c/hiv transgenic mice is abolished by mutation of its sh3-binding domain, and disease development is delayed in the absence of hck. *Journal of virology* **2001**, *75*, 9378-9392 DOI: 10.1128/JVI.75.19.9378-9392.2001.

532. Hioe, C.E., *et al.* Hiv envelope gp120 activates lfa-1 on cd4 t-lymphocytes and increases cell susceptibility to lfa-1-targeting leukotoxin (ltxa). *PloS one* **2011**, *6*, e23202 DOI: 10.1371/journal.pone.0023202.

533. Arthos, J., *et al.* Hiv-1 envelope protein binds to and signals through integrin alpha4beta7, the gut mucosal homing receptor for peripheral t cells. *Nature immunology* **2008**, *9*, 301-309 DOI: 10.1038/ni1566.

534. Vasiliver-Shamis, G., *et al.* Human immunodeficiency virus type 1 envelope gp120-induced partial t-cell receptor signaling creates an f-actin-depleted zone in the virological synapse. *Journal of virology* **2009**, *83*, 11341-11355 DOI: 10.1128/jvi.01440-09.

535. Roy, N.H., *et al.* Ezrin is a component of the hiv-1 virological presynapse and contributes to the inhibition of cell-cell fusion. *Journal of virology* **2014**, *88*, 7645-7658 DOI: 10.1128/JVI.00550-14.

536. Jolly, C., *et al.* Human immunodeficiency virus type 1 assembly, budding, and cell-cell spread in t cells take place in tetraspanin-enriched plasma membrane domains. *Journal of virology* **2007**, *81*, 7873-7884 DOI: 10.1128/jvi.01845-06.

537. Symeonides, M., *et al.* Evidence showing that tetraspanins inhibit hiv-1-induced cell-cell fusion at a post-hemifusion stage. *Viruses* **2014**, *6*, 1078-1090 DOI: 10.3390/v6031078.

538. Sol-Foulon, N., *et al.* Zap-70 kinase regulates hiv cell-to-cell spread and virological synapse formation. *The EMBO journal* **2007**, *26*, 516-526 DOI: 10.1038/sj.emboj.7601509.

539. Starling, S., *et al.* Lfa-1 engagement triggers t cell polarization at the hiv-1 virological synapse. *Journal of virology* **2016**, *90*, 9841-9854 DOI: 10.1128/JVI.01152-16.

540. Kumari, S., *et al.* T cell antigen receptor activation and actin cytoskeleton remodeling. *Biochimica et biophysica acta* **2014**, *1838*, 546-556 DOI: 10.1016/j.bbamem.2013.05.004.

541. Wang, J.H., *et al.* Macropinocytosis and cytoskeleton contribute to dendritic cell-mediated hiv-1 transmission to cd4+ t cells. *Virology* **2008**, *381*, 143-154 DOI: 10.1016/j.virol.2008.08.028.

542. Larsson, M., *et al.* Molecular signatures of t-cell inhibition in hiv-1 infection. *Retrovirology* **2013**, *10*, 31 DOI: 10.1186/1742-4690-10-31.

543. Choe, E.Y., *et al.* Hiv nef inhibits t cell migration. *The Journal of biological chemistry* **2002**, *277*, 46079-46084 DOI: 10.1074/jbc.M204698200.

544. Park, I.W., *et al.* Hiv-1 nef-mediated inhibition of t cell migration and its molecular determinants. *Journal of leukocyte biology* **2009**, *86*, 1171-1178 DOI: 10.1189/jlb.0409261.

545. Nobile, C., *et al.* Hiv-1 nef inhibits ruffles, induces filopodia, and modulates migration of infected lymphocytes. *Journal of virology* **2010**, *84*, 2282-2293 DOI: 10.1128/JVI.02230-09.

546. Stolp, B., *et al.* Hiv-1 nef interferes with t-lymphocyte circulation through confined environments in vivo. *Proceedings of the National Academy of Sciences of the United States of America* **2012**, *109*, 18541-18546 DOI: 10.1073/pnas.1204322109.

547. Cernuda-Morollon, E., *et al.* Rac activation by the t-cell receptor inhibits t cell migration. *PloS one* **2010**, *5*, e12393 DOI: 10.1371/journal.pone.0012393.

548. Coiras, M., *et al.* Modifications in the human t cell proteome induced by intracellular hiv-1 tat protein expression. *Proteomics* **2006**, *6 Suppl 1*, S63-73 DOI: 10.1002/pmic.200500437.

549. Lopez-Huertas, M.R., *et al.* Modifications in host cell cytoskeleton structure and function mediated by intracellular hiv-1 tat protein are greatly dependent on the second coding exon. *Nucleic acids research* **2010**, *38*, 3287-3307 DOI: 10.1093/nar/gkq037.

550. Vene, R., *et al.* Hiv-tat dependent chemotaxis and invasion, key aspects of tat mediated pathogenesis. *Clinical & experimental metastasis* **2000**, *18*, 533-538.

551. Fackler, O.T., *et al.* Modulation of the immunological synapse: A key to hiv-1 pathogenesis? *Nature reviews. Immunology* **2007**, *7*, 310-317 DOI: 10.1038/nri2041.

552. Thoulouze, M.I., *et al.* Human immunodeficiency virus type-1 infection impairs the formation of the immunological synapse. *Immunity* **2006**, *24*, 547-561 DOI: 10.1016/j.immuni.2006.02.016.

553. Vasiliver-Shamis, G., *et al.* Hiv-1 virological synapse is not simply a copycat of the immunological synapse. *Viruses* **2010**, *2*, 1239-1260 DOI: 10.3390/v2051239.

554. Abraham, L., *et al.* Hiv-1 nef: A multifaceted modulator of t cell receptor signaling. *Cell communication and signaling : CCS* **2012**, *10*, 39 DOI: 10.1186/1478-811X-10-39.

555. Collette, Y., *et al.* Physical and functional interaction of nef with lck. Hiv-1 nef-induced t-cell signaling defects. *The Journal of biological chemistry* **1996**, *271*, 6333-6341.

556. Haller, C., *et al.* Hiv-1 nef employs two distinct mechanisms to modulate lck subcellular localization and tcr induced actin remodeling. *PloS one* **2007**, *2*, e1212 DOI: 10.1371/journal.pone.0001212.

557. Pan, X., *et al.* Hiv-1 nef compensates for disorganization of the immunological synapse by inducing trans-golgi network-associated lck signaling. *Blood* **2012**, *119*, 786-797 DOI: 10.1182/blood-2011-08-373209.

558. Rudolph, J.M., *et al.* Inhibition of t-cell receptor-induced actin remodeling and relocalization of lck are evolutionarily conserved activities of lentiviral nef proteins. *Journal of virology* **2009**, *83*, 11528-11539 DOI: 10.1128/JVI.01423-09.

559. Debaisieux, S., *et al.* Hiv-1 tat inhibits phagocytosis by preventing the recruitment of cdc42 to the phagocytic cup. *Nature communications* **2015**, *6*, 6211 DOI: 10.1038/ncomms7211.

560. Raborn, E.S., *et al.* Cannabinoid inhibits hiv-1 tat-stimulated adhesion of human monocyte-like cells to extracellular matrix proteins. *Life sciences* **2014**, *104*, 15-23 DOI: 10.1016/j.lfs.2014.04.008.

561. Lafrenie, R.M., *et al.* Hiv-1-tat modulates the function of monocytes and alters their interactions with microvessel endothelial cells. A mechanism of hiv pathogenesis. *Journal of immunology* **1996**, *156*, 1638-1645.

562. Matzen, K., *et al.* Hiv-1 tat increases the adhesion of monocytes and t-cells to the endothelium in vitro and in vivo: Implications for aids-associated vasculopathy. *Virus research* **2004**, *104*, 145-155 DOI: 10.1016/j.virusres.2004.04.001.

563. Lafrenie, R.M., *et al.* Hiv-1-tat protein promotes chemotaxis and invasive behavior by monocytes. *Journal of immunology* **1996**, *157*, 974-977.

564. Pieper, G.M., *et al.* Transfection of human endothelial cells with hiv-1 tat gene activates nf-kappa b and enhances monocyte adhesion. *American journal of physiology. Heart and circulatory physiology* **2002**, *283*, H2315-2321 DOI: 10.1152/ajpheart.00469.2002.

565. de Paulis, A., *et al.* Tat protein is an hiv-1-encoded beta-chemokine homolog that promotes migration and up-regulates ccr3 expression on human fc epsilon ri+ cells. *Journal of immunology* **2000**, *165*, 7171-7179.

566. Prasad, A., *et al.* Slit2n/robo1 inhibit hiv-gp120-induced migration and podosome formation in immature dendritic cells by sequestering lsp1 and wasp. *PloS one* **2012**, *7*, e48854 DOI: 10.1371/journal.pone.0048854.

567. Anand, A.R., *et al.* Hiv-1 gp120-induced migration of dendritic cells is regulated by a novel kinase cascade involving pyk2, p38 map kinase, and lsp1. *Blood* **2009**, *114*, 3588-3600 DOI: 10.1182/blood-2009-02-206342.

568. Welch, M.D. Why should cell biologists study microbial pathogens? *Molecular biology of the cell* **2015**, *26*, 4295-4301 DOI: 10.1091/mbc.E15-03-0144.

569. McAllery, S.A., *et al.* The feasibility of incorporating vpx into lentiviral gene therapy vectors. *Molecular therapy. Methods & clinical development* **2016**, *5*, 16066 DOI: 10.1038/mtm.2016.66.

570. Adachi, A., *et al.* Production of acquired immunodeficiency syndrome-associated retrovirus in human and nonhuman cells transfected with an infectious molecular clone. *Journal of virology* **1986**, *59*, 284-291.

571. Hubner, W., *et al.* Sequence of human immunodeficiency virus type 1 (hiv-1) gag localization and oligomerization monitored with live confocal imaging of a replication-competent, fluorescently tagged hiv-1. *Journal of virology* **2007**, *81*, 12596-12607 DOI: 10.1128/jvi.01088-07.

572. Gray, L., *et al.* Tissue-specific sequence alterations in the human immunodeficiency virus type 1 envelope favoring ccr5 usage contribute to persistence of dual-tropic virus in the brain. *Journal of virology* **2009**, *83*, 5430-5441 DOI: 10.1128/jvi.02648-08.

573. Gomez, T.S., *et al.* Formins regulate the actin-related protein 2/3 complex-independent polarization of the centrosome to the immunological synapse. *Immunity* **2007**, *26*, 177-190 DOI: 10.1016/j.immuni.2007.01.008.

574. Sundstrom, C., *et al.* Establishment and characterization of a human histiocytic lymphoma cell line (u-937). *International journal of cancer* **1976**, *17*, 565-577 DOI: 10.1002/ijc.2910170504.

575. Schneider, U., *et al.* Characterization of ebv-genome negative "null" and "t" cell lines derived from children with acute lymphoblastic leukemia and leukemic transformed

non-hodgkin lymphoma. *International journal of cancer* **1977**, *19*, 621-626 DOI: 10.1002/ijc.2910190505.

576. Platt, E.J., *et al.* Effects of ccr5 and cd4 cell surface concentrations on infections by macrophagetropic isolates of human immunodeficiency virus type 1. *Journal of virology* **1998**, *72*, 2855-2864.

577. Wei, X., *et al.* Emergence of resistant human immunodeficiency virus type 1 in patients receiving fusion inhibitor (t-20) monotherapy. *Antimicrobial agents and chemotherapy* **2002**, *46*, 1896-1905 DOI: 10.1128/aac.46.6.1896-1905.2002.

578. Robinson, P.S., *et al.* Kidney-specific enzyme expression by human kidney cell lines generated through oncogene transfection. *Journal of cellular physiology* **1991**, *148*, 54-59 DOI: 10.1002/jcp.1041480107.

579. DuBridge, R.B., *et al.* Analysis of mutation in human cells by using an epstein-barr virus shuttle system. *Molecular and cellular biology* **1987**, *7*, 379-387 DOI: 10.1128/mcb.7.1.379.

580. Sarzotti-Kelsoe, M., *et al.* Optimization and validation of the tzm-bl assay for standardized assessments of neutralizing antibodies against hiv-1. *Journal of immunological methods* **2014**, *409*, 131-146 DOI: 10.1016/j.jim.2013.11.022.

581. Concordet, J.P., *et al.* Crispor: Intuitive guide selection for crispr/cas9 genome editing experiments and screens. *Nucleic acids research* **2018**, *46*, W242-w245 DOI: 10.1093/nar/gky354.

582. Hsu, P.D., *et al.* DNA targeting specificity of rna-guided cas9 nucleases. *Nature biotechnology* **2013**, *31*, 827-832 DOI: 10.1038/nbt.2647.

583. Huston, N.C., *et al.* Identification of guide-intrinsic determinants of cas9 specificity. *The CRISPR journal* **2019**, *2*, 172-185 DOI: 10.1089/crispr.2019.0009.

584. Sanjana, N.E., *et al.* Improved vectors and genome-wide libraries for crispr screening. *Nature methods* **2014**, *11*, 783-784 DOI: 10.1038/nmeth.3047.

585. Anderson, D.J. Modeling mucosal cell-associated hiv type 1 transmission in vitro. *The Journal of infectious diseases* **2014**, *210 Suppl 3*, S648-653 DOI: 10.1093/infdis/jiu537.

586. Ruggiero, E., *et al.* Virological consequences of early events following cell-cell contact between human immunodeficiency virus type 1-infected and uninfected cd4+ cells. *Journal of virology* **2008**, *82*, 7773-7789 DOI: 10.1128/jvi.00695-08.

587. Dale, B.M., *et al.* Cell-to-cell transfer of hiv-1 via virological synapses leads to endosomal virion maturation that activates viral membrane fusion. *Cell host & microbe* **2011**, *10*, 551-562 DOI: 10.1016/j.chom.2011.10.015.

588. Nagaraja, T., *et al.* The adaptor protein slp-76 regulates hiv-1 release and cell-to-cell transmission in t cells. *Journal of immunology* **2012**, *188*, 2769-2777 DOI: 10.4049/jimmunol.1102106.

589. Tardif, M.R., *et al.* Lfa-1 antagonists as agents limiting human immunodeficiency virus type 1 infection and transmission and potentiating the effect of the fusion inhibitor t-20. *Antimicrobial agents and chemotherapy* **2009**, *53*, 4656-4666 DOI: 10.1128/AAC.00117-09.

590. Jolly, C., *et al.* The regulated secretory pathway in cd4(+) t cells contributes to human immunodeficiency virus type-1 cell-to-cell spread at the virological synapse. *PLoS pathogens* **2011**, *7*, e1002226 DOI: 10.1371/journal.ppat.1002226.

591. Bosch, B., *et al.* A clathrin-dynamin-dependent endocytic pathway for the uptake of hiv-1 by direct t cell-t cell transmission. *Antiviral research* **2008**, *80*, 185-193 DOI: 10.1016/j.antiviral.2008.06.004.

592. Miyauchi, K., *et al.* Hiv enters cells via endocytosis and dynamin-dependent fusion with endosomes. *Cell* **2009**, *137*, 433-444 DOI: 10.1016/j.cell.2009.02.046.

593. Jones, D.M., *et al.* Dynamin-2 stabilizes the hiv-1 fusion pore with a low oligomeric state. *Cell reports* **2017**, *18*, 443-453 DOI: 10.1016/j.celrep.2016.12.032.

594. Chanput, W., *et al.* Thp-1 and u937 cells. In *The impact of food bioactives on health: In vitro and ex vivo models*, Verhoeckx, K.; Cotter, P.; Lopez-Exposito, I.; Kleiveland, C.; Lea, T.; Mackie, A.; Requena, T.; Swiatecka, D.; Wichers, H., Eds. Springer

Copyright 2015, The Author(s). Cham (CH), 2015; pp 147-159.

595. Liu, L., *et al.* The antiatherogenic potential of oat phenolic compounds. *Atherosclerosis* **2004**, *175*, 39-49 DOI: 10.1016/j.atherosclerosis.2004.01.044.

596. Liu, H., *et al.* Macrophage-derived mcpip1 mediates silica-induced pulmonary fibrosis via autophagy. *Particle and fibre toxicology* **2016**, *13*, 55 DOI: 10.1186/s12989-016-0167-z.

597. Phillips, D.M. The role of cell-to-cell transmission in hiv infection. *Aids* **1994**, *8*, 719-731 DOI: 10.1097/00002030-199406000-00001.

598. Wu, C., *et al.* Biogps: Building your own mash-up of gene annotations and expression profiles. *Nucleic acids research* **2016**, *44*, D313-316 DOI: 10.1093/nar/gkv1104.

599. Abraham, R.T., *et al.* Jurkat t cells and development of the t-cell receptor signalling paradigm. *Nature reviews. Immunology* **2004**, *4*, 301-308 DOI: 10.1038/nri1330.

600. Chen, J.L., *et al.* [advances in application of jurkat cell model in research on infectious diseases]. *Zhongguo dang dai er ke za zhi = Chinese journal of contemporary pediatrics* **2018**, *20*, 236-242.

601. Ashkenazi, A., *et al.* Viral envelope protein folding and membrane hemifusion are enhanced by the conserved loop region of hiv-1 gp41. *FASEB journal : official publication of the Federation of American Societies for Experimental Biology* **2011**, *25*, 2156-2166 DOI: 10.1096/fj.10-175752.

602. Choudhry, V., *et al.* Increased efficacy of hiv-1 neutralization by antibodies at low ccr5 surface concentration. *Biochemical and biophysical research communications* **2006**, *348*, 1107-1115 DOI: 10.1016/j.bbrc.2006.07.163.

603. Montefiori, D.C. Measuring hiv neutralization in a luciferase reporter gene assay. *Methods in molecular biology* **2009**, *485*, 395-405 DOI: 10.1007/978-1-59745-170-3_26.

604. Schober, P., *et al.* Correlation coefficients: Appropriate use and interpretation. *Anesthesia and analgesia* **2018**, *126*, 1763-1768 DOI: 10.1213/ane.0000000000002864.

605. Kerppola, T.K. Bimolecular fluorescence complementation (bifc) analysis as a probe of protein interactions in living cells. *Annual review of biophysics* **2008**, *37*, 465-487 DOI: 10.1146/annurev.biophys.37.032807.125842.

606. Chen, C., *et al.* Association of gag multimers with filamentous actin during equine infectious anemia virus assembly. *Current HIV research* **2007**, *5*, 315-323.

607. Gorry, P.R., *et al.* Macrophage tropism of human immunodeficiency virus type 1 isolates from brain and lymphoid tissues predicts neurotropism independent of

coreceptor specificity. *Journal of virology* **2001**, *75*, 10073-10089 DOI: 10.1128/jvi.75.21.10073-10089.2001.

608. Ibarrondo, F.J., *et al.* Hiv type 1 gag and nucleocapsid proteins: Cytoskeletal localization and effects on cell motility. *AIDS research and human retroviruses* **2001**, *17*, 1489-1500 DOI: 10.1089/08892220152644197.

609. Perrin-Tricaud, C., *et al.* Tagging the human immunodeficiency virus gag protein with green fluorescent protein. Minimal evidence for colocalisation with actin. *Virology* **1999**, *255*, 20-25 DOI: 10.1006/viro.1998.9573.

610. Stevenson, B.R., *et al.* Concentration-dependent effects of cytochalasin d on tight junctions and actin filaments in mdck epithelial cells. *Journal of cell science* **1994**, *107 (Pt 3)*, 367-375.

611. Cashin, K., *et al.* Alternative coreceptor requirements for efficient ccr5- and cxcr4-mediated hiv-1 entry into macrophages. *Journal of virology* **2011**, *85*, 10699-10709 DOI: 10.1128/jvi.05510-11.

612. Steckbeck, J.D., *et al.* Highly conserved structural properties of the c-terminal tail of hiv-1 gp41 protein despite substantial sequence variation among diverse clades: Implications for functions in viral replication. *The Journal of biological chemistry* **2011**, *286*, 27156-27166 DOI: 10.1074/jbc.M111.258855.

613. Sander, J.D., *et al.* Crispr-cas systems for editing, regulating and targeting genomes. *Nature biotechnology* **2014**, *32*, 347-355 DOI: 10.1038/nbt.2842.

614. Lino, C.A., *et al.* Delivering crispr: A review of the challenges and approaches. *Drug delivery* **2018**, *25*, 1234-1257 DOI: 10.1080/10717544.2018.1474964.

615. Cong, L., *et al.* Multiplex genome engineering using crispr/cas systems. *Science* **2013**, *339*, 819-823 DOI: 10.1126/science.1231143.

616. Joung, J., *et al.* Genome-scale crispr-cas9 knockout and transcriptional activation screening. *Nature protocols* **2017**, *12*, 828-863 DOI: 10.1038/nprot.2017.016.

617. Mathieson, T., *et al.* Systematic analysis of protein turnover in primary cells. *Nature communications* **2018**, *9*, 689 DOI: 10.1038/s41467-018-03106-1.

618. Guschin, D.Y., *et al.* A rapid and general assay for monitoring endogenous gene modification. *Methods in molecular biology* **2010**, *649*, 247-256 DOI: 10.1007/978-1-60761-753-2_15.

619. Doudna, J.A., *et al.* Methods in enzymology. The use of crispr/cas9, zfns, and talens in generating site-specific genome alterations. Preface. *Methods in enzymology* **2014**, *546*, xix-xx DOI: 10.1016/b978-0-12-801185-0.09983-9.

620. Didsbury, J., *et al.* Rac, a novel ras-related family of proteins that are botulinum toxin substrates. *The Journal of biological chemistry* **1989**, *264*, 16378-16382.

621. Troeger, A., *et al.* Hematopoietic-specific rho gtpases rac2 and rhoh and human blood disorders. *Experimental cell research* **2013**, *319*, 2375-2383 DOI: 10.1016/j.yexcr.2013.07.002.

622. Roberts, A.W., *et al.* Deficiency of the hematopoietic cell-specific rho family gtpase rac2 is characterized by abnormalities in neutrophil function and host defense. *Immunity* **1999**, *10*, 183-196 DOI: 10.1016/s1074-7613(00)80019-9.

623. Sugihara, K., *et al.* Rac1 is required for the formation of three germ layers during gastrulation. *Oncogene* **1998**, *17*, 3427-3433 DOI: 10.1038/sj.onc.1202595.

624. Fan, L., *et al.* The small rho gtpase rif and actin cytoskeletal remodelling. *Biochemical Society transactions* **2012**, *40*, 268-272 DOI: 10.1042/bst20110625.

625. Goggs, R., *et al.* The small gtpase rif is dispensable for platelet filopodia generation in mice. *PloS one* **2013**, *8*, e54663 DOI: 10.1371/journal.pone.0054663.

626. Hung, C.H., *et al.* Hiv-1 nef assembles a src family kinase-zap-70/syk-pi3k cascade to downregulate cell-surface mhc-i. *Cell host & microbe* **2007**, *1*, 121-133 DOI: 10.1016/j.chom.2007.03.004.

627. Mocsai, A., *et al.* The syk tyrosine kinase: A crucial player in diverse biological functions. *Nature reviews. Immunology* **2010**, *10*, 387-402 DOI: 10.1038/nri2765.

628. Schnoor, M., *et al.* Cortactin: Cell functions of a multifaceted actin-binding protein. *Trends in cell biology* **2018**, *28*, 79-98 DOI: 10.1016/j.tcb.2017.10.009.

629. Ammer, A.G., *et al.* Cortactin branches out: Roles in regulating protrusive actin dynamics. *Cell motility and the cytoskeleton* **2008**, *65*, 687-707 DOI: 10.1002/cm.20296.

630. Weed, S.A., *et al.* Cortactin localization to sites of actin assembly in lamellipodia requires interactions with f-actin and the arp2/3 complex. *The Journal of cell biology* **2000**, *151*, 29-40 DOI: 10.1083/jcb.151.1.29.

631. Daly, R.J. Cortactin signalling and dynamic actin networks. *The Biochemical journal* **2004**, *382*, 13-25 DOI: 10.1042/bj20040737.

632. Ritchie, C., *et al.* Analysis of hiv-1 gag protein interactions via biotin ligase tagging. *Journal of virology* **2015**, *89*, 3988-4001 DOI: 10.1128/JVI.03584-14.

633. Gomez, T.S., *et al.* Hs1 functions as an essential actin-regulatory adaptor protein at the immune synapse. *Immunity* **2006**, *24*, 741-752 DOI: 10.1016/j.immuni.2006.03.022.

634. Tremblay, M.J., *et al.* The acquisition of host-encoded proteins by nascent hiv-1. *Immunology today* **1998**, *19*, 346-351.

635. Gatfield, J., *et al.* Association of the leukocyte plasma membrane with the actin cytoskeleton through coiled coil-mediated trimeric coronin 1 molecules. *Molecular biology of the cell* **2005**, *16*, 2786-2798 DOI: 10.1091/mbc.e05-01-0042.

636. Zhang, L., *et al.* Proteomic analysis of pbmcs: Characterization of potential hiv-associated proteins. *Proteome science* **2010**, *8*, 12 DOI: 10.1186/1477-5956-8-12.

637. Mugnier, B., *et al.* Coronin-1a links cytoskeleton dynamics to tcr alpha beta-induced cell signaling. *PloS one* **2008**, *3*, e3467 DOI: 10.1371/journal.pone.0003467.

638. Mace, E.M., *et al.* Lytic immune synapse function requires filamentous actin deconstruction by coronin 1a. *Proceedings of the National Academy of Sciences of the United States of America* **2014**, *111*, 6708-6713 DOI: 10.1073/pnas.1314975111.

639. Mercenne, G., *et al.* Angiomotin functions in hiv-1 assembly and budding. *eLife* **2015**, *4*, DOI: 10.7554/eLife.03778.

640. Ernkvist, M., *et al.* P130-angiomotin associates to actin and controls endothelial cell shape. *The FEBS journal* **2006**, *273*, 2000-2011 DOI: 10.1111/j.1742-4658.2006.05216.x.

641. Schafer, D.A., *et al.* Dynamics of capping protein and actin assembly in vitro: Uncapping barbed ends by polyphosphoinositides. *The Journal of cell biology* **1996**, *135*, 169-179 DOI: 10.1083/jcb.135.1.169.

642. Bombardier, J.P., *et al.* Single-molecule visualization of a formin-capping protein 'decision complex' at the actin filament barbed end. *Nature communications* **2015**, *6*, 8707 DOI: 10.1038/ncomms9707.

643. Barrero, C.A., *et al.* Hiv-1 vpr modulates macrophage metabolic pathways: A silac-based quantitative analysis. *PloS one* **2013**, *8*, e68376 DOI: 10.1371/journal.pone.0068376.

644. Hubberstey, A.V., *et al.* Cyclase-associated proteins: Capacity for linking signal transduction and actin polymerization. *FASEB journal : official publication of the Federation of American Societies for Experimental Biology* **2002**, *16*, 487-499 DOI: 10.1096/fj.01-0659rev.

645. Ono, S. The role of cyclase-associated protein in regulating actin filament dynamics - more than a monomer-sequestration factor. *Journal of cell science* **2013**, *126*, 3249-3258 DOI: 10.1242/jcs.128231.

646. Hubberstey, A., *et al.* Mammalian cap interacts with cap, cap2, and actin. *Journal of cellular biochemistry* **1996**, *61*, 459-466 DOI: 10.1002/(sici)1097-4644(19960601)61:3%3c459::aid-jcb13%3e3.0.co;2-e.

647. Santos, S., *et al.* Virus-producing cells determine the host protein profiles of hiv-1 virion cores. *Retrovirology* **2012**, *9*, 65 DOI: 10.1186/1742-4690-9-65.

648. van Buul, J.D., *et al.* Rhog regulates endothelial apical cup assembly downstream from icam1 engagement and is involved in leukocyte trans-endothelial migration. *The Journal of cell biology* **2007**, *178*, 1279-1293 DOI: 10.1083/jcb.200612053.

649. Schaefer, A., *et al.* Actin-binding proteins differentially regulate endothelial cell stiffness, icam-1 function and neutrophil transmigration. *Journal of cell science* **2014**, *127*, 4470-4482 DOI: 10.1242/jcs.154708.

650. Luo, Y., *et al.* Hiv-host interactome revealed directly from infected cells. *Nature microbiology* **2016**, *1*, 16068 DOI: 10.1038/nmicrobiol.2016.68.

651. Okada, M. Regulation of the src family kinases by csk. *International journal of biological sciences* **2012**, *8*, 1385-1397 DOI: 10.7150/ijbs.5141.

652. Chan, E.Y., *et al.* Quantitative analysis of human immunodeficiency virus type 1-infected cd4+ cell proteome: Dysregulated cell cycle progression and nuclear transport coincide with robust virus production. *Journal of virology* **2007**, *81*, 7571-7583 DOI: 10.1128/JVI.00288-07.

653. Jockusch, B.M., *et al.* The profile of profilins. *Reviews of physiology, biochemistry and pharmacology* **2007**, *159*, 131-149 DOI: 10.1007/112_2007_704.

654. Alkam, D., *et al.* Profilin1 biology and its mutation, actin(g) in disease. *Cellular and molecular life sciences : CMLS* **2017**, *74*, 967-981 DOI: 10.1007/s00018-016-2372-1.

655. Bear, J.E., *et al.* Ena/vasp: Towards resolving a pointed controversy at the barbed end. *Journal of cell science* **2009**, *122*, 1947-1953 DOI: 10.1242/jcs.038125.

656. Dominguez, R. Actin filament nucleation and elongation factors--structure-function relationships. *Critical reviews in biochemistry and molecular biology* **2009**, *44*, 351-366 DOI: 10.3109/10409230903277340.

657. Schirenbeck, A., *et al.* The bundling activity of vasodilator-stimulated phosphoprotein is required for filopodium formation. *Proceedings of the National Academy of Sciences of the United States of America* **2006**, *103*, 7694-7699 DOI: 10.1073/pnas.0511243103.

658. Applewhite, D.A., *et al.* Ena/vasp proteins have an anti-capping independent function in filopodia formation. *Molecular biology of the cell* **2007**, *18*, 2579-2591 DOI: 10.1091/mbc.e06-11-0990.

659. Nolz, J.C., *et al.* The wave2 complex regulates actin cytoskeletal reorganization and crac-mediated calcium entry during t cell activation. *Current biology : CB* **2006**, *16*, 24-34 DOI: 10.1016/j.cub.2005.11.036.

660. Litschko, C., *et al.* Differential functions of wave regulatory complex subunits in the regulation of actin-driven processes. *European journal of cell biology* **2017**, *96*, 715-727 DOI: 10.1016/j.ejcb.2017.08.003.

661. Hart, T., *et al.* High-resolution crispr screens reveal fitness genes and genotype-specific cancer liabilities. *Cell* **2015**, *163*, 1515-1526 DOI: 10.1016/j.cell.2015.11.015.

662. Flint, M., *et al.* A genome-wide crispr screen identifies n-acetylglucosamine-1-phosphate transferase as a potential antiviral target for ebola virus. *Nature communications* **2019**, *10*, 285 DOI: 10.1038/s41467-018-08135-4.

663. Hart, T., *et al.* Evaluation and design of genome-wide crispr/spcas9 knockout screens. *G3 (Bethesda, Md.)* **2017**, *7*, 2719-2727 DOI: 10.1534/g3.117.041277.

664. Poirier, J.T. Crispr libraries and screening. *Progress in molecular biology and translational science* **2017**, *152*, 69-82 DOI: 10.1016/bs.pmbts.2017.10.002.

665. Rees, M. A design study of a system for detecting extraterrestrial intelligent life University, S., Ed. 1971.

666. Yu, X., *et al.* Icam-1 in hiv infection and underlying mechanisms. *Cytokine* **2019**, *125*, 154830 DOI: 10.1016/j.cyto.2019.154830.

667. Sanders, R.W., *et al.* Differential transmission of human immunodeficiency virus type 1 by distinct subsets of effector dendritic cells. *Journal of virology* **2002**, *76*, 7812-7821.

668. Pelchen-Matthews, A., *et al.* Beta2 integrin adhesion complexes maintain the integrity of hiv-1 assembly compartments in primary macrophages. *Traffic* **2012**, *13*, 273-291 DOI: 10.1111/j.1600-0854.2011.01306.x.

669. Lachambre, S., *et al.* Preliminary characterisation of nanotubes connecting t-cells and their use by hiv-1. *Biology of the cell* **2014**, *106*, 394-404 DOI: 10.1111/boc.201400037.

670. Ferron, F., *et al.* Structural basis for the recruitment of profilin-actin complexes during filament elongation by ena/vasp. *The EMBO journal* **2007**, *26*, 4597-4606 DOI: 10.1038/sj.emboj.7601874.

671. Courtemanche, N. Mechanisms of formin-mediated actin assembly and dynamics. *Biophysical reviews* **2018**, *10*, 1553-1569 DOI: 10.1007/s12551-018-0468-6.

672. Barzik, M., *et al.* Ena/vasp proteins enhance actin polymerization in the presence of barbed end capping proteins. *The Journal of biological chemistry* **2005**, *280*, 28653-28662 DOI: 10.1074/jbc.M503957200.

673. Stradal, T.E., *et al.* Regulation of actin dynamics by wasp and wave family proteins. *Trends in cell biology* **2004**, *14*, 303-311 DOI: 10.1016/j.tcb.2004.04.007.

674. Kelly, M.L., *et al.* Mouse models of pak function. *Cellular logistics* **2012**, *2*, 84-88 DOI: 10.4161/cl.21381.

675. Snapper, S.B., *et al.* N-wasp deficiency reveals distinct pathways for cell surface projections and microbial actin-based motility. *Nature cell biology* **2001**, *3*, 897-904 DOI: 10.1038/ncb1001-897.

676. Shinya, E., *et al.* Hemopoietic cell kinase (hck) and p21-activated kinase 2 (pak2) are involved in the down-regulation of cd1a lipid antigen presentation by hiv-1 nef in dendritic cells. *Virology* **2016**, *487*, 285-295 DOI: 10.1016/j.virol.2015.10.023.

677. Zoughlami, Y., *et al.* Regulation of cxcr4 conformation by the small gtpase rac1: Implications for hiv infection. *Blood* **2012**, *119*, 2024-2032 DOI: 10.1182/blood-2011-06-364828.

678. Fomina, A.F., *et al.* Regulation of membrane trafficking and subcellular organization of endocytic compartments revealed with fm1-43 in resting and activated human t cells. *Experimental cell research* **2003**, *291*, 150-166 DOI: 10.1016/s0014-4827(03)00372-0.

679. Pelchen-Matthews, A., *et al.* The protein tyrosine kinase p56lck inhibits cd4 endocytosis by preventing entry of cd4 into coated pits. *The Journal of cell biology* **1992**, *117*, 279-290 DOI: 10.1083/jcb.117.2.279.

680. Schmedt, C., *et al.* Csk controls antigen receptor-mediated development and selection of t-lineage cells. *Nature* **1998**, *394*, 901-904 DOI: 10.1038/29802.

681. Grishkan, I.V., *et al.* Helper t cells down-regulate cd4 expression upon chronic stimulation giving rise to double-negative t cells. *Cellular immunology* **2013**, *284*, 68-74 DOI: 10.1016/j.cellimm.2013.06.011.

682. Phipps, D.J., *et al.* Hiv infection in vitro enhances the activity of src-family protein tyrosine kinases. *Aids* **1996**, *10*, 1191-1198.

683. McCarthy, S.D., *et al.* C-src protein tyrosine kinase regulates early hiv-1 infection post-entry. *Aids* **2016**, *30*, 849-858 DOI: 10.1097/qad.0000000000001028.

684. Pan, S., *et al.* Involvement of the conserved adaptor protein alix in actin cytoskeleton assembly. *The Journal of biological chemistry* **2006**, *281*, 34640-34650 DOI: 10.1074/jbc.M602263200.

685. Addi, C., *et al.* Actin, microtubule, septin and escrt filament remodeling during late steps of cytokinesis. *Current opinion in cell biology* **2018**, *50*, 27-34 DOI: 10.1016/j.ceb.2018.01.007.

686. Hogue, I.B., *et al.* Gag induces the coalescence of clustered lipid rafts and tetraspanin-enriched microdomains at hiv-1 assembly sites on the plasma membrane. *Journal of virology* **2011**, *85*, 9749-9766 DOI: 10.1128/jvi.00743-11.

687. Grover, J.R., *et al.* Roles played by capsid-dependent induction of membrane curvature and gag-escrt interactions in tetherin recruitment to hiv-1 assembly sites. *Journal of virology* **2013**, *87*, 4650-4664 DOI: 10.1128/jvi.03526-12.

688. von Schwedler, U.K., *et al.* Functional surfaces of the human immunodeficiency virus type 1 capsid protein. *Journal of virology* **2003**, *77*, 5439-5450 DOI: 10.1128/jvi.77.9.5439-5450.2003.

689. Narayan, K., *et al.* Multi-resolution correlative focused ion beam scanning electron microscopy: Applications to cell biology. *Journal of structural biology* **2014**, *185*, 278-284 DOI: 10.1016/j.jsb.2013.11.008.

690. Narayan, K., *et al.* Focused ion beams in biology. *Nature methods* **2015**, *12*, 1021-1031 DOI: 10.1038/nmeth.3623.

691. Valcu, M., *et al.* Data transformation practices in biomedical sciences. *Nature methods* **2011**, *8*, 104-105 DOI: 10.1038/nmeth0211-104.

692. Fedorov, A., *et al.* 3d slicer as an image computing platform for the quantitative imaging network. *Magnetic resonance imaging* **2012**, *30*, 1323-1341 DOI: 10.1016/j.mri.2012.05.001.

693. Bishop, A.L., *et al.* Rho gtpases and their effector proteins. *The Biochemical journal* **2000**, *348 Pt 2*, 241-255.

694. Smith, J.M., *et al.* Iqgaps choreograph cellular signaling from the membrane to the nucleus. *Trends in cell biology* **2015**, *25*, 171-184 DOI: 10.1016/j.tcb.2014.12.005.

695. Abel, A.M., *et al.* Iqgap1: Insights into the function of a molecular puppeteer. *Molecular immunology* **2015**, *65*, 336-349 DOI: 10.1016/j.molimm.2015.02.012.

696. Malarkannan, S., *et al.* Iqgap1: A regulator of intracellular spacetime relativity. *Journal of immunology* **2012**, *188*, 2057-2063 DOI: 10.4049/jimmunol.1102439.

697. Li, S., *et al.* Gastric hyperplasia in mice lacking the putative cdc42 effector iqgap1. *Molecular and cellular biology* **2000**, *20*, 697-701 DOI: 10.1128/mcb.20.2.697-701.2000.

698. Wang, S., *et al.* Iqgap3, a novel effector of rac1 and cdc42, regulates neurite outgrowth. *Journal of cell science* **2007**, *120*, 567-577 DOI: 10.1242/jcs.03356.

699. Kim, H., *et al.* Iqgap1 in microbial pathogenesis: Targeting the actin cytoskeleton. *FEBS letters* **2011**, *585*, 723-729 DOI: 10.1016/j.febslet.2011.01.041.

700. Watanabe, T., *et al.* Iqgaps as key regulators of actin-cytoskeleton dynamics. *Cell structure and function* **2015**, *40*, 69-77 DOI: 10.1247/csf.15003.

701. Milev, M.P., *et al.* Characterization of staufen1 ribonucleoproteins by mass spectrometry and biochemical analyses reveal the presence of diverse host proteins associated with human immunodeficiency virus type 1. *Frontiers in microbiology* **2012**, *3*, 367 DOI: 10.3389/fmicb.2012.00367.

702. Mateer, S.C., *et al.* Actin filament binding by a monomeric iqgap1 fragment with a single calponin homology domain. *Cell motility and the cytoskeleton* **2004**, *58*, 231-241 DOI: 10.1002/cm.20013.

703. Adachi, M., *et al.* Involvement of iqgap family proteins in the regulation of mammalian cell cytokinesis. *Genes to cells : devoted to molecular & cellular mechanisms* **2014**, *19*, 803-820 DOI: 10.1111/gtc.12179.

704. Hedman, A.C., *et al.* The biology of iqgap proteins: Beyond the cytoskeleton. *EMBO reports* **2015**, *16*, 427-446 DOI: 10.15252/embr.201439834.

705. Hart-Smith, G., *et al.* Detection and characterization of low abundance glycopeptides via higher-energy c-trap dissociation and orbitrap mass analysis. *Journal of the American Society for Mass Spectrometry* **2012**, *23*, 124-140 DOI: 10.1007/s13361-011-0273-y.

706. Weiss, W.A., *et al.* Recognizing and exploiting differences between rnai and small-molecule inhibitors. *Nature chemical biology* **2007**, *3*, 739-744 DOI: 10.1038/nchembio1207-739.

707. Pedersen, E., *et al.* Rho gtpase function in development: How in vivo models change our view. *Experimental cell research* **2012**, *318*, 1779-1787 DOI: 10.1016/j.yexcr.2012.05.004.

708. Balasubramanian, M.K., *et al.* The schizosaccharomyces pombe cdc3+ gene encodes a profilin essential for cytokinesis. *The Journal of cell biology* **1994**, *125*, 1289-1301 DOI: 10.1083/jcb.125.6.1289.

709. Haugwitz, M., *et al.* Dictyostelium amoebae that lack g-actin-sequestering profilins show defects in f-actin content, cytokinesis, and development. *Cell* **1994**, *79*, 303-314 DOI: 10.1016/0092-8674(94)90199-6.

710. Severson, A.F., *et al.* A formin homology protein and a profilin are required for cytokinesis and arp2/3-independent assembly of cortical microfilaments in c. Elegans. *Current biology : CB* **2002**, *12*, 2066-2075 DOI: 10.1016/s0960-9822(02)01355-6.

711. Witke, W., *et al.* Profilin i is essential for cell survival and cell division in early mouse development. *Proceedings of the National Academy of Sciences of the United States of America* **2001**, *98*, 3832-3836 DOI: 10.1073/pnas.051515498.

712. Ding, Z., *et al.* Silencing profilin-1 inhibits endothelial cell proliferation, migration and cord morphogenesis. *Journal of cell science* **2006**, *119*, 4127-4137 DOI: 10.1242/jcs.03178.

713. Gouin, E., *et al.* Actin-based motility of intracellular pathogens. *Current opinion in microbiology* **2005**, *8*, 35-45 DOI: 10.1016/j.mib.2004.12.013.

714. Small, J.V. Pushing with actin: From cells to pathogens. *Biochemical Society transactions* **2015**, *43*, 84-91 DOI: 10.1042/bst20140184.

715. Damsky, C.H., *et al.* Is there a role for actin in virus budding? *The Journal of cell biology* **1977**, *75*, 593-605.

716. Jouvenet, N., *et al.* African swine fever virus induces filopodia-like projections at the plasma membrane. *Cellular microbiology* **2006**, *8*, 1803-1811 DOI: 10.1111/j.1462-5822.2006.00750.x.

717. Kolesnikova, L., *et al.* Budding of marburgvirus is associated with filopodia. *Cellular microbiology* **2007**, *9*, 939-951 DOI: 10.1111/j.1462-5822.2006.00842.x.

718. Kolesnikova, L., *et al.* Influenza virus budding from the tips of cellular microvilli in differentiated human airway epithelial cells. *The Journal of general virology* **2013**, *94*, 971-976 DOI: 10.1099/vir.0.049239-0.

719. Carpenter, J.E., *et al.* Egress of light particles among filopodia on the surface of varicella-zoster virus-infected cells. *Journal of virology* **2008**, *82*, 2821-2835 DOI: 10.1128/jvi.01821-07.

720. Korobova, F., *et al.* Arp2/3 complex is important for filopodia formation, growth cone motility, and neuritogenesis in neuronal cells. *Molecular biology of the cell* **2008**, *19*, 1561-1574 DOI: 10.1091/mbc.E07-09-0964.

721. Norris, A.D., *et al.* The arp2/3 complex, unc-115/ablim, and unc-34/enabled regulate axon guidance and growth cone filopodia formation in caenorhabditis elegans. *Neural development* **2009**, *4*, 38 DOI: 10.1186/1749-8104-4-38.

722. Lee, K., *et al.* Self-assembly of filopodia-like structures on supported lipid bilayers. *Science* **2010**, *329*, 1341-1345 DOI: 10.1126/science.1191710.

723. Yang, C., *et al.* Novel roles of formin mdia2 in lamellipodia and filopodia formation in motile cells. *PLoS biology* **2007**, *5*, e317 DOI: 10.1371/journal.pbio.0050317.

724. Block, J., *et al.* Filopodia formation induced by active mdia2/drf3. *Journal of microscopy* **2008**, *231*, 506-517 DOI: 10.1111/j.1365-2818.2008.02063.x.

725. Schirenbeck, A., *et al.* The diaphanous-related formin ddia2 is required for the formation and maintenance of filopodia. *Nature cell biology* **2005**, *7*, 619-625 DOI: 10.1038/ncb1266.

726. Harris, E.S., *et al.* Assembly of filopodia by the formin frl2 (fmnl3). *Cytoskeleton* **2010**, *67*, 755-772 DOI: 10.1002/cm.20485.

727. Johnston, S.A., *et al.* Arp2/3 complex activity in filopodia of spreading cells. *BMC cell biology* **2008**, *9*, 65 DOI: 10.1186/1471-2121-9-65.

728. Bashour, A.M., *et al.* Iqgap1, a rac- and cdc42-binding protein, directly binds and cross-links microfilaments. *The Journal of cell biology* **1997**, *137*, 1555-1566 DOI: 10.1083/jcb.137.7.1555.

729. Yamashiro, S., *et al.* Localization of two iqgaps in cultured cells and early embryos of xenopus laevis. *Cell motility and the cytoskeleton* **2003**, *55*, 36-50 DOI: 10.1002/cm.10109.

730. Swart-Mataraza, J.M., *et al.* Iqgap1 is a component of cdc42 signaling to the cytoskeleton. *The Journal of biological chemistry* **2002**, *277*, 24753-24763 DOI: 10.1074/jbc.M111165200.

731. Bensenor, L.B., *et al.* Iqgap1 regulates cell motility by linking growth factor signaling to actin assembly. *Journal of cell science* **2007**, *120*, 658-669 DOI: 10.1242/jcs.03376.

732. Brandt, D.T., *et al.* Get to grips: Steering local actin dynamics with iqgaps. *EMBO reports* **2007**, *8*, 1019-1023 DOI: 10.1038/sj.embor.7401089.

733. Pelikan-Conchaudron, A., *et al.* The iqgap1 protein is a calmodulin-regulated barbed end capper of actin filaments: Possible implications in its function in cell migration. *The Journal of biological chemistry* **2011**, *286*, 35119-35128 DOI: 10.1074/jbc.M111.258772.

734. Mogilner, A., *et al.* The physics of filopodial protrusion. *Biophysical journal* **2005**, *89*, 782-795 DOI: 10.1529/biophysj.104.056515.

735. Yang, S., *et al.* Molecular mechanism of fascin function in filopodial formation. *The Journal of biological chemistry* **2013**, *288*, 274-284 DOI: 10.1074/jbc.M112.427971.

736. Gallop, J.L., *et al.* Phosphoinositides and membrane curvature switch the mode of actin polymerization via selective recruitment of toca-1 and snx9. *Proceedings of the National Academy of Sciences of the United States of America* **2013**, *110*, 7193-7198 DOI: 10.1073/pnas.1305286110.

737. Takano, K., *et al.* Efc/f-bar proteins and the n-wasp-wip complex induce membrane curvature-dependent actin polymerization. *The EMBO journal* **2008**, *27*, 2817-2828 DOI: 10.1038/emboj.2008.216.

738. Pichot, C.S., *et al.* Cdc42-interacting protein 4 promotes breast cancer cell invasion and formation of invadopodia through activation of n-wasp. *Cancer research* **2010**, *70*, 8347-8356 DOI: 10.1158/0008-5472.can-09-4149.

739. Daste, F., *et al.* Control of actin polymerization via the coincidence of phosphoinositides and high membrane curvature. *The Journal of cell biology* **2017**, *216*, 3745-3765 DOI: 10.1083/jcb.201704061.

740. Zhang, L., *et al.* Phosphatidylinositol 4, 5 bisphosphate and the actin cytoskeleton. *Sub-cellular biochemistry* **2012**, *59*, 177-215 DOI: 10.1007/978-94-007-3015-1_6.

741. Janmey, P.A., *et al.* Regulation of actin assembly by pi(4,5)p2 and other inositol phospholipids: An update on possible mechanisms. *Biochemical and biophysical research communications* **2018**, *506*, 307-314 DOI: 10.1016/j.bbrc.2018.07.155.

742. Rocha-Perugini, V., *et al.* Pip2: Choreographer of actin-adaptor proteins in the hiv-1 dance. *Trends in microbiology* **2014**, *22*, 379-388 DOI: 10.1016/j.tim.2014.03.009.

743. Ono, A. Relationships between plasma membrane microdomains and hiv-1 assembly. *Biology of the cell* **2010**, *102*, 335-350 DOI: 10.1042/bc20090165.

744. Johnson, J.L., *et al.* C-terminal di-arginine motif of cdc42 protein is essential for binding to phosphatidylinositol 4,5-bisphosphate-containing membranes and inducing cellular transformation. *The Journal of biological chemistry* **2012**, *287*, 5764-5774 DOI: 10.1074/jbc.M111.336487.

745. Choi, S., *et al.* Iqgap1 is a novel phosphatidylinositol 4,5 bisphosphate effector in regulation of directional cell migration. *The EMBO journal* **2013**, *32*, 2617-2630 DOI: 10.1038/emboj.2013.191.

746. Ramalingam, N., *et al.* Phospholipids regulate localization and activity of mdia1 formin. *European journal of cell biology* **2010**, *89*, 723-732 DOI: 10.1016/j.ejcb.2010.06.001.

747. Heckman, C.A., *et al.* Filopodia as sensors. *Cellular signalling* **2013**, *25*, 2298-2311 DOI: 10.1016/j.cellsig.2013.07.006.

748. Bornschlogl, T., *et al.* Filopodial retraction force is generated by cortical actin dynamics and controlled by reversible tethering at the tip. *Proceedings of the National Academy of Sciences of the United States of America* **2013**, *110*, 18928-18933 DOI: 10.1073/pnas.1316572110.

749. Grikscheit, K., *et al.* Formins at the junction. *Trends in biochemical sciences* **2016**, *41*, 148-159 DOI: 10.1016/j.tibs.2015.12.002.

750. Carramusa, L., *et al.* Mammalian diaphanous-related formin dia1 controls the organization of e-cadherin-mediated cell-cell junctions. *Journal of cell science* **2007**, *120*, 3870-3882 DOI: 10.1242/jcs.014365.

751. Atkins, B.D., *et al.* Inhibition of cdc42 during mitotic exit is required for cytokinesis. *The Journal of cell biology* **2013**, *202*, 231-240 DOI: 10.1083/jcb.201301090.

752. Wei, B., *et al.* Unique spatiotemporal activation pattern of cdc42 by gef1 and scd1 promotes different events during cytokinesis. *Molecular biology of the cell* **2016**, *27*, 1235-1245 DOI: 10.1091/mbc.E15-10-0700.

753. Zhu, X., *et al.* Proper regulation of cdc42 activity is required for tight actin concentration at the equator during cytokinesis in adherent mammalian cells. *Experimental cell research* **2011**, *317*, 2384-2389 DOI: 10.1016/j.yexcr.2011.06.019.

754. Miki, H., *et al.* Induction of filopodium formation by a wasp-related actin-depolymerizing protein n-wasp. *Nature* **1998**, *391*, 93-96 DOI: 10.1038/34208.

755. Lommel, S., *et al.* Actin pedestal formation by enteropathogenic escherichia coli and intracellular motility of shigella flexneri are abolished in n-wasp-defective cells. *EMBO reports* **2001**, *2*, 850-857 DOI: 10.1093/embo-reports/kve197.

756. Mattila, P.K., *et al.* Missing-in-metastasis and irsp53 deform pi(4,5)p2-rich membranes by an inverse bar domain-like mechanism. *The Journal of cell biology* **2007**, *176*, 953-964 DOI: 10.1083/jcb.200609176.

757. Lim, K.B., *et al.* The cdc42 effector irsp53 generates filopodia by coupling membrane protrusion with actin dynamics. *The Journal of biological chemistry* **2008**, *283*, 20454-20472 DOI: 10.1074/jbc.M710185200.

758. Qualmann, B., *et al.* Syndapin isoforms participate in receptor-mediated endocytosis and actin organization. *The Journal of cell biology* **2000**, *148*, 1047-1062 DOI: 10.1083/jcb.148.5.1047.

759. Popov, S., *et al.* Hiv-1 gag recruits pacsin2 to promote virus spreading. *Proceedings of the National Academy of Sciences of the United States of America* **2018**, *115*, 7093-7098 DOI: 10.1073/pnas.1801849115.

760. Goh, W.I., *et al.* Mdia1 and wave2 proteins interact directly with irsp53 in filopodia and are involved in filopodium formation. *The Journal of biological chemistry* **2012**, *287*, 4702-4714 DOI: 10.1074/jbc.M111.305102.

761. Freed, E.O. Hiv-1 gag: Flipped out for pi(4,5)p(2). *Proceedings of the National Academy of Sciences of the United States of America* **2006**, *103*, 11101-11102 DOI: 10.1073/pnas.0604715103.

762. Cherbas, L., *et al.* Cell lines. *Methods (San Diego, Calif.)* **2014**, *68*, 74-81 DOI: 10.1016/j.ymeth.2014.01.006.

763. Risbridger, G.P. Human cell lines as tools of our trade: "Laying it on the (cell) line". *Molecular endocrinology (Baltimore, Md.)* **2015**, *29*, 1-2 DOI: 10.1210/me.2014-1376.

764. Browne, S.M., *et al.* Selection methods for high-producing mammalian cell lines. *Trends in biotechnology* **2007**, *25*, 425-432 DOI: 10.1016/j.tibtech.2007.07.002.

765. Swiech, K., *et al.* Recombinant glycoprotein production in human cell lines. *Methods in molecular biology* **2015**, *1258*, 223-240 DOI: 10.1007/978-1-4939-2205-5_12.

766. Niu, N., *et al.* In vitro human cell line models to predict clinical response to anticancer drugs. *Pharmacogenomics* **2015**, *16*, 273-285 DOI: 10.2217/pgs.14.170.

767. Genzel, Y. Designing cell lines for viral vaccine production: Where do we stand? *Biotechnology journal* **2015**, *10*, 728-740 DOI: 10.1002/biot.201400388.

768. Kaur, G., *et al.* Cell lines: Valuable tools or useless artifacts. *Spermatogenesis* **2012**, *2*, 1-5 DOI: 10.4161/spmg.19885.

769. Geraghty, R.J., *et al.* Guidelines for the use of cell lines in biomedical research. *British journal of cancer* **2014**, *111*, 1021-1046 DOI: 10.1038/bjc.2014.166.

770. Zhang-Lab_Resource. Lenticrisprv2 and lentiguide-puro: Lentiviral crispr/cas9 and single guide rna. http://genome-engineering.org/gecko/wp-content/uploads/2013/12/lentiCRISPRv2-and-lentiGuide-oligo-cloning-protocol.pdf

771. Laguette, N., *et al.* Samhd1 is the dendritic- and myeloid-cell-specific hiv-1 restriction factor counteracted by vpx. *Nature* **2011**, *474*, 654-657 DOI: 10.1038/nature10117.

772. Lahouassa, H., *et al.* Samhd1 restricts the replication of human immunodeficiency virus type 1 by depleting the intracellular pool of deoxynucleoside triphosphates. *Nature immunology* **2012**, *13*, 223-228 DOI: 10.1038/ni.2236.

773. Hofmann, H., *et al.* The vpx lentiviral accessory protein targets samhd1 for degradation in the nucleus. *Journal of virology* **2012**, *86*, 12552-12560 DOI: 10.1128/jvi.01657-12.

774. Bobadilla, S., *et al.* Efficient transduction of myeloid cells by an hiv-1-derived lentiviral vector that packages the vpx accessory protein. *Gene therapy* **2013**, *20*, 514-520 DOI: 10.1038/gt.2012.61.

775. Durand, S., *et al.* Tailored hiv-1 vectors for genetic modification of primary human dendritic cells and monocytes. *Journal of virology* **2013**, *87*, 234-242 DOI: 10.1128/jvi.01459-12.

776. Aiken, C. Pseudotyping human immunodeficiency virus type 1 (hiv-1) by the glycoprotein of vesicular stomatitis virus targets hiv-1 entry to an endocytic pathway and suppresses both the requirement for nef and the sensitivity to cyclosporin a. *Journal of virology* **1997**, *71*, 5871-5877.

777. van Wilgenburg, B., *et al.* Efficient, long term production of monocyte-derived macrophages from human pluripotent stem cells under partly-defined and fully-defined conditions. *PloS one* **2013**, *8*, e71098 DOI: 10.1371/journal.pone.0071098.

778. Richter, C., *et al.* Generation of inducible immortalized dendritic cells with proper immune function in vitro and in vivo. *PloS one* **2013**, *8*, e62621 DOI: 10.1371/journal.pone.0062621.

779. Kim, J.H., *et al.* High cleavage efficiency of a 2a peptide derived from porcine teschovirus-1 in human cell lines, zebrafish and mice. *PloS one* **2011**, *6*, e18556 DOI: 10.1371/journal.pone.0018556.

780. Mateyak, M.K., *et al.* Eef1a: Thinking outside the ribosome. *The Journal of biological chemistry* **2010**, *285*, 21209-21213 DOI: 10.1074/jbc.R110.113795.

781. Suter, D.M., *et al.* Rapid generation of stable transgenic embryonic stem cell lines using modular lentivectors. *Stem cells (Dayton, Ohio)* **2006**, *24*, 615-623 DOI: 10.1634/stemcells.2005-0226.

782. Sunseri, N., *et al.* Human immunodeficiency virus type 1 modified to package simian immunodeficiency virus vpx efficiently infects macrophages and dendritic cells. *Journal of virology* **2011**, *85*, 6263-6274 DOI: 10.1128/jvi.00346-11.

783. Cohen, J. Crispr is too fat for many therapies, so scientists are putting the genome editor on a diet. https://www.sciencemag.org/news/2018/08/crispr-too-fat-many-therapies-so-scientists-are-putting-genome-editor-diet

784. Moyes, K.W., *et al.* Genetically engineered macrophages: A potential platform for cancer immunotherapy. *Human gene therapy* **2017**, *28*, 200-215 DOI: 10.1089/hum.2016.060.

785. Shen, C.C., *et al.* Synthetic switch to minimize crispr off-target effects by self-restricting cas9 transcription and translation. *Nucleic acids research* **2019**, *47*, e13 DOI: 10.1093/nar/gky1165.

786. Roth, T.L., *et al.* Reprogramming human t cell function and specificity with non-viral genome targeting. *Nature* **2018**, *559*, 405-409 DOI: 10.1038/s41586-018-0326-5.

787. Hultquist, J.F., *et al.* Crispr-cas9 genome engineering of primary cd4(+) t cells for the interrogation of hiv-host factor interactions. *Nature protocols* **2019**, *14*, 1-27 DOI: 10.1038/s41596-018-0069-7.

788. DiTommaso, T., *et al.* Cell engineering with microfluidic squeezing preserves functionality of primary immune cells in vivo. *Proceedings of the National Academy of Sciences of the United States of America* **2018**, *115*, E10907-e10914 DOI: 10.1073/pnas.1809671115.

789. Prel, A., *et al.* Highly efficient in vitro and in vivo delivery of functional rnas using new versatile ms2-chimeric retrovirus-like particles. *Molecular therapy. Methods & clinical development* **2015**, *2*, 15039 DOI: 10.1038/mtm.2015.39.

790. Lu, B., *et al.* Delivering sacas9 mrna by lentivirus-like bionanoparticles for transient expression and efficient genome editing. *Nucleic acids research* **2019**, *47*, e44 DOI: 10.1093/nar/gkz093.

791. Cudmore, S., *et al.* Viral manipulations of the actin cytoskeleton. *Trends in microbiology* **1997**, *5*, 142-148 DOI: 10.1016/s0966-842x(97)01011-1.

792. Aspenstrom, P. Formin-binding proteins: Modulators of formin-dependent actin polymerization. *Biochimica et biophysica acta* **2010**, *1803*, 174-182 DOI: 10.1016/j.bbamcr.2009.06.002.

793. Manes, S., *et al.* Pathogens: Raft hijackers. *Nature reviews. Immunology* **2003**, *3*, 557-568 DOI: 10.1038/nri1129.

794. van Rheenen, J., *et al.* Pip2 signaling in lipid domains: A critical re-evaluation. *The EMBO journal* **2005**, *24*, 1664-1673 DOI: 10.1038/sj.emboj.7600655.

795. Eira, J., *et al.* The cytoskeleton as a novel therapeutic target for old neurodegenerative disorders. *Progress in neurobiology* **2016**, *141*, 61-82 DOI: 10.1016/j.pneurobio.2016.04.007.

796. Sequeira, V., *et al.* The physiological role of cardiac cytoskeleton and its alterations in heart failure. *Biochimica et biophysica acta* **2014**, *1838*, 700-722 DOI: 10.1016/j.bbamem.2013.07.011.

797. Hall, A. The cytoskeleton and cancer. *Cancer metastasis reviews* **2009**, *28*, 5-14 DOI: 10.1007/s10555-008-9166-3.

798. Schwegmann, A., *et al.* Host-directed drug targeting of factors hijacked by pathogens. *Science signaling* **2008**, *1*, re8 DOI: 10.1126/scisignal.129re8.

799. Kaufmann, S.H.E., *et al.* Host-directed therapies for bacterial and viral infections. *Nature reviews. Drug discovery* **2018**, *17*, 35-56 DOI: 10.1038/nrd.2017.162.

800. Hawn, T.R., *et al.* New tricks for old dogs: Countering antibiotic resistance in tuberculosis with host-directed therapeutics. *Immunological reviews* **2015**, *264*, 344-362 DOI: 10.1111/imr.12255.

801. Chiang, C.Y., *et al.* Mitigating the impact of antibacterial drug resistance through host-directed therapies: Current progress, outlook, and challenges. *mBio* **2018**, *9*, DOI: 10.1128/mBio.01932-17.

802. Schein, C.H. Repurposing approved drugs on the pathway to novel therapies. *Medicinal research reviews* **2019**, DOI: 10.1002/med.21627.

803. Pagano, M.A., *et al.* Viral proteins and src family kinases: Mechanisms of pathogenicity from a "liaison dangereuse". *World journal of virology* **2013**, *2*, 71-78 DOI: 10.5501/wjv.v2.i2.71.

804. Van den Broeke, C., *et al.* Rho'ing in and out of cells: Viral interactions with rho gtpase signaling. *Small GTPases* **2014**, *5*, e28318 DOI: 10.4161/sgtp.28318.

805. Guarino, M. Src signaling in cancer invasion. *Journal of cellular physiology* **2010**, *223*, 14-26 DOI: 10.1002/jcp.22011.

806. Molinie, N., *et al.* The arp2/3 regulatory system and its deregulation in cancer. *Physiological reviews* **2018**, *98*, 215-238 DOI: 10.1152/physrev.00006.2017.

807. Jansen, S., *et al.* Paving the rho in cancer metastasis: Rho gtpases and beyond. *Pharmacology & therapeutics* **2018**, *183*, 1-21 DOI: 10.1016/j.pharmthera.2017.09.002.

808. Cha, Y., *et al.* Drug repurposing from the perspective of pharmaceutical companies. *British journal of pharmacology* **2018**, *175*, 168-180 DOI: 10.1111/bph.13798.

809. Maldonado, M.D.M., *et al.* Targeting rac and cdc42 gtpases in cancer. *Cancer research* **2018**, *78*, 3101-3111 DOI: 10.1158/0008-5472.can-18-0619.

810. De, P., *et al.* Rac1 takes the lead in solid tumors. *Cells* **2019**, *8*, DOI: 10.3390/cells8050382.

811. Ji, J., *et al.* Rac1 is correlated with aggressiveness and a potential therapeutic target for gastric cancer. *International journal of oncology* **2015**, *46*, 1343-1353 DOI: 10.3892/ijo.2015.2836.

812. Marei, H., *et al.* Rac1 in human diseases: The therapeutic potential of targeting rac1 signaling regulatory mechanisms. *Small GTPases* **2017**, *8*, 139-163 DOI: 10.1080/21541248.2016.1211398.

813. Xiao, X.H., *et al.* Regulating cdc42 and its signaling pathways in cancer: Small molecules and microrna as new treatment candidates. *Molecules (Basel, Switzerland)* **2018**, *23*, DOI: 10.3390/molecules23040787.

814. Peretti, A.S., *et al.* The r-enantiomer of ketorolac delays mammary tumor development in mouse mammary tumor virus-polyoma middle t antigen (mmtv-pymt) mice. *The American journal of pathology* **2018**, *188*, 515-524 DOI: 10.1016/j.ajpath.2017.10.018.

815. Zhang, Y., *et al.* Focus on cdc42 in breast cancer: New insights, target therapy development and non-coding rnas. *Cells* **2019**, *8*, DOI: 10.3390/cells8020146.

816. Vallianou, N.G., *et al.* Statins and cancer. *Anti-cancer agents in medicinal chemistry* **2014**, *14*, 706-712.

817. del Real, G., *et al.* Statins inhibit hiv-1 infection by down-regulating rho activity. *The Journal of experimental medicine* **2004**, *200*, 541-547 DOI: 10.1084/jem.20040061.

818. Caffo, L., *et al.* Simvastatin and ml141 decrease intracellular streptococcus pyogenes infection. *Current pharmaceutical biotechnology* **2019**, DOI: 10.2174/1389201020666190618115154.

819. Johnson, M., *et al.* Iqgap1 regulation and roles in cancer. *Cellular signalling* **2009**, *21*, 1471-1478 DOI: 10.1016/j.cellsig.2009.02.023.

820. White, C.D., *et al.* Iqgaps in cancer: A family of scaffold proteins underlying tumorigenesis. *FEBS letters* **2009**, *583*, 1817-1824 DOI: 10.1016/j.febslet.2009.05.007.

821. Cui, X., *et al.* Elevated iqgap1 and cdc42 levels correlate with tumor malignancy of human glioma. *Oncology reports* **2017**, *37*, 768-776 DOI: 10.3892/or.2016.5341.

822. Zeng, F., *et al.* Ras gtpase-activating-like protein iqgap1 (iqgap1) promotes breast cancer proliferation and invasion and correlates with poor clinical outcomes. *Medical science monitor : international medical journal of experimental and clinical research* **2018**, *24*, 3315-3323 DOI: 10.12659/msm.909916.

823. Wang, X.X., *et al.* Targeted knockdown of iqgap1 inhibits the progression of esophageal squamous cell carcinoma in vitro and in vivo. *PloS one* **2014**, *9*, e96501 DOI: 10.1371/journal.pone.0096501.

824. Su, D., *et al.* Knockdown of iqgap1 inhibits proliferation and epithelial-mesenchymal transition by wnt/beta-catenin pathway in thyroid cancer. *OncoTargets and therapy* **2017**, *10*, 1549-1559 DOI: 10.2147/ott.s128564.

825. Fan, J., *et al.* Mir124 inhibits cell growth through targeting iqgap1 in colorectal cancer. *Molecular medicine reports* **2018**, *18*, 5270-5278 DOI: 10.3892/mmr.2018.9518.

826. Leung, J., *et al.* Interaction of moloney murine leukemia virus matrix protein with iqgap. *The EMBO journal* **2006**, *25*, 2155-2166 DOI: 10.1038/sj.emboj.7601097.

827. Gladue, D.P., *et al.* Interaction between core protein of classical swine fever virus with cellular iqgap1 protein appears essential for virulence in swine. *Virology* **2011**, *412*, 68-74 DOI: 10.1016/j.virol.2010.12.060.

828. Dolnik, O., *et al.* Interaction with tsg101 is necessary for the efficient transport and release of nucleocapsids in marburg virus-infected cells. *PLoS pathogens* **2014**, *10*, e1004463 DOI: 10.1371/journal.ppat.1004463.

829. Dolnik, O., *et al.* Marburg virus inclusions: A virus-induced microcompartment and interface to multivesicular bodies and the late endosomal compartment. *European journal of cell biology* **2015**, *94*, 323-331 DOI: 10.1016/j.ejcb.2015.05.006.

830. Lu, J., *et al.* Host iqgap1 and ebola virus vp40 interactions facilitate virus-like particle egress. *Journal of virology* **2013**, *87*, 7777-7780 DOI: 10.1128/jvi.00470-13.

831. Morita, E., *et al.* Human escrt and alix proteins interact with proteins of the midbody and function in cytokinesis. *The EMBO journal* **2007**, *26*, 4215-4227 DOI: 10.1038/sj.emboj.7601850.

832. Dussupt, V., *et al.* The nucleocapsid region of hiv-1 gag cooperates with the ptap and lypxnl late domains to recruit the cellular machinery necessary for viral budding. *PLoS pathogens* **2009**, *5*, e1000339 DOI: 10.1371/journal.ppat.1000339.

833. Welch, M.D., *et al.* Interaction of human arp2/3 complex and the listeria monocytogenes acta protein in actin filament nucleation. *Science* **1998**, *281*, 105-108 DOI: 10.1126/science.281.5373.105.

834. Suzuki, T., *et al.* Neural wiskott-aldrich syndrome protein is implicated in the actin-based motility of shigella flexneri. *The EMBO journal* **1998**, *17*, 2767-2776 DOI: 10.1093/emboj/17.10.2767.

835. Paterson, H.F., *et al.* Microinjection of recombinant p21rho induces rapid changes in cell morphology. *The Journal of cell biology* **1990**, *111*, 1001-1007 DOI: 10.1083/jcb.111.3.1001.

836. Shalloway, D., *et al.* Molecular cloning and characterization of the chicken gene homologous to the transforming gene of rous sarcoma virus. *Cell* **1981**, *24*, 531-541 DOI: 10.1016/0092-8674(81)90344-5.

837. Wickramarachchi, D.C., *et al.* Immune pathology associated with altered actin cytoskeleton regulation. *Autoimmunity* **2010**, *43*, 64-75 DOI: 10.3109/08916930903374634.

838. Zumla, A., *et al.* Host-directed therapies for infectious diseases: Current status, recent progress, and future prospects. *The Lancet. Infectious diseases* **2016**, *16*, e47-63 DOI: 10.1016/s1473-3099(16)00078-5.